AD-763 918

SYMPOSIUM ON ACOUSTIC FATIGUE

Advisory Group for Aerospace Research and Development

May 1973
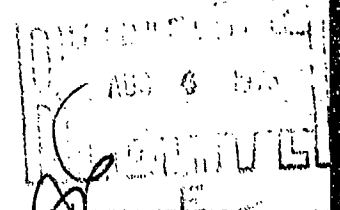
AGARD

ADVISORY GROUP FOR AEROSPACE RESEARCH & DEVELOPMENT

7 RUE ANCELLE · 92200 · NEUILLY SUR SEINE · FRANCE

AGARD CONFERENCE PROCEEDINGS No. 113

on

Symposium on Acoustic Fatigue

NORTH ATLANTIC TREATY ORGANIZATION

DISTRIBUTION AND AVAILABILITY

AGARD-CP-113

NORTH ATLANTIC TREATY ORGANIZATION

ADVISORY GROUP FOR AEROSPACE RESEARCH AND DEVELOPMENT

(ORGANISATION DU TRAITE DE L'ATLANTIQUE NORD)

AGARD Conference Proceedings No.113

SYMPOSIUM ON ACOUSTIC FATIGUE

THE MISSION OF AGARD

The mission of AGARD is to bring together the leading personalities of the NATO nations in the fields of science and technology relating to aerospace for the following purposes:

— Exchanging of scientific and technical information;

— Continuously stimulating advances in the aerospace sciences relevant to strengthening the common defence posture;

- Improving the co-operation among member nations in aerospace research and development;

— Providing scientific and technical advice and assistance to the North Atlantic Military Committee in the field of aerospace research and development;

— Rendering scientific and technical assistance, as requested, to other NATO bodies and to member nations in connection with research and development problems in the aerospace field;

— Providing assistance to member nations for the purpose of increasing their scientific and technical potential;

— Recommending effective ways for the member nations to use their research and development capabilities for the common benefit of the NATO community.

The highest authority within AGARD is the National Delegates Board consisting of officially appointed senior representatives from each member nation. The mission of AGARD is carried out through the Panels which are composed of experts appointed by the National Delegates, the Consultant and Exchange Program and the Aerospace Applications Studies Program. The results of AGARD work are reported to the member nations and the NATO Authorities through the AGARD series of publications of which this is one.

Participation in AGARD activities is by invitation only and is normally limited to citizens of the NATO nations.

PREFACE

The Structures and Materials Panel's Working Group on Acoustic Fatigue, under the Chairmanship of Mr A.H.Hall, has for many years been organising AGARD support for international collaboration in formulating and resolving problems relating to acoustic fatigue. In the year before this Symposium the Working Group's co-ordinator, Professor B.L.Clarkson, prepared an inventory of acoustic fatigue test facilities and this has been of great assistance to specialists in giving them a better understanding of each other's experimental observations and procedures. In addition National Co-ordinators, appointed by six of the NATO nations, have been providing basic data and reviewing the preparation of data sheets on acoustic fatigue topics. The objective of the present Symposium was to bring together many of these specialists and others in order to review progress in the development of design procedures for the avoidance of acoustic fatigue and to discuss the presentation of the series of AGARD data sheets. Some of these data sheets, published as AGARDograph 162, were discussed at the Symposium and others are to be issued in 1973.

The Symposium revealed that, since the Panel first illuminated this design p⌐ ⌐m some years ago, considerable progress has been made in the understanding of acoustic loadings, the response of structures to those loadings and the methods by which the integrity of acoustically loaded structures may be assessed.

The panel is grateful to Mr Hall, his Working Group, Professor Clarkson, The National Co-ordinators, authors and attendees, for the high quality of the papers presented and of the discussion which ensued from them.

CONTENTS

ALLOCUTION D'OUVERTURE

par

René LOUBET
"AEROSPATIALE" - Bureau d'Etudes
Boite Postale 3153
31053 - TOULOUSE CEDEX

RESUME

La complexité croissante des problèmes rencontrés en particulier dans le domaine de la fatigue acoustique, conduit à un grand nombre d'études et de travaux divers, par exemple sur les matériaux nouveaux, les solutions constructives, les méthodes de prévision.

Ceci oblige dans les perspectives actuelles, élargies par la coopération effective entre les Nations, à un effort croissant dans le domaine des contacts et de l'expression correcte des besoins, d'autre part, à un effort de vulgarisation des méthodes et moyens propres aux Spécialistes de la fatigue acoustique.

C'est à un membre français de l'Organisation de Cooperation de l'AGARD qu'a été réservé l'honneur d'ouvrir la séance inaugurale des travaux du "Symposium de Fatigue Acoustique". Je m'acquitte donc, très volontiers, de cette première et traditionnelle mission.

Avec tout autant de conviction, et cette fois au nom des Toulousains, je tiens à souhaiter aux congressistes la bienvenue dans notre ville qui apprécie cette occasion de vous accueillir; TOULOUSE que l'on qualifie volontiers de Capitale française de l'Aéronautique et de l'Espace, puisqu'effectivement elle possède la majorité des Centres Nationaux Officiels de Recherches et d'Essais, les grandes Ecoles formant les ingénieurs de l'aviation et qu'elle est le principal foyer d'activité de plusieurs de nos grandes sociétés dont l'AEROSPATIALE.

Bien qu'aucun d'entre vous ne l'ignore, comment ne pas évoquer aussi cette histoire si riche, non seulement de "machines" parmi les plus audacieuses en leur temps qui aient été conçues et pilotées, mais a'' i d'hommes et d'entreprises légendaires au temps des premiers pas de l'aviation civile et jusqu'aux développements que vous savez.

TOULOUSE a certes des lettres de noblesse plus anciennes, mais reconnaissons que ce sont bien les envols de "CARAVELLE", "CONCORDE" et très bientôt du dernier né "l'AIRBUS" qui consacrent ou ont connaître cette vocation prestigieuse aux yeux du monde. Ces mêmes grands noms, en contrepartie, obligent chaque jour TOULOUSE à se montrer digne de son passé, digne des possibilités actuelles techniques et industrielles déjà élargies à l'échelle de la Coopération effective entre Européens, en attendant plus, évolution que tous comprennent et que même les plus fidèles au passé reconnaissent comme nécessaire, tant le bénéfice en est évident.

Pour en venir à notre sujet, je voudrais souligner combien cette tendance à la coopération effective des firmes et des nations, influence les perspectives d'avenir. Sur le plan général, les projets, hier irréalisables sont aujourd'hui possibles et concrétisés. Il y a, dans le rythme du progrès et dans la carrière de chacun, la même discontinuité que dans les moyens d'étude et de production. Les techniques nouvelles s'imposent nombreuses et de plus en plus complexes, faisant grossir et proliférer les familles de spécialistes. Comme il est essentiel de contrôler, d'orchestrer l'action des spécialistes en vue d'une efficacité optimum de l'ensemble, il se pose une question essentielle de liaison, de clarté de langage.

Les données de travail doivent avoir des bases solides, les efforts doivent rester parfaitement coordonnés, sans que l'initiative soit étouffée, les échanges d'idées nombreux et efficaces.

Enfin, le moment venu, les responsables disposent du résultat de recherches menées parfois à des milliers de kilomètres par des hommes isolés et qui le resteraient si leurs travaux n'avaient pas été orientés et compris.

Pour cela, rien ne remplace les contacts directs et leur importance va donc en croissant; des réunions comme celle que nous allons tenir ici en fournissent l'occasion, il faut la saisir.

La fatigue acoustique illustre bien la nécessité d'information réciproque, condition de succès.

Il se trouve que les perspectives, en matière de fatigue acoustique et d'aviation civile, sont larges et relativement précises. Le développement des propulseurs, des matériaux, des formules nouvelles d'appareils, fait l'objet de prévisions à moyen terme dépourvues de mystère. C'est ainsi que la protection contre le bruit est le grand sujet du moment et cela ne peut qu'accroître, je suppose, l'importance des écrans.

Parmi les perspectives que je dois évoquer, la plus importante pour nous, est probablement celle de l'apparition des matériaux nouveaux, en particulier les composites à base de fibres de carbone et de bore.

Confrontés aux matériaux classiques, ils vont prendre une place grandissante, en permettant un gain de poids spectaculaire sur les Structures, environ 25% pour donner un ordre de grandeur.

Il convient donc d'approfondir leur étude en fatigue acoustique pour deux raisons principales et étroitement dépendantes :

D'abord, parce que nombre d'applications parmi celles déjà tentées, concernent précisément des structures sollicitées en acoustique. Citons, par exemple, les revêtements d'avion V/STOL, les carénages de soufflantes de turbo-réacteurs, les gouvernes du type élevon d'avion supersonique, etc....

En second lieu, parce que les caractéristiques des composites en fatigue acoustique sont tout spécialement intéressantes, les coefficients d'amortissement sont bien supérieurs à ceux des éléments métalliques et les mécanismes de rupture en flexion se traduisent par une baisse progressive de rigidité plutôt que par la progression de criques macroscopiques.

Au stade expérimental actuel, on est passé de la plaque à des éléments de structure assez importants, tels que : caisson de voilure, élevon complet du type "CONCORDE". Sur le plan théorique, on est obligé d'appliquer la théorie des plaques anisotropes, les modes et les fréquences propres étant parfois très différents de ceux des plaques métalliques isotropes. Dans les bureaux d'études et les usines, on aborde sérieusement la phase expérimentale qui doit permettre l'avènement d'une nouvelle gamme de produits au stade de la production, dans la période des cinq prochaines années.

L'importance des travaux que méritent ces matériaux, est aussi accrue du fait des longévités de plus en plus élevées que l'on demande aux constructeurs de garantir. Ceci suppose connus les résultats d'essais d'endurance représentatifs, compte tenu non seulement des sollicitations mécaniques, mais aussi des effets "temps – température" ou autres, rencontrés en exploitation. On sait que les métaux se prêtent en général à une importante contraction des temps d'essai, moyennant par exemple, une élévation de température.

Les matériaux organiques, à priori, ne respectent pas les mêmes lois; seule une expérimentation rigoureuse, parfaitement contrôlée, pourra répondre à ce genre de questions si elles sont bien posées par les vrais intéressés et éviter du même coup, à plus ou moins long terme, des déboires ruineux.

Nous pouvons évoquer, à cette occasion, cette difficulté permanente rencontrée en fatigue, et encore plus en fatigue acoustique; je veux parler de l'imprécision des calculs, des règles de cumul et bien sûr, des résultats expérimentaux. Ceci est la conséquence de la complexité des charges et de leur caractère aléatoire et des conditions d'essais en général : il y a un art de la fatigue acoustique, à côté de la science.

Lorsqu'on est pressé d'obtenir un résultat, il n'est pas rare qu'on accepte un certain nombre d'hypothèses simplificatrices sur les spectres d'excitation, les dimensions, les conditions aux limites de l'éprouvette, etc.... En outre, on majore l'intensité des charges.

Malgré les précautions prises, le résultat est contestable en valeur absolue surtout si l'éprouvette est compliquée. S'il s'agit de très longs essais, l'erreur relative sur l'endurance due à un défaut global, ou local, du spectre ou de l'éprouvette tend à croître. Une contrainte résiduelle d'usinage ou de formage peut avoir des conséquences déterminantes. Il est toujours plus ou moins difficile de faire un bilan complet des causes d'erreurs et, seuls des essais comparatifs peuvent analyser les problèmes.

Il y a beaucoup à faire pour éviter les déceptions dans ce domaine puisque les moyens théoriques et pratiques existent. Que peut-on attendre d'une méthode donnée, de telle installation d'essai ? La jeune science des sollicitations et des réponses acoustiques n'a pas encore atteint son plein épanouissement. Les publications du type AGARDOGRAPH apportent un élément de rigueur mis à la portée d'un plus grand nombre, dans un esprit de synthèse et de compréhension.

Je souhaite à tous, pour terminer, de trouver dans ce congrès, la meilleure occasion de collaboration efficace, en exprimant leurs besoins, leurs possibilités, leurs conclusions, pour un rendement accru de nos efforts.

INFLUENCE OF THE GROUND ON THE NEAR FIELD NOISE
LEVELS OF JET-SUPPORTED V/STOL AIRCRAFT

by

Dr.-Ing. Rudolf Scholten

Leiter der Abteilung
"Strukturdynamik und Akustik"

DORNIER AG
FRIEDRICHSHAFEN
DEUTSCHLAND

SUMMARY

A method for calculating the near field noise level of
a free jet (without ground effect) by means of a modified
Lighthill theory using measured reference sound fields will
be explained.

The shortcomings of the reference fields used to date as well
as means to eliminate them will be shown. In addition, a possi-
bility for determining, with sufficiently good practical accu-
racy, the frequency spectra in the near sound field by means
of a modified Strouhal number will be described. Then, the
validity of the "modified Lighthill theory" will be proven by
means of two greatly differing engine jets.

This will be followed by a discussion of comprehensive measured
data of "wall jet sound fields" (sound fields of an engine jet
directed vertically towards the ground) and the influence of the
essential parameters affecting the sound field. The measured
results will also be compared to the calculations.

And finally, it will be demonstrated on the V/STOL aircraft
DORNIER Do 31 that the ground effect can lead to a considerably
increased noise level, and that the calculation method yields
good practical results, even with a relatively complicated system
of engine jets.

Many novel problems are encountered in the VTOL as compared to the CTOL technique,
of which the noise problem is of singular importance.

1) Much more noise energy is radiated on account of the
   installed high engine power required for vertical
   take-off and landing.

2) Due to the ground influence the noise levels can
   considerably increase in the near field, i.e. within
   reach of the airframe, during take-off and landing.

We found with the Dornier Do 31 (Fig. 1), that noise fatigue failures occured within a
very short time on the airframe.

Therefor it is important for the project and design engineer, to know such loads at an
early date to ensure a fail-safe design of the airframe with respect to noise fatigue.

A practical method for estimating the noise levels on the airframe, which also takes the
influence of the ground into account, is needed for that purpose.

FREE JET

We employ a semi-empiric method for the calculation of the noise level of a free undis-
turbed engine jet. This method is based on the Lighthill theory [1] which states that the
total radiated noise energy of an engine jet is proportional to the eighth power of the
jet velocity.

For the noise intensity, which is proportional to the quadratic mean of the sound pressure,
the Lighthill formula reads:

$$ I \sim K \frac{\rho_i^2}{c_o^5} \frac{D^3}{r^2} a^3 \left[\frac{v}{v_i} \right]^8 \sim \frac{\overline{p^2}}{\rho_o c_o} $$

(1)

This formula however is only valid in the far field, which is of relevance for the presently much discussed noise pollution and of special interest in the VTOL technique [2].

We assume this formula to be valid for any point within the near field if the velocity exponent is a function of the location.

We say further:
The noise fields of two engine jets with different nozzle diameters are similar to each other. The law of similarity is the modified Lighthill formula.
The velocity exponent is the same at same nozzle diameter-related locations (Fig. 2).

If the noise field and the velocity exponent field of a so-called reference engine are known, unknown noise fields of engine jets can be determined using the following equation:

$$L_k = L' + 10\log_{10} \frac{\rho_{1k}^2 \; a_{ok}^4 (v_k/a_{ok})^{N_k}}{\rho_1'^2 \; a_0'^4 (v'/a_0')^{N'}} \tag{2}$$

Calculations with the available reference fields of a Rolls Royce Avon engine and the fields given in the RAeS data sheets sometimes showed noise levels which deviated so much from the measured ones as not to be acceptable for practical purposes (> 12 dB). The deviation of the velocity exponents of these two reference fields made even the similarity theory questionable (Fig. 3).

In order to solve this problem, we performed tests on two extremely different engines, Marboré and Orenda [3], [4].

A test rig was built for the Marboré engine (Fig. 4) which allowed both free jet and wall jet investigations to be carried out, all relevant parameters having been varied. The noise measurements on the Orenda engine were performed with an existing ground erosion test rig (Fig. 5). A total of 8 free jet noise fields at H = 6 m, and 20 wall jet noise fields were measured (H_D/D of 3 - 28).

It could be demonstrated with the free field measurement that the law of similarity is nevertheless valid. For both engine jets, Marboré and Orenda, the velocity exponents N at equal R/D (Fig. 3) are the same:

$$N_k(r, r_k) = N'(\frac{D'}{D_k} r_k) \tag{3}$$

The analysis of the frequency spectra (Fig. 6) showed that despite the relatively great nozzle plane height of 6 m from the ground a reflection influence was still present in the measured free fields. The overall sound pressure field of the Orenda engine could however easily be corrected by iteration to an absolute free field, and introduced as a new reference field.

The comparison of the measured fields with those calculated by means of the new reference fields showed that the maximum deviations in the noise levels of these extremely different engine jets (Marboré/Orenda) amount to less than 3 dB (Tab. 1).

This now allows the calculation of the OASPL fields of free jets with an accuracy sufficient for practical purposes.

In principle, it should also now be possible to determine the frequency spectra in this way by means of one third octave sound pressure level reference fields. However, as can easily be shown, it is not possible to determine the influence of the nozzle diameter on the frequency distribution in this way.

Therefore it is advisable, and also more economical, to start from non-dimensional reference spectra. A Strouhal number modified by v. Gierke [5] proved to be the most useful transfer function:

$$S_{mod} = \frac{fD}{v} \sqrt{\frac{T_s}{T_0}} \tag{4}$$

The spectra, first however, had to be corrected to pure free jet spectra, since part of the measured spectra contained, as mentioned above, considerable ground reflection influences.

The correction of the overall noise level was relatively simple. The spectra, however, cannot be corrected in this way. The procedure given by Hoch & Thomas [6], which allows a correction by means of the autocorrelation function, cannot be employed here either, as it assumes a spherosymmetric noise propagation.

This assumption can be made for great distances from the nozzle, but not for the near field because of the marked directional characteristic of the jet noise field.

However by introducing a weighting function f (ε) which contains the directional characteristic, this procedure can also be used for the near field, even if there is no spherosymmetry:

$$\Delta L \, [dB] = 10 \, \log \left[1 + \bar{z}^2 + 2\bar{z} \left(\frac{\sin\alpha \frac{\Delta R}{\lambda_i}}{\alpha \frac{\Delta R}{\lambda_i}} \cos\beta \, \frac{\Delta R}{\lambda_i} \right) \right] \tag{5}$$

with

$$\bar{z} = \frac{f(\psi)}{z} \qquad \text{and} \qquad f(z) = \frac{p_r}{p_d} \tag{6}$$

Using the correction curves (Fig. 7) the measured frequency spectra can now be corrected to the pure free jet, and nondimensional reference spectra can be established for any point of the near field, on the basis of which the frequency distribution of the calculated OASPL can then be determined.

WALL JET

The noise field of an engine jet directed vertically towards the ground is completely different from that of a free jet in its overall level, as well as in the directional characteristic and the frequency distribution.

In the case of an engine jet directed vertically towards the ground, the noise level is essentially composed of three parts (Fig. 8):

a)   the direct free jet noise

b)   the ground-reflected noise

c)   the noise generated by the turbulent area on the ground.

As tests with the wall jet revealed, the noise generated by the turbulent area on the ground is only of significance for high jet velocities if the height of the nozzle plane above the ground becomes $H_D/D < 5$, i.e. if the jet core is cut by the ground. Such a low nozzle plane height above the ground in connection with high jet velocities however is not practicable in the VTOL technique for many reasons (e.g. recirculation, ground erosion).

The main part of the level increase for wall jets is thus to be attributed to ground reflection.
The measured wall jet noise fields show particularly in case of great jet velocities, a marked noise level increase in direction of the reflected maximum propagation of the free jet noise field (Fig. 9). The reflected noise can be simulated by an imaginary noise field equal to and mirrored by that of the free jet.

This allows the application of the calculation method explained above without modification, simple by superimposing the noise levels of a mirrored free engine jet on the free field noise levels of the real jet (Fig. 10). The comparison of the calculation with the measurement proves that the wall jet noise field can really be calculated in this way if $H_D/D > 5$ and assuming a rigid reflection surface (e.g. concrete).

All measured wall jet fields were calculated for all H_D/D at the highest and lowest jet velocity and compared with the test results. The maximum deviations between measurements and calculations were in all cases less than ± 3 dB.

A major result of the parametric investigation was the fact that with high jet velocities, level increase of more than 18 dB within the range of the airframe can occur on account of the ground influence.

This means that in practice noise fatigue failures can occur in a very short time, if for example a free field noise level of 145 dB were used as design parameter for the structure without taking the ground influence into account.

The frequency spectra in the wall jet noise field can also be determined by superimposing the free direct and reflected sound (Fig. 11). The investigations show that apart from the enormous level increase, the frequency spectrum is also displaced in direction of the structural resonance frequencies of conventional aircraft skin panels. The ground reflection influence thus has a doubly negative effect with respect to noise fatigue.

Finally, it is illustrated by means of the Dornier Do 31 that even with more than 1 engine jet the calculation method still gives good results which are sufficiently accurate for practical purposes. In the case of the Do 31, there are 16 jets in all, and even here, the maximum deviations between measured and calculated levels were not greater than ± 3 db (Fig. 12).

LIST OF SYMBOLS

Symbol	Unit	Description
a	[m/s]	speed of sound
D	[m]	jet diameter
f	[Hz]	frequency
H	[m]	hight above the ground
j	[kp/ms]	intensity
K	[-]	Lighthills-constant
L	[dB]	sound pressure level
N	[-]	velocityexponent
OASPL		overall sound pressure level
p	[kp/m^2]	pressure
R, r	[m]	radius
SPL	[dB]	1/3 oktav level
T	[$^\circ$K]	absolut temperature
v	[m/s]	relative jet velocity
λ	[m]	wave length
ρ	[kps^2/m^4]	density

INDICES

Index	Description
a	direct
n	ref. to the nozzle
F	in the free field
i	1/3 oktave number
k	jet number
M	ref. to the microphone
r	reflected
o	ambient
1	in the expandet jet
'	ref. to the reference field

REFERENCES

[1]   M.J. Lighthill

"On Sound Genera d Aerodynamically"
Proc. Roy. Soc. A, Vol. 211, 1952; Vol. 222, 1954

[2]   R. Scholten u. M. Flemming

"Lärmprobleme der VTOL-Technik in Gegenwart und Zukunft,
im Hinblick auf die Erfahrungen mit dem VTOL-Strahltrans-
porter DORNIER Do 31"
Kampf dem Lärm Heft 6 Dez. 1969

[3]   Dornier Bericht Nr. 67/27 u. 69/9

"Untersuchungen über die theoretische und experimentelle
Bestimmung von Schallpegelkonturen im Bereich des Boden-
einflusses an Flugzeugzellen"
Dez. 1967 / 1969

[4]   R. Scholten

"Untersuchungen über den Bodeneinfluß auf die Schallpegel
und deren Frequenzverteilung im Nahfeld eines senkrecht
gegen den Boden gerichteten Triebwerksstrahles"
Diss. Techn. Universität Berlin, Fachbereich Verkehrswesen,
1971

[5]   H.E. Gierke

"The Noise Field of a Turbo-Jet Engine"
J. Ac. Soc. Amer., 24, 162, 1952

[6]   R. Hoch, P. Thomas (SNECMA)

"Influence Les Reflexions sur Les Spectres de Pression
Acoustique Les Jets"
1968

FIG. 1 : DO 31-E3

$$N_k(\Theta; r_k) = N'\left(\Theta; \frac{D'}{D_k} r_k\right)$$
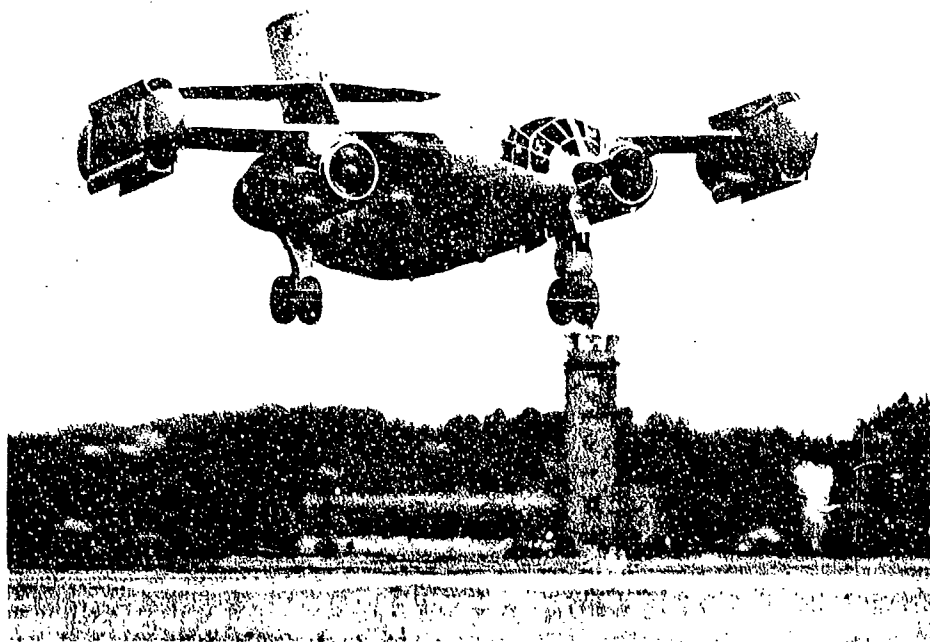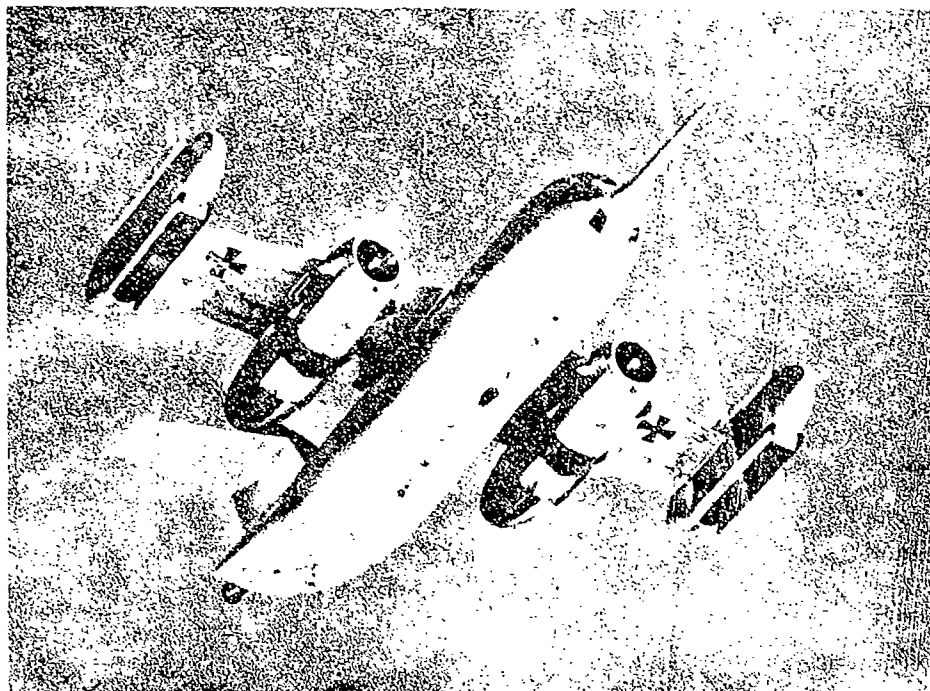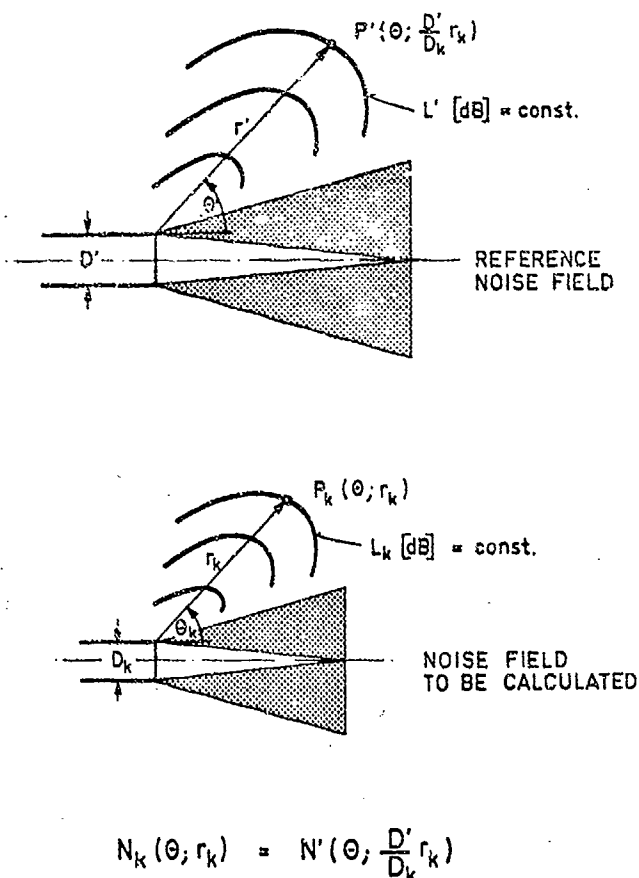
FIG. 2 : SIMILARITY OF JET NOISE FIELDS

R/D = 30
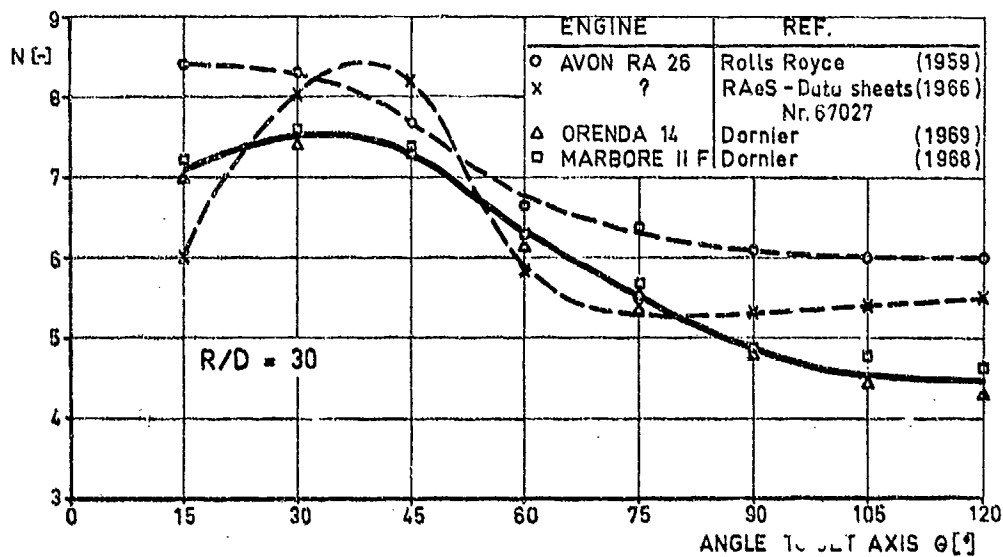
FIG. 3 : VELOCITY EXPONENTS OF THE OVERALL SOUND
PRESSURE LEVELS
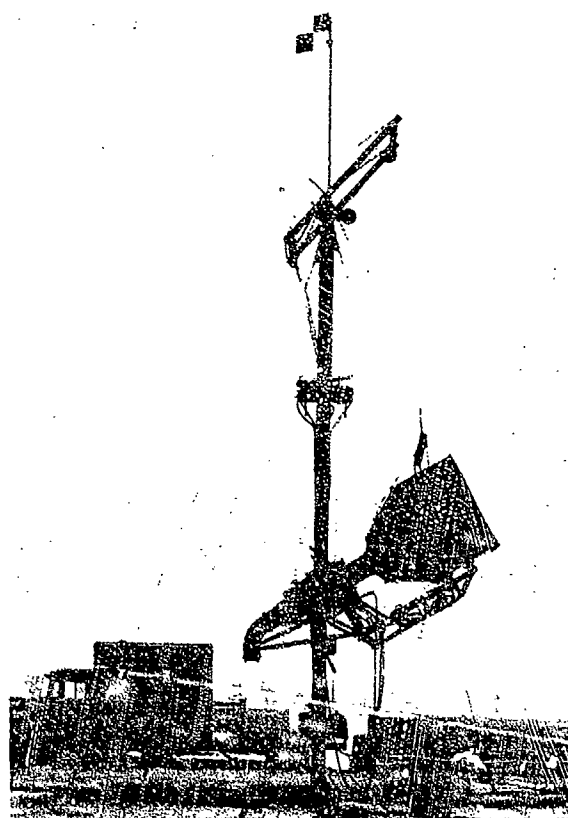
FIG. 4 : MARBORE TEST RIG
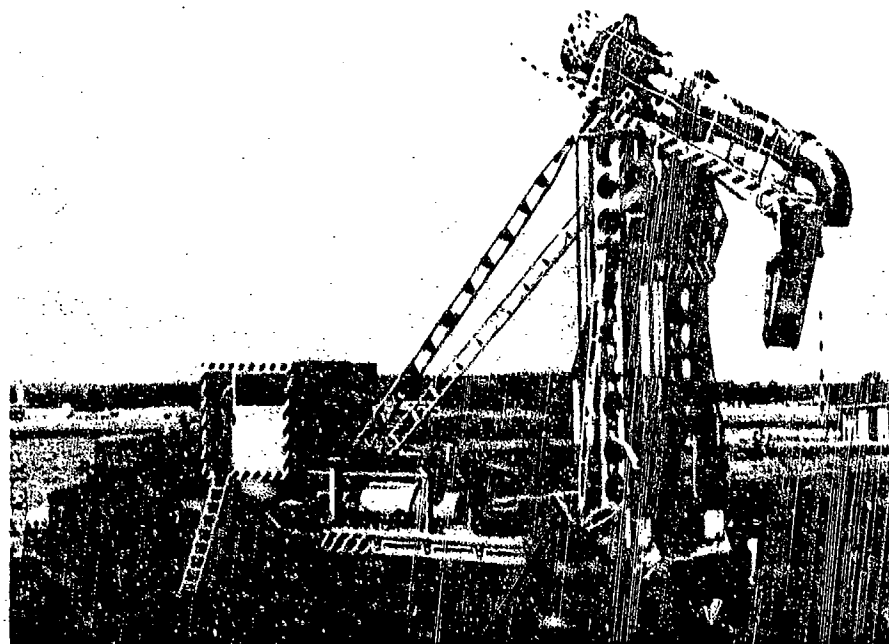
FIG. 5 . ORENDA TEST RIG
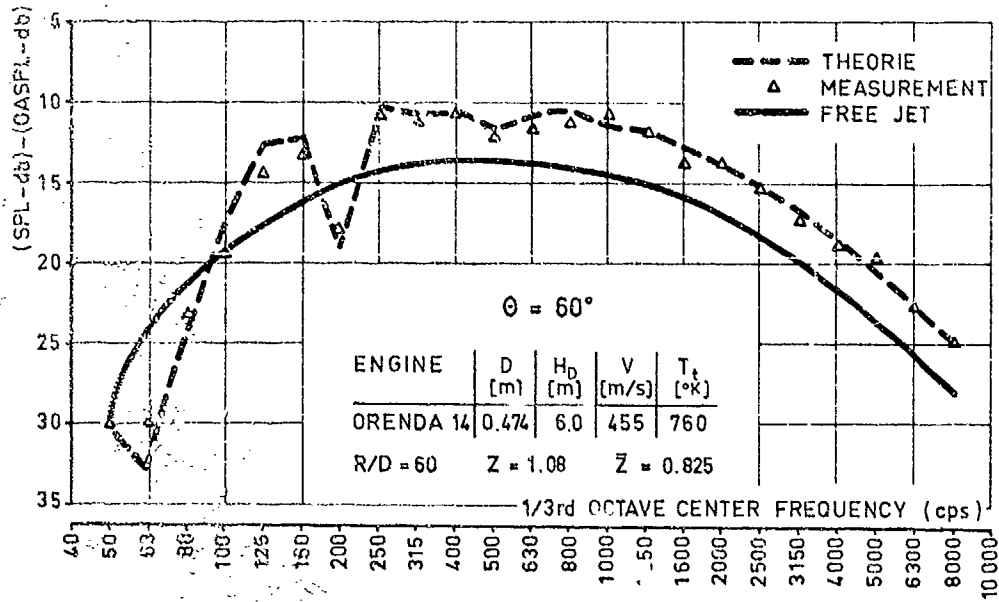
FIG. 6 : INFLUENCE OF GROUND REFLEXION

Θ	$\frac{R}{D}$	D = 0.215 m T_t = 785 °K v = 430 m/s		difference	D = 0.215 m T_t = 670 °K v = 240 m/s		difference
		measured	calculated		measured	calculated	
[°]	—	dB	dB	dB	dB	dB	dB
	5	138.5	140.0	+ 1.5	125.0	123.0	- 2.0
30	30	127.99	126.6	- 1.3	111.1	108.9	- 2.2
	60	121.1	121.5	+ 0.4	104.5	102.2	- 2.3
	5	129.5	132.0	+ 2.5	119.0	119.2	+ 0.2
60	30	120.4	121.7	+ 1.3	108.4	107.1	+ 0.7
	60	114.7	116.2	+ 1.5	101.0	102.1	+ 1.1
	5	125.1	126.2	+ 0.9	116.0	115.5	- 0.5
90	30	114.8	114.9	+ 0.1	103.2	103.6	+ 0.4
	60	109.9	110.6	+ 0.7	98.3	99.5	+ 0.8

ENGINE : MARBORE II F

TAB. 1 : FREE-JET OVERALL SOUND PRESSURE LEVELS

GEOMETRICAL CONDITIONS
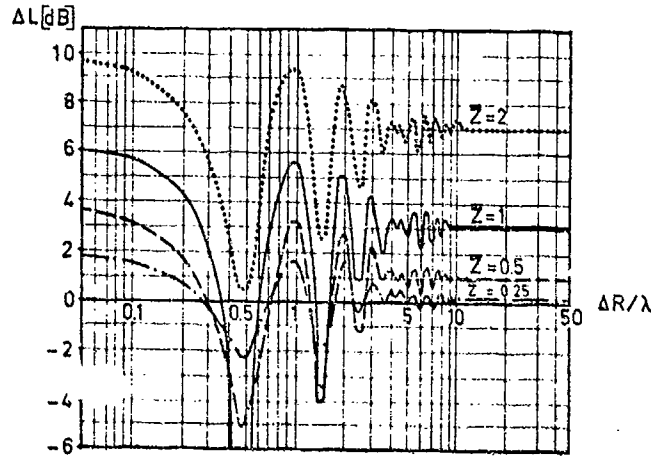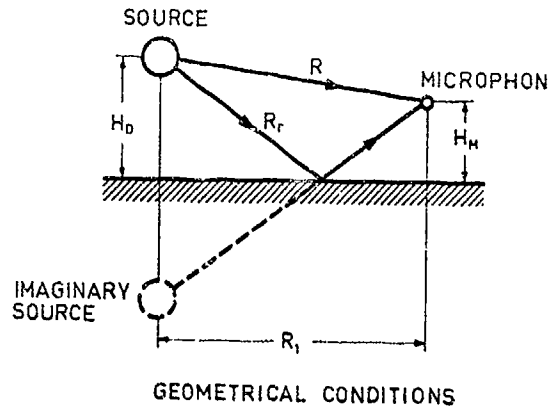
CORRECTIONS FOR 1/3rd OCTAVE
SOUND - PRESSURE - LEVEL SPECTRA

FIG. 7 : GROUND REFLEXION
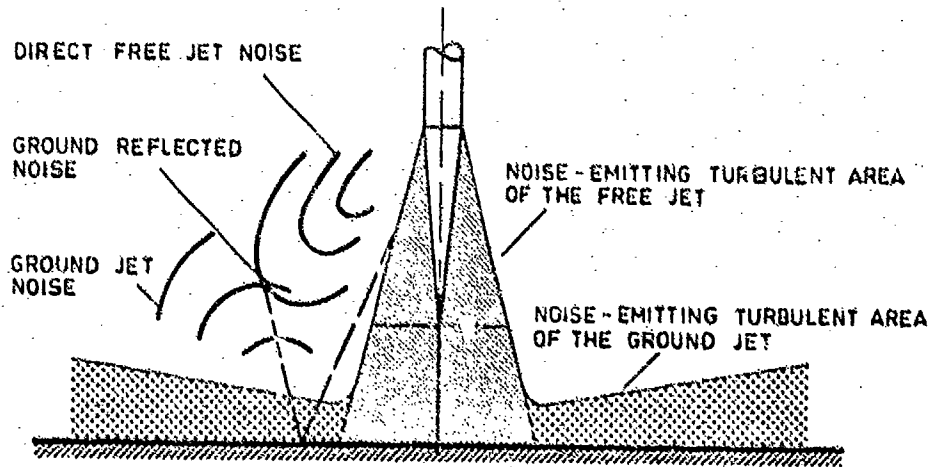
FIG. 8 : COMPOSITION OF THE WALL-JET NOISE FIELD

ENGINE : MARBORE II F   (OASPL IN dB)

D   = 0.215 m
V   = 430 m/s
T_t = 760 °K
H_D/D = 9

FIG. 9 : MEASURED WALL-JET NOISE FIELD

ENGINE : MARBORE II F   (OASPL IN dB)

D   = 0.215 m
V   = 430 m/s
T_t = 760 °K
H_D/D = 9
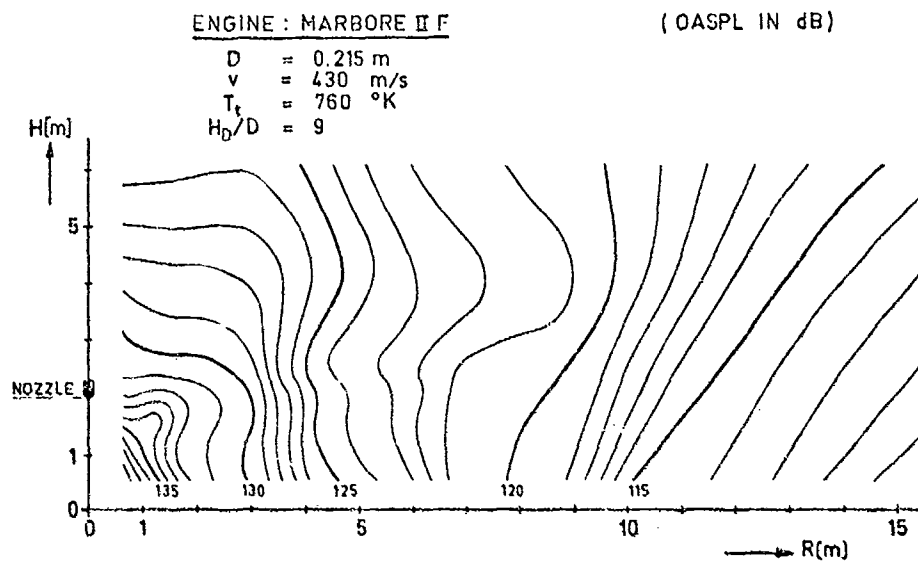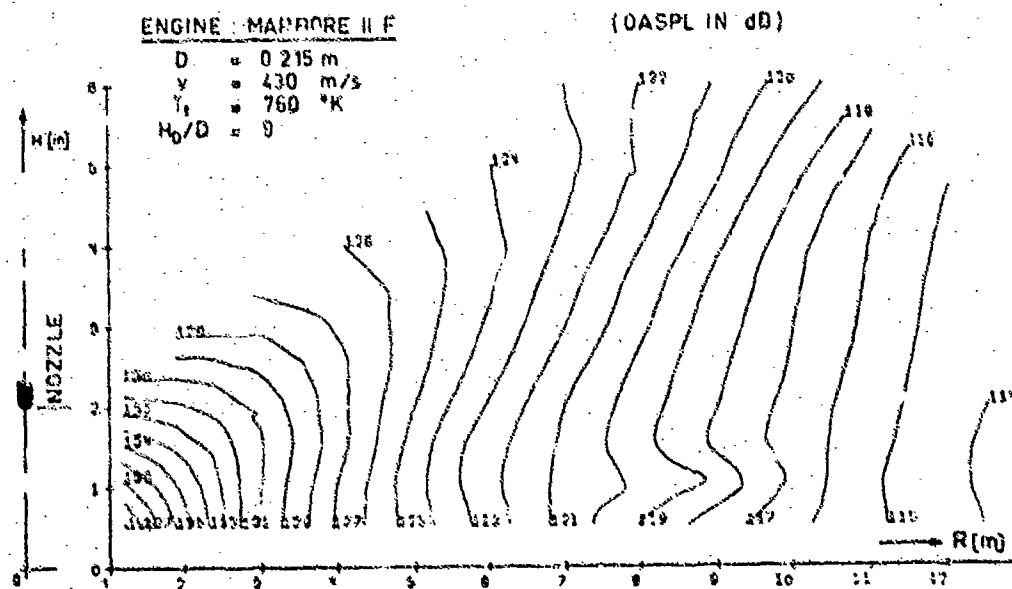
FIG. 10 : CALCULATED WALL-JET NOISE FIELD

ENGINE : MARBORE II F

SPL[dB]
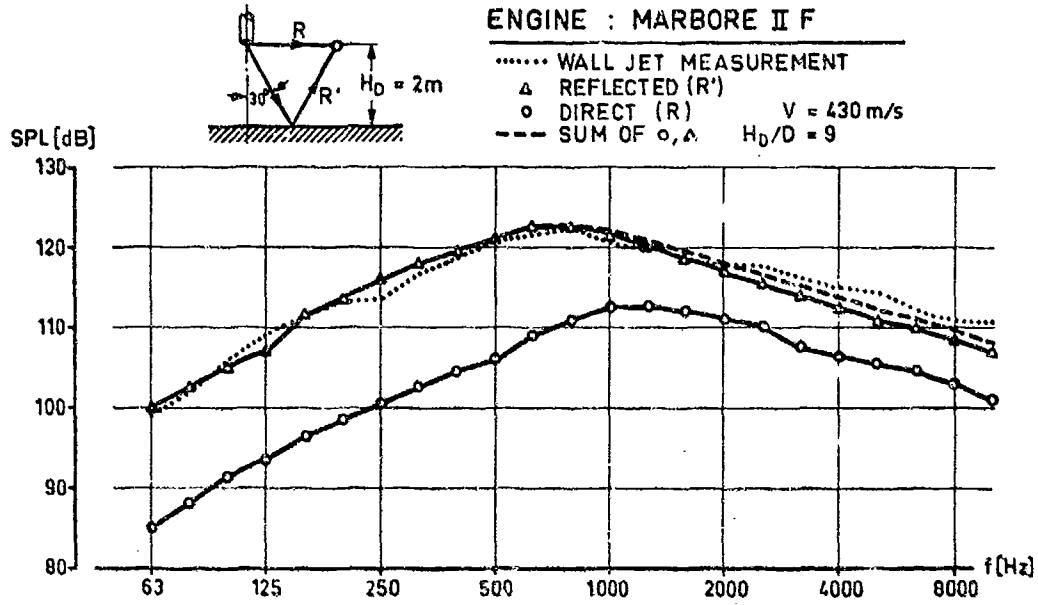
FIG. 11 : WALL-JET SPECTRA
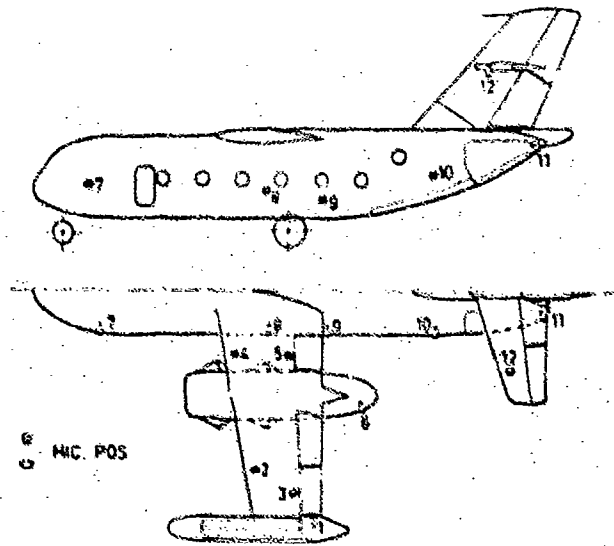
MICROPHON NUMBER		1	2	3	4	5	6	7	8	9	10	11	12
MEASURED OASPL	L(dB)	127	140	148	-	138	145	144	45	147	144	143	145
CALCULATED OASPL WITHOUT GROUND REFLECT	L(dB)	138	133	136	136	131	135	148	136	135	134	131	127
INCREASE OF OASPL BY GROUND REFLECTION	ΔL(dB)	8	12	11	11	11	5	6	5	5	6	7	13
INCREASE OF OASPL BY FAN NOISE	ΔL(dB)	-	-	-	-	-	-	3	3	1	-	-	-
INCREASE OF OASPL BY CASCADE NOISE	ΔL(dB)	-	-	-	1	1	-	-	1	1	1	-	-
INCREASE OF OASPL BY STRUCTURAL REFLECTION	ΔL(dB)	1	1	1	1	1	1	1	3	3	1	1	1
CALCULATED OASPL	L(dB)	146	147	150	145	147	149	161	148	145	144	142	143

FIG. 12 : COMPARISON OF CALCULATED AND MEASURED
NOISE LEVELS AT THE DO 31-E3 DURING
VTO IN H=0

DYNAMIC LOADING OF AIRCRAFT SURFACES DUE TO JET EXHAUST IMPINGEMENT

by

D. L. Lansing, J. A. Drischler, T. J. Brown,[*] and J. S. Mixson
NASA Langley Research Center
Hampton, Virginia, U.S.A.

SUMMARY

High-lift wing concepts being considered for application to commercial STOL transports are discussed. The flow patterns which produce dynamic loads on these wings are indicated. Measurements of surface pressure and acceleration on a one-half-scale model of an externally blown double-slotted flap are reported. Root-mean-square values, power spectra, and scaling parameters are shown.

SYMBOLS

a_{rms}	Root-mean-square value of acceleration
D_1	Diameter of bypass nozzle
f	Frequency, Hz
g	Acceleration of gravity
M	Mach number
M_n	Generalized mass
P_{rms}	Root-mean-square value of pressure
q	Dynamic pressure
$\vec{r}, \vec{r}_0$	Position vectors of points on a structure
U	Velocity of core jet or simple circular jet
$\alpha_n(\vec{r})$	Normal mode
γ_n	Damping factor
$R(\vec{r},)$	Power spectral density of displacement
$\Pi_a(f)$	One-third-octave band power spectra of acceleration
$\Pi_p(f)$	One-third-octave band power spectra of surface pressure
$\phi(\vec{r}, \vec{r}', \omega)$	Cross power spectral density of surface pressure
ω	Frequency, radian/sec
ω_n	Natural frequency

INTRODUCTION

The powered lift systems presently being considered for use on commercial STOL vehicles obtain additional lift by deflecting the flow of a jet exhaust with one or more turning flaps. For these systems, large areas of the wing and flap are immersed within the turbulent flow of the jet exhaust. Consequently, these surfaces are exposed to high-intensity dynamic loadings which have the potential of inducing high vibration levels and sonic fatigue in flight-weight aircraft structures. The loadings are random in nature and nonuniformly distributed due to the complex flow patterns which form around the flaps. Very little information is available on the properties of these loads. Hence, it is difficult for the structural dynamicist to design optimal flap systems.

The present paper will first point out some of the high-lift wing concepts now under consideration and the principal features of their associated flow fields for the purpose of indicating the diversity of loading actions and structural arrangements encountered in the STOL flap loads problem. Then, some measurements of surface pressure and acceleration on a one-half-scale model of an externally blown double-slotted flap are presented. Root-mean-square values, power spectra, and scaling parameters are discussed for the loads and response.

[*] Langley Directorate, U.S. Army Air Mobility R & D Laboratory.

HIGH-LIFT WING CONCEPTS AND ASSOCIATED FLOW FIELDS

Several high-lift wing concepts being considered for lift augmentation on STOL aircraft are shown in Figure 1.

For the conventional jet flap and the augmenter wing shown at the left of the figure, air is ducted from the engines to the wing where it is exhausted at high pressures and velocities through a slot in the trailing edge. For the conventional jet flap, the Coanda effect causes the lower part of the flow to attach to the flap. The upper portion of the flow will mix with the ambient air in the manner of a free jet. For the augmenter wing, the slot exhaust is confined between upper and lower set of flaps which direct the flow downward.

In contrast to these arrangements, the high-lift wings in the right of the figure use low-velocity air directly from the exhaust of a low-pressure-ratio fan engine. For the externally blown flap concept, the exhaust jet impinges on several flaps which redirect most of the flow downward but allow some air to pass through slots and spread over the upper flap surface. For the upper surface blowing concept shown here, the flow would attach to the upper surface of the wing and be turned downward with the aid of several flaps.

The principal sources of the turbulent pressure fluctuations which generate dynamic loads on these high-lift wing systems are the jet exhaust including upstream turbulence and turbulent mixing and boundary layers on the wing and flap surfaces. Since the flaps operate at high angles of attack during landing approach, separated flow may also occur. As a result of the diversity of configurations and operating conditions, these sources of pressure fluctuations occur in various combinations as shown in Figure 2.

For the externally blown flap, the lower surface of the wing and the flaps are exposed to the turbulent mixing region of the jet. If the flaps are sufficiently close to the jet exit plane, part of the flaps will be impinged by the jet core. Flow over the flaps may become separated producing localized regions of intense fluctuating pressures.

For the conventionally blown flap and some upper surface blowing configurations, the jet core attaches to the upper surface of the wing and flaps producing a region of relatively less turbulence directly in contact with the surface. If the core region terminates on or separates away from the surface ahead of the trailing edge, as may occur on a sufficiently long flap, the aft portion of the surface will be exposed to a different type of flow which experiment indicates involves significantly higher turbulence levels. The trailing edge itself is the interface between a boundary-layer flow and a free mixing region. The transition in flow regimes at this point may be a significant source of fluctuating loads.

Thus, each of the high-lift wing concepts has a number of sources of turbulent pressure fluctuations whose relative importance will vary with the specific geometry and operating conditions. Considerable research is required before a quantitative understanding of the associated dynamic load patterns is achieved.

LITERATURE REVIEW

The flow field which results when a fluid jet impinges on a solid surface is known as a "wall jet." Consequently, the flow fields around high-lift wings are wall jets of varying degrees of complexity. The literature on wall jets is extensive. A bibliography and review of work up through 1960 is contained in Reference 1. Other papers of interest on wall jets and some related studies on high-lift wings are contained in References 2-10. The work on wall jet flow fields is primarily concerned with mean and turbulent velocity profiles, shear distributions, and turbulence intensities and scales. Some of the recent studies on high-lift wings have been concerned with the noise that is produced by such flow fields. Theoretical and experimental investigations of the intensity, distribution, and statistical properties of turbulent pressures on surfaces impinged by jets are contained in References 3, 4, 7, and 10. Data are meager and generally have not been taken with the needs of the structural dynamicist or the STOL loads problem in mind. Calculated and measured responses of a simple panel to jet impingement loads are presented in Reference 11.

EXTERNALLY BLOWN FLAP TESTS

Test Setup and Instrumentation

Measurements of fluctuating surface pressure and acceleration were obtained on a partial span model of a double-slotted externally blown flap. The engine exhaust was simulated with a six-to-one bypass ratio nozzle using air at ambient temperature. Figure 3 is a photograph of the test arrangement. Figure 4 is a cross-sectional sketch taken in a plane through the jet exhaust and normal to the wing plane. During the tests, the first and second flaps were deflected at angles of 30° and 60°, respectively, to the wing chord line. In this position the core of the inner circular jet impinged near the leading edge of the second flap. Tests were conducted at core jet Mach numbers of 0.55, 0.73, 0.90, and 1.09. These Mach numbers were calculated from measured values of the nozzle pressure ratio and correspond to the Reynolds numbers of 7.1×10^6, 9.7×10^6, 12.3×10^6, and 14.9×10^6, respectively, based on the diameter of the bypass nozzle.

The span of the model was 2.74 m (9 ft). With flaps retracted the model chord is 2.08 m (82 in.). The chord of the first and second flaps is 0.53 m (21 in.) and 0.56 m (22 in.), respectively. The diameter of the core nozzle is 0.20 m (8 in.) and the outer diameter of the bypass nozzle is 0.58 m (23 in.).

As shown in Figure 4, nine surface pressure transducers were flush mounted in the flap and wing skins to measure fluctuating surface pressures. An accelerometer was mounted within the second flap to measure vibration levels.

The model is constructed of heavy gage sheet metal. The flap skin panels, supporting rib structure, and skin mounting brackets are 0.23 cm (0.09 in.) steel plate. The accelerometer was placed within the second flap about one-third chord back from the leading edge on one of the outer skin mounting brackets.

The tests described here were conducted at the Lewis Research Center by R. G. Dorsch, W. J. Kreim, and W. A. Olsen as part of NASA's STOL technology development program. Further description of the test arrangement and the results of noise measurements are given in Reference 12.

Surface Pressure Intensities

The distribution of the values of the fluctuating pressure coefficient over the flaps is shown in Figure 5. These values are the root-mean-square values of surface pressure normalized to the dynamic pressure q calculated from core jet exit velocity and ambient density. This type of normalization with respect to dynamic pressure has been used (for example, in Refs. 10, 13, 14, and 15) for various types of flow induced fluctuating loads. Although measurements of the local dynamic pressure and local static pressure at each transducer would have provided further insight into the detailed development of the flow field, these quantities were not measured. Therefore, it was convenient to use the simple normalization based on jet exit dynamic pressure which is compatible with other researchers.

Values of the fluctuating pressure coefficient remained essentially constant for all four jet velocities at any transducer with the exception of the one transducer near the leading edge on the lower surface of the second flap. At this transducer, the value of the fluctuating pressure coefficient ranged from 0.066 at a core jet Mach number of 0.52 to 0.126 at a Mach number of 1.09. This behavior may result from the impingement of the core of inner jet on the leading-edge portion of the second flap.

The lowest values of the fluctuating pressure coefficient, and, hence, the dynamic surface loads, were obtained on the upper side of the first flap and in the slot between the first flap and wing. The highest values occurred in the region of the impingement of the core jet. The pressure on the upper surface of the second flap near the leading edge is comparable to the pressure on the underside of the flaps directly exposed to the jet exhaust. This is probably a result of turbulent flow through the slot between flaps. Unnormalized values of the root-mean-square pressures are given for reference in Table I.

The surface pressure transducers were selected to have low sensitivity to acceleration. Moreover, calculation of the coherence functions for the accelerometer and nearby pressure transducers showed no significant degree of correlation. Thus, it is concluded that flap vibrations had no appreciable effect on the pressure measurements.

The fluctuating pressure coefficients measured on the flaps are compared with fluctuating pressure coefficients measured in a free jet, Reference 15, a wall jet, Reference 10, a 1/15-scale model triple-slotted externally blown flap, and in turbulent boundary layers, References 13 and 14, in Figure 6. The unpublished data on the 1/15-scale model were taken by R. E. Hayden, Y. Kadman, and R. C. Chanaud of Bolt Beranek and Newman, Inc. These results are expected to be released shortly in a NASA contractor report. The Mach number M and dynamic pressure q are based on free-stream conditions for the boundary layer and on the jet exit conditions in all other cases.

It is realized that the flow field in the turbulent boundary layer is essentially different from the other four situations. However, it is included because it is an extensively studied source of sonic fatigue loads which is familiar to many aircraft designers and therefore is useful as a reference point. The blocked areas for the externally blown flap model data indicate the range of pressure coefficients measured and jet exit Mach number tested.

The figure brings out the wide range of loading values found on externally blown flaps. The maximum pressure coefficients measured on flaps are 5 to 30 times as large as those measured in turbulent boundary layers. These maximum values are of the same order of magnitude for both of the models and the wall jet. In all three of these experiments, the distance from the jet exit plane to the impinged surfaces was five to nine jet diameters.

Comparison of the results obtained for the free jet and the wall jet shows that surface pressures in the wall jet can be appreciably higher than in the jet alone.

Surface Pressure Spectra

Some examples of one-third-octave band power spectra, $G_p(f)$, of the surface pressures are shown in Figure 7. The spectra have been normalized with respect to the square of the dynamic pressure. This ratio is plotted against Strouhal number, $D_j f/U$, based on the bypass nozzle diameter D_j, 0.76 m, and the exit velocity U of the core jet. The hatching indicates the region into which the individual spectra at the four jet Mach numbers fall.

As indicated by the sketch to the upper right, hatched region (A) refers to the pressure transducer on the upper surface near the leading edge of the second flap whereas region (B) refers to the transducer on the lower surface of the trailing edge of the first flap. Although the root-mean-square values at these two transducers are about the same, the spectral shapes are noticeably different. The upper surface transducers which are shielded from the direct jet exhaust all have a rather broad spectrum with a flat maximum and appreciably high-frequency content, whereas the lower surface transducers in the jet flow have a peaked spectrum with a more rapid decay at higher frequencies. The peak in the spectra obtained at the lower surface transducers occurred at frequencies under 500 Hz which indicates the relatively low-frequency nature of this type of loading.

Acceleration Intensity and Spectra

The root-mean-square values of acceleration, a_{rms}, measured on the second flap are indicated by the circled data points in Figure 8. These values are normalized with the acceleration of gravity, g. The

measured acceleration includes the response produced by the jet impingement loads just discussed and possibly mechanical vibration transmitted to the model through the ground support and pylon between the nozzle and wing.

The measured accelerations range from 4 g's at the lowest Mach number of 0.52 to 64 g's at the highest Mach number of 1.09. Since the accelerometer is mounted on a heavy bracket used to attach the outer skin to a rib support, these accelerations are occurring at a very substantial structural member. The potential for vibration induced damage on the light flight-weight construction at high engine power settings is evident.

Also shown in the figure as a straight dashed line arbitrarily drawn between the data points is an M^4 power law. It is seen that the measured values follow this trend quite well. Since this is an empirically determined relationship for a very limited amount of data, considerable caution is required in trying to extrapolate these results to other Mach numbers on this configuration or to other configurations.

Figure 9 shows one-third-octave band power spectra, $\Pi_a(f)$, of the acceleration. These spectra are normalized by the square of the acceleration of gravity and the 8th power of the jet Mach number. This latter factor is based on the variation of a_{rms} with Mach number shown in Figure 8. The spectra collapse quite well at frequencies above about 1000 Hz and clearly separate at lower frequencies where the lower jet Mach numbers are associated with relatively larger amounts of low-frequency vibration. All four spectra have peaks at frequencies of 200, 400, 600, and 1000 Hz. Since the frequencies at which these peaks occur are independent of jet exit velocity, they are presumably associated with some structural frequencies of the model.

PREDICTION OF RESPONSE TO FLAP LOADS

Predicting the response of a structure to applied loads using modal theory requires a knowledge of the load distribution and frequency content. For randomly applied loads, such as jet impingement surface pressures, this information is contained in the cross power spectral density.

The way in which the cross power spectral density of the loading enters into calculations of structural response can be seen from the following equation which has been derived by Powell, Reference 16, and others for the response of beams, plates, and shells to random loads:

$$\Pi(\bar{r},\omega) = \sum_n \sum_n \frac{a_n(\bar{r})a_m(\bar{r}) \int_S \int_{S'} a_n(\bar{r}_o)a_m(\bar{r}_o')\Phi(\bar{r}_o,\bar{r}_o',\omega)dS_o \, dS_o'}{M_n \left| \omega_n^2 - \omega^2 - i\eta_n \omega_n \omega \right| M_m \left| \omega_m^2 - \omega^2 - i\eta_m \omega_m \omega \right|}$$

In order to calculate the power spectral density of the displacement, $\Pi(\bar{r},\omega)$ one must evaluate a double integral involving the cross power spectral density of the random applied loads, $\Phi(\bar{r},\bar{r}',\omega)$, and the normal modes, $u_n(\bar{r})$. Consequently, some tractable mathematical representation of $\Phi(\bar{r},\bar{r}',\omega)$ is most desirable for analytical studies.

Extensive measurements of the cross power spectral density have been made in turbulent boundary layers, Reference 14. A simple analytical representation of the cross power spectral density was constructed and used for response calculations in Reference 17. A similar study of the response of a simple panel to wall jet pressures was carried out in Reference 11. However, very little data are available from which one can derive the cross power spectral density of the fluctuating pressures in simple wall jets. No much data exist for complex configurations such as high-lift wings. In the flap experiments discussed previously, the surface pressure transducers were too widely separated to obtain this type of information. This lack of loads data is an obvious gap which must be filled if sonic fatigue becomes a major consideration in the structural design of powered lift systems.

CONCLUDING REMARKS

This paper has indicated in a general way the sources of turbulent pressure fluctuations in the flow fields of several high-lift wing arrangements being considered for use on commercial STOL transports. Measurements of surface pressure and acceleration on a one-half-scale model of an externally blown flap have been presented. The high intensities of both the dynamic loads and structural response pose a serious challenge to the design of lightweight flap systems. The need for further research into the intensity distribution, spectra, and statistical properties of high-lift wing dynamic loads is evident.

REFERENCES

1. Gautner, J. W.
   Livingood, J. N. B.
   Hrycak, P.
   Survey of Literature on Flow Characteristics of a Single Turbulent Jet Impinging on a Flat Plate. NASA TN D-5652, February 1970.

2. Lilley, G. M.
   Hodgson, T. H.
   On Surface Pressure Fluctuations in Turbulent Boundary Layers. College of Aeronautics, Cranfield, CoA Note No. 101, April 1960

3. Coradia, S. W.
   Colwell, G. T.
   Parametric Study of a Two Dimensional Turbulent Wall Jet in a Moving Stream With Arbitrary Pressure Gradient. AIAA Journal, Vol. 9, No. 11, November 1971.

4. Hayden, R. E.
   Noise From Interaction of Flow With Rigid Surfaces: A Review of Current Status of Prediction Techniques. Bolt Beranek and Newman, Inc., Report No. 2276 (Prepared for NASA Under Contract NAS1-9559-14), NASA CR-2126, 1972.

5. Patel, R. P.
   Turbulent Jets and Wall Jets in Uniform Streaming Flow. The Aeronautical Quarterly, Vol. XXII, November 1971.

6. Gruschka, H. D.
   Schrecker, G. O.

   Aeroacoustic Characteristics of Jet Flap Type Exhaust. AIAA Paper No. 72-130. Presented at AIAA 10th Aerospace Sciences Meeting, San Diego, California, January 17-19, 1972.

7. Hayden, R. E.

   Sound Generation by Turbulent Wall Jet Flow Over a Trailing Edge. M.S. Thesis, Purdue University, 1969.

8. Wagner, F. R.

   The Sound and Flow Field of an Axially Symmetric Free Jet Upon Impact on a Wall. NASA Technical Translation F-13,942, October 1971.

9. Grosche, F. R.

   On the Generation of Sound Resulting From the Passage of a Turbulent Air Jet Over a Flat Plate of Finite Dimensions. R.A.E. Translation No. 1460, October 1970.

10. Strong, D. R.
    Siddon, T. E.
    Chu, W. T.

    Pressure Fluctuations on a Flat Plate With Oblique Jet Impingement. Institute for Aerospace Studies, University of Toronto. Technical Note No. 107, February 1967.

11. Maestrello, L.
    Gedge, M. R.
    Reddaway, A. R. F.

    The Response of a Simple Panel to the Pseudo-Sound Field of a Jet. Aerodynamic Noise. H. S. Ribner, Ed., Proceedings of an AFOSR-UTIAS Symposium held at Toronto, Canada, May 20-21, 1968.

12. Dorsch, Robert G.
    Kreim, Walter J.
    Olsen, William A.

    Externally Blown-Flap Noise. NASA TM X-67991, January 1972.

13. Coe, Charles F.

    Surface Pressure Fluctuations Associated With Aerodynamic Noise. Basic Aerodynamic Noise Research, NASA SP-207, July 14-15, 1969.

14. Bull, M. K.

    Properties of the Fluctuating Wall-Pressure Field of a Turbulent Boundary Layer. University of Southampton, Department of Aeronautics and Astronautics, AASU Report 234, March 1963.

15. Fuchs, H. V.

    Measurement of Pressure Fluctuations Within Subsonic Turbulent Jets. J. Sound Vib., Vol. 22, No. 3, June 1972, pp. 361-378.

16. Powell, Alan

    On the Response of Structures to Random Pressures and to Jet Noise in Particular. Random Vibration, S. H. Crandall, Ed., Ch. 8, Vol. 1, MIT Press, 1958.

17. Crocker, M. J.

    The Response of a Supersonic Transport Fuselage to Boundary Layer and to Reverberant Noise. J. Sound Vib., Vol. 9, No. 1, 1969, pp. 6-20.
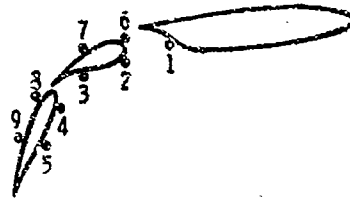
$P_{rms} \cdot 10^{-3}$, N/m^2				
TRANSDUCER	MACH NO			
	0.52	0.72	0.90	1.09
1	.20	.43	.83	1.17
2	.83	1.65	2.62	3.85
3	1.03	1.86	3.24	4.62
4	1.10	2.34	5.18	9.25
5	.69	1.31	2.62	3.45
6	.15	.26	.43	.54
7	.06	.10	.17	.23
8	.90	1.72	2.96	4.35
9	.52	.96	1.65	2.42

TABLE I.   ROOT-MEAN-SQUARE VALUES OF SURFACE PRESSURE

CONVENTIONAL JET FLAP   EXTERNALLY BLOWN FLAP

DUCTING

AUGMENTOR WING   UPPER SURFACE BLOWING
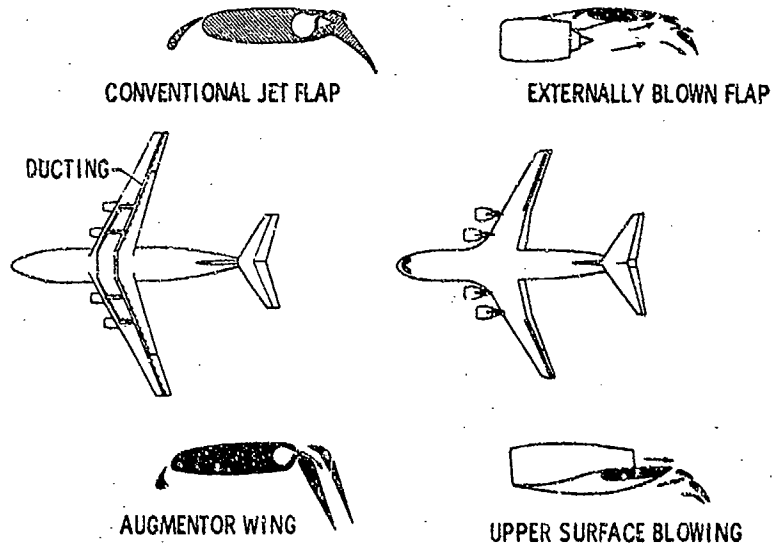
Figure 1.   High-lift wing concepts.

HIGH LIFT WINGS

MIXING

ATTACHMENT

IMPINGEMENT
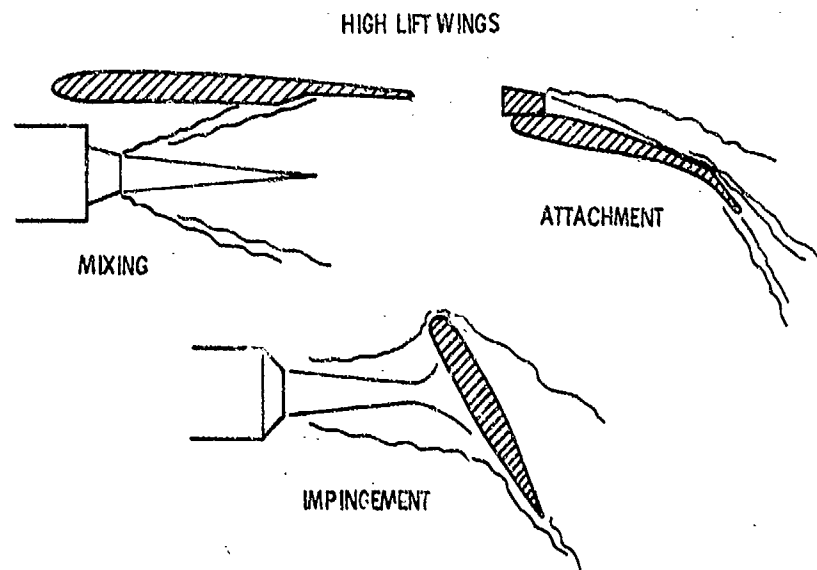
Figure 2.   Sources of turbulent pressure fluctuations.

Figure 3. Externally blown flap model.
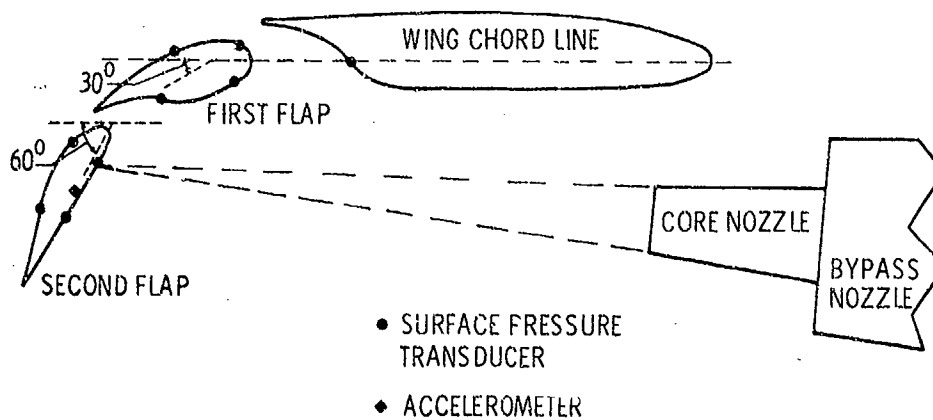
Figure 4. Test setup and instrumentation.

MEASURED VALUES OF p_{rms}/q
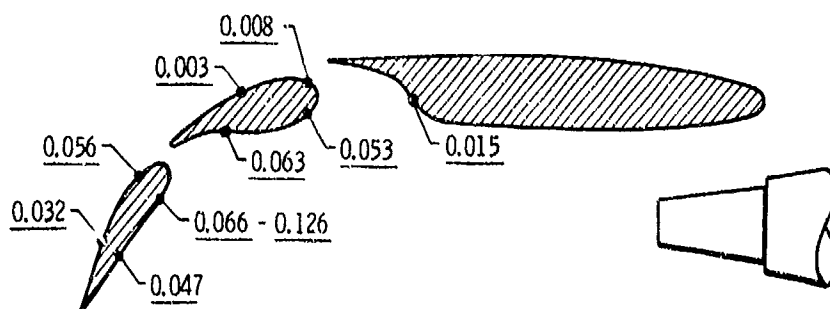
Figure 5. Fluctuating pressure coefficients on an externally blown flap.
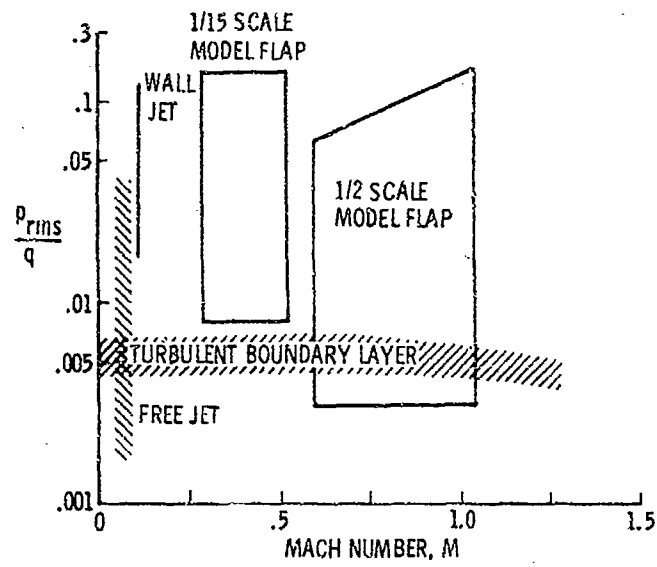
Figure 6. Comparison of fluctuating pressure coefficients.
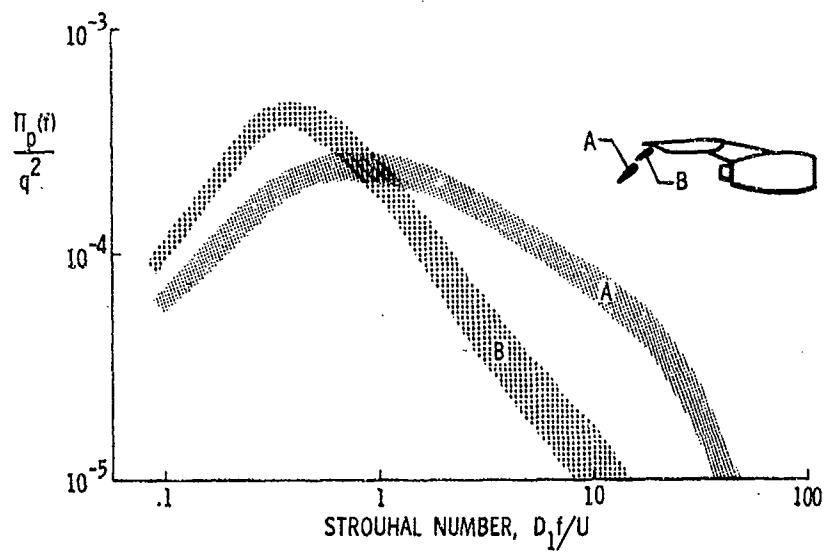
Figure 7. Power spectra of surface pressure.
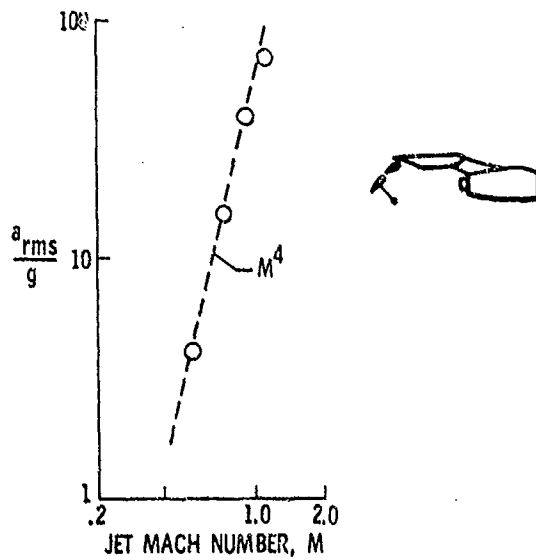
Figure 8. Root-mean-square values of acceleration.
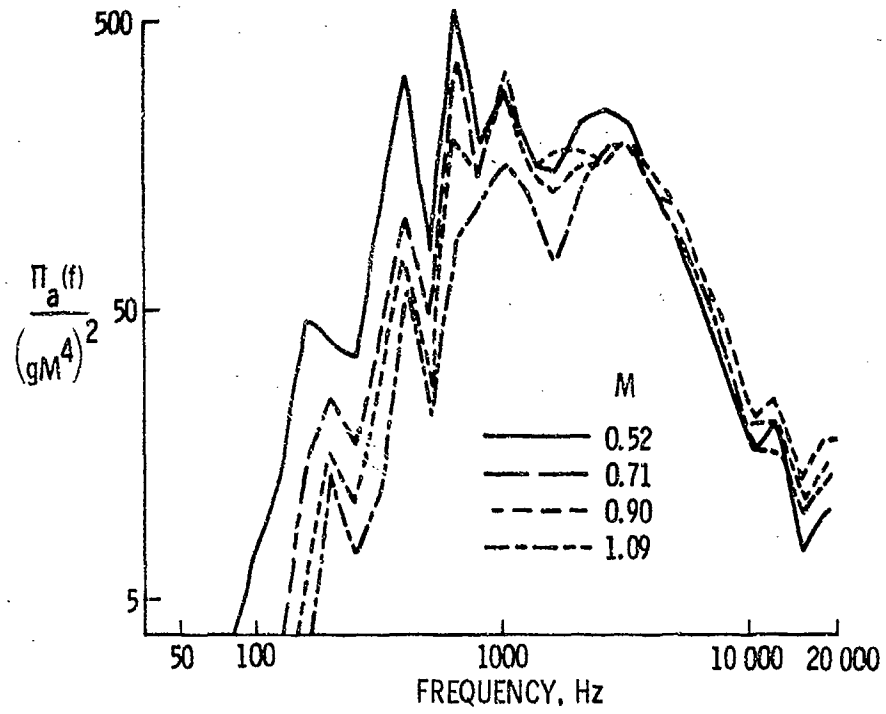
Figure 9. Power spectra of acceleration.

SURFACE PRESSURE FLUCTUATIONS FROM JET IMPINGEMENT
ON AN INCLINED FLAT PLATE

by

P.Westley, J.H.Woolley and P.Brosseau
Structures and Materials Laboratory
National Aeronautical Establishment
National Research Council of Canada
Ottawa K1A OR6, Canada

SUMMARY

More complete information on jet impingement pressure fluctuations is required by the structural designer of STOL aircraft that use externally blown flaps. This paper describes an experiment in which the surface pressure fluctuations on a flat plate were measured when an impinging cold air jet was blown at the plate with various speeds, inclination angles, and separation distances. The paper presents data on the surface sound pressure levels and their spectra.

SYMBOLS

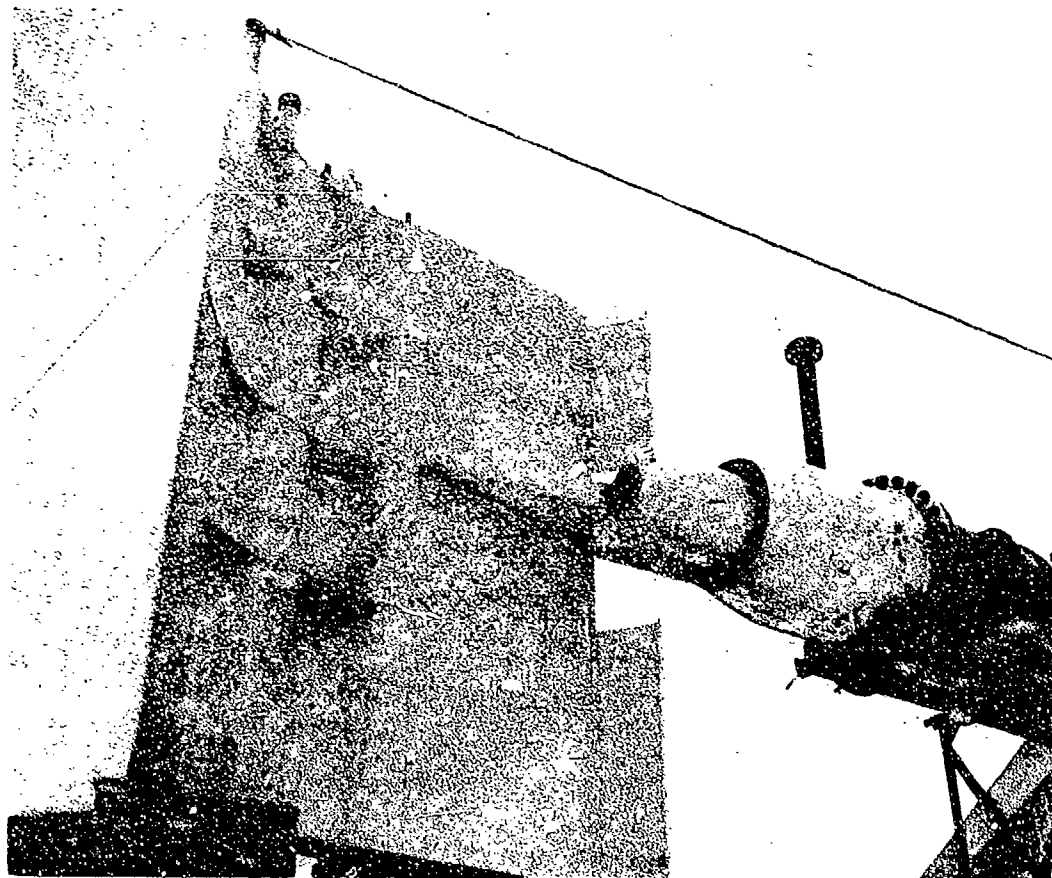|	
Δp	root mean square pressure fluctuation on plate at (X, Y)
P_A	ambient pressure
p	jet stagnation pressure
D	jet diameter
h	distance between nozzle and plate along j axis
β	angular distance between jet axis and plate
X, Y	rectangular coordinates on plate surface (origin at jet axis with OX in downstream direction.)
S.P.L.	sound pressure level, $\left(20 \log \frac{\Delta p}{.0002 \text{ dyne/cm}^2}\right)$
δ	distance upstream along plate axis of flow attachment point
r	radial distance

1 0   INTRODUCTION

The object of this investigation was to extend the data on the aerodynamic pressure fluctuations which occur over a solid surface when an air jet impinges on it. Some limited data exist on fully developed wall jets, but in most practical applications the problem is complicated by an inner impingement region which is dominated by the local conditions in the jet and an outer impingement region which is dominated by the developed wall jet.

Data on surface pressure fluctuations due to jet impingement are important in aircraft design applications where the jet exhaust strikes parts of the aircraft structure. The introduction of STOL aircraft with externally blown flaps is a topical example of jet impingement and one in which a light weight structure will encounter severe random loads.

The present investigation extends data on impingement surface pressure fluctuations by measuring the surface pressure fields over a flat plate when the velocity, inclination and distance of an impinging jet were varied over a range of operation conditions.

2.0   EXPERIMENTAL APPARATUS AND MEASUREMENTS

The jet impingement test rig is shown in section in Fig. 1 and in a general photograph in Fig. 2.

Dry compressed air, at a temperature of approximately 70°F, was supplied at various selected stagnation pressures, p, between 16 psia and 32 psia, to a contraction section and to a parallel nozzle with a circular exit of internal diameter, D, of 2.27 in.

The impingement plate consisted of a wooden rectangular plate, 90 in. x 60 in. x 1 in. which was mounted on an adjustable supporting frame that allowed the selection of various values of the impingement distance, h, and impingement angle, β.

The surface pressure fluctuations were measured with two flush mounted condenser microphones, ¼ in. diameter - B. & K.4136, which were fitted with protective grids and supported by rubber sleeves in 3/8 in. diameter holes distributed over the plate's surface.

The overall and 1/3 octave sound pressure levels were recorded at various points along the plate's centreline, $Y/D = 0$, for plate separation distances of $h/D = 3$ and 12, and over the whole of the plate for $h/D = 6$. The nozzle operating pressure ratios were $p/p_A = 1.26$, 1.54, 1.96 and 2.24, and the plate inclination angles were $\beta = 90^\circ$, 45° and $22\frac{1}{2}^\circ$.

Flow directions on the surface of the plate were made visible by an oil streak method.

3.0 RESULTS

3.1 Surface flow visualisation (Fig. 4-6)

Examples of surface flow visualisation are shown in the composite photographs of Fig. 4, 5 and 6 for the nozzle pressure ratio, $p/p_A = 2.24$. One notes a flow attachment point which is upstream of the plate's origin by a distance, $\delta = 0.0D$ for $\beta = 90^\circ$, $0.5D$ for $\beta = 45^\circ$, and $1.9D$ for $\beta = 22\frac{1}{2}^\circ$, with impingement distance of $h/D = 6$. As the impingement distance increases to $h/D = 12$, these values of δ increase to $0.0D$, $0.85D$ and $3.2D$ respectively for $\beta = 90^\circ$, 45° and $22\frac{1}{2}^\circ$. It will be noted that the surface flow diverges in approximately straight lines from the attachment point and that it terminates on the upstream side in a zero shear region of approximately parabolic shape.

3.2 Sound pressure level contours over plate (Fig. 4-6)

The overall sound pressure level contours on the plate are shown at 5 db intervals for the three flap angles, $\beta = 90^\circ$, 45° and $22\frac{1}{2}^\circ$, for the impingement spacing $h/D = 6$, and nozzle pressure ratio, $p/p_A = 2.24$, in Fig. 4, 5 and 6 respectively. The sound pressure level contours are symmetric about the origin for the normal impingement of $\beta = 90^\circ$ and become progressively extended in the downstream direction and laterally contracted as the flap angle is decreased to $\beta = 22\frac{1}{2}^\circ$. The 150 db contour extends along the longitudinal axis to $X/D = 7\frac{1}{4}$ for $\beta = 90^\circ$, to $X/D = 12$ for $\beta = 45^\circ$ and to $X/D = 16\frac{1}{2}$ for $\beta = 22\frac{1}{2}^\circ$. Laterally, the 150 db contour contracts from $Y/D = 7\frac{1}{4}$ for $\beta = 90^\circ$, to $Y/D = 6$ for $\beta = 45^\circ$, and to $Y/D = 4\frac{3}{4}$ for $\beta = 22\frac{1}{2}^\circ$. In general, for the impingement spacing of $h/D = 6$, two maxima sound pressure level points occur along the longitudinal axis and converge as β approaches 90°:-

169 db and 167 db at $X/D = -1/3$ and $+ 4\frac{1}{4}$ for $\beta = 22\frac{1}{2}^\circ$
174 db and 167 db at $X/D = -1/3$ and $+ 3\frac{1}{4}$ for $\beta = 45^\circ$
177 db at $X/D = 0$ for $\beta = 90^\circ$

3.3 Sound pressure levels along centreline - effect of β (Fig. 7-9)

The sound pressure levels along the centreline are shown in Fig. 7-9 for the impingement spacings of $h/D = 3$, 6 and 12 respectively. Double maxima appear at $X/D = \pm 1\frac{1}{4}$ for the smallest impingement spacing of $h/D = 3$ for $\beta = 90^\circ$, while at the largest impingement spacing of $h/D = 12$, the upstream maxima for $\beta = 22\frac{1}{2}^\circ$ and 45° have diminished to inflexions in the curves leaving a single maximum at the origin or upstream region. In general, it will be noted that the downstream sound pressure levels decrease, and that the upstream sound pressure levels increase with increase of the flap angle, β. These results appear to be consistent with the theory that the impinging jet acts effectively as a free jet until the stream is close to the inner impingement area. This implies that the initial flow conditions at the inner impingement regi. would be closely related to those found in the potential core, the surrounding free shear region or the fully developed jet flow when the impingement plate was removed.

3.4 Sound pressure levels along centreline - effect of h/D (Fig. 10-12)

The sound pressure levels along the centreline for impingement spacings of $h/D = 3$, 6 and 12 are compared in Fig. 10-12 for the various flap angles. The most significant observation is that the overall sound pressure levels appear to be almost independent of values of the impingement spacings, $h/D = 3$, 6 and 12, for the wall jet regions that are downstream of the inner impingement area, i.e. approximately $X/D > 2\frac{1}{2}$ for $\beta = 90^\circ$, $X/D > 6$ for $\beta = 45^\circ$ and $X/D > 8$ for $\beta = 22\frac{1}{2}^\circ$.

3.5 Rate of change of sound pressure level along centreline - effect of X/D (Fig. 13-15)

The overall sound pressure levels for $h/D = 3$, 6 and 12 are plotted against the centreline distance, X/D, on a logarithmic scale in Fig. 13-15. In the fully developed wall jet regions the slopes of the curves approach approximately -12 db to -14 db per each doubling of the axial distance, X/D. Thus, for these regions, the root mean square sound pressure, Δp, is approximately inversely proportional to the square of the radial distance from the origin,

$$\text{i.e.} \quad \Delta p \propto \frac{1}{r^2}.$$

3.6 Sound pressure levels along the centreline for various nozzle pressure ratios. (Fig. 16-23)

The nozzle pressure ratios of p/p_A = 1.26, 1.54, 1.96 and 2.24 were chosen to cover a range of jet speeds from M = 0.40 to M = 1.14. These centreline distributions of sound pressure levels are shown in Fig. 16-18 for β = 90°, Fig. 19-21 for β = 45°, and Fig. 22-23 for β = 22½°. The sound pressure levels increase with increase of pressure ratio. The rate of increase is generally independent of the position along the centreline, although there appears to be a tendency for the increase to be less in the inner impingement area. The shapes of the curves of the sound pressure level distributions which were observed for p/p_A = 2.24 are generally preserved to the lowest nozzle pressure ratio.

3.7 Variation of sound pressure level with nozzle excess pressure ratio. (Fig. 24-26)

The sound pressure levels are plotted against the excess nozzle pressure ratio $\left(\dfrac{p - p_A}{p_A}\right)$ on a logarithmic scale, for various positions along the centreline for an impingement spacing h/D = 6 in Fig. 24-26. Generally, the rate of increase of sound pressure level is approximately 6 db per doubling of the excess nozzle pressure ratio,

$$\text{i.e.} \quad \Delta p \; \alpha \left(\frac{p - p_A}{p_A}\right).$$

3.8 1/3 octave sound pressure level spectra. (Fig. 27-34)

The 1/3 octave spectra of the sound pressure levels at various distances along the plate centreline are plotted for β = 90° in Fig. 27-29, for β = 45° in Fig. 30-32, and for β = 22½° in Fig. 33-34.

One would expect the plate surface spectra in the inner impingement areas to reflect the frequency distributions of the pressure fluctuations found at the end of the jet, i.e. two free shear layers and a potential core for h/D = 3, two coalescing shear layers for h/D = 6, and developed jet flow for h/D = 12. The disturbances in the inner impingement area will be deflected and convected along the plate, and at the same time a fully developed wall jet with high shear in the inner boundary and low shear in the outer free shear layer will begin to establish itself.

A typical spectrum of the developing wall jet is shown in Fig. 28 for h/D = 6, β = 90°, p/p_A = 2.24 at the point X/D = 6.9 and is marked A B C D E F. The portion A B covers a flat or slowly rising low frequency portion of the spectrum; over B C the spectra rises rapidly at approximately 6 db per octave to reach a maximum at C; over the middle frequency band C D the spectra falls gradually at rates between 0 and 3 db per octave; a second break point is reached at D and the spectrum falls more rapidly once more. In some cases, a high frequency peak develops at F. Similar peaks were noted in the upstream areas that have broken contours in Fig. 5 and 6, and the polyurethane foam layer shown in Fig. 1 was fitted to reduce possible flange reflections of these upstream high frequency components.

Comparisons of Fig. 27, 28 and 29 for β = 90° and h/D = 3, 6 and 12 indicate that, apart from X/D = 0 and 1.7, the spectra are very similar at similar values of X/D and hence largely independent of the impingement distance.

A feature of the spectra in Fig. 27-34 is that with decrease of X/D the maximum moves along the curve C C_1 C_2, which is an extension of B C, and that one general curve which approximately includes the maxima and the upward slopes, B C, of the spectra can be applied to all the figures. The effect of decreasing the flap angle from β = 90° through β = 22½° is to generally move the maximum, C, to higher sound pressure levels and to higher frequencies. Thus it appears that the wall jet spectra are only weakly dependent on the jet to wall impingement distance. It is likely that major features of the spectra may be transformed to non-dimensional form by the use of the downstream plate distance and plate inclination angle.

3.9 Impingement shock cell screech in subsonic jets. (Fig. 3)

As far as is known little information has been published on shock cell noise screech of impinging jets, although the importance of upstream reflectors on free overchoked jets has been pointed out by some investigators. During the present tests the authors heard screech tones which were indistinguishable from the shock cell noise of free jets. Significantly, some screech tones were present when the impinging jet was subsonic. Schlieren photographs of an impinging jet (see Fig. 3) indicate that a new type of shock cell can be formed in either subsonic or supersonic jets. In the subsonic case, the shock cells move towards the nozzle. The shock waves appear to interact with instability waves propagating down the jet's free layers and to radiate screech tones. These shock cells may be induced by standing waves formed between the impingement plate and the upstream flange of the nozzle. The conditions for impingement shock cells appear to be a short impingement distance of the order of h/D = 3, a normal or near normal impingement angle, and a reflecting surface which is close to the nozzle exit or half wavelength intervals upstream of it. An example of the impingement shock cell screech appears in the spectra at G_1 and G_2 in Fig. 27. The

phenomenon has been noted, particularly at subsonic jet nozzle pressure ratios for $\beta = 90^\circ$, h/D = 3, but it may appear to a limited extent at $\beta = 45^\circ$, h/D = 3 or $\beta = 90^\circ$, h/D = 6. It therefore appears that this new type of shock cell screech phenomenon is not limited to over or under expanded supersonic jets.

Impingement screech is highly dependent on reflecting surfaces close to or upstream of the jet and care should be taken in model tests to simulate such surfaces.

4.0 CONCLUSIONS

(1) An experimental investigation has been completed of the surface pressure fluctuations on a flat plate model which was being struck by an impinging cold air jet of diameter D = 2.27 in. The nozzle was placed at distances of h/D = 3, 6 and 12 from the impingement plate whose inclination was varied through angles of $\beta = 90^\circ$, 45° to $22\frac{1}{2}^\circ$. The nozzle's pressure ratio was varied from 1.26 to 2.24

(2) The flat plate may be divided into an inner impingement area which had pressure fluctuating conditions similar to those found within the impinging jet, while the remainder of the surface of the plate developed pressure fluctuation characteristic of a developed wall jet.

(3) The inner impingement area contained a typical maximum sound pressure level of 177 db for $\beta = 90^\circ$ at the nozzle pressure ratio of 2.24.

(4) The root mean square pressure fluctuations in the developed wall jet areas were insensitive to the nozzle's separation distance from the impingement plate, were inversely proportional to the square of the distance from the centre of the plate, and were directly proportional to the excess nozzle pressure ratio.

(5) The longitudinal extent of the 150 db sound pressure level contour on the plate for h/D = 6 was typically X/D = 7½ for $\beta = 90^\circ$, X/D = 12 for $\beta = 45^\circ$ and X/D = 16½ for $\beta = 22\frac{1}{2}^\circ$. The lateral extent was y/D = ±7½ for $\beta = 90^\circ$, Y/D = ±6 for $\beta = 45^\circ$, and Y/D = ±4½ for $\beta = 22\frac{1}{2}^\circ$.

(6) One third octave sound pressure level spectra have been presented and, although complex, appear capable of being partly reduced to a non-dimensional form using plate coordinates and flap angle.

(7) A new type of shock cell screech was discovered in impinging subsonic jets and emphasises the need to reproduce acoustically reflecting surfaces during the aerodynamic testing of model impinging jets. The discovery may have important applications in the clarification of the mechanism of shock cell screech.

5.0 BIBLIOGRAPHY

(1) KUHN, R.E. An investigation to determine conditions under which downwash from VTOL aircraft will start surface erosion from various types of terrain. NASA TN D-56, Sept. 1959.

(2) LILLEY, G.M. and HODGSON, T.H. On surface pressure fluctuations in turbulent boundary layers. College of Aeronautics, Cranfield, CoA Note No.101, Apr. 1960.

(3) HENDERSON, L.F. The impingement of a supersonic jet on a flat plate. Aeronautical Research Laboratories, Melbourne, Mech.Eng. Note 238, Feb. 1960.

(4) MERLE, M.Mlle. Rôle d'un baffle sur l'emission sonore d'un jet d'air sonique. Fourth International Congress on Acoustics, Copenhagen. 1962.

(5) ABBOTT, W.A. Studies of flow fields created by vertical and inclined jets when stationary or moving over a horizontal surface. HMSO CP No.911, Oct. 1964.

(6) COX, M. and ABBOTT, W.A. Studies of the flow fields created by single vertical jets directed downwards upon a horizontal surface. HMSO CP 912, Oct. 1964.

(7) COX, M. and ABBOTT, W.A. Jet recirculation effects in V/STOL aircraft. J.Sound and Vibration, Vol.3, No.3, 1966. pp.373-406.

(8) STRONG, D.R., SIDDON, T.E. and CHU, W.T. Pressure fluctuations on a flat plate with oblique jet impingement. Inst. for Aerospace Studies, University of Toronto, Tech. Note No.107, Feb. 1967.

(9) POLDERVAART, L.J., WIJNANDS, A.P.J. and JONGSMA, F.H.M. On the production of discrete frequencies in the noise spectrum of a supersonic jet. Physics Dept., Eindhoven University of Technology, 26 Nov. 1968.

(10)   WESTLEY, R. and WOOLLEY, J.H.   An investigation of the near noise
       fields of a choked axisymmetric air jet. AFOSR-UTIAS Symposium
       on Aerodynamic Noise, 20-21 May 1968. pp.147-167.

(11)   WESTLEY, R. and WOOLLEY, J.H.   The near field sound pressures of
       of choked jet during a screech cycle. AGARD CP 42, Paper 23,
       May 1969.

(12)   TYLER, R.A. and WILLIAMSON, R.G.   Observations of tunnel flow
       separation induced by an impinging jet.
       National Research Council of Canada, Aero Report LR-537, Apr. 1970.

(13)   SKIFSTAD, J.D.   Aerodynamics of jets pertinent to VTOL aircraft.
       J.Aircraft, Vol.7, No.3, May-June 1970. pp.193-204.

(14)   PERRY, D.H.   A review of some published data on the external-flow
       jet augmented flap. HMSO CP No.1194, Dec. 1970.

(15)   WESTLEY, R. and WOOLLEY, J.H.   Shock cell noise mechanisms - The
       near field sound pressures associated with a spinning screech mode.
       Conf. of Current Developments in Sonic Fatigue, Inst. of Sound and
       Vibration, University of Southampton, 6-9 July 1970.

(16)   SCHWANTES, E.   The propulsion jet of a VTOL aircraft.
       AGARD CP-91-71, Paper 15, Sept. 1971. pp.1-10.

(17)   DONALDSON, C.D. and SNEDEKER, R.S.   A study of free jet impingement.
       Part 1 Mean properties of free and impinging jets
       Part 2 Free jet turbulent structure and impingement heat transfer
       J. Fluid Mech. Vol.45, part 2, 1971. pp.281-319.
       J. Fluid Mech. Vol.45, part 3, 1971. pp.477-512.

(18)   WICKENS, R.G.   Preliminary aerodynamic data on quasi externally blown
       jet flap model. National Aeronautical Establishment, National
       Research Council of Canada, LTR-LA-91, Aug. 1971.

(19)   DORSCH, R.G., LASAGNE, P.L., MAGLIERI, D.J. and OLSEN, W.A.
       Flap Noise Panel. Aircraft Engine Noise Reduction Conference,
       Figure Preprints, NASA Lewis, May 1972.

(20)   DORSCH, R.G., KREIM, W.J. and OLSEN, W.A.   Externally-blown-flap noise.
       AIAA Paper No.72-129, Jan. 1972.
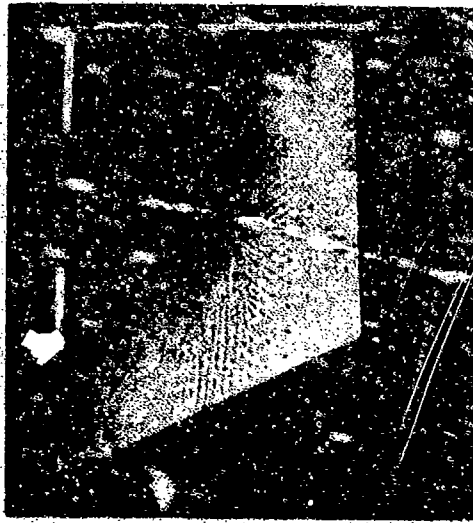
FIG. 2   JET IMPINGEMENT RIG
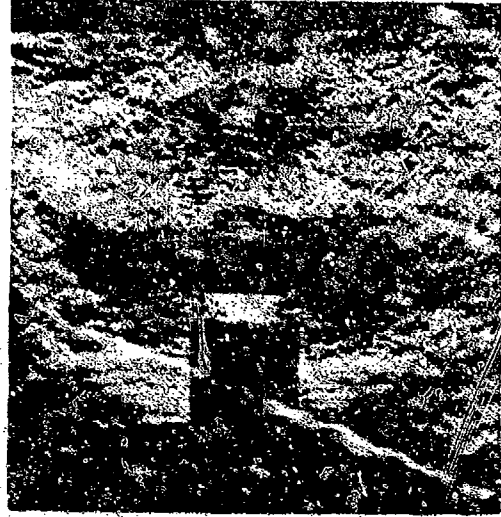
FIG. 3   SCREECH SHOCKS IN IMPINGING SUBSONIC JET

$M = 0.90, \, \theta = 90^{\circ}, \, \dfrac{h}{D} = 3$
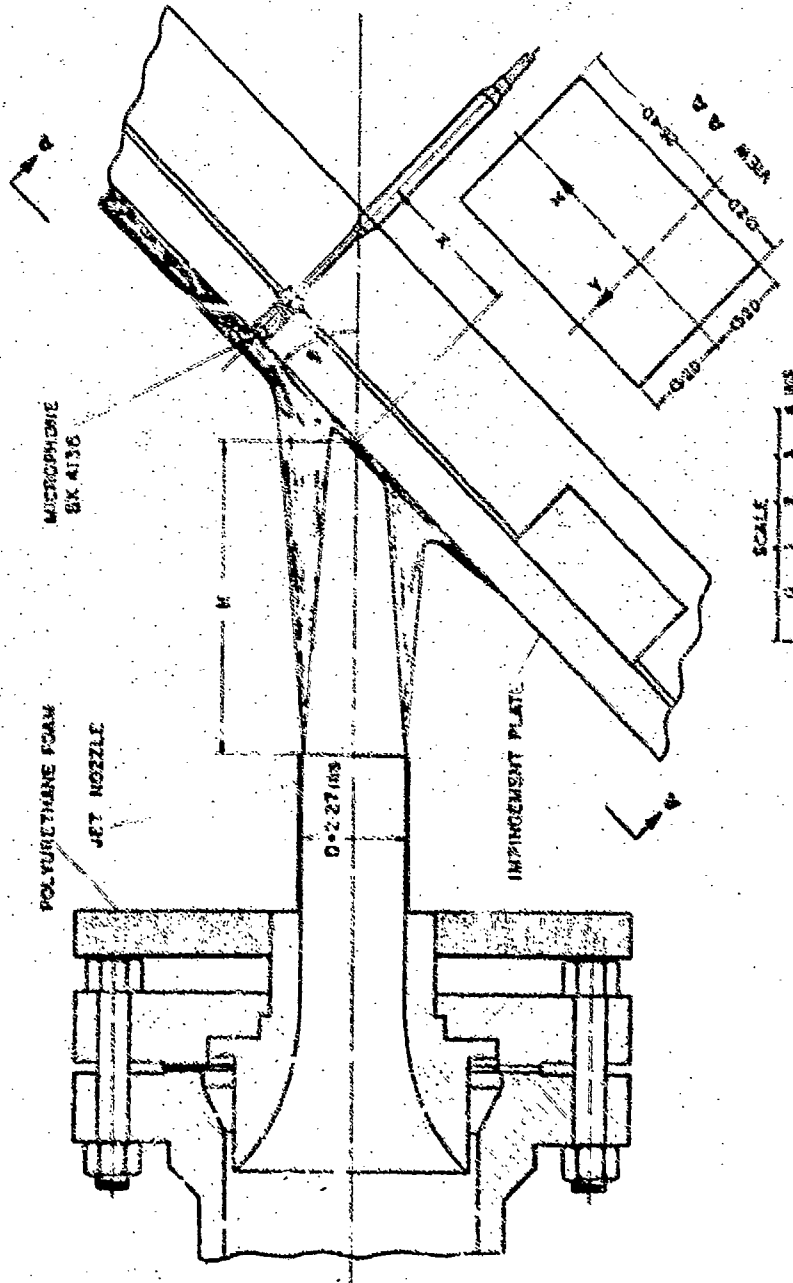
FIG. 1   JET IMPINGEMENT RIG
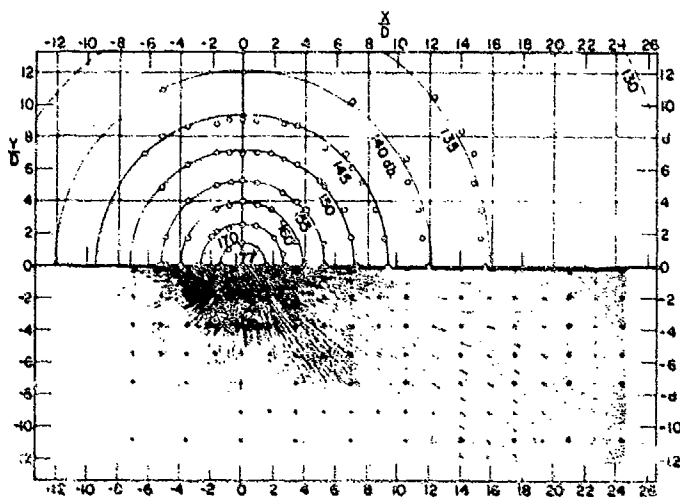
FIG. 4.   FLAP ANGLE, $\delta = 90^\circ$
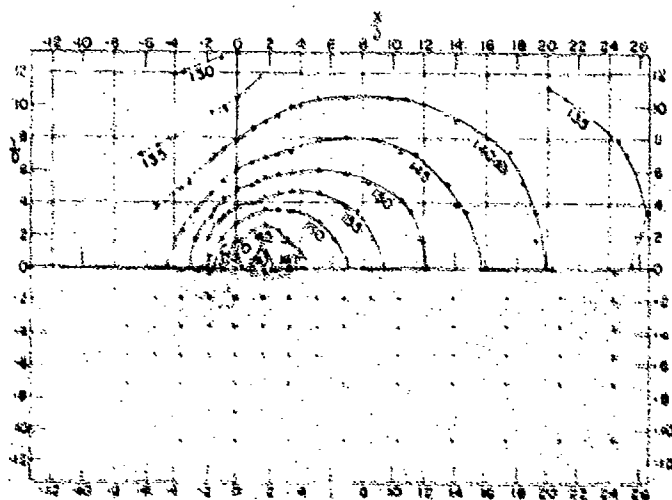
FIG. 5.   FLAP ANGLE, $\delta = 45^\circ$
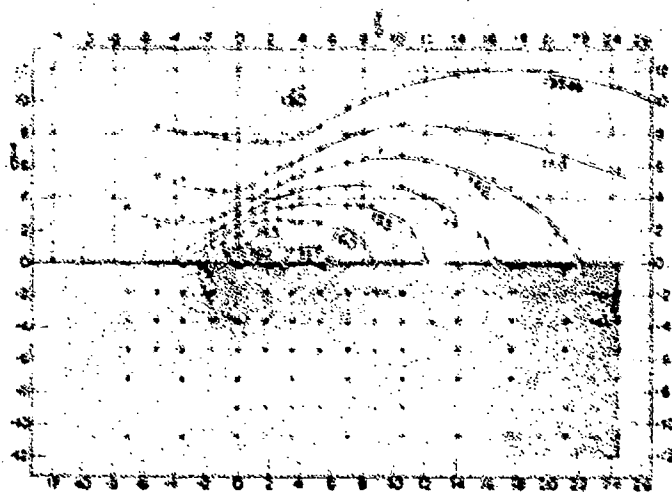
FIG. 6.   FLAP ANGLE, $\delta = 22\frac{1}{2}^\circ$

FIG. 4-6   SOUND PRESSURE LEVEL CONTOURS OVER FLAT PLATE.
(NOZZLE SEPARATION, $\frac{L}{D} = 6$; NOZZLE PRESSURE RATIO, $\frac{P_c}{P_A} = 2.74$)

FIG. 7   NOZZLE SEPARATION, $\frac{h}{D} = 3$
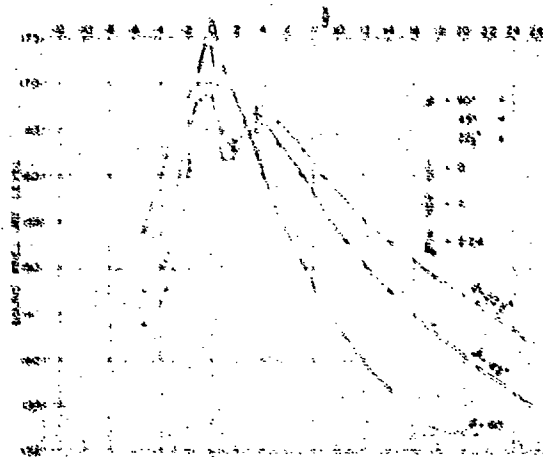
FIG. 8   NOZZLE SEPARATION, $\frac{h}{D} = 6$
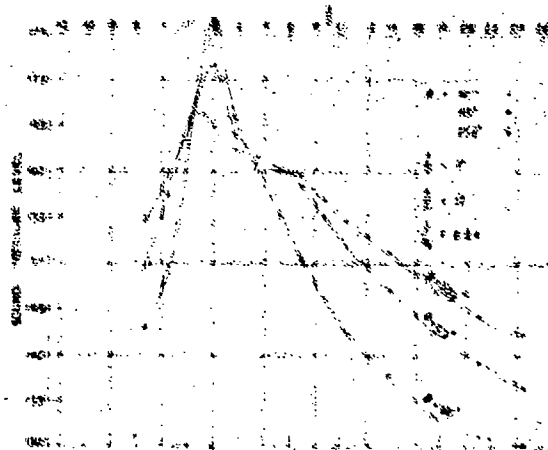
FIG. 9   NOZZLE SEPARATION, $\frac{h}{D} = 12$

FIG. 7-9   SOUND PRESSURE LEVEL ALONG CENTRELINE

(FLAP ANGLES, $\theta = 90°$, $45°$, $22\frac{1}{2}°$; NOZZLE PRESSURE RATIO, $\frac{P}{P_A} = 2.24$)
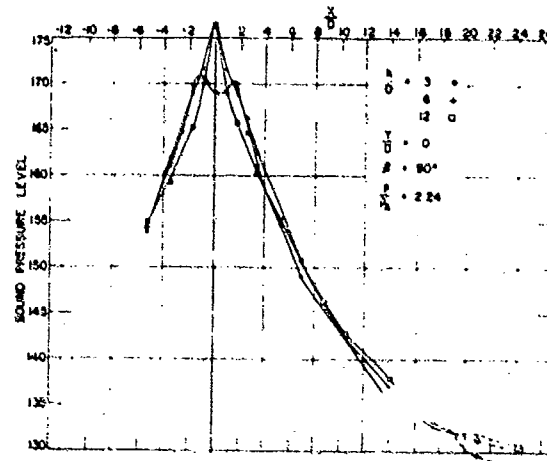
FIG. 10   FLAP ANGLE, β = 90°
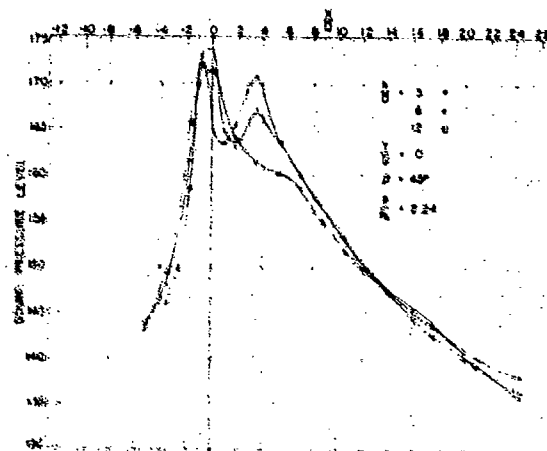
FIG. 11   FLAP ANGLE, β = 45°
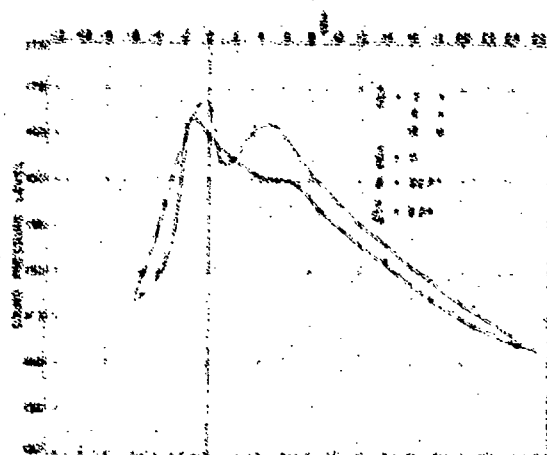
FIG. 12   FLAP ANGLE, β = 22½°

FIG. 10-12   SOUND PRESSURE LEVELS ALONG CENTRELINE

(NOZZLE SEPARATIONS, $\frac{h}{D}$ = 3, 6, 12; NOZZLE PRESSURE RATIO, $\frac{P}{P_A}$ = 2.24)
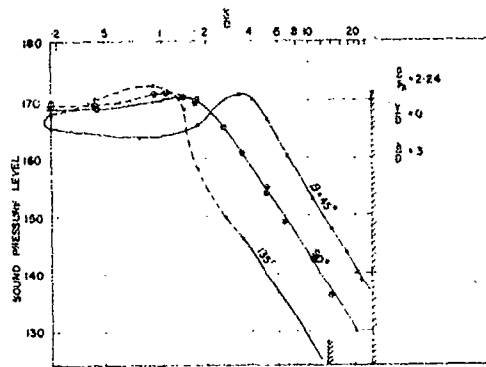
FIG. 13   NOZZLE SEPARATION, $\frac{h}{D} = 3$
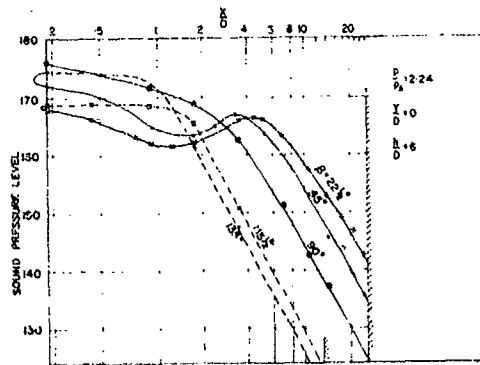
FIG. 14   NOZZLE SEPARATION, $\frac{h}{D} = 6$
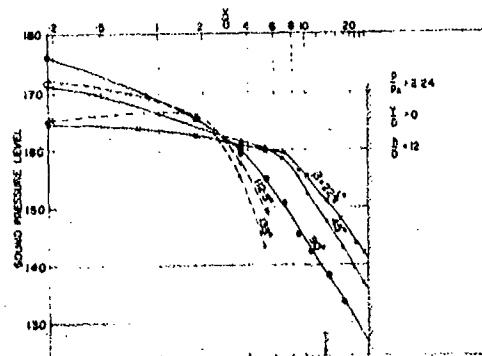
FIG. 15   NOZZLE SEPARATION, $\frac{h}{D} = 12$

FIG. 13-15   SOUND PRESSURE LEVELS ALONG CENTRELINE
(FLAP ANGLES, $\beta = 90^\circ$, 45°, $22\frac{1}{2}^\circ$; NOZZLE PRESSURE RATIO, $\frac{p}{p_A} = 2.24$)
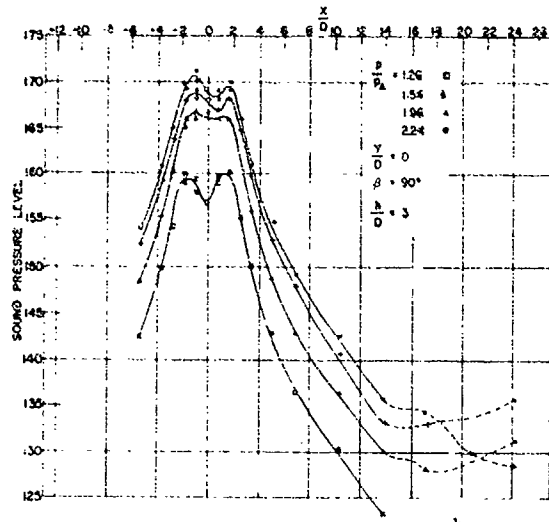
FIG. 16   NOZZLE SEPARATION, $\frac{h}{D} = 3$
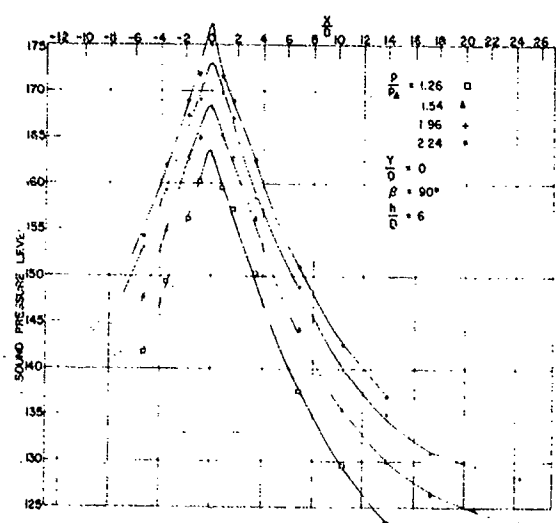
FIG. 17   NOZZLE SEPARATION, $\frac{h}{D} = 6$
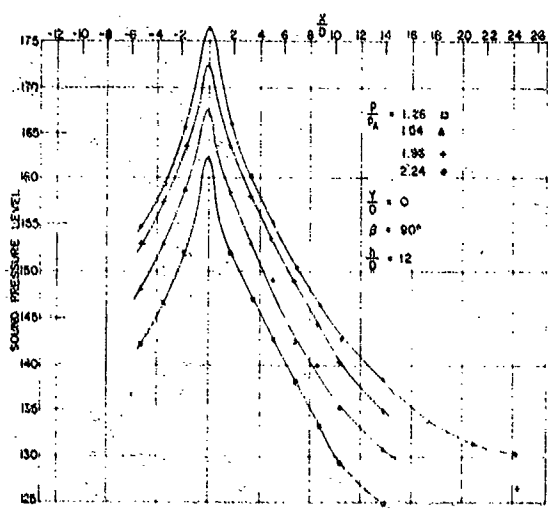
FIG. 18   NOZZLE SEPARATION, $\frac{h}{D} = 12$

FIG. 16 - 18   SOUND PRESSURE LEVELS ALONG CENTRELINE

(NOZZLE PRESSURE RATIOS, $\frac{p}{p_A} = 1.26,\ 1.54,\ 1.96,\ 2.24;$ FLAP ANGLE, $\beta = 90^{\circ}$)
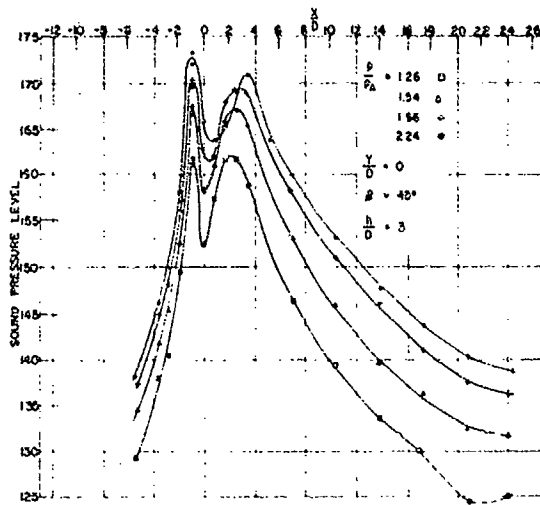
FIG. 19   NOZZLE SEPARATION $\frac{h}{D} = 3$
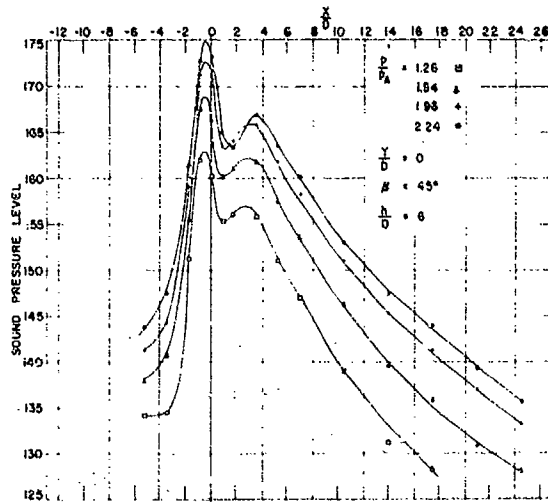
FIG. 20   NOZZLE SEPARATION $\frac{h}{D} = 6$
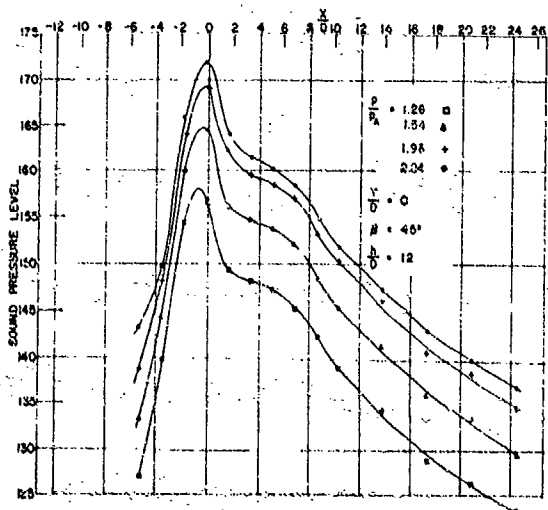
FIG. 21   NOZZLE SEPARATION $\frac{h}{D} = 12$

FIG. 19 - 21   SOUND PRESSURE LEVELS ALONG CENTRELINE

(NOZZLE PRESSURE RATIOS, $\frac{p}{p_A}$ = 1.26, 1.54, 1.96, 2.24; FLAP ANGLE, $\beta = 45^{\circ}$)
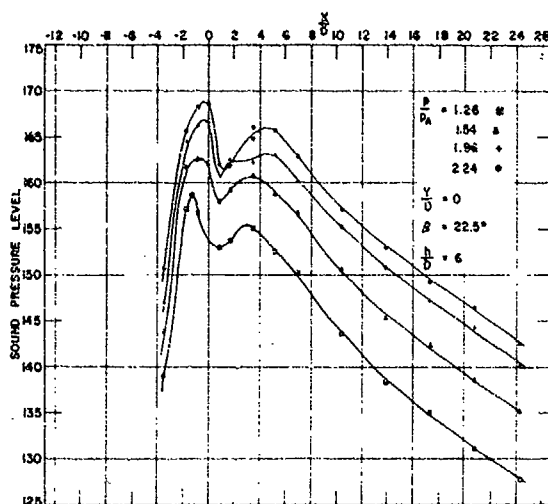
FIG. 22 NOZZLE SEPARATION, $\frac{h}{D} = 6$
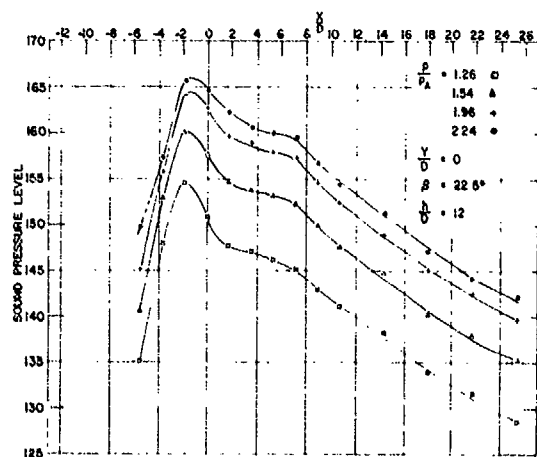
FIG. 23 NOZZLE SEPARATION, $\frac{h}{D} = 12$

FIG. 22-23 SOUND PRESSURE LEVELS ALONG CENTRELINE
(NOZZLE PRESSURE RATIOS, $\frac{p}{p_A} = 1.26, 1.54, 1.96, 2.24$; FLAP ANGLE, $\beta = 22.5°$)
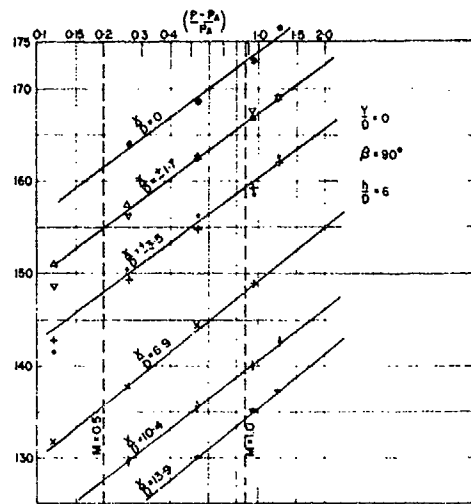
FIG. 24   FLAP ANGLE, $\beta = 90^\circ$
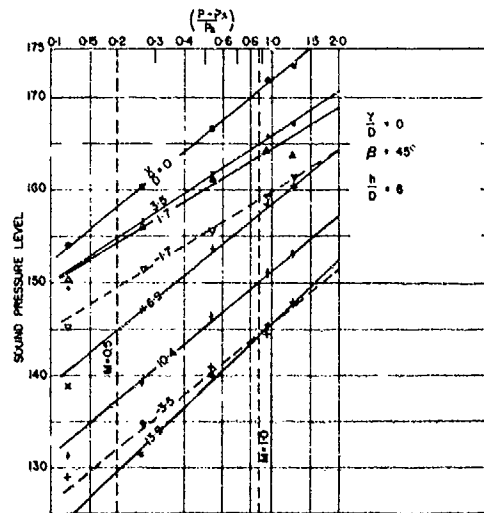
FIG. 25   FLAP ANGLE, $\beta = 45^\circ$
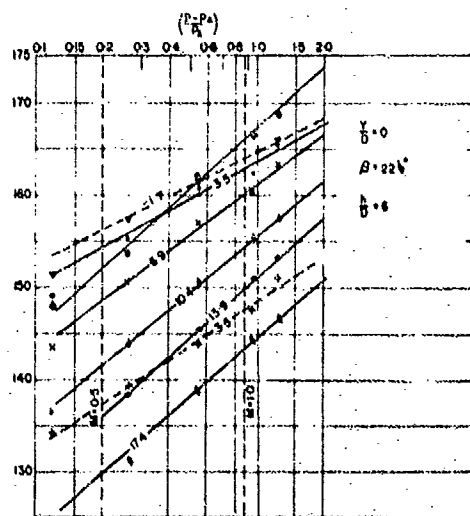
FIG. 26   FLAP ANGLE, $\beta = 22\frac{1}{2}^\circ$

FIG. 24-26   SOUND PRESSURE LEVELS VS.   NOZZLE EXCESS PRESSURE RATIO, $\dfrac{p - p_A}{p_A}$

(FLAP ANGLES, $\beta = 90^\circ$, 45°, $22\frac{1}{2}^\circ$; NOZZLE SEPARATION, $\frac{h}{D} = 6$)
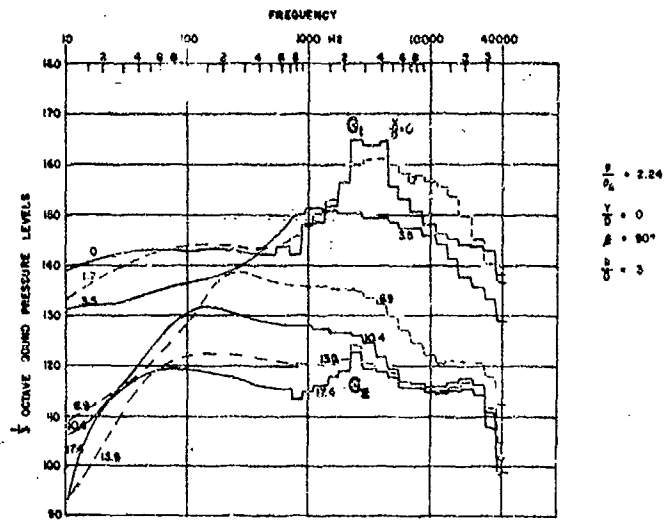
FIG. 27   NOZZLE SEPARATION, $\frac{h}{D} = 3$
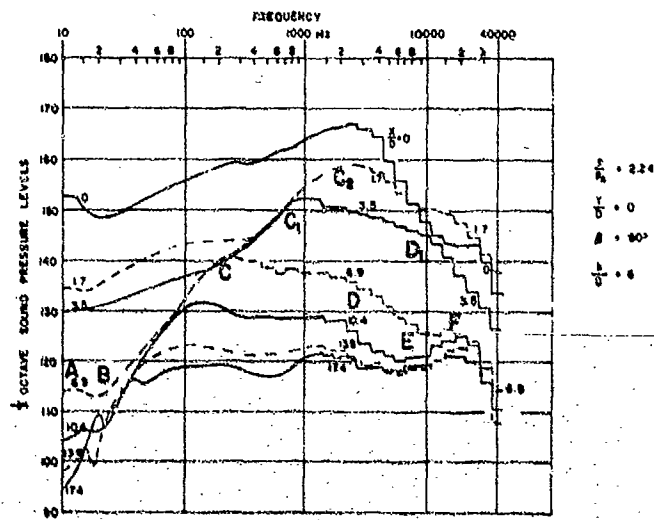
FIG. 28   NOZZLE SEPARATION, $\frac{h}{D} = 6$
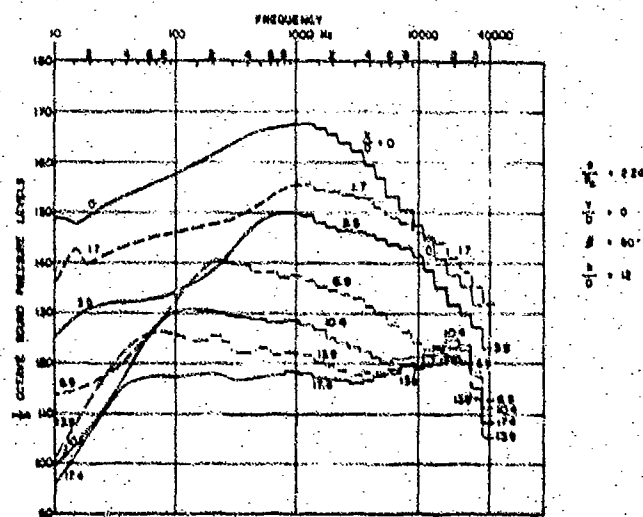
FIG. 29   NOZZLE SEPARATION, $\frac{h}{D} = 12$

FIG. 27-29   SPECTRA - 1/3 OCTAVE SOUND PRESSURE LEVELS.

(FLAP ANGLE, $\beta = 90^0$; NOZZLE PRESSURE RATIO, $\frac{p}{p_A} = 2.24$)

$\frac{X}{D} = 0, 1.7, 3.5, 6.9, 10.4, 13.9, 17.4$
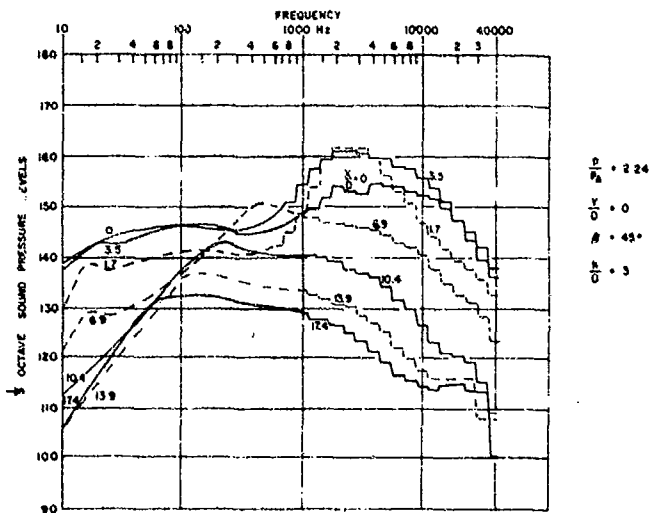
FIG. 30   NOZZLE SEPARATION, $\frac{h}{D} = 3$
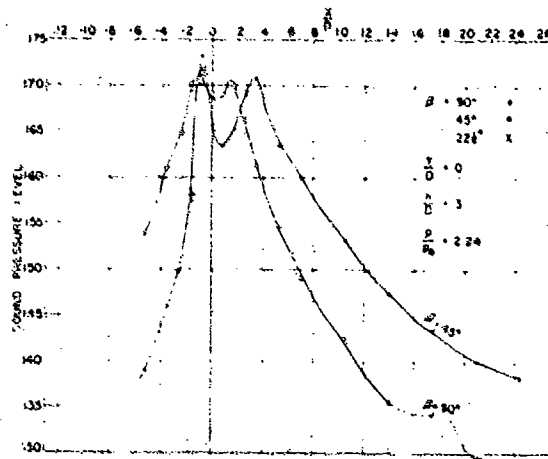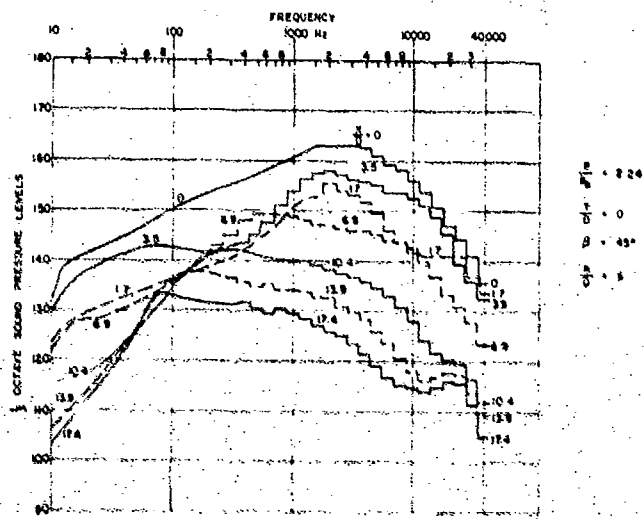

FIG. 31   NOZZLE SEPARATION, $\frac{h}{D} = 6$
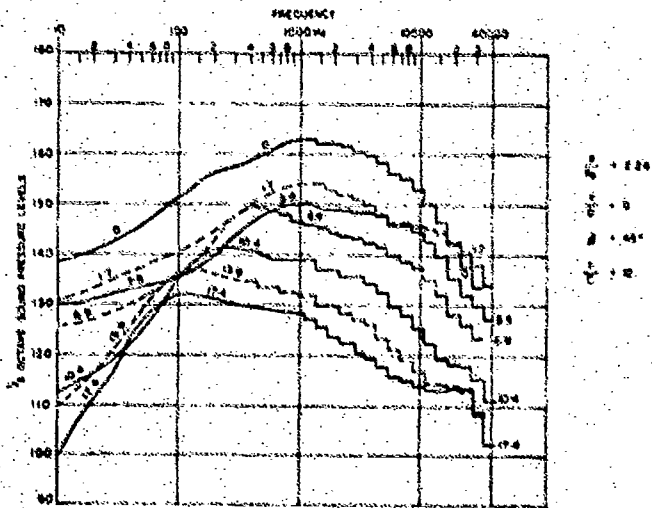
FIG. 32   NOZZLE SEPARATION, $\frac{h}{D} = 12$

FIG. 30 - 32   SPECTRA - $\frac{1}{3}$ OCTAVE SOUND PRESSURE LEVELS

(FLAP ANGLE, $\beta = 45°$; NOZZLE PRESSURE RATIO, $\frac{p}{p_A} = 2.24$;

$\frac{X}{D} = 0, 1.7, 3.5, 6.9, 10.4, 13.9, 17.4$;)
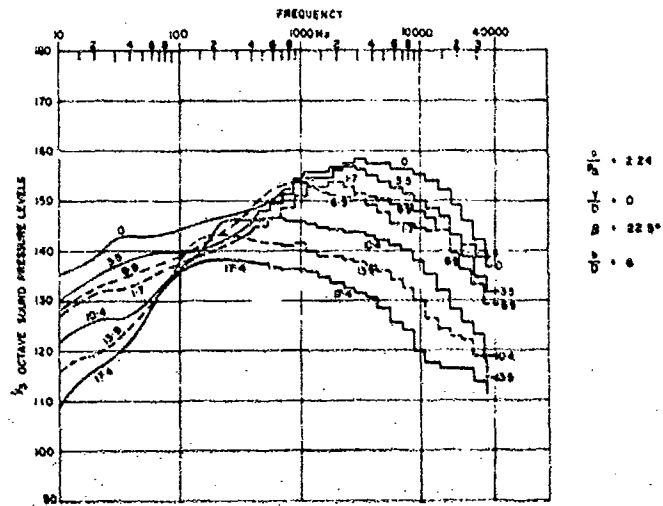
FIG. 33 NOZZLE SEPARATION, $\frac{h}{D} = 6$
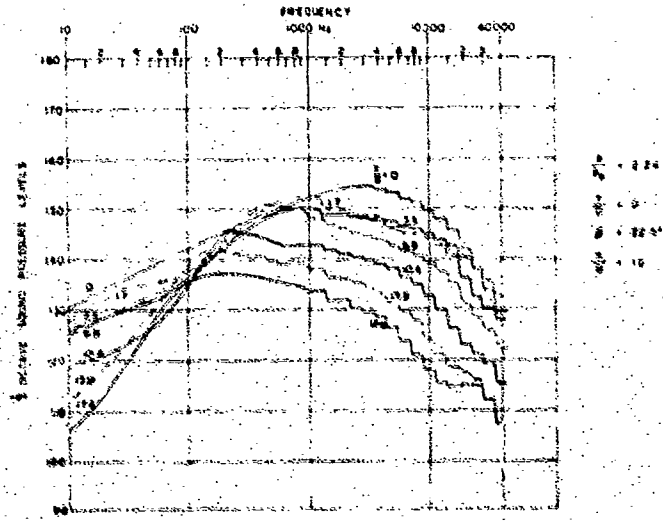
FIG. 34 NOZZLE SEPARATION, $\frac{h}{D} = 12$

FIG. 33 - 34 SPECTRA - $\frac{1}{3}$ OCTAVE SOUND PRESSURE LEVELS

(FLAP ANGLE, B = 22½°, NOZZLE PRESSURE RATIO, $\frac{P}{P_A}$ = 2.24;

$\frac{X}{D}$ = 0, 1.7, 3.5, 6.9, 10.4, 13.9, 17.4)

SESSION 1   DISCUSSION - LOADING ACTIONS

In reply to a question as to whether the relative phase of the reflected wave had been taken into account, Dr. Scholten said that they had used the autocorrelation function of the total pressure at each point and then transformed this to get pressure spectra.   The effect of the directivity of the fan noise component was also included.   Dr. Scholten was asked if there had been any failures of the structure at an early stage in the prototype development.   He replied that as the prototype had not been designed for a large number of flying hours an extensive programme of acoustic fatigue development work was not considered necessary before the prototype flew.   There were some failures in the conventional skin-stringer design of the engine pads.   They had used the earlier prediction methods but the acoustic pressure levels were higher than predicted by the free field method.   The loads here are very difficult to estimate because of the very near field effects and also the hydrodynamic pressures.   It was partly due to these difficulties that the work reported in this paper was done.

Mr. Lansing was asked if there had been any measurements of dynamic hinge moments on the model flaps.   He replied that these had not yet been done.   In answer to another question he stated that 'Koolite' pressure transducers had been used.   Mr. Coe added that these were of the semiconductor strain gauge type whose size varied down to 50 thousandths in.   The levels of acceleration measured on the model would not be representative of a real flight structure.   The model had been made of thick steel plate but even in this heavy structure the acceleration levels were very high.   Temperature measurements had been made on a half scale model at N.A.S.A. Ames.   The half scale model engine in this test had not been truly representative of the full scale engine.   In the model tests the region of impingement of the hot core jet had given rise to higher temperatures on the model flap than had been anticipated.   The estimated amount of mixing with the cold by pass flow must not have been fully achieved.   It is not yet known whether a similar problem would arise on the full scale configuration.

In reply to a question on the details of his pressure measurements, Mr. Westley said that he had tried to use microphones with their diaphragms flush to the plate surface.   This was satisfactory outside a radius of about two jet diameters from the centre of impact of the jet.   At closer positions, fine dust particles in the flow were sufficient to break the diaphragm.   It was decided, therefore to make the measurements with the standard grid in place over the microphone diaphragm.   He does not think that this has any significant effect on the results.   It was also stated that the manufacturers' data was used to make corrections for the influence of the static pressure in the flow on the microphone sensitivity.   Mr. Coe pointed out that the spectra had been analysed down to 10 Hz and questioned the validity of this because of the low frequency 'roll off' characteristics of the microphones.   Mr. Westley replied that there was a negligible effect of microphone size at the high frequency end of the spectra but the corrections had not yet been made for the low frequency end.

PRESSURE-FLUCTUATION INPUTS AND RESPONSE OF PANELS UNDERLYING ATTACHED AND SEPARATED SUPERSONIC TURBULENT BOUNDARY LAYERS

by

Charles F. Coe
Chief, Aeronautical Structures Branch
and
Wei J. Chyu, Scientist
Ames Research Center, NASA, Moffett Field, California 94035, USA

SUMMARY

The paper summarizes results of an investigation of surface pressure fluctuations and response of panels underlying attached and separated turbulent boundary layers and shock waves at NASA Ames Research Center. Extensive tests of a large assortment of axisymmetric and two-dimensional models have been conducted at transonic and supersonic Mach numbers to 3.6 to study the pressure fields. Assorted fixed-edge flat panels have been tested at Mach numbers from 1.6 to 3.6 in attached and completely separated flow fields and also in mixed flow with a step induced shock wave oscillating on the panels. The surface pressure fluctuations are described in terms of broadband rms, spectral density, and spatial correlation information. The effectiveness of parameters for scaling the pressure fluctuations is also illustrated. Measurements of the amplitude and strain response of the panels are compared with response computations by the normal mode method of analysis.

NOTATION (Note: All dimensions in standard metric units)

A	surface area of the panel	ℓ_1	panel length in x_1 direction
A_m	normalization factor for ϕ_m	ℓ_2	panel length in x_2 direction
$D = \dfrac{Eh^3}{12(1-\nu^2)}$	bending stiffness	m_σ	generalized mass for the σth mode
c	damping coefficient	M_∞	free stream Mach number
C_p	static pressure coefficient, $(p - p_\infty)/q_\infty$	p	local static pressure
d	thickness of panel	$\tilde{p}(x,t)$	pressure fluctuation acting on the panel
D	diameter	q_∞	free stream dynamic pressure
E	Young's modulus	$q_\sigma(t)$	generalized coordinates
f	frequency	$Q_\sigma(\omega)$	Fourier transform of q_σ
$f_\sigma(t)$	generalized force	$S(x',x'',\omega)$	two-sided cross spectral density function
$f\xi/U_c$	Strouhal number	$S(\xi,\omega)$	two-sided power spectral density function
$F_1 = \omega \ell_1/U_c$		S_s	flow separation length measured upstream from $x_s = 0$
$F_2 = \omega \ell_2/U_c$		t	time
F_σ	Fourier transform of f_σ	U	velocity
$G(\omega) = 2S(\omega)$	one-sided power spectral density function	$U_c(f)$	narrow-band convection velocity
$G(\xi,\omega) = 2S(\xi,\omega)$	one-sided cross spectral density	$w(x,t)$	displacement normal to the panel surface
h	shoulder height of cone frustum or two-dimensional wedge	$W(\xi,\omega)$	Fourier transform of w
$H_\sigma(\omega)$	frequency response function	x_s	longitudinal distance measured upstream from shoulder of cone frustum or two-dimensional wedge
$J_{\sigma\sigma'}(\omega)$	real part of longitudinal acceptance		
$J'_{\sigma\sigma'}(\omega)$	transversal acceptance	x_1	location on the panel in the longitudinal (or streamwise) direction
$k_{\sigma\sigma'}(\omega)$	negative of imaginary part of longitudinal acceptance	x_2	location on the panel in the lateral direction

$\underline{x}(x_1, x_2)$	coordinate referring to location on the panel		θ	angle of cone frustum or wedge
$y_1 = x_1/\ell_1$			ρ	correlation coefficient
$y_2 = x_2/\ell_2$			$\psi_\alpha(\underline{x})$	mode shape function of the panel
$\underline{y}(y_1, y_2)$	normalized coordinates referring to location on the panel		$\bar{\psi}_\alpha(\underline{y})$	mode shape function of a panel with unit dimensions
δ	boundary layer thickness		ω	angular frequency
δ^*	displacement boundary layer thickness		ω_α	natural frequency of the αth mode
$\delta_{\alpha\beta}$	Kronecker delta		ϕ	phase angle of cross spectral density function

$$\nabla^4 = \frac{\partial^4}{\partial x_1^4} + 2\frac{\partial^2}{\partial x_1^2}\frac{\partial^2}{\partial x_2^2} + \frac{\partial^4}{\partial x_2^4}$$

			Subscripts	
$\underline{\xi} = \underline{x}' - \underline{x}''$	coordinate referring to the separation distance of two points on the panel		norm	normalized quantity
			$\alpha = (m, n)$	mode index
$\eta_1 = y_1' - y_1''$			$\beta = (r, s)$	mode index
$\eta_2 = y_2' - y_2''$			o	quantity evaluated immediately ahead of detached shock wave
$\underline{\eta}(\eta_1, \eta_2) = \underline{y}' - \underline{y}''$			∞	quantity evaluated at the free stream
ϵ	strain		1	streamwise direction
μ	mass per unit area of the panel		2	lateral direction
ν	Poisson ratio		p	quantities related to the excitation field
ν_α	loss factor for the αth mode		d	quantities related to panel displacement
α	attenuation coefficient		ϵ	quantities related to strain
γ	coherence function			

1. INTRODUCTION

The pressure fluctuations in regions of attached and separated turbulent boundary layers and shock waves adjacent to surface of aerospace vehicles give rise to structural vibrations throughout atmospheric flight. The study of these excitations and resulting vibrations is of importance in determining stress, fatigue life of structures, and noise transmission into the interior of the vehicle. Unfortunately, the analysis of this type of vibration is complicated by the inherent random characteristics of the excitation pressure fields, and the difficulty of analytically describing the vibration of a realistic structure. For these reasons, early investigators of this problem considered only a hypothetical flow field and made the simplifying assumption that the structure, almost invariably either a beam or a rectangular panel, is infinitely large (refs. 1-3). This assumption gives rise to a solution in terms of the mean square displacement of the panel as a whole, but not the displacement as a function of location on the panel.

Investigations dealing with the excitation fields for the attached and separated turbulent boundary layers and regions of mixed flow, including oscillating shock waves, have been numerous (the references of refs. 4-6 yield an appropriate lengthy bibliography). A review of the literature indicates, however, that the required statistical information to describe the surface-pressure fluctuations is reasonably complete only for subsonic attached turbulent boundary layers. Investigations at transonic and supersonic speeds have primarily included measurements of pressure-fluctuation intensities and very limited analysis of power spectra and/or spatial correlation. With the exception of results in references 4-7, these latter forms of analyses have only been published for attached flow.

With respect to response, recent investigations have considered finite-size rectangular panels underlying subsonic attached turbulent boundary layers, but a simplifying assumption was made that the panels were simply supported (refs. 8-10). This assumption simplifies the algebra tremendously, permitting solutions to be expressed in closed forms; and although these analytical results give better agreement with experiment than those obtained with the infinite panel assumption, they tend to overestimate the response of a realistic panel. Previous analyses also failed to give an accurate prediction of the wave matching between the flexural wave of a panel and the pressure wave. The estimation of this wave matching is important particularly when the matching occurs at one of the resonant frequencies of the structure and this causes a large structural response. With the advent of modern high speed computers, a theoretical analysis of a finite rectangular panel with clamped edges under the excitation of a turbulent boundary

layer is now feasible. Analytical integration in closed forms are not necessary, since numerical integration can be carried out with no algebraic simplification of the integrand. This digital-computer-oriented approach has the following additional advantages over an analytical approach: (1) The transparency of the problem is preserved, as very often the physics of the problem is lost amongst a great length of closed-form mathematical formulae; (2) future developments are simplified as the basic computer program can be modified to describe different flow fields and/or different structures.

With the deficiencies in both the input and response problems in mind, a research program has been undertaken at NASA, Ames Research Center, to improve the statistical description of the random pressure fluctuations underlying attached and separated turbulent boundary layers and shock waves; and to improve the analytical capability for computation of the displacement and strain of realistic panel structures when excited by each of these flow fields. The investigations of pressure fluctuation inputs and response have spanned the subsonic, transonic, and supersonic speed ranges up to a Mach number of 3.5.

Sketches of models used for the investigation of pressure-fluctuation inputs are shown in Fig. 1. The basic configurations were 0.0508 m and 0.254 m diameter ogive cylinders and the Ames 9- by 7-foot and 8- by 7-foot supersonic wind tunnel (SWT) walls to investigate attached turbulent boundary-layers. Cone frustums ahead of axisymmetric rings and two-dimensional wedges of different heights and a variety of angles from 15° to 90° were added to the cylinders and walls to investigate regions of separated flow and shock waves. The different model sizes and tunnel walls provided large variations of the thicknesses of both the attached and separated boundary layers to investigate scaling relationships to establish the most effective parameters for nondimensionalization of the pressure fluctuations. The thickness of attached boundary layers, for example, varied from approximately 0.00466 m on the 0.0508 m diameter model to 0.135 m on the wind-tunnel wall. Separated-flow lengths ahead of 45° frustums and a 0.2032 m high 45° wedge varied from 0.041 m to 0.89 m.
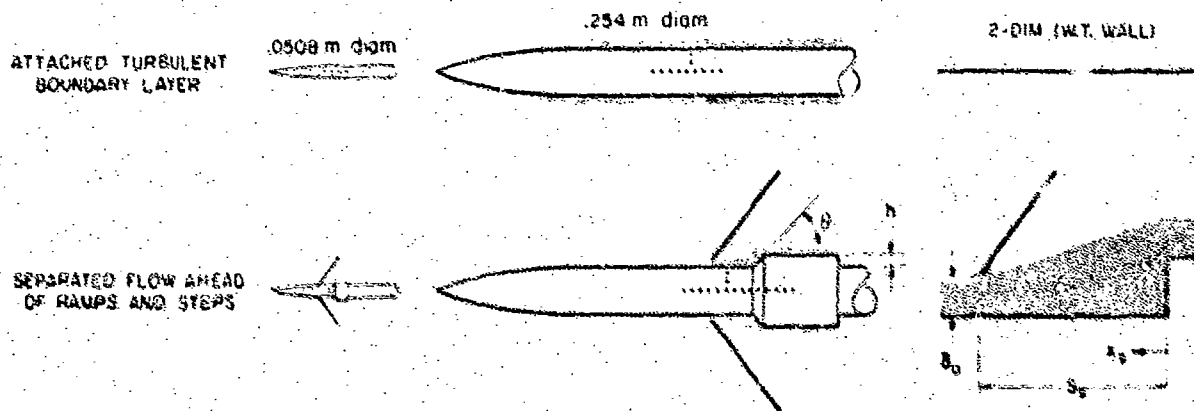
Figure 1. Configuration investigated for study of surface-pressure fluctuations.

The surface pressure fluctuations were measured with two different sizes of semiconductor type pressure transducers having sensing diameters of 0.00279 m and 0.00121 m. The transducers were mounted flush or slightly submerged to the surface in longitudinal, lateral, and diagonal arrays. In addition, detailed static-pressure distributions and boundary-layer measurements were obtained. More details on the test procedure, data acquisition and analysis, and overall scope of the pressure-fluctuation investigation can be found in references 4 and 7.

For the response part of the research, the first step in the program was to develop the analytical capability and a practical computer program for computation of the amplitude response of a clamped-edge panel. The excitation of a subsonic attached turbulent boundary layer was considered first because of the availability of corresponding excitation data by Bull (ref. 11), and response measurements by Wilby (ref. 10). The method of analysis (method of normal mode used together with the technique of spectral analysis) and comparisons with Wilby's response data are shown in reference 12. These initial results show favorable comparisons between the computed and measured response.

The analysis and computer program have subsequently been expanded to include the amplitude and strain response of simply-supported and clamped-edge panels excited by supersonic attached and separated turbulent boundary layers. Corresponding experiments have been conducted to measure the amplitude and strain response of a variety of panels with different length-to-width ratios and thicknesses. Panel lengths and widths varied from 0.1524 m to 0.3048 m and thicknesses varied from 0.5588×10⁻³ m to 2.254×10⁻³ m. The tests were conducted in the same facilities (9- by 7-foot SWT and 8- by 7-foot SWT) used for the supersonic pressure-fluctuation studies between Mach numbers of 1.6 and 3.5. An illustration of the test set up for separated flow is shown in Fig. 2. The panel response tests were conducted with the 0.2032-m high 90° step, whereas pressure fluctuations were also measured ahead of 23° and 45° wedges. Separated flow lengths ahead of the steps varied from approximately 0.91 m to 1.10 m depending on Mach number and the attached boundary layer thickness.

Three test conditions with the panels underlying attached flow, separated flow, and mixed flow with an oscillating shock wave were investigated. Attached flow was obtained by removing the step. Separated flow was obtained with the step positioned as shown in Fig. 2 so that the panel was about one-third the distance between the shock wave and the step. The step was moved further downstream to position the shock wave on the panels.

Panel displacements were measured with non-contacting capacitance probes that could be remotely positioned to different panel coordinate positions. A steady-state cavity pressure was carefully maintained at wall static pressure at the streamwise midpoint near the lower edge of the panels for all test conditions.

The analyses of all the results of the pressure fluctuation and panel response investigations are not complete. However, a large amount of data have been amassed for attached and separated flows at supersonic speeds, and therefore these data and the corresponding panel response measurements and analyses are the subject of this paper.

2. PRESSURE-FLUCTUATION INPUTS

2.1 Broadband Characteristics

The surface-pressure fluctuations measured in attached flow on the walls of Ames wind tunnels are shown in Fig. 3 along with comparative data from a few other investigations. The data presented are considered by the authors to most reliably represent the broadband intensities of the pressure fluctuations, $\sqrt{\bar{p}^2}/q_\infty$, for the Mach number range from 0 to 3.5. Many more data points could be added to the figure from other earlier investigations, but the spread of data would then be increased markedly. Most of the other available data considered have been rejected because of uncertain effects of transducer size, installation, and extraneous noise. The data from the Ames 9- by 7-foot SWT and 8- by 7-foot SWT and the XB-70 represent measurements at several locations on a rigid plate in the tunnel wall and on the aircraft. The spread in data of about 30% (3 dB) is typical and is believed due to a nonuniformity in the unsteady pressure field. The fact that data can be consistently repeated within 0.3 dB when different transducers of the same kind are installed at a specific location on the wind tunnel wall supports this argument. Generally, the wind tunnel and flight data in Fig. 3 compare favorably, and both show about a 30% decrease in $\sqrt{\bar{p}^2}/q_\infty$ between Mach numbers of 1 and 2.5. At $M > 2.5$ the available wind tunnel data show a tendency for $\sqrt{\bar{p}^2}/q_\infty$ to increase slightly from a minimum of about 0.0035 at $M = 2.5$ to about 0.004 at $M = 3.5$.

Figure 2. Panel-response test installation.

Figure 3. Broadband characteristics of pressure fluctuations underlying attached turbulent boundary layers.

Typical longitudinal distributions of mean static and fluctuating pressures illustrative of the separated flow on the models of this investigation are shown in Fig. 4 (the effect of diameter and frustum height in Fig. 4(a) and the effect of Mach number on the flow field in the vicinity of the response-test panel is shown in Fig. 4(b)). As previously described (refs. 4 and 14), the mean static pressure, initially at free-stream static pressure, increases rapidly as the flow encounters the detached frustum shock near the separation point and then approaches a plateau as the transition from attached to separated flow is completed. The static-pressure coefficients in the region of the plateau were nearly the same on all the axisymmetric models, but were approximately 20% lower than the corresponding measurements on the two-dimensional wall. The locations of the static-pressure rise associated with the shocks and separation points were not scaled by the x_s/h parameter. Further study of the shock separation distances has shown that the differences are due to the variation of h/δ_0 on these models rather than to Reynolds number effects.

The characteristic feature of the broadband pressure fluctuations (Fig. 4(a)) can be related to features of the mean static-pressure distributions. The pressure fluctuations increase rapidly at the shock, as identified by the rapid pressure rise, and reach a maximum intensity where the slope of the static-pressure curve is maximum. In the fully separated region, the fluctuating pressure descends from this maximum to a plateau level. Correspondingly in this same region the static pressure decreases toward a plateau level. It can be noted that the plateau level was relatively independent of the shoulder height of the frustum that caused the separation on the 0.254-m-diameter model. The lower fluctuating-pressure intensities on the 0.0508-m-diameter model were found to be due to an insufficient frequency range of the recorded data. The higher fluctuating pressures on the two-dimensional model are associated

a) Effect of diameter and frustum/wedge height.

b) Effect of Mach number.

Figure 4. Longitudinal distribution of steady and fluctuating static pressures in region of separated flow.

with the higher static pressures in the separated flow region on the two-dimensional model. Generally, the Mach number effects on the broadband pressure fluctuations (Fig. 4(b)) in the separated flow are not significant, however, there is a trend showing a slight increase in intensity with increasing Mach number.

2.2 Power Spectral Densities

Power spectra representative of pressure fluctuations in the vicinity of supersonic separated flow are shown in Fig. 5. The curves show the distinct differences in shapes and mean-square amplitudes that distinguish separated flow spectra from spectra measured in regions of the nearby shock wave and attached turbulent boundary layer. Shock spectra are characterized by a very steep slope and high intensities at low frequencies. The lowest frequencies in these data are 10 Hz. The separated-flow spectra were at least one decade lower than the shock spectra at low frequencies. Having a less steep slope, however, the separated-flow spectra crossed the shock spectra, and were the highest spectral intensities obtained at intermediate and high frequencies. The power spectra of the pressure fluctuations beneath the attached boundary layer were more than two decades lower than the separated-flow spectra at low frequencies. Although all the spectra appear to be converging toward a common level and slope at higher frequencies, there was still at least one decade difference between the attached and separated flow spectra at the highest frequencies of this investigation. The spectra labeled "intermittent shock" illustrate the effect of an intermittent excursion of the shock to the maximum limit of its upstream oscillation. Only the very low frequency components of the pressure fluctuations are increased in intensity, while the intermediate and high frequencies retain the intensities of the attached boundary layer.

2.2.1 Nondimensionalization of Power Spectra

Many geometric and flow parameters were considered for the nondimensionalization of pressure fluctuations when presented in the frequency domain. Various combinations of length and velocity were applied to the generally accepted reduced frequency parameter having the form (frequency × length/velocity). The mean-square amplitudes per unit reduced frequency were nondimensionalized by (pressure)^2. Some of the

Figure 5. Typical power spectra of pressure fluctuations underlying supersonic flow.

reduced-frequency parameters investigated were: $f\delta_0/U_\infty$, $f\delta_0^*/U_\infty$, fS_s/U, $f(S_s - x_s)/U$, $f\delta/U$, and $f\delta/U_\infty$.

It became evident early in the investigation that there was no reduced-frequency or spectral-density parameter that was the most effective for scaling the data from the many models, particularly for separated flow, for the full range of frequencies considered. (Certain characteristics of the pressure fluctuations were found to be different within different ranges of reduced frequencies.) It was clear however, that the parameters $f\delta/U$ and $f(S_s - x_s)U$ involving local boundary-layer thickness or flow-separation dimensions and local velocity were best for scaling frequencies in separated flow. In this paper, since both attached and separated boundary layers are considered, the nondimensionalization of spectra are illustrated in terms of $f\delta/U$. The data used for the response computation are also presented in terms of $f\delta/U_\infty$ since the local velocity in the separated region is frequently not available and also since differences in scaling with U vs U_∞ are relatively minor. Also minor differences were found in the effectiveness of free-stream versus local dynamic pressure for scaling the spectral density; therefore, the choice has been made in favor of the more conveniently available q_∞.

Local boundary layer thicknesses used for scaling the pressure-fluctuation data were based on measurements of boundary-layer profiles for all the attached-flow test cases and on profiles measured within the separated flow region on the d = 0.254 m, h = 0.0508 m, θ = 45° model. The separated-flow boundary layer measurements are shown in Fig. 6 to illustrate that the boundary-layer growth rearward from the separation point was sufficiently linear to allow a simple linear interpolation of local boundary-layer thickness. Local boundary-layer thicknesses in separated flow were therefore estimated for all the models from the relationship $\delta = \delta_0 + h (S_s - x_s)/S_s$.
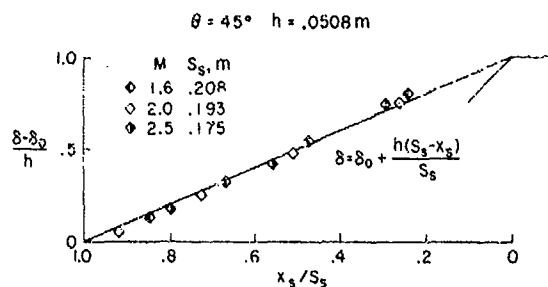
Figure 6. Boundary-layer thickness of separated flow.

Typical scaling of spectral measurements obtained on the different models at M = 2.0 is illustrated in Fig. 7. The spectrum selected for each model represents an approximate mean of from 10 to 20 measurements, and in most of the separated flow cases the mean spectrum was obtained near the center of the separated flow region. The closeness of fit of the spectra scaled by the reduced frequency parameter $f\delta/U$ (Fig. 7) illustrates about the best attainable collapse of data. Most of the separated flow results fit within a factor-of-two spread on the mean-squared spectral density scale. This is considered a good fit of random dynamic data obtained on so many different models, and indicates relative independence of the pressure-fluctuation characteristics on geometry.
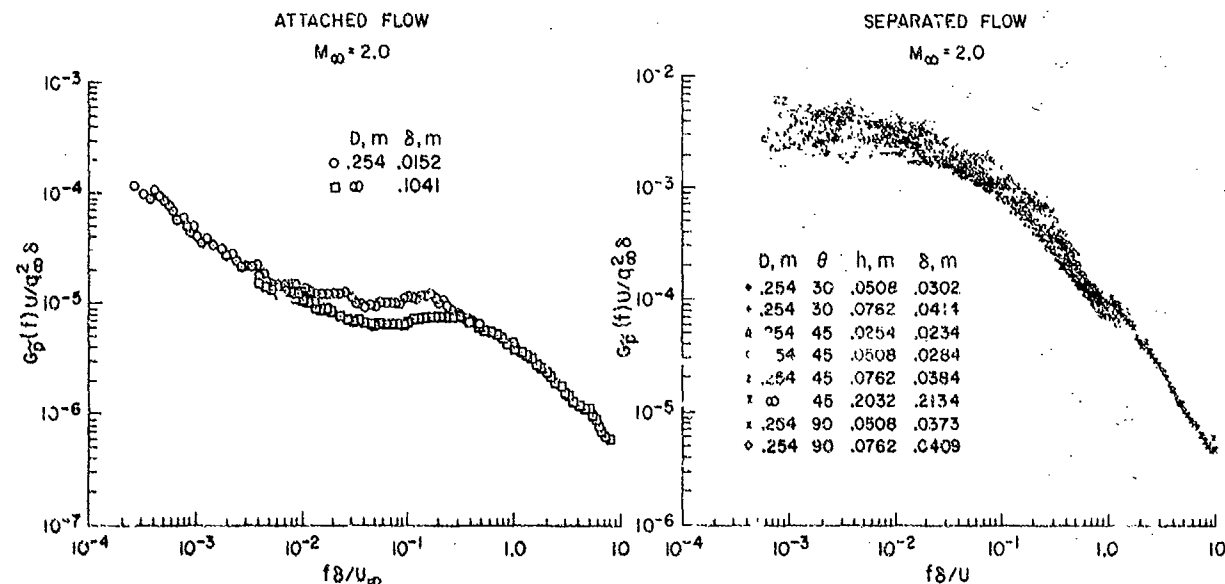
Figure 7. Scaling of power spectra.

2.2.2 Mach Number Effects of Power Spectra

The variation of power spectra in attached and separated flows between Mach numbers of 1.6 and 3.5 is shown in Fig. 8. Each of these spectra represents an average of from 10 to 20 spectra measured on a rigid plate installed in the "panel-response" test fixture in the walls of the Ames 9- by 7-foot SWT and 8- by 7-foot SWT. These data form the basis of the representation of the excitation spectrum used for panel response calculations. Note that the data are not dimensionalized by free-stream velocity.

The power spectra for attached flow generally are very similar for all Mach numbers with the exception of a slightly lower measured spectrum at M = 3. There is a reasonably consistent trend at low reduced frequencies,
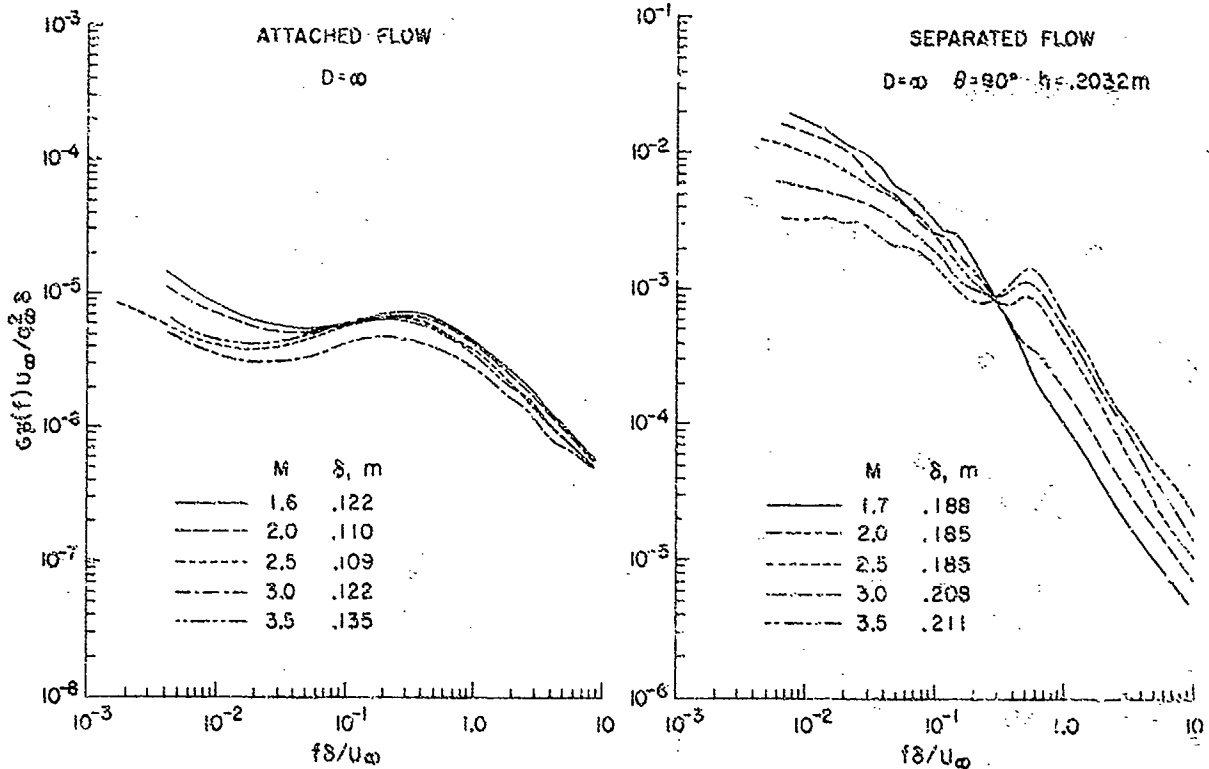
Figure 8. Variation of power spectra with Mach number.

$f\delta/U_\infty < 0.05$, that indicates a reduction in spectrum level with increasing Mach number. These variations should be taken lightly, however, because of reduced statistical accuracy of analysis at the lower frequencies. In contrast with the attached flow case the power spectra measured in the separated flow show a very consistent variation with Mach number. The spectral levels decrease with increasing Mach number at $f\delta/U_\infty < 0.3$ and increase with increasing Mach number at $f\delta/U_\infty > 0.3$. These results illustrate the separation of frequency regimes at $f\delta/U_\infty = 0.3$. In each regime the pressure fluctuations are dependent upon different phenomena. The surface pressure measurements in the lower frequency region are mainly sensitive to the transmitted fluid fluctuations in the turbulent flow of the separated boundary layer; the radiated energy is negligible. In the higher frequency region, it is believed that the surface pressure fluctuations are strongly influenced by an eddy Mach wave radiation phenomena. This phenomena was investigated by Ffowcs-Williams (ref. 16), and although his results do not apply to the study of surface pressure fluctuations a study currently in progress by Dr. Richard D. Rechtien of the University of Missouri, Rolla, Missouri, (NASA-Ames Grant) indicates a dependence of these data on Mach wave radiation.

2.3 Spatial Correlation of Pressure Fluctuations

Chyu and Hanly (ref. 4) presented some data from this investigation that showed the power and cross spectra and space-time correlations of fluctuating pressures underlying the supersonic attached boundary layer on the 0.254-m diameter ogive cylinder and the separated boundary layer ahead of the 0.0508-m high frustum. Among other things, they investigated the co- and quad-spectral density and coherence as functions of a wave number parameter $f\xi_1/U_c(f)$. Illustrative coherence functions are shown in Fig. 9. The results indicate a similarity between the coherence measurements in attached and separated flow at supersonic Mach numbers, but only if the velocity term is $U_c(f)$. The use of convection velocity instead of free-stream velocity is necessary, since for separated flow, $U_c(f)$ varies significantly with frequency. The general trends of the data are also similar to the subsonic-flow measurements by Bull (ref. 11). It can be seen that the envelope of the coherence functions for various spatial distances ξ_1/δ^* decreases exponentially with increasing frequency, however, the envelope unfortunately represents the coherence only at high frequencies.

Chyu and Au-Yang (ref. 12) used Bull's coherence data to represent the subsonic attached-boundary-layer spatial correlation for application to the response computation. The fact that the coherence functions do not collapse complicates the empirical expression
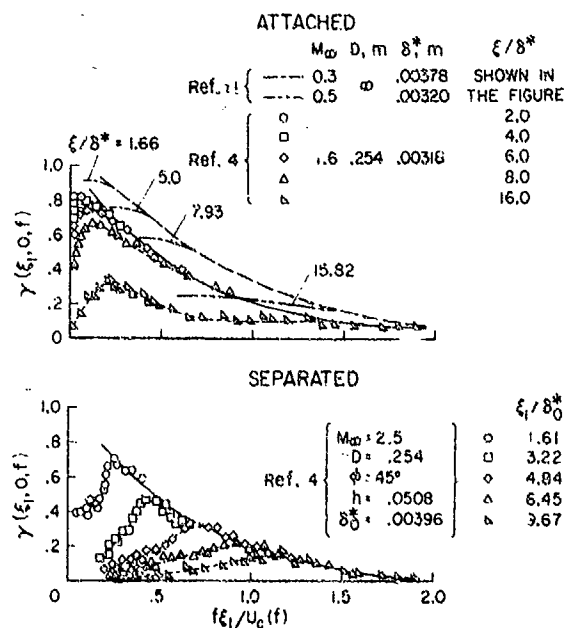
Figure 9. Longitudinal coherence of pressure fluctuations.

of correlation, and therefore, a different approach has more recently been investigated. As suggested by Rechtien the normalized moduli of the cross spectral densities, $|G_p(\xi, f)|_{norm}$, for available or selected transducer spacings have been curve-fitted to the exponential function $|G_p(\xi, f)|_{norm} \approx e^{-\xi\alpha}$ by the method of least squares to obtain a non-dimensional attenuation-coefficient function $\alpha(\xi, f)\delta$. Typical moduli of the cross-spectral densities of the pressure fluctuations in separated flow that were used for the evaluation of the attenuation coefficient are shown in Fig. 10.

Figure 11 shows the attenuation-coefficient function measured in separated flow on the 0.254-m diameter model with the 0.0508-m high 45° frustum shoulder to illustrate its effectiveness of describing spatial correlation. The function is shown to be reasonably independent of the number of moduli, the transducer spacing, or the reference locations involved in the curve fitting. These results indicate that the flow is relatively homogeneous within the limited area of the separated flow region where the measurements were obtained. It appears that the attenuation coefficients decreased slightly at higher frequencies as the larger transducer spacings were used in the analysis. The variation is considered insignificant, however, in light of the state of the art of the structural part of the problem of predicting response to random turbulence. Attenuation coefficients obtained from transducer arrays oriented longitudinally, diagonally, and laterally to the free-stream flow indicate that the decay of correlated turbulence was independent of orientation at $f\delta/U < 0.06$. The predominant turbulence is therefore nonconvective at the lower frequencies, and contours of equal spatial correlation would be circular. At $f\delta/U > 0.06$ the attenuation coefficients were progressively lower as the angularity of the transducer orientation changed from lateral to longitudinal, indicating extended correlation in the direction of free-stream flow.
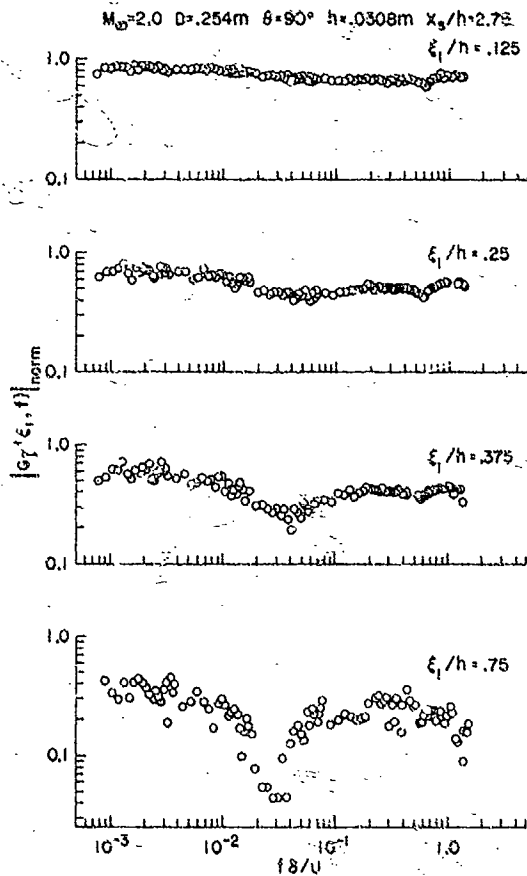
Figure 10. Variation of normalized cross spectra with longitudinal spacing of transducers in separated flow.
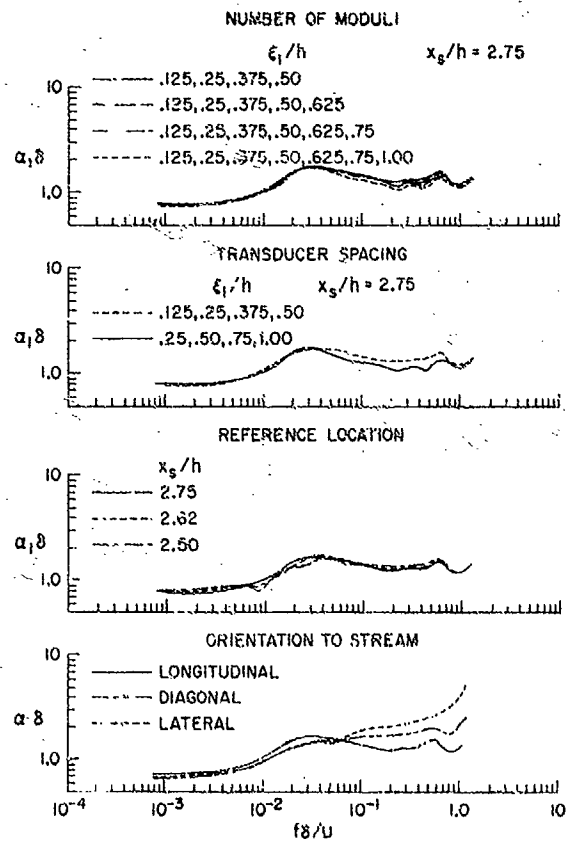
Figure 11. Attenuation coefficients measured on the 0.254-m diameter model in the region of separated flow, h = 0.0508 m, φ = 45°.

A comparison of longitudinal attenuation coefficient functions obtained on the different models in separated flow is shown in Fig. 12 to illustrate the effectiveness of $\alpha\delta$ for scaling for separated flow. The results indicate that the nondimensionalized attenuation coefficients were in relatively good agreement, showing a total spread between all the curves of generally less than a factor of two.

Typical longitudinal attenuation coefficients at Mach numbers from 1.6 to 3.5 are shown in Fig. 13 for both attached and separated flow on the wind tunnel walls. As with the spectra (Fig. 8) the separated flow data show a more consistent variation with Mach number than the attached flow data, particularly at the lower frequencies. The results show that the pressure fluctuations in attached flow were most highly correlated at $f\delta/U_\infty \approx 0.4$; whereas, in separated flow the maximum correlation occurred at the lowest frequencies. The dips in separated flow $\alpha\delta$ curves in the frequency range $0.3 < f\delta/U_\infty < 1.3$ indicate increased correlation that is believed to result from the Mach wave radiation phenomena discussed in connection with the observed Mach number effects on power spectra.

$M_\infty = 2.5$ $\theta = 45°$

D, m	h, m	δ, m
---- .0508	.0102	.0056
------ .254	.0254	.0138
——— .254	.0508	.02.4
········· ∞	.2032	.1056
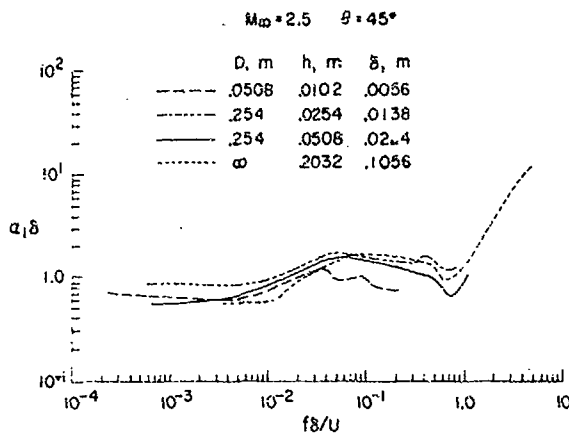
Figure 12. Scaling of attenuation coefficients.

2.4 Phase Angles of Cross Spectra

The convection of turbulence in attached and separated boundary layers results in an angle of phase between spatially correlated components of pressure. Since this phase angle can result in matching of panel flexural waves and pressure waves and thus cause an enhancement of response, it is necessary that it be accounted for in response computations. Convection of the surface-pressure fluctuations can be studied directly in terms of convection velocities or in terms of the phase angles of the cross spectra. The broadband convection velocity derived from space-time correlations is the most convenient description of convection characteristics for attached flow, but Chyu and Hanly (ref. 4) showed that it is inappropriate for separated flow since convection velocities vary with frequency.

ATTACHED FLOW

$D = \infty$

M	δ, m
——— 1.6	.122
——— 2.0	.110
·——·· 2.5	.109
——— 3.0	.122
——— 3.5	.135

SEPARATED FLOW

$D = \infty$ $\theta = 90°$ $h = .2032$ m

M	δ, m
——— 1.7	.188
——— 2.0	.185
·······2.5	.185
——— 3.0	.203
——— 3.5	.211
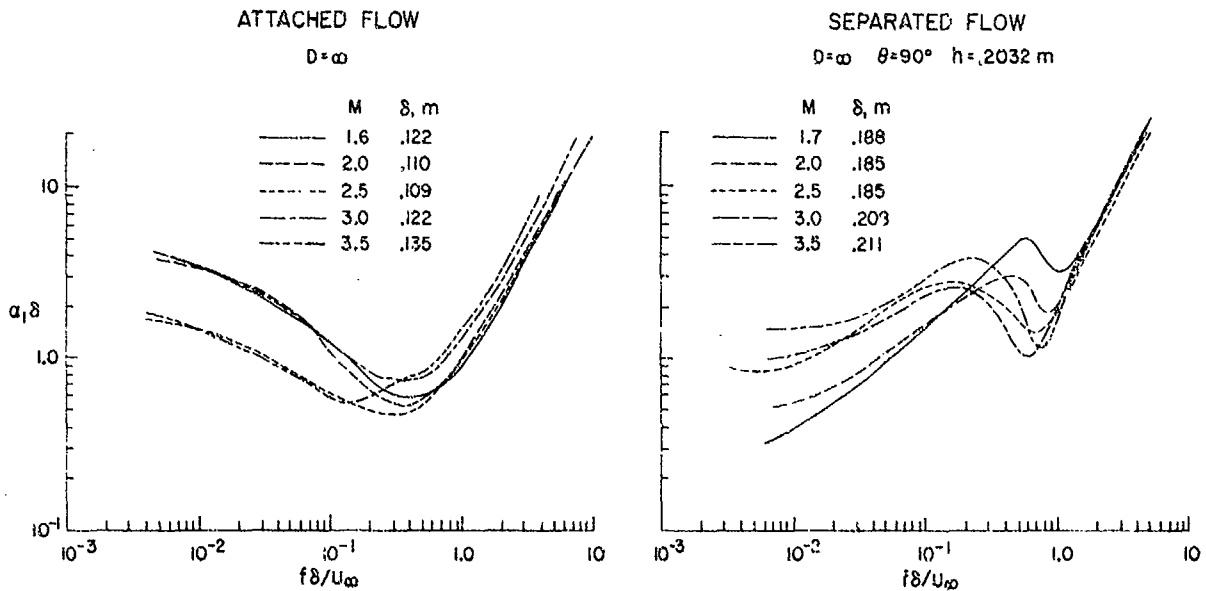
Figure 13. Effect of Mach number on longitudinal attenuation coefficients.

Typical phase angles that result from convection of the turbulence in separated flow are shown in Fig. 14. The data were obtained on the 0.254-m diameter model with axisymmetric flow and show the effects of the angular orientation of a transducer array to the free-stream flow direction. At low frequencies, f < 300 Hz, the phase angles were zero for all angular orientations. A zero phase angle indicates a zero or infinite speed of convection of the pressure fluctuations between two points, as would exist with a stationary pulsating bubble or for normal incidence of an acoustic radiation process. The equivalent of the pulsating bubble could occur if the turbulence is related to fore-and-aft oscillations of the detached shock wave. The phase-angle measurements generally indicate an absence of lateral convection in the separated flow over the full range of frequencies investigated. This result was evidenced by the near zero lateral measurements and by the agreement between longitudinal and diagonal measurements of θ/ξ_1 (phase angle per meter of longitudinal component of transducer spacing).

$M_\infty = 2.0$ $\theta = 45°$ $h = .0508$ m

o LONGITUDINAL	
□ DIAGONAL	ϕ/ξ_1
◊ LATERAL	ϕ/ξ_2

2.5 Narrow-Band Convection Velocities

When significant phase angles are measured, they can be converted to convection velocities, as defined by $360 \, f(\xi/\phi)$, and thus reveal the narrow-band convection characteristics of the turbulence. Figure 15 shows that on the 0.254-m diameter model, the convection velocities of the pressure field in separated flow varied from a minimum of approximately 0.2 U at $f\delta/U \approx 0.6$ to a plateau

Figure 14. Typical phase angles of cross spectra of pressure fluctuations underlying separated flow.

TRANSDUCER SPACING

$M_\infty = 2.0$ $h = .0508$ $x_s/h = 2.75$

ξ_i/h	
—·—·—	.12
—··—··—	.25
———	.37
--------	.50
———	.62
— — —	.75
—— ——	1.00

REFERENCE LOCATION

$M_\infty = 2.0$ $h = .0508$ $\xi_i/h = .375$

	x_s/h	x_2/h
———	2.75	0
———	2.75	.375
—·—·—	2.62	0
--------	2.12	0

FRUSTUM - SHOULDER HEIGHT

$M_\infty = 2.0$

	h, m	x_s/h	ξ_i/h
———	.0102	2.95	1.00
--------	.0254	3.06	1.00
———	.0508	2.75	.50
—·—·—	.0762	2.00	.67
—— ——	.2032	2.27	.50
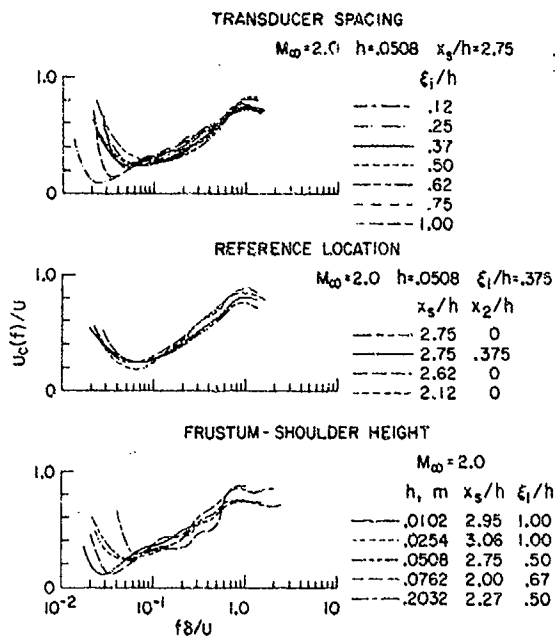
Figure 15. Typical narrow-band convection velocities.

near 0.8 U at $f\delta/U \approx 0.8$. The variation of convection speed with frequency infers that the predominant turbulence at different frequencies between $0.03 < f\delta/U < 0.8$ is generated at different levels of the boundary layer ranging from slightly above the zero velocity line to the free-shear layer. Upstream convection was not detected between points within the separated flow region. The turbulent eddies generated in the reverse flow region apparently contribute little to the wall-pressure fluctuations. With the exception of the low frequency region of $f\delta/U < 0.06$, the convection velocities were relatively unaffected by transducer spacing or reference location. It is also shown that they can be effectively scaled by the reduced frequency parameter $f\delta/U$.

Representative narrow-band convection velocities in attached and separated flows on the walls of the 9- by 7-foot SWT and 8- by 7-foot SWT at the location of the panel response test fixture are shown in Fig. 16. It can be seen that for attached flow there was no significant variation in the ratio of convection velocity to free-stream velocity ($U_c(f)/U_\infty \approx 0.75$) with frequency or Mach number. The variation of convection velocity with frequency in separated flow was previously discussed in connection with Fig. 15. This variation with frequency was relatively unaffected by Mach number at $f\delta/U_\infty < 0.6$. The plateau values of nearly constant U_c/U_∞ at $f\delta/U_\infty > 1.0$, however, varied inversely with Mach number (with the exception of the $M_\infty = 3.5$ data) so that the absolute convection velocity, U_c, was nearly constant. The convection velocity in this plateau region varied from approximately 354 m/sec (1150 fps) at $M_\infty = 1.7$ to 366 m/sec (1200 fps) at $M_\infty = 3.0$. The reduced frequencies where the beginning of the plateau occurs can be identified with changes in the characteristics of the power spectra and attenuation coefficients.

ATTACHED FLOW

$D = \infty$

	M	δ, m
———	1.6	.122
———	2.0	.110
--------	2.5	.109
—·—·—	3.0	.122
—··—··—	3.5	.135

SEPARATED FLOW

$D = \infty$ $\theta = 90°$ $h = .2032$ m

	M	δ, m
———	1.7	.188
———	2.0	.185
--------	2.5	.185
—·—·—	3.0	.208
—··—··—	3.5	.211

Figure 16. Variation of narrow-band convection velocities with Mach number.

2.6 Representation of Surface-Pressure Fluctuations

The fundamental information needed to describe the excitation of a structure underlying a turbulent flow is the cross spectral density of the fluctuating pressures.

In a homogeneous turbulence the cross spectra can be expressed in the form

$$\frac{S_p(\xi_1, \xi_2, \omega)}{S_p(\omega)} = \left| \rho_{\tilde{p}}(\xi_1, \xi_2, \omega) \right| e^{-i\omega\xi_1/U_c} \tag{1}$$

where $\left| \rho_{\tilde{p}}(\xi_1, \xi_2, \omega) \right|$ is the cross correlation coefficient between two points separated by distance ξ_1 and ξ_2 in the x_1 and x_2 directions. Experimental data have also shown that the correlation coefficient can be separated in coordinates as follows:

$$\left| \rho_{\tilde{p}}(\xi_1, \xi_2, \omega) \right| = \left| \rho_{\tilde{p}}(\xi_1, 0, \omega) \right| \left| \rho_{\tilde{p}}(0, \xi_2, \omega) \right| \tag{2}$$

where $\left| \rho_{\tilde{p}}(\xi_1, 0, \omega) \right| = \exp\left[-\alpha_1 \xi_1\right]$ and $\left| \rho_{\tilde{p}}(0, \xi_2, \omega) \right| = \exp\left[-\alpha_2 \xi_2\right]$.

The convection velocity U_c is related to the phase angle ϕ of the cross spectral density of the fluctuating pressure by $U_c = 360 \, f\xi_1/\phi$. For this investigation, it has been chosen to represent U_c in terms of ϕ since U_c varies significantly with f for separated flow and since $\phi \to 0°$, $U_c \to \infty$. It should also be noted that ϕ/ξ_1 is an independent function of f and is therefore not scaled by a reduced frequency parameter.

To derive expressions that represent the selected functions used to describe the fluctuating pressures in supersonic attached and separated turbulent boundary layers, the large amount of experimental data previously discussed have been averaged at each test Mach number (1.6, 2.0, 2.5, 3.0, 3.5) and approximate means of the envelopes of these data have been curve-fitted as shown in Fig. 17.
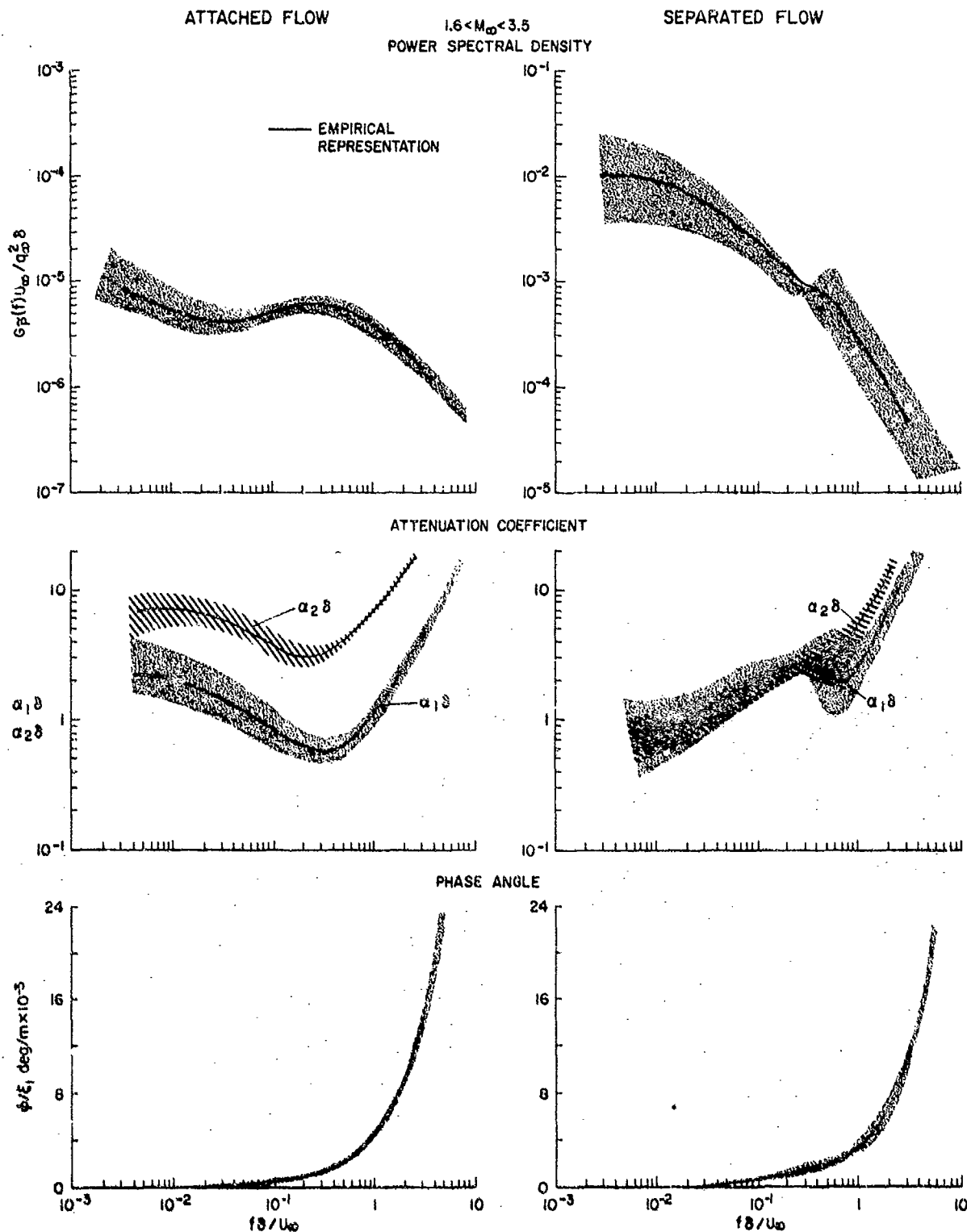
Figure 17. Representation of surface-pressure fluctuations.

The empirical formulae that express the power spectrum, attenuation coefficients, and phase angles for attached and separated flows are as follows:

a) For attached flow

Power Spectrum

$$G_{\tilde{p}} U_\infty / q_\infty^2 \, \delta = \exp\{-12.470 - 0.639x - 0.269x^2 + 0.015x^3 + 0.017x^4 + 0.002x^5\} \tag{3}$$

Attenuation Coefficients

$$\alpha_1 \delta = \exp\{0.060 + 0.941x + 0.380x^2 - 0.023x^3 - 0.020x^4 - 0.002x^5\} \tag{4}$$

$$\alpha_2 \delta = \exp\{2.163 + 1.291x + 0.262x^2 - 0.132x^3 - 0.043x^4 - 0.0033x^5\} \tag{5}$$

Phase Angle

$$\phi/\xi_1 = 39.37\{115.14 + 131.99x + 69.89x^2 + 18.84x^3 + 2.44x^4 + 0.12x^5\} \text{ deg/m} \tag{6}$$

b) For separated flow

Power Spectrum

$$G_{\tilde{p}} U_\infty / q_\infty^2 \, \delta = \exp\{-8.094 - 1.239x - 0.295x^2 - 0.090x^3 - 0.014x^4 - 0.001x^5\} \tag{7}$$

Attenuation Coefficients

$$\alpha_1 \delta = \exp\{1.031 + 0.666x + 0.645x^2 + 0.270x^3 + 0.043x^4 + 0.002x^5\} \tag{8}$$

$$\alpha_2 \delta = \exp\{1.797 + 1.239x + 0.536x^2 + 0.122x^3 + 0.010x^4\} \tag{9}$$

Phase Angle

$$\phi/\xi_1 = 39.37\{90.54 + 89.28x + 50.47x^2 + 15.69x^3 + 2.32x^4 + 0.13x^5\} \tag{10}$$

Where for both a) and b) above: $x = \log_e(f\delta/U_\infty)$

3. RESPONSE OF FLAT CLAMPED-EDGE PANELS

3.1 Method of Analysis

The displacement $w(\underline{x}, t)$ of a vibrating panel (Fig. 18), is assumed to obey the classical thin plate equation

$$\mu \ddot{w} + c\dot{w} + B\nabla^4 w = \tilde{p}(\underline{x}, t) \tag{11}$$

where μ and B are constants and independent in the present analysis. It is assumed further that $w(\underline{x}, t)$ can be expanded in terms of $\psi_\alpha(\underline{x})$ as follows:

$$w(\underline{x}, t) = \sum_\alpha q_\alpha(t)\psi_\alpha(\underline{x}) \tag{12}$$

Figure 18. Schematic of a panel with flow excitation.

Here ψ_α is assumed to be properly normalized and separable in coordinates, i.e.,

$$\int_A \psi_\alpha(\underline{x}) \, \psi_\beta(\underline{x}) \, dx = \delta_{\alpha\beta} \tag{13}$$

and

$$\psi_\alpha(\underline{x}) = \psi_m(x_1)\psi_n(x_2) \tag{14}$$

It can be shown that for a panel with clamped edges ψ_m takes on different forms according to whether m is even or odd:

a) If m is odd,

$$\psi_m(x_i) = \frac{1}{A_m \sqrt{\ell_i}} \cos \gamma_m \left(\frac{x_i}{\ell_i} - \frac{1}{2}\right) + K_m \cosh \gamma_m \left(\frac{x_i}{\ell_i} - \frac{1}{2}\right) \tag{15}$$

where γ_m are the roots of the equation

$$\tan \frac{\gamma_m}{2} + \tanh \frac{\gamma_m}{2} = 0$$

and

$$K_m = \frac{\sin(\gamma_m/2)}{\sinh(\gamma_m/2)}$$

b) If m is even,

$$\psi_m(x_i) = \frac{1}{A_m \sqrt{\ell_i}} \sin \gamma_m \left(\frac{x_i}{\ell_i} - \frac{1}{2}\right) + K_m \sinh \left(\frac{x_i}{\ell_i} - \frac{1}{2}\right) \tag{16}$$

where γ_m are the roots of the equation

$$\tan \frac{\gamma_m}{2} - \tanh \frac{\gamma_m}{2} = 0$$

By using the orthogonality condition of the mode-shape function, the normalizing factors A_m can be found to be

$$A_m = \frac{\sqrt{2}\,\gamma_m}{Z_m}$$

where

$$Z_m = \gamma_m + \sin \gamma_m + K_m^2 (\sinh \gamma_m + \gamma_m) \quad \text{if } m \text{ is odd}$$

$$= \gamma_m - \sin \gamma_m + K_m^2 (\sinh \gamma_m - \gamma_m) \quad \text{if } m \text{ is even}$$

The generalized coordinates $q_\alpha(t)$ satisfies the Lagrange equation

$$m_\alpha \ddot{q}_\alpha(t) + C_\alpha \dot{q}_\alpha(t) + K_\alpha q_\alpha(t) = f_\alpha(t) \tag{17}$$

where the generalized mass

$$m_\alpha = \mu \int_A \psi_\alpha^2(\underline{x})d\underline{x} = \mu$$

$$K_\alpha = m\omega_\alpha^2$$

$$f_\alpha(t) = \int_A \bar{p}(\underline{x},t)\psi_\alpha(\underline{x})d\underline{x}$$

and

$$C_\alpha = \frac{K_\alpha \nu_\alpha}{\omega}$$

here ν_α is the combined loss factor for both structural and viscous damping. The present state of art requires that ν_α must be measured experimentally. The Fourier transform of the Lagrange Eq. (17) takes the form

$$Q_\alpha(\omega) = H_\alpha(\omega)F_\alpha(\omega) \tag{18}$$

where

$$H_\alpha(\omega) = \frac{i}{m_\alpha[(\omega_\alpha^2 - \omega^2) + i\nu_\alpha\omega^2]} \tag{19}$$

Equations (12) and (18) together give

$$W(\underline{x}, \omega) = \sum_\alpha H_\alpha(\omega) F_\alpha(\omega)\psi_\alpha(\underline{x}) \tag{20}$$

The displacement power-spectral density is related to $W_T(\underline{x}, \omega)$ by

$$S_d(\underline{x}, \omega) = \lim_{T \to \infty} \frac{\pi}{T} W_T^*(\underline{x}, \omega) W_T(\underline{x}, \omega) \tag{21}$$

where W_T is the truncated Fourier transform of w. Equations (17), (18), (20), and (21) together give the displacement power spectral density in the form:

$$S_d(\underline{x}, \omega) = S_p(\omega) \sum_\alpha \bar\psi_\alpha^2(y) \left|H_\alpha(\omega)\right|^2 J_{mm}(F_1) J_{nn}(F_2)$$

$$+ S_p(\omega) \sum_{\alpha \neq \beta} \frac{\bar\psi_\alpha(y)\bar\psi_\beta(y) J_{ns}(F_2) [g_{\alpha\beta} J_{mr}(F_1) + h_{\alpha\beta} k_{mr}(F_1)]}{m_\alpha m_\beta (g_{\alpha\beta}^2 + h_{\alpha\beta}^2)} \tag{22}$$

where

$$g_{\alpha\beta} = (\omega_\alpha^2 - \omega^2)(\omega_\beta^2 - \omega^2) + \nu_\alpha \nu_\beta \omega_\alpha^2 \omega_\beta^2$$

$$h_{\alpha\beta} = \nu_\alpha \omega_\alpha^2 (\omega_\beta^2 - \omega^2) - \nu_\alpha \omega_\beta^2 (\omega_\alpha^2 - \omega^2)$$

$$J_{mr}(F_1) = 2 \int_0^1 \int_0^{y_1''} \bar\psi_m(y_1')\bar\psi_r(y_1'') \left|\rho_p\left(\eta_1, 0, \frac{\pi F_1}{2}\right)\right| \cos\frac{\pi F_1 \eta_1}{2} \, dy_1' \, dy_1'' \quad \text{if } m + r \text{ even}$$

$$= 0 \quad \text{if } m + r \text{ odd} \tag{23}$$

$$J_{ns}(F_2) = 2 \int_0^1 \int_0^{y_2''} \bar\psi_n(y_2')\bar\psi_s(y_2'') \left|\rho_p\left(0, \eta_2, \frac{\pi F_2}{2}\right)\right| dy_2' \, dy_2'' \quad \text{if } n + s \text{ even}$$

$$= 0 \quad \text{if } n + s \text{ odd} \tag{24}$$

and

$$k_{mr}(F_1) = 2 \int_0^1 \int_0^{y_1''} \bar\psi_m(y_1')\bar\psi_r(y_1'') \left|\rho_p\left(\eta_1, 0, \frac{\pi F_1}{2}\right)\right| \sin\frac{\pi F_1 \eta_1}{2} \, dy_1' \, dy_1'' \quad \text{if } m + r \text{ odd}$$

$$= 0 \quad \text{if } m + r \text{ even} \tag{25}$$

Here $\bar\psi_n(y)$ are the normalized mode-shape functions, expressed by Eqs. (15) and (16) with t replaced by unity. The physical significance of the structural acceptances J_{mr} is discussed by Ref. 12. The pressure correlation coefficients ρ_p are experimentally shown to be related to the cross spectral density of the fluctuating pressure in a homogeneous turbulence and can be expressed by

$$\frac{S_p(\zeta_1, \zeta_2, \omega)}{S_p(\omega)} = \left|\rho_p(\zeta_1, 0, \omega)\right| \left|\rho_p(0, \zeta_2, \omega)\right| e^{-i\omega\zeta_1/U_c} \tag{26}$$

The strains in the x_1 and x_2 directions of a rectangular plate are related to the displacement w by

$$\epsilon_1 = \frac{(1/2)d}{1 - \nu^2}\left(\frac{1}{r_1} + \nu\frac{1}{r_2}\right), \qquad \epsilon_2 = \frac{(1/2)d}{1 - \nu^2}\left(\frac{1}{r_2} + \nu\frac{1}{r_1}\right) \tag{27}$$

where

$$\frac{1}{r_1} = -\frac{\partial^2 w}{\partial x_1^2}, \quad \frac{1}{r_2} = -\frac{\partial^2 w}{\partial x_2^2}$$

are the curvatures in x_1 and x_2 directions. The strain spectrum can be obtained by

$$S_{\epsilon_i}(\underline{x}, \omega) = \lim_{T \to \infty} \frac{\pi}{T} E_{i_T}^*(\underline{x}, \omega) E_{i_T}(\underline{x}, \omega) \tag{28}$$

where E_{i_T} is the truncated Fourier transform of ϵ_i in Eq. (27), and can be expressed by

$$E_1(\underline{x}, \omega) = \sum_\alpha H_\alpha(\omega) F_\alpha(\omega) \phi_1^\alpha$$

and $\tag{29}$

$$E_2(\underline{x}, \omega) = \sum_\alpha H_\alpha(\omega) F_\alpha(\omega) \phi_2^\alpha$$

where

$$\phi_1^\alpha = \frac{(1/2)d}{1 - \nu^2}\left(\frac{\partial^2 \psi_\alpha}{\partial x_1^2} + \nu \frac{\partial^2 \psi_\alpha}{\partial x_2^2}\right)$$

$$\phi_2^\alpha = \frac{(1/2)d}{1 - \nu^2}\left(\frac{\partial^2 \psi_\alpha}{\partial x_2^2} + \nu \frac{\partial^2 \psi_\alpha}{\partial x_1^2}\right) \tag{30}$$

Equations (28-30) together with the expression for ψ in Eqs. (15) and (16) give the strain power spectrum

$$S_{\epsilon_i}(\underline{x}, f) = A S_p(f) \sum_\alpha [\phi_i^\alpha(\underline{x})]^2 |H_\alpha(f)|^2 I_{mm}(F_1) I_{nn}(F_2)$$

$$+ 2 A S_p(f) \sum_{\alpha\beta} \frac{\phi_i^\alpha(\underline{x}) \phi_i^\beta(\underline{x}) I_{nn}'(F_2) \{s_{\alpha\beta} I_{mr}(F_1) + h_{\alpha\beta} k_{mr}(F_1)\}}{m_\alpha m_\beta (\Omega_{\alpha\beta}^2 + h_{\alpha\beta}^2)} \tag{31}$$

5.2 Response Measurements and Computations

As briefly described in the introduction, tests have been conducted to measure the displacement and strain response of several panels of different lengths, widths, and thicknesses in supersonic attached and separated flows and in mixed flow with a shock wave positioned on the panels. The response tests of the total input-response investigation have only recently been completed and therefore the following results are somewhat preliminary. All the panels tested were constructed of magnesium having the following properties:

$$E = 4.48 \times 10^{10} \ N/m^2$$

$$\rho = 1750 \ Kg/m^3$$

$$\nu = 0.35$$

The first panels selected for analysis had the same dimensions with $\ell_1 = 0.3046$ m, $\ell_2 = 0.2266$ m, $\ell_1/\ell_2 = 4/3$, but two different thicknesses $d = 0.00115$ m and $d = 0.00235$ m.

It was recognized prior to the tests that the installation of strain gages on the panels could affect the stiffness and symmetry of response and therefore could compromise the comparison between measurements and computations. Since strain is a key element in fatigue, however, it was considered more important to include the strain gages to verify the strain computations. It would have been desirable to conduct separate displacement response tests, but this was economically impractical.

5.2.1 Systems Damping

In Eq. (19) ν_α is the combined loss factor for the complete structural airstream system. The loss factor therefore takes into account the effect of hysteretic damping as well as viscous damping. The latter includes the interaction of panel motion on the flow field within and outside the boundary layer, and the effect of acoustical radiation

6-16

into the interior of the structure (cavity) and into the exterior flow field. Although the development (by Dowell, ref. 17) of an analytical method for the determination of the aerodynamic damping part of the loss factor is in progress, the present state of a : requires that ν_η must be estimated from experience or measured experimentally.

The loss factors used for the computations of panel response as presented in this paper have been measured from the autocorrelations of the response-time histories for the specific panels of interest. Representative loss-factor measurements for a 0.3048-m long, 0.2286-m wide by 0.00235-m thick magnesium panel are shown in Fig. 19 for both attached and separated flows. The results indicate that only the damping of the first mode is significantly higher than the damping of all other modes. The first mode damping was slightly higher in separated flow than in attached flow, but all other modes were relatively unaffected by the flow condition. The effects of Mach number are not clearly defined although it is evident that the effects are not large for the range of Mach numbers investigated. It is expected that the damping would increase significantly for the attached flow case at $1.6 > M > 1.0$. Muhlstein (ref. 18) has shown total-system-damping measurements in attached flow at Mach numbers between 1.1 and 1.4 that decrease a full decade between $M = 1.1$ and $M = 1.4$. His results at $M = 1.4$, although for a much thinner boundary layer relative to the panel length, are consistent with the results in Fig. 19.

Figure 19. Damping of the panel/air-stream system in terms of loss factor.

3.2.2 Displacement Response

Illustrative measurements and computations of the power-spectral densities of displacement of the 0.00118-m thick panel are shown in Fig. 20 for $M_\infty = 2.5$. Measurements are shown for the probe locations indicated in the inset panel sketches. Corresponding computations for the same locations are shown only for the peak displacements at measured resonance frequencies. The computer program computes the complete spectrum, but this has been omitted to simplify the figures. The results show similar trends between attached and separated flows in the response of most modes as a function of frequency. The first mode predominated the displacement, as would be expected. The relative displacements between attached and separated flows are in the same proportion as the input spectra (Fig. 17). Thus the spatial correlation differences between attached and separated flows have only a subtle influence on the response characteristics. It was originally planned to present longitudinal and lateral acceptances as a function of frequency to illustrate spatial correlation effects, but these results were not available in time to be included in the paper.

The comparison between measured and computed displacement spectral densities at resonance generally shows similar trends with frequency with the computed displacements from about two to ten times higher than the measured displacements. Although the comparative results are considered good and within state of art for random excitation and response phenomena, the anxious and optimistic investigator always hopes for better agreement. The first suspicions are usually directed to searching for computational errors. In this case the computer program and measured spectra have been repeatedly checked. As an example the comparable measured spectra have been obtained by three different analysis systems (2 digital and 1 analog). It is believed that the major differences in computed and measured results are due to the assumptions in the analytical method that the flow field is uniform and homogeneous. An obvious major source of panel response asymmetry is the longitudinal pressure variation on the panel in separated flow (Fig. 4(b)). A slight lateral variation in static pressure was also found on the wind-tunnel wall in the region of the panel for the attached flow case. These effects are somewhat accounted for, but not entirely, by computing the response spectra at the measured natural frequencies. The effects of the strain-gages mounted on the panel are also not accounted for.

3.2.3 Strain Response

Typical measurements and computations of strain response power spectral densities are shown in Fig. 21. The most significant feature of the strains is that the first mode is not the dominant mode as shown in the case for the displacement response. This result is expected since the strains are proportional to the local panel curvature associated with the response mode. In the displacement response the differences between the attached and separated flow are consistent with the difference in the excitation spectra. There is also about the same order of differences between computations and measurements of strain. A few characteristics of the spectra indicate panel distortion and asymmetry of modes as discussed in 3.2.2. An example is the measurement of a significant strain response for the 1-2 mode at the panel center point which should be on a node line.

3.3 Effect of Flow Field on Displacement Response

Comparisons of the displacement responses of two panels (d = 0.00118 m and d = 0.00235 m), due to the excitations of attached and separated and mixed flows at $M_\infty = 2.5$ are shown in Fig. 22. The results show that the response amplitudes were approximately the same for both the separated flow and mixed flow cases even though the excitation spectra are significantly different in the region of the shock wave (Fig. 5). The increase in mixed flow spectra at $f <$ ... Hz is consistent with the higher excitation spectra at these low frequencies. It is interesting that there was apparently no higher degree of coupling of the shock oscillations in mixed flow with the panel response than occurred in the fully separated flow case. For the mixed flow case, the shock wave was positioned near the center of the panel. The extent of the shock wave oscillations relative to the panel length can be seen in the longitudinal distribution of the fluctuating pressures shown in Fig. 4.

ATTACHED FLOW $M_\infty = 2.5$ $q_\infty = 2170\,N/m^2$ SEPARATED FLOW

$l_1 = 0.3048\,m$ $l_2 = 0.2286\,m$ $d = 0.00118\,m$
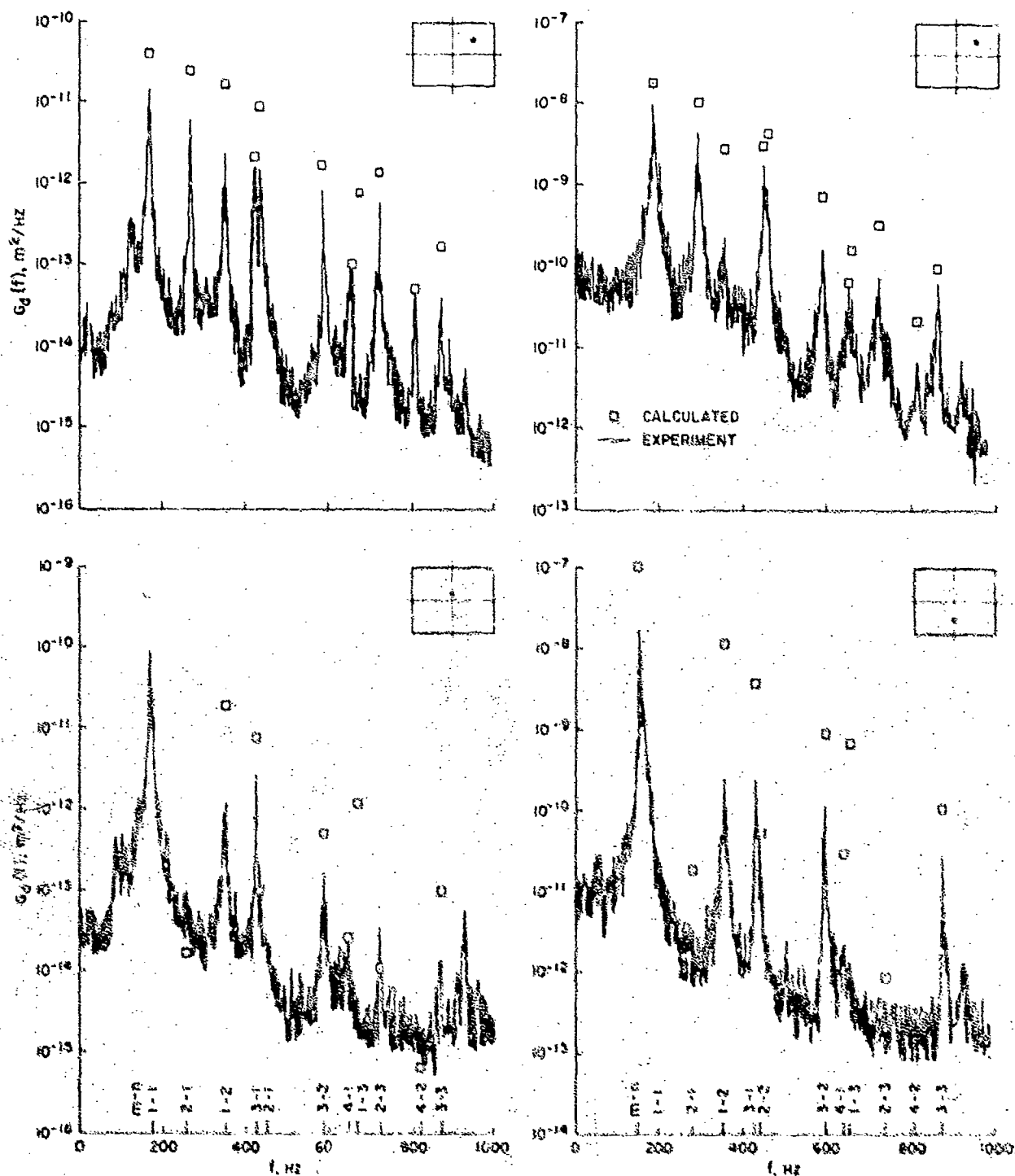
Figure 50. Power spectral densities of displacement response.

The ratio between the attached flow and separated flow response spectra are approximately the same for both panel thicknesses, as would be expected; except that an unexplained broadband mode of vibration occurred at $f \approx 190$ Hz on the $d = 0.00235$ m panel. Significant differences in resonant frequencies can be noted for each of the flow cases. The frequencies also do not scale directly with thickness or with the same scale factor for all modes for the two panel thicknesses. These characteristics can be due to stiffness changes resulting from unsymmetrical loading or midplane stresses due to thermal effects, or due to changes in excitation; however, the distortion of the mode shapes by the unsymmetrical loading on the panels as discussed in 3.2.2 is considered to be the most probable cause.

4. CONCLUDING REMARKS

A large amount of experimental data have been studied to determine the characteristics of surface-pressure fluctuations underlying supersonic attached and separated turbulent boundary layers ($M_\infty = 1.6$ to 3.5). The most effective parameters for making the characteristics dimensionless have been established. Empirical formulae have been derived to represent the nonsteady pressure fields in each of the flow regions. A method of analysis of the amplitude

ATTACHED FLOW $M_\infty = 2.5$ $q_\infty = 2170$ N/m^2 SEPARATED FLOW

$l_1 = 0.3048$ m $l_2 = 0.2286$ m $d = 0.00118$ m
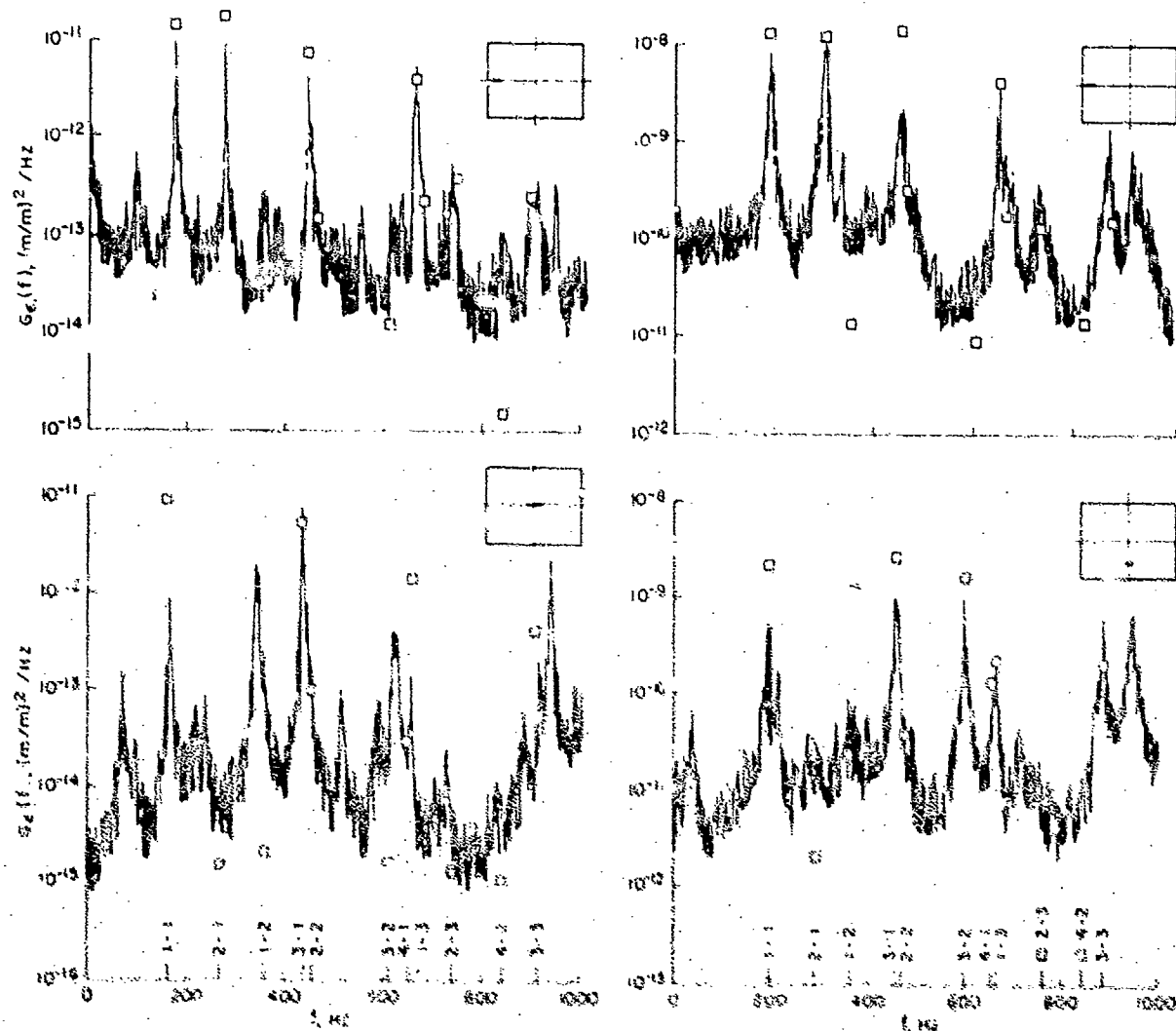
Figure 21.   Power spectral densities of stress response.

and strain response of flat clamped-edge panels has also been described, and comparisons have been made between response measurements and computations for panels underlying both the attached and separated flows.

The results of the pressure-fluctuation studies have shown that the turbulence generated within attached or separated flow is relatively homogeneous although some nonuniformities of the fluctuating pressures have been identified. The statistical characteristics that describe the surface fluctuating pressures can be effectively scaled by the reduced frequency parameters $f\delta/U$ or $f\delta/U_\infty$. An attenuation-coefficient function $\eta\beta$ representing the decaying exponential of the moduli of the cross spectra has been shown to be an appropriate function to describe the spatial correlation of the unsteady pressure fields. Observed irregularities in the shapes of power spectra and attenuation coefficients and convection velocities as a function of frequency can be attributed to changes in the predominant sources of the fluctuating pressures in different frequency zones.

The results of the panel response studies indicate that the method of analysis predicts the relative levels of response of most modes for either attached or separated flow, but generally, over-predicts the mean-square amplitudes or strains. It is believed that the differences between computations and measurements result primarily from the assumption in the analysis that the flow fields are uniform and homogeneous, whereas, in the experiments significant nonuniform steady-state loading occurred. The differences in panel response between attached and separated flows are consistent with the approximate three decade change in the excitation spectra. The response of panels to the oscillation of mixed flow with an oscillating shock wave near the center of the panels was not significantly different than the response to separated flow even though the excitation in the region of a shock wave has higher amplitude and different frequency content. Indications are that the shock oscillations did not couple to any degree with the panel motions. The damping of panel-airstream system was relatively invariant with Mach number at constant total pressure between $M_\infty = 1.6$ and $M_\infty = 3.5$. The damping of the first resonant mode was about 25% higher for separated flow than for attached flow, but otherwise the damping of all modes was about the same for either flow conditions.

M=2.5 l_1=0.3048m l_2=0.2286m

d=0.0018 m q_∞ = 2170 N/m²   d=0.00235 m
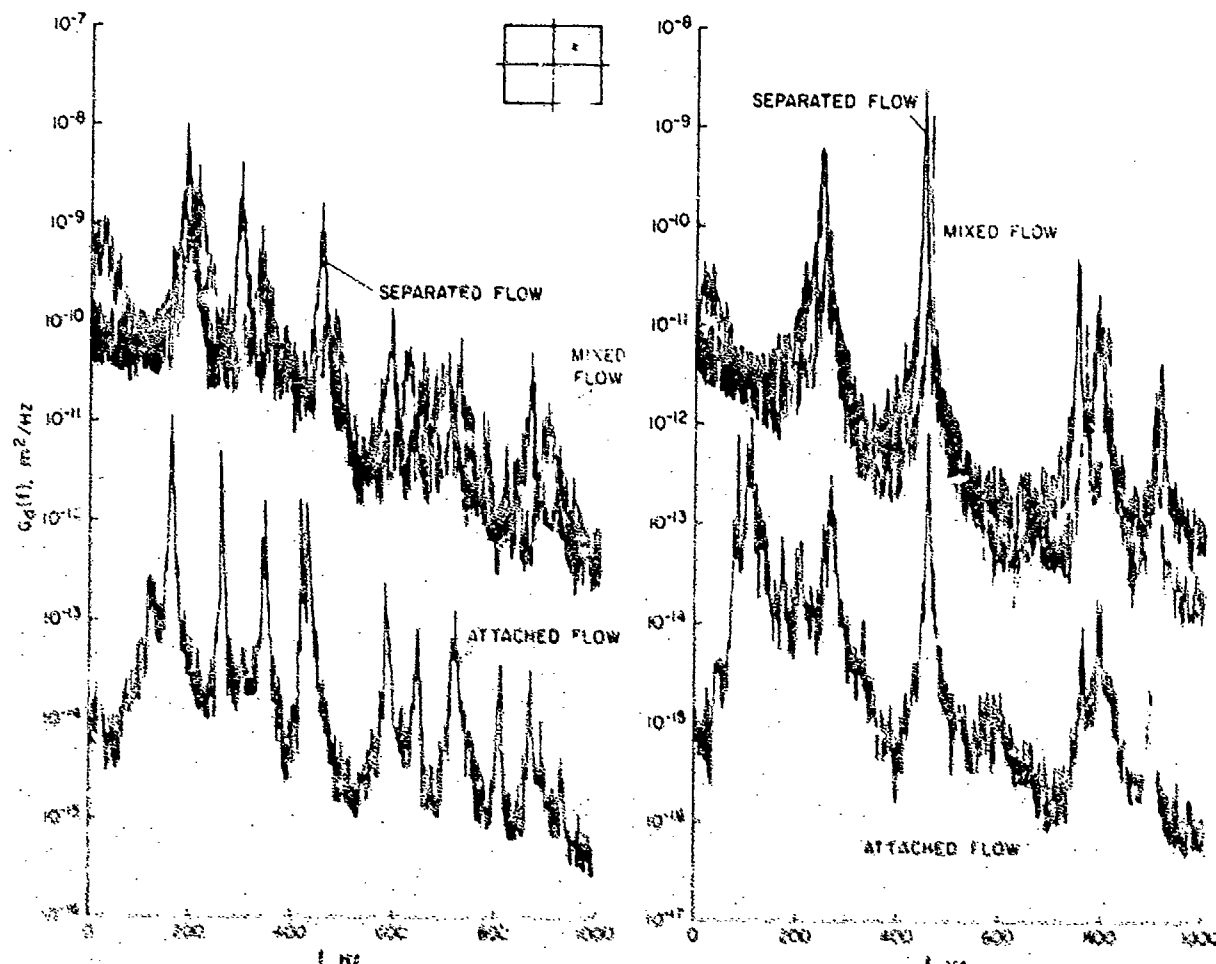
Figure 22. Comparison of panel response due to excitations of attached and separated boundary layer and oscillating shock waves.

5. REFERENCES

1. Corcos, G. M. and Liepmann, H. W.: On the Contribution of Turbulent Boundary Layers to the Noise Inside a Fuselage. NACA TM 1420, 1956.

2. Ribner, H. S.: Boundary-Layer-Induced Noise in the Inte... of Aircraft. University of Toronto, U. T. I. A. Report 37, 1956.

3. Kraichnan, R. H.: Noise Transmission from Boundary Layer Pressure Fluctuations. J. Acoust. Soc. Am. 1 Jan. 1957.

4. Chyu, W. J. and Hanly R. D.: Power- and Cross-Spectra and Space-Time Correlations of Surface Fluctuating Pressures at Mach Numbers Between 1.6 and 2.5. NASA TN D-7440.

5. Speaker, W. F. and Ailman, C. M.: Spectra and Space-Time Correlations of the Fluctuating Pressures at a Wall Beneath a Supersonic Turbulent Boundary Layer Perturbed by Steps and Shock Waves. Douglas Rep., SM-49806, Nov. 1965.

6. Lowson, M. V.: Prediction of the Inflight Fluctuating Pressures on Space Vehicles. Wyle Laboratories Report, WR 65-26, Dec. 1965.

7. Coe, C. F.: Surface-Pressure Fluctuations Associated with Aerodynamic Noise. NASA SP-207, pp. 409-424, 1969.

8. Strawderman, W. A.: Turbulent-Induced Plate Vibrations: An Evaluation of Finite and Infinite-Plate Models. J. Acoust. Soc. Am., Vol. 45, No. 5, Part 2. 1969.

9. Berich, D. J.: Spatial Correlation in Acoustic-Structural Coupling. J. Acoust. Soc. Am., 36, 1 Jan. 1964.

10. Wilby, J. F.: The Response of Simple Panels to Turbulent Boundary Layer Excitation, AFFDL-TR-67-70, Oct. 1967.

11. Bull, M. K.: Wall-Pressure Fluctuations Associated with Subsonic Turbulent Boundary-Layer Flow, J. Fluid Mech., Vol. 28, PT. 4, pp. 719, 1967.

12. Chyu, W. J. and Au-Yang, M. K.: Random Response of Rectangular Panels to the Pressure Field Beneath a Turbulent Boundary Layer in Subsonic Flows. NASA TN D-6970, 1972.

13. Willmarth, W. S. and Roos, F. W.: Resolution and Structure of the Wall Pressure Field Beneath a Turbulent Boundary Layer. J. of Fluid Mech., Vol. 22, Part I, pp. 81-94, 1965.

14. Belcher, P. M.: Predictions of Boundary-Layer Turbulence Spectra and Correlations for Supersonic Flight, 5e Congres International D'Acoustique, Liege, Sept. 1965.

15. Chapman, D. R.; Kuehn, D. M.; and Larson, H. K.: Investigation of Separated Flows in Supersonic and Subsonic Streams With Emphasis on the Effect of Transition. NACA TR-1356, 1958.

16. Ffowcs-Williams, J. W.: The Mach Wave Field Radiated by Supersonic Shear Flows, Journal of Fluid Mechanics, Vol. 21, No. 4, pp. 641-657, 1964.

17. Dowell, E. H.: Theoretical Panel Vibration and Flutter Studies Relevant to Space Shuttle, AIAA Paper No. 72-350, AIAA/ASME/SAE 13th Structures, Structural Dynamics, and Materials Conference, 1972.

18. Muhlstein, Lado: Experimental Evaluation of the Aerodynamic Damping of Skin Panels at Low Supersonic Mach Numbers. AIAA Paper No. 72-402. AIAA/ASME/SAE 13th Structures, Structural Dynamics, and Materials Conference, 1972.

ACCURATE FINITE ELEMENT MODELLING OF FLAT AND CURVED STIFFENED PANELS

by

G.M. Lindberg
Research Officer
National Research Council of Canada
Ottawa, Ontario, Canada. K1A 0R6

SUMMARY

Three different stiffener models have been evaluated
for use in studying the dynamics of stiffened plates. The
more exact, 'complete' beam finite element seems to work well,
although the ad-hoc, T-beam approach gives nearly the same
results. Both analyses over predict the predominately stiffener
modes. The 'simple' beam element underestimates a number of
frequencies and should probably not be used. A rectangular
cylindrical shell finite element has been derived and it has
been used to study the dynamics of singly curved stiffened
panels. The major effect of curvature is to increase the
lowest frequencies and to broaden the banded nature of the
results. Higher frequencies are little affected by changes in
curvature.

1.0 INTRODUCTION

The dynamic analysis of stiffened structures continues to be the subject of
considerable research effort. Many techniques for predicting natural frequencies and
mode shapes have been formulated; notably the transfer matrix approach [Ref. 1-3], the
wave approach [Ref. 4,5], the "exact" approach [Ref. 6,7] and the finite element approach
[Ref. 8-22].

The finite element method is the most general approach, since there are no
restrictions on shape or boundary conditions. The accuracy of the method depends upon
the precision of the elements adopted and upon the number of elements used; these sources
of error are well understood and there are adequate guidelines available to ensure
accurate solutions. Clear guidelines do not exist however for choosing the type of
stiffener element to be utilized and, more importantly, the method to be employed for
linking the stiffener elements to the plate elements. This paper investigates various
stiffener models and assesses their relative merits. As well, the effects of curvature
on stiffened plate vibrations is briefly explored.

2.0 FINITE ELEMENT MODELLING OF STIFFENED PLATES

2.1 Literature Review

Lindberg and Olson [8] carried out one of the earliest stiffened plate finite
element dynamic analyses. They used non-conforming plate elements, assumed there was no
stiffener bending and used a simple torsional beam element with warping accounted for
approximately. All in-plane motion was neglected.

More recently, Yurkovich et al. [9] employed a non-conforming, non-converging
triangular plate bending element together with a beam element that included bending torsion
and warping effects. They concluded that warping has a significant effect on frequencies
when open section stiffeners are used. Rudder [10] has carried out a detailed analysis of
a general, thin-walled, open-section stiffener element including all bending, torsion and
warping effects. This stiffener is linked to a modified conforming plate element.
Unfortunately, all in-plane motion is neglected, so the in-plane displacements of the beam
along the connect line are constrained to be zero.

Olson and Lindberg [11-13] have made a second study of a 5-bay stiffened panel.
They used high-precision, conforming, triangular plate elements and accounted for beam
bending in two directions plus beam torsion. They neglected beam warping, since their
stiffener cross-section was solid and rectangular. In-plane motions were again neglected.
Olson and Hazell [14] found that this analysis was not suitable for all stiffened plates,
since the stiffener bending did not account for the added stiffness of the plate material
adjacent to the stiffeners. This effect was accounted for in an ad-hoc manner, following
Timoshenko and Goodier [15], by calculating the beam bending moment of inertia for an
equivalent T-beam.

In all the above, in-plane displacements have been neglected, even though the
eccentric stiffeners provide coupling between in-plane and out-of-plane displacements. For
static solutions of stiffened plates [16-22], where solutions are much less costly, the
in-plane stiffness of the plate is generally included. Stiffener finite elements have been
obtained in two ways; firstly, by defining the beam stiffness matrix about its centroid
and then shifting the axis to the connect line via a transformation [21] or secondly, by
defining the strain energy of the beam element with respect to the connect line.

2.2 Models Employed in This Study

Three finite element models are considered in this paper, the 'simple' model proposed by Olson and Lindberg, [11-13] the ad-hoc, T-beam approach used by Olson and Hazell [14] and a new 'complete' approach developed herein. All three models employ rectangular conforming finite elements to model the plate portions of the structure. These elements [23] are based upon an out-of-plane displacement function containing a complete quartic polynomial plus higher order terms and in-plane displacement functions containing complete cubic polynomials plus higher order terms. The generalized coordinates for each element are the normal displacement, its two first derivatives plus its three second derivatives at each corner plus the two in-plane displacements and their two first derivatives at each corner for a total of 48 degrees of freedom. A suitable equating of generalized coordinates at adjacent element nodes provides continuity of displacements and normal slope between the elements. When in-plane motion is neglected, only the bending part of the element stiffness matrix is used. These elements are fully compatible with the triangular elements used earlier, [11-14].

The 'simple' beam element model of Olson and Lindberg is depicted in Fig. 1 where the coordinate system is defined through the centroid of the rectangular stiffener. The normal displacement is taken as a quintic polynomial and the rotation is assumed to be cubic to permit the beam and plate finite elements to be linked together in a conforming fashion. In-plane displacements are neglected. The generalized coordinates used at each end are the deflection and its first two derivatives in the direction of the beam plus the rotation and its first derivative. Equating these variables with the corresponding ones on an adjacent plate element provides continuity of bending deflections everywhere between the two elements. The strain energy expression for the beam element is

$$U = \frac{EI_{xx}}{2} \int_0^\ell w_{yy}^2 \, dy + \frac{GJ}{2} \int_0^\ell \phi_y^2 \, dy + \frac{EI_{zz}h^2}{8} \int_0^\ell \phi_{yy}^2 \, dy \tag{1}$$

where $I_{xx} = bh^3/12$, is the bending inertia about the x-x axis, J is the torsion constant, defined approximately [24] as

$$J = \frac{hb^3}{3} - \frac{64b^4}{\pi^5} \tanh \frac{\pi h}{2b} \tag{2}$$

for a beam of rectangular cross-section and $I_{zz} = hb^3/12$ the area moment of inertia about the z-z axis.

The kinetic energy is simply

$$T = \frac{\rho bh\omega^2}{2} \int_0^\ell w^2 dy + \frac{\rho I_o \omega^2}{2} \int_0^\ell \phi^2 dy \tag{3}$$

where $I_o = bh(b^2+4h^2)/12$ is the rotational moment of inertia about the point 0 in Fig. 1. The strain energy of warping is neglected but could easily be incorporated by adding to Eq. (1).

$$U_{warp} = \frac{EC_{ws}}{2} \int_0^\ell \phi_{yy}^2 \, dy \tag{4}$$

where C_{ws} is the warping constant.

This model has two major defects; firstly in-plane motions are neglected and secondly the out-of-plane stiffness of the beam will inevitably be underestimated.

Olson and Hazell [14] modified this model by choosing an ad-hoc bending stiffness for the beam and attached plate, following Ref. [15]. This approach defines the effective bending moment of inertia of the stiffener as that of a T-beam where the arms of the T are portions of the adjacent plates, some 9% of the stiffener length in width. This ad-hoc bending stiffness was used as I_{xx} in Eq. (1).

The third model considered in this paper includes the effects of the in-plane motions and the subsequent coupling between axial, bending and rotational displacements in the beam. Consider the beam shown in Fig. 2, where the coordinate system passes through the connection point at the top of the beam. To match the cubic in-plane displacements and rotation, and the quintic out-of-plane displacement of the plate element, w is chosen to be a quintic polynomial, while u, v and ϕ are chosen to be cubic. Then the strain energy expression for the element becomes

$$U = \frac{EI_{xxo}}{2} \int_0^\ell w_{yy}^2 \, dy - \frac{EAh}{2} \int_0^\ell v_y w_{yy} \, dy + \frac{EA}{2} \int_0^\ell v_y^2 \, dy + \frac{GJ}{2} \int_0^\ell \phi_y^2 \, dy + \frac{EI_{zz}}{2} \int_0^\ell u_{yy}^2 \, dy$$

$$+ \frac{EI_{zz}h^2}{8} \int_0^\ell \phi_{yy}^2 \, dy + \frac{EI_{zz}h}{2} \int_0^\ell u_{yy} \, \phi_{yy} \, dy \tag{5}$$

where $I_{xxo} = bh3/3$ is the bending moment of inertia about the connection line and A is the cross-sectional area of the stiffener. If all in-plane moments of inertia are to be neglected (to reduce the subsequent eigenvalue problem size), the kinetic energy remains that of Eq. (3). The above derivation holds only for symmetrical stiffeners; in general there would be complete coupling between u, v, w and φ.

The beam and plate elements of all three models are linked similar fashion. Care is taken to ensure continuity between elements so that a conforming finite element model is obtained. The finite width of the stiffener is also accounted for. Complete details of linkage may be found in Ref. [11-13].

In all cases studied herein, in-plane inertias are neglected. This permits a reduction of eigenvalue problem size by the use of matrix partitioning without the introduction of any further approximation.

3.0 FLAT PLATE EXAMPLE PROBLEM

The flat, five-bay stiffened panel shown in Fig. 3 was analyzed using all three models. This is the same panel previously studied by Olson and Lindberg [11-13] and good experimental results are available. Only one quarter of the plate had to be analyzed since the total problem was broken down into four sub-problems by invoking the double symmetry of the problem. The finite element grid used in this analysis is also shown in Fig. 3. The properties of the plate are as follows:

$$L = 21", \ W = 8", \ t = 0.050", \ b = 0.25", \ h = 0.50",$$
$$E = 10^7 \ \text{psi}, \ \rho = 0.000262 \ \text{lb sec}^2/\text{in}^4, \ \nu = 0.3.$$

The frequency results of this analysis are given in Table I, together with the theoretical and analytical results of Ref. [11-13]. For the 'simple' model, the results of this analysis and that of Ref. [11-13] are very close. The results found using triangular plate bending elements are slightly higher than those found using rectangular plate bending elements since rectangular elements impose fewer constraints on total energy.

The results found using the 'simple' representation are quite good, although there is a tendency for the predicted frequency bands to be smaller than the experimentally found ones. As well, several modes are under predicted, contrary to the expected over prediction of a conforming model. This is especially true for the predominantly stiffener bending modes 11-14 and confirms that the bending stiffness of this model is underestimated.

The results of the T-beam, ad-hoc model and the 'complete' model are remarkably close to each other. In general, the results using these models are slightly higher than those found using the 'simple' model and the width of each band of frequencies is somewhat larger. Hence they are closer to the experimental results. For the predominately stiffener bending modes 11-14 (and to a lesser extent for modes such as 20-24 with a fair amount of predicted stiffener bending), the 'complete' model over predicts the frequencies (w.r.t. experimental results) by approximately 15%. The reason for such large differences, as explained in Section 3.1, is that the experimental boundary conditions are not completely rigid and the beam element used in the 'complete' model is very sensitive to small variations in the rotational restraint of the boundary condition.

The first few mode shapes found with the 'simple' representation and the 'complete' model are given in Fig. 4. The mode shapes predicted with the 'complete' model are much more realistic than those of the 'simple' model, confirming that the 'complete' model works well. The mode shapes found using the ad-hoc model are similar to those found using the 'complete' model.

3.1 Effect of Rotational Restraint on Beam Stiffeners

It is impossible to construct an infinitely rigid clamped boundary condition because of the finite modulus of elasticity of any clamping material. The effect of this finite modulus has been studied by Lindberg [25] and by Matusz et al. [26]. The rotational edge constraint for a beam may be expressed in non-dimensional form as

$$M = \frac{EI}{L^2} \xi \ \theta \tag{6}$$

and Matusz et al. have shown that $\xi = 2.262 \ L^2/bh$ for a half plane support and $\xi = 1.579 \ L^2/bh$ for a quarter plane support. As well, they have shown that a finite support must be at least five times the depth of the beam or plate before it can be considered 'infinite'. Lindberg has found a similar result for the rotational restraint of a half plane and also indicates that a typical experimental value for this rotational restraint is 1/2 to 1/3 of the theoretical value. Typically this finite rotational restraint causes a reduction in natural frequencies of some 1-4%.

To establish the effect of boundary conditions for this particular case, the dynamics of a stringer alone with varying rotational end constraints was studied, using both 'simple', uncoupled beam elements and 'complete', coupled beam elements. Four finite elements were used to model the beam and the first two vertical bending and two lateral bending modes are presented in Fig. 5. For clamped boundary conditions, ($\xi \to \infty$) the two sets of natural frequencies are nearly the same (except for the second lateral

bending mode). The 'simply supported' boundary conditions (in the vertical direction) differ however, so a difference in the vertical bending frequencies predicted by the two models is found.

Most interestingly, however, the 'complete' model is much more sensitive to a slight reduction in the vertical rotational restraint at the boundaries than the simple model. For example, for $\xi = 1160$, the theoretical limit of Eq. (6), the vertical bending frequencies predicted by the 'simple' model have dropped an expected 0.7% but the frequencies predicted by the 'complete' model have dropped 2.6%. For a value of $\xi = 400$, a realistic experimental value [25], the frequencies predicted by the 'simple' model are lower by 2% while those predicted by the 'complete' model are 7%.

The boundary of the experimental model is quite massive, but it is still only 1" thick by 4" wide. Since the stiffeners are 0.5" deep, it is clear that the experimental boundary condition does not approach the theoretical best limit. It is for this reason that the finite element results of the 'complete' model (Table I) are considerably higher than the experimental results for the predominately stiffener modes.

4.0 ANALYSIS OF CURVED STIFFENED PLATES

Many stiffened aircraft structures are curved in one direction. At present, the only analysis methods available are the transfer matrix approach [1,27] and finite element methods. The transfer matrix method is quite cumbersome and only limited results have been presented.

For this study the flat plate element used herein is converted into a rectangular cylindrical shell finite element following the theory of Ref. [27]. This element remains compatible with the triangular element of Ref. [27]. The 'complete' stiffener model derived in Section 2 is used to model stiffeners placed along the generators of a cylindrical shell. The analysis of a stiffened cylindrical shell then proceeds following Section 2, with one modification made before linking beam and shell elements together. The x-component of the rotation vector of the shell is defined as $-w_x + u/R$ while it is simply $-\phi$ or $-w_x$ for the beam. Hence a simple transformation must be applied to transform the local degrees of freedom of the beam element to match those of the shell element. This transformation is not given here but is similar to that used in Ref. [28].

4.1 Curved Models Studied

The geometry of the five-bay panel of Section 3 was selected for study with two different radii of curvature, $R = 40"$ and $R = 20"$. A finite element grid similar to that for Section 2 was used and full use of symmetry was made. Again in-plane inertia was neglected so that matrix partitioning could be used to reduce eigenvalue problem sizes.

The frequency results for these two cases are given in Table II and partially plotted in Fig. 6. As expected, the addition of the curvature affects only the lowest modes. Many of the higher modes, especially the stiffener modes remain virtually unchanged. However, since the lowest modes tend to be the most critical ones, it is significant that the banded nature of the frequencies tends to broaden as the radius of curvature is decreased. The first few mode shapes for these curved models are plotted in Fig. 4. There is little change in these mode shapes, even though the natural frequencies have risen significantly.

4.2 Comparison with Data Sheets

The AGARD Acoustic Fatigue Data Sheets [29] give methods for estimating the natural frequencies of both flat periodic skin-stringer structures and simple singly-curved plates. The predictions for the three plates studied herein are also given in Table II. It is interesting to see that the finite element results are generally bracketed by the data sheet results.

5.0 CONCLUDING REMARKS

Three different stiffener models have been evaluated for use in studying the dynamics of stiffened plates. The more exact, 'complete' beam finite element seems to work well, although the ad-hoc, T-beam approach gives nearly the same results. Both analyses over predict the predominately stiffener modes. The mode shapes predicted by these two models are more realistic than those predicted by the 'simple' beam element. The 'simple' beam element also underestimates a number of frequencies and should probably not be used.

A rectangular cylindrical shell finite element has been derived and it has been used to study the dynamics of singly curved stiffened panels. The major effect of curvature is to increase the lowest frequencies and to broaden the banded nature of the results. Higher frequencies are little affected by changes in curvature. Curvature appears to have little effect on the mode shapes.

6.0 REFERENCES

1. Lin, Y.K. and Donaldson, B.K., "A Brief Survey of Transfer Matrix Techniques with Special Reference to the Analysis of Aircraft Panels", J. of Sound and Vibration, Vol. 10, No. 1, January 1969, pp. 103-143.

2. Mercer, C.A. and Seavey, C., "Prediction of Natural Frequencies and Normal Modes of Skin-Stringer Panel Rows", J. of Sound and Vibration, Vol. 6, No. 1, January 1967, pp. 149-162.

3. Clarkson, B.L. and Cicci, F., "Methods of Reducing the Response of Integrally Stiffened Structures to Random Pressures", Paper 69-Vibr-26, 1969, American Society of Mechanical Engineers.

4. Sen Gupta, G., "Natural Flexural Waves and the Normal Modes of Periodically Supported Beams and Plates", J. of Sound and Vibration, Vol. 13, No. 1, September 1970.

5. Sen Gupta, G., "Natural Frequencies of Periodic Skin Stringer Structures Using a Wave Approach", J. of Sound and Vibration, Vol. 16, No. 4, June 1971.

6. Wittrick, W.H. and Williams, F.W., "Natural Vibrations of Thin, Prismatic Flat-Walled Structures", in Proceedings of the IUTAM Symposium on High Speed Computing of Elastic Structures, Liège, Belgium, 23-28 August 1970. Published by University of Liège, 1972.

7. Long, B.R., "A Stiffness-Type Analysis of the Vibration of a Class of Stiffened Plates", J. of Sound and Vibration, Vol. 16, No. 3, 1971, pp. 323-335.

8. Lindberg, G.M. and Olson, M.D., "Vibration Modes and Random Response of a Multi-Bay Panel System Using Finite Elements", Aeronautical Rept. LR-492, 1967, National Research Council of Canada.

9. Yurkovich, R.N., Schmidt, J.H. and Zak, A.R., "Dynamic Analysis of Stiffened Panel Structures", J. of Aircraft, Vol. 8, No. 3, 1971, pp. 149-155.

10. Rudder, Jr., F.F., "Study of Effects of Design Details on Structural Response to Acoustic Excitation", NASA Contractor Report, NASA CR-1959, March 1972.

11. Olson, M.D. and Lindberg, G.M., "Free Vibrations and Random Response of an Integrally Stiffened Panel", Proceedings of Conference on Current Developments in Sonic Fatigue, University of Southampton, July 6-9, 1970.

12. Olson, M.D. and Lindberg, G.M., "Free Vibrations and Random Response of an Integrally Stiffened Panel", Aeronautical Rept. LR-544, 1970, National Research Council of Canada.

13. Olson, M.D. and Lindberg, G.M., "Jet Noise Excitation of an Integrally Stiffened Panel", J. of Aircraft, Vol. 8, No. 11, November 1971, pp. 847-855.

14. Olson, M.D. and Hazell, C.R., "Real-Time Vibration Analysis of Rib-Stiffened Plates by Holographic Interferometry", Presented at the International Symposium on Experimental Mechanics, University of Waterloo, Canada, June 12-16, 1972.

15. Timoshenko, S.P. and Goodier, J.N., "Theory of Elasticity", 3rd Ed., McGraw-Hill, New York, 1970, Sec. 95.

16. Gustafson, W.C. and Wright, R.N., "Analysis of Skewed Composite Girder Bridges", J. of Str. Div., ASCE, Vol. 94, April 1968.

17. Mehrain, M., "Finite Element Analysis of Skew Composite Plates", Ph.D. Dissertation, University of California, Berkeley, California, 1967.

18. McBean, R.P., "Analysis of Stiffened Plates by Finite Element Method", Ph.D. Dissertation, Stanford University, 1968.

19. McBean, R.P., "Finite Element Analysis of Stiffened Plate", Presented at the Annual Conference of Eng. Inst. of Canada, Ottawa, September 1970.

20. Bhalla, D.S.B., "Analysis of Stiffened and Unstiffened Slabs", Engineering Report for Degree of Master of Engineering, University of Ottawa, June 1972.

21. Tinawi, R.A., "Behaviour of Orthotropic Bridge Decks", Ph.D. Thesis, McGill Univ., May 1972.

22. Wegmuller, A.W. and Kostem, C.N., "Effect of Imperfections on the Static Response of Beam-Slab Type Highway Bridges", in Proceedings of the Specialty Conference on The Finite Element Method in Civil Engineering, Edited by J.O. McCutcheon, et al., McGill Univ., June 1-2, 1972.

23. Lindberg, G.M., Hrudey, T.M. and Cowper, G.R., "Refined Finite Elements for Folded Plate Structures", in Proceedings of the Specialty Conference on the Finite Element Method in Civil Engineering, Edited by J.O. McCutcheon, et al., McGill Univ., June 1-2, 1972.

24. Sokolnikoff, I.S., "Mathematical Theory of Elasticity", 2nd Ed., McGraw-Hill, New York, 1956.

25. Lindberg, G.M., "Lumped Parameter Methods Applied to Elastic Vibrations", Ph.D. Thesis, University of Cambridge, England, November 1963.

26. Matusz, J.M., O'Donnell, W.J. and Erdlac, R.J., "Local Flexibility Coefficients for the Built-In Ends of Beams and Plates". American Society for Mechanical Engineers, J. of Eng. for Ind., Vol. 91, Series B, 1969, p. 614.

27. Lindberg, G.M. and Olson, M.D., "A High-Precision Triangular Cylindrical Shell Finite Element", AIAA Journal, Vol. 9, No. 3, 1971, pp. 530-532.

28. Lindberg, G.M. and Cowper, G.R., "An Analysis of a Cylindrical Shell with a Pear-Shaped Cross Section. - Lockheed Sample Problem No. 1". Structures Lab. Memo. ST-139, June 1971, National Research Council of Canada.

29. Thomson, A.G.R., "Acoustic Fatigue Design Data, Part I", AGARD Structures and Materials Panel AGARDograph No. 162, AGARD-AG-162-Part I, May 1972.

TABLE I: Comparison of Frequencies for Flat Five-Bay Panel

Mode	Symmetry x	y	Experiment (Hz)	Ref. 11-13 Theory (Hz)	'Simple' Theory (Hz)	Ad-Hoc T-Beam (Hz)	'Complete' Theory (Hz)
	1	1					
1	S	S	609	623.50	616.9	620.2	620.0
2	A	S	634	630.98	626.2	639.1	640.0
3	S	S	651	638.65	636.0	663.2	665.9
4	A	S	669	673.78	670.7	689.2	691.8
5	S	S	682	673.79	670.7	691.6	695.4
	1	2					
6	S	A	897	915.47	905.8	906.3	906.1
7	A	A	910	920.53	911.4	913.3	913.2
8	S	A	917	926.71	918.4	922.2	922.3
9	A	A	928	935.04	926.8	930.2	930.3
10	S	A	945	935.35	927.3	931.7	932.0
		1	Stiffener Bending				
11	A	S	1175	1160.8	1156.0	1445.6	1497.7
12	S	S	1245	1210.5	1203.8	1467.6	1508.2
13	A	S	1330	1288.4	1276.6	1503.2	1522.0
14	S	S	1429	1394.6	1388.9	1622.6	1651.3
	1	3					
15	S	S	1324	1329.3	1303.9	1303.8	1303.7
16	S	S	1333	1332.5	1306.8	1310.6	1310.8
17	A	S	1345	1333.0	1308.6	1306.8	1306.8
18	S	S	1350	1338.2	1313.3	1315.0	1315.2
19	A	S	1375	1340.8	1319.6	1314.2	1314.4
	2	1					
20	A	S	1604	1606.6	1582.7	1628.9	1651.5
21	S	S	1674	1748.5	1725.0	1909.5	1998.9
22	A	S	1982	1924.3	1897.6	2050.2	2114.5
23	S	S	2185	2107.7	2075.7	2218.7	2270.4
24	A	S	2353	2258.6	2220.1	2370.0	2413.7
	1	4					
25	S	A	1909	1913.1	1878.5	1878.6	1878.4
26	A	A	1923	1914.3	1880.4	1880.7	1880.6
27	S	A	1940	1915.6	1882.7	1883.4	1883.4
28	A	A	1968	1917.5	1885.0	1885.7	1885.7
29	S	A	1985	1917.6	1885.3	1886.3	1886.3
	2	2					
30	A	A	1968	2102.6	1999.9	2006.1	2005.5
31	S	A	1992	2104.0	2004.2	2027.0	2027.3
32	A	A	2020	2105.3	2008.4	2053.0	2054.6
33	S	A	2034	2173.9	2060.7	2083.7	2085.1
34	A	A	2055	2173.9	2060.7	2085.6	2087.4

TABLE II: Curvature Effects Upon Frequences of Five-Bay Stiffened Panels

			FINITE ELEMENT RESULTS			DATA SHEET RESULTS			
								Single Panel Bounds	
Mode	Symmetry x	Symmetry y	Flat Plate (Hz)	R = 40" (Hz)	R = 20" (Hz)	Stiffened Flat Plate (Hz)	Flat Plate (Hz)	R = 40" (Hz)	R = 20" (Hz)
	1	1							
1	S	S	620.1	666.0	781.9	590		Simply Supported	
2	A	S	640.1	707.6	868.7	620	363	430	510
3	S	S	665.9	782.5	1034.5	660		Clamped	
4	A	S	691.9	900.0	1292.3	690	725	1060	1530
5	S	S	695.4	986.8	1486.0	700			
	1	2							
6	S	A	906.1	1007.1	1254.7	750			
7	A	A	913.2	1040.4	1337.6	770		Simply Supported	
8	S	A	922.4	1089.6	1460.5	810	580	770	1020
9	A	A	930.4	1138.3	1585.1	840		Clamped	
10	S	A	932.0	1158.2	1637.9	850	940	1260	1680
		1	Stiffener Bending						
11	A	S	1497.7	1487.6	1501.4				
12	S	S	1508.2	1507.0	1537.9				
13	A	S	1522.0	1528.8	1582.0				
14	S	S	1651.3	1657.6	1700.1				
	1	3							
15	S	S	1303.7	1424.3	1732.1				
16	A	S	1306.8	1441.8	1778.5			Simply Supported	
17	S	S	1310.8	1464.8	1839.6		943	1220	1520
18	A	S	1314.4	1485.0	1895.3			Clamped	
19	S	S	1315.2	1492.8	1916.0		1320	1640	2020
	2	1							
20	A	S	1651.5	1655.0	1676.8	1580			
21	S	S	1998.9	2004.8	2066.4	1670		Simply Supported	
22	A	S	2114.5	2116.4	2137.6	1780	1230	1360	1360
23	S	S	2270.4	2273.3	2292.7	1870		Clamped	
24	A	S	2413.7	2425.9	2451.7	1910	1890	2040	2070
	1	4							
25	S	A	1878.4	2001.9	2329.1				
26	A	A	1880.6	2012.9	2361.9			Simply Supported	
27	S	A	1883.4	2026.5	2402.5		1450	1750	2030
28	A	A	1885.7	2037.5	2435.8			Clamped	
29	S	A	1886.3	2041.3	2448.1		1870	2870	3130
	2	2							
30	A	A	2005.5	2022.8	2074.8	1910			
31	S	A	2027.3	2049.3	2118.0	2000		Simply Supported	
32	A	A	2054.6	2078.3	154.7	2100	1450	1610	1670
33	S	A	2085.2	2110.4	2188.5	2190		Clamped	
34	A	A	2087.4	2112.3	2190.5	2220	2100	2280	2350

68

FIG. 2: 'COMPLETE' BEAM ELEMENT AND STIFFENER GEOMETRY

FIG. 1: 'SIMPLE' ELEMENT AND STIFFENER GEOMETRY
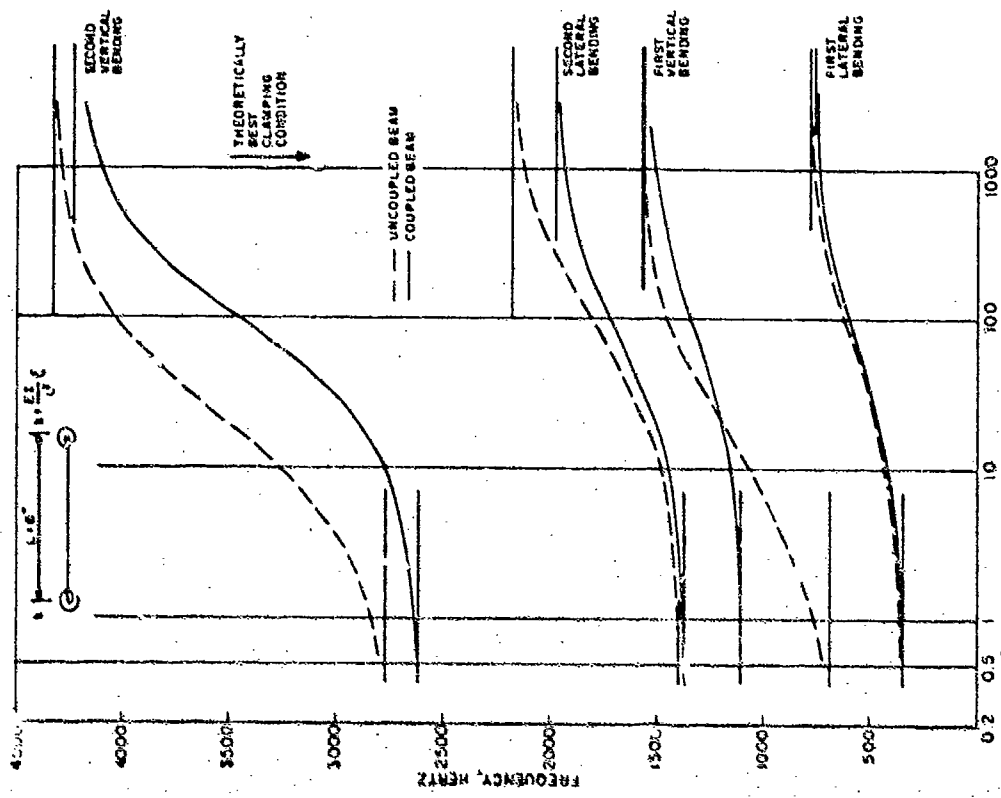
FIG.5: ELASTIC RESTRAINT EFFECT ON STIFFENER VIBRATIONS

PANEL GEOMETRY

FINITE ELEMENT GRIDWORK

FIG.3: FIVE-BAY STIFFENED PANEL

781.9

868.7

1034.5

1292.3

1486.0

CURVED PANEL
R = 20"

666.0

707.6

782.5

900.0

986.8

CURVED PANEL
R = 40"

620.1

640.1

665.9

691.7

695.4

FLAT PLATE
"COMPLETE" THEORY

616.9

626.2

636.0

670.7

670.7
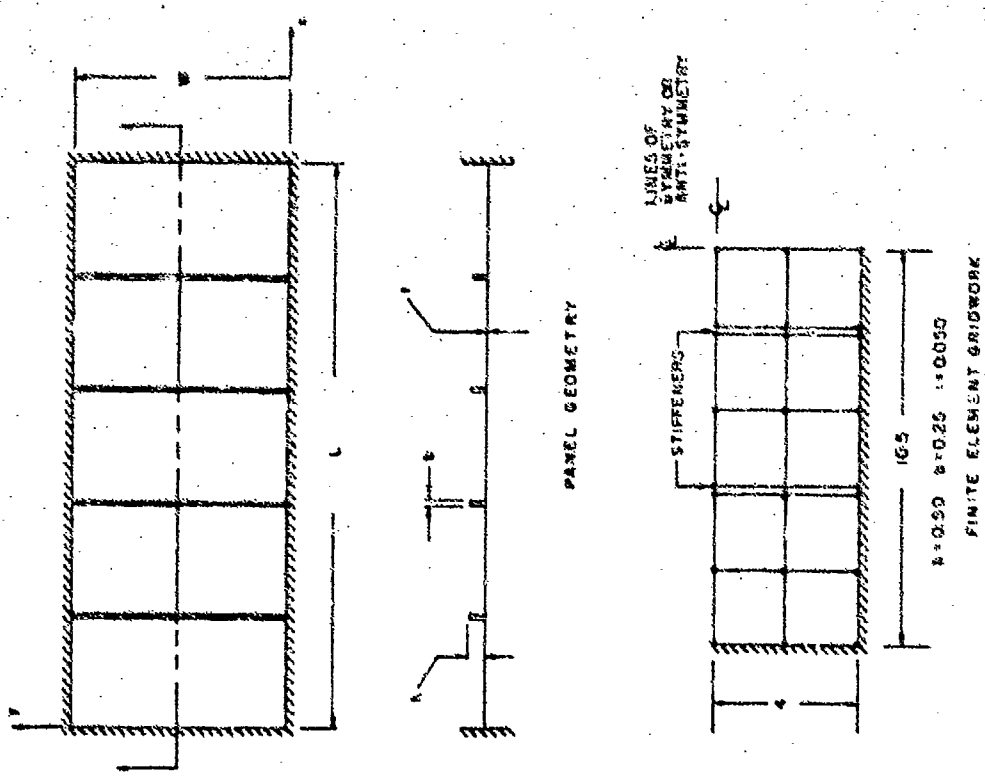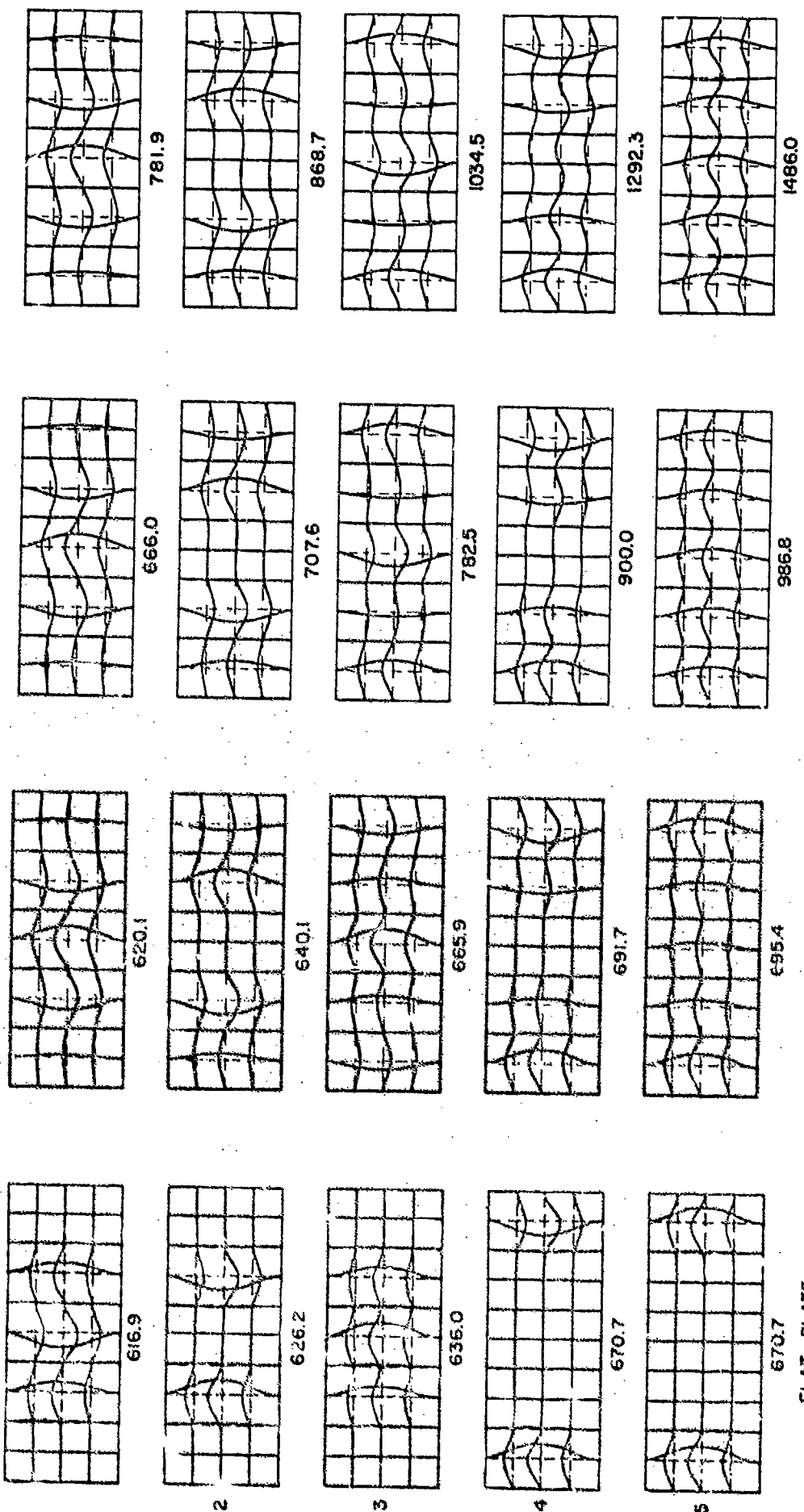
FLAT PLATE
"SIMPLE" STIFFENERS

2

3

4

5

MODE SHAPES OF THE STIFFENED PANELS

FIG. 4 (a)

FIG 4 (b)   MODE SHAPES OF THE STIFFENED PANELS
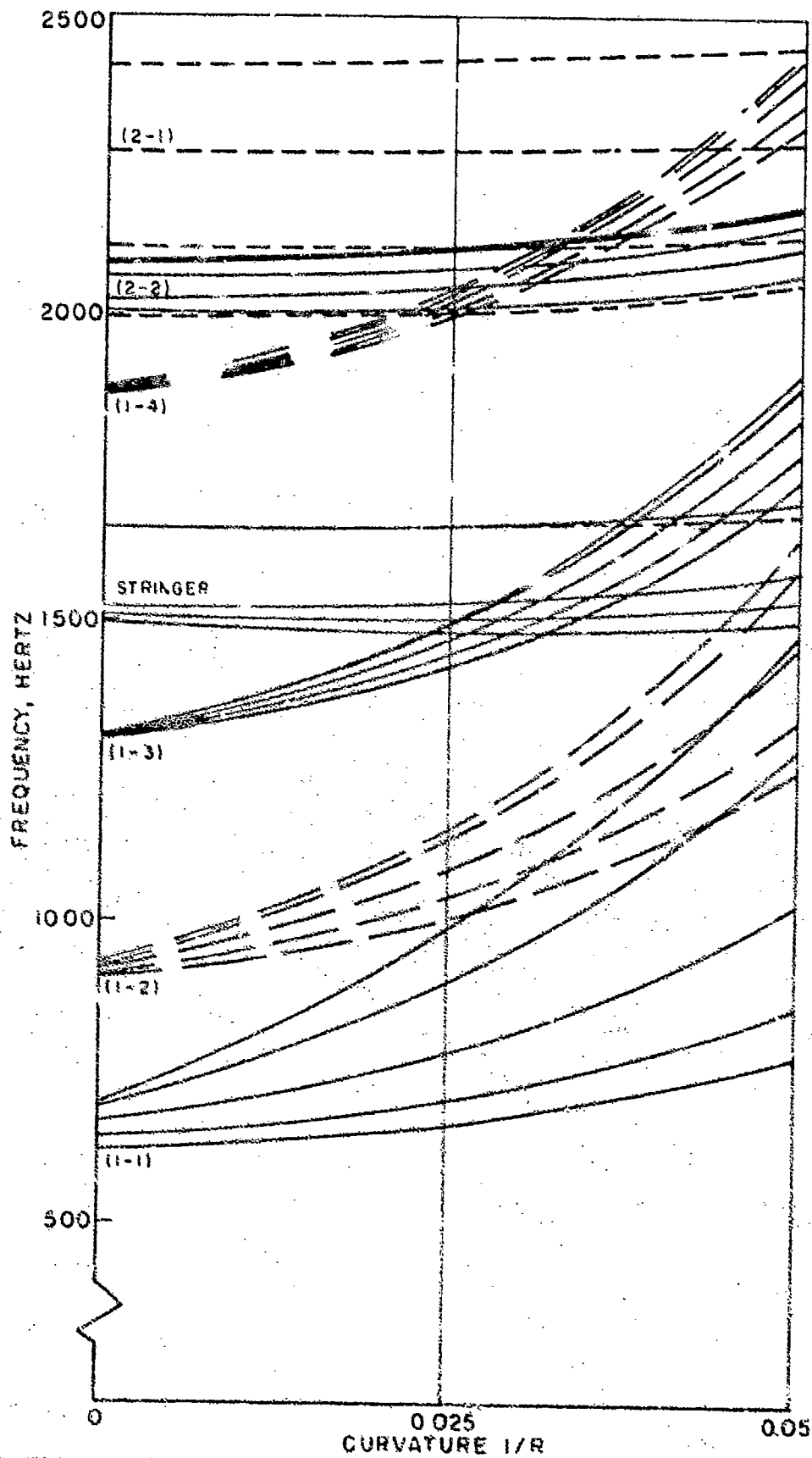
FIG.6: EFFECT OF CURVATURE ON FREQUENCIES OF FIVE-BAY PANEL

RESPONSE AND FATIGUE CHARACTERISTICS OF
LIGHT ALLOY MACHINED PLANK STRUCTURES

by

D.C.G. Eaton
Head of Structural Acoustics Group
British Aircraft Corporation, Ltd.,
Commercial Aircraft Division
Filton House
Bristol BS99 7AR,
England

SUMMARY

Light alloy integrally machined planks as used in current aircraft practice usually exhibit different vibration characteristics compared with those of equivalent fabricated 'conventional' structures. These features are reviewed together with the related acoustic fatigue implications.

Methods of predicting dynamic stresses are considered and comparisons made with practical results. Some aspects of the fatigue behaviour particularly related to machined structures as derived from coupon and siren tests are outlined.

A current research programme which is aimed at providing information for the formulation of design guides is described.

Possible problems associated with noise induced crack propagation in machined plank structures are discussed.

1. INTRODUCTION

Light alloy machined planks are now used extensively in aircraft construction and frequently replace the more conventional fabricated structures which consist of rolled or extruded stringers riveted to skins. Applications are to be found in fuselage, fin, tailplane and wing construction. Whilst the dynamic behaviour of the fabricated structure is in general terms well known, and there is extensive inservice experience of the acoustic fatigue behaviour, the corresponding data for machined plank formats is rather sparse. Apart from ad hoc laboratory investigations by aircraft manufacturers comparatively little systematic study has so far been attempted. Of this, work at the Institute of Sound and Vibration Research is the most noteworthy (e.g. references 1,2) which has concentrated on methods of response attenuation for existing structures. Recently, work has commenced on more detailed studies of the response and fatigue behaviour with a view to providing design guides for the basic structure and methods of response suppression (reference 3).

An attempt is made here to briefly review the practical aspects and the various investigations that have or are taking place. Consideration is also given to methods of stress prediction for use at the design stage, including the importance of substructure design.

The potential of palliative methods for existing structures is explored including the use of damping treatments and intermediate frames.

The influence of locked in stresses and other related features on the fatigue behaviour is considered in the light of various test findings.

Finally, noise damage aspects of "safe-life" and "fail-safe" philosophy are briefly reviewed and a current programme of work to explore this area is outlined.

2. SOME PRACTICAL CONSIDERATIONS AND THEIR INFLUENCE ON THE DYNAMIC AND FATIGUE BEHAVIOUR

Due to both problems and facilities associated with the design and manufacture of machined planks the dynamic behaviour can differ markedly from that of its fabricated counterpart. For example, the absence of stringer "feet" for riveting purposes permits closer pitching of the integral stringers. From machining aspects it is obviously simpler to gang-mill a smooth upstanding leg rather than introduce a bulbed or angled boom as would be found in the extruded or rolled version (figure 1). This results in stringers with comparitively low flexural and torsional stiffnesses. As a result the machined stiffeners no longer ac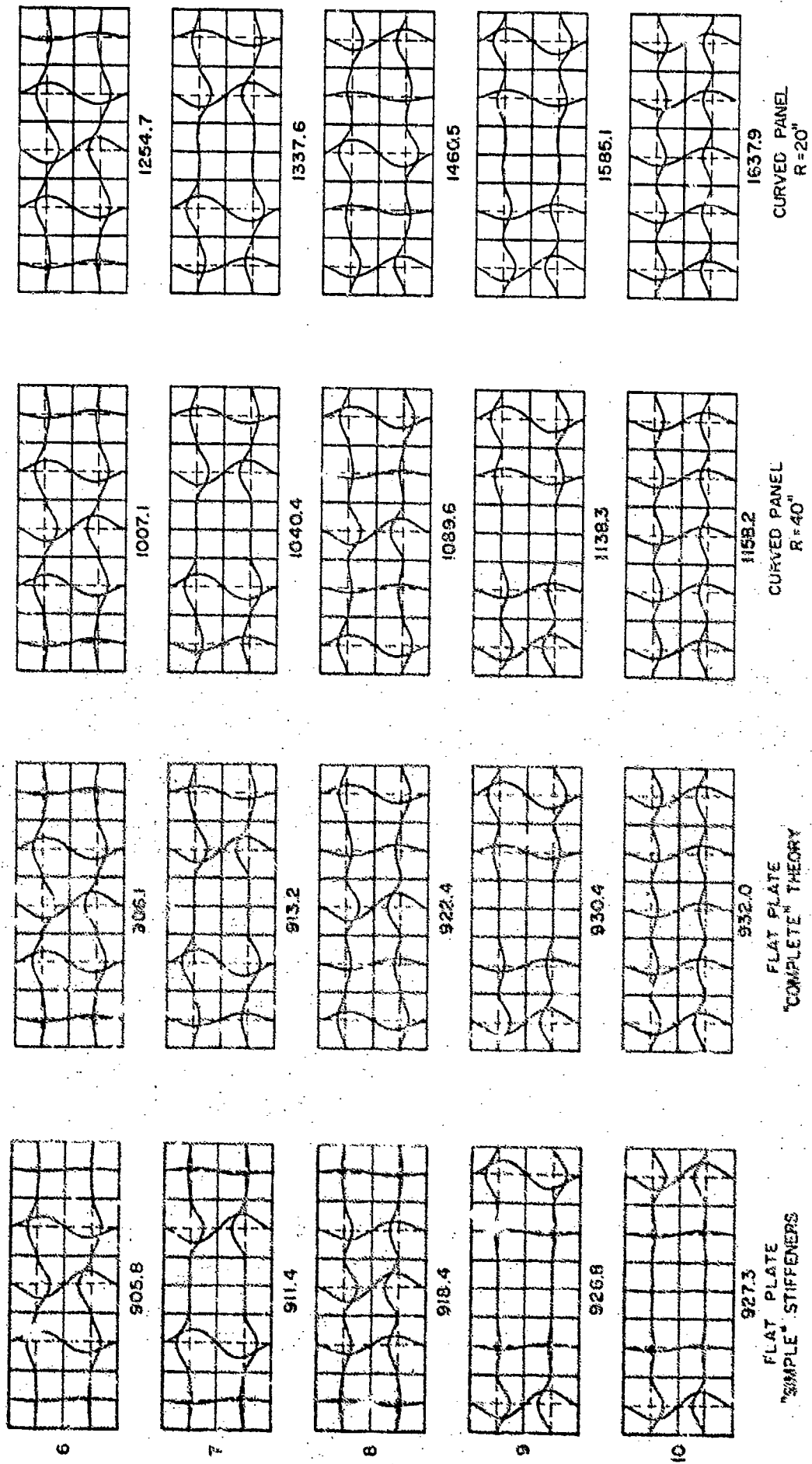t as "nodes" in the important modes of vibration, the plank tending to behave as an orthotropic plate (figure 2). In these circumstances stresses in the stiffener extremities can be of a similar magnitude to those in the skin normal to the stringer edge (the usual failure location in fabricated structure).

As a result cracks can initiate at the stringer free edge subsequently spreading down into the skin. This is obviously of potential importance in areas of high noise environment. The examples in figures 2 and 3 as derived from tests (references 4,5) serve to illustrate this.

A similar source of fatigue was found when attempting to use a machined plank configuration in the design of lightly statically loaded control surface skins. This introduced a matrix of shallow stiffening in the "waffle plate" design illustrated in figure 4 (reference 5). Again, "orthotropic plate" vibration initiated premature failures at the free edges of the stiffeners. Similar failures

have been experienced in aircraft usage (fairings) where shallow integral stiffening has effectively been introduced by chemically etching pockets in thick skins.

Of course the advent of numerically controlled tape machining lessens the practical problem of introducing bulbed stiffeners. If sufficiently enhanced stiffening is realised then the dynamical behaviour will revert to the type observed with fabricated configurations (e.g. reference 6). However, the damping of an integrally machined structure is low due to the few attachments required, and skin and substructure response may still be substantial. In practice there may also be other reasons for avoiding enhanced stiffening. For example, if a doubly curved panel is required, sizeable forming stresses are likely to be incurred. Such forming stresses can produce a serious reduction in the fatigue life. This is dealt with in section 3.3.

3. THE EVOLUTION OF STRUCTURAL DESIGN GUIDES

3.1 GENERAL REQUIREMENTS. As with most acoustic fatigue problems a detailed analysis of the structural dynamics and fatigue behaviour involves a large number of parameters. A thorough analytical solution is therefore intractable. For example, there are the usual evaluation difficulties associated with the determination of modal characteristics, joint acceptance properties and fatigue lives.

In order to produce design guides one needs to establish the simplest model, which will provide assessments of dynamic stress and stress reversal accumulation to appropriate engineering accuracy, and compile reliable fatigue data. In the following sections these requirements are reviewed and the topics of a detailed study, which is currently in progress, are highlighted.

3.2 DYNAMIC STRESS PREDICTION. As suggested in figure 1, the response is likely to be multimodal. Attempts have and are being made to produce theoretical models which will describe this behaviour, in particular, using transfer matrix and finite element methods (e.g. references 1,3,7). Currently such methods consider the dynamic properties of the plank alone, its periphery being restrained from vertical movement. Such approaches have obvious limitations as an easy design aid and there are the latent hazards of ill conditioning, computer storage overflow, etc. when marked changes in configuration are considered. In parallel with these studies attempts continue with simpler configurations which it is hoped may provide workable models. It is with these this review provides examples.

The simplest is a single degree of freedom configuration as suggested by Clarkson for flat planks (reference 8) and further studied by Arcas (reference 9). Here a Rayleigh-Ritz approach is adopted and used to examine the behaviour of a single skin-stiffener bay. The assumed mode shape represents the deformation under a uniform pressure loading.

A similar approach has been used to examine a corresponding configuration having shallow curvature (reference 3). Brief details of the theoretical model are indicated in figure 5. Comparisons have been made with experimental data derived from siren and jet noise response tests carried out with a doubly curved panel (the curvature was slight in the stiffener direction). The specimen was a multiple skin-stiffener-frame combination. Its dimensions varied and a typical range is quoted in figure 2. In addition, at one stage of the testing, the frame pitch was halved by the incorporation of intermediate frames (giving effectively an eleven inch pitch).

Initial application of the curved model with either simply supported or fully fixed boundaries at the frame locations did not produce satisfactory results particularly as the trend was contrary to expectations when the frame pitch was increased (figure 6). It was felt that due to curvature effects associated with over predominance of the panel "breathing mode" the plate edge restraint at the stiffener boundary was more pronounced than would occur in a typical multi-bay configuration (figure 5). As a result, Walker (reference 3) carried out an examination of the flexural mode of an eight bay system using a transfer matrix analysis which appears to confirm this hypothesis. The effect of frame bay variation on the modal frequency in both instances is shown in figure 7. Since the 'error' was associated only with radius terms in the strain energy expression attempts were made to vary this parameter and the result is also shown in figure 7. For the stiffener bay configuration considered, an 'effective radius' could in fact be established.

The results of using this effective radius to determine the dynamic stress are presented in figure 8. It is immediately apparent that a more realistic assessment of the stress is now realised as the frame pitch is increased. The predictions of the refined method have again been compared with the test data. In this instance a mean of the simply supported and fully fixed mode stress predictions have been used in the comparison which is shown in figure 9. It is evident that an enhanced correlation has been realised which is in fact comparable with those obtained for other forms of structure by Clarkson and Arcas. This is demonstrated by the statistical assessment given in figure 10 which follows the approach suggested by Arcas in reference 9. Probability distributions based on an assumed normal density are compared.

A number of additional features are of possible interest in assessing the adequacy of the model of the curved configuration:

On average, stiffener stresses were overestimated by 65% between frames and underestimated by 40% in the vicinity of frames.

Skin stresses were underestimated by 25% between frames, this figure increased to 96% adjacent to frames.

It seems likely that stresses adjacent to frames are influenced by frame flexure.

Using the predominant frequency observed in the measurements rather than the predicted frequency was found to have little effect on the correlation.

The test panel was to some extent lacking in symmetry (a feature not uncommon in aircraft construction). This may have tended to break up the modal pattern of the type shown in figure 1. For structures of a fully repetitive nature a less encouraging result might be obtained.

These initial findings suggest that a single degree of freedom model can be used for stress prediction in a design analysis for a limited range of structural dimensions. It seems likely that modifications to the model may be required for different regimes of the structural parameters. Obviously correlation with test data for a wider range of structural parameters is required (see section 3.4).

None of the approaches considered permits examination of the influence of the sub structure in any detail. Examples of the importance of this aspect are to be found in references 10 and 11. In reference 10 Abrahamson and Clarkson have examined the coupled rib and plank vibration of box structures.

Limited test evidence suggests that there may be stronger coupled frame and stiffened skin vibrations with machined plank formats than occurs with corresponding conventional constructions. In order to examine theoretically the importance of frame vibration, investigations have commenced where the machined plank is treated as an orthotropic plate (reference 3). This assumption is based on the plate-like behaviour described earlier. The coarsening of the plank description permits a more detailed examination of the frame behaviour in a Rayleigh-Ritz analysis. It has the further advantage that, in a number of cases under consideration, some of the joint acceptance properties may be evaluated from programmes already available for cylinder and plate modes.

A particular example is briefly considered in section 4. It is intended to extend this approach to a more general consideration of the influence of frame design.

3.3 FATIGUE DATA. A certain amount of fatigue data has been compiled from ad hoc siren tests and coupon tests in which the specimens are subjected to narrow band loading provided by electro mechanical vibration exciters. These coupons have been of two types as shown in figure 11. They are subjected to zero mean stress (except for any locked-in stresses associated with the manufacturing process). All the quoted information has been derived for type RR 58 material.
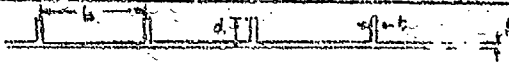
These investigations have established two tentative bounding curves (figure 12). The upper bound is for structural regions having no stress concentrations. The lower bound is for structures containing substantial locked in stresses incurred during the forming process. The effects o these can usually be reduced by local shot peening or stress relieving. It is thought that results for configurations containing stress concentrations (e.g. riveted joints) should lie nearer to the upper bound.

It is apparent from these curves that, if by careful design and manufacture undue stress concentrations are avoided, this type of construction can withstand higher dynamic stresses than its fabricated counterpart (e.g. an allowable threshold stress might be 3,000 Lb/ins^2 r.m.s. as against 2,000 Lb/ins^2 in conventional structures).

3.4 ASSESSMENT OF RESPONSE AND FATIGUE PREDICTIONS LEADING TO STRUCTURAL DESIGN GUIDES. In order to provide more general data on the response and fatigue behaviour of machined planks a number of test panels have been fabricated containing a range of structural dimensions. By the use of typical aircraft structural stability criteria a set of panels has been devised which in the main are representative of configurations found in practice. By subsequently incorporating intermediate frames on certain specimens it has been possible to further extend the range of the parameters to provide further information for assessments of the dynamic behaviour.

These panels which are currently under test are listed in the table below. Each panel has seven skin-stiffener bays, two basic frames and peripheral supporting frames. They are constructed in L 93 material.

Table: Structural Test Panel Dimensions (inches)

Panel Number	1	2	3	4	5	6	7	8	9
Panel Curvature Radius	∞	∞	∞	∞	∞	∞	57.6	57.6	57.6
Frame Pitch	20	20	20	20	20	10	20	20	10
Stringer Pitch, b	5.25	5.25	5.25	4.0	4.0	4.0	5.25	4.0	4.0
Stringer Thickness, t	0.18	0.18	0.085	0.085	0.085	0.085	0.085	0.085	0.085
Stringer Height, d	1.0	0.7	0.7	0.7	0.5	0.5	0.7	0.5	0.5
Skin Thickness, h	0.07	0.07	0.057	0.057	0.057	0.057	0.057	0.057	0.057
Stability Designed	✓	✓	✓	✓		✓	✓		
Comments	Panel 6 is derived from 5 and Panel 9 from 8 by addition of intermediate frames								

The basic panels (i.e. excluding the intermediate frame variants) have been subjected to a jet noise response test in which extensive strain measurements were taken and the associated structural noise levels and spatial correlations recorded.

Resonance tests, which have commenced, are to be conducted on all the panels. In the main these will concentrate on the frequency regions of greatest interest as determined from the theoretical studies and the jet noise tests.

This is to be followed by siren acoustic fatigue tests on a selection of these panels. The siren spectrum will be shaped to excite similar structural response characteristics as observed in the jet noise tests. Further fatigue data are being realised from coupon tests of the type described in section 3.3. Some studies of the effects of stress concentrations and locked in stresses due to the presence of attachments are intended using the configuration shown in figure 11.

On completion of these investigations it is expected to understand the dynamic behaviour as incurred in practice. The existing or modified theoretical models can then be used with greater confidence in design analyses.

The detailed fatigue data derived for L.93 material will form an important reference for future fatigue assessments. These results should also shed some light on the possible differences realised in fatigue results from multimode and single mode of response tests.

4. PALLIATIVE METHODS FOR EXISTING STRUCTURES

4.1 GENERAL BACKGROUND. As with any other form of construction there is always the risk that unexpected acoustic fatigue problems will arise during the service life of an aircraft. These will require remedial measures which can be applied quickly and with the minimum of disruption to the existing structure.

Artificial damping treatments have rarely been used as an integral part of primary structure due to reservations concerning their resistance to creep, contamination, temperature variations and other factors. However, an application as an additional secondary item presents fewer hazards. Work at Southampton University (e.g. references 1 and 2) has considered a number of damping treatments in this category. One of these techniques involving the use of a constrained layer has recently been tried out with one of the test panels referred to in section 3.4 and some interim findings are referred to by way of an example of a potential palliative. This is described in section 4.2.

The other more frequently experienced approach is to enhance the local structural stiffness at the expense of a weight penalty. Inevitably there is a need to establish a minimum weight configuration. An example of current work for machined planks is summarised in section 4.3.

4.2 THE USE OF A CONSTRAINED DAMPING LAYER. The technique makes use of a damped sandwich beam which is attached to the free edges of the stiffeners in the middle of the frame bay (figure 13). Most of the damping is thought to come from the shearing deformations associated with lateral displacements of the stiffener edges. The shearing deformation associated with flexure of the beam is probably secondary. Detailed investigations are being conducted by Coote (references 2,12) who supplied the beams for the test in question. No attempt was made to optimise the beam configuration (it is thought that stiffer face plates might increase the efficiency of the damper) which was placed across the centres of the three frame bays of panel 7 (see section 3.4).

The panel was subjected to frequency response tests with and without the beams in situ, the strain levels being recorded at a number of stations. Figure 13 shows an average curve for the ratio of the stress before and after treatment. It is apparent that the greatest damping occurs at the lower frequencies where, although the panel and stiffeners are primarily bending, sizeable relative movements of the stiffeners may be incurred. At the higher frequencies predominantly torsional motion of the stiffeners can arise. If these are in antiphase then energy dissipation can occur.

The success of the method depends on the modes of vibration likely to cause failures. The panel bending modes are usually of importance.

4.3 APPLICATION OF INTERMEDIATE FRAMES. Results from siren and jet noise tests carried out on a fuselage specimen have indicated that the introduction of intermediate frames reduces the plank stresses by between 30% and 50% depending on the measurement location. Initial studies using the theoretical model shown in figure 14 have indicated a similar reduction for modes involving frame flexure. Results for the frame twisting mode are not yet available.

5. EFFECTS OF NOISE ON CRACK PROPAGATION

Systematic experimental studies of the propagation of cracks by noise have been restricted in the main to those in flat uniform plates either unloaded or subjected to uniaxial or biaxial loads simulating cabin pressurisation stresses (References 13,14). Yet comparatively little work has been carried out to examine the effects of adjacent fabricated structures.

Attempts have been made to relate these results to the practical aircraft configuration and thereby forecast propagation rates in conjunction with 'fail-safe' investigations. This topic is the subject of further appraisal by Kirkby (reference 15) whose tentative findings suggest that on occasions noise induced propagation might be of comparable importance with that induced by the quasi-static forces that normally define the loading environment. As far as the author is aware such aspects have not been the subject of study in the case of machined structure and at this stage one can only conjecture potential problems.

The application of machined structure can largely obviate the regions of stress concentration found in conventional riveted structure. This includes the elimination of joggles and other sharp radii and the reduction of the number of rivets and their holes and so on. In addition some 'redundant' structure is eliminated such as backing angles. Thus in safe-life terms the machined configuration has the definite advantage that sources of crack nucleation are fewer.

However, once damage has been initiated for any reason, including the effects of non-acoustic sources, the resistance to crack propagation appears to be less. There are fewer inherent crack stoppers and less redundant structure to offer an alternative loadpath. Fortunately, in the case of wing and fin structures there is still a high degree of redundant structure and in the potentially sensitive area of less redundancy, viz the pressurised fuselage structure, the noise levels are usually sizeably lower.

A criterion from a fail-safe approach might be that the structure should be capable of carrying load whilst containing a crack not readily observed by visual means and that it should not grow to catastrophic proportions between major aircraft inspections. Such a crack might be some six to ten inches in length depending on its location. This length might be reached more quickly than normally envisaged from quasi-static load effects. The directionality of the crack path and its ability to circumnavigate potential crack stoppers may be modified by the noise loading. Figures 1,2 and 3 provide some indication of possible damage characteristics. Crack growth beyond a ten inch length has been considered. With some machined plank structures the configuration will not necessarily be sufficiently "detuned" and can therefore still respond in a resonant fashion to the acoustic excitation.

In order to assess the importance of these features a test programme has commenced. The importance of sequential noise and quasi-static loads (pressurisation, gust, landing loads, etc.) on crack growth is to be examined in a siren using a biaxial loading rig and specimen configuration as shown in figure 15. This rig has recently been calibrated and the first crack propagation tests are about to commence.

At a later stage it is intended to conduct tests on a pressure shell specimen containing typical planks and substructure. Again a sequential loading will be applied, the noise being supplied by peripherally mounted sirens. This test will allow such features as the effects of curvature and substructure to be studied. It will also permit an examination of the effects of noise on extensively cracked panels (e.g. crack length ≥ 10 inches).

Ad hoc tests are proceeding on miscellaneous specimens to establish the rate and directional behaviour of cracking in various structural configurations. This work is aimed primarily at maintenance and reliability aspects and includes testing of repair schemes.

6. FINAL REMARKS

This paper has reviewed the facets of acoustic fatigue related to typical light alloy machined plank structures.

Some methods of stress prediction which avoid many of the complicating features associated with response to noise have been considered. An example related to curved planks has been compared with test data with encouraging results. Such methods appear to have good potential but require further ratification.

The limited fatigue data that are available indicate that if care is taken during design and manufacture this form of structure has advantages over equivalent fabricated structures in terms of 'safe-life' criteria.

A damping treatment which does not affect the strength of the main structure and which could be readily introduced as a modification to an existing structure has been the subject of an initial examination. Results are quite promising and warrant further study.

Possible problems associated with crack propagation due to noise have been discussed and current investigations outlined.

A series of theoretical and experimental investigations which are proceeding are expected to greatly assist in the compilation of design guides.

7. REFERENCES

1. Clarkson, B.L., and Cicci, F. "Methods of Reducing the Response of Integrally Stiffened Structures to Random Pressures". TRANS ASME Paper No. 69 - Vibr - 26 (1969).

2. ., C.T. I.S.V.R. Southampton University Unpublished Data.

3. British Aircraft Corporation, Ltd. Procurement Executive, Ministry of Defence, reference K41A/384/0843a2 (1972). Unpublished Data.

4. Wagner, J.G., "Quelques Considerations sur Le Fatigue Acoustique". 5th I.C.A.F. Symposium: "Aircraft Fatigue Design, Operational and Economic Aspects", Melbourne 1967.

5. Matthews, L.J., Michaelides, L.G., Walker, G., and Eaton, D.C.G. British Aircraft Corporation Ltd., unpublished data.

6. Olson, M.D., Lindberg, G.M., "Free Vibrations and Random Response of an Integrally Stiffened Panel" Conference Proceedings Southampton 1970. "Current Developments in Sonic Fatigue"

7. Lin, Y.K., and Donaldson, B.K., "A Brief Survey of Transfer Matrix Techniques with Special Reference to the Analysis of Aircraft Panels" J. Sound Vib. (1969) Vol.10 No.1.

8. Clarkson, B.L., "Stresses in Skin Panels Subjected to Random Acoustic Loading" The Aeronautical Journal, Volume 72 No. 695 1968.

9. Arcas, Noe, "Prediction of Stress and Fatigue Life of Acoustically-Excited Aircraft Structures" Shock and Vibration Bulletin No. 39 Part 3 (1969)

10. Clarkson, B.L., and Abrahamson, A.L., "Response of Skin/Rib Structures to Jet Noise". Conference Proceedings, Southampton 1970 "Current Developments in Sonic Fatigue"

11. Eaton, D.C.G., "Development and Testing of Concorde Structure from Noise Aspects", Environmental Engineering Vol. 9 September, 1969

12. Coote, C.T., "Measurement of the Damping Properties of Silicone-based Elastomers over Wide Temperature Ranges". Journal of Sound and Vibration Volume 21 Number 2 (1972)

13. Mills, D., "Acoustically Propagated Cracks in Biaxially Tensioned Plates. Ph.D. Thesis, University of Southampton, 1970.

14. Jost, G.S., "Fatigue Crack Growth under Random Combined Stress Conditions". Ph.D. Thesis, University of Southampton 1969

15. Kirkby, W.T., R.A.E. Technical Report in course of Preparation.

16. Galletly, G.D., "On the In-Vacuo Vibrations of Simply Supported Ring Stiffened Shells", Proc. of 2nd U.S. National Congress of Applied Mechanics pp. 225-231, 1954

17. Miller, P.R., "Free Vibrations of a Stiffened Cylindrical Shell", A.R.C. R & M 3154 (1958)

ACKNOWLEDGEMENTS

310Hz

STRINGER TWISTING MODE

TYPICAL
INTERMEDIATE
MODES

600Hz

STRINGER BENDING MODE
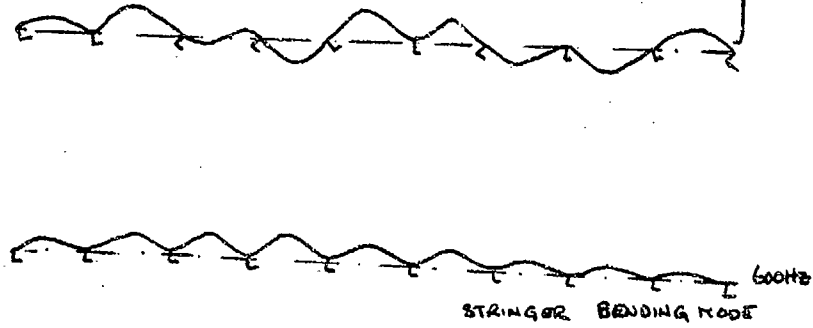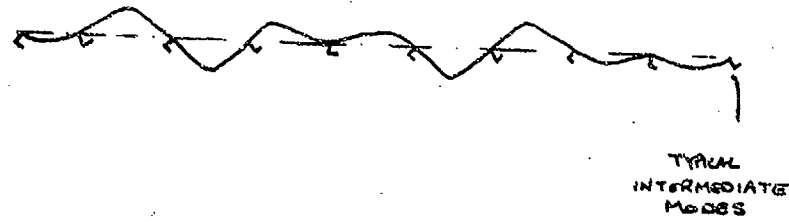
Conventional Structure Typical Modes of Response
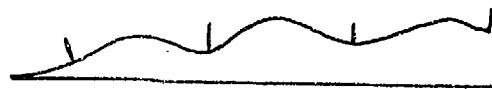
Symmetric modes
other half of panel
identical.

RING   FRAME
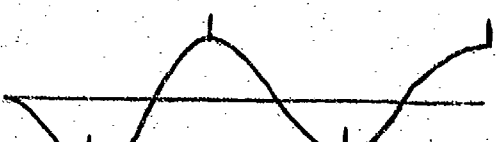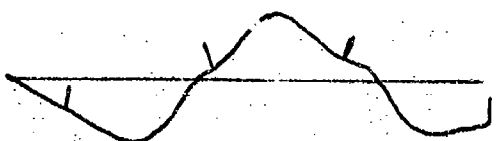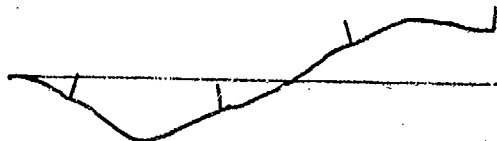
The modes shown are typical
of those predicted for
the panels whose dimensions
are summarised in table.

In the case of panels
the first overtone mode
as shown below — — — —
will differ in detail
because of the reduced
flexural stiffness. — — —

FRAME   FRAME

Machined plank structure typical modes of response.

CRACKING
INITIATED AT
THE FREE EDGE
OF THE
STIFFENER
MIDWAY BETWEEN
FRAMES.
AFTER A
FURTHER 4 HOURS
OF TESTING
DAMAGE HAD
EXTENDED
EXTENSIVELY
AS SHOWN

5 ins

7.5 ins

5.7 ins
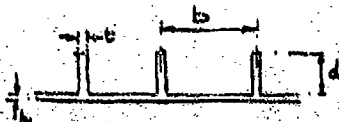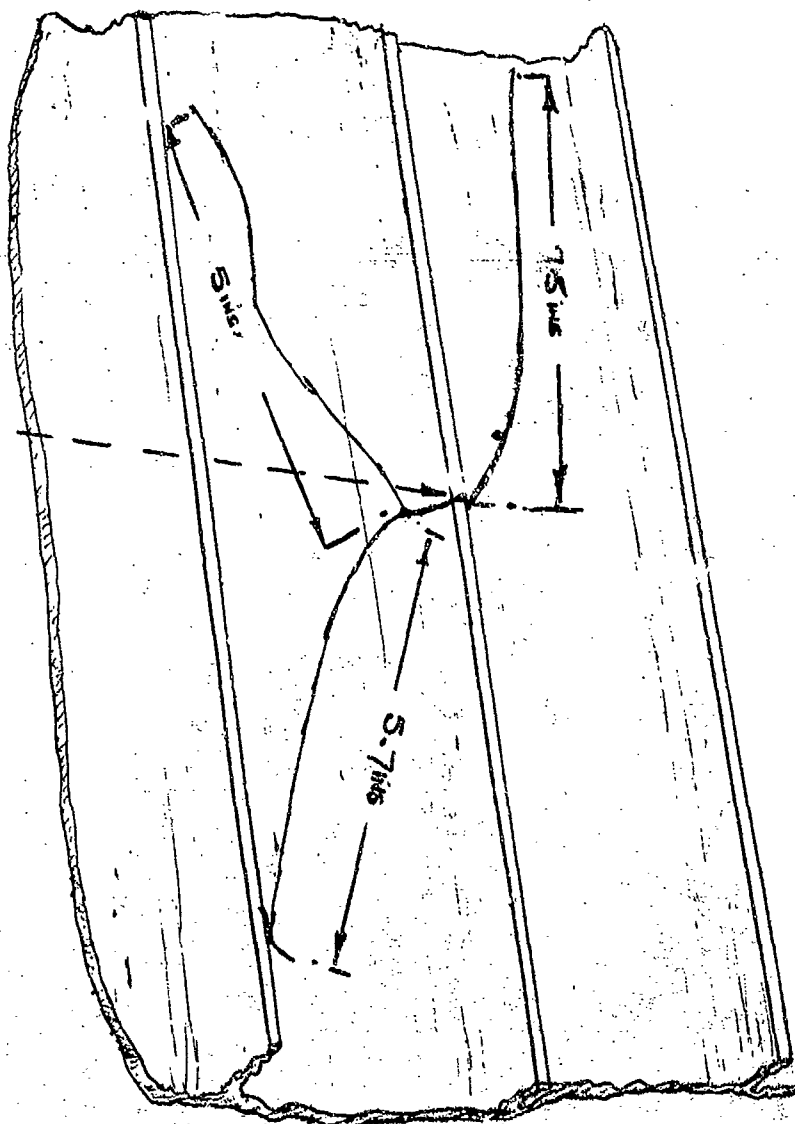
TYPICAL PANEL DIMENSIONS

FRAME PITCH .... 22 ins
PANEL CURVATURE (Average) .... 45 ins
STRINGER PITCH, b .... 3.5 - 4.5 ins
STRINGER THICKNESS, t .... 0.08 ins
STRINGER HEIGHT, d' .... 0.75 - 1.0 ins
SKIN THICKNESS, h .... 0.05 - 0.07 ins

FIG.2 ACOUSTIC FATIGUE OF FUSELAGE SIREN TEST SPECIMEN. The extent of the damage shown
was reached after 81 hours of testing under broadband noise of about 162 dB. The fatigue
was aggravated by the presence of locked-in forming stresses.

Box Structure Test Specimen
with Four Ribs & Machined Skins

Tested in a Siren Facility
for 20 hours with Broad-
band Noise   163 dB
Estimated Free Edge Stress
at Failure Point – 6,000 lb/in^2 r.m.s.
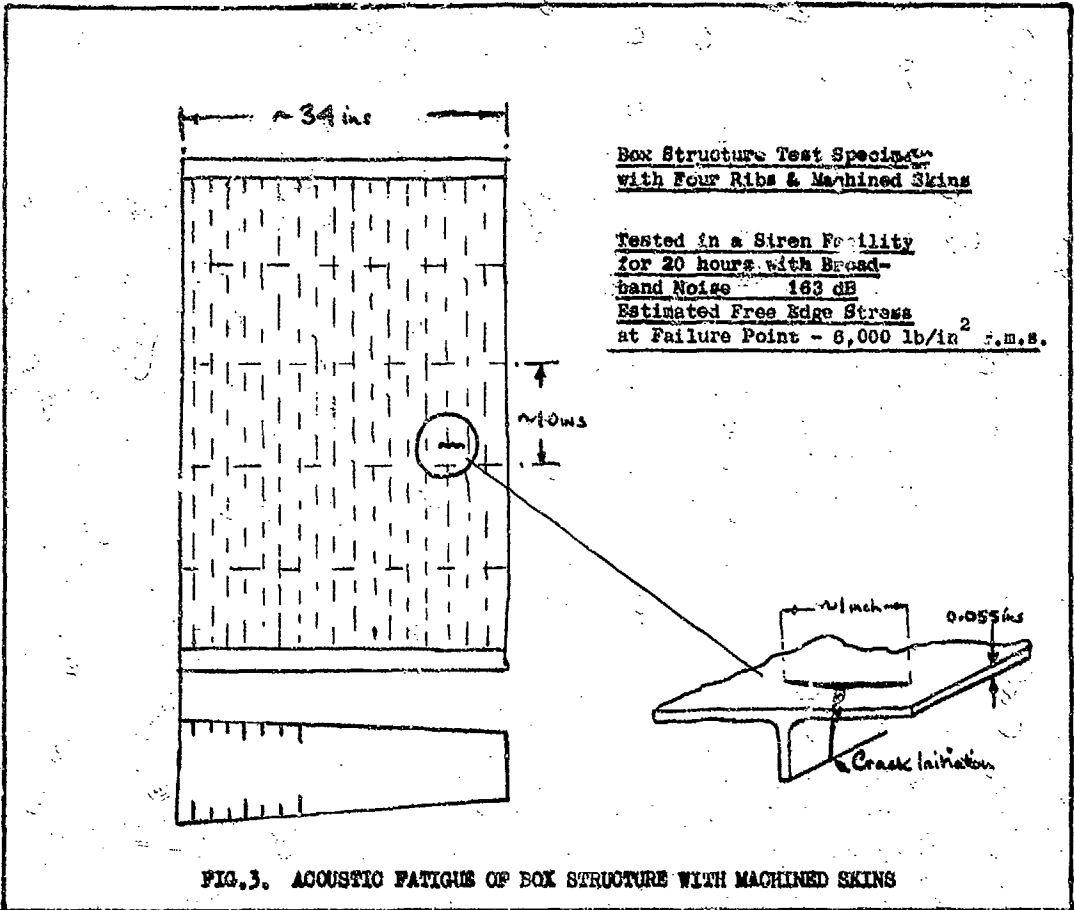
FIG. 3. ACOUSTIC FATIGUE OF BOX STRUCTURE WITH MACHINED SKINS

Siren Test Failure of
Waffle Plate After 10 Hours
At 160 dB Broadband Noise

A-A Skin/Stiffener Dimensions
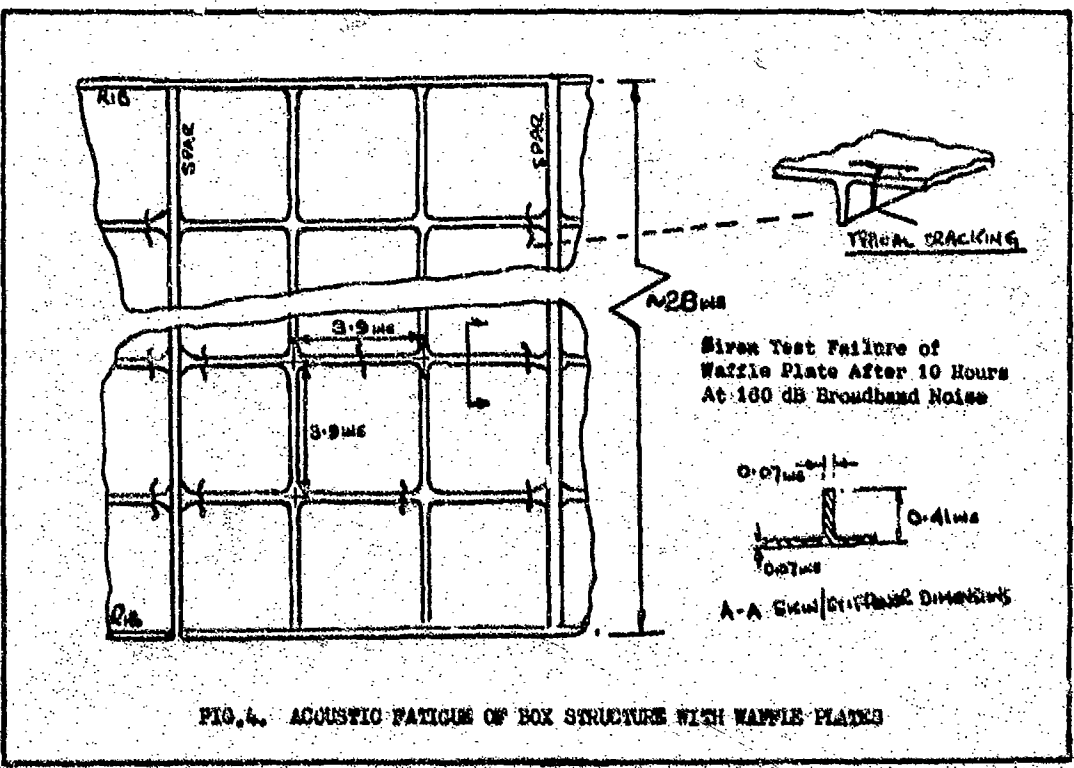
FIG. 4. ACOUSTIC FATIGUE OF BOX STRUCTURE WITH WAFFLE PLATES

$$w(x,s,t) = F(x) \cdot f(s) \cdot q_3(t)$$

$$u(x,s,t) = \frac{\partial F(x)}{\partial x} \cdot F(s) q_1(t)$$
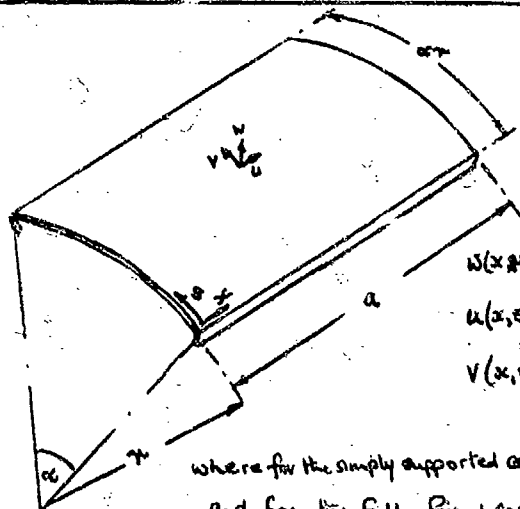
$$V(x,s,t) = F(x) \cdot \frac{\partial f(s)}{\partial s} \cdot q_2(t)$$

where for the simply supported case at the frames $F(x) = \sin\frac{\pi x}{a}$

and for the fully fixed case at the frames $F(x) = 1 - \cos\frac{2\pi x}{a}$

$$f(s) = K + 1 - \cos\frac{2\pi s}{a\gamma}$$

N.B. In determining the resonant frequency of the system by the Rayleigh-Ritz method no serious loss of accuracy is incurred by the omission of the K term in the F(s) expression of the 'U' coordinate.

The usual shallow shell expressions were used to evaluate the plate strain energy. Only 'vertical' flexure was included in the stiffener strain energy expression.

TRANSFER MATRIX MODEL.

THESE BAYS OMITTED

SINGLE DEGREE OF FREEDOM, SINGLE BAY MODEL.
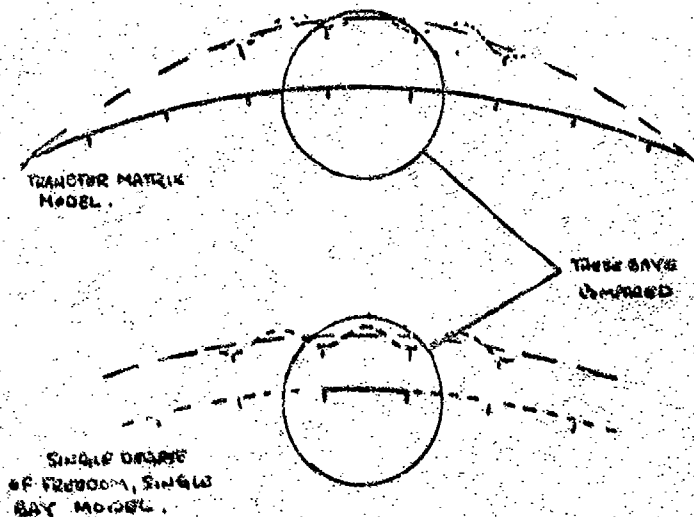
FIG 8. BRIEF OUTLINE OF SINGLE DEGREE OF FREEDOM CURVED PANEL MODEL. The exaggeration of the 'breathing mode' in the single bay model compared with that set up in the multibay version (transfer matrix) is also indicated.

FIG. 6. COMPARISON OF PREDICTED AND MEASURED STRAINS USING UNMODIFIED
SINGLE DEGREE OF FREEDOM CURVED PLANK MODEL.

FIG 7 COMPARISON OF FREQUENCIES FOR ORIGINAL RAYLEIGH-RITZ SINGLE BAY MODEL TRANSFER MATRIX MODEL; AND EFFECTIVE RADIUS MODEL.

FIG.8. EFFECT OF EFFECTIVE RADIUS ON DYNAMIC STRESS.

FIG 9. CORRELATION OF MEASURED AND PREDICTED STRAIN, VARIOUS RELATIVE VALUES.

FIG 11 COUPON SPECIMENS USED IN FATIGUE TESTS

The specimen is subjected to narrow band excitation centred
on its fundamental resonant frequency.

FIG 12 Estimated upper and lower bounds of Fatigue Data for typical light
Alloy machined structure as derived from coupon and sinon specimen
tests.

FREQUENCY RESPONSE TEST
Average curves of strain
and acceleration attenuation
from measurements at several
panel locations.

ε_1, g_1 basic plank strain and acceleration

ε_2, g_2 damped plank strain and acceleration

CONSTRAINED DAMPING LAYER CONFIGURATION

In the particular test the reduction in response is most marked at the lower frequencies due possibly to relative stiffener edge displacement.

There is possibly little relative movement at the middle frequencies and model coupling may occur. But the apparent increase in response is not yet understood.

Higher frequency attenuation may be attributable to relative movement of stiffeners as stiffeners twist.

FIG.13. RESULTS OF . TESTS OF 1.0 INCH WIDE CONSTRAINED LAYERS ON PLANK FREQUENCY RESPONSE CHARACTERISTICS.

$$I = \frac{td^2}{3} \qquad J = \frac{dt^2}{3}$$

Assumed orthotropic plate strain energy expression used in Rayleigh-Ritz analysis:

$$\Pi_p = \int_0^\ell \int_0^{2\pi} \frac{1}{2a} \left\{ C_x a^2 \left(\frac{\partial u}{\partial x}\right)^2 + C_\phi \left(\frac{\partial v}{\partial \phi} + w\right)^2 + (C_x + C_\phi)\nu a \frac{\partial u}{\partial x}\left(\frac{\partial v}{\partial \phi} + w\right) \right.$$

$$\left. + \frac{Eh}{2(1+\nu)}\left(\frac{\partial u}{\partial \phi} + a\frac{\partial v}{\partial x}\right)^2 \right\} dx\, d\phi$$

$$+ \frac{1}{2a^2}\int_0^\ell \int_0^{2\pi}\left\{ D_x a^3 \frac{\partial^2 w}{\partial x^2}\left(a\frac{\partial^2 w}{\partial x^2} - 2\frac{\partial u}{\partial x}\right) + D_\phi\left(w + \frac{\partial^2 w}{\partial \phi^2}\right)^2 + (D_x + D_\phi)\nu a^2 \frac{\partial^2 w}{\partial x^2}\left(\frac{\partial^2 w}{\partial \phi^2} - \frac{\partial v}{\partial \phi}\right) \right.$$

$$\left. + \frac{D_{x\phi}}{2}\left[\left(a\frac{\partial^2 w}{\partial x \partial \phi} + \frac{\partial u}{\partial \phi}\right)^2 + 3a^2\left(\frac{\partial^2 w}{\partial x \partial \phi} - \frac{\partial v}{\partial x}\right)^2\right]\right\} dx\, d\phi$$

where $C_x = \frac{Eh}{1-\nu^2} + \frac{EA}{b}$; $C_\phi = \frac{Eh}{1-\nu^2}$; $D_x = \frac{Eh^3}{12(1-\nu^2)} + \frac{EI}{b}$; $D_\phi = \frac{Eh^3}{12(1-\nu^2)}$; $D_{x\phi} = \left\{\frac{Eh^3}{12(1+\nu)}\left(\frac{Eh^3}{12(1+\nu)} + \frac{GJ}{b}\right)\right\}^{\frac{1}{2}}$

Expressions for the bending and twisting energies of the frame are derived from a method which is effectively an extension of the expressions of Galletly and Miller as given in references 16 and 17.

Modes for the model mentioned in section 4.3 assume the main frames provide fully-fixed boundary conditions. Two types of mode are considered involving either bending or twisting of the intermediate frame:

$$w = F(x) \cdot F(\Theta)\, q_2(t)$$

$$v = F(x) \cdot \frac{\partial F(\Theta)}{\partial \Theta}\, q_2(t) \qquad \text{where } q_i(t) \text{ are normal coordinates}$$

$$u = \frac{\partial f(x)}{\partial x} \cdot F(\Theta) \cdot q_1(t) \qquad \text{where } F(\Theta) = \cos n\Theta$$

and $F(x)_1 = \lambda + \Delta_1 \psi_1$ mode 1,n

$F(x)_2 = \lambda + \Delta_2 \psi_2$ mode 2,n

$$\lambda = x^4 - 2\ell x^3 + \ell^2 x^2$$

$$\psi_1 = \frac{2x^3}{\ell^2} - \frac{3x^2}{\ell^2} + 1$$
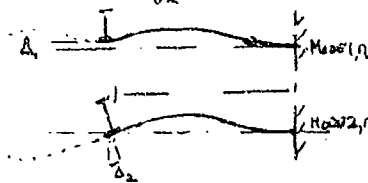
$$\psi_2 = \frac{x^3}{\ell^2} - \frac{2x^2}{\ell} + x$$

For 'repetitive' structures Galletly (reference 16) has suggested suitable cylinder mode shapes which are currently being used for more general investigations.

FIG.14. APPLICATIONS OF AN ORTHOTROPIC PLATE MODEL FOR COUPLED FRAME – PLATE MODES

SLOTS IN SPECIMEN
ENHANCE DIRECTIONALITY
OF LOAD PATH

FULCRUM

HYDRAULIC
JACKS

LOADING
PLATENS

REPRESENTATIVE
AREA APPROX.
20 INS x 20 INS

MAIN SUPPORT
STANCHIONS
ARE BOLTED TO
THE FLOOR
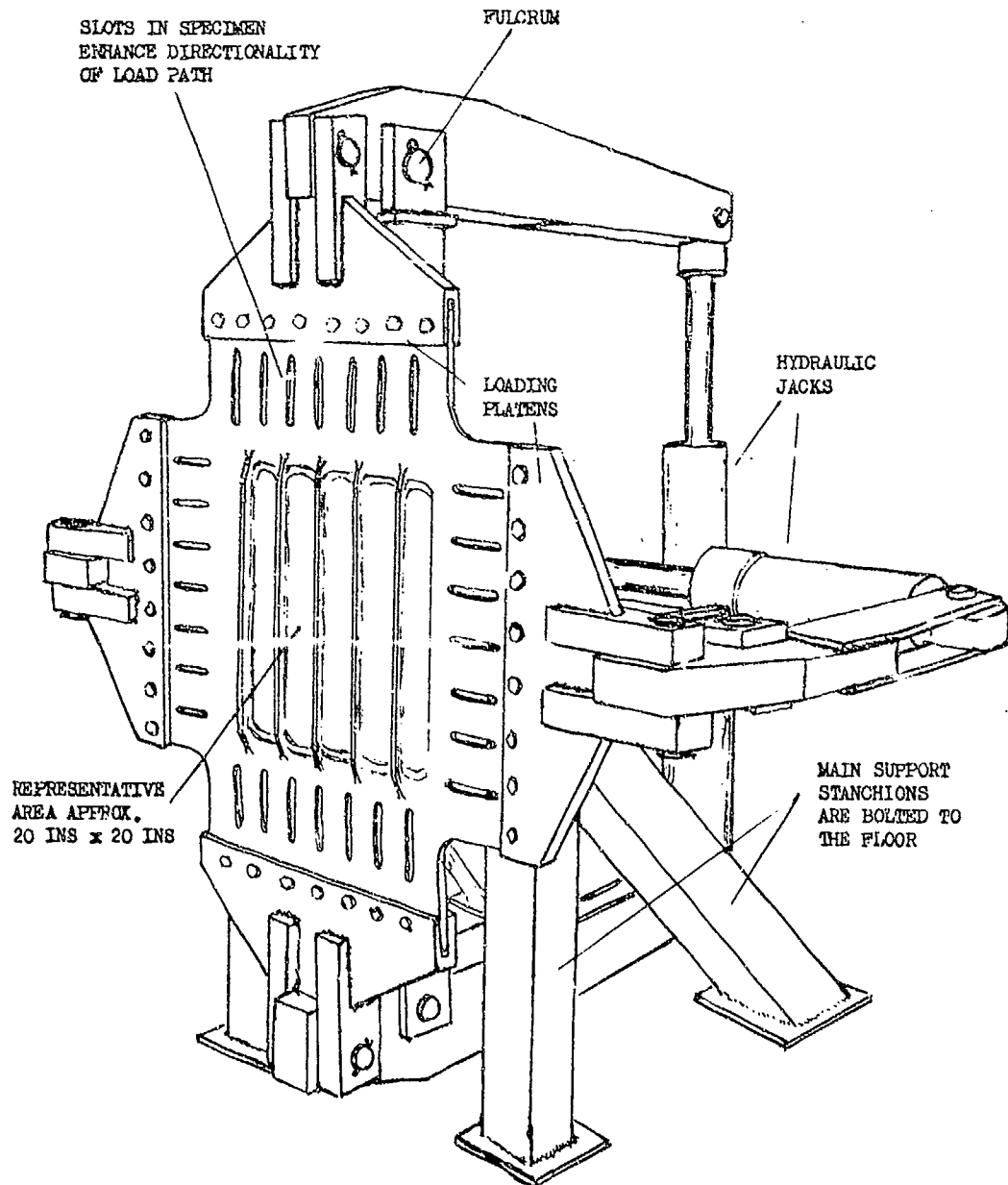
FIG. 16. BIAXIAL LOADING RIG & MACHINED PLANK SPECIMEN FOR USE IN SIREN TESTS.
The rig has been designed to operate in a confined space. For clarity the specimen
face is shown reversed in the loading platens compared with the normal test
configuration.

RECHERCHE EXPERIMENTALE DE LA TENUE DES STRUCTURES D'AVION A LA FATIGUE ACOUSTIQUE

par

Jean GAY
AEROSPATIALE - Bureau d'Etudes
Boite Postale 3153
31053 - Toulouse Cedex

RESUME

La recherche expérimentale de la tenue des structures d'avion à la fatigue acoustique est délicate. Sa réussite nécessite la connaissance de principes de base qu'il est nécessaire d'appliquer avec discernement à chaque cas spécifique.

L'objectif de cette communication est l'exposé des données de base qu'il est nécessaire de connaitre, et des conditions d'essais qu'il faut choisir pour un traitement correct du problème.

Les données de base sont :

- les sources d'excitation
- les conditions de vol
- les zones critiques de l'avion

desquelles découlent les conditions d'essais :

- type d'essais
- niveau d'excitation
- spectre d'excitation
- durée de l'essai
- définition des éprouvettes
- choix des moyens d'essais
- processus d'essais

1. SOMMAIRE

Les excitations acoustiques de niveaux élevés engendrent dans les zones d'avion qui les subissent, des réponses dynamiques plus ou moins importantes, suivant la conception, la nature et les caractéristiques d'amortissement des structures sollicitées.

Ce phénomène, s'il n'est pris en considération, peut provoquer des dommages allant de la simple crique à la détérioration rapide d'un élément (gouverne par exemple).

Sur des pièces simples, certaines méthodes théoriques permettent d'évaluer d'une manière satisfaisante la résistance à la fatigue sonore. Il n'en est pas de même sur des ensembles aussi complexes que des structures d'avion.

Dans ces conditions, le plus sûr moyen d'investigation est :

" L ' E X P E R I M E N T A T I O N "

L'objectif de cette communication est l'exposé des principes de base qui régissent sa bonne réalisation.

2. VUE SYNOPTIQUE DU PROBLEME

Le traitement du problème implique la connaissance des informations suivantes :

```
┌─────────────────────────────────┐
│        DONNEES  DE BASE          │
├─────────────────────────────────┤
│  - sources d'excitation          │
│  - conditions de vol             │
│  - zones critiques de l'avion    │
└─────────────────────────────────┘
```

d'où découlent

```
┌─────────────────────────────────┐
│        CONDITIONS  D'ESSAIS      │
├─────────────────────────────────┤
│  - type d'essais                 │
│  - niveau d'excitation           │
│  - spectre d'excitation          │
│  - durée de l'essai              │
│  - définition des éprouvettes    │
│  - choix des moyens d'essais     │
│  - processus d'essais            │
└─────────────────────────────────┘
```

3. DONNEES DE BASE

A. SOURCES D'EXCITATION

Les excitations qui influencent la tenue en fatigue acoustique des structures proviennent principalement de deux sources :

- le bruit de jet
- les écoulements aérodynamiques { tourbillons
couches limites

Ces excitations peuvent être évaluées par calcul, ou mieux, mesurées sur avion, banc d'essai ou maquette.

Les sources secondaires comme le conditionnement d'air, les alternateurs, etc ... posent des problèmes locaux dont l'étude et le traitement ne sont pas exposés ici.

B. CONDITIONS DE VOL ET ZONES CRITIQUES DE L'AVION

La connaissance de l'évolution des excitations en fonction de la trajectoire est indispensable. C'est elle qui permet de définir :

- le niveau global d'excitation
- les temps d'exposition à un niveau donné
- les zones critiques de l'avion.

Elle permet également, dans certains cas, de définir une équivalence : heures d'essais – heures de vol.

A titre d'exemple, la figure 1 donne pour le cas de "CONCORDE" :

- une schématisation de ces excitations sur une trajectoire type
- une représentation des zones de l'avion respectivement intéressées par chaque excitation.

Pour ce cas spécifique, les trois sources d'excitations ont des influences variables :

a) le champ de pressions sonores créé par le jet des réacteurs a des effets particulièrement sensibles pendant les points fixes, le décollage, l'atterrissage et la mise en reverse des réacteurs. Les zones de structure plus particulièrement affectées sont celles situées au niveau et en arrière des tuyères.

b) la couche limite turbulente agit pendant toute la durée de la croisière, principalement sur le fuselage.

c) le tourbillon de bord d'attaque a des effets comptables seulement pendant les vols à grande incidence. Seule la voilure est influencée par ce phénomène.

4. CONDITIONS D'ESSAIS

A. TYPE D'ESSAIS

Deux grandes familles d'essais sont à considérer :

- les essais sélectifs
- les essais qualificatifs

Les essais sélectifs ont pour but la comparaison de différentes conceptions structurales ou l'étude de paramètres particuliers. Ils ne demandent pas une connaissance parfaite des sources d'excitation. Celles-ci , ainsi que les temps d'essais, peuvent être choisis arbitrairement, tout en restant cependant dans des limites acceptables de similitude.

Les essais qualificatifs doivent permettre l'estimation de la vie en fatigue acoustique d'éléments réels ou d'éprouvettes représentatives, en tenant compte au maximum des conditions d'excitation de l'avion étudié.

B. NIVEAUX D'EXCITATION

Essais sélectifs : la finalité de ces essais est d'obtenir la rupture des éprouvettes. Une méthode consiste à choisir un niveau de bruit supérieur à celui mesuré ou estimé sur l'avion intéressé. Généralement, un niveau global de 6 dB supérieur au niveau réel est choisi, ce qui se traduit par une multiplication par deux environ des contraintes dynamiques.

Une autre méthode consiste à effectuer H heures d'essais au niveau réel N
H heures d'essais au niveau .... N + 3 dB
H heures d'essais au niveau .... N + 6 dB

Elle permet de cerner d'une manière plus fine que dans le cas précédent, l'initiation des dommages.

D'autres combinaisons sont possibles. L'art de l'expérimentateur est justement de choisir la meilleure en fonction des qualités escomptées de ses structures.

Essais qualificatifs : pour ces essais, il est souhaitable de choisir comme niveau global d'excitation le maximum atteint ou escompté au cours de la mission type de l'avion considéré. Comme on verra plus loin, il sera alors nécessaire d'établir une relation entre les temps d'essais et les temps de vol.

C. SPECTRE D'EXCITATION

Essais sélectifs : pour ces essais, il est recommandé de reproduire le spectre d'excitation réel. Cela n'est pas toujours possible. A défaut, un spectre à niveau sensiblement constant dans la gamme des fréquences de résonance des structures étudiées est acceptable.

Essais qualificatifs : la connaissance du spectre d'excitation dans la zone intéressée de l'avion et sa reproduction la plus fidèle possible par les moyens d'essais, sont indispensables à la bonne représentativité de l'expérimentation, surtout si l'analyse montre que le spectre est riche en fréquences discrètes.

D. DUREE DE L'ESSAI

Essais sélectifs : les essais sont conduits en général, jusqu'à rupture des éprouvettes, ce qui arrive fréquemment. Etant donné les conditions sévères auxquelles elles sont soumises. Si la rupture ne se produit pas et si les contraintes dynamiques mesurées en cours d'essais sont relativement stables, il est peu probable que des dommages se produisent après cent heures d'endurance. Cette limite peut être raisonnablement fixée pour des essais sélectifs.

Essais qualificatifs : le problème est plus complexe, car il s'agit de fixer une vie en fatigue acoustique de la structure acceptable en exploitation. Tout réside dans l'équivalence heures d'essais - heures de vol. Pour certains avions, cela est relativement facile à définir. Prenons par exemple le cas du CONCORDE et reportons-nous à la figure 1. Cette image montre que pendant le point fixe et le décollage, soit 1 minute environ, il existe des pressions sonores de plus de 15 dB, supérieures à celles engendrées au cours des autres configurations de vol.

Les contraintes dynamiques dues aux excitations acoustiques sont faibles par rapport aux contraintes statiques. Elles se situent au voisinage de la limite de fatigue du matériau. Il en découle que des structures définies pour résister à des pressions aléatoires de niveau N ne sont pratiquement pas affectées par des niveaux de 10 dB inférieurs.

D'où, pour CONCORDE, l'équivalence :

- 1 minute d'essai avec niveau de bruit global correspondant au régime max réacteur ≈ 1 vol

- 1 heure d'essai avec niveau de bruit global correspondant au régime max réacteur ≈ 60 vols

- 400 heures d'essai avec niveau de bruit global correspondant au régime max réacteur = 24000 vols, soit la vie de l'avion, facteur de dispersion non compris.

Pour d'autres types d'avion, où les différentes sources d'excitation ont des niveaux du même ordre, l'équivalence est beaucoup plus difficile à établir. Par exemple, pour CARAVELLE, il n'a pas été possible de réaliser à priori, une équivalence "essais jet-noise - heures de vol". Celle-ci n'a pu être estimée qu'à postériori en établissant une relation entre les dommages relevés sur un certain nombre d'éléments d'avions en service, et ceux détectés sur les éléments similaires essayés à la fatigue sonore. Cette équivalence varie d'ailleurs d'un élément à un autre. Elle était par exemple de :

$$1 \text{ H d'essai} \sim 35 \text{ heures de vol sur le saumon de plan fixe}$$
$$1 \text{ H d'essai} \sim 10 \text{ heures de vol sur le volet de profondeur}$$

E. DEFINITION DES EPROUVETTES

Essais sélectifs : les éprouvettes doivent être la copie fidèle des solutions structurales étudiées. Le moindre détail a son importance. Leurs dimensions devront être suffisantes pour obtenir des réponses dynamiques réalistes. Si la structure étudiée comporte des cadres et lisses formant maillage, l'éprouvette devra en posséder plusieurs, afin d'éliminer les conditions limites et de ne considérer pour l'exploitation des résultats, que les mailles centrales. La comparaison de différentes solutions structurales n'est vraiment probante que si les éprouvettes de chacun des types étudiés ont des masses unitaires équivalentes.

Essais qualificatifs : les éprouvettes seront, si possible, des éléments "grandeur" (gouverne par exemple), de manière à ne pas négliger les formes propres d'ensemble, sur lesquelles se superposent les vibrations de maillon. A défaut d'éléments réels, choisir toujours des éprouvettes dont les dimensions les plus grandes possibles, seront compatibles avec l'installation d'essais.

F. MOYENS D'ESSAIS

Plusieurs moyens d'essais peuvent être utilisés comme source d'excitation :

a) réacteurs : pour simuler un bruit de jet, la source d'excitation la plus réaliste est, bien sûr, le réacteur de l'avion étudié. Ce type d'installation bien que séduisant, présente cependant des inconvénients : prix d'achat et d'entretien élevés, limitation de niveau de bruit, souplesse d'utilisation, etc ...

b) générateurs de bruit à haut niveau sonore : ces générateurs permettent de réaliser en laboratoire des ambiances acoustiques à niveau sonore élevé, simulant aussi bien les spectres de bruit des jets, que ceux des écoulements aérodynamiques tourbillonnaires. Quel que soit le générateur utilisé : sirène, haut-parleur, etc ..., une installation d'essai d'ambiance acoustique à haut niveau sonore peut se représenter par le schéma ci-dessous :

chambre réverbérante

adaptateur

générateur de bruit

tunnel a ondes progressives

adaptateur

veine guide d'ondes

chambre réverbérante
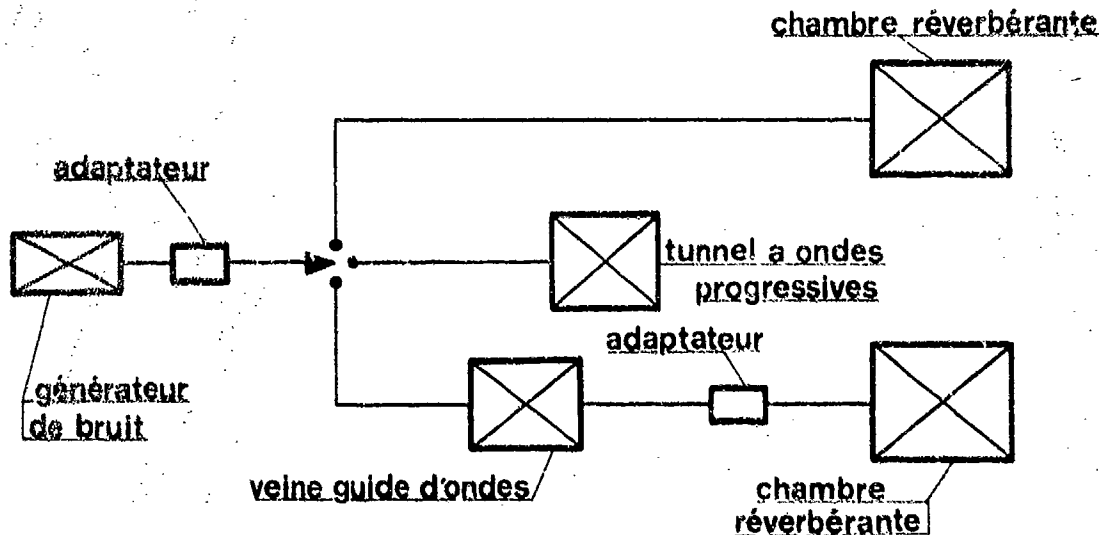
- la chambre peut être entièrement réverbérante ou comporter une terminaison absorbante.

- les tunnels à ondes progressives sont constitués par une partie servant de chambre d'expérimentation suivie d'une deuxième partie absorbante.

Les dimensions des chambres et tunnels sont variables. Les niveaux sonores dépendent des dimensions et du générateur.

Configurations d'essais :

Pour les essais acoustiques, plusieurs configurations peuvent être adoptées.

a) incidence normale
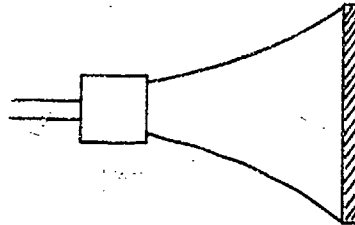
b) incidence rasante
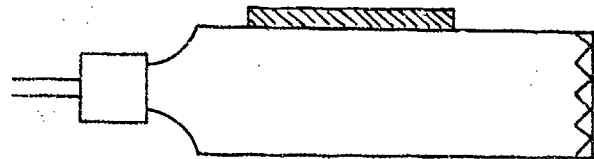
c) chambre réverbérante
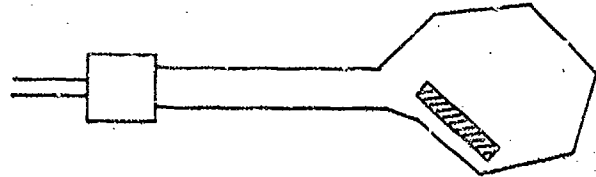
- l'incidence normale : dans cette configuration, l'éprouvette ferme totalement le pavillon et la réflexion du bruit sur la structure produit un renforcement de la pression et par conséquent, une plus grande intensité sur l'éprouvette pour des conditions données du générateur. Ceci a pourtant un inconvénient majeur dans le fait qu'une résonance due au couplage structure-pavillon peut se produire.

- l'incidence rasante : là, la possibilité de couplage n'existe plus mais le renforcement des pressions est supprimé. Les niveaux sont inférieurs de 5 à 6 dB aux précédents.

- la chambre réverbérante : dans cette configuration, le bruit excite l'éprouvette en incidence aléatoire. Pour de nombreux techniciens de l'Aéronautique, cette configuration est la plus réaliste.

Comme on le voit, chaque solution présente avantages et défauts.

C'est à l'expérimentateur de bien connaître son installation pour en atténuer les inconvénients et à en tirer le maximum d'avantages.

C. PROCESSUS D'ESSAIS

Le processus classique d'un essai acoustique est le suivant :

- essai de résonance
- essai de réponse
- essai d'endurance

a) essai de résonance : cet essai a pour but de définir le comportement dynamique de la structure étudiée :

- fréquences de résonances,
- formes propres,

dont la connaissance est très utile dans beaucoup de cas, pour expliquer l'origine des dommages obtenus au cours de l'essai d'endurance.

b) essai de réponse : l'éprouvette est placée dans le champ sonore d'un réacteur de l'avion étudié. Sa position par rapport à la source de bruit est identique à celle occupée sur avion par la structure intéressée.

- un micro, placé à quelques centimètres de la structure, enregistre le bruit dont l'analyse permet de définir le spectre d'excitation

– des jauges extensométriques, collées sur la structure en des points caractéristiques, permettent d'enregistrer la réponse dynamique des structures (spectre, niveau de contraintes).

Ces paramètres : niveau et spectre d'excitation,
niveau et spectre de réponse,
servent de référence à l'essai d'endurance.

c) essai d'endurance : quel que soit le générateur et l'installation acoustique utilisée, la première phase de l'essai d'endurance consiste à reproduire les spectres d'excitation et de réponse mesurés au cours de l'essai de réponse. Cette opération, souvent assez longue, n'est réglée que par des lois empiriques. Elle demande de la part de l'expérimentateur une bonne connaissance de son installation d'essai.

La figure 2 montre le spectre de bruit (analyse en 1/3 d'octave) relevé à 50 mm d'une structure excitée par un réacteur simple flux et sa reproduction, sur la même structure, dans la chambre réverbérante d'une installation à hauts niveaux sonores.

Figure 3 : de la même manière, la figure 3 montre la réponse d'une jauge.

Comme on le constate, la reproductibilité des phénomènes réels peut être assurée par une installation à hauts niveaux sonores et l'essai d'endurance entrepris avec le maximum de garanties. Des contrôles fréquents, au moins toutes les quinze minutes pendant les premières heures d'essais sont absolument indispensables. Trop confiants des expérimentateurs ont eu la désagréable surprise de trouver leur éprouvette en fort mauvais état après des temps d'essais très courts

5. CONCLUSION

Vingt minutes ne permettent que de brosser un tableau très schématique de ce que peut être la recherche expérimentale de la tenue des structures à la fatigue acoustique.

Les quelques règles énoncées ne doivent être considérées que comme une trame sur laquelle chaque cas particulier peut être adapté.

Plus qu'à de grandes théories, la réussite d'un essai sera due aux moyens mis en oeuvre et au bon sens des expérimentateurs.

Les installations à hauts niveaux sonores sont de merveilleux moyens d'investigation qui mettent en évidence les moindres défauts d'échantillonnage ou de conception des structures.

Les profits qui en résultent sont grands et permettent sur les structures fortement sollicitées dynamiquement d'éviter bien des déboires en exploitation.

REPARTITION DES EXCITATIONS
AU COURS D'UN VOL

NIVEAU D'EXCITATION

REACTEURS

TOURBILLONS

TOURBILLONS

COUCHE LIMITE

1   34'   2ᴴ30'

TEMPS
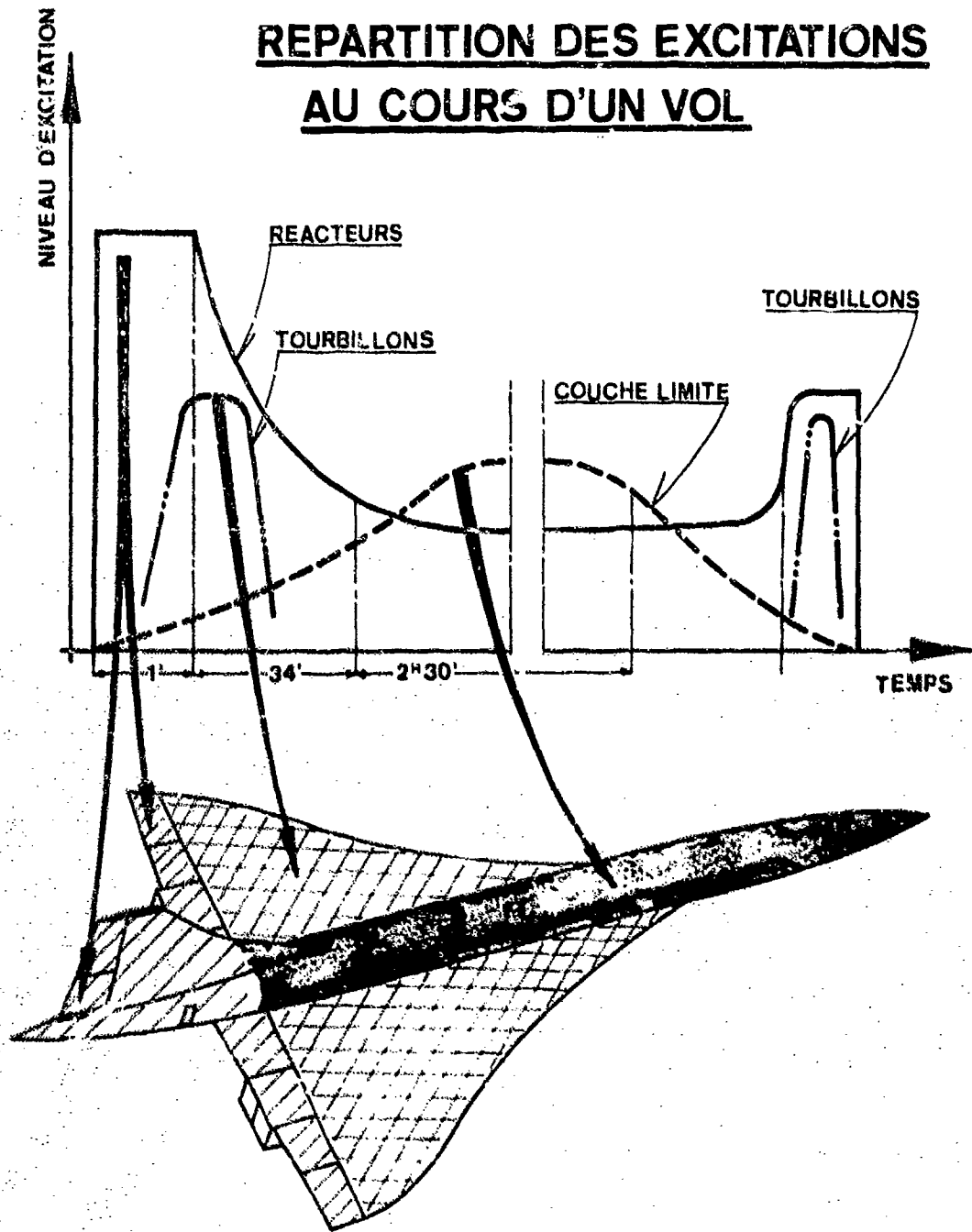
FIGURE 1

SPECTRES RELEVES A 50ᴹᴹ D'UNE STRUCTURE
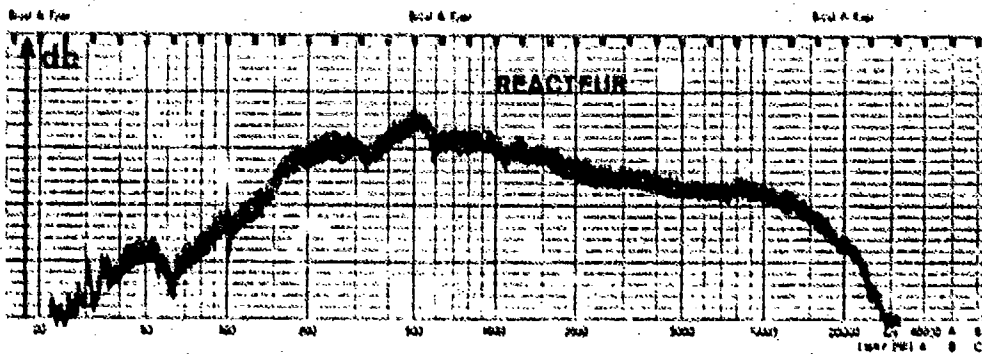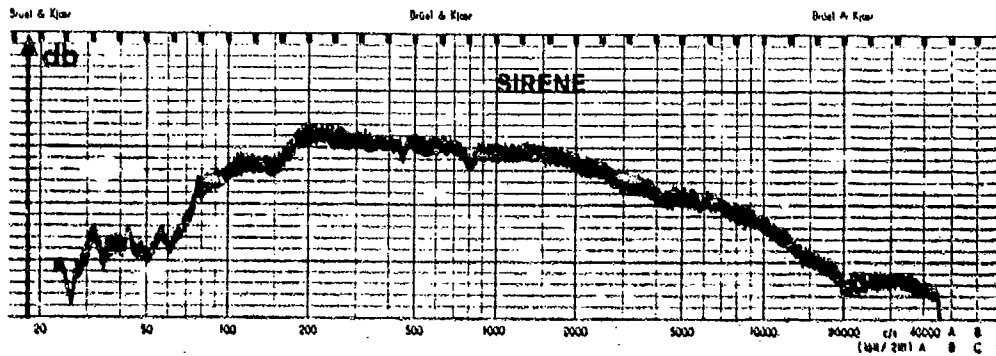
FIGURE 2

CONTRAINTES RELEVEES SUR UNE STRUCTURE

EXCITATION PAR SIRENE

EXCITATION PAR REACTEUR
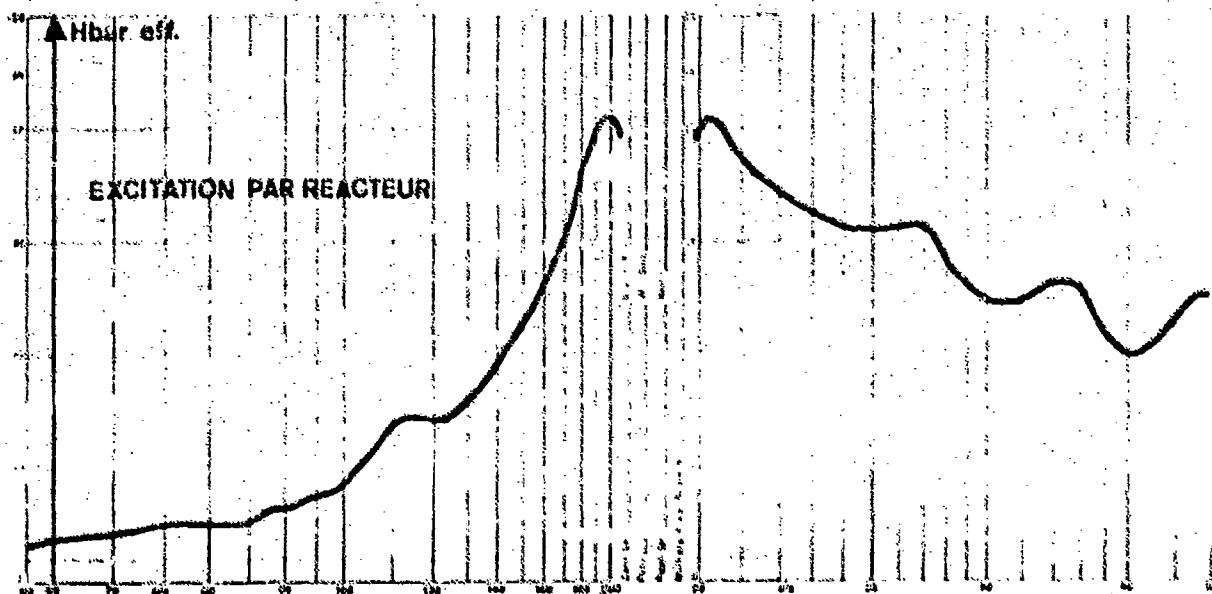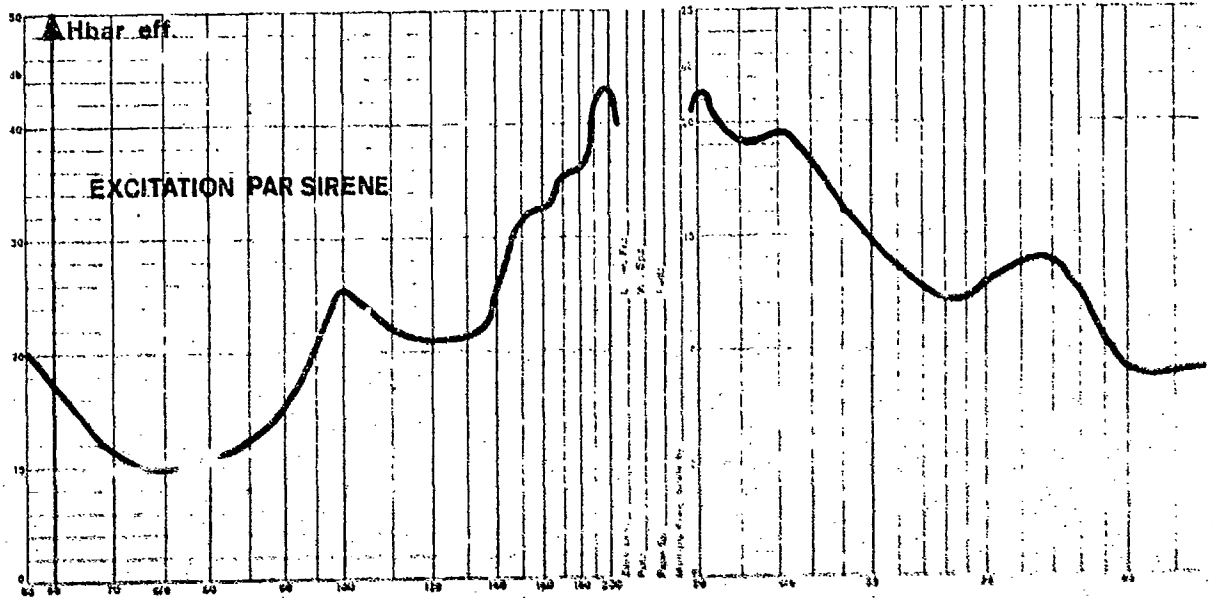
FIGURE 3

SESSION 2   DISCUSSION - RESPONSE OF STRUCTURES

Mr. Coe was asked several questions relating to the analysis techniques and instrumentation which he had used.   He replied that the excitation spectra had been analysed on a hybrid system. It was essentially an analogue system incorporating true integration to give the required statistical accuracy.   Digital control logic was used to change the integration time, frequency bandwidth, and to control the centre frequency stepp' ;.   Th bandwidth was increased from 2 Hz at low frequencies to 800 Hz at 20,000 Hz. The output was in digital form. The strain data were analysed on the General Radio Time Data System. Smoothing wa not used so that the absolute magnitude of the peaks in the spectra could be estimated more accura.ely. The overall strain levels were measured independently and found to agree with the integrate' spectra to withi: 20%

Dr. Lindberg was asked several questions about the computational procedures which he had used. He replied that he had considered four sub cases of symmetry with different boundary conditions in order to obtain all the lower order modes.   He had neglected inplane inertias.   Matrix condensa-tion and eigenvalue economisers had been used to reduce the problem down to about 50 degrees of freedom.   The running time on the IBM 360/6' machine was in the range 3 to 7 minutes with the eigenvalue extraction procedure taking up most of the time. No advantage had been taken of the repetitive nature of the structure to reduce the number of degrees of freedom. A sub structure analysis could have been used to give some saving in computer time but this could not give the time savings of the Wittrick method or the wave propagation method of Dr. Mead. He had not yet done the calculations necessary to determine the effect of curvature on the mode shapes but he did not think that anything dramatic would happen.   Questioned on details of his representation, Dr. Lindberg replied that he had used a T beam representation of the stringer. He had included 9% of the width of the panel with the flange of the T beam and found that this gave good agreement with the experimental results. He also said that he had not yet made any estimations or measurements of stress response. Mr. Bayerdorfer referred to the Vernier work which showed that the ratio of stress in the skin at the middle of the stringer and frame attachment lines changes very significantly with curvature. Dr. Lindberg had not yet studied this effect.

Mr. Bacon was asked if he had compared the structural efficiencies of built up and honeycomb structures designed to resist acoustic fatigue. He replied that the choice had been done on the basis of design for static loads rather than acoustic fatigue.

Mr. Kirkby questioned Mr. Cay on the philosophy of the qualification testing described in the paper. The test times used do not a,ear to allow for scatter in fatigue performance. Mr. Cay replied that he had tested at higher noise levels and used a factor of 3 on life. Mr. Coe commented on the possibility of interaction between the structural vibration and fluid flow at transonic speeds. This could cause a much reduced damping and hence higher stress levels as the aircraft passed through the transonic flight regime.

DESIGN DATA FOR ACOUSTIC FATIGUE

by

A.G.R. Thomson   and   R.F. Lambert

Engineering Sciences Data Unit Ltd
251-259 Regent Street, London W1R 7AD

SUMMARY

The AGARD Cooperative Project on Acoustic Fatigue Data Sheets is described and the items prepared under Phase 1 of the Project are discussed with particular reference to their basis and derivation. Areas where additional research is needed to improve the data sheets are highlighted. An Appendix gives a derivation of simplified equations used in the data sheets for estimating the natural frequencies of honeycomb panels.

1 INTRODUCTION

This paper describes the acoustic fatigue data sheets prepared by ESDU under the AGARD Cooperative Project on Acoustic Fatigue Data Sheets and amplifies some points of their history and technical basis.

The Engineering Sciences Data Unit of the Royal Aeronautical Society has for many years produced evaluated data for use in many fields of engineering design, including aircraft fatigue. During this period a technique of preparing authoritative design data and methods has been developed whereby a permanent technical staff work with the guidance and advice of specialist voluntary working groups drawn from industry, universities and research establishments. This technique is designed to ensure as far as possible that the topics chosen for data sheet treatment are relevant to design needs, both in content and method of presentation, that the methods presented are technically sound and that relevant and up-to-date research information and practical experience are fully taken into account in their preparation. The information thus produced is presented in a form aimed at convenient design use, omitting unnecessary detail, and attempting to cover the full practical range of design variables, but pointing out limitations in the validity of the data where appropriate.

2. DEVELOPMENT OF THE AGARD COOPERATIVE PROJECT ON ACOUSTIC FATIGUE DATA SHEETS

In 1965 some acoustic fatigue specialists in the U.K. approached the Royal Aeronautical Society to enquire into the possibility of preparing data sheets on acoustic fatigue as part of the well established series on conventional fatigue that had been started in the 1930s. The Society's Fatigue Committee, after studying the possibilities, undertook to prepare an initial batch of acoustic fatigue data sheets provided that the work did not interfere too much with progress on their heavy programme of work on conventional fatigue problems. Accordingly the R.Ae.S. Acoustic Fatigue Panel was formed to carry out the task.

The procedure for design of components liable to acoustic fatigue was envisaged schematically as shown in Figure 1. Not all areas of the design procedure are amenable to data sheet treatment, but much of the part enclosed by the shaded line in Figure 1 contains subject matter which requires quantitative analysis by methods which had by the mid-sixties become sufficiently well evaluated to be consolidated into convenient data sheet form. A pattern emerged of classifying suitable data sheet material into one or other of the following categories.

LOADING ACTIONS e.g. sound pressure levels due to jet noise
NATURAL FREQUENCIES of various idealised component geometries
STRESS RESPONSE of these components to a given loading action
FATIGUE LIFE ESTIMATION of various component parts
MISCELLANEOUS e.g. introductory material, general definitions, conversions of units etc.

The R.Ae.S. Acoustic Fatigue Panel drew up a programme of data sheet work on those lines and although ESDU Staff could not, at that time, provide much assistance from resources which were already stretched by a heavy programme of conventional fatigue work, due to the enthusiasm and hard work of the Acoustic Fatigue Panel an initial group of eleven Data Items was prepared, approved by the Fatigue Committee and issued in just two years from the original suggestion for the work. A further three items were issued a year later.

At the same time the AGARD Structures and Materials Panel had been concerned with activities in acoustic fatigue since 1960 and had achieved considerable success in coordinating and encouraging acoustic fatigue research in the NATO Nations. By 1960

the Panel's Specialist Group on Design in Acoustic Fatigue, under the Chairmanship of the Panel's Coordinator in Acoustic Fatigue, Professor B.L. Clarkson, was able to report during the 28th Panel Meeting in Dayton the identification of six subject areas in which sufficient research results had been accumulated of a suitable kind to warrant their immediate consolidation and presentation in design data sheet form.

Arising from this a project was initiated under which ESDU agreed to revise and extend the existing data sheets with the support and collaboration of AGARD. The project was to be managed by a collaborative structure as shown in Figure 2 and was to be carried out in two phases.

The subjects chosen for the first phase of the project were

(a)   Jet noise near field prediction

(b)   Stress response of flat stiffened panels

(c)   Stress response of curved stiffened panels

(d)   Natural frequencies of flat and curved honeycomb panels

(e)   Stress response of honeycomb panels

(f)   Random S-N curves for light alloys

Data Sheets on the first three of these were issued as AGARDograph-162 Part 1 in May 1972, and the remainder have been completed and are scheduled for publication in the Autumn of 1972. The design information arising from Phase 1 is discussed in the following sections.

3.   NEAR-FIELD JET NOISE ESTIMATION

Several methods of estimation of near-field jet noise were already available and a choice from these was made in the light of a comparison (Reference 16) of the predictive accuracy of four of the most widely used techniques. The near-field noise contours predicted by each method were compared with results from recent full scale and hot model tests representative of current-technology engines. The comparison was made on the basis of both shape of the contours, judged subjectively, and the magnitude of the noise levels.

Two of the methods, namely the existing R.Ae.S. data sheet method and the method developed by H.E. Plumblee at Lockheed-Georgia which were developed in the late 1960s, gave significantly better predictions, not surprisingly, than methods developed a decade earlier at WADC and Rolls-Royce. The R.Ae.S. method gave good predictions particularly at low axial distance from the jet nozzle, and gave contour shapes in closer agreement with the test results than Plumblee's method and did not require the use of a computer for the predictions. Accordingly the existing R.Ae.S. method was amended, to indicate its limitations more thoroughly, and adopted for the AGARD data sheets in Section 2   Reference 1.

However it is considered that Plumblee's method could be further developed to give significantly better predictions than the other methods examined as it is more soundly based theoretically, and has considerable flexibility in varying the coefficients in the basic equations used. One line of development that has been suggested is to modify the method to use an extended or multiple source rather than a point source.

The R.Ae.S. method is empirically based on a set of reference near-field noise contours and spectra compounded at a datum jet velocity and density using measurements available in 1967 from several different engines. The reference levels thus obtained are corrected for the actual jet velocity using a space and velocity dependent velocity index derived empirically and given in graphical form. A correction for jet temperature is made by way of jet density in the usual way. Further corrections are suggested for reflections from adjacent surfaces. The spectrum shapes are assumed to vary axially but not radially.

The method allows calculation of spectrum levels at a given point in the near field very quickly and with acceptable accuracy but it would be useful to supplement it at a later date with a computer program to give the complete field. Further work is required to improve the accuracy of prediction under reheat conditions.

4.   NATURAL FREQUENCIES OF SKIN-STRINGER PANELS

In a preliminary estimate of stresses in the skin of acoustically excited skin-stringer panels it is normally sufficient to consider vibration only in the 'stringer-bending' mode of the complete panel, in which individual plates may be assumed to vibrate in their fundamental fixed-edge mode. However interpretation of experimental results, or more complete analysis of skin-stringer panels calls for a detailed knowledge of the frequencies of the many modes of vibration of the complete panel, for example those shown in Figure 3. The calculation of these modes in the general case

is arduous, but fortunately many examples of panels in aircraft structures may be regarded as periodic, i.e. consisting of a side-by-side assemblage of identical plate/ stiffener elements. In this case the calculations can be considerably simplified, using a wave approach, as shown by Mead and Sen Gupta (Reference 4). This method has been adapted into data sheet form in Section 3 of Reference 1, employing a modified form of presentation of the design curves which avoids the need for graphical construction inherent in the source references.

The design curves in the data sheet were computed by ESDU using the University of London Atlas computer.

5.   NATURAL FREQUENCIES OF SINGLY-CURVED PANELS

Section 4 of Reference 1 gives a method of calculating the natural frequencies of rectangular singly-curved plates with simply-supported or fully fixed edges.

For the simply-supported case, the natural frequencies are obtained from the exact solution of the simplified equation of motion given by Flügge (Reference 6). In simplifying the equations of motion the panels are considered to be thin and shallow and shear deflection and rotory inertia terms are neglected.

Webster's double power series method is used for the fixed edge case. The method of solution, based on the Rayleigh-Ritz method, is described in Reference 7. The accuracy of the solution depends on the number of terms used in the power series and this is generally limited by the computer store available and computing costs. It is further limited by the fact that the equations may become ill-conditioned as the number of terms is increased. The design curves in Reference 1 were computed by ESDU using a program provided by Nottingham University which was modified to run on the University of London Atlas computer. The number of terms used in the power series was increased (generally up to four terms in each direction) until the change in predicted frequency was small enough to be insignificant for general design purposes.

As fixed-edge plate mode shapes do not have definable numbers of half-waves in the two principal orthogonal directions, modes are identified by the symmetry or anti-symmetry in each of the principal directions across the panel. Representative computed mode shapes are illustrated in the data sheet in the form shown in Figure 4.

6.   STIFFENED PANEL STRESS RESPONSE TO ACOUSTIC LOADING

Design data in Section 5 of Reference 1, giving root mean square stresses in stiffened panels, are based on a simple unimodal response theory. It is assumed that the individual plates in the panel vibrate predominantly in their fundamental fixed-edge mode. This restricts the use of the data to panels where the stiffeners are sufficiently rigid in bending to give approximately fixed-edge conditions for individual plates. It is further assumed that the pressure is uniform and in phase over the whole of an individual plate, and that the spectrum level of acoustic pressure is constant over the frequency range close to the fundamental natural frequency of the panel. .

The r.m.s. stress at the middle of the rivet-line along the longer edge is obtained directly from a nomograph. The stress at the rivet line was chosen as the reference stress because failures generally originate at that position and it usually corresponds with, or is sufficiently close to, the failure line position at which S_{rms}-N data are available from coupon tests for life estimation.

Guidance is given on applying a factor to obtain approximate root mean square stresses in the case of control surfaces, and other box-type structures, where two plates are joined by ribs. It is intended to extend the method to such structures using a more refined approach in Phase 2 of the Cooperative Project.

The accuracy of the method was assessed by comparison with the limited available measured data, using a typical value of structural damping ratio of 0.017. For flat panels the estimated stress values were within a factor of two either way of the measured values, but for curved panels the data tended to overestimate stress.

A comparison of estimated and measured rivet line stresses for aircraft tailplanes and control surfaces showed that for root mean square stresses below 100 MN/m^2 the predictive accuracy is of the same order as found for flat panels. Above this stress level the theory tends to underestimate the measured stresses. In estimating the box structure stresses the panels were assumed to be flat since curvature was small and varied over the panel surface.

7.   RANDOM LOADING S-N CURVES FOR ALUMINIUM ALLOYS

The random loading S-N data given in Section 1 of Reference 2 are a compilation of available experimental results obtained from reversed bending tests on coupon specimens subjected to narrow band random loading. Because of the limited amount of data available a meaningful statistical analysis is not possible. Data are grouped according to specimen type, rivet type and material specification and a least-squares line is drawn through each set of data.

The only data available in sufficient quantity for guidance in design against acoustic fatigue are from reversed bending tests about a zero mean stress. In the absence of test data it is recommended that allowances for variation of mean stress be made using constant amplitude fatigue data replacing alternating stress values by root mean square values. Data for correction for mean stress variation for constant amplitude loading may be found in Reference 6.

Only test data for aluminium-copper alloys has been included in the AGARDograph. Some data were available for aluminium-zinc alloys (D.T.D. 687 and 7075) but were not included as these materials have poor crack propagation properties, compared with aluminium-copper alloys, which make them generally less suitable for use in an acoustic environment, although the life to first crack in these aluminium-zinc alloys is similar to that for aluminium-copper alloys.

Some data from push-pull tests were available (References 7 and 8) but these also were not included. A comparison between reversed bending and push-pull data did not show the expected trend of lower lives, at a given stress level for the push-pull tests. This trend was expected since in axial loading tests the volume of material stressed to a maximum is much greater than in reversed bending tests, hence there is a higher probability of a flaw being present in the highly stressed region.

Data are given in the AGARDograph for three types of specimen, representative of sheet alloy in bending without stress concentration, riveted-skin joints and rib-flange connections.

During the initial stages of data correlation for riveted-skin specimens the reference stress was taken at the rivet line. Because of different types of construction, and consequent differences in stress concentration factors in the rivet area, it was not possible to obtain agreement between results from different test facilities by this method and it was found necessary to use the stress at the failure line as the reference stress.

When comparing random loading S-N data from different sources, differences in testing technique contribute to considerable scatter. One of these differences is in the definition of failure which is usually detected by changes in resonant frequency and damping. A further difference is in the definition of number cycles to failure which may be the number of positive peaks or the total number of zero crossings with positive slope or, in narrow-band tests, the product of the test specimen resonant frequency and the time to failure.

In random vibration fatigue tests the applied load spectrum is truncated to a prescribed factor of the r.m.s. The stress truncation level for data presented in the AGARDograph varied between ± 3 and ± 4.5 times the root mean square value. This range accounts for some of the scatter and perhaps much of the discrepancy between results from different laboratories. Further work in quantifying the effect appears to be necessary.

Because of the scatter in test results and possible differences in test methods it would be useful to check to what extent the test facilities and test technique affects the scatter in data. This could be done by testing a number of specimens, made by one manufacturer to a standard specification from the same batch of material, in each test facility.

8. NATURAL FREQUENCIES OF SANDWICH PANELS

Section 2 of Reference 2 gives graphs and a nomograph for estimating the natural frequencies of flat or curved sandwich panels with cores of zero flexural stiffness. For practical purposes cores of honeycomb, expanded plastic, end-grain balsa etc. can be regarded as having zero flexural stiffness, and the data have been derived with honeycomb cores primarily in mind. The data were based on Jacobson's work (Reference 11), but some simplifications and extensions were made that warrant further explanation here. Details are given in Appendix A. The rather complicated equations obtained by Jacobson (Equations 16, 17 and 18 of Reference 8) for the natural frequency of a simply-supported curved sandwich panel, in which the face plates carries all the bending moment and an orthotropic core carries all the shear load, can be broken down to the form:

$$f = f_u C_1 \left(C_2^2 + C_3 C_4 \right)^{1/2} \qquad (8.1)$$

where f is the natural frequency of the sandwich panel and f_u is a reference

natural frequency, taken as that of a solid panel of the same density and Young's modulus as the sandwich panel face plates and of thickness equal to the distance between the mid-planes of the face plates. The factor C_1 is a function of core and

faceplate thicknesses and densities and takes account of the differences in stiffness and density of the sandwich panel and the reference model. The parameter C_2 takes

account of the shear flexibility of the sandwich panel, while C_3 is a function of

aspect ratio in a curved panel and C_4 a function of the curvature.

Broken down into this form, the frequency f_u can be obtained from existing data sheets, while C_1, C_2, C_3 and C_4 can each be presented in simple graphical form and the frequency of the sandwich panel thus obtained from Equation 8.1.

The method of prediction for flat panels has been validated for aluminium alloy honeycomb panels using experimental data by Ballentine (Reference 12). The comparison between calculated and measured frequencies is shown in Figure 5. The panels tested had reduced thickness edges, and in calculating the frequencies it was assumed that the edges were simply-supported at the attachment lines. The finite rotational stiffness at the edges can account for the general slight underestimate of frequency. Taking the ratio of bending stiffnesses at the edge and at the full section (for panels of similar design) as a measure of rotational restraint at the edges, Figure 6 shows the effect of rotational restraint quite distinctly. Nevertheless the results do confirm that it is sufficiently accurate for design purposes to assume simple-support conditions at the edges of honeycomb panels with reduce thickness edges unless heavy doublers are used at the edges or the face-plates are abnormally thick compared with the panel depth.

It may be noted from Figure 5 that the frequencies in the (1,2) mode are distinctly underestimated compared with those in the (2,1) mode. Examination of the individual test results suggests that the effect of core orthotropy may be insufficiently accounted for in the theory e.g. experimental frequencies for the (2,1) and (1,2) modes in a given square panel differed more than could be explained by the difference between shear moduli in the two directions. This point may warrant further investigation when very accurate estimates of natural frequency are required, but the discrepancies are not though to be significant in the context of acoustic fatigue life estimation.

9.   SANDWICH PANEL STRESS RESPONSE TO ACOUSTIC LOADING

Design data for the stress response of sandwich panels under the action of jet noise given in Section 3 of Reference 2 are also based on Jacobson's work (Reference 11). In this theory unimodal response is assumed. Other basic assumptions are uniform spectral density of acoustic pressure over the panel, facing plates of equal thickness, shallow curvature and simply-supported edge conditions.

The response mode for both flat and curved panels is taken to be the fundamental mode having one half wave in each of the principal directions across the panel. The unimodal response assumption restricts the range of applicability of the design data to cases where the fundamental frequency is well separated from the higher mode frequencies. This condition is best satisfied when panels are flat and square. Further tests are required to determine the accuracy of the theory for panels of aspect ratio greater than 2.0 and for all ranges of panel curvature.

The data give an estimate of stress at the panel centre. The stresses at the edges are dependent on detail design of the edge attachments. For typical panels with reduced thickness edges there is an additional factor illustrated in Figure 7 which should be considered when estimating panel centre stresses.
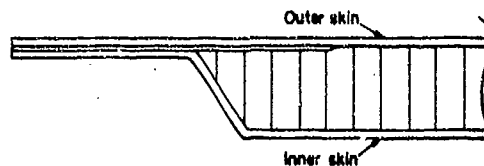
TYPICAL REDUCED THICKNESS PANEL EDGE

In the basic theory the panel is assumed to be supported at the neutral axis and midplane, or membrane stresses which would occur if the supports were rigid in the plane of the panel are quite negligible for deflections of the magnitude induced acoustically. However if the panel is supported rigidly in translation in the plane of one of the face-plates, as in the usual panned configuration, Sweers (Reference 13) has suggested that the situation is quite different. The in-plane stress due to deflection remains insignificant, but now the outer face plate strain is constrained to zero for supports rigid in translation. This results in a relief of stress in the centre of the outer face plate and an increase of stress in the inner face-plate. Experimental evidence for this effect is conflicting, but it seems clear that the ratio of stresses in the inner and outer face plates will depend quite strongly on the degree of in-plane restraint of the support, and this could account for observed discrepancies between data from different sources.

If this effect really does exist to any marked extent it is important and deserves further investigation.

10. CONCLUSIONS

To date eight data sheets for design against acoustic fatigue have been prepared, completing Phase 1 of the AGARD Cooperative Project on Acoustic Fatigue Data Sheets. Work is in hand in the preparation of further design data under Phase 2 of the Project which will deal with

(a) Near-field compressor noise prediction

(b) Natural frequencies and stress response of stiffened panels with stringers of low bending stiffness

(c) Natural frequencies and stress response of box and control surface structures

(d) Structural damping

(e) Random S-N curves for titanium alloys.

Users of the data are encouraged to advise the Engineering Sciences Data Unit of their experiences in using the data and to draw attention to any additional information which may be of value in future extensions and amendments.

11. REFERENCES

1. Thomson, A.G.R.
   Lambert, R.F.
   Sen Gupta, G.
   Acoustic fatigue design data – Part 1.
   AGARD-AG-162 – Part 1, 1972.

2. Thomson, A.G.R.
   Lambert, R.F.
   Acoustic fatigue design data – Part 2.
   AGARD-AG-162 – Part 2, 1972.

3. Riley, M.P.
   Near-field jet noise prediction techniques.
   British Aircraft Corporation Ltd, Acoustic Laboratory
   Report A.R. 324, 1971.

4. Mead, D.J.
   Sen Gupta, G.
   Wave group theory applied to the response of finite
   structures. Conference on Current Developments in
   Sonic Fatigue, I.S.V.R., Southampton University,
   July 1970.

5. Clarkson, B.L.
   Stresses in skin panels subjected to random acoustic
   loading. J.R. Aeronaut. Soc., Vol.72, No.695,
   pp.1000-1010, November 1968.

6.   –
   The effect of mean stress on fatigue strength.
   Engineering Sciences Data Item Nos. A.00.01 and
   A.00.02, March 1963.

7. Williams, T.R.G.
   Fatigue under sinusoidal and narrow-band random
   conditions. J. Sound Vib., Vol.11, No.2, pp.251-261,
   February 1970.

8. Williams, T.R.G.
   Sova, J.A.
   Studies of fatigue damage in aluminium alloys.
   J. Sound Vib., Vol.16, No.2, pp.283-291, May 1971.

9. Flügge, W.
   Stresses in shells. p.219. Springer-Verlag, Berlin,
   1960.

10. Webster, J.J.
    Free vibrations of rectangular curved panels.
    Int. J. Mech. Sci., Vol.10, No.7, pp.571-582, July 1968.

11. Jacobson, M.J.
    Stress and deflection of honeycomb panels loaded by
    spatially uniform white noise. AIAA Journal, Vol.6,
    No.8, pp.1503-1510, August 1968.

12. Ballentine, J.R.
    et al.
    Refinement of sonic fatigue structural design criteria.
    AFFDL-TR-67-156, 1967.

13. Sweers, J.E.
    Prediction of response and fatigue life of honeycomb
    sandwich panels subjected to acoustic excitation.
    Acoustic fatigue in aerospace structures.
    Syracuse University Press, 1965.

14.   –
    Natural frequencies of uniform flat plates.
    Engineering Sciences Data Item No. 66019, 1966.

FIGURE I.

AGARD STRUCTURES AND
MATERIALS PANEL

WORKING GROUP ON
ACOUSTIC FATIGUE

Chairman: Mr A.H.Hall

Finance
Overall approval

Set scope, programme of work,
format and vetting as required

SPECIALIST GROUP ON
DESIGN IN ACOUSTIC FATIGUE

Chairman: Prof B.L.Clarkson

NATIONAL COORDINATORS					
Canada	France	Germany	Italy	UK	US

Provide basic data in the form of
laboratory reports and source liaison
as required; comment on drafts

R.Ae.S.
Acoustic
Fatigue
Panel

Chairman:
Prof B.L.Clarkson

E S D U

1. Collect basic data from Contact Men and world
   literature

2. Analyse basic data to Specialist Group programme

3. Prepare draft Data Sheets

4. Present drafts to R.Ae.S. Acoustic Fatigue Panel and
   discuss

5. Present finalised drafts to Specialist Group and discuss

6. Arrange printing of final Data Sheets

FIGURE 2   MANAGEMENT OF PROJECT

Mode 1
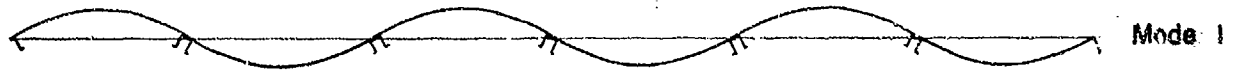
Stringer torsion mode

Mode 2

Mode 3
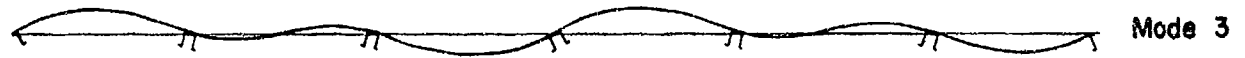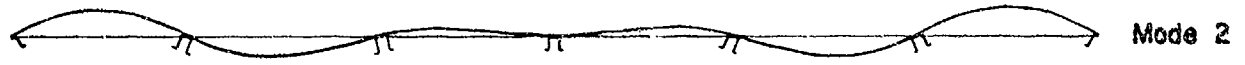
An intermediate mode

Mode 4

Mode 5

Mode 6
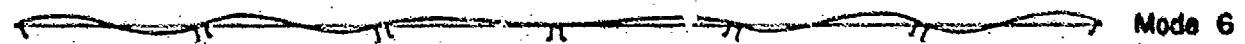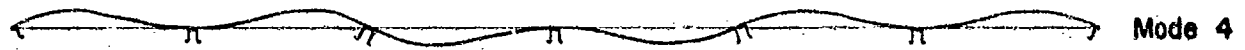
Stringer banding mode

FIGURE 3. TYPICAL MODE SHAPES OF A SIX-SPAN SKIN-STRINGER PANEL
(ONLY THE FIRST GROUP IS SHOWN)

FIGURE 4. SHAPES FOR SECOND ANTISYMMETRIC-SYMMETRIC MODE (PLATES WITH ALL EDGES FIXED)
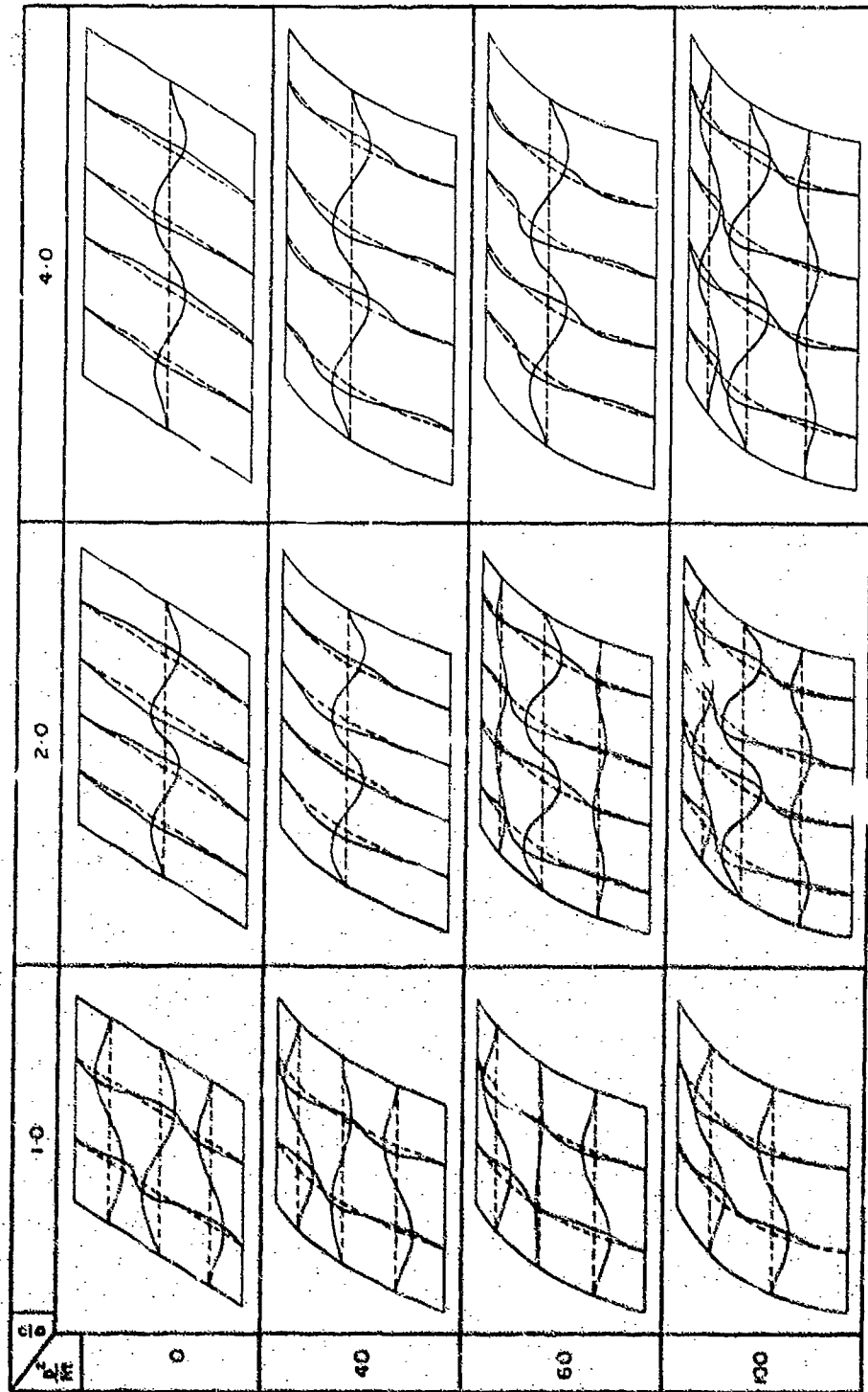
$\frac{b}{R} = 0.1$, $t = 1.27\,mm(0.05\,in)$
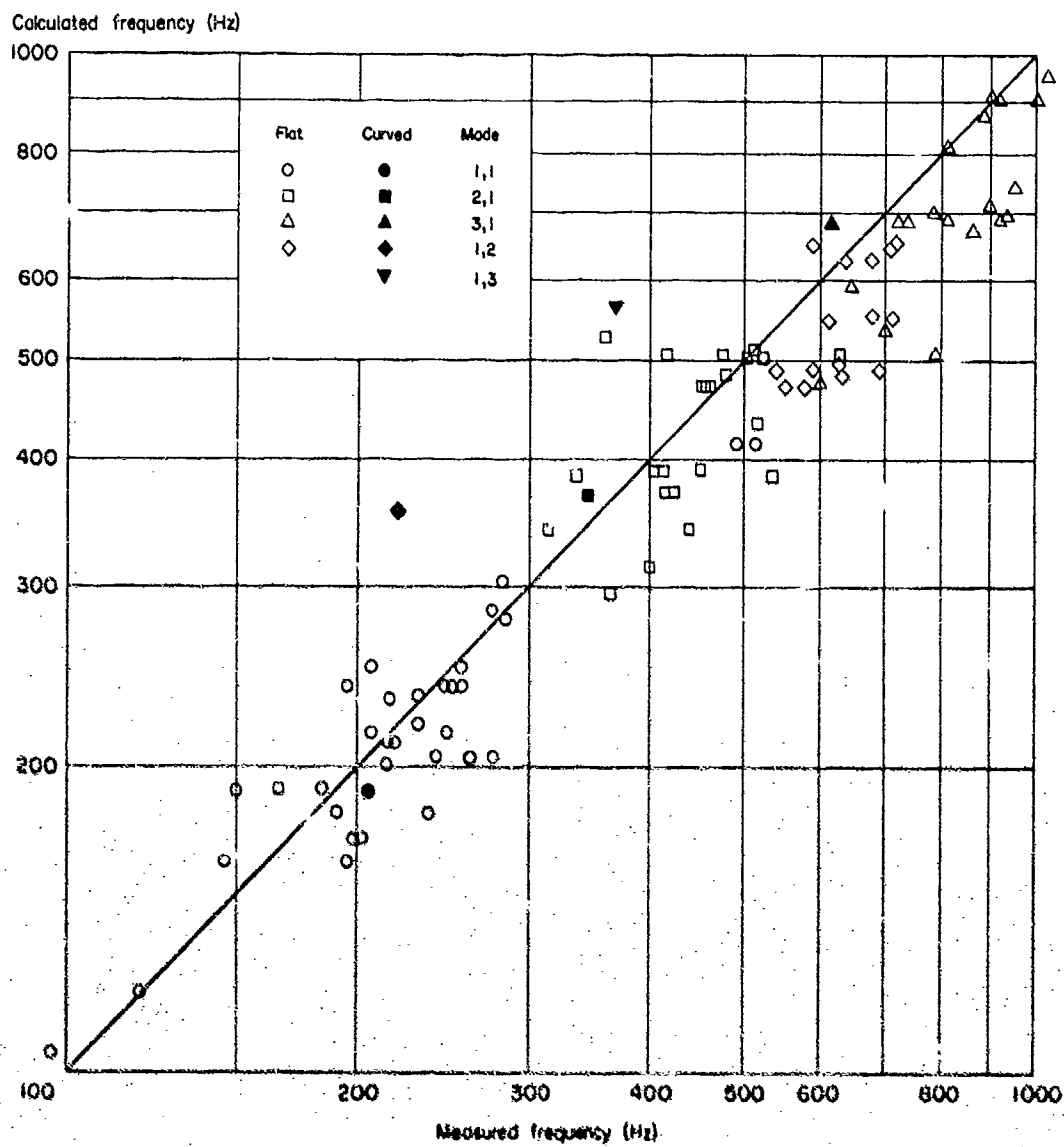
FIGURE 5. COMPARISON OF CALCULATED AND MEASURED NATURAL FREQUENCIES
OF SIMPLY-SUPPORTED HONEYCOMB SANDWICH PANELS
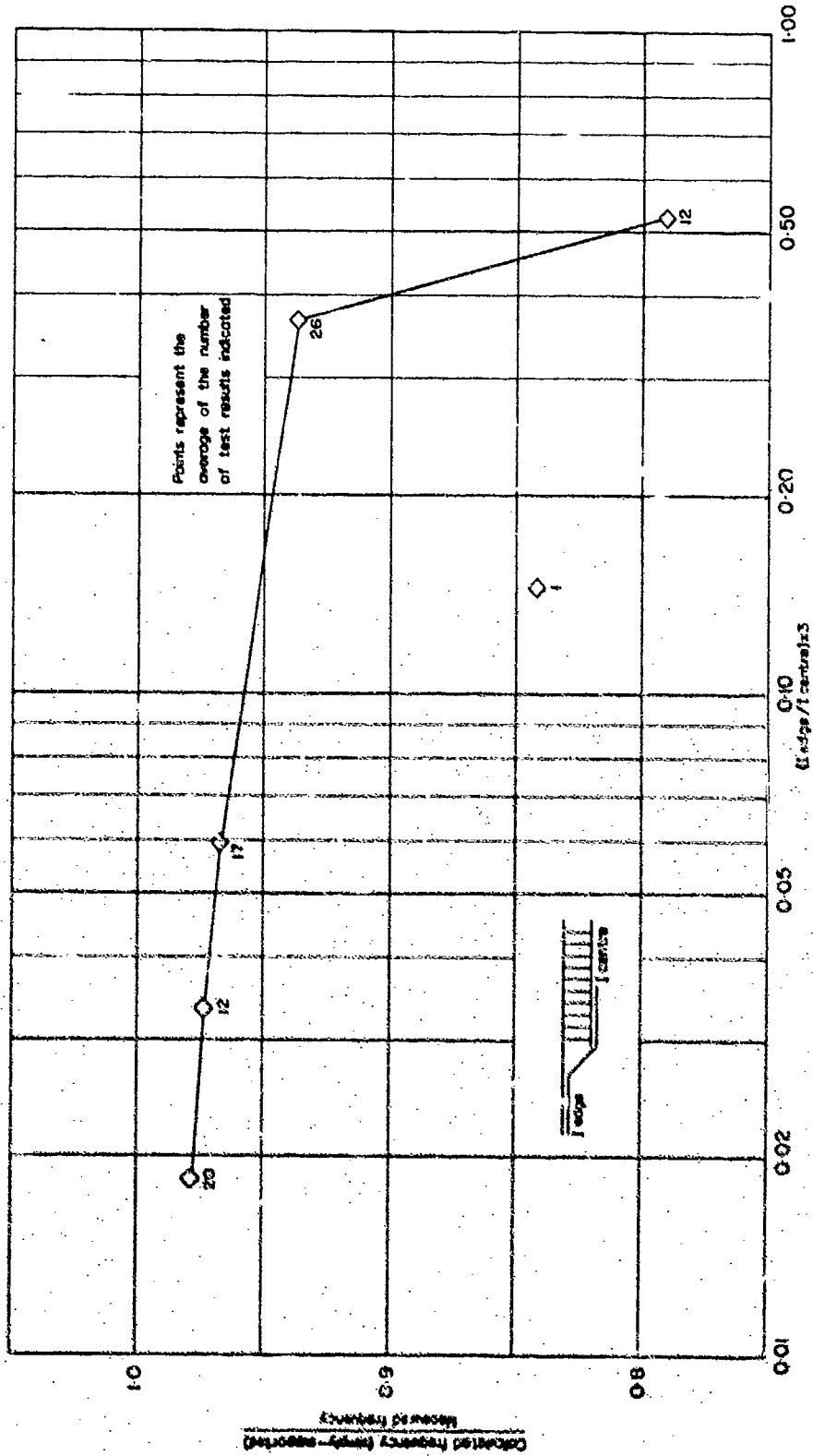
FIGURE 6. EFFECT OF EDGE STIFFNESS ON NATURAL FREQUENCY OF NOMINALLY SIMPLY-SUPPORTED HONEYCOMB PANELS

'Outer' face plate

'Inner' face plate

S_o

+

Face-plate stress

O

'Outer' face plate

−

S_i

'Inner' face plate
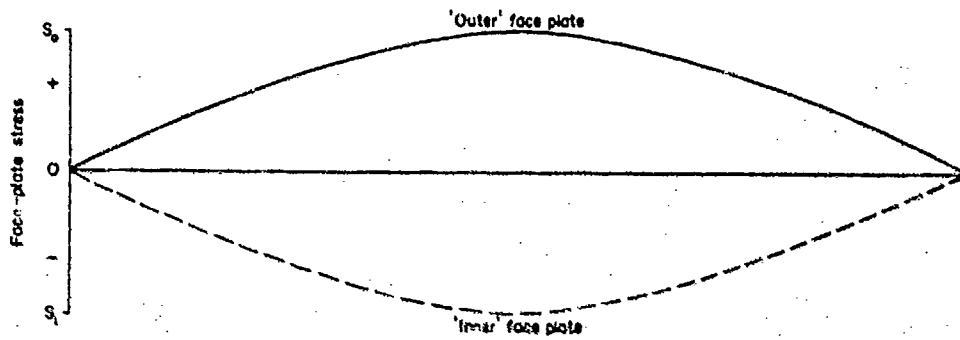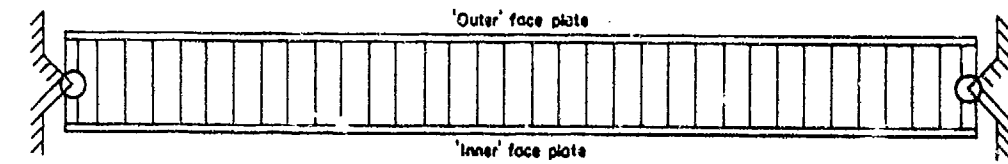
SIMPLE IDEALISATION

Edges free in rotation, fixed in translation, hinged at mid-plane. Total strain along mid-plane very small for small deflections, mid-plane stress negligible.

'Outer' face plate

'Inner' face plate

'Outer' face plate

Face-plate stress
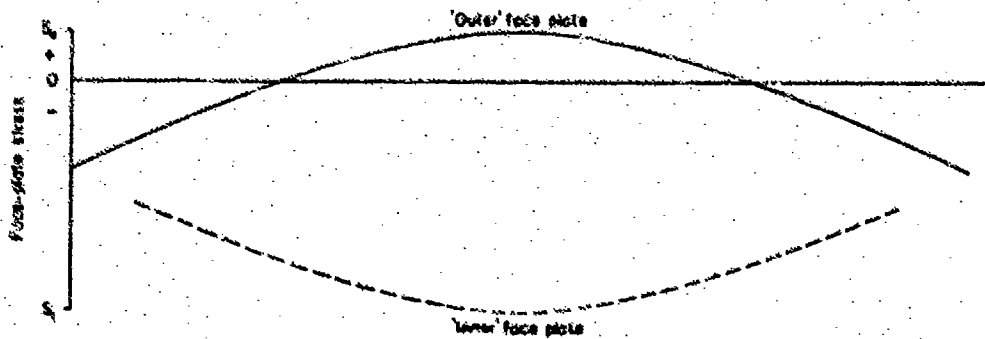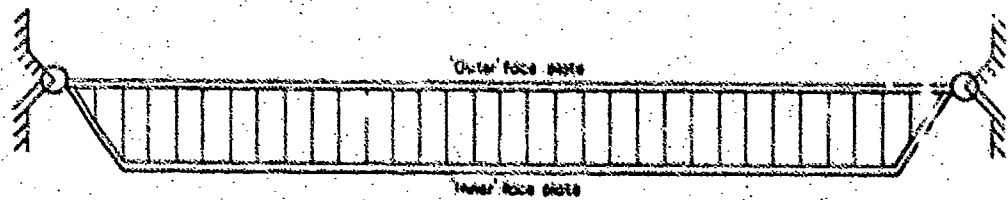
'Inner' face plate

IDEALISATION FOR FINNED PANELS

Edges free in rotation, fixed in translation, hinged in plane of outer face plate. Total strain in plane of outer face plate very small for small deflections, hence centre stress in outer face plate is relieved.

FIGURE 7.

APPENDIX A

DERIVATION OF SIMPLIFIED EQUATIONS FOR NATURAL FREQUENCIES
OF FLAT HONEYCOMB PANELS

A1. NOTATION

c_1 density factor $\left\{ \dfrac{6}{\left(2 + \dfrac{\rho_c}{\rho_f}\dfrac{h}{t}\right)} \right\}^{1/2}$

c_2 shear stiffness factor, $\left\{ 1 + \dfrac{m^2\pi^2 D}{h}\left(\dfrac{1+\mu^2}{G_a^2}\right) \right\}^{-1/2}$

c_3 panel curvature parameter

D bending rigidity

E Young's modulus

E_f Young's modulus of face-plate material

G shear modulus of isotropic core

G_a, G_b transverse shear moduli of orthotropic core in a- and b-directions respectively

G_o effective shear modulus of orthotropic core

J non-dimensional parameter

K_3, K_4 non-dimensional parameters

M_o mass density per unit area of panel

T stiffness ratio parameter $G_a a^2 h/D\pi^3$

a length of straight edge of panel

b length of curved edge of panel

f_c natural frequency of curved sandwich panel

f_f natural frequency of flat sandwich panel, neglecting shear deformation

f_{fs} natural frequency of flat sandwich panel, taking account of shear deformation

f_a natural frequency of flat solid panel of thickness $(h + t_f)$

f_t natural frequency of flat solid panel of thickness t

m, n number of half waves along sides of lengths a and b respectively

t thickness of solid panel

t_f face-plate thickness

γ ratio of core shear moduli, G_b/G_a

μ aspect ratio of nodal pattern, an/mb

ρ mass density of panel

ρ_c mass density of sandwich panel core

ρ_f mass density of sandwich panel faceplates

σ Poisson's ratio

A2. FREQUENCY EQUATIONS FOR FLAT PANEL

The well known equation for the natural frequency of a simply-supported flat rectangular panel neglecting shear deflections, is

$$f_t = \frac{\pi}{2a^2} \sqrt{\frac{D}{M_o}} \cdot m^2(1+\mu^2) \ . \tag{A1}$$

Charts for rapid evaluation of this equation are readily available, e.g. in Reference 14.

In the case of a solid panel of thickness $t = h+t_f$, modulus E_f and density ρ_f,

$$\left[\frac{D}{M_o}\right]_t = \frac{E_f t^3}{12(1-\sigma^2)\rho_f t} \ .$$

For a sandwich panel (with a core rigid in shear, but of zero flexural stiffness) of core thickness h and faceplate thickness t_f,

$$\left[\frac{D}{M_o}\right]_f = \frac{E_f t_f (h+t_f)^2}{2(1-\sigma^2)(\rho_c h + 2\rho_f t_f)}$$

Hence

$$\frac{f_f}{f_t} = \left\{ \left[\frac{D}{M_o}\right]_f \bigg/ \left[\frac{D}{M_o}\right]_t \right\}^{1/2} = \left\{ \frac{6}{\left(2+\frac{\rho_c}{\rho_f}\frac{h}{t}\right)} \right\}^{1/2}$$

or

$$f_f = f_t C_1 \ . \tag{A2}$$

A3. EFFECT OF FINITE CORE SHEAR STIFFNESS

For a sandwich panel having an isotropic core of zero flexural stiffness, and taking shear deformation into account, Equation 7 of Reference 11 can be written in the form

$$f_{fs} = f_f \bigg/ \left\{ 1 + \frac{m^2\pi^2 D}{h} \frac{1+\mu^2}{G^2} \right\}^{1/2} = f_t C_1 C_2 \ . \tag{A3}$$

A4. EFFECT OF CORE ORTHOTROPY

Examination of experimental results (Reference 12) suggests that orthotropy of the core can have a significant effect on the natural frequencies of honeycomb panels of practical dimensions. It is common design practice to ignore the directional effects of core orthotropy in calculating the natural frequencies by using an effective value of core shear modulus $G_c = \sqrt{G_a G_b}$ in place of G in Equation A3. While this

approximation gives satisfactory results for the fundamental mode of nearly square panels, it cannot be expected to apply with any accuracy to deep panels with high aspect ratio, or to modes with high ratio of wavelengths in the principle directions, when the frequency is affected much more by shear stiffness in the short direction than the long direction.

Accordingly an attempt was made to improve upon the use of an effective modulus $G_c = \sqrt{G_a G_b}$ in Section 2 of Reference 2.

Jacobsen (Reference 11, equations 16 to 18) gives equations for the fundamental frequency of a flat or curved rectangular panel with an orthotropic core. For a flat panel these equations can be reduced to

$$f_{fs} = f_t C_1 \left\{ \tau K_3 + \gamma \mu K_4 + (1+\mu^2 \gamma) \right\} = f_t C_1 C_2$$

where

$$K_3 = -\frac{2a^2}{J} \left(2a\gamma + \left[\left(2a^2 + 1 - \sigma - \gamma\mu^2(1+\sigma) \right) \bigg/ \tau \right] \right) \ .$$

$$K_4 = -\frac{2a^2}{J} \left\{ 2a\mu\gamma + \left(\left\{ a\gamma \left(1+\mu^2(1-\sigma) \right) - \mu(1+\sigma) \right\} \bigg/ \tau \right) \right\}$$

and
$$J = 4\pi^2\gamma + (2\pi/T)\left\{2\mu^2+1-\sigma\cdot\gamma\left[2+\mu^2(1-\sigma)\right]\right\} - (F/T^2)$$

where
$$F = \mu^2(1+\sigma)^2 - \left[2\mu^2+(1-\sigma)\right]\left[2+\mu^2(1-\sigma)\right] \quad .$$

Thus C_2', (corresponding to C_2 in Equation A3) is a complicated function of γ, μ, σ and T which contains too many variables for presentation in simple graphical form.

An approximation to C_2' was therefore sought and the expression

$$C_2 = \left\{1 + \frac{\pi^2 D}{h}\left(\frac{m^2}{G_a a^2} + \frac{n^2}{G_b b^2}\right)\right\}^{\cdot/2}$$

suggested itself intuitively. This can be written in the form

$$C_2 = \left\{1 + \frac{\pi^2 D}{ha^2}\frac{(m^2+\mu^2 n^2)}{G_c}\right\}^{-1/2} , \qquad (A4)$$

where
$$G_c = G_a \frac{(1+\mu^2)}{(1+\mu^2/\gamma)} \quad . \qquad (A5)$$

Equations A4 and A5 are readily presentable in graphical form.

Comparison of C_2 with C_2' computed for ranges of values of γ, μ and T and for $\sigma = 0.3$ showed that $C_2 = C_2'$ within 1 per cent over the range of the variables covered in Reference 2, Section 2. Accordingly this approximation was adopted in the data sheet.

It should be noted that Jacobsen's equations were derived for the fundamental mode only (m=n=1 in the expression for μ). The validity of extending their use to higher modes, i.e. taking $u = an/mb$ rather than a/b, in Reference 2, Section 2 is confirmed by comparison with Ballentine's experimental results as shown in Figure 5.

ESTIMATES OF THE RESPONSE OF BOX TYPE STRUCTURES
TO ACOUSTIC LOADING

by

Brian L. Clarkson
Director and Professor of Vibration Studies,
Institute of Sound and Vibration Research
University of Southampton
England

1. INTRODUCTION

In flight vehicle structures, acoustic loading due to jet or rocket engines, boundary layer pressure fluctuation, or separated flow causes high frequency vibration of the surface skin structure and also the internal support members. The design of the internal support structure to withstand this induced vibration presents considerable difficulty because of its dependence on the fine detail of the local design.

In typical configurations, the skin is relatively stiff and the stresses induced by noise are usually very low. The internal rib structure, however, is relatively light and is prone to acoustic fatigue damage. In addition to the lightening holes and stiffeners, the rib often has many small cut outs to allow the skin stiffeners to pass through. In some cases the skin stiffeners are attached to the rib web by means of cleats. The rib structure is thus a very complicated one and often contains many points of high stress concentration which can initiate acoustic fatigue failures. Where failures have occurred in fins or tail-planes, they have usually been in the internal structure or have started internally.

When such a structure is excited by broadband pressures such as jet noise, a complicated form of vibration takes place. The skins vibrate as interconnected stiffened plates between the ribs and the internal rib structure also vibrates. The frequencies of lowest local coupled modes of this structure are usually in the acoustic frequency range (100 to 1000 Hz). The response spectrum for each component usually shows several predominant peaks. Although the skin must be forcing the ribs to vibrate the peaks in the skin and rib spectra do not generally coincide in frequency. Naturally there is a coupling but the predominant peaks are not the same in the two parts of the structure. Because of the coupling through the ribs, both skins vibrate at about the same level even when the excitation is only applied direct to one side.

Acoustic loading on such a structure results in continuously distributed pressures which have a random time history. Because of the wide frequency range of the forcing pressures, many normal modes of the structure are excited. The spatial relationship of the pressures (or cross spectral density) is an important parameter in determining which modes of vibration of the structure are predominant in the response. However in design methods this fine detail of the forcing function cannot usually be included in the analysis.

This paper reports on a study of the vibration response of the internal ribs of a structure representing possible design variants for a tailplane. The test specimen was designed in such a way that the ribs could be changed. Thus the effect of different internal designs could be studied experimentally. A semi empirical method similar to that used in the AGARD Data Sheets on Acoustic Fatigue is proposed and the estimates are compared with the experimental results.

2. DESIGN OF THE TEST SPECIMEN

A multicell box structure, typical of aircraft construction was made and tested in the high intensity noise facility of the NASA Langley Research Center. The test specimen, shown in Figure 1, was designed to have relatively stiff boundary members, seven internal ribs and unstiffened skins. The skins were stiffened locally over the rib flange attachment to increase the rib in-plane bending stiffness. To avoid the introduction of extra (and indeterminate) damping, the specimen was designed to be tested in a free free mode.

The design objectives for the specimen were:

1. Major coupled skin-rib modes of vibration in the range 100-500 Hz.

2. Overall free free modes (bending normal to ribs) of the specimen to be higher than 500 Hz (impracticable to make it much higher than about 500 Hz).

3. Overall bending (in-plane bending of ribs) to be higher than 500 Hz (probably about 700 Hz in this design).

4. Coincidence effects (matching of sound and vibration wavelengths) should not occur at frequencies below about 750 Hz.

The ribs and skins were fastened together by bolts so that a range of rib designs could be tested in the same overall configuration. The first set of ribs were plain unstiffened plates with bent-over flanges. Later designs in the series included stiffeners, lightening holes, etc. This paper reports the results of three rib designs.

Figure 2 shows the specimen installed in the high intensity noise facility at the NASA Langley Research Center. The specimen is suspended by two steel ropes in the wall of the duct carrying the noise. A light seal between the specimen and the wall is achieved by strips of foam plastic. This does not add any structural restraint to the edges nor increase the damping significantly. The high intensity travelling wave sound field in the duct is created by two air modulators. The spectrum of the acoustic pressures on the specimen is shown in Figure 3. This shows that acoustical energy is present over a wide frequency range and thus many modes of the structure are excited simultaneously.

The strains induced in the structure were measured by foil strain gauges on the outer surface of the skins and on one of the centre ribs. Four miniature gauges were placed in the bend radius of the rib flange in an attempt to measure the local strains in the region of the attachment of the rib web to the skin.

The three rib designs tested to date are illustrated in figure 4, and figure 5 shows the strain gauges installed on rib design no. 2. Figure 6 shows the strain gauge positions on rib designs no. 1 and no. 5.

3. ESTIMATION OF RESPONSE LEVELS

A simplified theory is derived on the assumption that the major part of the response results from the contribution of one predominant mode (see for example reference 2). The tests on full scale structures have shown that in certain types of structure (usually large skin plates) the response spectrum may only have one major peak resulting from one mode of vibration. In other structures, such as control surface skin plating, there may be many peaks in the response spectrum. Even in this case, however, the simple theory gives a reasonable estimate of the overall stress level. Nevertheless it is clearly necessary to examine the application of the theory in a wide range of structures to establish the limitations.

3.1 Single Mode Response: Skin Structure

On the assumption that there is only one significant mode contributing to the response and that the acoustic pressures are exactly in phase over the section of structure, a simplified expression for the root mean square stress in directly excited skin structure can be written as:

$$\sqrt{\overline{\sigma^2(t)}} = \left[\frac{\pi}{4\delta} \, f_r \, G_p(f_r) \right]^{\frac{1}{2}} \sigma_0 \tag{1}$$

where
δ = viscous damping ratio

f_r = frequency of predominant mode

$G_p(f_r)$ = spectral density of pressure at frequency f_r

σ_0 = stress at point of interest due to a uniform static pressure of unit magnitude.

This expression was first derived from the consideration of a single degree of freedom system by Miles (1). This has been shown to give reasonable estimates of the skin stresses in uniform thickness and stiffened plate structures (2).

3.2 Application to Control Surfaces: Skins

In the case of control surfaces, two skins are attached together by ribs and thus both skins and ribs vibrate because of the mechanical coupling between them. Even when the sound pressures are much greater on one side of the control surface, due to acoustic shielding, the stresses in both skins are very similar. These types of structure are not so amenable to the simple form of analysis outlined in section 3.1, as now the energy incident on one skin, minus the reflected energy, is absorbed by two vibrating skins and the interconnecting ribs. Consequently, the stress level must be less than half and is possibly about one third of that which would have been induced in a single plate. Making the assumption that the stress is reduced to one-third of the single plate case the root mean square stress in the skin is then given by

$$\sqrt{\overline{\sigma^2(t)}} = \frac{1}{3} \left[\frac{\pi}{4\delta} \, f_r \, G_p(f_r) \sigma_0^2 \right]^{\frac{1}{2}}. \tag{2}$$

This generally applies to tailplanes, elevators and flaps.

This method has been found to give reasonable estimates of the skin stresses in control surfaces (2) but of course in its simplest form it does not give estimates of the rib stresses. An extension of the simple procedure has been proposed (3) in which a Rayleigh-Ritz energy analysis is used to obtain slightly more realistic values for f_r and σ_0 in the equation above.

It is assumed that the structure is composed of a large number of similar bays and hence only one bay is considered in the analysis as shown in figure 7. Beam functions are used for the terms in the series expansion in the two orthogonal directions for the face plates and the ribs. Each function in the series representing the displacement along the line normal to the intersection of the skin and rib is chosen so as to give continuity of displacement, slope and bending moment at the junction. The objective here has been to develop a computer based model which is able to give good estimates of the stresses in the skin and rib at the junction line. It is therefore essential to have continuity of bending moment and hence equilibrium of stresses at this line.

The displacement functions have been chosen as follows:

$$w(xy) = \sum_{m=1}^{p} \sum_{n=1}^{q} A_{mn} X_m(x) Y_n(y) \qquad (3)$$

$$u(zy) = \sum_{m=1}^{p} \sum_{n=1}^{q} A_{mn} Z_m(z) Y_n(y) \qquad (4)$$

where $X(x)$, $Y(y)$, $Z(z)$ are beam functions

$$X_m(x) = \cos \delta_m \frac{x}{a} - \cosh \delta_m \frac{x}{a} + B_m \sin \delta_m \frac{x}{a} + D_m \sinh \delta_m \frac{x}{a} \qquad (5)$$

$$Z_m(z) = -\cos \zeta_m \frac{z}{d} + \cosh \zeta_m \frac{z}{d} + E_m \sin \zeta_m \frac{z}{d} + G_m \sinh \zeta_m \frac{z}{d} \qquad (6)$$

$$Y_n(z) = \cosh \gamma_r \frac{y}{b} - \cos \gamma_r \frac{y}{b} - \alpha_r (\sinh \gamma_r \frac{y}{b} - \sin \gamma_r \frac{y}{b}) \qquad (7)$$

...(ref. 4)

The fully fixed end beam function has been used for Y because it is considered that this is a closer representation of the fixing conditions at the spars. The series of values used for γ and α are as given in reference 4.

The boundary conditions at the junction of the skin and rib can now be used to determine the constants in equations 3 and 4. In addition to displacement and slope continuity, there must be moment equilibrium at the junction.

The estimates of the natural frequencies and mode shapes can now be obtained by equating the maximum strain energy with the maximum potential energy in free vibration. The unit stress parameter σ_0 is obtained by equating the work done by unit magnitude static pressure in moving through the displacement of the mode shape with the maximum strain energy in the mode.

4. EXPERIMENTAL RESULTS

In all cases the response spectra measured by the strain gauges show a multimodal form of response. Many modes of vibration are contributing to the overall stress at any point in the structure. The three tests were carried out at 140 dB, 139 dB and 149 dB overall sound pressure levels respectively. Therefore, for the purposes of comparison the results have been converted to a level equivalent to 140 dB overall excitation level on the assumption that the response of the structure is linear in this range. In the majority of cases two strain gauges are placed in similar positions - one set on the centre line of the specimen and one set 4 in. away from the centre line. Within the accuracy of the measurements the difference between these two sets of results is not considered to be significant. Tables 1 and 2 summarise the overall stress results for the three test specimens.

Table 1 gives the results for the skin strain gauges. This piece of structure and the gauges are identical in each of the three tests as only the ribs were changed to construct the second and fifth specimen. These results show that the two sets of strain gauges are giving similar results and therefore the average value is used when making general comparisons. In the second specimen the average levels are about 66% of those of specimen no. 1 and in the fifth specimen they are about 47% of specimen no. 1.

Table 2 gives the results for the rib strain gauges. In this case specimens no. 1 and 5 can be compared directly but in the case of the stiffened design (no. 2) the strain gauge positions are not directly comparable. Comparisons of average values here is not very useful as this would conceal the effect of the differences in detail design features.

The results given in Tables 1 and 2 show that the vibration stress levels are approximately equal in both skins. The maximum stress occurs over the edge of the skin doubler closest to the rib web. The stresses in the centre of the skin panel are some 20% lower than the maximum values. For the unstiffened ribs, the rib stresses show good consistency between the measurement at different positions and, as was expected, the highest stresses are in the bend radius. These are about twice the maximum skin stresses and 50% higher than the stresses at the centre line of the rib.

The shapes of the stress spectra at different points on the cross section of design no. 1 are illustrated in figure 8. These show that the predominant peaks in the skin spectra occur in the frequency range 140 to 200 Hz (max. peak around 164 Hz) with a second group of peaks in the range 200 to 250 Hz. In the rib the maximum occurs at about 250 Hz. There are other major peaks in the range 210 to 230 Hz and then another group at 150 to 200 Hz corresponding to the skin peaks. Without a much more detailed examination it is not possible to identify particular modes of vibration from these spectra.

The differences in the response of the three rib designs can be seen more clearly in the spectral analysis of the response at each gauge position. Typical results for the skin and rib are given in figures 9, 10 and 11. Figure 9 shows the strain response at the centre of the central skin panel in the direction normal to the ribs. By changing the rib structure supporting this skin the response spectra is changed to the shapes shown in figures 9(b) and 9(c). These are not drawn to the same scale and

therefore only a comparison of shape can be made. If they were to be drawn to the same scale the area of each diagram would be equal to the mean square stress. Figure 10 shows the strain spectra for the centre of the rib and figure 11 shows the spectra for the rib bend radius. Figure 10(c) shows the spectra of the strain at the rivet line in the centre of the stiffener. This spectra has a group of peaks corresponding to the rib web strain (as shown in figure 10(b)) but also a group of peaks in the region 400 to 500 Hz. This latter part of the response is associated with the bending of the stiffener itself. In designs 1 and 2 there is no significant difference in the strains in the bend radii adjacent to the inner and outer skins but in the case of the damped rib (design no. 5) the strain in the bend radius adjacent to the directly excited skin (fig. 11c) is about twice that in the opposite radius (figure 11d).

The spectra for design no. 1 show the two regions of main response, i.e. skin: 140 to 200 Hz and rib: 200 to 250 Hz. Reduction in the rib thickness and the addition of stiffeners (design no. 2) has moved the rib bend radii peaks downwards in frequency to the range 180 Hz to 220 Hz although the stiffeners themselves show a major peak in the region 400 to 500 Hz.

The spectra show that the overall damping has been changed by the change in the rib design. Estimates of the bandwidths of the peaks in the spectra suggest average damping values as follows:

$$\text{Design No. 1} \qquad \delta = 0.015 \text{ to } 0.020$$
$$\text{No. 2} \qquad \delta \approx 0.025$$
$$\text{No. 3} \qquad \delta \approx 0.035.$$

These values will be used in the estimation procedure.

5. ESTIMATES OF STRESS LEVELS

The approximate method given in the AGARD Data Sheets on Acoustic Fatigue (5) can be used to estimate the stresses in the skin covers of the box structure. For the internal structure, the Rayleigh Ritz method described in section 3.2 can be used. This latter method also gives an alternative estimate for the skin stresses.

5.1 AGARD Data Sheet Method

The structural dimensions are:

$$a = 33", \qquad b = 8", \qquad a/b = 4.125$$

$$t = 0.064".$$

Fundamental natural frequency (edges assumed fully fixed) = 220 Hz.

1/3 octave sound pressure level at 200 Hz centre frequency = 126 dB $\equiv$ 109.2 dB spectrum level.

Now using the Nomograph

$$\frac{b}{t} = 125; \qquad V = 0.99; \qquad \frac{t}{V} = 1.64 \text{ mm.}$$

$\therefore$ nominal r.m.s. stress at rivet line = 650 lb/in^2.

The effect of the outer skin and ribs is to reduce this stress by a factor of 3.

Thus the estimated nominal stress is 217 lb/in^2.

5.2 Rayleigh Ritz Method

In this case we use the basic equation (1) and compute σ_0 and f_r from the Rayleigh Ritz method. Computations for a model having the dimensions of the test specimen give results for the stress parameter σ_0 and the frequency of the first mode (3). When the damping of the specimen is taken into account the appropriate estimates can be made and compared with the experimental results as follows:

r.m.s. stress levels lb/in^2 140 dB overall sound pressure level

	Experimental		Estimates		
	r.m.s. stress average values	Damping	AGARD Data Sheet rms stress	Rayleigh Ritz σ_0	Mode 1 r.m.s. stress
Design No. 1.					
Skin centre	.417	0.017		246	16
rivet line	321		217	87	6
Rib centre	562			264	17
bend radius	864			446	29

	Experimental			Estimates		
	r.m.s. stress average values	damping	AGARD Data Sheet rms stress	Rayleigh Ritz σ_0		Mode 1 r.m.s. stress
Design No. 2.						
Skin centre	315	0.025		203		13
rivet line	186		179	72		5
Rib centre	933			218		14
bend radius	728			368		24
Design No. 5.						
Skin centre	194	0.035		171		11
rivet line	148		151	60		4
Rib centre	162			183		12
bend radius	605			310		20

These results show that the AGARD data sheet gives estimates for the skin rivet line stress which are within a factor of 2 of the measured stresses. This method in its present form is not able to predict the stresses in the internal structure. The Rayleigh Ritz method gives estimates for one mode only. The stress spectra show that many modes of vibration exist in the response and thus these estimates are much lower than the experimental results. To get a realistic value, the estimates would have to be multiplied by the number of modes having significant response. A factor of 15 or so would bring the estimates into the region of the measurements. Clearly this is an unsatisfactory procedure. One possibility is to use this method to indicate the ratio of stresses in the rib relative to the skin centre. The AGARD Data Sheets could then be used to estimate the skin centre stress.

CONCLUSIONS

The results reported in this paper show that the overall response of box type structures to acoustic loads can be reduced by changes in the internal rib structure. The skin stresses can be predicted by the AGARD Data Sheet method but present estimation methods are inadequate to predict the effect of changes in internal structural details.

ACKNOWLEDGEMENTS

REFERENCES

1. Miles, J.W. On Structural Fatigue under Random Loading. J. Aero. Sc. Vol. 21, p. 753-762 (1954).

2. Clarkson, B.L. Stress in Skin Panels Subjected to Random Acoustic Loading. AFML-TR-67-199.

3. Clarkson, B.L. Computer Based Analyses of the Response of Box Type Structures to Random Pressures. To be published in Int. Journal of Computers and Structures.

4. Young, D. Vibration of Rectangular Plates by the Ritz Method. J. App. Mech., Trans. ASME 72, 448, (1950).

5. AGARD Data Sheets on Acoustic Fatigue.

TABLE 1   <u>Overall r.m.s. stress levels in the skin at 140 dB excitation level</u>
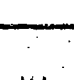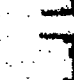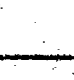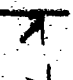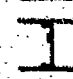
Gauge Position		No.	Design No. 1 stress lb/in²		Design No. 2 stress lb/in²	% of 1	Design No. 5 stress lb/in²	% of 1
	inner	1 3	484 463	474	372 336	354	75	355 255	305	64
	outer	13 15	432 506	469	224 381	— 303	65	181 261	221	47
	inner	9 11	348 403	376	209 224	217	58	172 166	169	45
	outer	21 23	379 412	396	172	172*	43	136	136*	34
	inner	2 4	300 299	300	224 217	221	74	189 156	173	58
	outer	14 16	320 402	361	227 187	207	57	166 183	175	48
	inner	10 12	298 332	315	142 175	159	50	114 130	122	39
	outer	22 24	280 338	309	183 153	168	54	118 122	120	39
	inner	5 7	402 349	376	295 254	275	73	189 172	181	48
	outer	17 19	438 476	457	314 295	354	77	213 201	207	45
	inner	6 8	139 163	151	149 161	155	102	75 88	82	54
	outer	18 20	138 143	141				69	69*	49
Average				100%			66%			47%

TABLE 2   <u>Overall r.m.s. stress levels in the rib at 140 dB excitation level</u>

Gauge Position	No.	Design No. 1 stress lb/in²		Design No. 2 stress lb/in²		Design No. 3 stress lb/in²	
	25 26	821 781	801	728	728*	432 648	490
	27 28	982 969	926			850 608	729
	30 32	581 542	562	28 27	933* 448	162	162*
	29 31	320 375	348			124 111	118
				29 30 31	459 127		

*only one reading.

Position of internal ribs (8" pitch)

3' 6"

6" 8" 8" 8" 8" 8" 8" 6"

5'0"

FIG. 1 MULTICELL BOX TEST SPECIMEN.
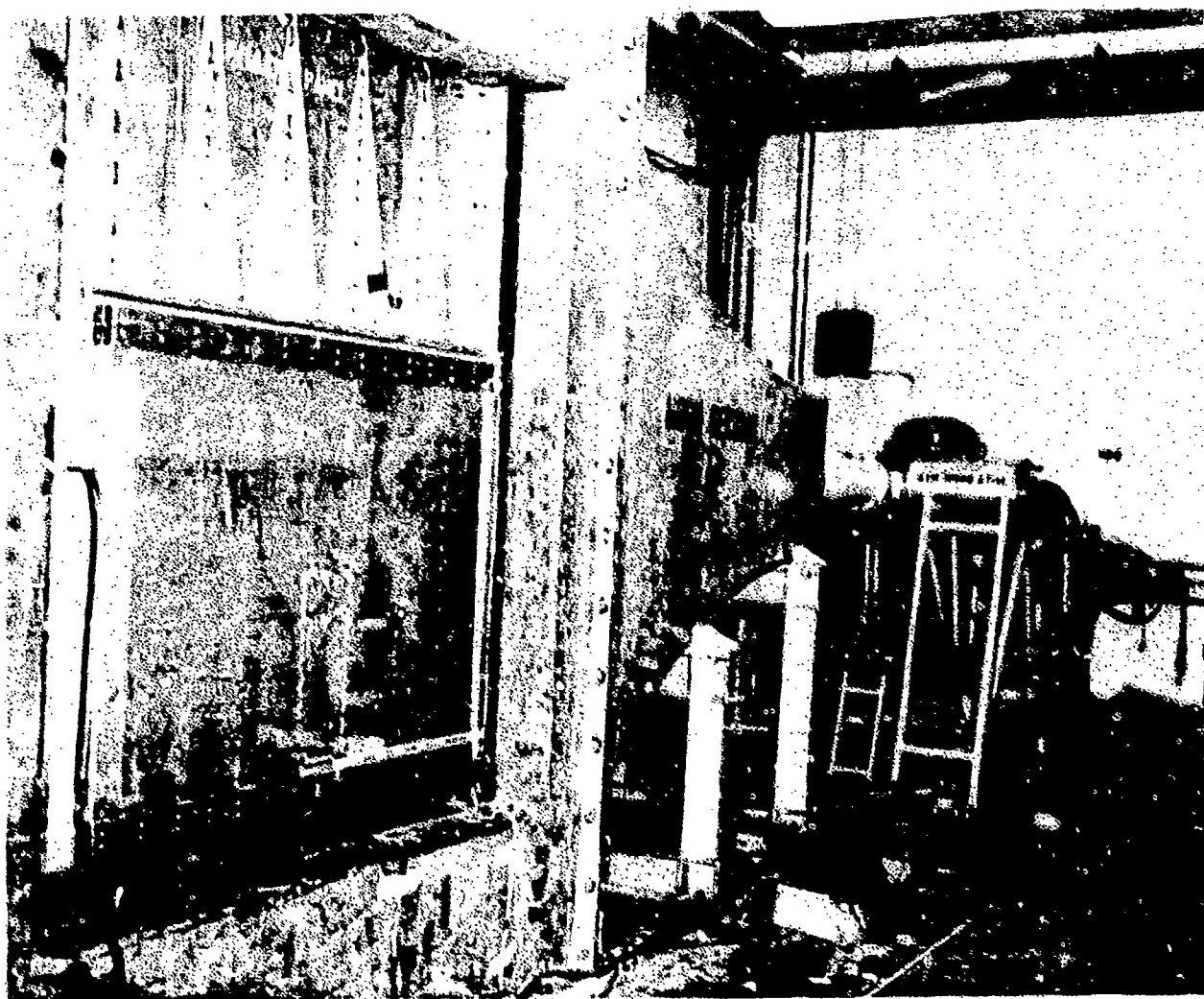
FIG. 2 TEST SPECIMEN INSTALLED IN N.A.S.A HIGH INTENSITY NOISE FACILITY.

FIG. 3   AE THIRD OCTAVE SPECTRUM OF ACOUSTIC PRESSURE.

0.045 in.

Double skin with
viscoelastic core

Design No 5
(Damped rib)

0.032 in.

Section A A

Design No 2
(Stiffened rib)

Clean attaching
stiffener web to skin

0.040 in.

Design No 1
(Plain rib)
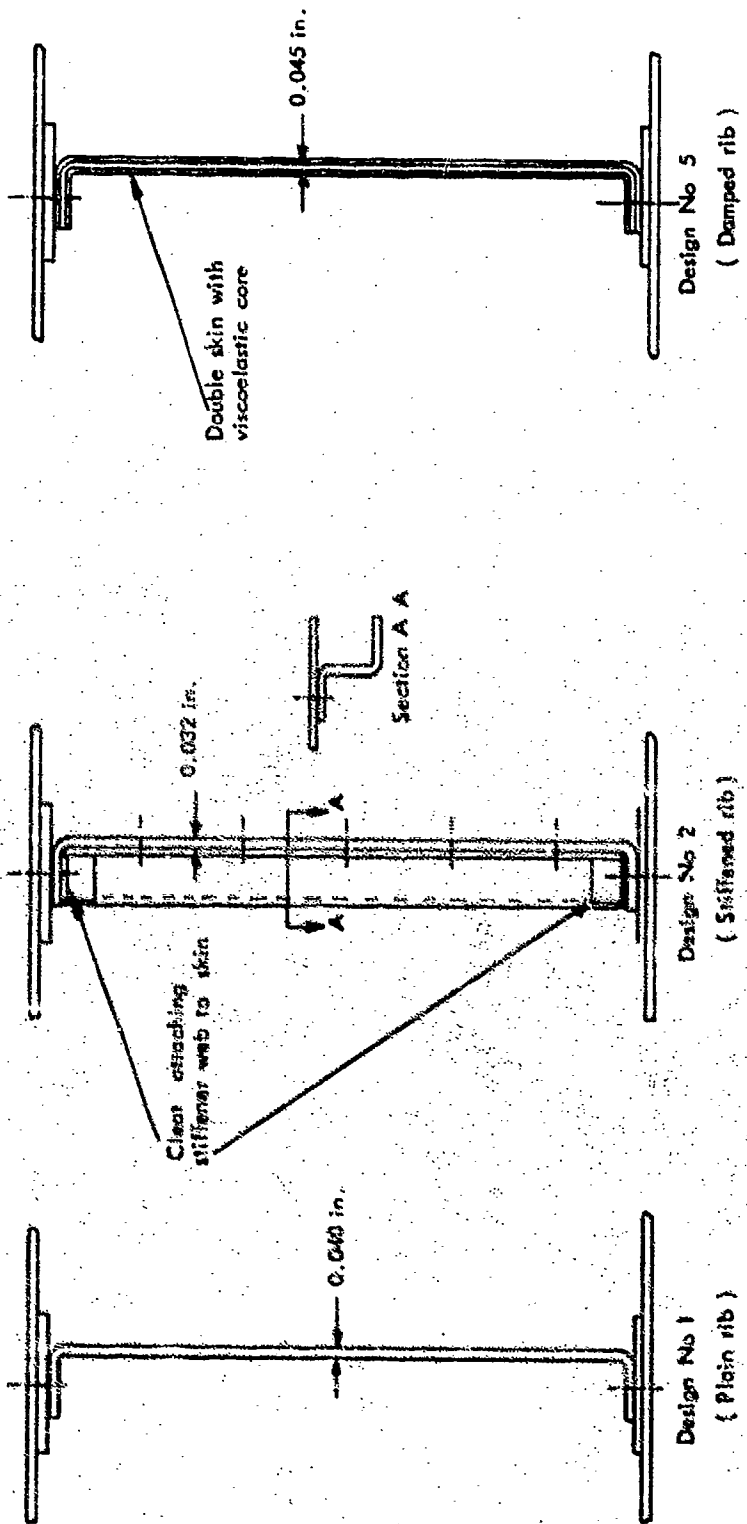
FIG. 4 RIB DESIGNS
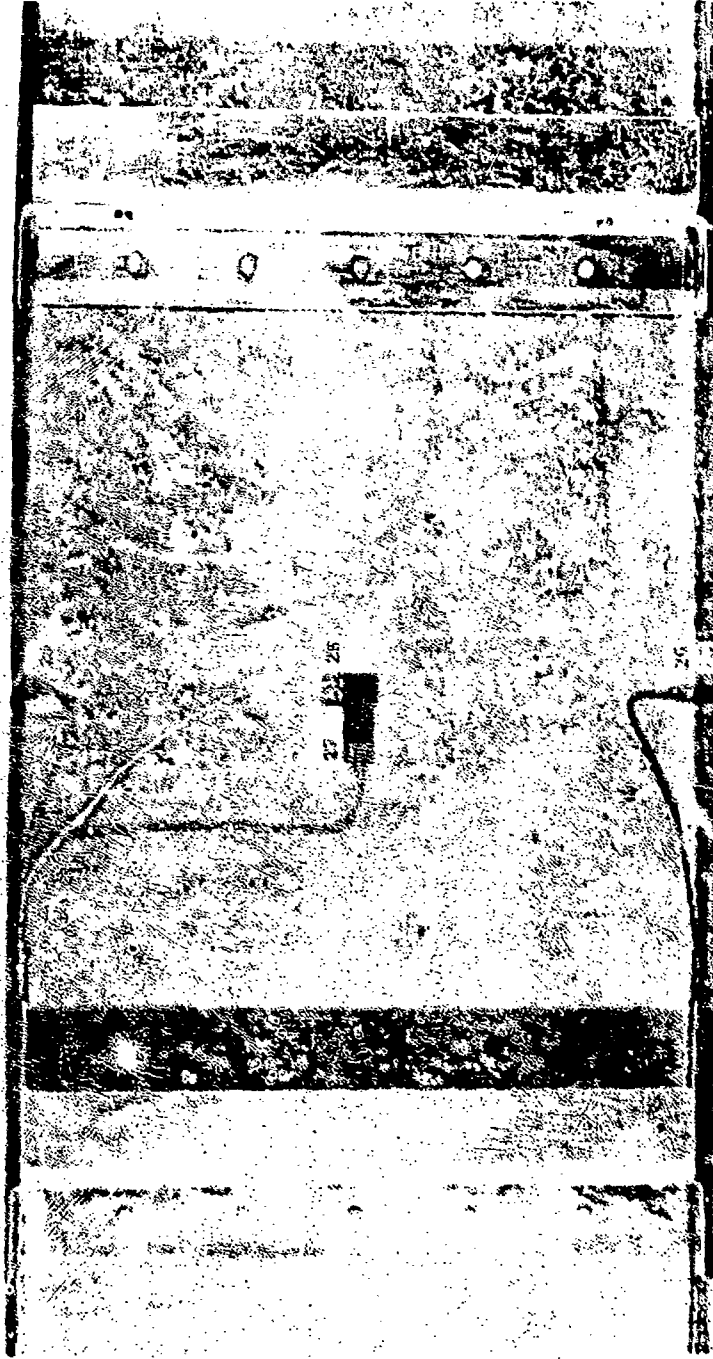
FIG. 5 STRAIN GAUGE INSTALLATION RIB DESIGN No 2.
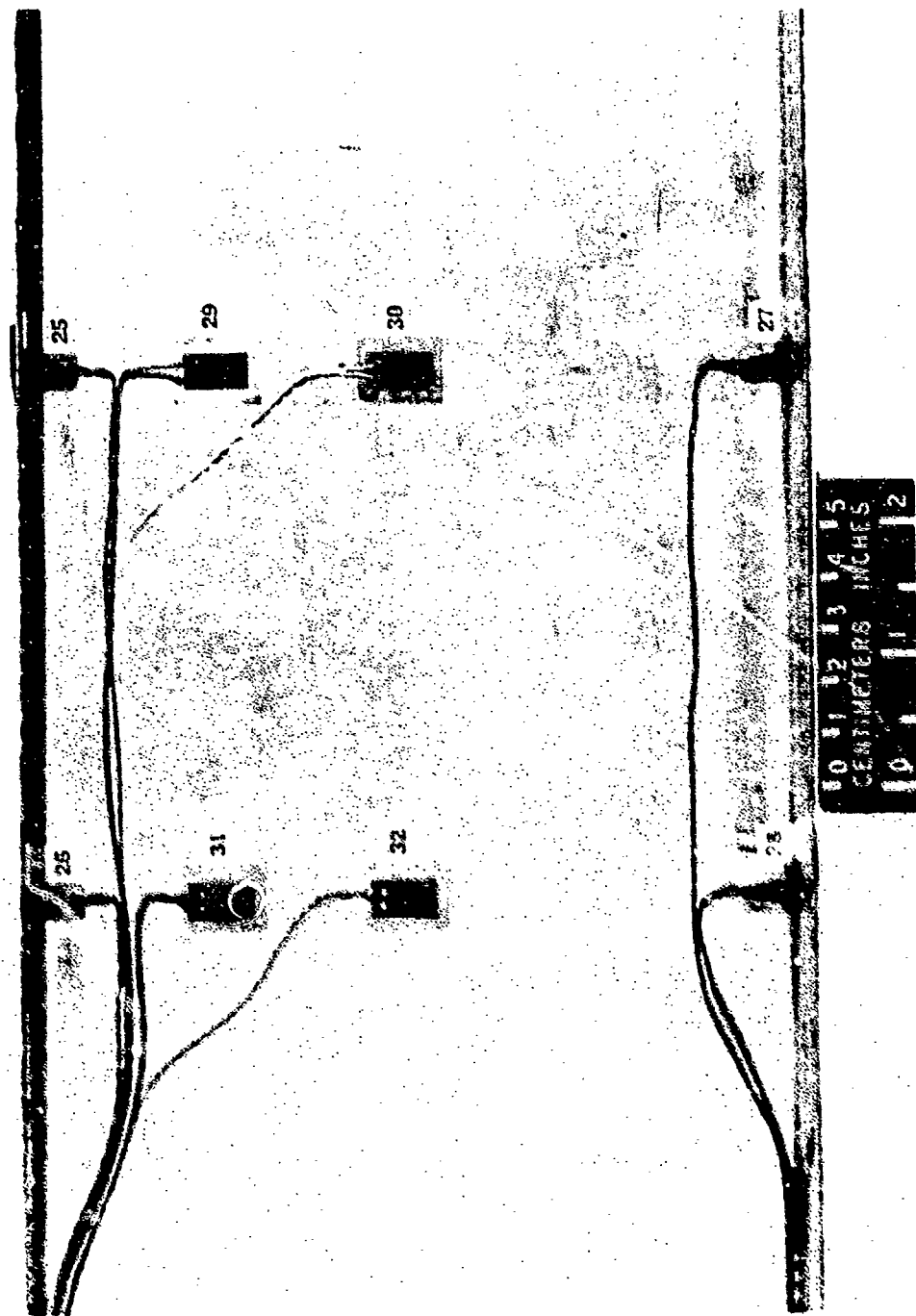
FIG. 6 STRAIN GAUGE INSTALLATION RIB DESIGN No 1&5.

$$U(z,y) = \Sigma \Sigma A_{mn} \ Z_m(z) \ Y_n(y)$$

$$\omega(x,y) = \Sigma \Sigma A_{mn} \ X_m(x) \ Y_n(y)$$
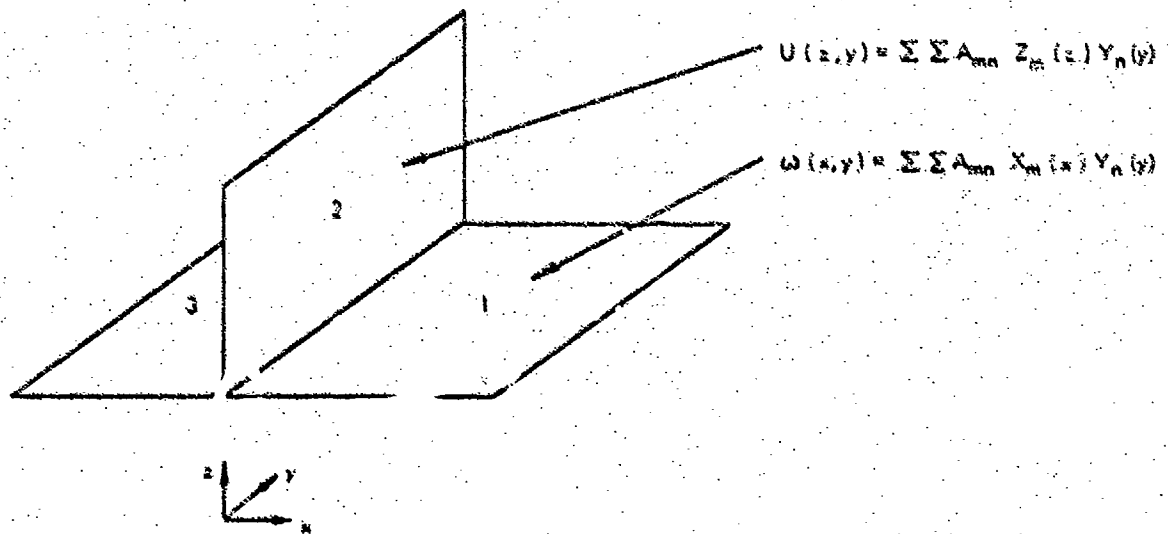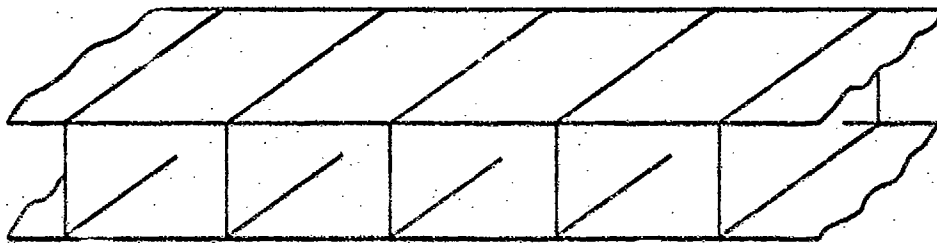
FIG. 7 THREE DIMENSIONAL MODEL USING INTERCONNECTED PLATES.
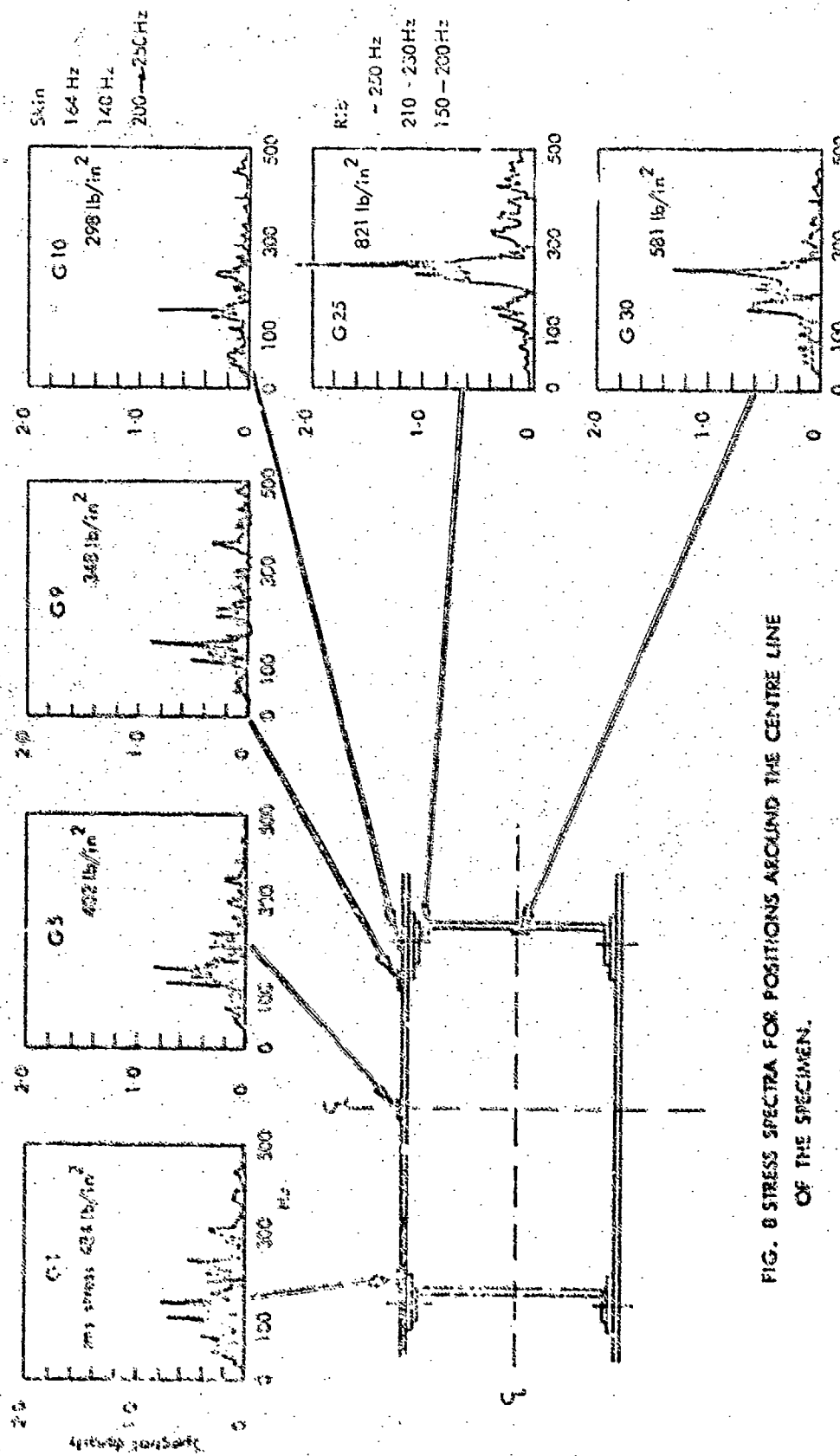
FIG. 8 STRESS SPECTRA FOR POSITIONS AROUND THE CENTRE LINE
OF THE SPECIMEN.
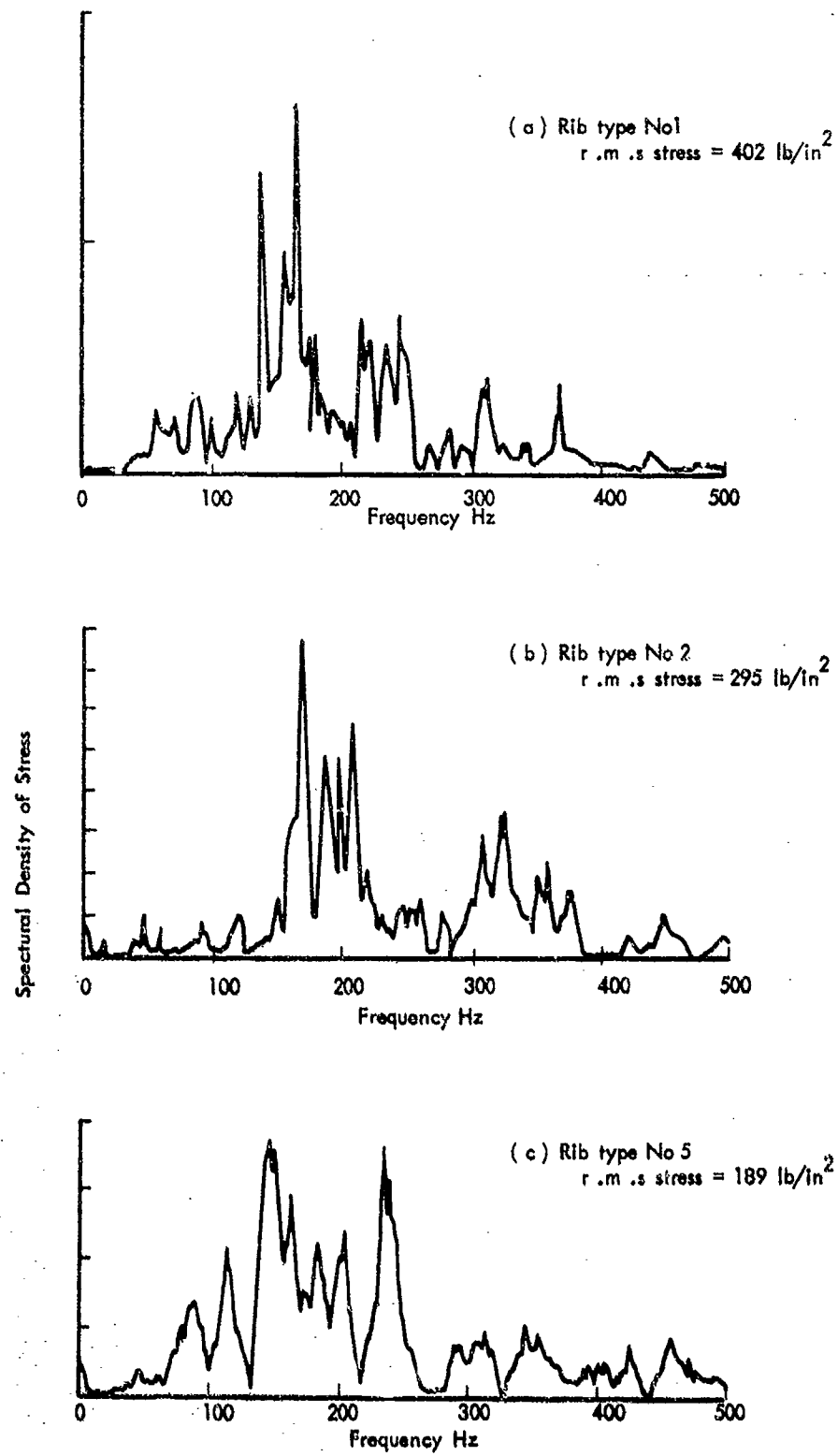
FIG. 9 SPECTRA OF STRAIN IN SKIN (gauge No 5)

(a) Rib type No 1
r.m.s stress = 581 lb/in^2

(b) Rib type No 2 (centre of rib web gauge No 28)
r.m.s stess = 933 lb/in^2

(c) Rib type No 2 (over centre of stiffener, gauge No30)
r.m.s stress = 127 lb/in^2

(d) Rib type No 5
r.m.s stress = 162 lb/in^2
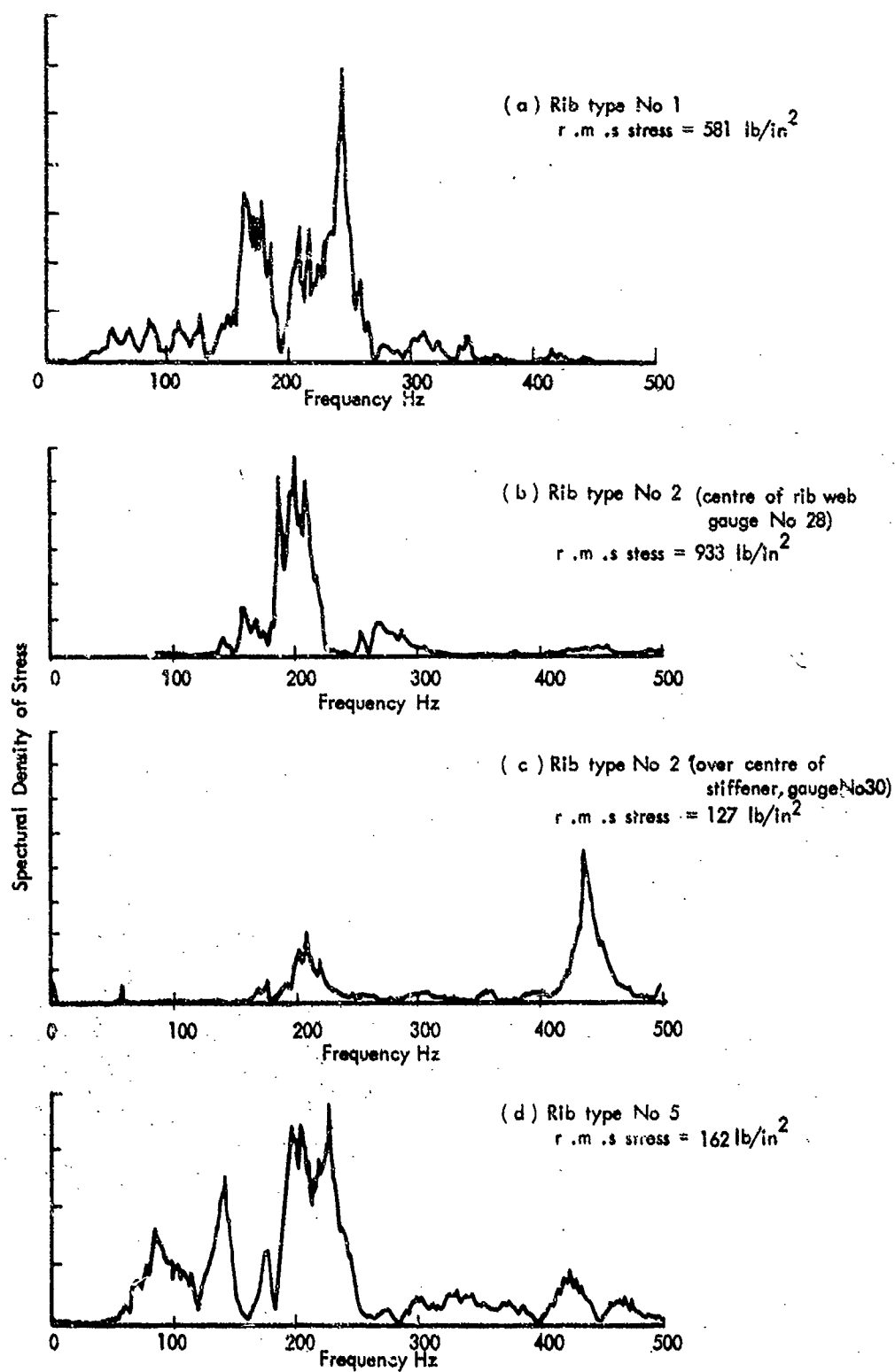
FIG.10 SPECTRA OF STRAIN AT MID DEPTH OF RIB (gauge No 30)

(a) Rib type No 1
r .m .s stress = 821 lb/ in^2

(b) Rib type No 2
r .m .s stress = 728 lb/ in^2

(c) Rib type No 5
(adjacent to excitation)
r .m .s stress = 850 lb/in^2

(d) Rib type No 5
(opposite side to excitation)
r .m .s stress = 432 lb/in^2

Spectural Density of Stress

Frequency Hz
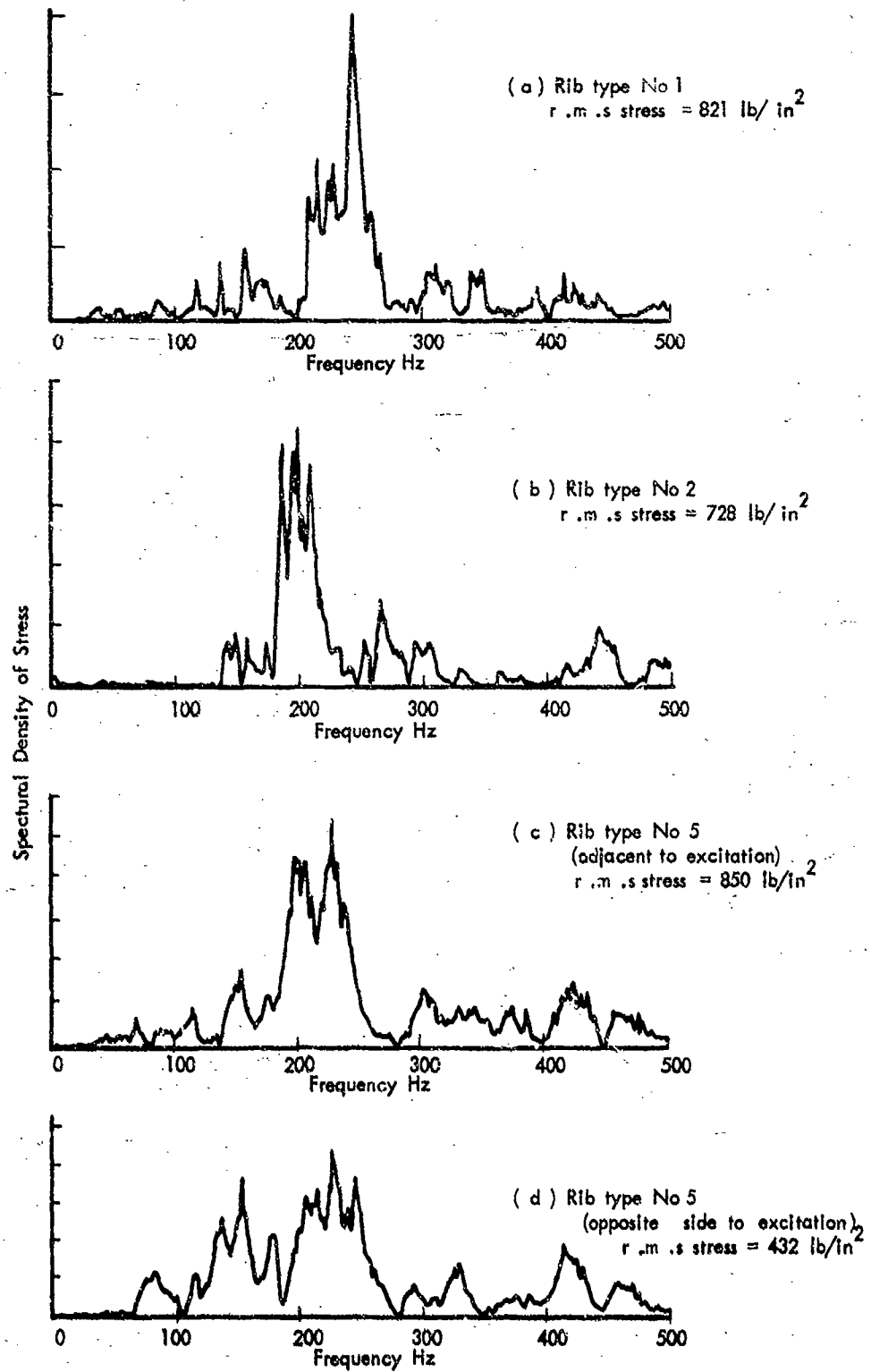
FIG. 11 SPECTRA OF STRAIN IN RIB BEND RADIUS (gauge No 25)

CORRELATION OF SONIC FATIGUE FAILURES IN LARGE
FAN ENGINE DUCTS WITH SIMPLIFIED THEORY

by

Jaak Soovere
Lockheed-California Company
Burbank, California 91503, U.S.A.

SUMMARY

The nature of the large fan jet engine intake duct noise and its effect on the duct structure are briefly described. A simple semi-empirical method is developed to predict the stresses in intake duct structure induced by fan noise. The predicted stresses at the failure location, show good correlation with random fatigue data for bending across the rivet line.

LIST OF SYMBOLS

a	constant
b, b_B	panel width, 'panel' circumferential width
D	flexural rigidity $= Eh^3/12(1 - \nu^2)$
d	ratio of curved panel to flat panel stiffness $= D_x/D$
E	Young's modulus
f	frequency, Hz
h	shell skin thickness
I, I_R	second moment of area of flat panel, ring
I_x	second moment of area through curved panel cross section
k, k_R	amplitude constant for shell, ring
$k_{m,n}$	panel bending wave numbers in the x and y directions respectively
ℓ	ring spacing or panel length
M_n	generalized mass
m,n	mode numbers in the x and y directions respectively
P_n, $\bar{P}$	generalized force, non dimensional generalized force
R	shell radius
u,v,w	shell modal displacements in the x, y and z directions respectively
x,y,z	shell coordinates in the axial, circumferential and radial directions respectively
y	distance from the ring neutral axis to the duct skin
α	constant
δ	viscous damping coefficient
ϵ, ϵ_{yR}	strain, ring strain
θ	angle subtended by the 'panel'
ν	Poisson's ratio
ρ	mass density
σ	stress
ω, ω_n	frequency, natural frequency in radians/sec.

1.   INTRODUCTION

The advent of the high by-pass ratio turbo-fan engine has been accompanied by a rapid rise in the noise level produced by the fan inside the engine intake duct. The intake duct noise has reached an intensity sufficient to produce large dynamic stresses, even in off-resonance intake duct vibration, which exceed the fatigue limit.

Engine intake duct failures, attributed to the high frequency fan noise, have occurred on many current aircraft. Little information concerning these failures (1) is available in current literature. No analytical design procedures, that can be applied in the early design stage, have been developed to eliminate these failures. The complex nature of the fan noise field, varying in its spectral content from engine to engine, indicates that a semi-empirical approach must be used to describe the duct structural response. In order to understand the effect of the fan noise on the surrounding duct structure, a brief description of the fan noise field is necessary.

2.   THE FAN NOISE

The intake duct noise environment is a function of the fan diameter, the fan RPM, the fan blade tip Mach number and the density of the air. At low fan speeds, the acoustic energy is concentrated at the fundamental blade passage frequency and its higher harmonics as illustrated in Figure (1). The corresponding noise field acting on the duct structure, can be visualised as the sum of lobed circumferential pressure patterns, containing a predominant single positive and negative lobe per blade. These lobes are in phase throughout the length of the duct and rotate at the fan RPM (2, 3). The intensity of the noise field decays rapidly with distance from the fan face.

When the blade tip speed exceeds Mach 1, shock waves with large crest factors are generated near the leading edge of the blades. The small differences in the geometry in each of the blades, produce shocks of unequal strengths. The stronger shocks travel faster than the weaker shocks which results in a progressively irregular circumferential pressure pattern, spiralling upstream (4) at the fan RPM. The angle of the spiral increases with blade tip Mach number. The acoustic pressure falls off initially, within one blade chord with the inverse of the distance from the fan face raised to the power of one half (4, 5) and thereafter as the inverse of the distance. In long ducts a further change in the decay rate is observed, Figure (2).

The spectral content in the fan noise is characterised by discrete frequency spikes at multiples of the individual blade rotational frequency, commonly referred to as buzz-saw, Figure (3). Once the blade tip speed exceeds Mach 1, propagation becomes possible at frequencies below the fundamental blade passage frequency. Each of the buzz-saw components has its own critical blade tip Mach number which must be exceeded if propagation is to take place. The theoretically predicted (2, 5) and measured variation of the critical blade tip Mach number for each of the buzz-saw components, are illustrated in Figure (4).

The spectral content of the fan noise is dependent not only on the fan RPM but also on the variation of the speed of sound with temperature and, therefore, with altitude. The propagation of the first few buzz-saw components is only possible at altitude. Because of the differences in blade geometry from engine to engine, no two engines will have the same spectral content in the fan noise. If the blade tolerances can be improved, the spectrum level of the buzz-saw components will be considerably reduced and the noise energy will instead be concentrated in the blade passage frequency and its higher harmonics.

3.   THE DUCT RESPONSE

The rotating fan pressure field induces a similarly rotating stress field in the duct structure. The circumferential r.m.s. stresses in both the rings and the shell remain essentially constant around the circumference of the duct.

The duct shell stress spectrum, in Figure (5), exhibits a similar spectral content to that of the fan noise, which leads to the conclusion of a forced shell response. A more detailed examination, however, indicates that some of the buzz-saw stress components are amplified over a small region of the circumferential mode number n. This region occurs in the vicinity of the shell resonances (7, 8) as illustrated in Figure (6). One or more buzz-saw components will coincide with the shell resonance at some engine settings, but the engine hunting about these settings would considerably reduce the dwell time on resonance.

The shell response to the fan noise at subsonic tip speed and indeed to the 'clean' engine fan noise at supersonic fan tip speed, exhibits a similar stress spectrum to that of the fan noise, with the highest stress occurring at the fundamental blade passage frequency. The duct response in this case is forced by the fan noise and is characterised by a very sharp spike in the response spectrum, Figure (7) and Reference (1).

4.   SIMPLIFIED SHELL THEORY

In the discussion following the presentation of Arnold's and Warburton's paper (8) on the experimental verification of the theory of cylindrical shells, a simple method of predicting simply supported shell frequencies was suggested. It was based on the method for predicting the frequencies of engine blades with curved cross sections. The stiffness of the blade was computed using the second moment of area about the neutral axis drawn through the curved cross section of the blade, Figure (8). Considering the expression for the frequency of a simply supported flat plate, given by

$$f = \frac{1}{2\pi}\left(\frac{D}{h\rho}\right)^{\frac{1}{2}} \left\{ \left(\frac{m\pi}{\ell}\right)^2 + \left(\frac{n\pi}{b}\right)^2 \right\} \tag{1}$$

the frequency is seen to be the sum of the two beam frequencies in the x and y directions. It should, therefore, be possible to predict the frequencies of curved shells by including the increase in the stiffness due to curvature, in a similar expression.

Szechenyi (9) suggested that the flexural stiffness of integrally stiffened panels can be represented by

$$Dx\ km^4 + 2\ Dxy\ km^2kn^2 + Dy\ kn^4$$

where it was assumed that the cross rigidity Dxy lies somewhere between Dx and Dy and can be approximated by

$$Dxy = (Dx\ Dy)^{\frac{1}{2}}. \tag{2}$$

Using the same approach, the expression for the frequency of a simply supported cylindrical shell or curved panel is reduced to that of a simply supported orthotropic flat plate and is given by

$$f = \frac{1}{2\pi}\left(\frac{D}{\rho h}\right)^{\frac{1}{2}} \left\{ \left(\frac{Dx}{D}\right)^{\frac{1}{2}} \left(\frac{m\pi}{\ell}\right)^2 + \left(\frac{n\pi}{b}\right)^2 \right\} \tag{3}$$

where

$$\frac{Dx}{D} = \frac{Ix}{I} = \frac{6R^2}{h^2}\left\{1 + \frac{\sin\theta}{\theta} - 2\left(\frac{\sin(\theta/2)}{\theta/2}\right)^2\right\}$$

$$+ \frac{3}{2}\left\{1 + \frac{\sin\theta}{\theta} - \frac{4}{3}\left(\frac{\sin(\theta/2)}{\theta/2}\right)^2\right\} \tag{4}$$

Dx/D is the ratio of the curved panel stiffness to the flat panel stiffness.

The accuracy of this method is illustrated in Figure (9), in which the frequencies predicted by Equation (3) are compared with those predicted by shell theory (7). Reasonably good agreement is obtained in the region where the bending strain energy predominates over the extensional strain energy. In general, this method is not as accurate in predicting the resonant frequencies of simply supported curved panels as the approximate method suggested by Szechenyi (9) and Armenakas (10), but it does result in a simple expression for the stresses in the curved panels and shells.

The equivalent orthotropic panel surface strain displacement relationships, in the axial and circumferential directions, are given by

$$\epsilon_x = -\frac{h}{2}\left(\frac{Ix}{I}\right)^{1/3} \frac{\partial^2 w(x,y)}{\partial x^2}$$

$$\epsilon_y = -\frac{h}{2} \frac{\partial^2 w(x,y)}{\partial y^2} \tag{5}$$

Using the normal mode approach, and assuming a predominant single mode response, a simply supported mode shape and harmonic motion, the maximum panel centre stresses are given by

$$\sigma_x = \frac{Eh\pi^2}{2(1-\nu^2)} \frac{\left\{\left(\frac{Ix}{I}\right)^{1/3}\left(\frac{1}{\ell}\right)^2 + \nu\left(\frac{1}{b}\right)^2\right\}P_n}{M_n\omega_n^2\left\{1 - \left(\frac{\omega}{\omega_n}\right)^2 + 2i\delta\frac{\omega}{\omega_n}\right\}}$$

$$\sigma_y = \frac{Eh\pi^2}{2(1-\nu^2)} \frac{\left\{\left(\frac{1}{b}\right)^2 + \nu\left(\frac{Ix}{I}\right)^{1/3}\left(\frac{1}{\ell}\right)^2\right\}P_n}{M_n\omega_n^2\left\{1 - \left(\frac{\omega}{\omega_n}\right)^2 + 2i\delta\frac{\omega}{\omega_n}\right\}} \tag{6}$$

where M_n, the generalized mass and P_n, the generalized force, are defined by

$$M_n = \int_A M(x,y)w_n^2(x,y)\,dA = a\rho b\ell h$$

$$P_n = \int_A P(x,y)w_n(x,y)\,dA = a\ell b P \tag{7}$$

On substituting Equations (3) and (7) into (6),

$$\sigma_x = \frac{6\alpha P}{\pi^2 aK(\omega)}\left(\frac{\ell}{h}\right)^2 \frac{\left\{\left(\frac{Ix}{I}\right)^{1/3} + \nu\left(\frac{\ell}{b}\right)^2\right\}}{\left\{\left(\frac{Ix}{I}\right)^{\frac{1}{3}} + \left(\frac{\ell}{b}\right)^2\right\}^2}$$

$$\sigma_y = \frac{6\alpha P}{\pi^2 aK(\omega)}\left(\frac{b}{h}\right)^2 \frac{\left\{1 + \nu\left(\frac{Ix}{I}\right)^{1/3}\left(\frac{h}{\ell}\right)^2\right\}}{\left\{1 + \left(\frac{Ix}{I}\right)^{\frac{1}{3}}\left(\frac{b}{\ell}\right)^2\right\}^2} \tag{8}$$

where

$$K(\omega) = \left\{1 - \left(\frac{\omega}{\omega_n}\right)^2 + 2i\delta\frac{\omega}{\omega_n}\right\}$$

Equation (8) is valid for both forced and resonant structural response.

5. APPLICATION OF THE THEORY

In using the above theory to define the stresses in the engine intake ducts, the format of Equation (8) is retained but the amplitude constant, k, and the curved panel to flat panel stiffness ratio, d, are now determined empirically from strain gauge measurements. In addition, the following assumptions must be made:

(a) The total displacement of the intake duct structure, is the sum of the ring displacement in which the duct skin acts essentially as an added mass, and the duct skin displacement relative to the adjacent rings.

(b) The average 'frozen' circumferential wavelength in the duct structure is equal to the distance between two adjacent blade tips. The effective circumferential 'panel' length b_B is, therefore, equal to half this distance.

(c) The small angle of the spiral has a negligible effect on the 'panel' centre stresses.

Assumption (b) is important as it defines the magnitude of the circumferential strain in the duct structure.   At subsonic blade tip speed this assumption is justified by the nature of the fan noise as described in Section 2 and verified by the measured strain data in Figure (7). At supersonic blade tip speed, even with relative motion between the individual shocks, the average number of shocks felt by the structure is still equal to the number of blades. The magnitude of the time averaged circumferential strain is, therefore, determined by the average frozen circumferential wave length which is equal to the distance between two adjacent blade tips.

On introducing the above assumptions into the theory, the axial and the circumferential 'panel' centre r.m.s. stresses are defined by

$$\sigma_x = k^\beta \left(\frac{\ell}{h}\right)^2 \frac{\{d^{1/3} + \nu(\frac{\ell}{b_B})^2\}}{\{d^\ell + (\frac{\ell}{b_B})^2\}^2}$$

(9)

$$\sigma_y = \frac{k_R \bar{y}\, b_B^{2} \ell^\beta}{I_R} + k^\beta \left(\frac{b_B}{h}\right)^2 \frac{(1 + \nu d^{1/3}(\frac{b_B}{\ell})^2)}{(1 + d^\ell (\frac{b_B}{\ell})^2)^2}$$

The parameter d is extracted from the strain gauge data using the following relationship:

$$d = \left(\frac{\ell}{b_B}\right)^6 \left(\frac{\varepsilon_x}{\varepsilon_y - \varepsilon_{yR}}\right)^3$$

(10)

and is plotted in Figure (10) against the 'panel' aspect ratio. The amplitude constant k is thereafter determined from

$$k = \frac{E\varepsilon_x}{(1 - \nu^2)} \left(\frac{h}{\ell}\right)^2 \frac{1}{\beta} \frac{(d^\ell + (\frac{\ell}{b_B})^2)^2}{d^{1/3}}$$

(11)

and is plotted in Figure (11) as a function of distance from the fan face. The amplitude constant k_R for the rings has a similar variation with distance from the fan face but of a different magnitude.

6. CORRELATION OF SIMPLE THEORY WITH SHELL THEORY

The shell theory in Reference (7) gives the following strain displacement relationships.

$$\varepsilon_x = \frac{\partial u}{\partial x} - z\frac{\partial^2 w}{\partial x^2}$$

(12)

$$\varepsilon_y = \frac{\partial v}{\partial y} + \frac{w}{R} - z\left(\frac{\partial^2 w}{\partial y^2} - \frac{1}{R}\frac{\partial v}{\partial y}\right)$$

The corresponding stress strain relationships are

$$\sigma_x = \frac{E}{1 - \nu^2}(\varepsilon_x + \nu\varepsilon_y)$$

(13)

$$\sigma_y = \frac{E}{1 - v^2} (\epsilon_y + v\epsilon_x)$$

Considering only the shell in between the rings, and assuming simply supported edges, the shell mode shapes are defined by

$$u = \bar{u} \cos \frac{ny}{R} \cos \frac{\pi x}{\ell}$$

$$v = \bar{v} \sin \frac{ny}{R} \sin \frac{\pi x}{\ell} \tag{14}$$

$$w = \bar{w} \cos \frac{ny}{R} \sin \frac{\pi x}{\ell}$$

Combining Equations (12), (13) and (14) and replacing n/R by π/b_B, the maximum axial shell stress is given by

$$\sigma_x = \frac{E z \bar{w} \pi^2}{(1 - v^2)\ell^2} \left\{ 1 + v(\frac{\ell}{b_B})^2 - \frac{1}{2} \frac{\ell}{\pi} \frac{\bar{u}}{\bar{w}} \right.$$

$$\left. + v(\frac{1}{2} \frac{\ell}{\pi} \frac{\ell}{b_B} \frac{\bar{v}}{\bar{w}} + (\frac{\ell}{\pi})^2 \frac{1}{2} \frac{1}{R}) \right\} \tag{15}$$

The equivalent expression from the simple theory is

$$\sigma_x = \frac{E z \bar{w} \pi^2}{(1 - v^2)\ell^2} \left\{ d^{1/3} + v(\frac{\ell}{b_B})^2 \right\} \tag{16}$$

On comparing equations (15) and (16) after substituting h/2 for z, it is observed that

$$d^{1/3} = 1 - \frac{2}{h} \frac{\ell}{\pi} \frac{\bar{u}}{\bar{w}} + v(\frac{2}{h} \frac{\ell}{\pi} \frac{\ell}{b_B} \frac{\bar{v}}{\bar{w}} + (\frac{\ell}{\pi})^2 \frac{2}{h} \frac{1}{R}) \tag{17}$$

The theoretically predicted variation of the stiffness parameter d, defined by Equation (17), with the 'panel' aspect ratio, is illustrated in Figure (10). The modal intensities $\bar{u}$, $\bar{v}$ and $\bar{w}$ used in Equation (17), are computed from the shell theory in Reference (7). The variation of the stiffness parameter d for the fixed fixed shell edge condition, is computed from the empirically determined equivalent wave length method given in Reference (8). On comparing the measured data with the predicted variation, a cross over from a fixed fixed to a simply supported edge condition is observed, for a 'panel' aspect ratio just greater than unity. This cross over point corresponds to the critical ring spacing, of an internally pressurized ring stiffened shell (11), beyond which the rings cease to have an effect on each other.

7.   PREDICTED CRITICAL DUCT STRESSES

Generally speaking the sonic fatigue critical stresses occur in regions of high stress concentration such as along rivet lines where the skin is attached to substructure. Because of the problems associated with instrumenting the flow side of the duct, all strain gauges in the measurement program were placed on the exterior surface of the duct. Biaxial gauges were located on the skin panels midway between adjacent rings and single gauges were located in the circumferential direction, on both the base and the top flanges of the rings, at various axial and circumferential positions along the duct. To obtain an estimate of the skin axial stresses at the ring rivet lines, the 'panel' edge to 'panel' centre stress ratio is obtained from Reference (12), for a flat panel with two opposite sides simply supported and the remaining two sides fixed. This ratio is plotted in Figure (12) as a function of panel aspect ratio. A ratio of 2 to 2.5 is indicated for the range of data considered in this paper.

A typical variation in the duct stresses with ring spacing, predicted by the semi-empirical theory at a distance of a half fan diameter from the fan face, is illustrated in Figure (13). The peak stresses are seen to occur at a ring spacing close to the 'panel' width b_B.

The critical axial shell stresses at the ring rivet lines, can be reduced by the addition of doublers to the duct shell below the rings (1). Alternatively all the circumferential and axial stresses in the duct structure, can be reduced by employing a ring spacing well below the 'panel' width b_B. The spectrum level of the fan noise at the blade passage frequency, may exceed the buzz-saw spectrum level by 6 to 15 dB, for engines operating at high subsonic and for clean engines, at supersonic blade tip speeds. Duct shell resonances must, therefore, be avoided in this region. This requirement generally places a lower limit on the acceptable ring spacing.

8. CORRELATION OF PREDICTED STRESSES WITH FAILURE DATA

During the development program, sonic fatigue failures were experienced by the duct. The nature of the cracks, which occurred in the skin at the ring rivet lines, indicated the axial stresses to be the critical stresses. The magnitude of edge stresses at the failure locations were predicted as described in this paper. Times to failure were converted to cycles of stress by means of time history plots of representative duct strains. The results are summarized in Figure (14). An analysis of the duct strain data shows the instantaneous strain to have a Gaussian density distribution, Figure (15). This justifies the use of random fatigue data in the design criteria. As can be noted in Figure (14), the failure stresses predicted by the semi-empirical approach shows good correlation with the random fatigue curve from Reference (13).

REFERENCES

1. I. Holehouse, Sonic Fatigue of Aircraft Structure Due to Engine Fan Noise.
   Conference on Sonic Fatigue, ISVR, England, 6-9th July 1970.

2. J.M. Tyler, T.C. Sofrin. Axial Flow Compressor Noise Studies.
   S.A.E. Trans., Vol. 70, p.309, 1962.

3. C.L. Morfey. Rotating Pressure Patterns in Ducts: Their Generation and Transmission.
   J. Sound Vib. Vol. 1, pp. 60-87. 1964.

4. T.G. Sofrin, G.F. Pickett. Multiple Pure Tone Noise Generated by Fans at Supersonic Tip Speeds.
   Symposium on Fluid Mechanics, September 1970. Pennsylvania State University.

5. C.L. Morfey, M.J. Fisher. Shock Wave Radiation from a Supersonic Ducted Rotor,
   J.R. Ae. Soc. Vol. 74, p. 580, July 1970.

6. S. Slutsky. Discrete Noise Generation and Propagation by a Fan Engine.
   Aerodynamic Noise, University of Toronto Press, 1969.

7. J.L. Sewall, E.C. Naumann. An Experimental and Analytical Vibration Study of the Cylindrical
   Shells With and Without Longitudinal Stiffeners.
   NASA TND-4705, September 1968.

8. R.N. Arnold, G.B. Warburton. Flexural Vibration of Thin Cylinders.
   Proc. Inst. Mech. Eng. Vol. 167, 1953.

9. E. Szechenyi. Approximate Methods for the Determination of the Natural Frequencies of
   Stiffened and Curved Plates.
   Conference on Sonic Fatigue, ISVR, England. 6-9th July 1970.

10. A.E. Armenakas. On the Accuracy of Some Dynamic Shell Theory.
    Proc. Am. Soc. Civ. Eng. 1967. J.E. Mec. 93, EM5. pp. 95-109.

11. R.J. Roark. Formulas for Stress and Strain.
    McGraw-Hill.

12. S. Timoshenko, S. Woinowsky-Krieger. Theory of Plates and Shells.
    McGraw-Hill (2nd Edition).

13. G.S. Johnson. Skin Cracking Due to Engine Noise.
    McDonnell Report 4685, August 1957.
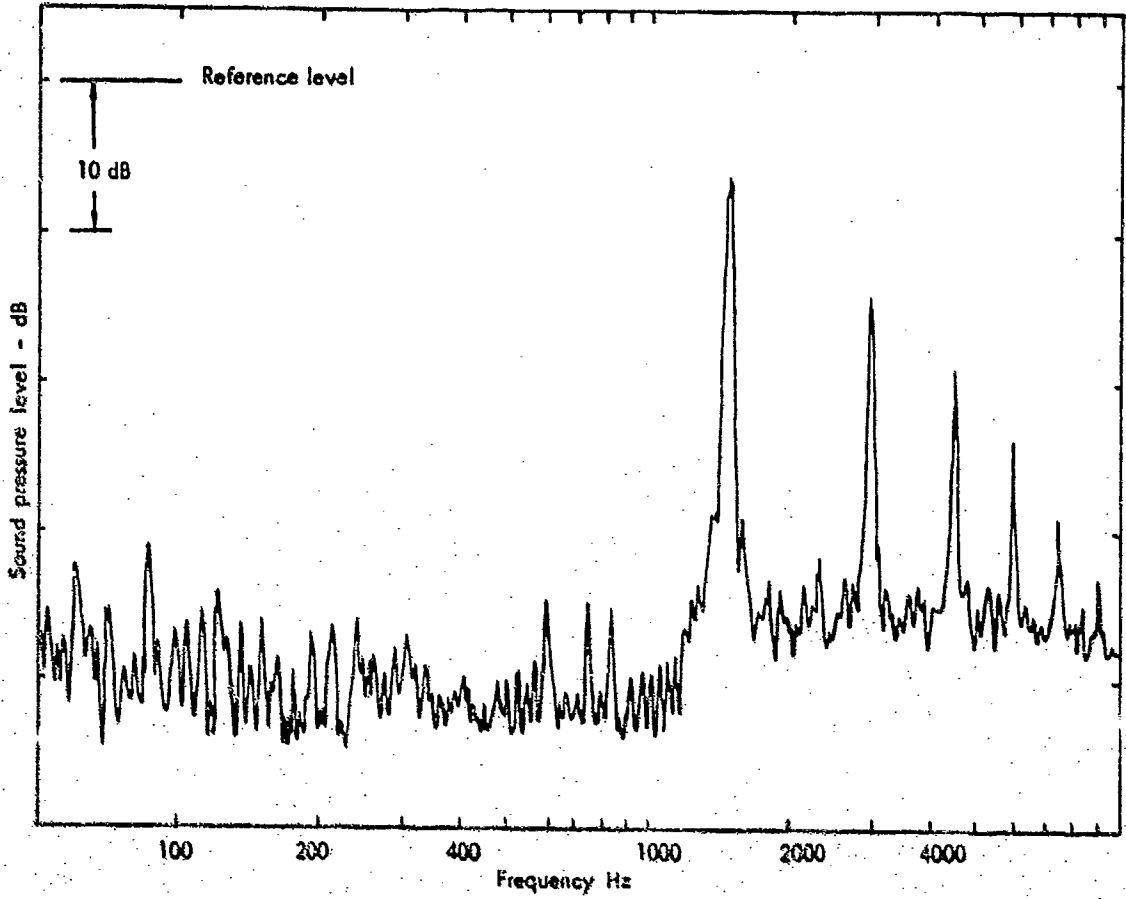
FIG 1 NARROW BAND ANALYSIS OF THE FAN NOISE AT SUBSONIC BLADE TIP SPEED
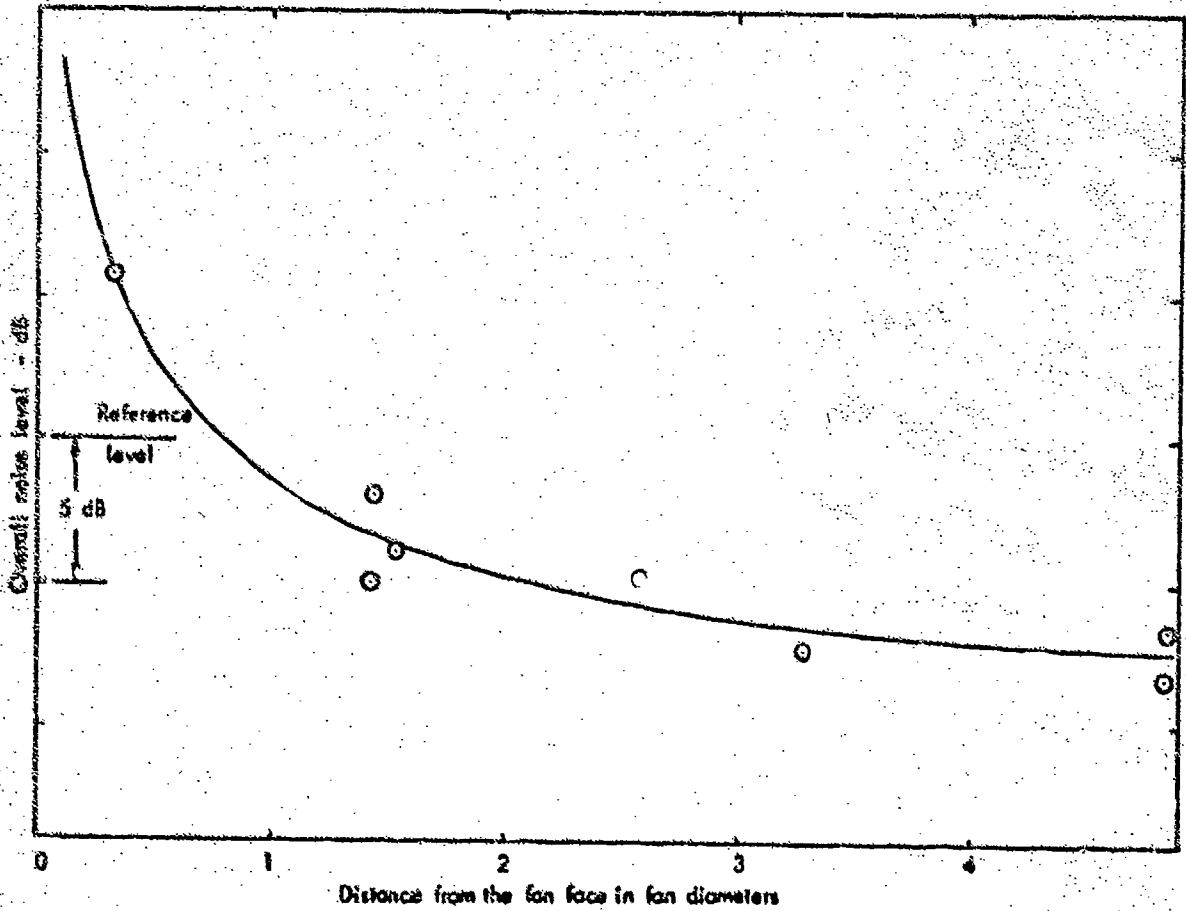
FIG 2 FAN OVERALL NOISE LEVEL AS A FUNCTION OF DISTANCE FROM THE FAN FACE
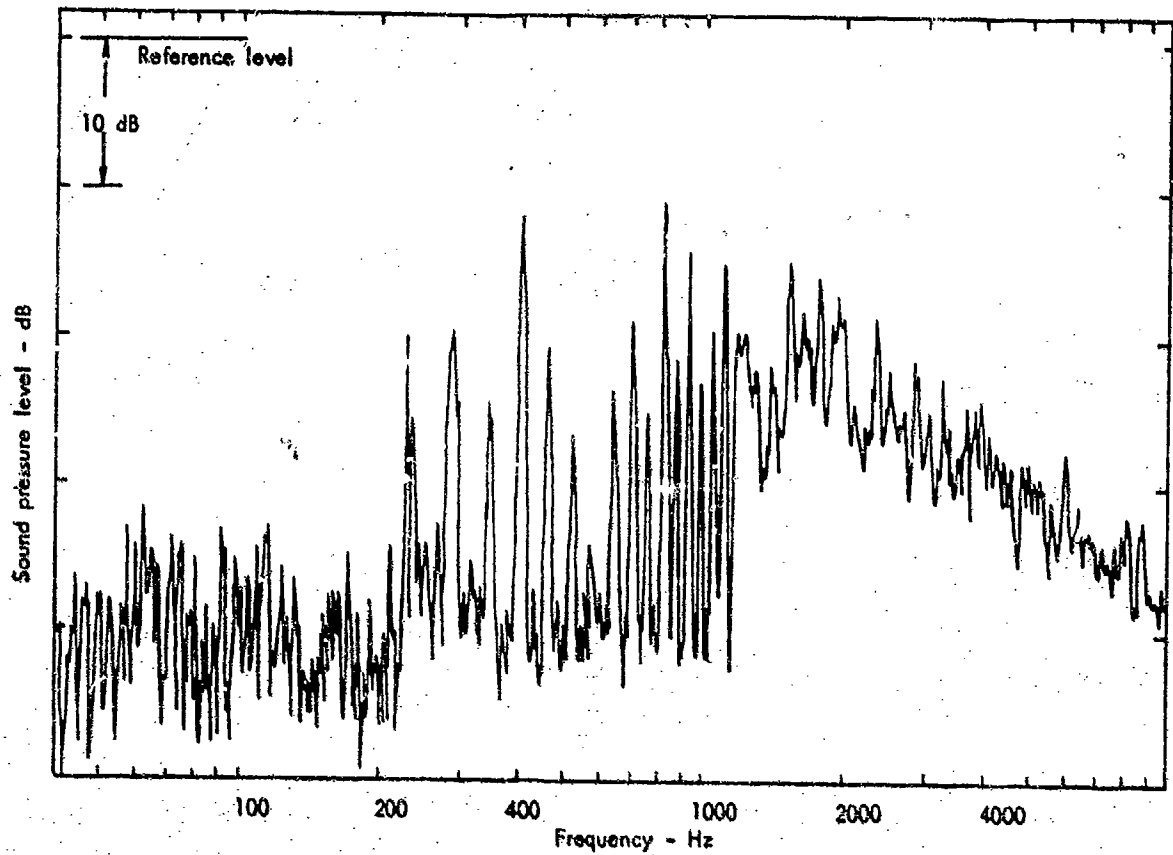
FIG 3 NARROW BAND ANALYSIS OF THE FAN NOISE AT SUPERSONIC BLADE TIP SPEED
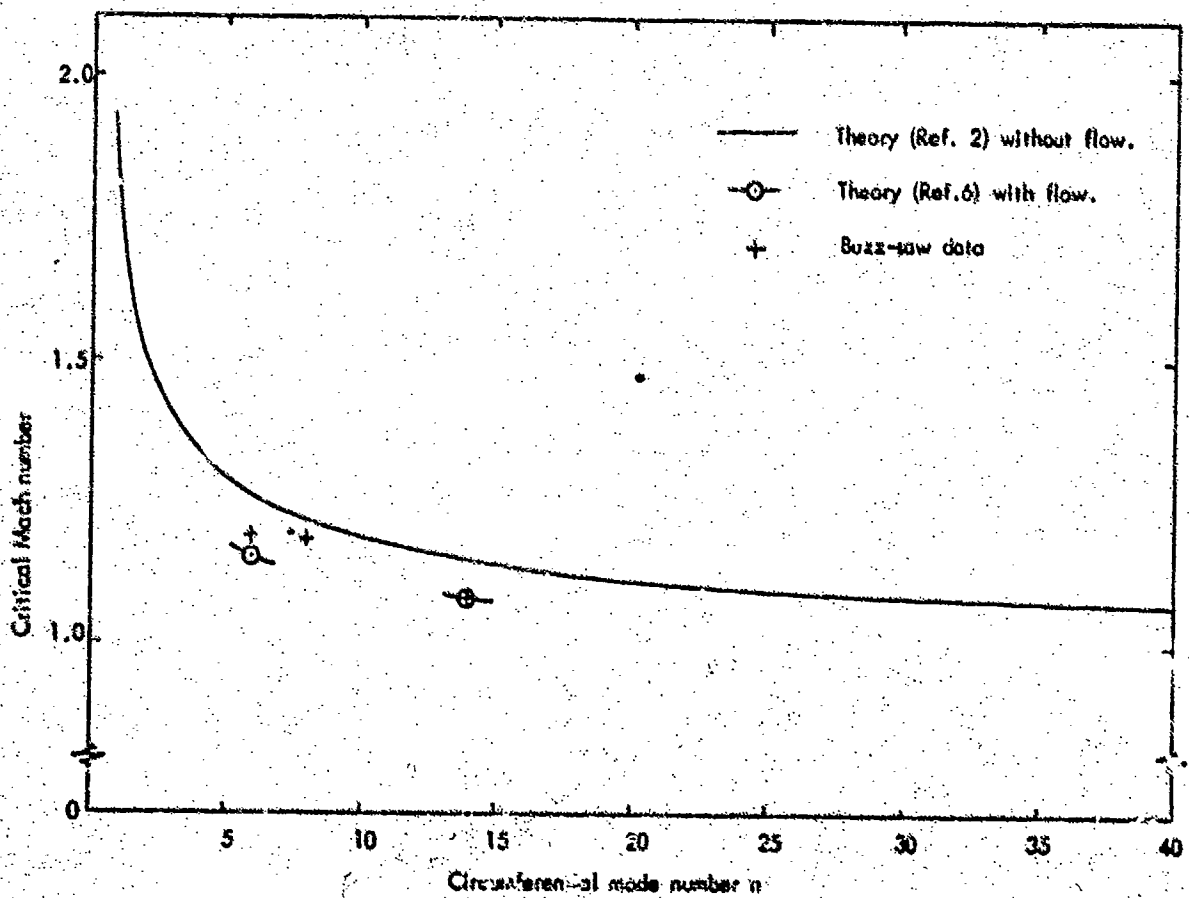
FIG 4 CRITICAL MACH NUMBER FOR CYLINDRICAL DUCTS WITH ZERO HUB TO TIP RATIO

4.3 in. Ring spacing
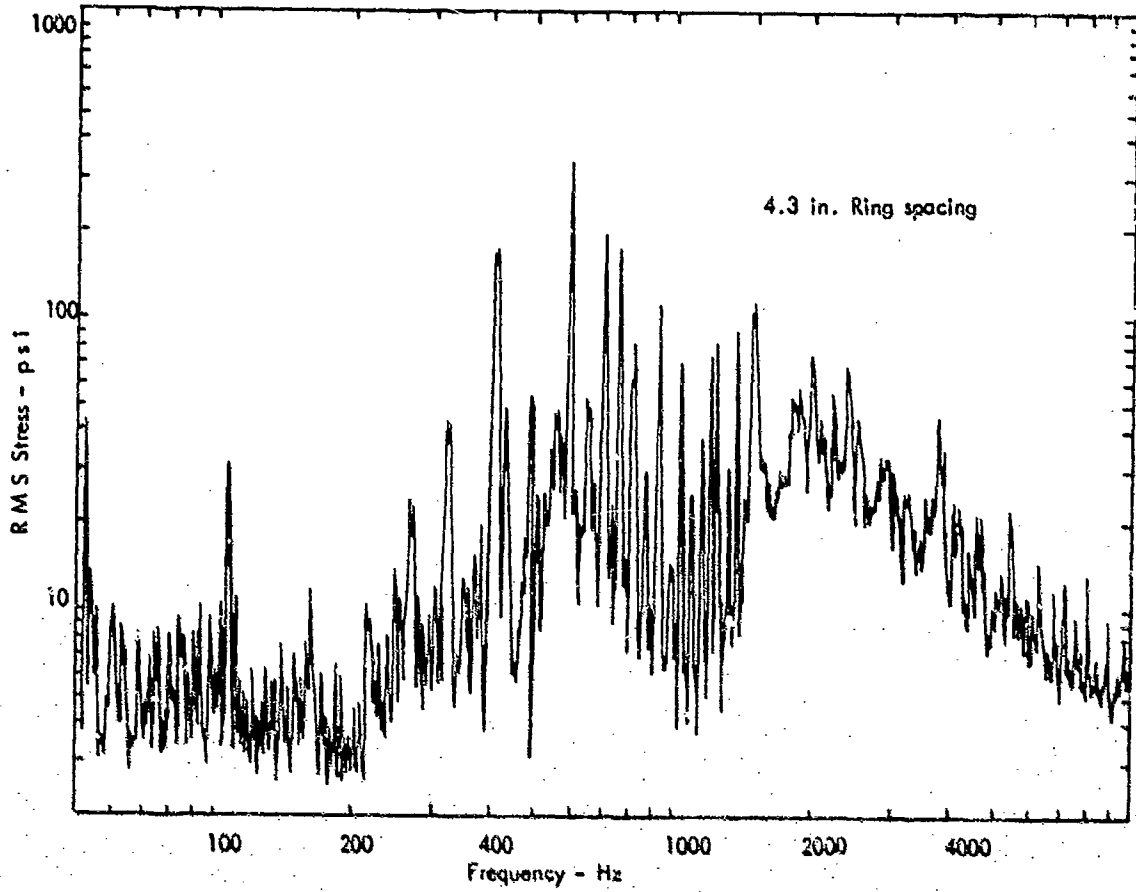
FIG 5 TYPICAL DUCT SHELL STRESS SPECTRUM

Buzz-saw

Ring spacing 4.3 in.
m = 1

Fixed Fixed
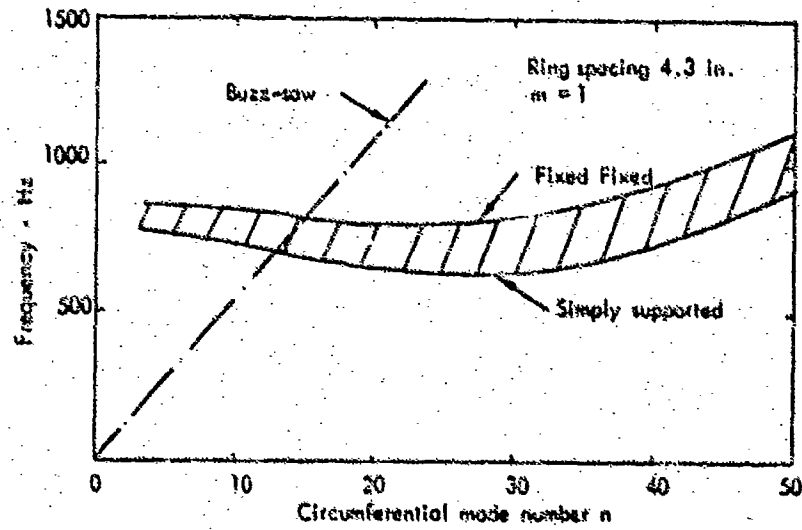
Simply supported

FIG 6 THEORETICAL SHELL RESONANT FREQUENCIES
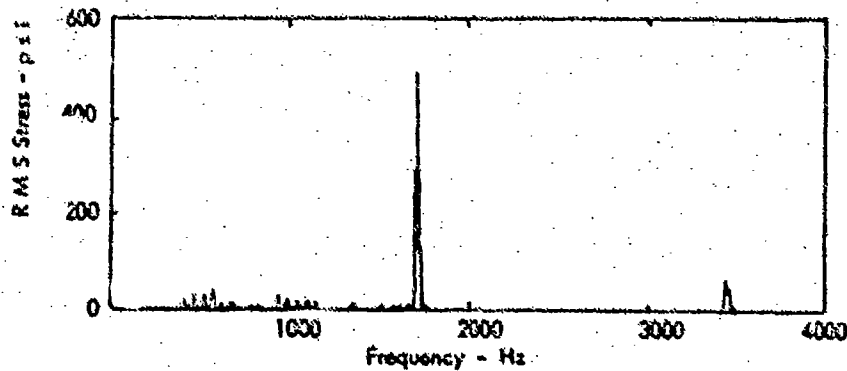
FIG 7 TYPICAL DUCT SHELL FORCED STRESS SPECTRUM
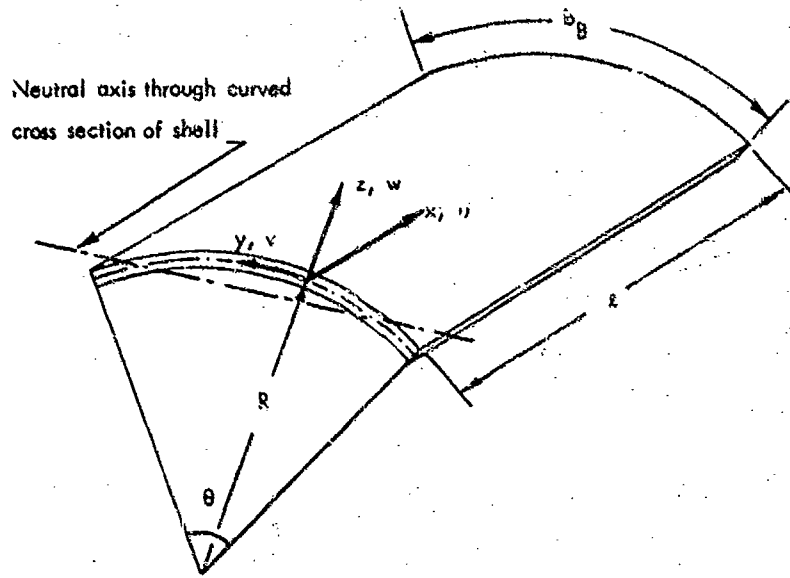
FIG 8 COORDINATE SYSTEM OF THE ' PANEL '
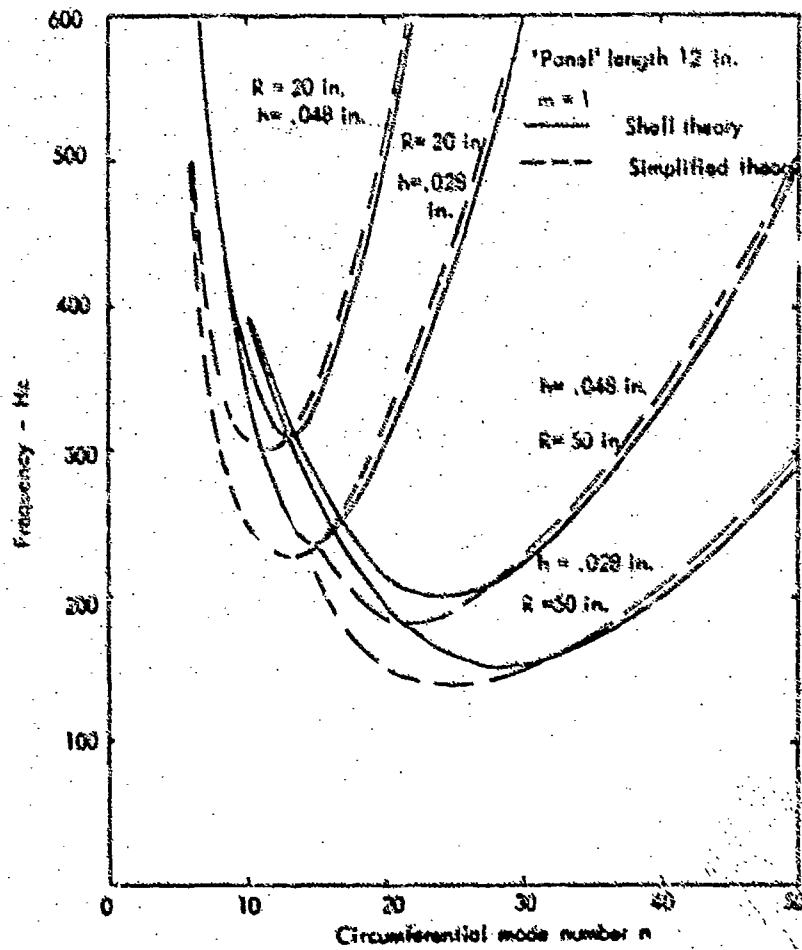
FIG 9 SIMPLY SUPPORTED SHELL RESONANT FREQUENCIES FROM SHELL
THEORY AND SIMPLIFIED THEORY
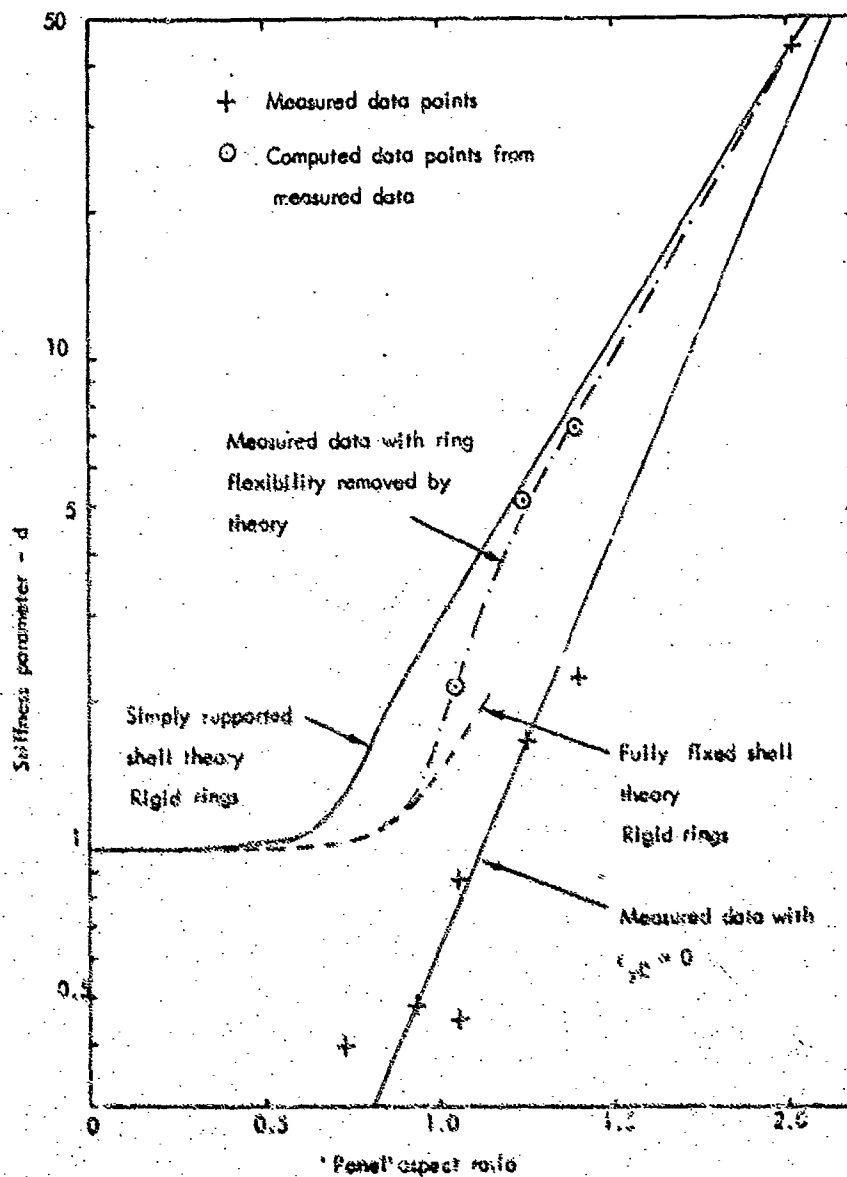
FIG 10 CURVED SHELL STIFFNESS PARAMETER AS A FUNCTION OF THE 'PANEL' ASPECT RATIO
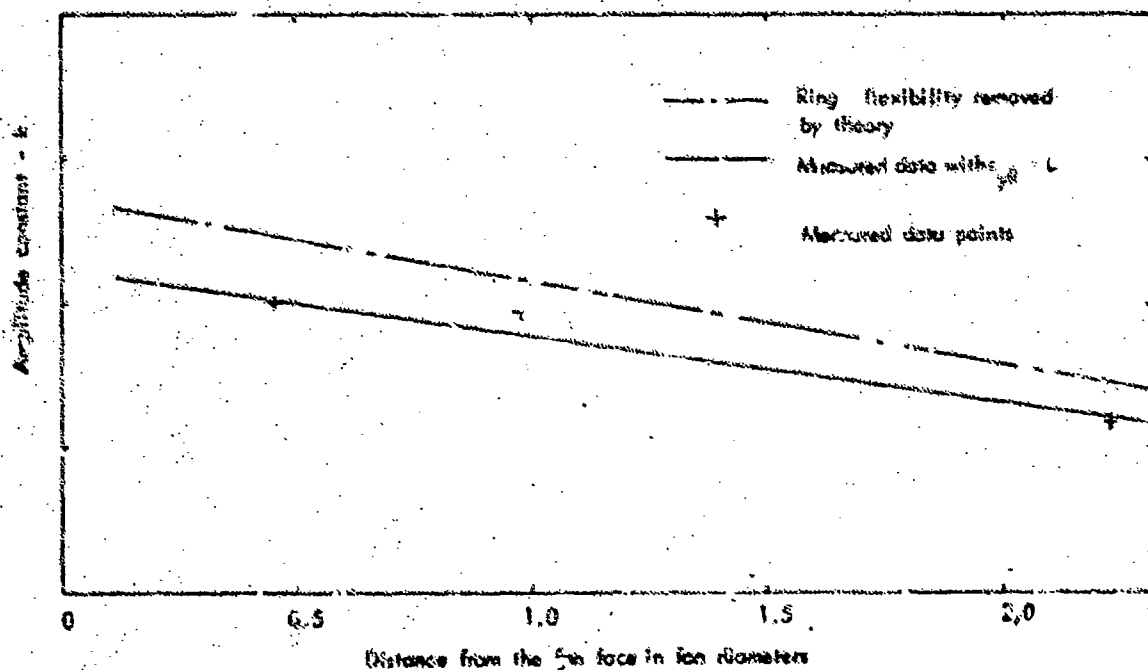
FIG 11 AMPLITUDE CONSTANT AS A FUNCTION OF DISTANCE FROM THE FAN FACE
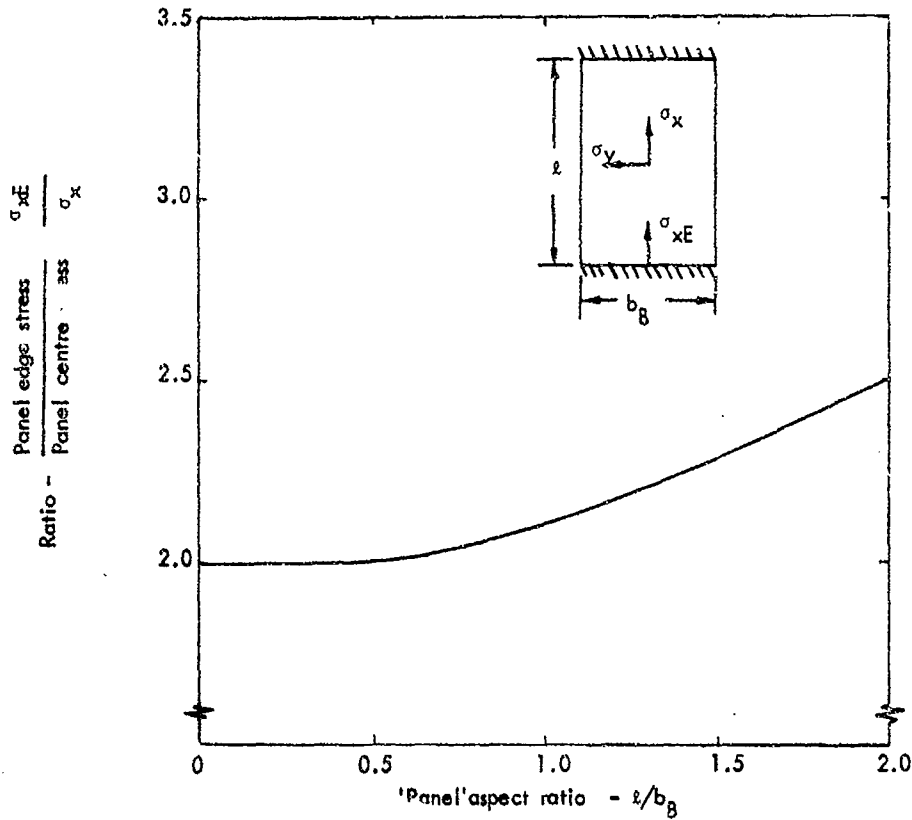
FIG 12 RATIO OF 'PANEL' EDGE TO CENTRE STRESS AS A FUNCTION OF 'PANEL' ASPECT RATIO
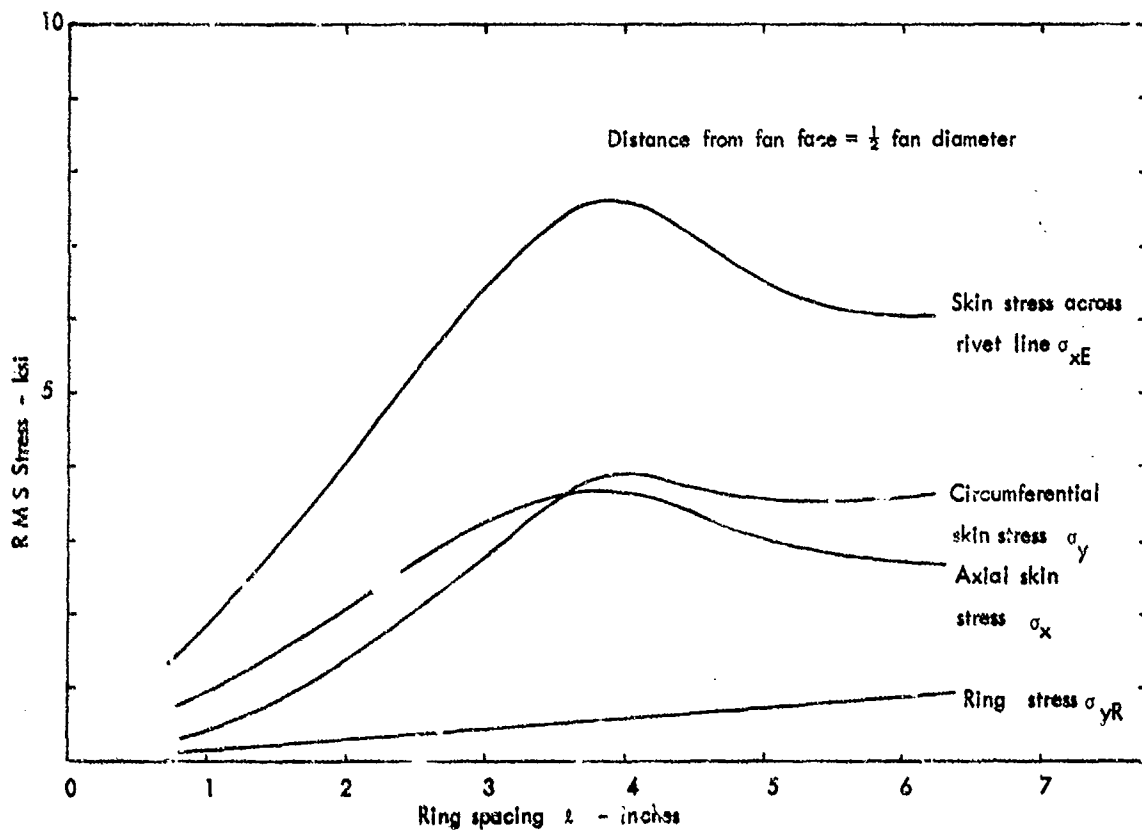
FIG 13 PREDICTED STRESSES IN THE INTAKE DUCT STRUCTURE AS A FUNCTION OF RING SPACING
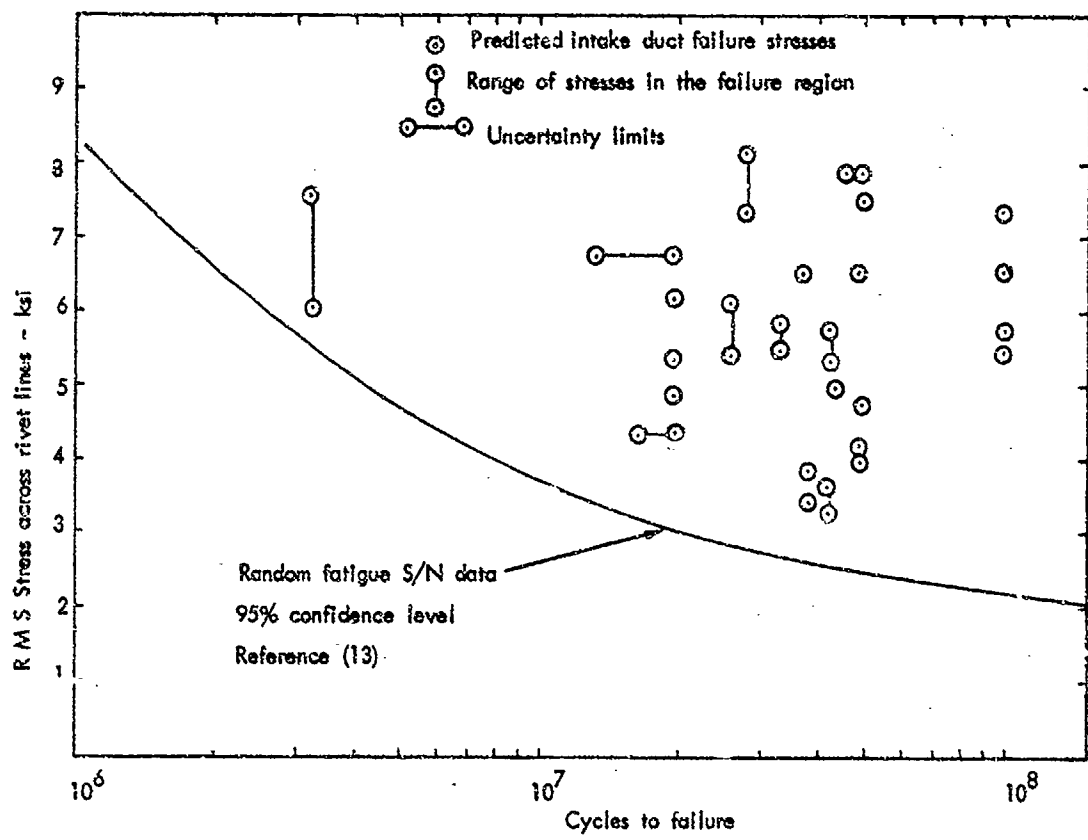
FIG 14 R M S STRESS ACROSS THE RIVET LINES AS A FUNCTION OF CYCLES TO FAILURE
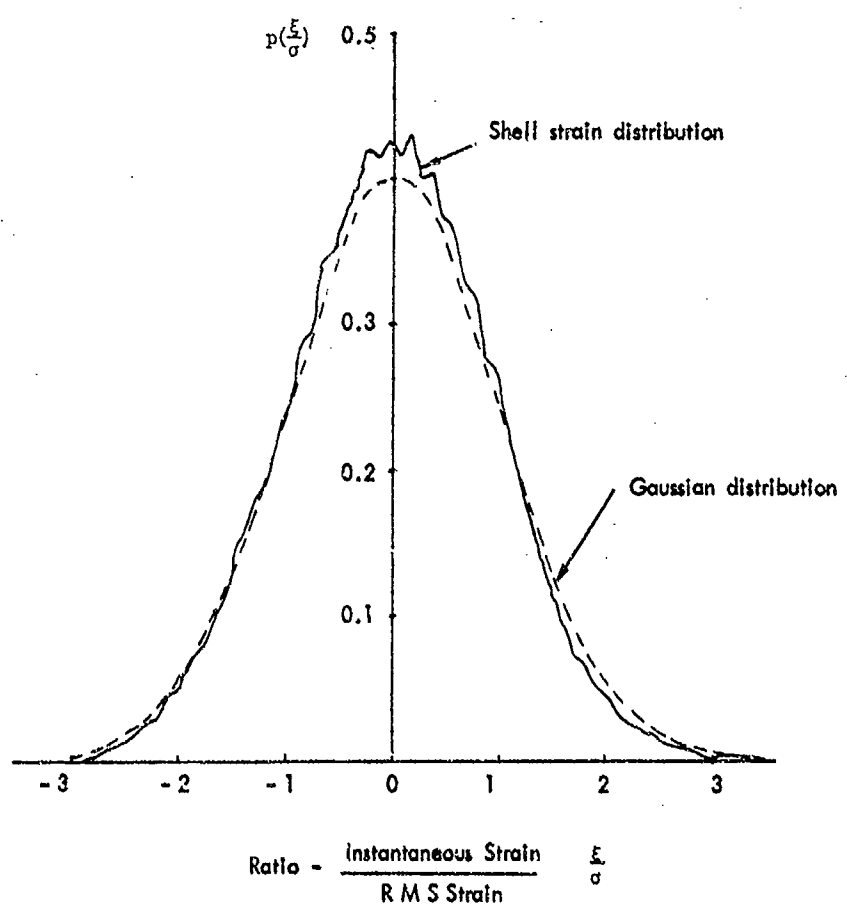
FIG 15 NORMALISED PROBABILITY DENSITY FUNCTION OF THE DUCT SHELL
STRAIN RESPONSE

SESSION 3   DISCUSSION - DESIGN METHODS

Mr. Thomson raised the question of definition of fatigue failure but no one was able to propose a generally accepted criterion. This point was discussed at some length in the general discussion period. He also drew attention to discrepancies in some of the data on the response of honeycomb panels. One worker had reported that there was a difference in the dynamic stress in the centre of the two face plates which could be as great as 2.5 to 1. Other workers had not made comparisons. Members having test programmes running in the near future agreed to check this point and report back to ESDU. They would also attempt to correlate any differences with differences in edge 'close cut' design. The first set of design data sheets for stiffened panels referred to panels having stiffeners which were stiff in bending. Although many designers do not use stiffeners which are weak in bending there is a need for a data sheet on this latter type of construction. Providing that the stress concentrations at the ends of the lighter stiffeners are adequately treated this type of design can be very efficient.

Mr. Soovere pointed out that the new generation of high bypass ratio engines give different stress time history patterns in intake stresses from those found in the intake structure of low bypass ratio engines. In the earlier generation of engines the spectra do not change significantly during flight, but in the new high bypass ratio engines there can be higher levels in flight than at take off because the fan has a higher speed in flight. The pressure loading spectra in intake ducts such as the S duct of the Lockheed Tristar changes with altitude. This is thought to be due to a change in the mode of propagation of sound in the duct.

EXPERIMENTALLY DETERMINED DAMPING FACTORS

by

J.A. HAY

Chief Acoustics Engineer,
British Aircraft Corporation Limited,
Commercial Aircraft Division,
Brooklands Road,
Weybridge KT13 0SF,
Surrey,
United Kingdom.

SUMMARY

The degree of damping present in a structure is a very important parameter in determining the response of the structure to acoustic excitation. Unfortunately, the prediction of the damping present in any particular structure is not generally possible from theoretical considerations. Nor, on the other hand, is there very much experimental data available upon which to base an assessment.

During the last few years, a certain amount of damping data has been collected for a variety of structural specimens tested in the acoustic facilities of the British Aircraft Corporation.

This paper presents the collection of results obtained, and compares them for the different categories of structures tested.

INTRODUCTION

The inherent structural damping is a very important factor in determining the response of a structure to acoustic excitation. Unfortunately, the magnitude of the damping cannot be reliably predicted, and there is a dearth of relevant experimental data.

Over the last six years or so, a number of structural specimens have been tested in the acoustic facilities of the British Aircraft Corporation. From many of these tests it has been possible to extract data relating to the degree of damping present and, in the absence of better information, this data is presented here.

DAMPING OF STRUCTURES

Damping is responsible for energy dissipation during deformation of a material. This energy dissipation can be achieved in several ways. There can be material damping, slip or friction damping at joints, or damping due to the environment.

If a perfectly elastic material is deformed by the application of an external force, the work done by the force during the deformation is stored in the material. When the external force is removed, this stored energy causes the material to oscillate about its relaxed position. This is an un-damped system. In a perfectly plastic material all the work done by the external force is dissipated and no energy is stored in the material. Hence, removal of the external force leaves the material in its deformed state. This is a completely damped system. In practice materials are neither perfectly elastic nor perfectly plastic, but display both of these properties to a limited extent. The ratio of the plasticity and elasticity of a particular material is used to describe the behaviour of the material and is called the damping, or loss factor of the material.

In a built-up structure the damping does not solely consist of material damping. Damping is also introduced by the interaction of the material with its environment. In this category are such things as friction damping at joints and edges and air damping. The parameter used to describe the damping of a system is the damping ratio. This ratio takes into account all the forms of damping present in a structure.

If we consider, for simplicity, a single degree of freedom, damped system undergoing vibration due to a sinusoidal forcing function, we have an equation of motion:

$$m\ddot{x} + C\dot{x} + Kx = F(t)$$

where C = the viscous damping coefficient.

This coefficient will take a value determined by the properties of the system under investigation and the restraint placed upon the system. We define the critical value of damping coefficient as the minimum value of coefficient which leads to a non-oscillatory solution to the equation above. This value will be $2\sqrt{mK}$. We then define damping ratio as the ratio of actual damping coefficient to the critical damping coefficient.

i.e. Damping ratio:
$$\delta = \frac{C}{2\sqrt{mK}}$$

Since the circular natural frequency of such a system is defined by the equation

$$\frac{K}{m} = \omega^2 n$$

we can re-write the value of critical damping as $C_{rit} = 2\, m\omega n$.

And the damping ratio can similarly be written as

$$= \frac{C}{2\, m\omega_n}$$

So, for a viscously damped system, where the damping coefficient is independent of frequency, the damping ratio is inversely proportional to frequency.

For a system in which hysteretic damping is predominant, i.e. one in which the energy dissipation is mainly achieved through material deformation and slippage at the joints, an equivalent viscous damping coefficient can be defined as:

$$C_{eq} = \frac{\alpha}{\pi\omega}$$

where α is a constant independent of frequency.

For a derivation of this equation see Ref. 2.

The equation of motion of an hysteretically damped system can then be written in the form.

$$m\ddot{x} + \frac{\alpha}{\pi\omega}\dot{x} + Kx = F(t)$$

and such a system has a damping ratio defined as

$$\delta = \frac{\frac{\alpha}{\pi\omega}}{2m\omega} \qquad = \frac{\alpha}{2\pi\, m\omega^2}$$

Thus, for a system with hysteresis damping, where the equivalent damping coefficient is inversely proportional to frequency, the damping ratio is inversely proportional to the square of the frequency.

In practical structures the damping will not be wholly viscous but a summation of all forms of damping. The equation of motion will similarly be more complex, but the definition of damping ratio remains the ratio of actual to critical damping, where the critical damping is that for the mode of vibration under consideration. The exact calculation of the damping ratio of a structure is therefore impossible for several reasons. The exact mode of vibration is unlikely to be known. The effective mass of the system, its spring rate in any direction, the friction at its joints and the magnitudes of the damping coefficients are also generally not known precisely.

Damping ratios are therefore generally obtained empirically. If we plot strain level in the structure against frequency we get "peaks" at resonant frequencies. Let f_0 be the frequency of the resonance i.e. the frequency at the point of highest strain. If we take f_1 and f_2 to be the frequencies at which the strain has fallen to 0.707 ($1/\sqrt{2}$), of its maximum value, then we can obtain an approximation to the damping ratio by using the formula

$$\delta = \frac{df}{2} \times \frac{1}{f_0} \qquad \text{where } df = f_1 - f_2$$

Damping ratios can also be obtained by more accurate methods, such as the vector plotting method of Ref. 1.

This thus takes into account all forms of damping, e.g. visco-elastic, coulomb, material, and all edge effects and structural restrictions. We therefore, arrive at an overall damping ratio for a structure or a part of it, without knowing any of the physical properties of the structure, by analysing the response in this manner.

TEST WORK

The specimens considered here are listed in Tables 1(a) to 1(c) . They were tested under conditions of acoustical excitation in "siren channel" facilities of which the channel shown in FIG. 1 is typical. The specimens were placed against the open side of the channel, and excited by travelling sound waves passing down the channel. Some of the specimens were tested using discrete frequency excitation, and some using broad band. On some specimens, both types of excitation were used. However, most of the data presented here has been derived from discrete frequency tests.

In obtaining the damping ratios from these results, the strain gauge recordings were analysed in two ways. The majority of the results given have been derived from the "half power" method described above, but some of them have been obtained by the "vector plotting" method. For a few cases both methods have been used and, in order to check how they compare, these have been plotted in FIG. 2. Whilst there are differences between the results of the two methods shown in this limited selection, there does not appear to be any bias towards one method giving consistently higher values than the other. Within the accuracy of the two methods, they appear to give comparable results.

RESULTS

The results of the analysis carried out to date are shown, for the various types of structures, in FIGS. 3 to 9.

The immediate impression given by this widely scattered data is not faviurable. However, in the hope of getting some semblance of order, it is possible to fall back on the theoretical trends outlined above in, for:-

(i) Viscous damping,

$$\delta \propto \frac{1}{(Freq)}$$

(ii) Hysteretic damping,

$$\delta \propto \frac{1}{(Freq)^2}$$

and, indeed, some of the sets do show a tendency to lower values as the frequency increases.

Attempting to fit lines of these two slopes quickly reveals that the former bears some resemblance to the trend of the results, whilst the latter appears to be too steep. Accordingly, lines of slope inversely proportional to the frequency were drawn through each set.

From these, it might be hoped that some consistent differences might evolve for the different types of structures. For instance, it is generally considered that machined skin structures will have less damping than rivetted structures with dry joints and that these, in turn, will be more lightly damped than rivetted structures incorporating jointing compounds. Regretfully inspection of the results in FIG. 10 reveals no such consistent variation and it can only be concluded that the scatter in these results is too large to differentiation for this sort.

So, finally, we can only offer as the best that can be deduced from this data, based on the assumptions that have been made, the mean line given in FIG. 11. This leaves the possibility of the real damping differing by a factor of 3 from this suggested curve, but it is the best that can be done until more data becomes available, or a better analysis can be made. To this end, the existing data is being re-analysed and, of course, more data is slowly becoming available from later tests.

CONCLUSIONS

In the absence of any reliable method for predicting structural damping, and of suitable experimental data, such data as exists in B.A.C. from acoustically excited structural specimens has been examined.

It is found that the scatter of this data is very large, and does not sensibly differentiate between different types of structure.

However, in the current situation where a dearth of data of any sort exists, values of the damping ratio given by the mean line in FIG. 11 are suggested for use until better data becomes available .

LIST OF REFERENCES

Reference 1.

C.C. Kennedy & C.D.P. Pancu.
The Use of Vectors in Vibration Measurement and Analysis.
J.A.S. Nov. 1947

Reference 2.

Leonard Meorovitch
Analytical Methods in Vibrations.
Macmillan.

ACKNOWLEDGEMENTS

RIVETTED STRUCTURES WITH VISCO-ELASTIC SEALANT (PLAIN SKINS)

SYMBOL	SPECIMEN	DETAILS OF CONSTRUCTION AND METHOD USED FOR DAMPING RATIOS
✕	R.Ae.S. Panels 1, 2, 6 & 7	Simple boxes with varying rib pitch and depth. Material L72, 0.048" thick. Mushroom and countersunk ⅛" rivets. Thickol sealant. Damping ratios obtained from plots of strain versus frequency, derived from discrete frequency testing.
⊙	R.A.e.S. Panels 3 and 5	As above, except for use of J.C.5 sealant.
▲	Monel & Light Alloy Rivet Panels 1 & 2	Simple boxes 42" long 10" wide and 6" deep. Materials Skin 2mm. thick CM001, webs, 10SWG L 72 100° c/s rivets. Viton sealant. Damping ratios from discrete frequency plots.
⊛	Rear Fuselage Single Curvature Panel.	Skin material CM001, thickness 0.036". Frames at 20" pitch. Skin attachment with mushroom head rivets. Viton sealant. Damping ratios from vector plots.
▽		As above re-skinned with 0.064" thick skin.
✚	Tail plane Torsion Box	

RIVETTED STRUCTURES WITH VISCO-ELASTIC SEALANT (MACHINED SKINS)

SYMBOL	SPECIMEN	DETAILS OF CONSTRUCTION AND METHOD USED FOR DAMPING RATIOS
◻	12 Bay Fin Box	Machined skin panels of CM001 0.057" thick rivetted to 4 spars and 5 ribs enclosing 12 bays with stringers parallel to spars. Countersunk rivets. Viton sealant. Damping ratios from discrete frequency plots.
⊗	9 Bay Fin Box	Upper fin box. Skin machined, .0124 to .074 thickness. Spars and ribs rivetted by cleats and booms. Viton Sealant. Damping from response vector plots.
▲	Double Curvature Rear Fuselage Panel	Three sections of machined CM003-4 skin and stringers rivetted together and to six representative frames. Monel rivets. Viton sealant. Damping from discrete frequency plots.

RIVETTED STRUCTURES WITH CHEMI-ETCHED SKINS

SYMBOL	SPECIMEN	DETAILS OF CONSTRUCTION AND METHOD USED FOR DAMPING RATIOS
⊕	Rear fuselage	Basic skin, .064" thick, CM001, chemi-etched between frames and stringers to 0.036". Frames at 20" pitch. 82° c/s rivets. Viton sealant. Damping ratios from response vector plots
▮		As above but using mushroom head rivets.
◇		As above but with intermediate cleated frames giving 10" frame pitch.
◭		As above but with Z section stringers.
⬤	Rear fuselage Double curvature	As above but with double curvature and incorporating a longitudinal and a circumferential skin joint and two stringer run-outs.
◉		As above but with cleated intermediate frames giving 10" pitch.

RIVETTED STRUCTURES WITH NO SEALANT (PLAIN SKINS)

SYMBOL	SPECIMEN	DETAILS OF CONSTRUCTION AND METHOD USED FOR DAMPING RATIOS
●	Monel and Light Alloy Rivets Panel 3.	As panels 1 and 2 but with no sealant in joints.

WELDED STRUCTURE, CHEMI-ETCHED SKIN

SYMBOL	SPECIMEN	DETAILS OF CONSTRUCTION AND METHOD USED FOR DAMPING FACTORS
◼	Rear fuselage Single curvature Panel	As previous specimen but skin attachment using spot welding instead of rivets.

STRUCTURES INCORPORATING RIVETS AND WELDING

SYMBOL	SPECIMEN	DETAILS OF CONSTRUCTION INCORPORATING RIVETS AND WELDING
◗	Intermediate Fuselage Panel	0.063" thick, CM001 skin. 16 'T' section stringers, spot welded to skin. Two frames rivetted to skin. Damping ratios from response vector plots.

HONEYCOMB STRUCTURES

SYMBOL	SPECIMEN	DETAILS OF CONSTRUCTION AND METHOD USED FOR DAMPING RATIOS
✚	Rudder Wedge	Wedge, 56" long, 34" high and 5" thick at root. CM001 chemi-etched skin. Interior material, NIDA 400 (2024), 0.25" honeycomb with 0.002" wall thickness, Adhesive 130. Damping ratios from strain frequency plots.
◆	Rudder Wedge	As above but with Bloomingdale F 996 adhesive and E142 MDS honeycomb.

Reverberant Chamber

Acoustic Termination Box

Working Section

Air Modulators

Horns

Siren Room
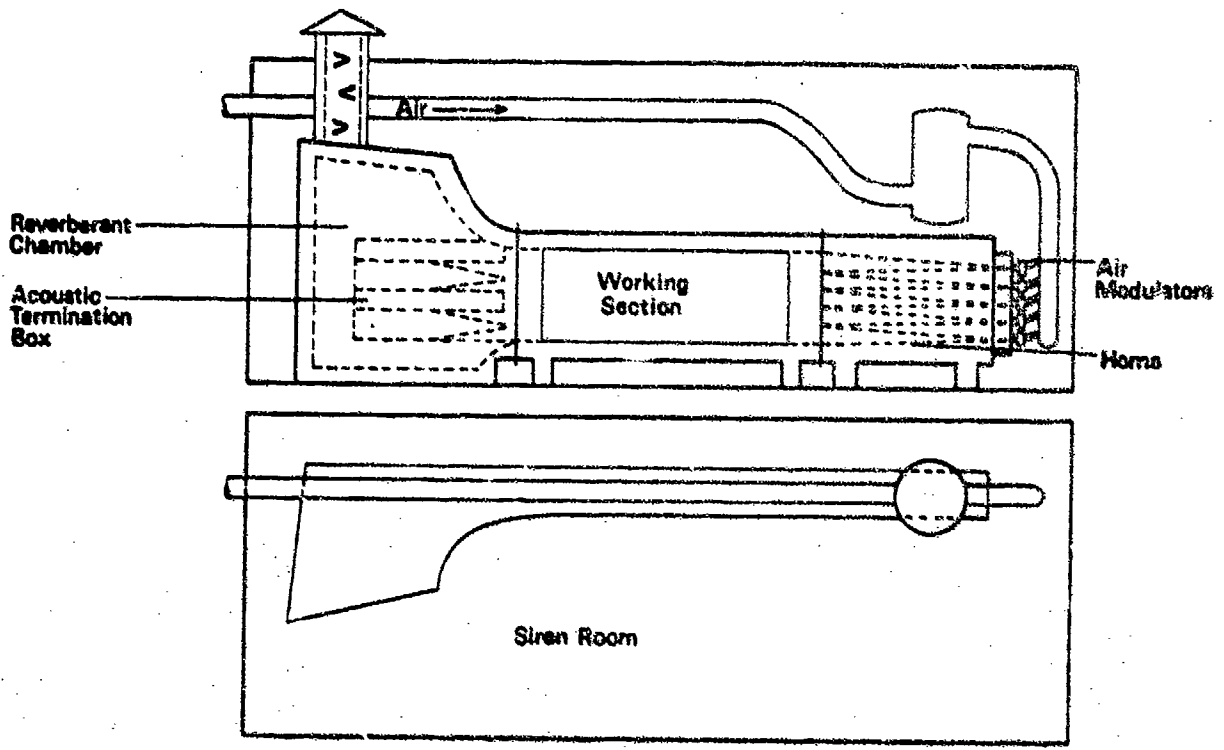
ACOUSTIC TEST CHANNEL FIG.1

VECTOR PLOT "Z"

HALF POWER "Z"

COMPARISON OF EXPERIMENTALLY DETERMINED VALUES OF "Z" FIG. 2
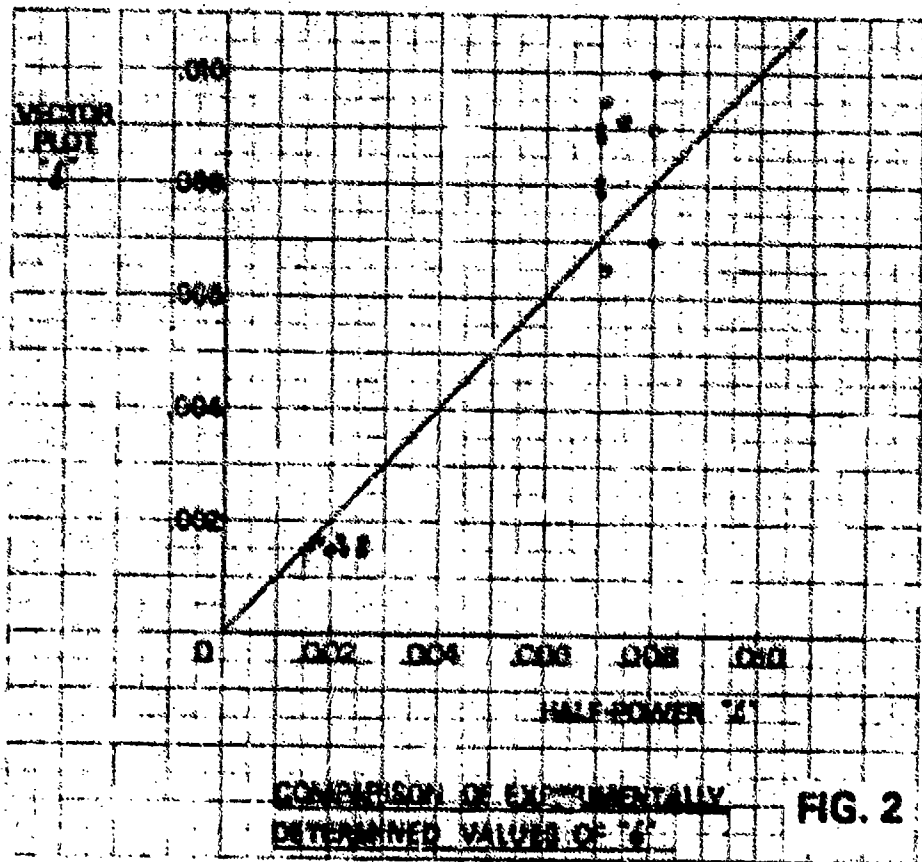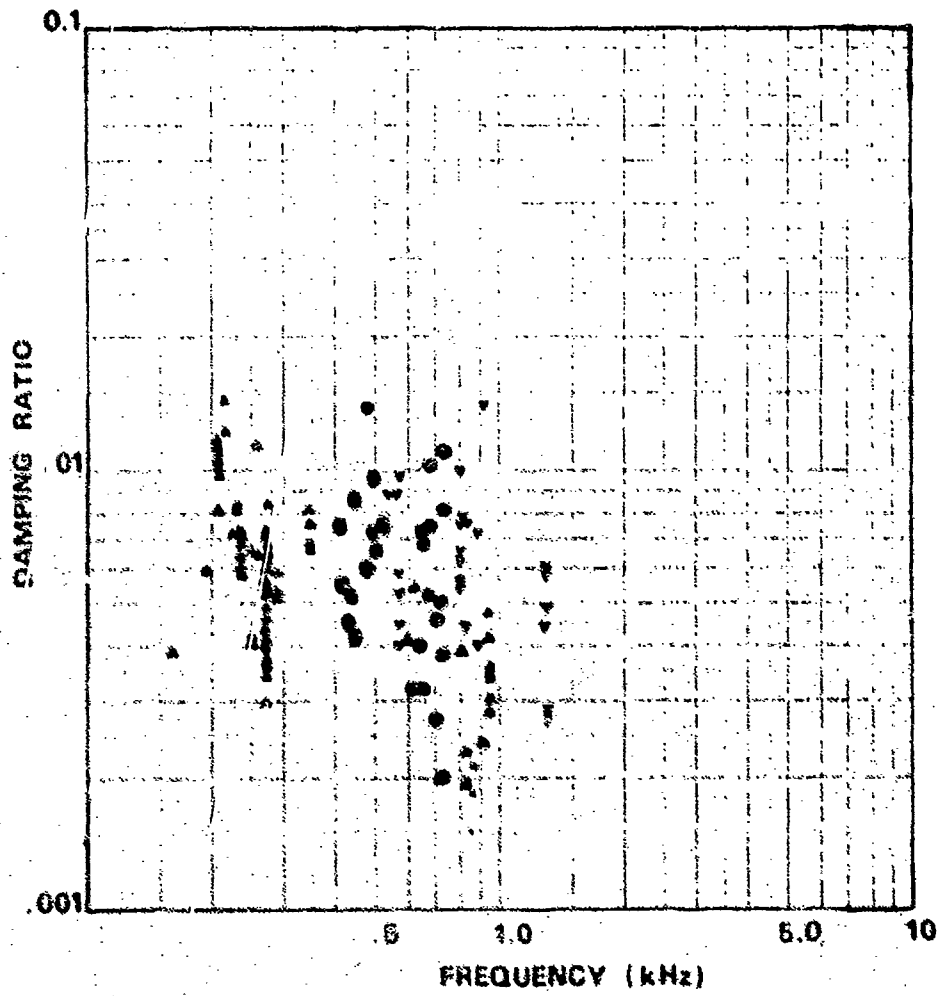
RIVETTED STRUCTURES WITH VISCO-ELASTIC SEALANT
(MACHINED SKINS)

FIG. 3
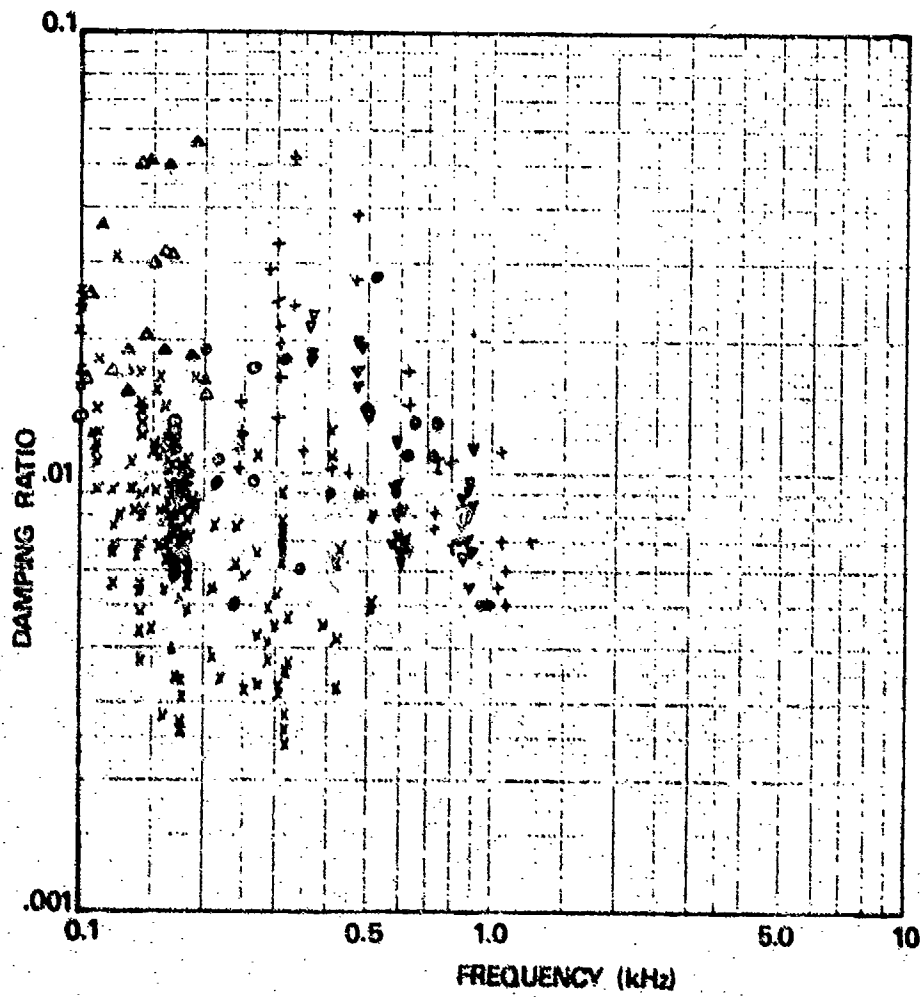
RIVETTED STRUCTURES WITH VISCO-ELASTIC SEALANT

(PLAIN SKINS)

FIG. 4
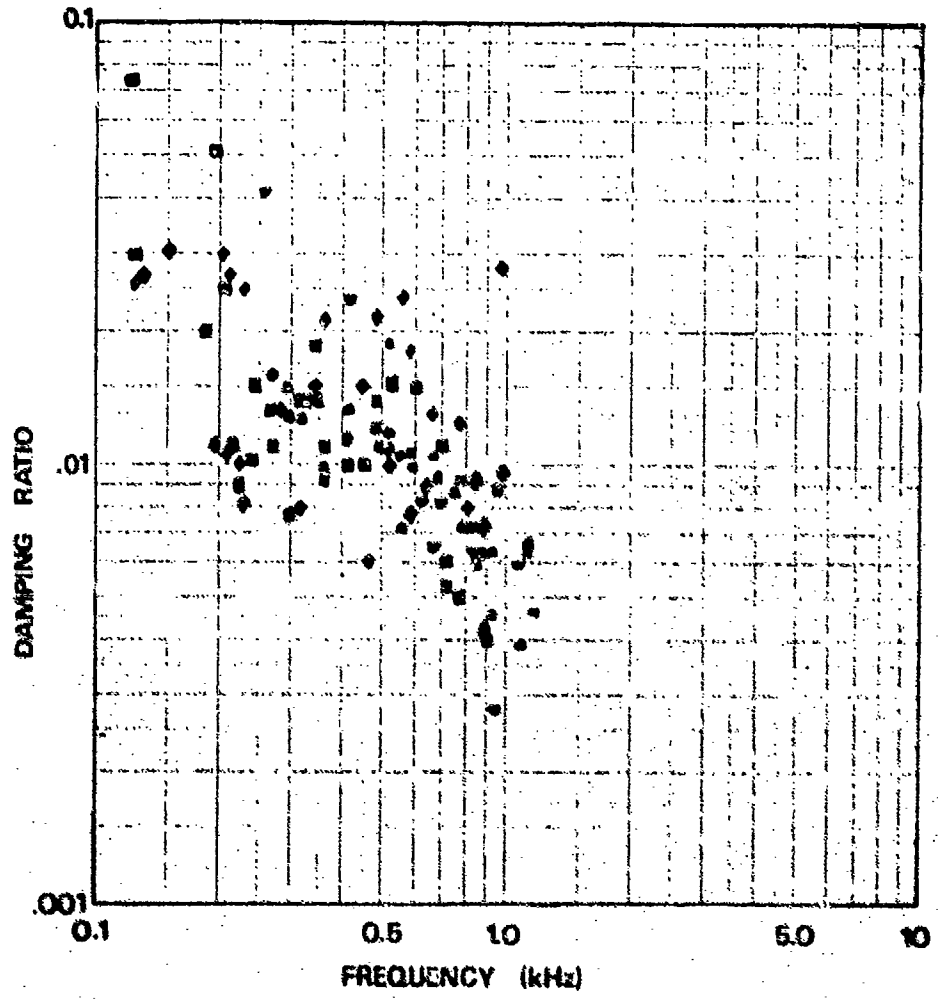
RIVETTED STRUCTURES WITH CHEMI-ETCHED SKINS

FIG. 5
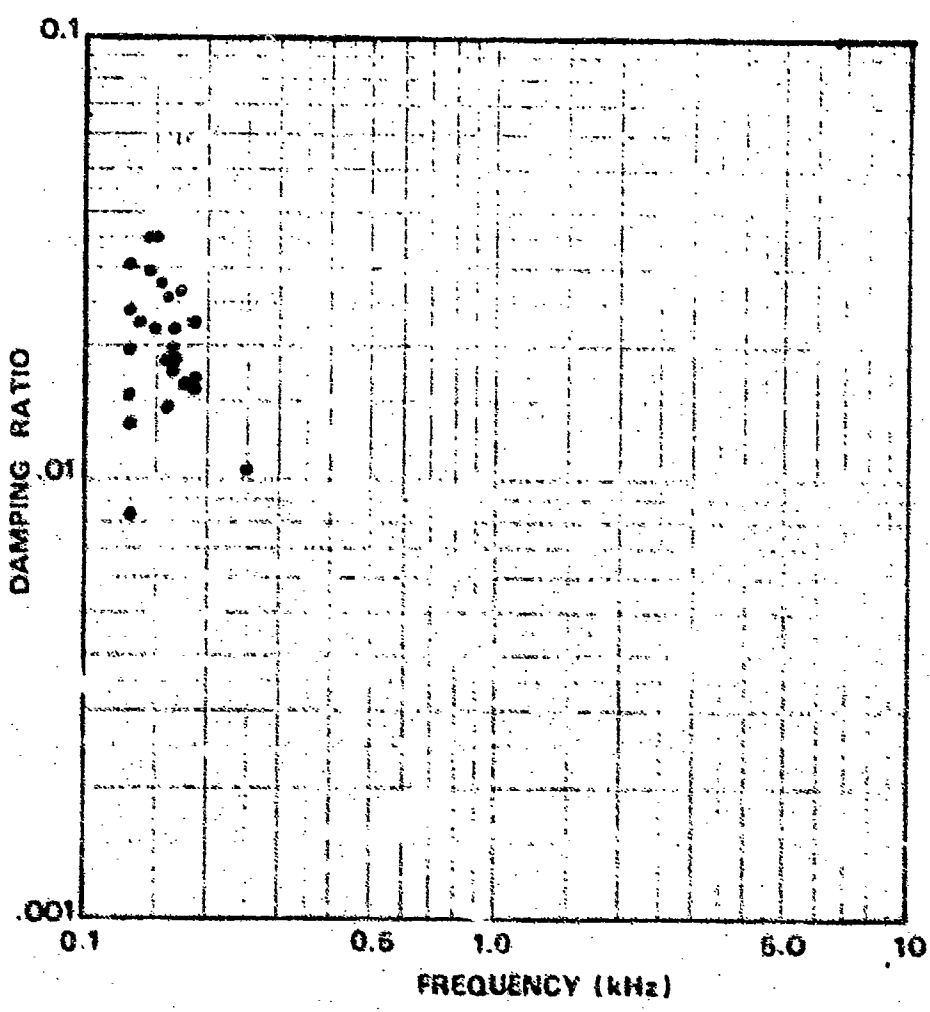
RIVETTED STRUCTURES WITH NO SEALANT (PLAIN SKINS)

FIG. 6
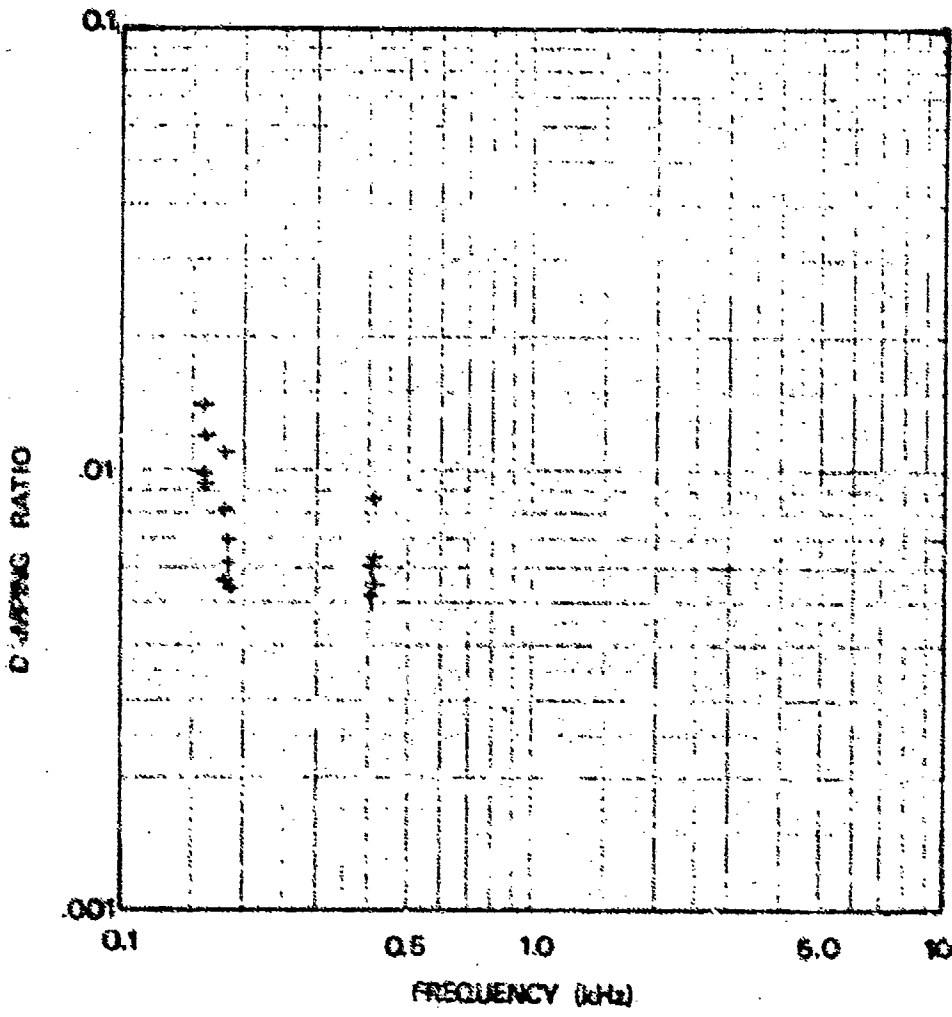
HONEYCOMB STRUCTURES

FIG.7
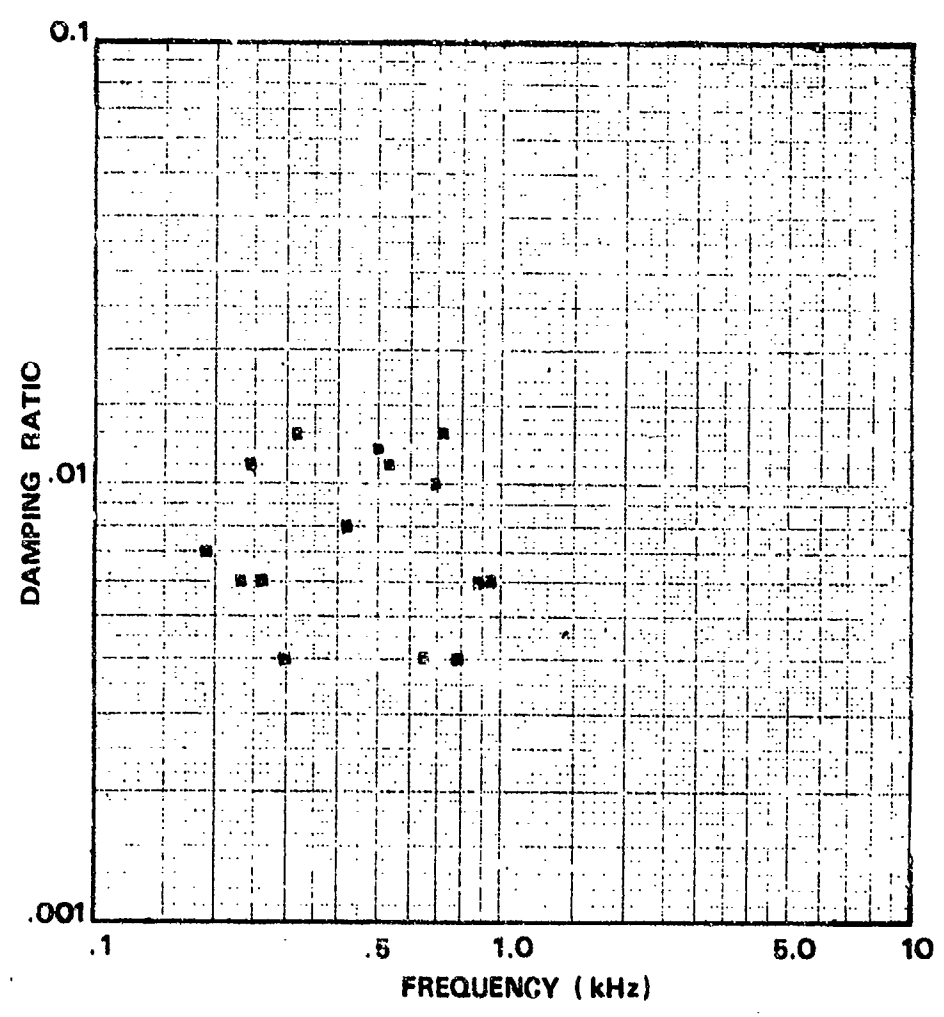
WELDED STRUCTURE, CHEMI-ETCHED SKIN

FIG .8
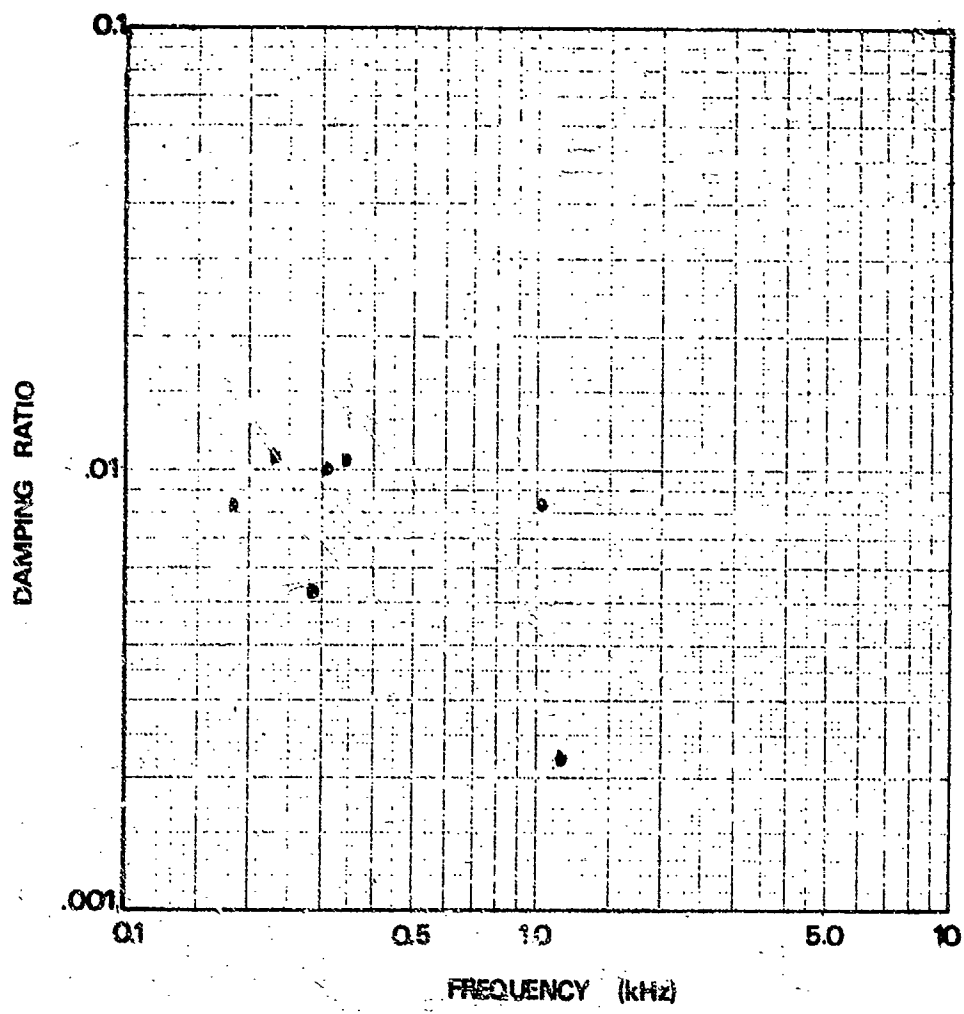
STRUCTURE INCORPORATING RIVETS AND WELDING

FIG. 9

DAMPING RATIO
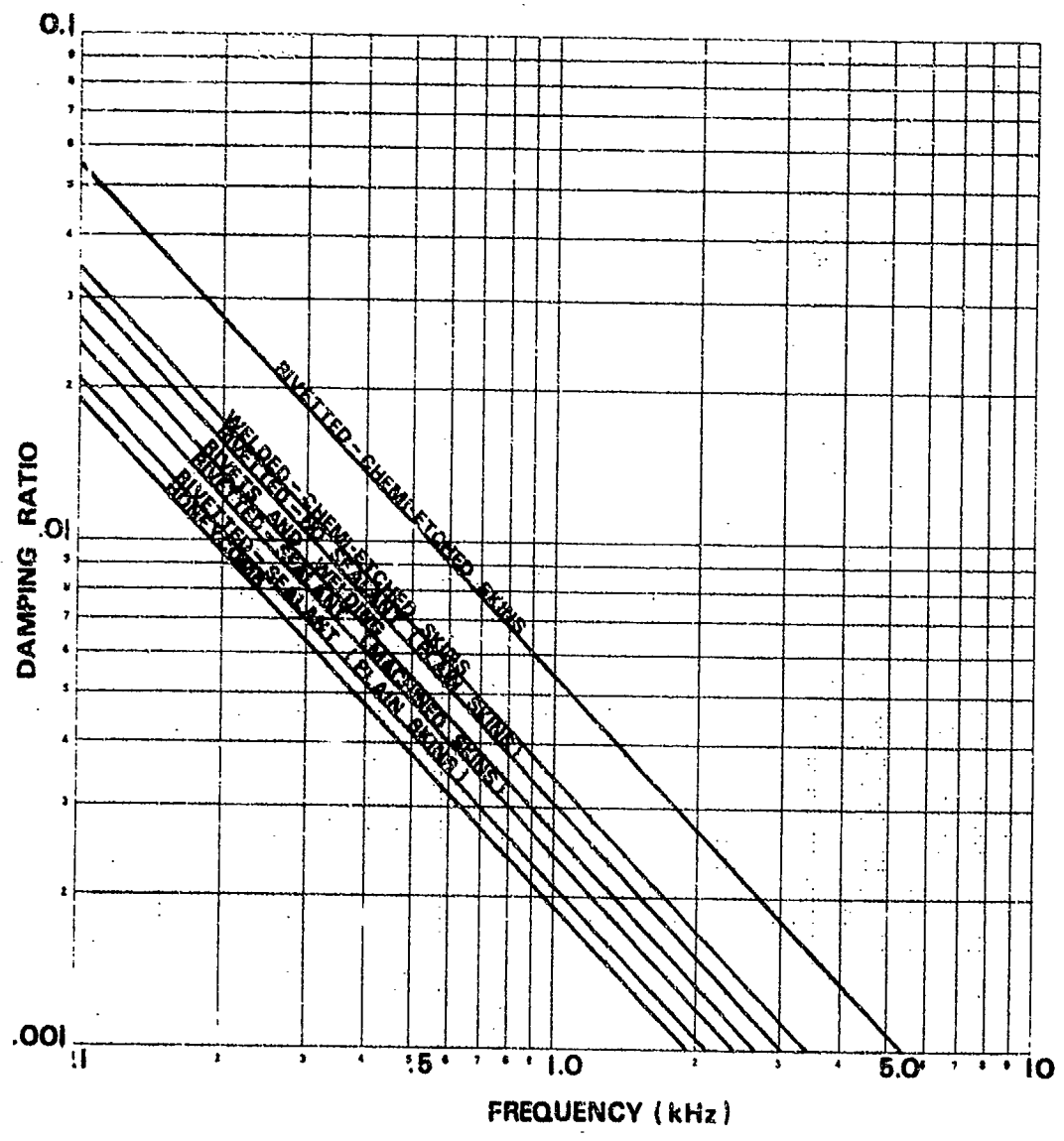
FREQUENCY (kHz)

COMARISON OF RESULTS

FIG.10
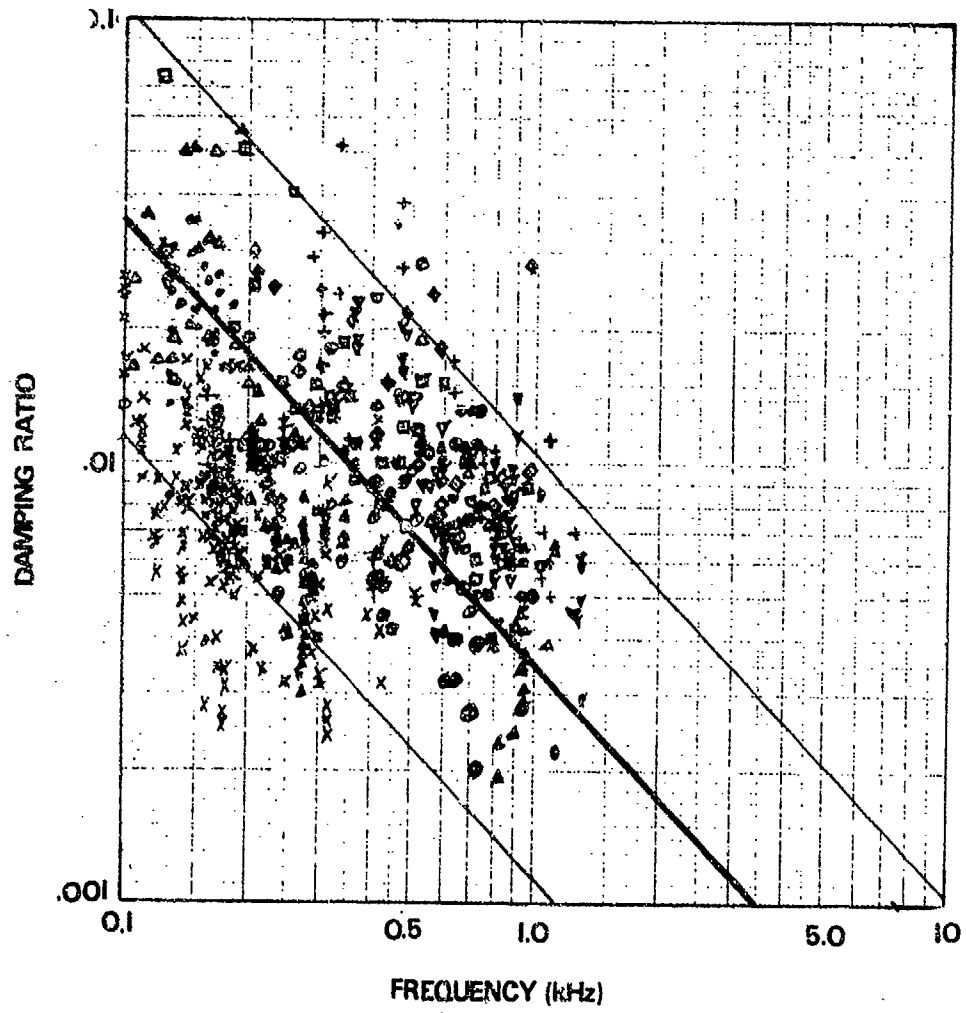
FREQUENCY (kHz)

PLOT OF DAMPING RATIOS v FREQUENCY

FIG. 11

DESIGN AND SONIC FATIGUE CHARACTERISTICS OF COMPOSITE MATERIAL COMPONENTS

by

N. D. Wolf
Supervisory Aerospace Engineer
Air Force Flight Dynamics Laboratory (FYA)
WPAFB, Ohio 45433
U.S.A.

and

M. J. Jacobson
Engineering Specialist
Northrop Corporation
Aircraft Division
Hawthorne, Calif 90250
U.S.A.

SUMMARY

This paper consists of a summary of two programs concerned with the design and acoustic testing of composite material components. Equations are presented for both a simplified theory and a more general theory in matrix form, for predicting natural frequencies, mode shapes and stresses in unstiffened and cross-stiffened advanced composite panels subjected to acoustic loads. Sonic fatigue test results on simple 8-ply boron-epoxy and 6-ply cross-stiffened graphite-epoxy panels are described. This includes panel damping values, fatigue life, stress data and a description, where appropriate, of panel fatigue failures. Also a series of 72 beam specimens was fatigue tested with shaker excitation to develop S-N data for various simulated joint configurations. The beams consisted of a graphite-epoxy or boron-epoxy material bonded or riveted to a graphite-epoxy or titanium alloy stiffener. S-N data up to 10^8 cycles were obtained. Frequencies and strains predicted by the analytical procedures are compared with experimentally measured values.

List of Symbols

D = Flexural rigidity, lb in

H = Torsional rigidity, lb in

$H(\Omega_o)$ = Nondimensional frequency response function

K = Generalized stiffness in fundamental mode, lb/in

L = Length of beam, in

M_i = Generalized mass in the ith mode, lb sec^2/in

M = Generalized mass in the fundamental mode, lb sec^2/in

M_o = Mass per unit area of plate, lb sec^2/in^3

N = Life, cycles

S = Strain, in/in

S_p = Spectral density of pressure, psi^2/Hz

S_w = Spectral density of deflection, in^2/Hz

$[Z]$ = Matrix of modal impedances, rad/sec^2

a = Edge of rectangular plate parallel to x-axis, in

b = Edge of rectangular plate parallel to y-axis, in

e_x, e_y = Extensional strain, in/in

h = Plate thickness, in

p_o = Amplitude of pressure, psi

t = Time (but t as a superscript means transpose), sec

w = Lateral deflection, in

x, y, z = Orthogonal rectilinear coordinates, in

α = Nondimensional beam function parameter

β = Beam function parameter, in^{-1}

γ = Beam function parameter, in^{-1}

Γ = Participation factor, in^2

γ_i = Nondimensional viscous damping factor in i^{th} mode

ζ = Nondimensional viscous damping factor

η = Generalized deflection coordinate, in

θ	= Nondimensional beam function parameter
τ	= Time, sec
ϕ	= Clamped-clamped beam function
ψ	= Clamped-clamped beam function
Ω	= Circular frequency, rad/sec
Ω_o	= Discrete driving circular frequency, rad/sec

1. INTRODUCTION

A great deal of effort over the past several years has been devoted to using fiber reinforced composite materials in aircraft design. Many materials have been considered but those presently being emphasized are boron, graphite and glass fibers with epoxy and aluminum matrices. Many of the material properties required to design structures constructed of composite materials have been investigated and are available. Design techniques as well as fabrication and manufacturing methods have been and are still being studied. Some of the advantages of fiber reinforced composite structures are the high strength-to-weight and stiffness-to-weight ratios and the tailorability of the strength properties. Some components, such as skin panels, substructural parts and fairings using composites, are being fabricated for present operational aircraft and are contemplated for use in future aircraft. A number of these components are presently being flight tested. It, therefore, is necessary to examine these materials and structural con-figurations for their characteristics when exposed to high intensity noise as some of these components may be exposed to this type of environment during their service life.

Previous comprehensive sonic fatigue investigations (see for example Reference 3) of fiber rein-forced composite structures have been limited to glass fiber reinforced panels. There are also sonic fatigue test results on boron epoxy and graphite epoxy panels. Since a complete theoretical solution of the structural response and fatigue life problem is not possible at high sound pressure levels due to the nonlinear relation between pressure and strain, a combined theoretical and experimental program (References 1 and 2) was initiated. The theoretical phase of the program developed a simple theory for the prediction of dynamic stresses in an unstiffened orthotropic plate subjected to a spatially uniform white noise envi-ronment. This phase of the work also included the use of a finite element computer program for the pre-diction of cross-stiffened panel response to acoustic excitation.

The initial part of the experimental program started with simple basic boron-epoxy panels to gain experience on how fiber reinforced composite structures reacted when loaded with high intensity noise. The panels were flat with fixed edge boundary conditions and were exposed to discrete frequency noise at their first mode resonant frequency. The basic purpose of these tests was to gain knowledge on such para-meters as panel mode shapes, panel damping, fatigue life, and the type of fatigue failures.

The next phase was to advance to more complicated structures such as multi-bay panels with stiff-eners and joints, more practical boundary conditions, and broad-band noise excitation to simulate a more realistic environment. Therefore, this part of the program consisted of testing three nine-bay, cross-stiffened, graphite-epoxy panels with six-ply skins. The panels were tested to obtain acoustic response and acoustic fatigue data.

A shaker test program was conducted to demonstrate that S-N data for acoustic fatigue predictions could be obtained by shaker specimen testing. In the shaker test program, six S-N curves were developed for two joint configurations, either bonded or riveted, and for three material combinations with six-ply skins.

The investigations and data presented in this paper are a summary of two programs which are described in detail in References 1 and 2. The program described in Reference 1 was conducted under Contract F33615-70-C-1463 by the Northrop Corporation for the Air Force Flight Dynamics Laboratory (AFFDL) and the program described in Reference 2 was an in-house exploratory development effort conducted by the AFFDL.

2. SUMMARY OF THEORY OF ORTHOTROPIC PANEL RESPONSE TO ACOUSTIC EXCITATION

The use of fiber reinforced composite materials for structural applications requires more com-plex analysis methods than in cases where metallic skin and internal structures are used. This is due to the corresponding analytical complexities associated with material properties and variations in fiber orientation through the laminate thickness. This section presents only a summary of the primary equations developed in Reference 1 for the following: (1) a simplified theory for predicting both the fundamental mode of an orthotropic plate and its response to acoustic excitation, and (2) the general theory for pre-dicting the natural modes and response of an orthotropic plate to acoustic excitation.

Section 6 will discuss and compare results found by using these equations and techniques in determining natural frequencies, mode shapes, and stresses for simple panels and cross-stiffened panels constructed of (1) an aluminum alloy and (2) a graphite-epoxy composite.

Simplified Theory

The simplified theory can be used in the design of individual bays of cross-stiffened orthotropic plates in cases when each of the bays responds principally in its fundamental mode as though it were clamped on all four edges. The main limitation of the simplified theory is that the stiffeners around the periphery of a bay are assumed to be rigid. Therefore, the design and analysis of the supporting struc-ture of cross-stiffened panels cannot be investigated with this theory. It appears that in many cases when the critical acoustic fatigue location in a cross-stiffened panel is in the skin at the joint with the supporting structure, the simplified theory can be applied in the acoustic design.

In Reference 1, the lateral deflection of the advanced composite plate with a coordinate system as given in Figure 1 is assumed unimodal and is expressed in terms of clamped-clamped beam functions for the 1-1 mode as follows:

$$w(x,y,t) = \phi(\beta x)\ \psi(\gamma y)\ \eta(t) \tag{1}$$

with $\phi(\beta x) = \cosh \beta x - \cos \beta x - \alpha(\sinh \beta x - \sin \beta x)$ (2)

and $\psi(\gamma y) = \cosh \gamma y - \cos \gamma y - \theta(\sinh \gamma y - \sin \gamma y)$ (3)

In the case of spatially uniform, time harmonic loading the pressure is

$$p(t) = p_0\ e^{i\Omega_0 t} \tag{4}$$

and the time function in the deflection equation (1) for the steady state case with no damping is

$$\eta(t) = \frac{p_0 \Gamma}{K}\ \frac{e^{i\Omega_0 t}}{1 - \left(\frac{\Omega_0}{\omega}\right)^2} \tag{5}$$

with $K = D_{xx} b\beta^4 a + 2H\alpha\beta\theta\gamma(2-\alpha\beta a)(2-\theta\gamma b) + D_{yy}\ a\gamma^4 b$ (6)

$$M = ab\ M_0 \tag{7}$$

$$\Gamma = \frac{16\alpha\theta}{\beta\gamma} \tag{8}$$

and $\omega^2 = \dfrac{K}{M}$ (9)

where ω is the natural circular frequency.

For the viscous damped case, the amplitude of the steady state solution is

$$\left|\eta(t)\right| = \frac{p_0 \Gamma}{K}\ \left|H(\Omega_0)\right| \tag{10}$$

with

$$H(\Omega_0) = \left\{\left[1 - \left(\frac{\Omega_0}{\omega}\right)^2\right]^2 + 4\ \zeta^2\left(\frac{\Omega_0}{\omega}\right)^2\right\}^{-\frac{1}{2}} \tag{11}$$

The absolute strains in the upper and lower plate surfaces in unimodal response under harmonic excitation at the fundamental frequency are also found in Reference 1 as follows

$$\left|e_x\right| = \frac{h\ p_0 \Gamma}{4\ K\ \zeta}\ \left|\psi\ \frac{d^2\phi}{dx^2}\right| \tag{12}$$

and

$$\left|e_y\right| = \frac{h\ p_0 \Gamma}{4\ K\ \zeta}\ \left|\phi\ \frac{d^2\psi}{dy^2}\right| \tag{13}$$

To determine the unimodal rms strain response to spatially uniform, time random loading, the $p_0\ e^{i\Omega_0 t}$ is replaced by $p(t)$ and the following equations from Reference 1 result for deflection and strain.

$$w^*(x,y,\Omega) = \phi\ \psi\ \frac{\Gamma\ H(\Omega)}{K}\ p^*(\Omega) \tag{14}$$

where the asterisk denotes the Fourier transform of the deflection and loading with

$$H(\Omega) = \left[1 - \left(\frac{\Omega}{\omega}\right)^2 + \frac{2i\ \zeta\ \Omega}{\omega}\right]^{-1} \tag{15}$$

The deflection spectral density in terms of the loading spectral density is

$$S_w = \left|\frac{\phi\ \psi\ \Gamma\ H(\Omega)}{K}\right|^2 S_p \tag{16}$$

and the mean square unimodal response is

$$\bar{w}^2 = \frac{\phi^2 \psi^2 \Gamma^2}{K^2} \int_0^\infty |H(\Omega)|^2 \, S_p(\Omega) \, d\Omega \tag{17}$$

For constant spectral density of the applied pressure (i.e. white noise)

$$\int_0^\infty S_p \, |H(\Omega)|^2 \, d\Omega = \frac{\pi \, \omega \, S_p}{4 \, \zeta} \tag{18}$$

The mean square strains at the surface with white noise excitation are

$$\bar{e}_x^2 = \frac{h^2 \, \Gamma^2 \, \psi^2}{4K^2} \left(\frac{d^2 \phi}{dx^2}\right)^2 \frac{\pi \, \omega \, S_p}{4 \, \zeta} \tag{19}$$

and

$$\bar{e}_y^2 = \frac{h^2 \, \Gamma^2 \, \phi^2}{4K^2} \left(\frac{d^2 \psi}{dy^2}\right)^2 \frac{\pi \, \omega \, S_p}{4 \, \zeta} \tag{20}$$

The strain calculations at the center of an edge of the plate have been calculated in Reference 1 and imply that the strain is larger at the center of the long edge than at the center of the short edge as is the case for isotropic plates of uniform thickness.

General Theory

The general theory, developed in Reference 1 and summarized below, is suitable for programming for digital computer calculations using the finite element technique. A drawback in attempting to apply the general theory is that the number of finite elements and node points may be prohibitive in a single computer run computation of several natural frequencies, mode shapes, and stresses at critical locations (of complex structures) where acoustic fatigue failures seem likely to occur. Thus major problems may arise when the equations of the general theory are applied in detailed stress analyses of fiber reinforced composite panels of nonuniform thickness and with attachments such as stringers, ribs and frames.

Natural frequencies and mode shapes can be obtained from the following matrix equation

$$[K] \, \{q^{(i)}\} = \bar{\omega}_i^2 [M] \, \{q^{(i)}\} \tag{21}$$

where

$[K]$ = stiffness matrix

$[M]$ = mass matrix

$\{q^{(i)}\}$ = the ith mode shape, the eigenvector

$\bar{\omega}_i$ = the ith natural frequency

The modal response in the frequency domain to a modal force $f(t)$ is obtained from the following

$$\{S_\xi\} = \lceil Z(\omega) \rfloor^{-1} [Q]^t \, \{S_f(\omega)\} \tag{22}$$

where

$\{S_\xi\}$ = Matrix of modal amplitudes in the frequency domain

$Z_j = (\bar{\omega}_j^2 - \omega^2 + 2_i \, \gamma_j \, \omega \, \bar{\omega}_j) \, M_j$

$[Q]$ = $[\{q^{(1)}\}, \{q^{(2)}\} \ldots]$

$\{S_f(\omega)\}$ = Fourier transform of $f(t)$

The cross-power spectral density of the deflection is

$$[\phi_d(\omega)] = [Q] \, \lceil Z(\omega) \rfloor^{-1} [Q]^t \, [\phi_f(\omega)] \, [Q] \, \lceil Z(\omega) \rfloor^{-1*} [Q]^t \tag{23}$$

where $[\phi_f(\omega)]$ is a complex matrix whose elements $\phi_{f_{ij}}(\omega)$ may be expressed as the Fourier transform of

the cross-correlation function $R_{f_i f_j}$

$$\phi_{f_{ij}}(\omega) = \frac{1}{\pi} \int_{-\infty}^{\infty} R_{f_i f_j}(\tau) e^{-i\omega\tau} d\tau \tag{24}$$

The stress-deflection, moment-deflection, or shear-deflection is

$$\sigma = \lfloor B \rfloor \{d\} \tag{25}$$

where $\lfloor B \rfloor$ is called the stress matrix when σ is a stress.

The power spectral density of a stress, moment, or shear is

$$\phi(\omega) = \lfloor B \rfloor \{\phi_d\} \lfloor B \rfloor^t \tag{26}$$

The mean square stress is

$$\overline{\sigma}^2 = \lfloor B' \rfloor \{X\} \lfloor B' \rfloor^t = \sum_i \sum_j B_i X_{ij} B_j \tag{27}$$

where

$$\lfloor B' \rfloor = \lfloor B \rfloor \{Q\}$$

$$[X] = \int_0^{\infty} \lceil Z(\omega) \rfloor^{-1} [E] [Z*]^{-1} d\omega$$

$$X_{ij} = E_{ij} C_{ij} = E_{ji}^* C_{ji} = X_{ji}^*$$

$$[E] = [Q]^t \{\phi_f\} [Q]$$

$$C_{ij} = \frac{2\pi (\gamma_i \overline{\omega}_i + \gamma_j \overline{\omega}_j)/M_i M_j}{[\overline{\omega}_i^2 - \overline{\omega}_j^2]^2 + 4\overline{\omega}_i \overline{\omega}_j \{(\gamma_i^2 + \gamma_j^2) \overline{\omega}_i \overline{\omega}_j + \gamma_i \gamma_j (\overline{\omega}_i^2 - \overline{\omega}_j^2)\}}$$

$$\{\phi_f\} = \lceil A \rfloor \{\phi_p\} \lceil A \rfloor$$

where

A_{ii} = the area under pressure associated with joint i and

$\{\phi_p\}$ = the power spectral density matrix of the applied pressure.

It is also shown in Reference 1 that $\overline{\sigma}^2$ is a function of real components and not imaginary components of elements of the spectral density matrix $\{\phi_f\}$. Therefore

$$\overline{\sigma}^2 = \lfloor B' \rfloor \{Re~X\} \lfloor B' \rfloor^t = \sum_i \sum_j B_i' ~Re~(X_{ij}) ~B_j' \tag{28}$$

Method of Applying the General Theory

By properly choosing boundary conditions of a quadrant of a panel array that is symmetrical about both of its center lines, only the quadrant itself rather than the full panel is needed in the modal analysis of the symmetrical modes. Since only those modes that are symmetrical about both centerlines of the full panel are excited in many test and service conditions, the analysis of only one quadrant of a panel array is adequate in many practical cases.

The damping factors that are needed as input for the response calculations may be obtained in resonance tests under discrete frequency excitation.

The pressure cross-spectral density $\phi_{f_{ij}}$ may be obtained from the analysis of test data or from equation 24 after some theoretical cross-correlation function $R_{f_i f_j}$ is assumed. The former approach may

carried out by making a record on tape of pressure signals at locations i and j on the panel and then using standard data analysis equipment to obtain the real and imaginary parts of the cross-spectral density of the pressure.

In equation (27) $\overline{\sigma}$ may be an rms stress, moment, or shear. The amount of computation in the use of this equation may be reduced by ignoring modal coupling and computing the deflection, moment, and shear response of one mode at a time. It is shown in Reference 4 that the modal coupling may be relatively unimportant.

3. SONIC FATIGUE CHARACTERISTICS OF SIMPLE BORON-EPOXY COMPOSITE PLATES

The objective of the acoustic tests of the flat boron-epoxy composite panels was to determine panel mode shapes, panel damping, fatigue life and the type of failure when exposed to acoustic excitation.

Description of Flat Panel Specimens

The dimensions of these plates were nominally 12 X 14 inches and 0.040 inches thick. They were manufactured by laminating together 8 plies of orthotropic boron-epoxy material in a 0° - 90° layup symmetrical about the mid-plane. The outer plys had a fiber orientation of 0°. The matrix material was Narmco 5505 and the boron content was 50% by volume.

Test Procedure

These panels were subjected to a sonic fatigue test in a progressive wave acoustic test chamber. A total of twelve panels was tested one at a time under periodic excitation with a SPL range of 158 dB to 164 dB. The panels were mounted in a picture frame arrangement and were tested with all edges clamped. This mounting is shown in detail in Figure 2. Because of the mount, the effective panel size was reduced to 9 X 11 inches. All tests were conducted with this arrangement except the panel damping tests. Mode shapes and natural frequencies of these panels were obtained by using loudspeaker excitation and measuring acceleration amplitude and phase angle between a fixed and roving accelerometer. Mode shapes were also obtained by using a laser beam interferometric technique. Reference 2 provides details of both methods. Panel damping values were obtained by exciting the panels in the free-free mode using the logarithmic decrement method. Before and during the initial part of the high SPL tests to measure panel fatigue life, panel strain values were measured. After the strain gages failed, usually during the early part of the test, panel amplitude and frequency were monitored using a non-contacting displacement probe. Visual inspections of the panels were made frequently to determine if fatigue failures had resulted. Failures were defined as cracks or ply delaminations.

Test Results

The results of the panel mode shape and resonant frequency studies are presented in Figure 3 for a typical panel.

With the panel suspended from elastic cord to simulate a free-free condition, panel damping factors ranged from about 0.004 at 65 Hz to 0.003 at 400 Hz. These values were measured at low SPL's ranging from 125 to 138 dB. With the panel mounted in the picture frame arrangement in the side wall of the progressive wave test section, a panel damping factor of 0.028 was measured at a SPL of 125 dB and a resonant frequency of 127 Hz.

Strain measurements were recorded prior to endurance testing at 4 dB increments starting at 130 dB. Peak strain values are given in Table I for frequencies of maximum response for strain gage locations Nr 1 through 4 shown in Figure 2. It is also shown in Table I that the peak frequency response of these panels ranged from 138 Hz at a SPL of 130 dB to 270 Hz at a SPL of 162 dB.

Figure 4 shows a typical sound input spectrum for the 162 dB run and Figure 5 a typical strain gage response spectrum for gage Nr 1 at an input SPL of 162 dB.

Endurance testing results for the boron-epoxy composite panels are given in Figure 6. Also presented in this figure are calculated endurance results based upon strain response measurements for aluminum alloy (2024-T3) panels for a K_t value of two. These panels were 0.050 inches thick and were tested under the same conditions as the fiber reinforced composite panels. These results are presented for comparison purposes.

An attempt was made during these tests to determine panel crack or failure propagation rates. This was accomplished by using a sequence camera and photographing the failure at selected time intervals as it started and propagated. Complete results of these tests are given in Reference 2.

Discussion of Test Results

The variation in panel damping was due to the manner in which the panel was mounted during the damping measurement process. In the case where the panel was mounted in the free-free condition the damping factors were less than one-half of one percent of critical and only structural damping was being measured. In the case where the panel was mounted in the picture frame the damping factor was about 3 percent of critical. This increase was attributed to friction in the joint between the panel and mounting frame and possibly to the difference in the panel mode shapes.

The shift in resonant frequency (Table I) at peak response as a function of SPL was due to the non-linear response of the panels. This was verified by the amplitude "jump" phenomenon observed during preliminary sweep frequency runs to determine the frequency of peak response used for the endurance testing.

Figure 6 shows the endurance life of the 8 ply boron-epoxy panels to be greater than 10^8 cycles at a SPL of 158 dB. This corresponded to a measured peak strain value of ± 2150 μ in/in at gage position Nr 1. In comparison, the aluminum panel which was 25 percent thicker, had a peak strain at gage position Nr 1 of ± 1350 μ in/in. This corresponded to a life of approximately 6 X 10^5 cycles for 2024-T3 aluminum with a K_T value of 2.

The visible point of incipient failure in the boron composite panels typically appeared as a crack in the outer ply immediately adjacent and parallel to the clamped boundary. Generally, the failure would progress through the remaining plys and, if undetected, often result in the complete disintegration of a small concentrated area near the boundary. This was sometimes accompanied by severe delamination of the outer ply. A typical boron composite panel failure is shown in Figure 7.

4. BEAM SPECIMEN SHAKER TESTS

There were two principal objectives of the shaker tests. First, to obtain experimental S-N data for different joint configurations and material systems to determine the relative advantages of the various types of specimens. Second, to demonstrate that experimental S-N data could be obtained and applied in the design of joints of fiber reinforced composite panels in acoustic environments without resorting to acoustic tests. The use of shaker tests was employed to obtain S-N data for the joint assemblies because shaker test programs are less costly for a fixed number of test specimens and can provide stress or strain versus life data for a joint assembly that are applicable to joints in panels under acoustic loading.

Description of Beam Specimens

In order to conduct shaker tests to obtain acoustic design information, it was necessary to establish carefully the specimen design and test procedure for shaker excitation. The designs of the acoustic test specimens (cross-stiffened panels) and the shaker test specimens were based on obtaining experimentally the same key parameters (including modes of failure) in the acoustic specimens as in the shaker specimens. By following this procedure, considerable acoustic design information can be obtained by conducting shaker tests to supplement the data generated in the acoustic tests.

The shaker test specimen design was based on the location of the first acoustic fatigue failure of the joint assembly of the cross-stiffened acoustic test panel described in Section 5. A detailed stress analysis was conducted on two cases: (1) a beam of unit width with geometrical and elastic properties of a section taken between the T-sections and (2) a beam of unit width with geometrical and elastic properties of a section taken between the I-beams of the nominal 10 X 7 inch central bay of the acoustic test panel. The analysis was performed by considering the beam clamped at both ends and loaded by a uniform unit static pressure. Based upon the results of this analysis which is detailed in Reference 1, it was determined that the initial acoustic fatigue failures in the test panel should be expected near the T-section stiffeners rather than near the I-beam stiffeners. Therefore the design considering the T-section details was chosen as the shaker test specimen design. Specimen details are given in Figure 8.

In the shaker test program, an adhesive-bonded joint was used for one joint configuration and a riveted joint for the other. These two configurations are typical of configurations projected for use in aircraft applications. In addition, the following material combinations were used: (1) graphite-epoxy skin to graphite-epoxy stiffeners, (2) graphite-epoxy skin to titanium alloy stiffeners, and (3) boron-epoxy skin to titanium alloy stiffeners. The stiffeners refer to shaker specimen components that simulate either ribs, spars, or stringers. The Fothergill/Harvey Courtaulds HT-S/4617 graphite-epoxy system and the Narmco 5505 boron-epoxy system were selected as the composite materials for the test program. FM-123-2 adhesive was chosen for bonding the fiber reinforced composite skins to the internal structure in joint assemblies of the shaker specimens. FM-123-2 was chosen because of its low modulus and relatively low curing temperature (250°).

Test Procedures

The shaker specimens were fatigue tested either individually or three at a time by clamping the web section of the simulated stiffener to a test fixture mounted on top of a shaker. See Figure 9 for the details of this arrangement. The ends of the beam were free and the tests were conducted by exciting the second symmetrical bending mode with the response frequency being about 200 Hz. The shaker tests were conducted under narrow-band random excitation with a 20 Hz bandwidth signal. See Figure 10 for a typical base acceleration input.

Three types of transducers were used to monitor the specimen response, accelerometers, strain gages, and a capacitive displacement probe. The primary measurement was the strain response of the specimen. Input vibration levels were set and controlled to produce predetermined strain levels. The other transducers were used to maintain this strain response after the failure of the strain gages.

For a S-N curve of a joint assembly to have meaning, it is necessary to define S. In simple coupon fatigue tests of homogeneous materials, S is usually defined as the applied stress. However, for the joint assemblies of panels and beams such as were tested in this program under acoustic or shaker excitation, S is more difficult to define. For example, if failures occur in the skin, S should be related in some manner to the stress or strain in the skin; if failures occur in the adhesive, S should be related in some manner to the stress or strain in the adhesive. The generalization of this concept is that S should be related to the stress or strain in the fatigued component of the joint assembly. The experimental fatigue failures in the shaker test program were instrumental in defining S as the strain in the outer surface layer of the skin (where fatigue failures occurred) of the joint assembly. The reference strain was measured at the location shown in Figure 11. A typical spectral shape of the rms strain response at the reference location is shown in Figure 12 for a base acceleration of 10g's.

Fatigue Failures

The fatigue failures of all shaker specimens initiated in the skin. For the bonded specimens, the failure location was at the ends of the bonded joint connecting the skin to the T-sections. For the riveted specimens, the failure location was at the end of the bonded attachment connecting the skin to the backup detail that had been bonded to the skin prior to the riveting.

Prior to the start of tests, it was decided that a test would be terminated at 10^8 cycles if no failure occurred, if a drop of 20 percent in the response frequency from its value at the beginning of the fatigue test occurred, or if a failure was observed. An observed failure was defined as a visible crack (without the use of a microscope) of approximately 0.01 inch. During the tests, when a crack was approximately 0.01 inch long, it would often propagate rapidly with a simultaneous sharp drop in the response frequency.

Discussion of Shaker S-N Data

The S-N data obtained in the shaker tests are presented in Figure 13. The number of test cycles to failure was computed by summing the products of the specimen natural frequency and the duration that the response remained at that frequency. Frequency changes were noted during the tests and the total number of cycles to failure calculated.

An objective of the shaker test program was to obtain S-N curves with sets of six-ply specimens that simulated a portion of the bonded joints used in the acoustic test program. The S-N curves of Figure 13 are useful because they indicate life that can be expected from a larger population of different types of test specimens. Because of the few specimens in each set, the confidence levels associated with life predictions based on the S-N shaker specimen test results are significantly lower than the confidence levels associated with material allowables for the design of metallic aircraft structural elements. However, it does appear that the rms fatigue strain at 10^8 cycles under the narrow band random loading of the six-ply $(90/\pm45)_S$ graphite-epoxy and boron-epoxy laminates is at least ten percent of the static, ultimate tensile strain of the six-ply laminates.

The test results show that the riveted fiber reinforced composite specimens had longer lives than non-riveted specimens. The longer life of the riveted specimens has been attributed to less stress concentration at the edges (of the bonded area) where the fatigue failures initiated in the skins of the shaker specimens. Less stress concentration at the edges of the bonded areas is expected when the load transfer is from the stiffeners through the three rivets into the backup plates and into the graphite-epoxy or boron-epoxy skins. The backup plates which were bonded to the skin are desirable when using countersunk rivets in thin skins.

Based on the test data, in general, the vibration specimens with graphite-epoxy skins have longer life when the stiffeners are titanium alloy rather than graphite-epoxy. The differences in life at a given strain have been attributed to the graphite-epoxy stiffener being more flexible than the titanium alloy stiffener. Hence, the strain across the specimen width (in the vicinity of a fatigue failure) is less uniform and consequently results in a higher stress concentration (and shorter life) at the edge of the width of the bonded areas (where all fatigue failure initiated) of the specimens with graphite-epoxy stiffeners. The preceding implies that the specimen life is dependent on the stress concentration at the edges of the width of the bonded areas (where fatigue failures have initiated) of the vibration specimens. The use of the titanium alloy stiffeners and the use of rivets with titanium alloy back-up plates bonded to the skin apparently reduced the stress concentration and led to longer lives.

5. SONIC FATIGUE TESTS ON CROSS-STIFFENED PANELS WITH JOINTS

The basic objective of the acoustic test of the cross-stiffened graphite-epoxy composite panels was to obtain dynamic and sonic fatigue characteristics of the joint assemblies.

Description of Cross-stiffened Panel Specimens

Three acoustic test panels were assembled with 6 ply $(0/\pm45)_S$ graphite-epoxy skin and 6 ply $(\pm45/0)_S$ graphite epoxy I-beams and T-sections. In the assembled panels, the I-beams simulated the ribs and the T-sections simulated stringers. The graphite-epoxy system used was the same as described for the beam specimens. Each acoustic test panel was cross-stiffened and contained nine rectangular bays in a three by three array. See Figure 14, which is a schematic of the panel. The central panel bay and the skin and joint assemblies enclosing the bay were considered as being within the "test section" part of the panel.

Test Procedure

The acoustic panels were subjected to a sonic fatigue test in a progressive wave acoustic test chamber. They were tested singly to a broad-band excitation with an overall SPL of 166 dB. For the resonant frequency and modal surveys, the panels were excited by loudspeaker excitation and the resonant frequencies were determined by accelerometers and the mode shapes by using the Chladni pattern technique. Damping factors were obtained by using the logarithmic decrement method, utilizing the oscillograph decay record taken from the accelerometer signals during the modal survey. Experimental strain versus acoustic pressure data were also recorded starting at 136 dB with 3 dB increments to determine if nonlinear effects were present. Visual inspections were used to detect acoustic fatigue failures, which were defined as the first observation of a fatigue crack or delamination. In addition, visual inspections were made when unexpected strain or pressure fluctuations occurred. Strain gages were mounted on the panel and their locations are shown in Figure 14.

Test Results

Representative detailed results from the acoustic test are described in the following. Panel resonances and their associated mode shapes are given in Figure 15 for Panel Nr 2.

Damping factors associated with the decay of panel resonances obtained by using the logarithmic decrement method are given in Table II for Panels Nr 1, 2, and 3.

Strain readings taken at 3 dB increments are given in Table III for a selected number of gages on the skin for Panel Nr 2. Also the spectral density of the acoustic pressure is given in Figure 16 for an overall SPL of 139 dB, and the strain spectral density for gage Nr 2 at an overall SPL of 139 dB and 166 dB respectively in Figures 17 and 18.

The acoustic fatigue test on the three panels was conducted at an overall SPL of 166 dB. The first panel experienced a premature failure that was attributed to a design and manufacturing deficiency that was corrected for the next two panels. The second and third panels each survived 100 hours of exposure to the broad-band high intensity noise environment.

Acoustic Test Conclusions

The tests demonstrated that high quality, graphite-epoxy panels with thin 6-ply skins can be exposed to a high intensity broad-band acoustic environment for at least 10^8 cycles without experiencing acoustic fatigue failures in the skin and/or in the joints. The strain and life data obtained in the acoustic tests of the last two panels showed rather close agreement. The nominal bay dimensions chosen for the panels were typical of dimensions in thin-skinned metallic, aircraft structures. The strains developed in the acoustic tests were too low to produce acoustic fatigue failures and therefore it was not possible to compare directly the lives of the vibration specimens in the program with the acoustic panels. However, by fabricating acoustic panels with larger bays it should be possible in acoustic tests to obtain cross-stiffened panel failures under multimodal strain response at some average frequency, that can be compared directly with vibration specimen failures under unimodal strain response. Such tests would produce more data to assess the usefulness of the procedure described below for predicting acoustic fatigue life based on the average response frequency and the overall rms response strain.

The absence of an acoustic fatigue failure in these panels was predicted based upon a three-step procedure. First, experimental overall rms strains in the panel skin were obtained at acoustic fatigue-critical locations at the reference SPL which in this case was 166 dB. Second, the number of cycles of acoustic response was calculated as the product of an average frequency of response times the time duration of acoustic exposure at 166 dB. Third, the combination of rms strain from Step 1 and cycles of response from Step 2 was compared with the experimental S-N data (Figure 13) that were obtained in the shaker tests of specimens with graphite-epoxy skins and stiffeners.

6. APPLICATION OF ANALYSIS METHODS

The objective of the analytical effort was to develop a procedure to predict the natural frequencies, mode shapes, and stress-strain response of flat cross-stiffened, fiber reinforced composite panels subjected to random acoustic excitation. Equations for these predictions were presented in Section 2. Since there are only limited experimental data available to assess adequately the validity of these equations as applied to cross-stiffened fiber reinforced composite panels, the approach taken in this program was to investigate analytically several problems that could be solved for both isotropic panels and fiber reinforced composite panels. The isotropic panels were considered first. Then, with these results to serve as a guide, the investigation was extended to include the vibration characteristics and dynamic response of composite panels to random acoustic excitation.

The Northrop Corporation had available at the beginning of this effort a digital computer program referred to as REDYN that was capable of performing the calculations required by the general theory. Other digital computer programs having a similar capability are available and can be used in the same manner that REDYN was used. It is the intent of the following to present only a summary of the results of the various computational procedures, and the methods of utilizing REDYN for performing these calculations can be found in Reference 1.

Application to Isotropic Plates

The theory was first applied to a square 21 X 21 X 0.10 inch flat, unstiffened, aluminum alloy plate clamped on all four edges. Natural frequencies, mode shapes, deflections, and strains were computed by different methods. The results of the various calculations are given in Table IV. The deflections and strains are based on fully correlated white noise and computed for the center of a plate.

The closest agreement to the fundamental frequency obtained with beam functions (i.e., the simplified theory) occurred with the rectangular finite elements and implies that the rectangular option of REDYN is preferable to the triangular option.

When 36 nodes and 25 square elements were used with REDYN and when the distance between nodes was reduced by 50 percent, the fundamental frequency was increased approximately three percent; i.e., the frequency was increased from 77.7 Hz to 79.7 Hz (see Table IV). In other words, by utilizing the conditions of symmetry and using the same number of nodes for the eigenvalue problem, a three percent change in natural frequency occurred. Therefore, fundamental frequencies obtained with REDYN where conditions of symmetry are nonexistent and a full plate analysis is required, are considered satisfactory.

The mode shapes along a center line of the plate were calculated using (1) the clamped-clamped beam function approach and (2) REDYN with triangular and with rectangular elements with only one quadrant of the plate and conditions of symmetry. The results are presented in Table V and are normalized to unity at the center of the plate.

The finite element approach and the beam function approach are both approximate analytical methods. Convergence of the lowest frequency and modal shape has not been shown because of limitations on the storage capacity of computers. However, the close agreement between the results (natural frequency, strain, deflection, and mode shape) obtained with the beam function method and the rectangular finite element (REDYN) method indicates that both give good results.

A study is described in Reference 1 to determine the effect of finite element node location on the calculation of natural frequency, stress, and deflection of a cross-stiffened panel subjected to acoustic loading using both REDYN and the clamped-clamped beam function method. Based upon the results of this study (Table XXIII of Reference 1) and since no experimental data were available, the conclusion was drawn that the finite element analysis and the simplified theory using beam functions could be used for the dynamic analysis of cross-stiffened panels. However, this procedure may produce an unsatisfactory dynamic description of the fundamental mode of some cross-stiffened plates, and it will be necessary to develop a criterion to determine when the simplified theory can be used to predict the fundamental frequency of a cross-stiffened plate. Until this is developed, it appears that the simplified theory produces an upper bound on this frequency.

Application to Fiber Reinforced Composite Panels

Using the results of the previous section as a guide, the theory was now used to predict the free vibrations and the strain-stre's response of fiber reinforced composite panels subjected to random acoustic excitation.

The simplified theory and the finite element approach with REDYN were first used t compute the fundamental frequency and strain in an orthotropic plate that was clamped on all four edges. The model used was intended to simulate the central bay of the cross-stiffened, graphite-epoxy test panels previously described. The central bay dimensions used for this solution were 6 X 9 inches to account for the I-beam and T-section flanges which supported the nominal 7 X 10 inch central bay by approximately 0.5 inches around the periphery and thereby reduced the unsupported area of the panel. The computed fundamental frequency and the unimodal strain response at the edges of the long and short edge of the plate are given in Table VI. The strain gage response for gages Nr 2 and 7 is also given in Table VI for acoustic test panels Nr 2 and Nr 3.

The linear, finite element program REDYN was also used to predict (Table VI) the fundamental frequency and strain response near strain gages Nr 2 and 7, in the skin of the central bay of the acoustic test panels. The finite element model, in this case, designed for the analysis represented only one quadrant of the complete cross-stiffened panel with bound v conditions chosen to produce symmetrical response about the panel centerlines and zero deflection and slope at the other two edges. Reference 1 gives the complete details of this model. It should be noted that the theoretical strains were at the centroids of small finite elements that included the location of strain gages Nr 2 and 7.

There is agreement between the theoretical frequencies given in Table VI and these in turn agree with the experimental values. There is also general agreement between the strains predicted by the beam function approach and both finite element calculations for the simple plate and the cross-stiffened panel; however, these do not agree with the experimental values. This disagreement is of the same order of magnitude as discrepancies between theoretical strains and experimental stresses reported by previous investigators for the dynamic behavior of isotropic panels. This disagreement may be due to the following (1) nonlinear strain-pressure relationship, (2) local strain at the periphery of the cross-stiffened panel may be significantly influenced by the local geometry that has not been modeled in the dynamic analysis (the model for the cross-stiffened panel is a little better in this respect) and (3) the acoustic pressure may not be considered spatially uniform. It may be possible in the future to reduce these differences by using a finer grid in the finite element analysis and by accounting for the deviations from the assumed fully correlated loading conditions.

7. CONCLUSIONS

Two methods of analysis have been developed for predicting linear strain response to acoustic excitation. The simplified theory will predict the unimodal response at the fundamental frequency of a flat, rectangular, orthotropic plate subjected to fully correlated, white noise excitation and clamped on all four edges. At the present time there is no criterion to indicate when the simplified theory is applicable to the design of skins of cross-stiffened, fiber reinforced composite panels.

The second method consisted of applying an available, linear, finite element, dynamic stress analysis computer program for predicting the natural frequencies and the multi-modal, stress response in the skin and internal structure of orthotropic plates subjected to broad-band acoustic pressure excitation. This method of analysis provided satisfactory agreement between predicted and experimental fundamental frequencies. A comparison of the predicted strains in the panel skins at low excitation levels and strains in the skins of the flat, acoustic test panels showed satisfactory agreement in the sense that percentage differences between predicted and experimental values were approximately the same as the differences that have been documented during acoustic fatigue investigations conducted with metallic panels during the last several years.

Sonic fatigue test programs were conducted on simple flat boron-epoxy and cross-stiffened flat graphite-epoxy composite test panels. These programs yielded data on the dynamic characteristics of these panels such as resonant frequencies, mode shapes, panel damping factors and dynamic strain response. Panel endurance data and the types of fiber reinforced composite panel failures that may result from high intensity noise were also obtained.

Six S-N curves for shaker specimens that simulated joints in composite panels with different material systems and different attachments and stiffeners were obtained in the test program. From these tests it was concluded that S-N data obtained by shaker testing can be substituted for S-N data obtained under more expensive acoustic panel tests. Also it appears practical to conduct a series of shaker tests and vary important items such as the method of attachment, the orientation of plies in fiber reinforced composite skins, and the stacking sequence of the plies in order to obtain experimental S-N data to compare advantages and disadvantages of various types of joint assemblies. In general, where the location of failure is at a joint assembly in a thin skin and possibly in the joint attachment of an acoustically loaded panel, it appears that the strain at the failure location results from simple bending and the use the use of S-N curves obtained under essentially simple bending conditions appears feasible in the prediction of the panel life.

Based upon the acoustic test results of this program, it appears that flat simple boron-epoxy and thin-skinned graphite-epoxy cross-stiffened panels attached to composite or metallic material structure are attractive for use in high intensity noise environments.

REFERENCES

1. Technical Report AFFDL-TR-71-126, Jacobson, M. J., "Advanced Composite Joints; Design and Acoustic Fatigue Characteristics", Wright-Patterson Air Force Base, Ohio, April 1972.

2. Test Report AFFDL/FYA-72-2, (in preparation), Rupert, C. L., "Sonic Fatigue and Response Tests of Boron Composite Panels", Wright-Patterson Air Force Base, Ohio.

3. Technical Report AFFDL-TR-68-107, Jacobson, M. J., "Acoustic Fatigue Design Information for Fiber Reinforced Structures", Oct 1968.

4. AIAA J., Vol. 6, Nr 8, pp 1503-1510, Jacobson, M. J., ". . and Deflection of Honeycomb Panels Loaded by Spatially Uniform White Noise", Aug 1968.

Figure 1. Geometry and Coordinate System of Rectangular Plate
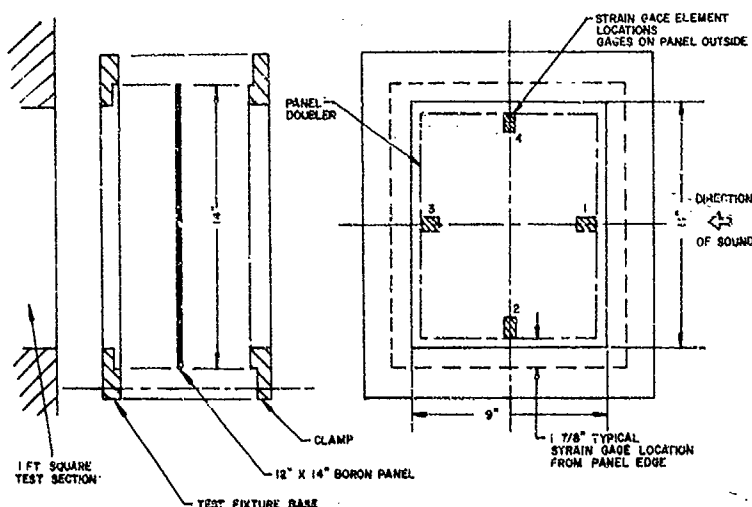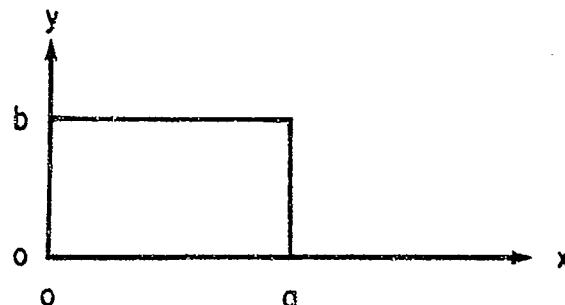
Figure 2. Boron-Epoxy Test Panel, Mounting Fixture and Strain Gage Locations
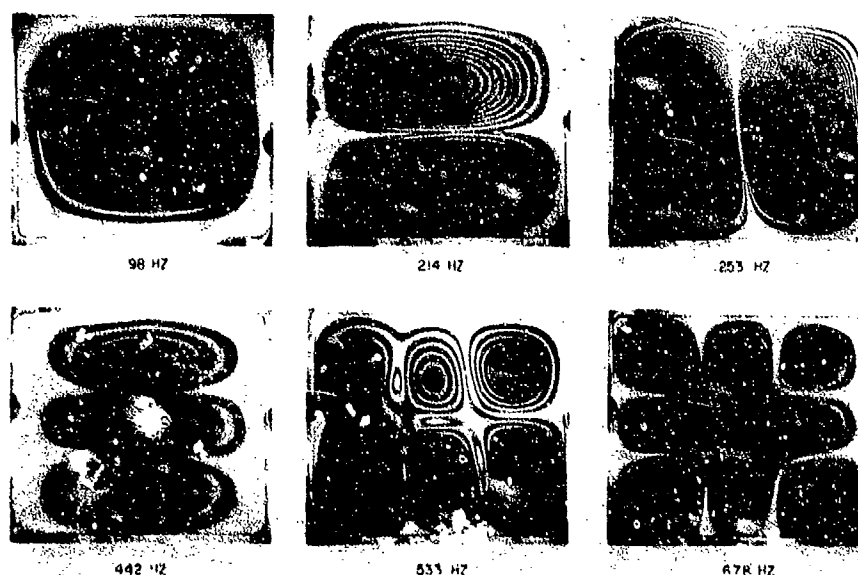
Figure 3. Typical Boron-Epoxy Panel Mode Shapes and Resonant Frequencies
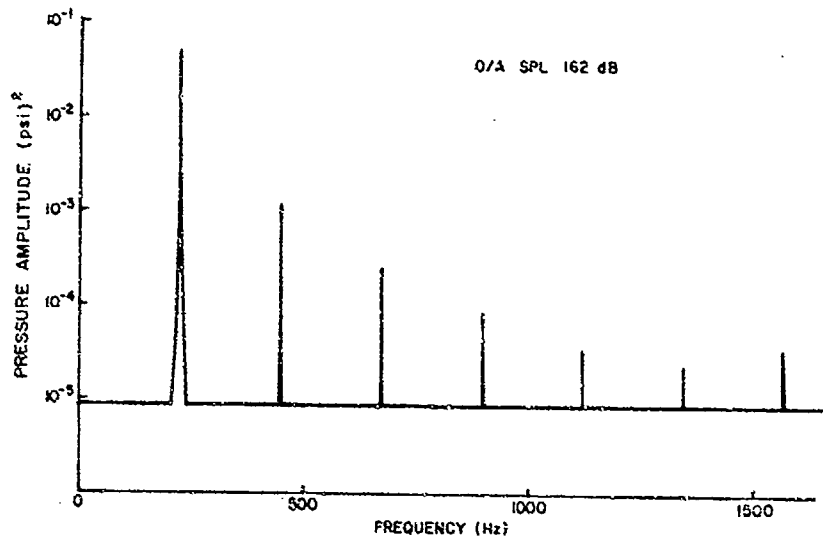
Figure 4. Typical Pressure Spectrum for Boron-Epoxy Panel
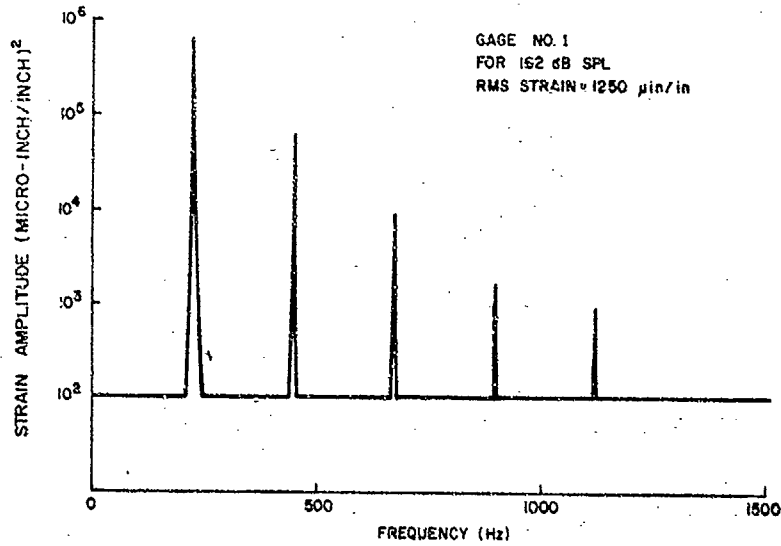
Figure 5. Typical Strain Spectrum for Boron-Epoxy Panel
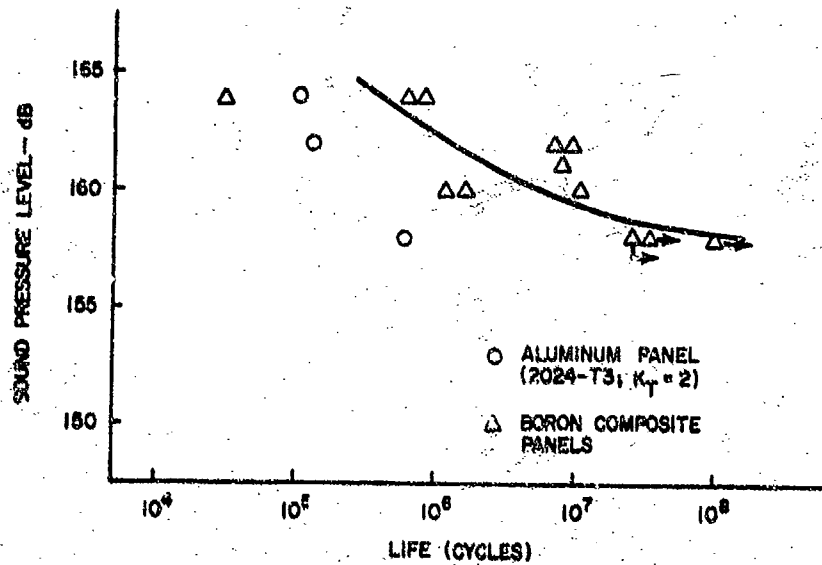
Figure 6. Boron-Epoxy and Aluminum Panel Fatigue Data
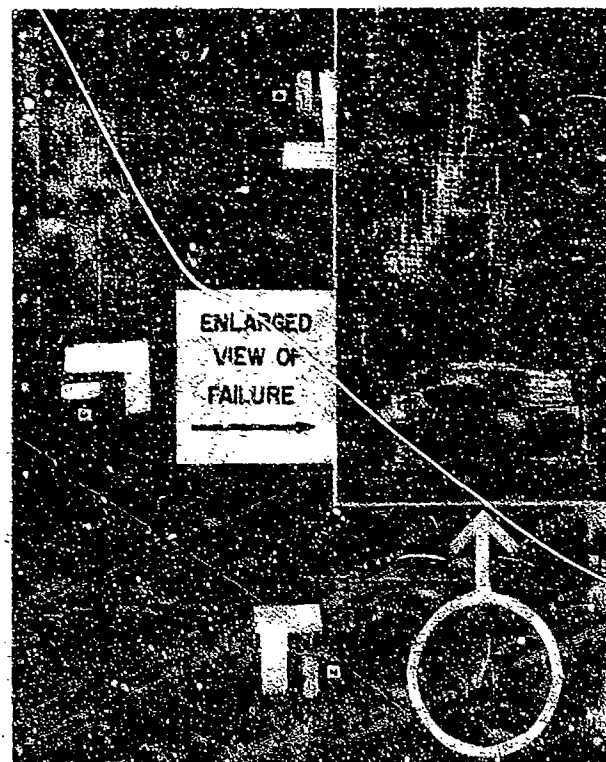
Figure 7. Typical Boron-Epoxy Panel Failure

BONDED STRINGER SPECIMEN

RIVETED STRINGER SPECIMEN

SKIN 6 PLY $[90/\pm 45]_s$

SKIN 6 PLY $[90/\pm 45]_s$

MATERIAL	
SKIN	STRINGER
GRAPHITE-EPOXY	GRAPHITE-EPOXY
GRAPHITE-EPOXY	TITANIUM ALLOY
BORON-EPOXY	TITANIUM ALLOY

MATERIAL	
SKIN	STRINGER
GRAPHITE-EPOXY	GRAPHITE-EPOXY
GRAPHITE-EPOXY	TITANIUM ALLOY
BORON-EPOXY	TITANIUM ALLOY
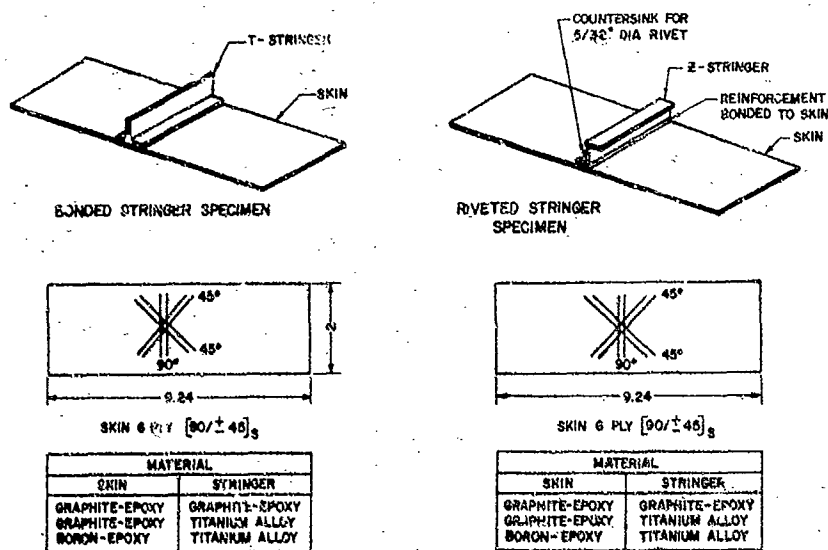
Figure 8. Beam Specimens for Shaker Tests

Figure 9. Single Specimen Mounted for Shaker Fatigue Test
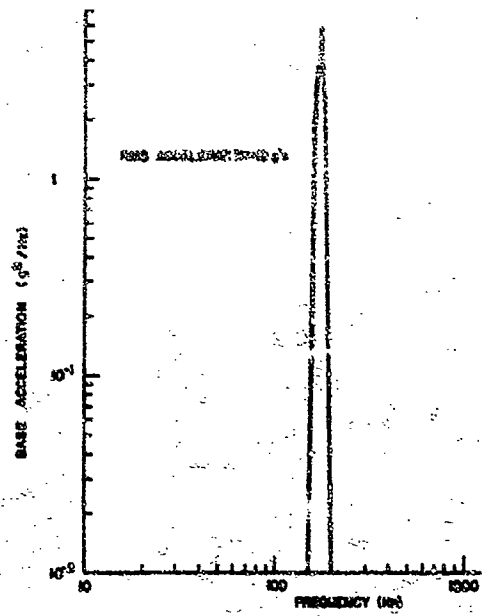
Figure 10. Base Acceleration for Typical Shaker Specimen (10 g Run)
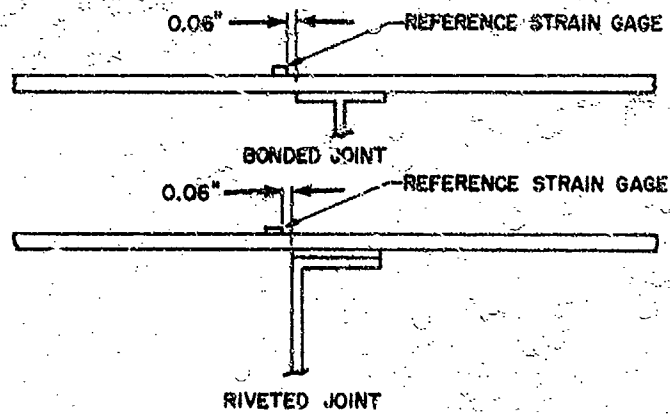
Figure 11. Strain Gage Locations on Shaker Specimens
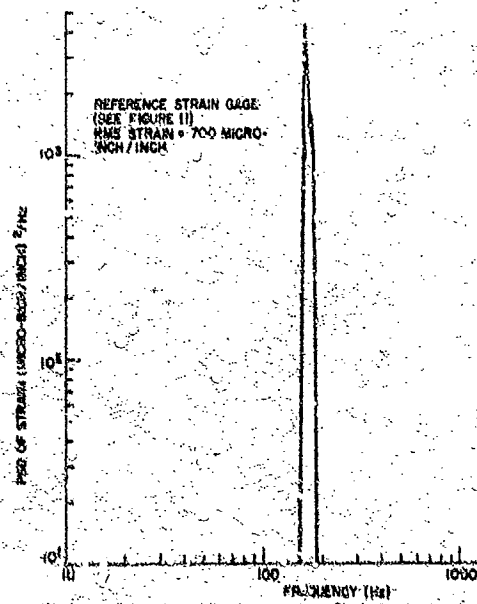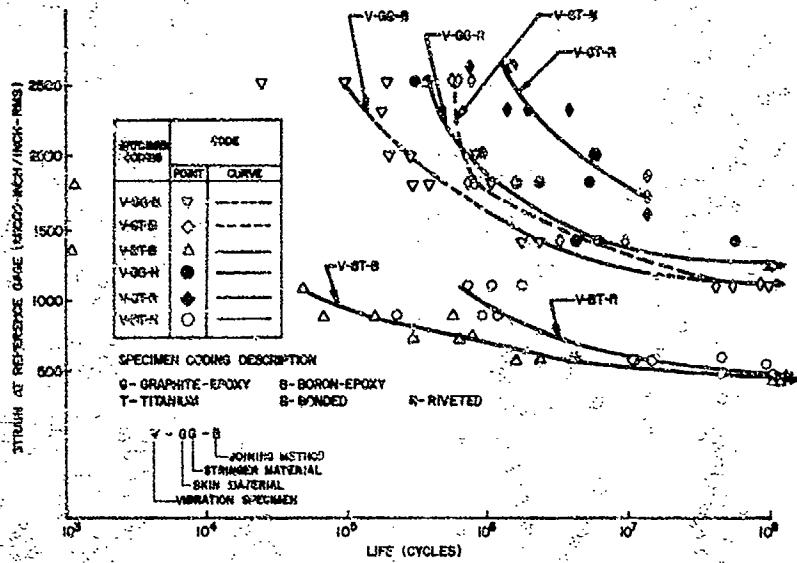
Figure 13. Summary of Shaker S-N Data
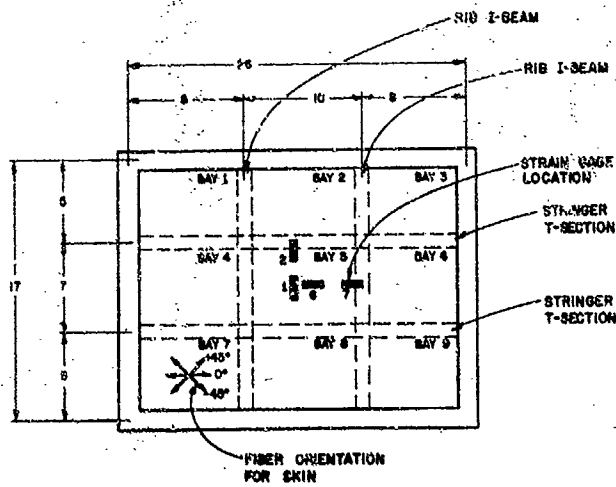
NOTES: 1. ALL STRAIN GAGES SHOWN ARE ON THE EXPOSED SURFACE OF THE SKIN.
2. ALL DIMENSIONS ARE NOMINAL.

Figure 14. Schematic of Graphite-Epoxy Advanced
Composite Panel with Selected Strain Gage Locations
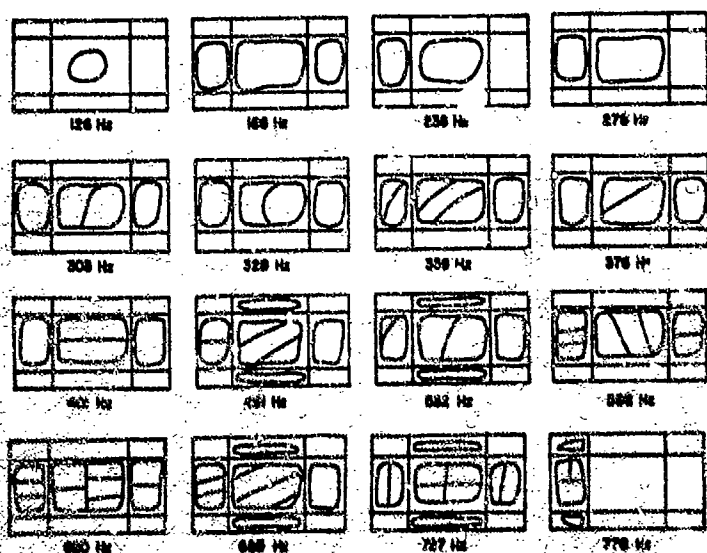
Figure 15. Mode Shapes and Resonant Frequencies of Panel V-2
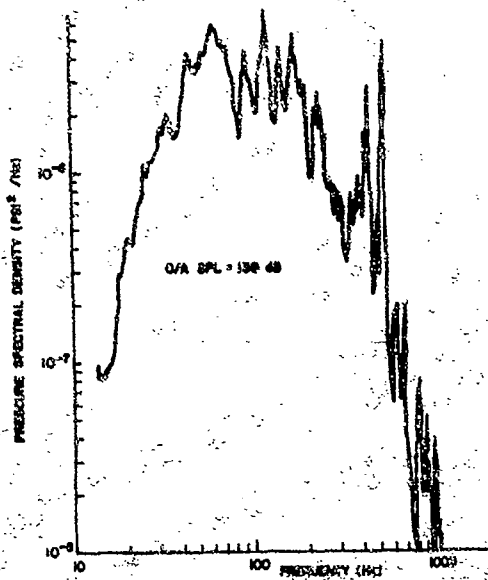
Figure 16. Pressure Spectral Density
for Graphite-Epoxy Panel Nr 2
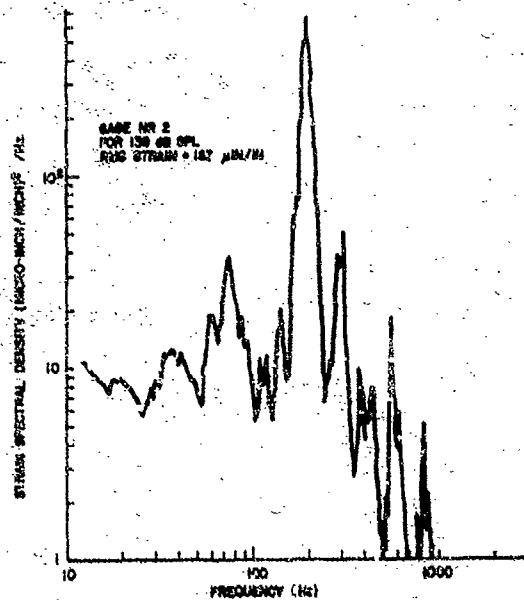
Figure 17. Strain Spectral Density
for Graphite-Epoxy Panel Nr 2
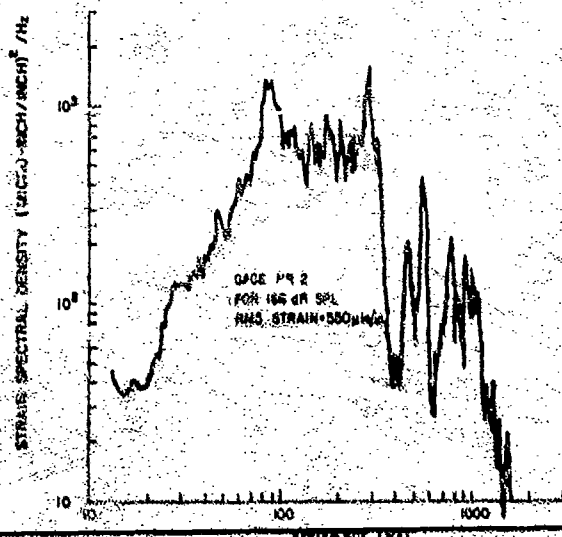
Figure 18. Strain Spectral Density
for Graphite-Epoxy Panel Nr 2

TABLE I TYPICAL PANEL STRAIN GAGE RESPONSE DATA

SPL dB	Freq Hz	Peak Strain - Microinches/Inch			
		GAGE NR			
		1	2	3	4
130	138	±280	±110	±210	±90
134	155	440	180	330	180
138	170	550	240	410	-
142	180	650	320	470	-
146	194	960	400	650	-
150	225	1250	620	1070	-
154	233	1400	700	1100	-
158	260	2150	1000	1550	-
162	270	2700	-	-	-
164	-	-	1750	-	-

TABLE II DAMPING FACTORS

BAY NR	4			5			6			8		
PANEL NR	1	2	3	1	2	3	1	2	3	1	2	3
Frequency (Hz)	184	187	177	184	187	170		177				
Damping Factor	.023	.016	.013	.017	.017	.013		.012				
Frequency (Hz)	233	238										
Damping Factor	.014	.032										
Frequency (Hz)				277						277		
Damping Factor				.017						.015		
Frequency (Hz)				343					348			
Damping Factor				.017					.015			

TABLE III STRAIN GAGE RESPONSE
(MICRO-INCH/INCH-RMS) FOR PANEL NR 2

Strain Gage Nr	Overall Sound Pressure Level (dB re 0.0002 dynes/cm^2)										
	136 dB	139 dB	142 dB	145 dB	148 dB	151 dB	154 dB	157 dB	160 dB	163 dB	166 dB
1	88	112	128	152	176	200	225	260	275	300	330
2	114	160	210	260	310	345	400	450	500	545	600
6	68	80	90	104	114	120	140	150	160	190	210

TABLE IV COMPARISON OF FREQUENCIES, DEFLECTIONS and STRAINS

	REDYN					Clamped-Clamped Beam Function	Experimental
Element Type/Nr	Triangular/50	Triangular/72	Rectangular/25	Rectangular/36	Rectangular/25		
Nodes	36	49	36	49	36		
Quadrants	1 + Symmetry	1 + Symmetry	1 + Symmetry	4	4		
Frequency Hz	76.1	77.0	79.7	78.4	77.7	80.7	76.0
Deflection in (rms)		0.061	0.057	0.059	0.050	0.056	
Principal Strain µ in/in		85.	106.	98.5	96.5	110	

TABLE V THEORETICAL MODE SHAPES

LOCATION	DEFLECTION		
$\frac{x}{L}$	Beams Functions (in.)	REDYN, 36 Nodes, Triangular Elements, One Quadrant (in.)	REDYN, 36 Nodes Rectangular Elements, One Quadrant (in.)
0.0	.00	.00	.00
0.1	.14	.12	.13
0.2	.43	.39	.41
0.3	.67	.69	.71
0.4	.94	.97	.92
0.5	1.00	1.00	1.00

TABLE VI COMPARISON OF EXPERIMENTAL RESULTS OF CROSS-STIFFENED PANELS WITH ANALYTICAL CALCULATIONS

Approach	Method	Acoustic Loading dB	Fundamental Freq. Hz	Strain at Center of Short Side Gage #7 µ in/in	Strain at Center of Long Side Gage #2 µ in/in
Theoretical	Simplified Method (Beam Functions)	139[1]	182	180	406
Theoretical	Finite Element (REDYN) Unstiffened Plate	139[1]	180	180	348
Theoretical	Finite Element (REDYN) Cross-Stiffened Panel	139[1]	165	168	304
Experimental	Test Panel #2	139	187	96	160
Experimental	Test Panel #3	139	170	74	164

1 - The acoustic loading was characterized as fully correlated white noise and the pressure PSD was estimated from the data analysis of the pressure applied to acoustic panel Nr 3 during the 139 OB SPL run.

SESSION / DISCUSSION - DAMPING AND COMPOSITE STRUCTURES

    Commenting on Mr. Hay's paper, Dr. Mead said t! damping measurements from response tests carried out in travelling wave tube test faciliti would be complicated by the fact that some modes of vibration of the structure would have high acoustic damping. This is likely to be more significant at lower frequencies and therefore the damping values measured at low frequencies may well be exaggerated. There are several damping mechanisms present which depend on frequency and mode wavelength in different ways. For example, shear damping is likely to be dependent on wavelength squared whereas damping due to bending moments on joints is independent of wavelength. It therefore seems unrealistic to look for a simple frequency law. Dr. White commented on the effect of non-linearity of joints and added that there is also a possibility of non-linear stiffness being significant in some of the modes. This affects the way in which damping can be derived from the vector diagrams. The maximum amplitude and the maximum rate of change of arc length do not occur at the same frequencies. Mr. Hay replied that in some tests there were results for different levels of excitation and so it might be possible to look at the effect of amplitude and hence see if there is any marked non-linearity effect appearing. In reply to another question, Mr. Hay said that the data presented was for a mixture of modes. It was not easy to identify the modes but it might be possible to indicate which are the lower order modes.

    Mr. Wolf was questioned on the details of the experimental procedure used in his work. He replied that all the failures were in the skin material for both bonded and rivetted constructions. Stress concentrations were present which are not reflected in the S-N data. No measurements were made of the stress distribution in the skin over the stiffener. It was suggested that the rivetted specimen appeared to have a longer life than the bonded specimen on the S-N plot because the tests were done on the basis of controlling the strain at a point some distance from the stress concentration. The different strain gradients in the two types of attachments could result in unfair comparisons. In reply to a question on failure determination, Mr. Wolf said that a frequency change of about 20% was deemed to define failure. All failures were at the edge of the panels. Attempts were made to position the failures at the centre of the panel by using doublers at the edges. They also tried to get information on crack propagation rates by using holes to initiate cracks. This was not very successful. In reply to another question, Mr. Wolf said that they had tried to monitor the strain on the Boron panels but it was very difficult to keep the strain gauges on the panel. They lasted for only about 2 minutes at the higher strain levels. Reference 2, which is in the course of preparation, will give the strain data which is considered to be reliable. Non-contacting displacement transducers were also used on the beam tests. The stiffness properties of the composite were determined from mechanical tensile tests as described in reference 1.

SONIC FATIGUE OF DIFFUSION-BONDED
TITANIUM SANDWICH STRUCTURE

I. Holehouse
Technology Staff Engineer
Rohr Industries, Inc.
Chula Vista, California 92012
U.S.A.

SUMMARY

Titanium honeycomb sandwich structure is being increasingly demanded for aerospace structural applications. A major limitation in meeting this demand has been the availability of a joining system capable of realizing the structural and thermal properties of titanium alloys. Four systems are available; adhesive bonding, aluminum brazing, resistance welding and diffusion bonding. Of these, only resistance welding and diffusion bonding have the full temperature capability of titanium and it is believed that diffusion bonding has structural advantages, particularly in sonic fatigue. This paper deals with the sonic fatigue characteristics of titanium sandwich utilizing a "Liquid Interface Diffusion" (LID) bonding process. Sixteen test panels were subjected to sound levels of up to 170db for extended time periods. Various failure modes and times to failure were observed. Sufficient strain and acoustic data were taken to develop a semi-empirical design analysis nomograph. The analytical approach taken utilized a single degree of freedom random response equation combined with a finite element approach for determining natural frequencies and static stress values. The effect of skin repairs and facing-to-core bond voids were investigated by testing panels with programmed defects. Sonic fatigue testing was also performed on titanium honeycomb sandwich panels reinforced with graphite-epoxy laminates.

1. INTRODUCTION

The analytical approaches used to determine the natural frequencies, static stresses and dynamic stresses for the test panel configurations are presented in the first section. The second section deals with the experimental approach, and includes the test results. The analytical and experimental results are then brought together in a series of regression analyses to provide simplified equations for calculating frequencies and stress levels. These equations are then used to generate design nomographs which are presented in Section 5, with a recommended design procedure. The effects of panel fabrication defects on sonic fatigue life are discussed in the experimental section.

2. THEORETICAL APPROACH

2.1 INTRODUCTION

Although acoustically-induced vibrations usually consist of several response modes, fatigue damage is usually dominated by one mode. This enables a single-degree-of-freedom theory to be used to estimate dynamic stress levels. Natural frequency and static stress components of the dynamic stress equation are determined using finite-element structural analysis computer programs.

2.2 GENERAL THEORY

Miles (Reference 1) has developed a single-degree-of-freedom response equation for the mean square stress:

$$\sigma^2(t) = \frac{\pi}{4\zeta} f_r \ G(f_r)\sigma_0^2 \tag{1}$$

where f_r = the natural frequency of the fundamental mode in Hz

$G(f_r)$ = spectral density of the acoustic pressure at the frequency f_r

σ_0 = static stress due to a uniform unit static pressure load

ζ = damping ratio

Equation 1 has found widespread application in sonic fatigue analysis. However, in order to utilize it, the following assumptions are made:

a) Only one response mode affects fatigue life. This is usually assumed to be the fundamental with fully-fixed edges.

b) The vibration mode shape is identical to the deflection mode under a uniform static pressure load.

c) Acoustical pressures are exactly in phase over the whole panel.

d) The spectral density of the acoustical pressure is constant in the frequency range near the fundamental frequency of the panel.

The assumptions in "a" have a self-cancelling tendency. Neglecting secondary response modes leads to underestimating overall response stresses. Assuming full fixation at the panel edges leads to an overestimate of edge stresses.

In structural design work, the damping ratio (r) is estimated from previous experience and is usually in the region of 0.02 to 0.05. The determination of natural frequencies (f_r) and static stresses (σ_o) is described in the following paragraphs.

2.3 FREQUENCY ANALYSIS

Works by Abel (Reference 2) and Ahmed (Reference 3) were used to calculate natural frequencies. Reference 2 was available at the beginning of the program and was used for initial frequency estimates. It is limited to axisymmetrical structures and loadings. In order to use this method for flat plates, a near infinite radius cylinder was analyzed and an aspect ratio correction applied based on Reference 4. Abel's method has the advantage of simplicity and short computer time (less than one minute per case). Later in the program Ahmed's method was used. This work is more complex and does not have the axisymmetical limitation. The two methods gave similar values for fully-fixed edges. However, Abel's program could not be used for low aspect ratio simply-supported flat plates because the appropriate boundary conditions along the short edges could not be simulated. Since only fixed edges were to be considered in the final analysis and a computer program based on Abel's work was available, these frequencies were used in the subsequent dynamic stress calculations. Figures 1 and 2 (from Reference 5) were used to determine core shear modulus and core density values, respectively. Corrugated foil values were used. Table 1 lists panel configurations and shows a comparison of calculated frequencies using Reference 2 and 3.

Table 1
Calculated Frequencies

CONFIG. NUMBER	PANEL DEPTH (IN.)	FACING THICKNESS (IN.)	CORE				CLAMPED FREQUENCIES	
			CELL SIZE (IN.)	FOIL THICKNESS	DENSITY LB/FT^3	SHEAR MODULUS LB/IN.^{2}	ABEL (Hz)	AHMED (Hz)
1	1/8	.005	3/16	.002	6.8	73,000	121	-
2	1/4	.003	3/16	.0015	5.1	55,000	287	299
3	1/4	.008	1/4	.003	7.7	82,500	276	287
4	1/4	.012	3/16	.002	6.9	73,000	294	302
5	1/4	.020	3/16	.0015	5.1	55,000	308	307
6	1/4	.020	3/16	.002	6.9	73,000	309	308
7	1/4	.020	1/4	.003	7.7	82,500	308	307
8	1/2	.008	3/16	.0015	5.1	55,000	494	524
9	1/2	.012	3/16	.0015	5.1	55,000	514	544
10	1/2	.020	1/4	.003	7.7	82,500	523	547

In order to construct a frequency design nomograph (paragraph 5.1) a simplified equation was obtained (paragraph 4.2) by regressing the frequencies calculated using Reference 2 against the program input parameters.

2.4 STATIC STRESS ANALYSIS

Reference 3 was used for estimating stresses in the honeycomb panels under a uniform static pressure of 1 lb/ft^2. Later in the program NASTRAN (a large general-purpose computerized structural analysis system based on finite-element techniques and developed by NASA--Reference 6) was used. The general acceptance of NASTRAN in the American aerospace industry enables it to be used on product designs without specific justification. For this reason it is used to generate the static stresses used in the final dynamic stress equation. NASTRAN or similar general-purpose programs are widely used in industry for static analysis and some duplication of effort (e.g., modelling) is avoided if the same program is used to generate static stress values in support of sonic fatigue analysis

The general assumptions made in this analysis are:

a) Linear elasticity theory applies.

b) The core is orthotropic.

c) Normal strains in the core are negligible.

d) The core is incapable of carrying in-plane loads.

e) Plane surfaces remain plane.

Triangular and rectangular elements were used. Both included uncoupled membrane and bending stresses and have five degrees of freedom per node.
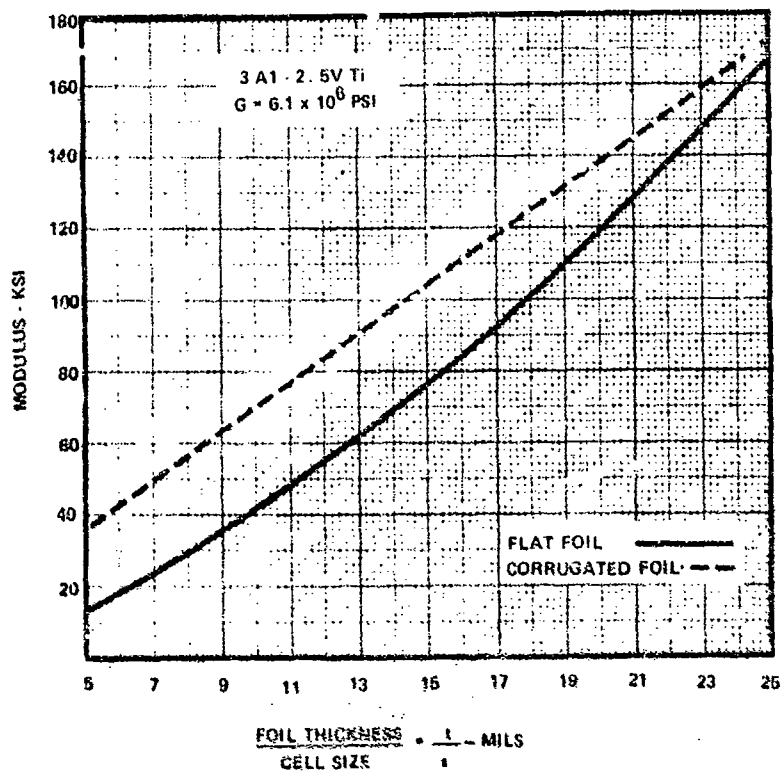
Figure 1   Core Shear Modulus
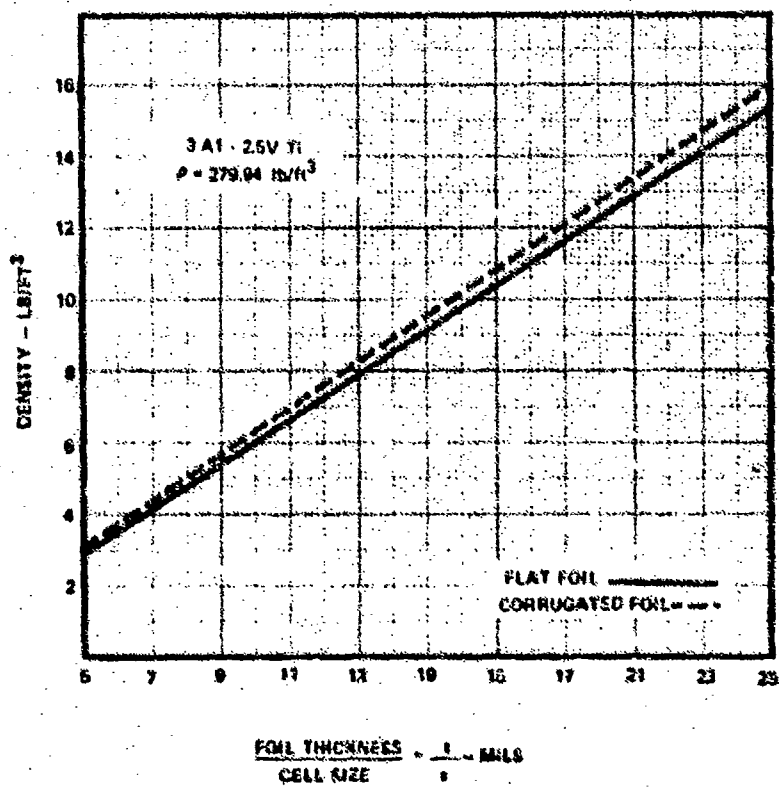
Figure 2. Core Density.

The following element properties were used in the computations:

6Al-4V Titanium Facings	3Al-2.5V Titanium 3/16 x .002 Core
$E = 16 \times 10^6$ lb/in^2	$\Sigma = 0$
$G = 6.2 \times 10^6$ lb/in^2	$G = 43,800$ lb/in^2 (Transverse)
$\rho = 0.16 \times$ lb/in^3	

The orthotropic core limitation is not generally representative of honeycomb core. Shear modulus values in the transverse direction are 60% of the values in the ribbon direction for the core used in this program. The values given in Figure 2 are for the ribbon direction. Since the comparison between analytical and experimental data was to be made in the transverse direction, the 60% values were used in estimating static stress levels. However, such a change in the core shear modulus had only a 2% effect on the facing stress values. Because of this minimal effect of shear modulus on stress, the differences in shear moduli for the different honeycomb cores were neglected in the static stress analysis. In the worst case, this represented a 2% loss of accuracy.

Table 2 shows a comparison between Ahmed's and NASTRAN static stress values at the center of a clamped panel for a uniform static pressure of 1 lb/ft^2.

Table 2
Static Stresses Due to Uniform Pressure of 1 Lb/Ft^2

PANEL DEPTH (IN.)	FACING THICKNESS (IN.)	STRESSES (LB/IN^2)	
		NASTRAN	AHMED
1/8	.005	104.0	-
1/4	.008	33.9	33.1
1/4	.012	22.6	21.5
1/4	.020	13.7	13.2
1/2	.008	17.0	16.7
1/2	.012	11.4	11.1
1/2	.020	6.9	6.7

Center stresses rather than edge stresses are shown because they were eventually used in regressing against the test data. Edge stresses were highly dependent upon edge doubler configurations which in turn varied with the facing thickness. Stress distributions were obtained for each panel in order to relate center stresses to the maximum stresses in the panels. Figure 3 shows the distribution for panel number 4, which has .012" facings with 0.016 edge doublers.
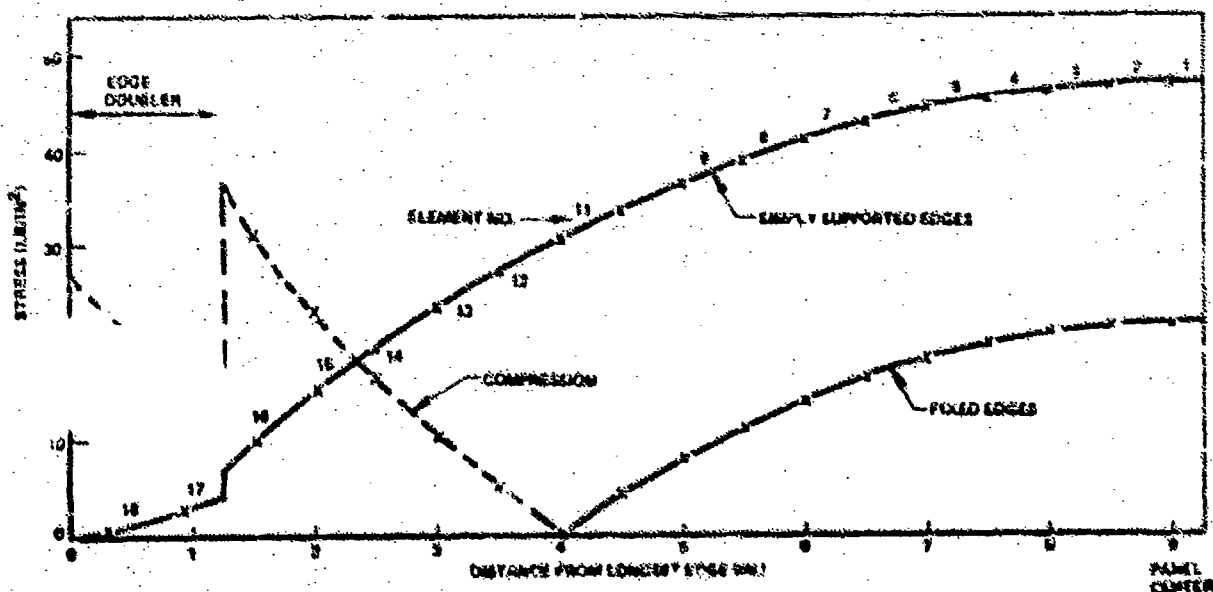
Figure 3. Static Stress Distribution for Panel No. 4.

Static stress values were then calculated for various overall panel sizes and aspect ratios and a multiple regression analysis performed between the calculated values and the program input parameters (paragraph 6.3). This analysis was used to generate a static stress design nomograph (paragraph 5.2).

3. EXPERIMENTAL APPROACH

3.1 INTRODUCTION

The objective of the experimental investigation was to obtain structural response and fatigue life data for the titanium honeycomb panels under random acoustic loading. The data form the empirical basis for a simplified sonic fatigue design nomograph.

Sixteen panels comprising 10 different configurations were tested in a "progressive-wave tube." Two panels had controlled core-to-facing voids, one had a facing repair and one had a potted insert. Also tested were two panels with graphite-epoxy reinforced facings. Thirteen of the panels were tested to failure.

3.2 TEST PANEL DESIGN

The 10 configurations tested are given in Table 1. Each panel measured 25.25" x 18.5" with 6Al-4V titanium facings and 3Al-2.5V titanium core (corrugated). Full-depth close outs were used to represent a clamped condition when mounted in the "progressive-wave tube." Edge doublers were typical of design practice, being 1-1/4" wide with their thickness corresponding to facing thickness as follows:

Facing Thickness	Doubler Thickness
.005	.012
.008	.012
.013	.016
.020	.070

Panel area densities ranged from 1/4 to 1-3/4 lb/ft^2.

3.3 CORE-TO-FACING BOND

Four joining systems are available for titanium honeycomb sandwich: adhesive bonding, aluminum brazing, resistance welding and diffusion bonding. Of these, only resistance welding and diffusion bonding realize the full temperature capability of titanium alloys. The panels used in this program were diffusion bonded using a "Liquid Interface Diffusion" process (LID). The LID joining concept utilizes an electroplate of selected materials applied to the faying surfaces. The bonding is performed at 1700°F. in a high vacuum furnace. The LID elements are then diffused into the substrate and diluted to a point where degradation of base material is minimized.

In addition to high strength, LID joints have an important weight saving advantage over brazed and welded joints. The absence of a fillet keeps the LID joint weight down to 1/250 lb/ft^2. Welded joints add 1/8 lb/ft^2 and bonded and brazed joints typically add 1/10 lb/ft^2. This weight saving approaches 40% in lightweight engine ducts.

3.4 INSTRUMENTATION

Each panel was instrumented with six strain gauges: a biaxial at the panel center and a single axis gauge at the center of, and normal to, each side. Small (1/8") strain gauges were used to avoid excessive strain averaging effects. Three microphones were used to monitor acoustic levels in the "progressive-wave tube." Noise levels and spectra quoted in the test results are from a microphone located at the panel center.

3.5 TEST PROCEDURE

The panels were subjected to broad-band random noise at grazing incidence in a "progressive-wave tube" at the McDonnell-Douglas acoustics facility in Santa Monica, California. A maximum exposure time of 20 hours was set for each operating sound pressure level (corresponds to greater than 10^7 cycles for the panel designs tested). This time was shortened when it was apparent from the strain levels that the possibility of a fatigue failure was remote. Whenever this was done, testing was continued at a higher sound pressure level. When a panel showed no signs of damage after 20 hours at 170db (the maximum capacity of the test facility), this overall level was maintained and the frequency spectrum narrowed to either 1/3 or 1 octave centered around the maximum structural response frequency.

The panels were mounted so as to closely resemble fixity at the edges. During installation the strain gauges were monitored to detect any preload. It is important that a good fit exist between the panel and the fixture to preclude premature edge failures. In order to ensure that the panel response was not unduly affected by resonances in the test fixturing, accelerometers were used to monitor fixture response. No significant influence was detected.

Testing started with a sine sweep at 140db from 50 to 1,000 Hz to determine natural frequencies. This was followed by a "linearity" check with random excitation from 140 to 165db in 5db steps for 10-second intervals. The acoustic levels for subsequent endurance runs were selected on the basis of the strain levels measured during the linearity check.

Data reduction was accomplished in "real-time" during testing. Strain and acoustic levels were also recorded on magnetic tape.

Detailed inspections of the test panels, including "tap" testing for voids, were carried out at intervals ranging from 10 seconds at the beginning of endurance runs up to one hour as the test progressed. Strains were continually monitored during testing. Any change in overall stress levels or frequencies was

3.5   DATA REDUCTION

Overall levels, spectra and phase changes were measured for all microphone and strain gauge outputs. Figures 4, 5 and 6 show a sine sweep, noise and strain spectra and a phase plot, respectively, for panel number 4. The phase plots between microphone and strain gauge outputs were generated to distinguish between "forced" and "resonant" response peaks. In order to optimize the statistical accuracy of the spectrum analysis it is desirable to use the maximum filter bandwidth, compatible with good resolution, in order to permit the maximum averaging time for a given total analysis time. To accomplish this, 2, 5, 10, 20 and 50 Hz filters were used to generate spectra for a given data point. Each major response peak was reduced to a spectrum level, assuming a flat spectrum across the filter bandwidth, by subtracting $10 \log_{10}$ (filter bandwidth) decibels from the measured value. Spectrum levels derived from the 2, 5 and 10 Hz filtered levels were virtually identical, 20 Hz levels were lower. Accordingly, the 10 Hz filter was used.
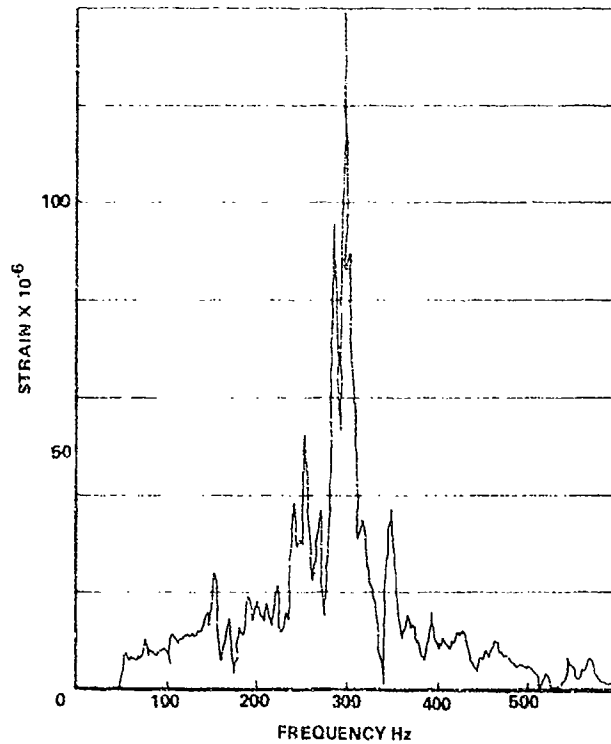
Figure 4.   Sine—Sweep.
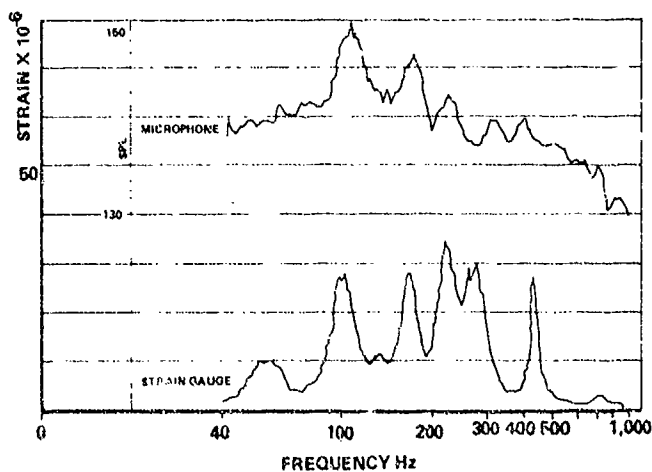
Figure 5.   Noise and Strain Spectra at 170 db.
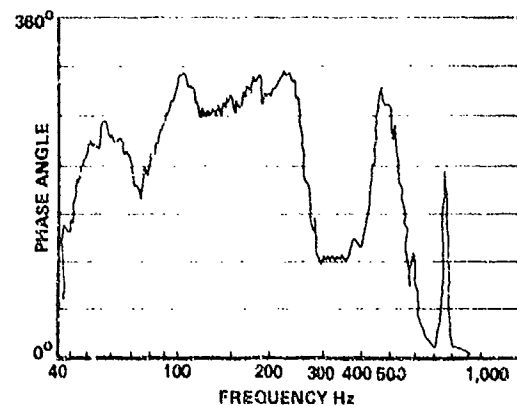
Figure 6.   Phase Angle – Microphone/Strain Gauge.

3.7   TEST RESULTS

The results of the progressive wave tube tests are summarized in Table 3. Panel configurations are given in Table 1. Panel 2A was the same as 2 with a four-ply $(0^\circ-90^\circ-90^\circ-0)$ graphite-epoxy laminate bonded to one facing. Panel 2B was the same as 2A with a two-ply $(0^\circ-90^\circ)$ laminate added to the other face. Panel 3 had a two-inch circular skin patch at the panel center. Panel 4B had a potted insert at the center. Panel 5A had a 2" x 1" void at the center and Panel 9 had a thin 5-inch-long edge void.

Table 3
Sonic Fatigue Test Results

PANEL NUMBER	NATURAL FREQUENCY (Hz)	SOUND PRESSURE LEVEL (db)	CENTER STRESS OVERALL RMS) (LB/IN^2)	DURATION	MODE OF FAILURE
1	150	150 155 160	3,360 6,250 12,500	10 hours 20 hours 30 minutes	None None Delamination
2	200	160 165	3,000 9,600	6 hours 2 minutes	None Facing Failure at Edge
2A (Graphite on one face)		160 165	2,300 3,700	–	–
2B (Graphite on both faces)		160 165	640 1,040	–	–
3 (Facing repair)	200	160 165	1,500 2,640	10 hours 10 hours	None Edge Failure
3A	200	160 165	3,200 7,200	5 hours 2 hours	None Edge Failure
4	285	160 165	1,360 2,560	5 hours 18 hours	None Core Failure
4A	285	165 170	2,240 3,040	20 hours 1 hour	None Edge Failure
4B (Potted Inserts)	150	155 160 165	1,280 2,560 5,900	5 hours 2 hours 22 minutes	None None Delamination
5	295	165 170	1,100 2,240	10 hours 3 minutes	None Delamination
5A (Programmed Voids)	295	165 168 170	1,110 1,900 3,160	10 hours 1 hour 25 minutes	None None Delamination at Edge
6	290	165 170 170 (1 Octave)	1,600 2,260 3,000	10 hours 20 hours 8 hours	None None None Edge Failure
7	290	165 170 170 (1 Octave)	1,440 2,210 3,680	1 hour 20 hours 2 hours	None None None (Test Discontinued)
8	380	160 165 170	700 1,170 1,950	10 hours 7 hours 8 hours	None None Facing Failure
9 (Edge Voids)	425	165 170	880 1,280	10 hours 18 minutes	None Delamination
10	390	165 170 170 (1/3 Octave)	480 960 3,200	10 hours 20 hours 2 hours	None None Facing Failure Near Edge

3.8 DISCUSSION OF TEST RESULTS

The test data clearly show diffusion-bonded titanium sandwich structure to be suitable for application in high-intensity acoustic environments. A variety of modes of failure are indicative of a good balance between facing material, core and bond strengths as well as in the detail design of the edge doublers and closeouts.

Table 4 shows a comparison between measured and calculated frequencies.

Table 4
Comparison Between Calculated and Measured Frequencies

CONFIGURATION NUMBER	PANEL DEPTH	FACING THICKNESS	CALCULATED FREQUENCIES		MEASURED FREQUENCIES
			CLAMPED (REFERENCE 2)	SIMPLY SUPPORTED (REFERENCE 3)	
1	1/8	.005	121	---	150
2	1/4	.008	287	177	200
3	1/4	.008	276	177	200
4	1/4	.012	294	220	285
5	1/4	.020	308	290	295
6	1/4	.020	309	290	290
7	1/4	.020	308	290	290
8	1/2	.008	494	346	380
9	1/2	.012	514	424	425
10	1/2	.020	523	----	390

The measured values fall between the clamped and simply-supported values with the exception of configurations 1 and 10. The high-measured frequency in the first case was probably due to the influence of the edge doublers and closeouts extending into the extremely light panel.

The measured overall stress levels are consistently lower than those calculated using Miles' equation. Comparing stresses at the panel centers, the measured values were 1/2 and 1/4 of the calculated values for the 1/4" and 1/2" panels respectively. This indicates that the response stresses are more sensitive to changes in core depth than indicated by Miles' equation. This comparison was made using the measured frequencies in Miles' equation.

The direct relationship between overall stress and the acoustic spectrum level at the maximum response frequency was held within 15% for most data points. Damping ratios were between 0.03 and 0.07, with an average value of 0.05. These are relatively high values for progressive wave tube tests, but are not untypical of full-scale measurements on aircraft structures. The effect of core density (and therefore core shear modulus) on the overall stresses was greater than expected.

The test data show that the fatigue characteristics improve with decreasing facing thickness. There are several possible explanations for this. LID joints have relatively small fillets resulting in a notch effect. This effect is offset slightly with thinner facings. Another factor may be the acicular (Widmanstätten) microstructure in the facings at the bond lines. This results in locally improved fracture toughness and fatigue characteristics. This effect penetrates a constant 0.005" and therefore has a greater effect on thinner facings. In order to plot the maximum stress in the panels against cycles to failure, stress distribution graphs (such as Figure 3), were used to relate measured stresses at the panel centers to maximum values at the edge doubler. These values were used in the dynamic stress nomograph (Figure 10). The fatigue data indicate that the LID titanium panels realize a comparable proportion of the base material fatigue properties as adhesive bonding does for aluminum.

Panel 5A had a 2" by 1" void at the center of one face. This doubled the local facing stress but did not result in a premature failure. Failure occurred at the edge of the panel, without any propagation of the void having occurred. Panel 9, which had a 5-inch-long edge void, delamination prematurely. Obviously, edge void criteria need to be more stringent than with center voids. The facing repair on Panel 3 had no detrimental effect on response or fatigue life. Panel 4B with the potted insert suffered skin delamination around the edge of the potting, but the failure was not premature. No deterioration of the potting compound was experienced.

The graphite-epoxy reinforcement gave encouraging results, particularly when both facings were treated. Panel 2A was originally tested with the graphite layers terminating just short of the edge doublers. This resulted in a negligible reduction in the response levels. The layers were then extended over the edge doublers to provide a load path into the panel fixturing. This resulted in the values shown in Table 3. The graphite added on Panel 2B was equivalent in weight to increasing the facing thickness of panel 2 from .008" to .016". The stress level at 165db was reduced from 9,600 lb/in^2 to 1,040 lb/in^2. Increasing the facing thickness from .008" (Panel 2) to .020" (Panel 5) reduced the stress to 1,100 lb/in^2. Thus, the graphite demonstrated a significant strength/weight improvement over 6Al-4V titanium alloy.

During the development of the LID process, several panels with marginal mechanical properties were sonic fatigue tested. The results showed that slight variations in mechanical properties result d in major sonic fatigue life differences. Failure times varied from 35 seconds to 12 hours at similar response levels. These early tests helped to establish the necessary quality control and bonding process parameters in order to ensure consistently good sonic fatigue performance.

4. REGRESSION ANALYSIS

4.1 INTRODUCTION

It is rare that sonic fatigue test data fall neatly into the simplified equations used in most practical design work. Different structural concepts and their respective applications often show sufficiently unique characteristics to make an individual regression analysis of test data a preferable basis for a design method than a generalized theory. Reference 7 provides such a theory for aluminum skin-stringer and s. wich structures. The regression analyses in this section form the basis of a sonic fatigue design technique for titanium sandwich structures (outlined in Section 5).

Multiple regression analysis techniques have become very easy to use with the availability of "canned" digital computer programs. However, unless the underlying statistical nature of these techniques and their limitations are well understood, erroneous conclusions can easily be reached. The first dynamic stress regression in this program used the acoustic load as an independent variable, along with the relevant structural parameters. A statistically significant and accurate equation was obtained. However, the load had an inverse relationship with the stress. Upon reflection, it was realized that this was because the stiffer test panels were subjected to higher loads to produce significant stress levels. Consequently, the regression analysis associated high sound levels with low stresses. In such an obvious case, the error is easily detected, but a not so obvious case may easily go unnoticed. Any relati n between the dependent and an independent variable should be examined to determine if it is basically al and whether it stems from a meaningful relationship in the data, or from a peculiar characteristic of the test program. In the example cited, the problem was overcome by dividing the acoustic load into the dependent variable.

Another problem in regression analysis is the elimination of "outliers." The overall accuracy of an equation can often be improved by eliminating highly deviant data points. When this is done, however, the "T" and "F" values should be rechecked for significance (the smaller the sample size the greater the "T" and "F" values needed for a given level of significance.

A standard IBM "Stepwise Multiple Regression" program capable of handling curvilinear and second-degree polynomial functions was used in these analyses. The following statistical parameters are quoted for each regression:

> Multiple Correlation Coefficient — Indicates degree of correlation between dependent and independent variables.

> "F" Value — Indicates the reliability of the regression equation (analysis of variance).

> "T" Value — Indicates the reliability of the relationship between the particular independent variable and the dependent variable.

> Standard Error — Is the standard deviation of the residual (errors).

> Durbin-Watson Statistic — Indicates degree of autocorrelation in error terms. A good statistic implies a high confidence level for "F" and "T" tests.

4.2 NATURAL FREQUENCIES

The frequencies calculated using Reference 2 (Table 1) were regressed against the core depth (h) and the facing thickness (t). Typical variations in core properties have negligible effect on frequencies. The following relationship gave the best results:

$$f = 2,239 \, h^{0.913} \, t^{0.194} \tag{2}$$

The following statistical data apply to this equation:

Multiple Correlation Coefficient	0.990
"F" Value for Analysis of Variance	221.588
Standard Error of Estimate	23.800

Variable	Regression Coefficient	Std. Error of Reg. Coeff.	Computed "T" Value
h	0.91266	0.04414	20.675
t	0.19404	0.04891	3.967

Average % Deviation	6%
Durbin-Watson Statistic	2.0

Combining this equation, which is for a fixed-panel size of 18.5" by 22.25", with the frequency equation in Reference 4, the following equation is obtained:

$$f = 2.88Kn \, \frac{h^{0.913} \, t^{0.194}}{b^2} \tag{3}$$

Where b is the length of the smallest side. Figure 7 (from Reference 4) gives values of Kn for various aspects ratios.

Equation (3) forms the basis of the frequency design nomograph given in Section 5 (Figure 8).
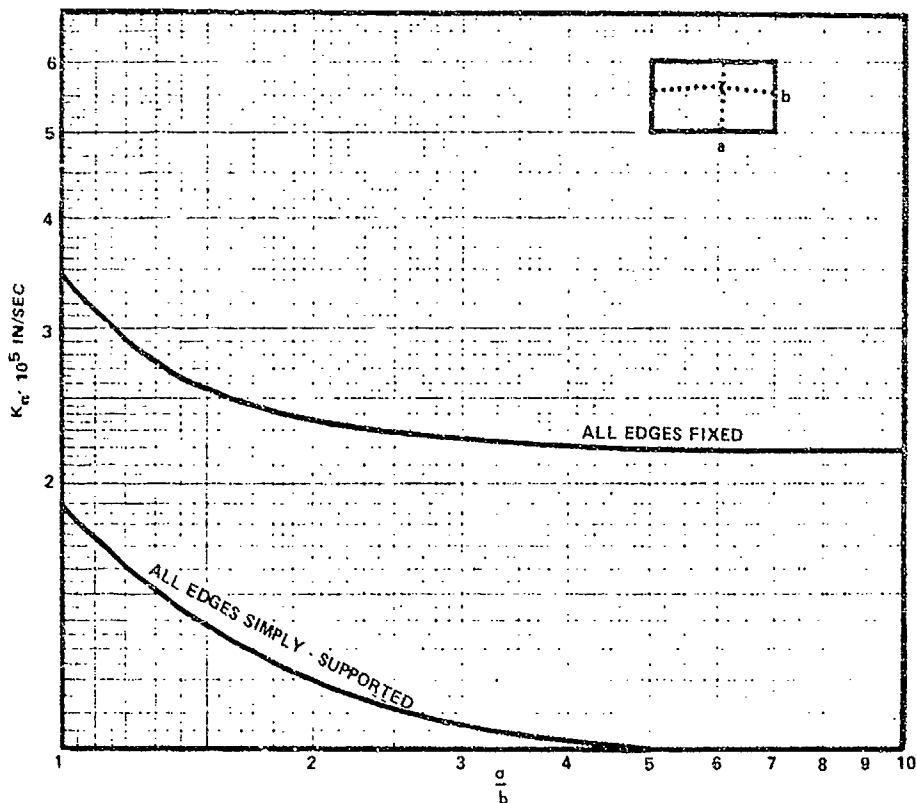
Figure 7.

4.3 STATIC STRESSES

The maximum edge stresses in a clamped panel with no edge doubler were calculated using NASTRAN and regressed against core depth (h) and facing thickness (t). Additional computations were performed for various overall panel sizes to permit the panel width (b) and the aspect ratio (a/b) to be included. The following relationship was obtained:

$$\sigma_o = 3.96 \times 10^{-4} \frac{b^2 \, (a/b)^{0.792}}{ht} \qquad (4)$$

Where σ_o is the stress at the center of, and normal to, the longest side due to a uniform pressure load of 1 lb/ft^2.

The following statistical data apply to this equation:

Multiple Correlation Coefficient. 0.998

"F" Value for Analysis of Variance. 1168.932

Standard Error of Estimate. 414.245

Variable	Regression Coefficient	Std. Error of Reg. Coeff.	Computed "T" Value
b	2.00617	0.04242	47.288
a	0.79272	0.07862	10.083
h	-0.97856	0.00581	-168.407
t	-0.97532	0.00644	-151.481

Average % Deviation 6%

Durbin-Watson Statistic 1.1

Equation (4) forms the basis of the static stress nomograph given in Section 5 (Figure 9).

4.4 DYNAMIC STRESSES

The measured overall rms stresses given in Table 3 were regressed against various panel parameters in the following form:

$$\frac{\sigma_{rms}}{\sigma_o L} = fn \, (f, \, h, \, t, \, \zeta, \, \rho_c) \qquad (5)$$

Where L is the acoustic spectrum level in (lb/ft^2)/Hz

Although a good curve fit was obtained (7% average deviation), low T statistic values were obtained for t and ζ indicating a lack of significance. They were subsequently dropped from the analysis. Because of the high interdependence between frequency (f) and core depth (h), "Multicollinearity" problems were encountered during regression indicating that only one of these two variables was required. Thus, final regression was made against frequency and core density only. (Core density and core shear modulus values are readily interchangeable from Figures 1 and 2.) The elimination of core depth (h) and facing thickness (t) from the dynamic stress regression did not exclude their effects, but simply limited them to their contribution via static stress values (σ_o) and frequencies (f). The following relationship was obtained:

$$\text{Log}_{10} \frac{\sigma_{rms}}{\sigma_o} = 2.47 - 0.00147f - 0.0395 \rho_c$$

The following statistical data apply to this equation:

Multiple Correlation Coefficient. 0.991

"F" Value for Analysis of Variance. 303.822

Standard Error of Estimate. 3.781

Variable	Regression Coefficient	Std. Error of Reg. Coeff.	Computed "T" Value
f	-0.00147	0.00007	-22.616
ρ_c	-0.03953	0.00839	- 4.710

Intercept   2.47208

Average % Deviation 4.5%

Durbin-Watson Statistic 1.14

The above equation simplified to the form:

$$\sigma_{rms} = \frac{296.5\sigma_o L}{(1.0034^f)(1.095^{\rho_c})} \tag{6}$$

Where L is in lb/ft^2 and σ_o is the stress due to a static uniform pressure of 1 lb/ft^2. The value of σ_{rms} corresponds to the location of σ_o. Usually, maximum values are used, which for a flat rectangular panel occur at the center of and normal to the longest side. Equation (6) forms the basis of the dynamic stress design nomograph in Section 5 (Figure 10).

5. DESIGN NOMOGRAPHS

Three design nomographs are presented in this section, based on Equations (3, 4 and 6) developed in Section 4. The frequency and static stress nomographs are for flat clamped panels only. The dynamic stress nomograph, although developed from flat panel data, may be applied to curved panels, cylinders and for various edge conditions. However, in such cases it should be used with caution since there is no empirical supporting data.

The basic estimating procedure for flat plates is to use Figures 8 and 9 to estimate the frequency (f) and static stress value (σ_o) and then to input those values into Figure 10 to obtain the overall rms stress (σ_{rms}) and fatigue life. The static stress nomograph is for the maximum edge stress with no doubler. In practical designs, edge doublers are invariably used and the thickness and width of these doublers affect the maximum edge stresses. Consequently, a general design method should make an allowance for these effects. Typically, edge doublers range from 1" to 2" in width, having a thickness equal to, or one gauge higher than, the facing thickness. When such doublers are used, multiply the stress obtained from Figure 9 by 0.7.

The majority of aerospace structures do not consist simply of flat rectangular panels. They are often curved or have cutouts and fittings, etc. The recommended design procedure in these cases is to bypass the frequency and static stress nomographs and use a general-purpose structural analysis computer program (such as NASTRAN) to determine frequencies and maximum static stress values. Input these values directly into Figure 10 to obtain the maximum overall rms stress and corresponding fatigue life.

The design nomographs can be applied to titanium sandwich structures utilizing core-to-facing joining systems other than LID. However, the fatigue curve portion of the dynamic stress nomograph may not be applicable.
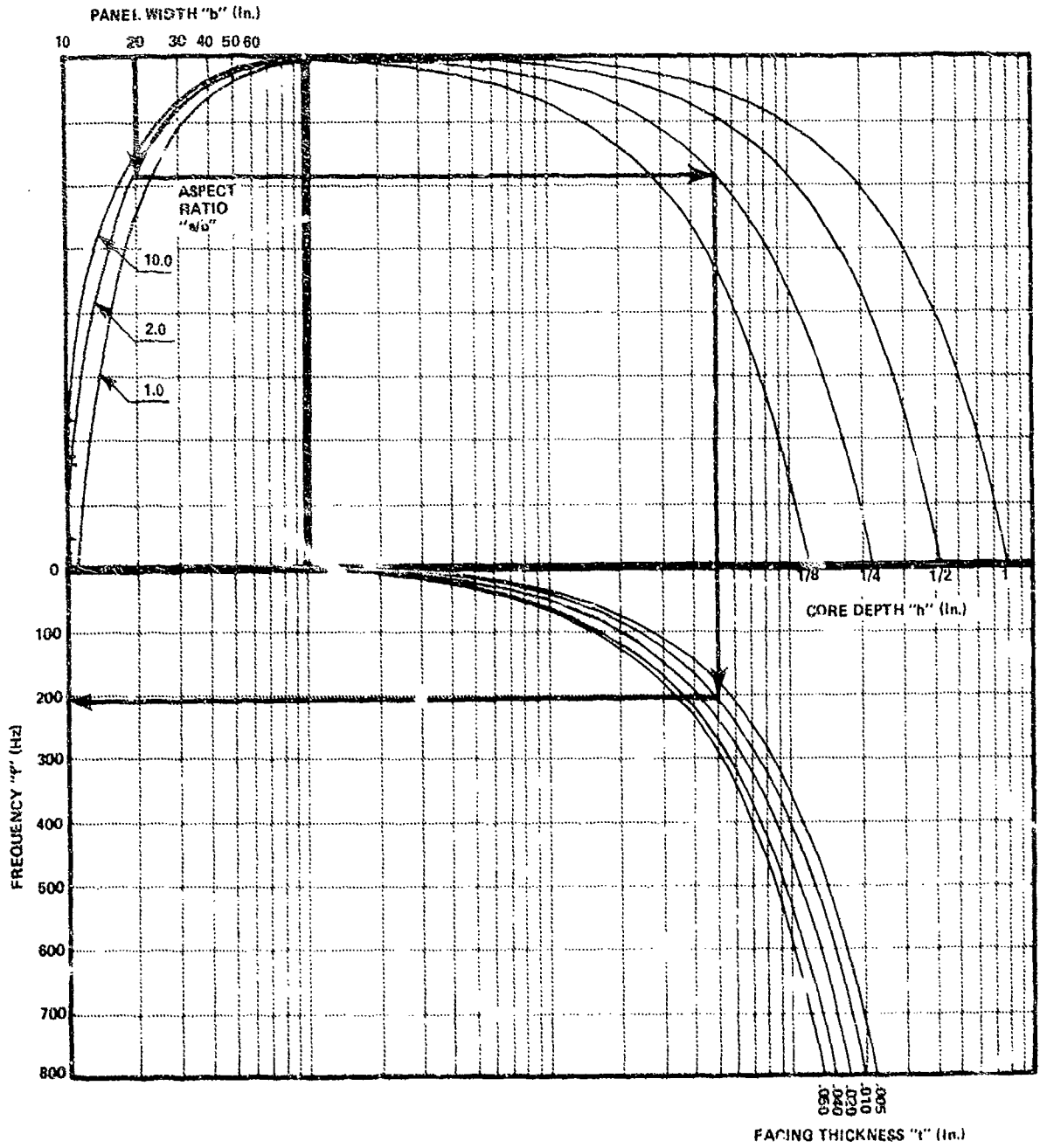
Figure 8. Frequency Nomograph.
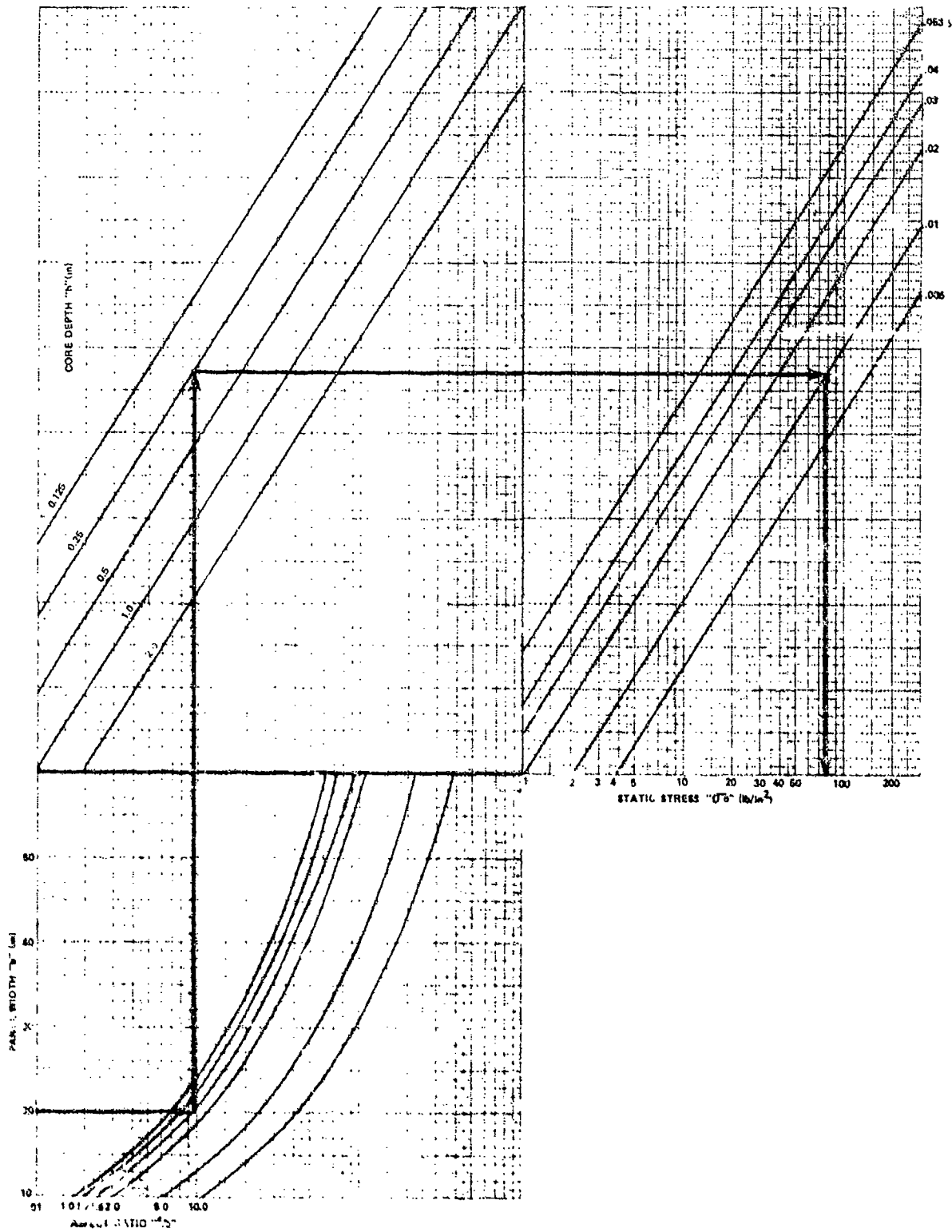
Figure 9: Static Stress Nomograph.
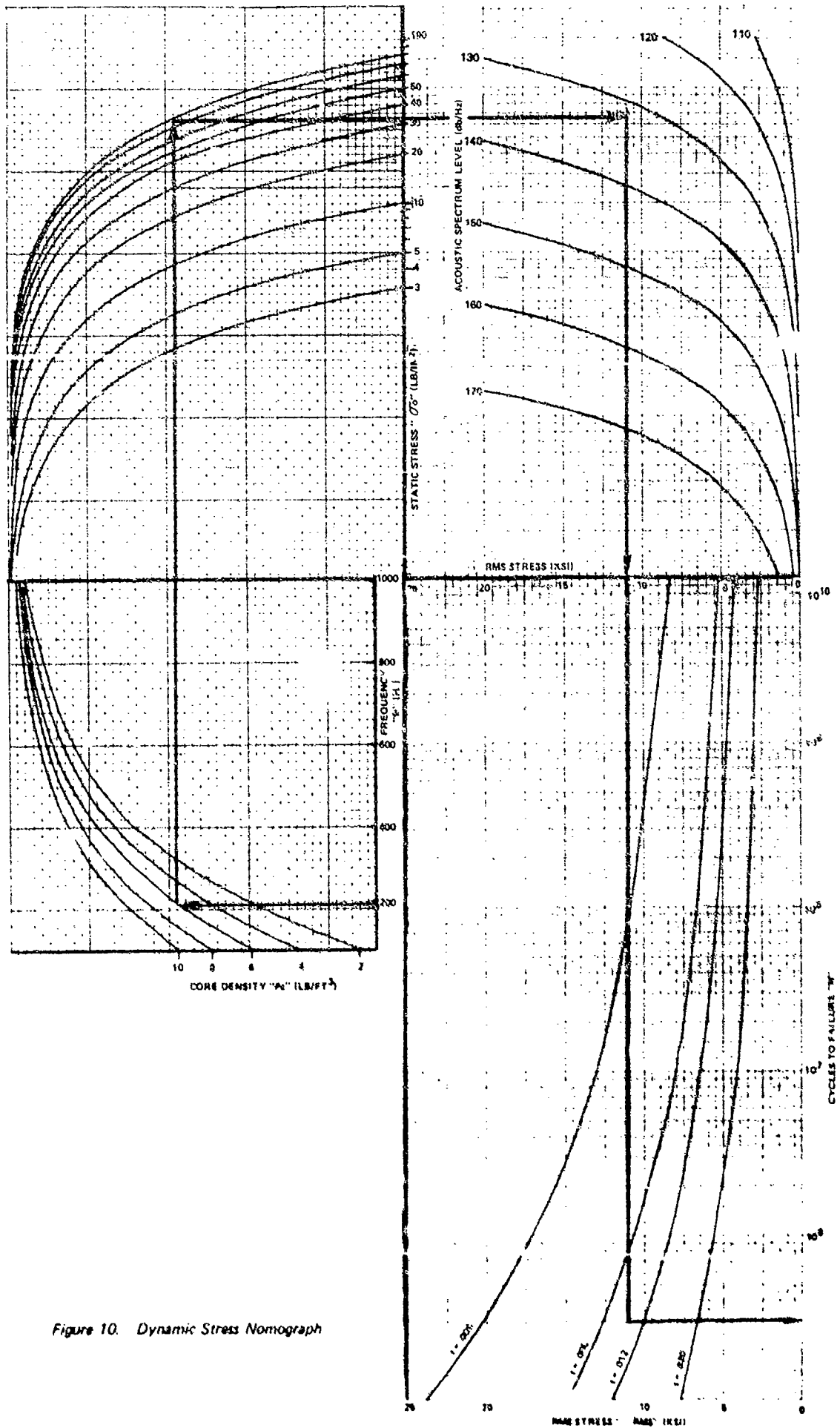
Figure 10. *Dynamic Stress Nomograph*

REFERENCES

1. Miles, J. W. -- "On Structural Fatigue Under Random Loading," Journal of Aeronautical Sciences, Volume 21, November 1954.

2. Abel, J. F. -- "Static and Dynamic Analysis of Sandwich Shells With Viscoelastic Damping," University of California at Berkeley, Report N58-34285, August 1968.

3. Ahmed, K. M. -- Ph.D. Thesis, Institute of Sound and Vibration Research, University of Southampton, England 1971.

4. Royal Aeronautical Society -- "Data Sheets on Acoustic Fatigue," No. 66019, 1966.

5. Hallam, R. -- "Analysis of Advanced Honeycomb Cores--Theoretical Core Properties," Rohr Industries, Inc., Chula Vista, California, Report No. 831-047, May 1971.

6. Macneal, R. H. -- "The NASTRAN Theoretical Manual," NASA Report No. SP-221, September 1970.

7. Ballentine, J. R. -- et al "Refinement of Sonic Fatigue Structural Design Criteria," Air Force Report AFFDL-TR-67-156, January 1968.

"ACOUSTIC FATIGUE TEST ON THE VFW-FOKKER
VAK 191 B STRUCTURAL COMPONENTS"

Pietro SELVAGGI
Chief Engineer, Technical Staff – Structures
AERITALIA – Uffici di Torino-C.so Marche, 41
10146 TORINO – ITALY

Angelo LOREA

Research Engineer
FIAT – Laboratori Gasdinamica – Strada del Drosso 145
10100 TORINO – ITALY

SUMMARY

Near field noise and temperature measurements on 1/4 scale model of the VFW-FOKKER VAK 191 B aircraft indicated that critical environments will be induced on aircraft structural components during the VTO and STO configurations.
This paper reports the results of the structural response and endurance test performed at FIAT on a fuselage skin panel and on a wing trailing edge flap.
The noise and temperature simulation procedure and the experimental facilities arranged for testing purpose are also briefly described.

1. INTRODUCTION

The design of acoustic fatigue resistant structures frequently results from static loads considerations and the acoustic fatigue problem is taken into account by best available design criteria and design practices.
Subsequently, during the development phase of the aircraft, tests are conducted in order to verify the capability of structural components to withstand acoustically induced loads without cracking and, if necessary, to improve the basic design.
Sometime, the problem can get more complicated if other environments, such as high temperatures, act on the structure in combination with the acoustic excitation.
In these cases endurance tests with temperature and noise simulation will lead to suggestion for design changes.
During the development of the V/STOL VAK 191 B aircraft, a joint project between the two Companies VFW and FIAT, it was anticipated that critical thermal and acoustic environments would be induced on certain local structural areas during the VTO and STO configurations.
Near field noise and temperature measurements on a quarter-scale aircraft model indicated that the lower front fuselage panels and the wing trailing edge flaps would be exposed simultaneously to high temperatures and high sound pressure levels (reference 1).
For the lower fuselage panels however, the thermal environments were considered not so significant as for the wing trailing edge flaps and were not simulated in the acoustic tests.
The test time, defined on the basis of the required safe life flying hours of the prototype aircraft, was 30 hours.
This time, covering 360 VTOL and 540 STOL flights, was determined assuming a total time of 6 hours spent in the take-off and landing configurations, and a scatter factor of 5.

2. TEST SPECIMENS ARRANGEMENT AND ACOUSTIC TEST FACILITY.

The test specimen were represented by the actual aircraft structural components.
The fuselage panel, including radar antenna, consisted of a rectangular 700 x 680 mm curved plate with stringers and frame sections and was installed, as shown in Fig. 1, in the acoustic test section in such a way that the convex side was excited by the grazing incidence sound.
A special mounting frame was not required, as the panel surface area was selected sufficient to simulate the adjacent structure flexibility.
For the trailing edge flap, which consisted of a sandwich honeycomb structure, the installation was complicated by the necessity to reproduce the thermal effects.
A quartz lamp radiative heater was manufactured for this purpose, and it was placed inside the progression wave chamber as shown in Fig. 2.
The flap was fastened to the side of the test section in such a manner that it was allowed to expand under the thermal load without restriction.
The Acoustic Fatigue Facility of FIAT – Gasdynamic Laboratories was selected for these tests since it permitted the required noise levels to be generated.
In this Test Facility, whose general arrangement is illustrated in Fig. 3, the sound was generated by two different units:
- a system of six loud speakers for the preliminary experiments (structural response analysis), as comparatively low sound intensity, wide range of frequencies and considerable tone pureness were required.

- A system of six electropneumatic transducers (Pye-Ling) fed with compressed air for the endurance tests.

A typical example of sound field spectral analysis for transducers operating both sinusoidally and as wide band random noise generators is given in Fig. 4.

Further information about this facility is given in Reference 2.

3. PRELIMINARY EXPERIMENTS

As a starting point it was necessary to determine the natural frequencies of the structural components such that the excitation bandwidth could be placed over the range of these frequencies.

By means of electrical strain gages, located as shown in Figs. 5 and 6, the predominant resonant frequencies and the associated mode shapes could be found.

In order not to impair the fatigue life of the test specimens the response tests were performed at room temperature with low sound pressure levels.

To achieve more available structural response data, sinusoidal excitation at 125 dB OASPL and random excitation at 129 dB OASPL were adopted.

Under sinusoidal excitation, as presented in Figs. 7 and 8, the structural components revealed several natural frequencies distributed in the octave bands centered at 125, 250, 500 Hz.

This distribution was also confirmed by the structural response results obtained under random excitation and it suggested to perform the subsequent endurance tests with wide band random noise spectrum.

4. ACOUSTIC FATIGUE TESTS

Acoustic fatigue tests represented the concluding phase of the acoustic prevention programme for the VAK 191 B Aircraft.

The test conditions could be defined on the basis of the results of noise and temperature measurements performed on the aircraft model and of the preliminary experiments.

For simplicity purpose, it was decided to simulate only the most damaging fatigue environments which occurred during the take off and landing flight segments.

Thus the lower fuselage panel was tested under the noise spectrum of the VTOL configuration (Reference 3) as in this configuration the aircraft jets hit the ground normally and the sound intensity was found to be the maximum (151 dB OASPL). The test spectrum was well placed in the range of the predominant vibration modes of the panel and presented slight variations from the measured spectrum, as shown in Fig. 9.

Thermal loads were not simulated since it was predicted that they would have not affected the fatigue resistance of the panel.

During the test the strains on different significant points of the panel skin and stiffeners were recorded, and the strains spectral analysis (Figs. 10 and 11) indicated a maximum strain of 56 με RMS in the octave band centered at 500 Hz.

The panel was capable to withstand the test noise spectrum for the whole required time without appreciable fatigue damage, as it was demonstrated by visual inspections and by the continuous check of a natural frequency (361 Hz.) selected to detect any incipient failures.

For the trailing edge flap a more sophisticated test arrangement and procedures were required since the thermal loads could not be neglected.

In fact the measurements on the aircraft model (Reference 4) indicated that during the short take-off the lower flap surface, directly struck by the main jet exhaust, was subjected to a maximum heat flow of 340 Kw/m² combined with 158 dB OASPL.

During the vertical take-off, instead, the heating was found negligible and the sound intensity reached a maximum overall value of 150 dB.

Preliminary heating tests carried out on honeycomb sandwich panels, having structural characteristics similar to those of the flap, enabled to establish that, striking the panels with the STOL thermal flow, excessively high temperatures, which bonded honeycomb structure could not withstand, were reached in a very short time.

Thus, in order to clear the flap of the main jet exhaust, it was decided to recommend limitations on the flap and main jet deflections during the short take-off and to carry out the flap acoustic fatigue test under a constant temperature of 70 ÷ 75°C, this being the maximum allowed for the adhesive.

The wide band random noise spectra which were used in the tests (Figs. 12 and 13) and derived from the STOL and VTOL configurations, reproduced faithfully only the service sound pressures in the octave bands centered at 125 and 250 Hz., which covered the most important flap natural frequencies.

To obtain more realistic test conditions, the noise spectra were mixed according to the time spent in each take-off and landing configuration. During the test temperatures and strains of the flap surface were controlled by means of thermocouples and strain gages; the maximum strains measured were 68 με RMS (STOL) and 40 με RMS (VTOL) in the octave band centered at 250 Hz (Figs. 13 and 14).

Inspections performed both visually and with appropriate instruments (Bond-Tester, Eddy Sonic Resonator) demonstrated the capability of the flap to withstand the combined thermal and acoustic environment without fatigue damages or decay of the adhesive properties.

5. CONCLUDING REMARKS

In this paper the results of the acoustic fatigue tests performed on VFW –FOKKER VAK 191 B structural components have been briefly presented.

Some short remarks have also been made with regard to preliminary measurements and experiments carried out in order to investigate the most critical thermal – acoustic environments and define appropriate experimental procedures.

In particular it should be noted that many testing difficulties were encountered in the simulation of the combined environments and the arrangement of the test section.

However the results obtained, were satisfactory because not only did they complete an investigation on structural elements, but they also allowed the acquisition of useful data on the fatigue behaviour on honeycomb sandwich panels under thermal acoustic excitation.

6. REFERENCES

1. FIAT - Divisione Aviazione. Report N° 0021: Prove acustiche su un modello in scala 1/4 del VAK 191 B.

2. FIAT - Laboratori Gasdinamica."Acoustic fatigue test facility".

3. FIAT - Divisione Aviazione. Report N° C074: VAK 191 B. Prove di fatica acustica del pannello di fusoliera anteriore.

4. FIAT - Divisione Aviazione. Report N° 0079: VA   B. Prove di fatica acustico - termica del flap.

ACKNOWLEDGEMENTS
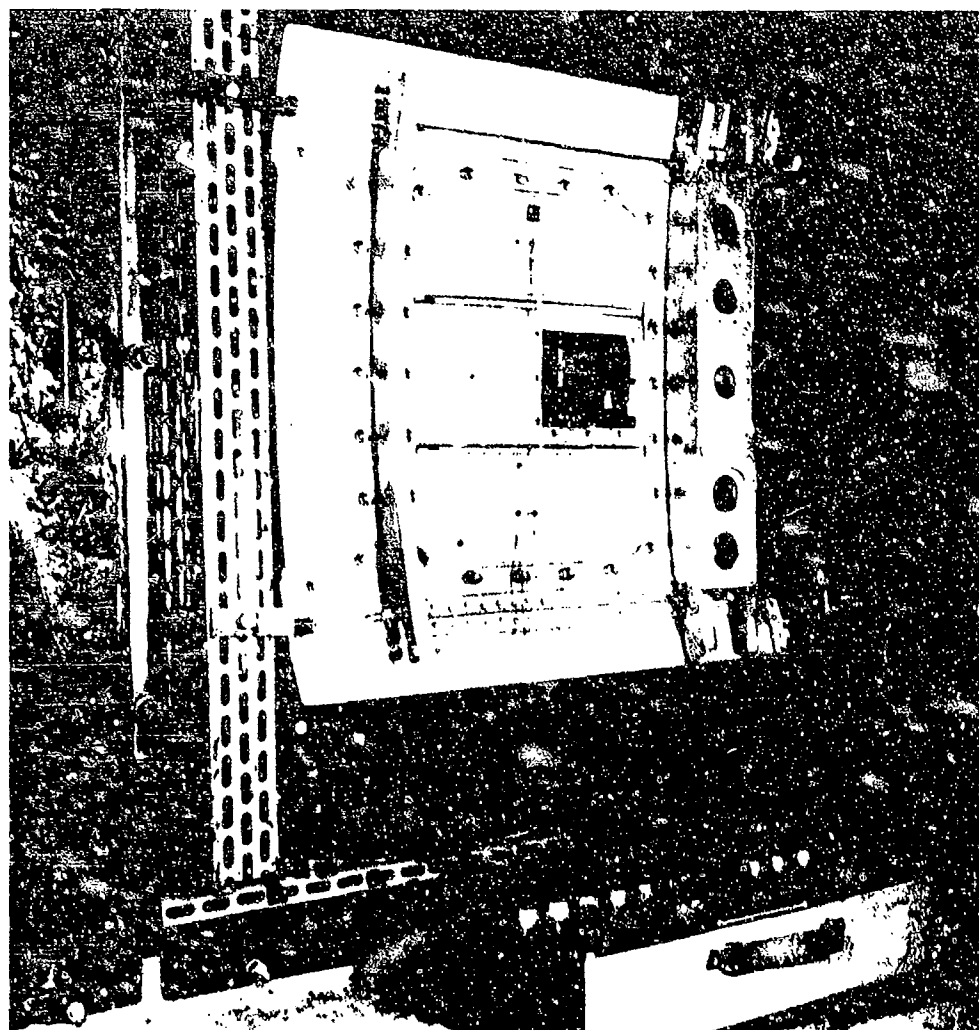
Fig 1 VAK 191 B FUSELAGE LOWER PANEL. Test installation
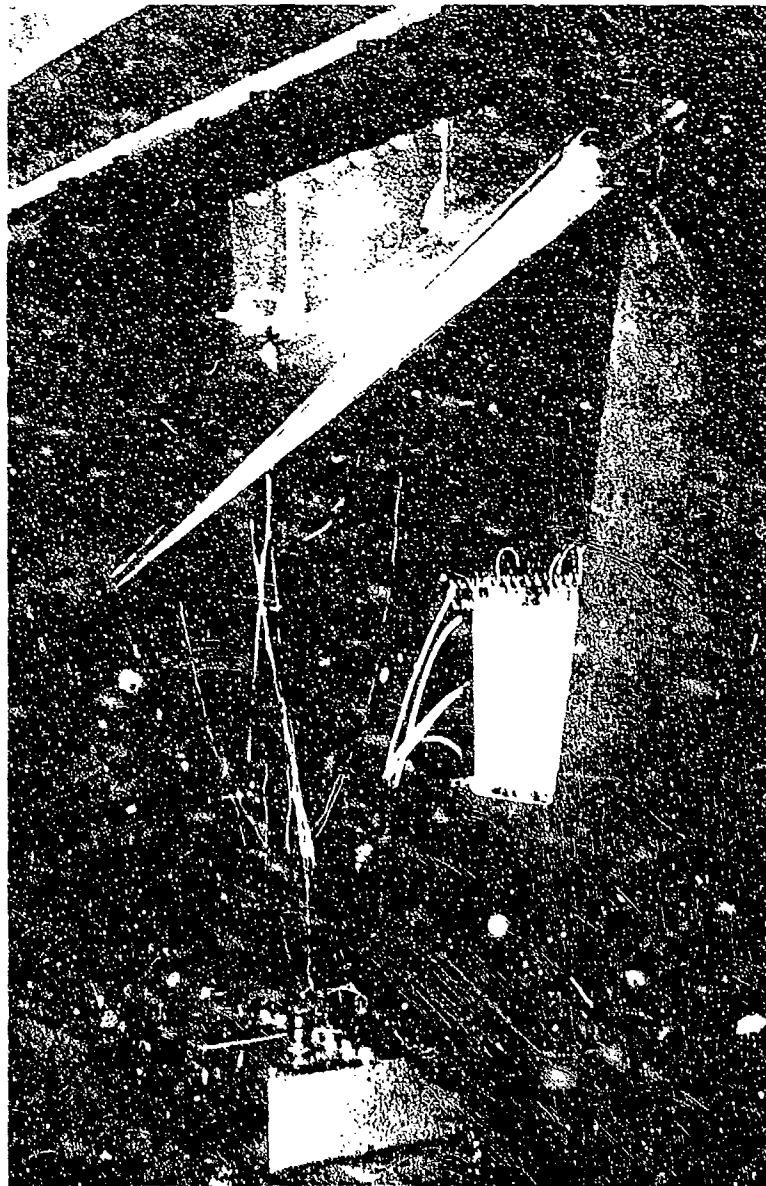
Fig 2 - JAK 39IB TRAILING EDGE FLAP Test Installation
   A TE rod Five heater

Scale

0   1   2   3   4 m.
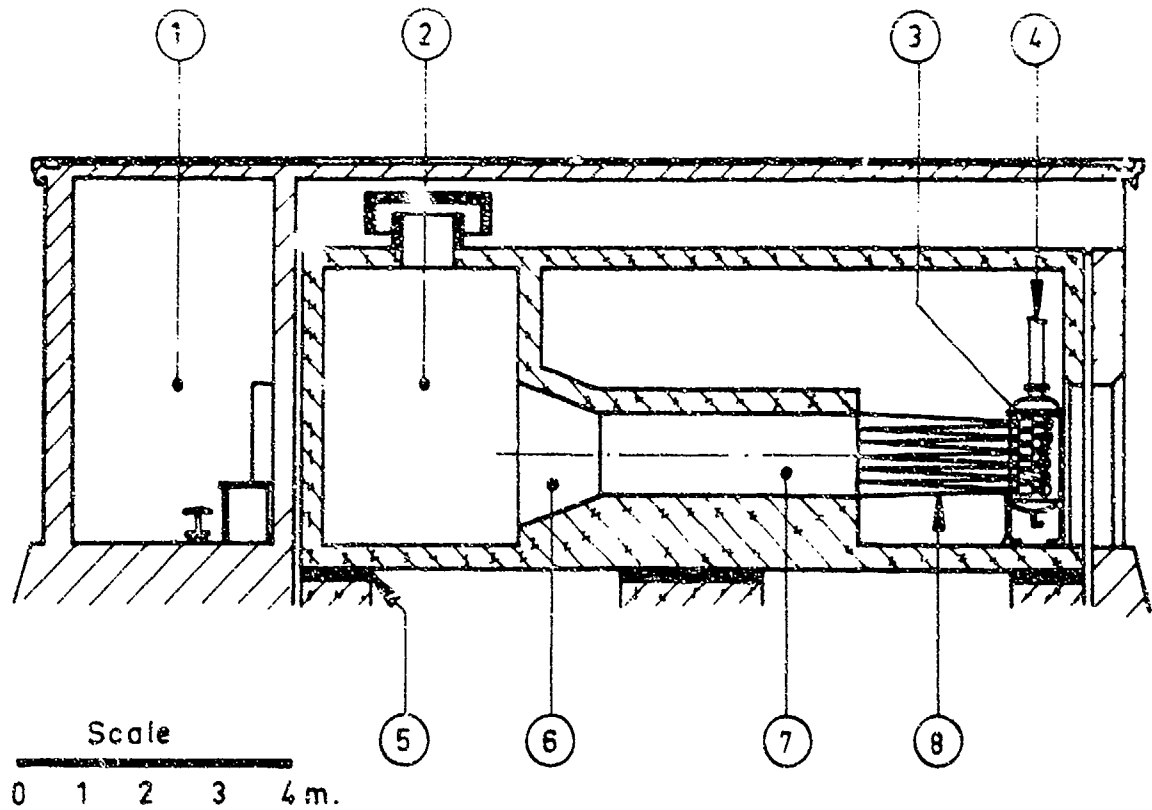
(1) Control room

(2) Reverberation room

(3) Electropneumatic transducers

(4) Air supply

(5) Resilient suspension

(6) Horn

(7) Progressive wave tube

(8) Horns

Fig. 3 - ACOUSTIC FATIGUE TEST FACILITY : General layout

A - SINUSOIDAL WAVEFORM

Sound pressure level [dB]
(ref. 0.0002 μ bar)

Frequency [Hz]

B- WIDE BAND RANDOM NOISE

1/3 Octave band sound pressure level [dB]
(ref. 0.0002 μ bar)

S.P.L. Overall = 168 dB

1/3 Octave band center frequency [Hz]
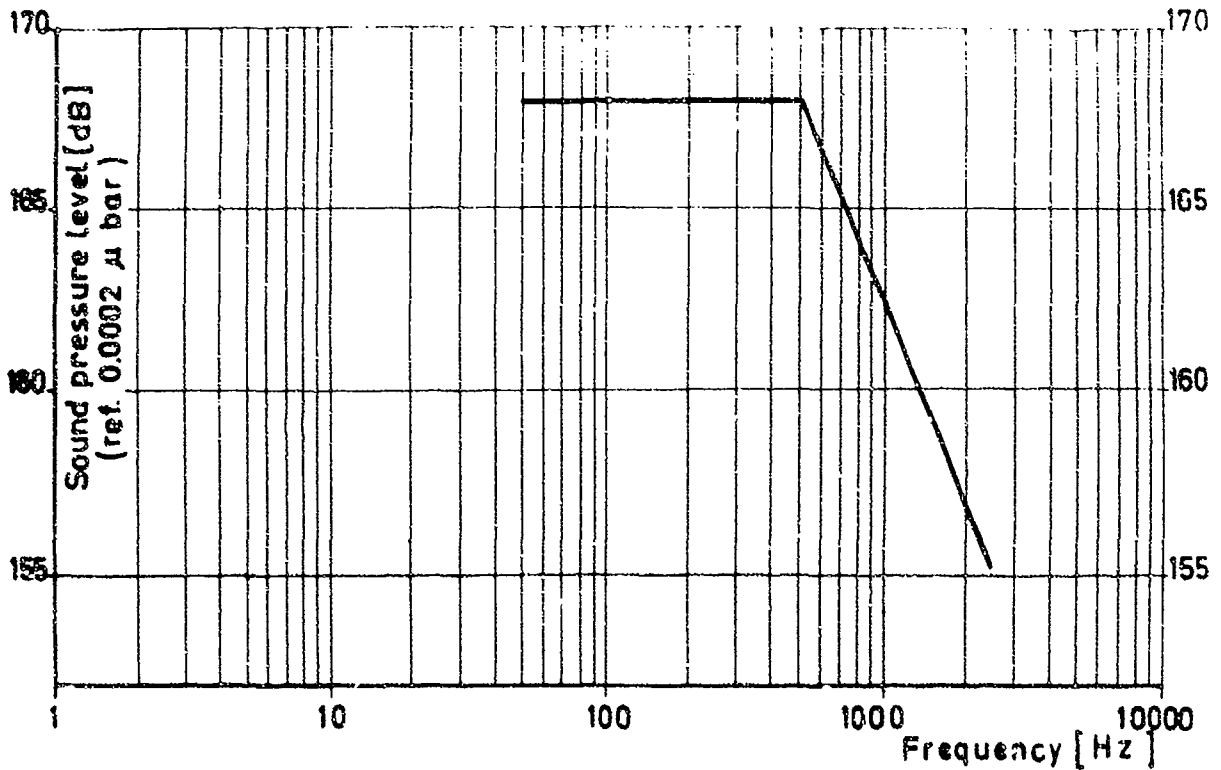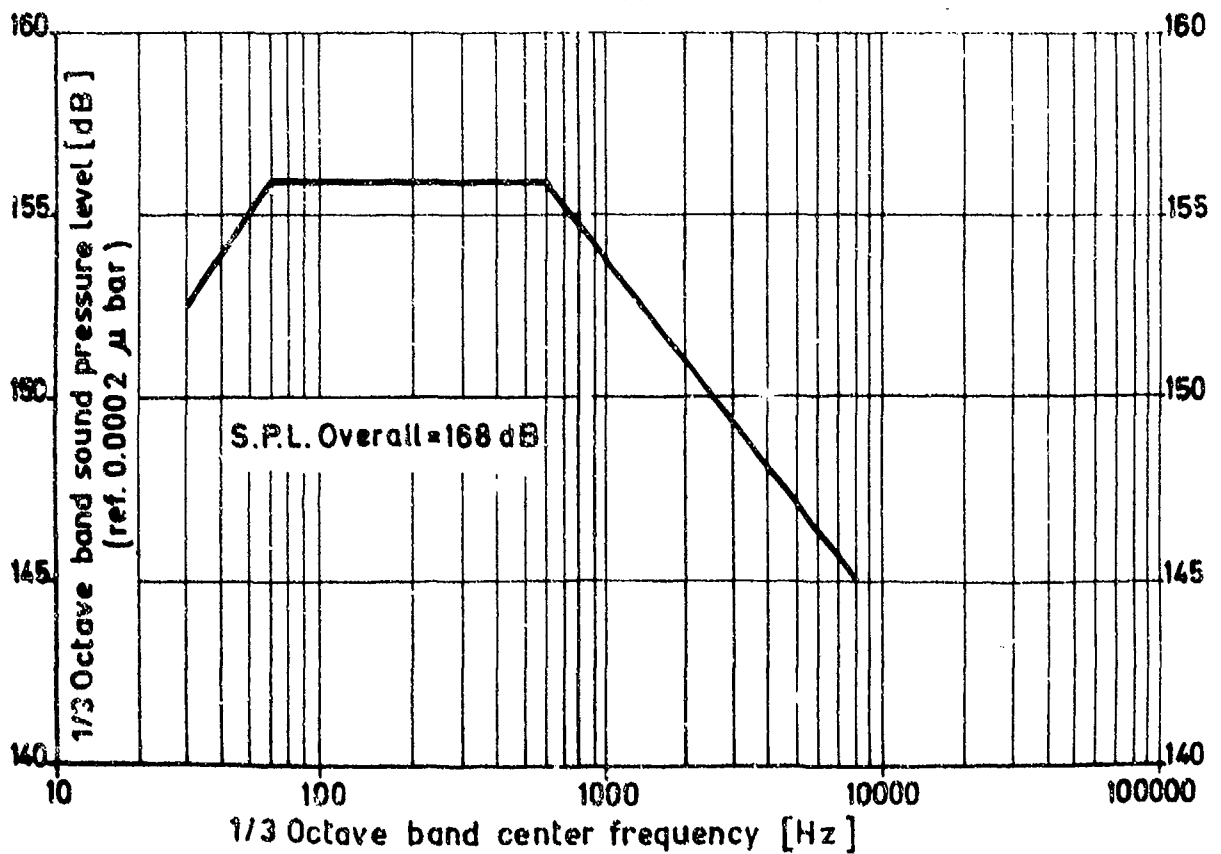
Fig. 4-VAK 191B-ACOUSTIC FATIGUE TEST FACILITY: Theoretical ratings in progressive wave tube
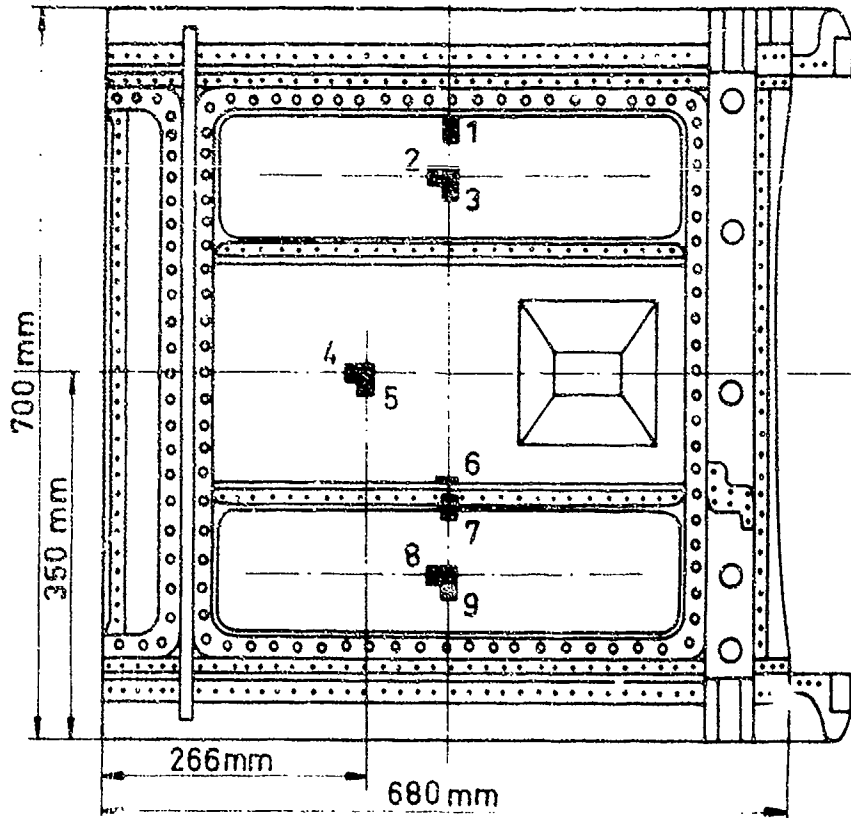
Fig. 5 - VAK 191 B : FUSELAGE LOWER PANEL : Strain gages positions
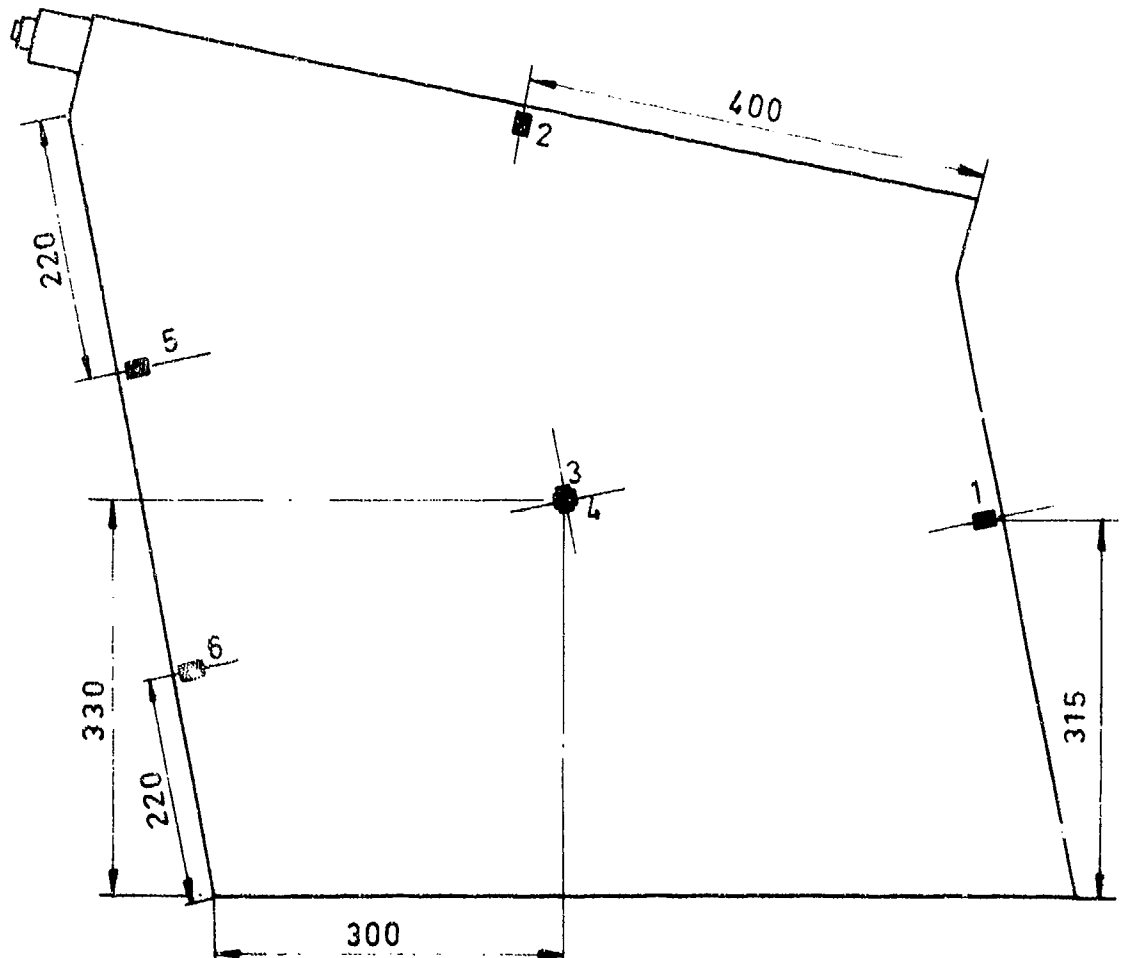
FIG.6 - VAK 191 B : TRAILING EDGE FLAP : Strain gages positions

Strain gage / Resonant Frequency[Hz]	1	2	3	4	5	6	7	8	9	Octave band [Hz]
184	10.70	2.00	3.02	1.00	1.00	6.30	3.23	1.00	3.04	125
324	1.00	1.00	6.62	1.00	3.66	10.60	1.00	1.00	3.96	250
334	4.25	2.04	5.20	1.00	2.60	10.00	2.82	1.00	7.25	
361	27.00	4.90	32.00	4.11	3.23	20.00	5.60	3.89	25.00	
392	12.60	5.12	16.00	1.50	1.00	4.73	5.35	3.26	14.00	
410	7.95	2.18	6.85	3.92	2.00	6.75	3.96	3.62	12.90	500
438	11.10	2.72	9.00	256	6.63	6.00	3.23	3.72	8.68	
480	4.55	1.50	8.85	4.45	6.62	5.12	4.60	4.66	15.80	
512	9.60	1.00	5.12	1.00	1.00	5.60	3.67	1.00	9.70	
520	12.60	1.00	8.15	1.00	1.00	4.45	2.90	1.00	7.53	
627	9.25	1.00	8.85	2.00	3.02	2.82	2.40	1.00	9.70	
685	9.80	1.00	8.20	6.62	2.00	1.00	1.00	1.00	3.15	
698	7.45	1.00	9.25	16.00	1.00	1.00	2.00	1.00	5.00	
729	14.50	9.00	7.95	10.00	4.26	2.82	7.10	3.37	10.22	
769	9.80	5.00	6.30	3.35	1.00	1.00	1.00	2.90	4.61	
1130	5.20	10.60	1.00	3.83	1.00	1.00	2.35	4.06	1.00	1000
1170	5.30	9.15	1.50	1.00	1.50	1.00	2.35	9.50	3.83	

Fig. 7 - VAK 191B : FUSELAGE LOWER PANEL : Strain response at the resonant frequencies

Strain gage / Resonant Frequency [Hz]	1	2	3	4	5	6	Octave band [Hz]
159	4.45	4.02	8.22	4.73	1.02	1.30	125
297	1.79	3.20	15.00	14.10	1.08	0.84	250
313	0.84	0.84	6.30	4.45	0.84	0.84	
482	1.42	0.84	0.94	0.84	0.84	0.84	500
520	1.06	0.84	0.84	1.06	0.84	1.44	
675	0.84	0.84	2.65	1.27	0.84	0.84	
777	0.84	0.84	0.84	1.27	0.84	0.84	

FIG. 8 - VAK 191 B: TRAILING EDGE FLAP: Strain response
at the resonant frequencies
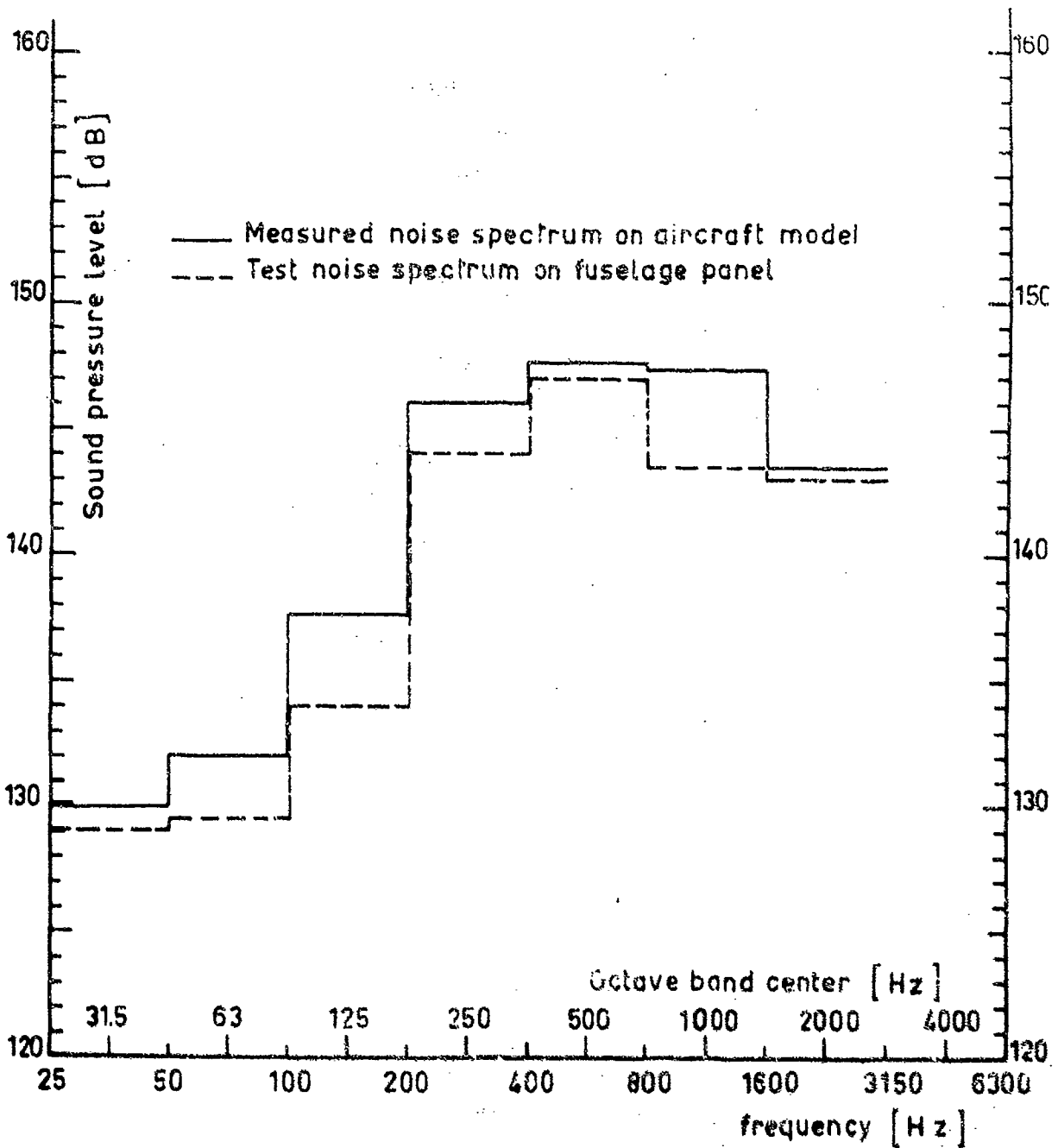
Fig.9 - VAK 191 B : FUSELAGE LOWER PANEL : Service noise spectrum and facility noise spectrum
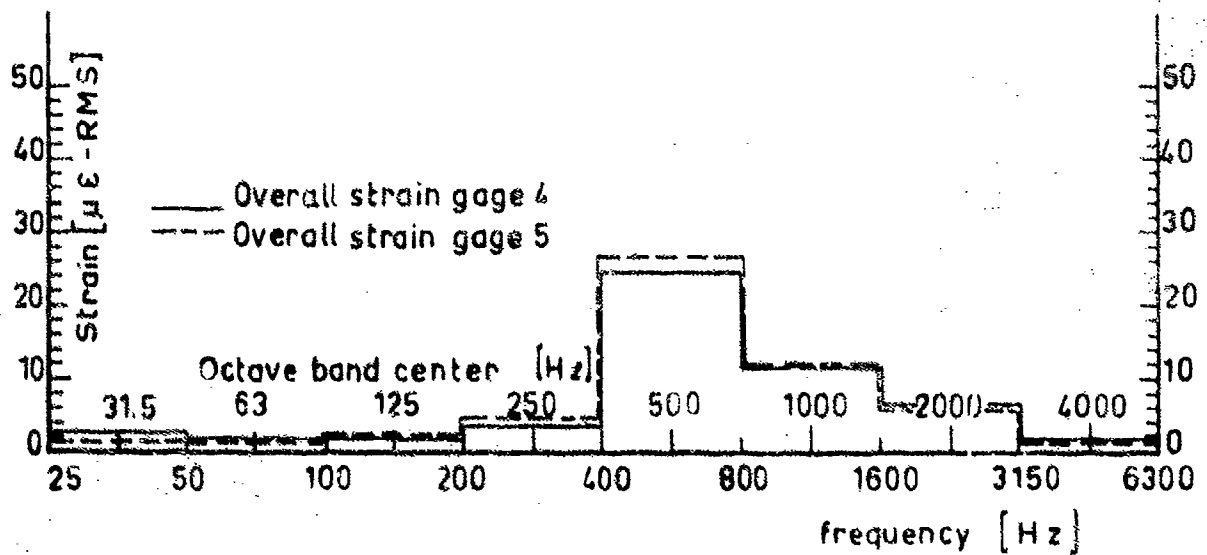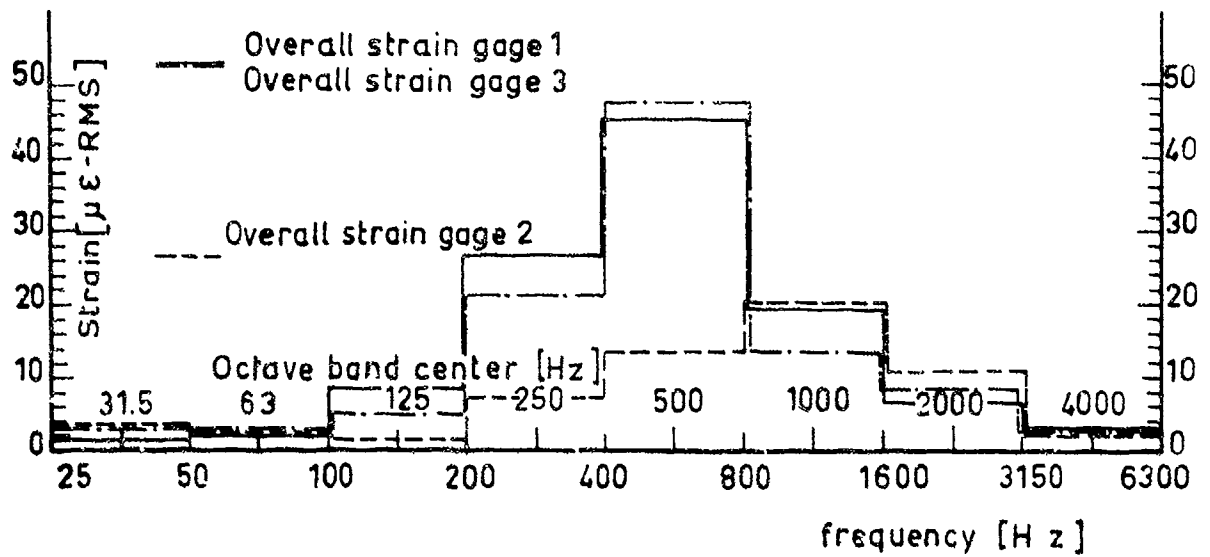
Fig.10 - VAK 191 B FUSELAGE LOWER PANEL ACOUSTIC FATIGUE TEST: Octave band strains analysis
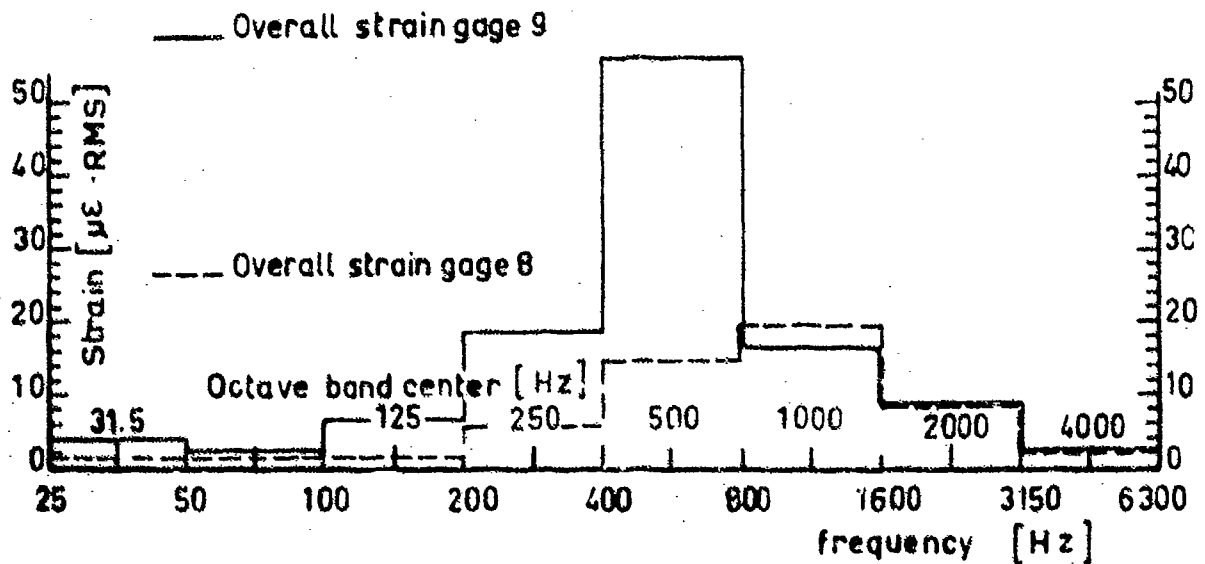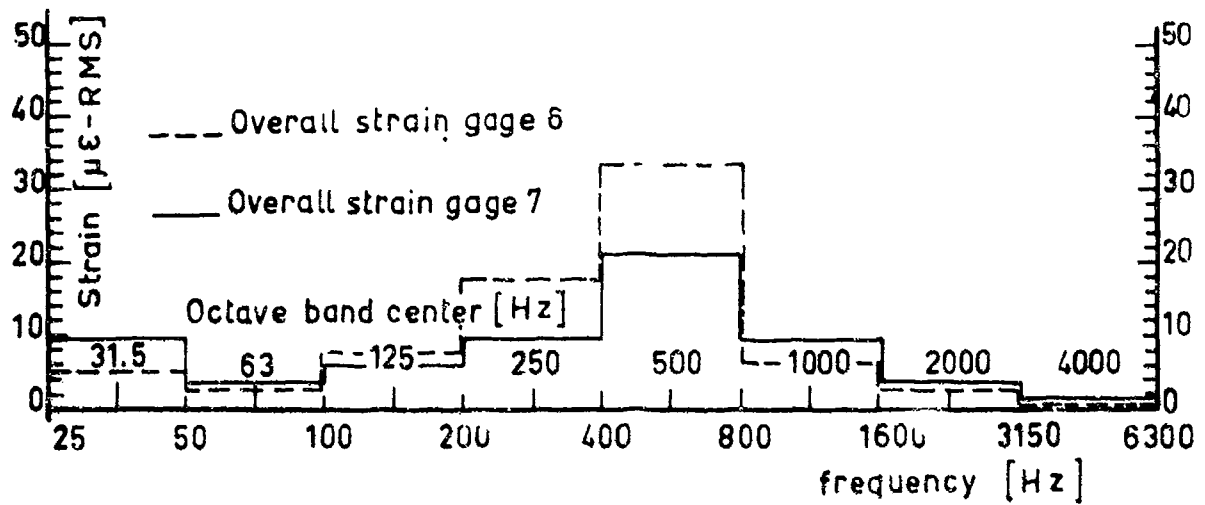
Fig. 11 - VAK 191 B FUSELAGE LOWER PANEL ACOUSTIC FATIGUE
TEST: Octave band strains analysis
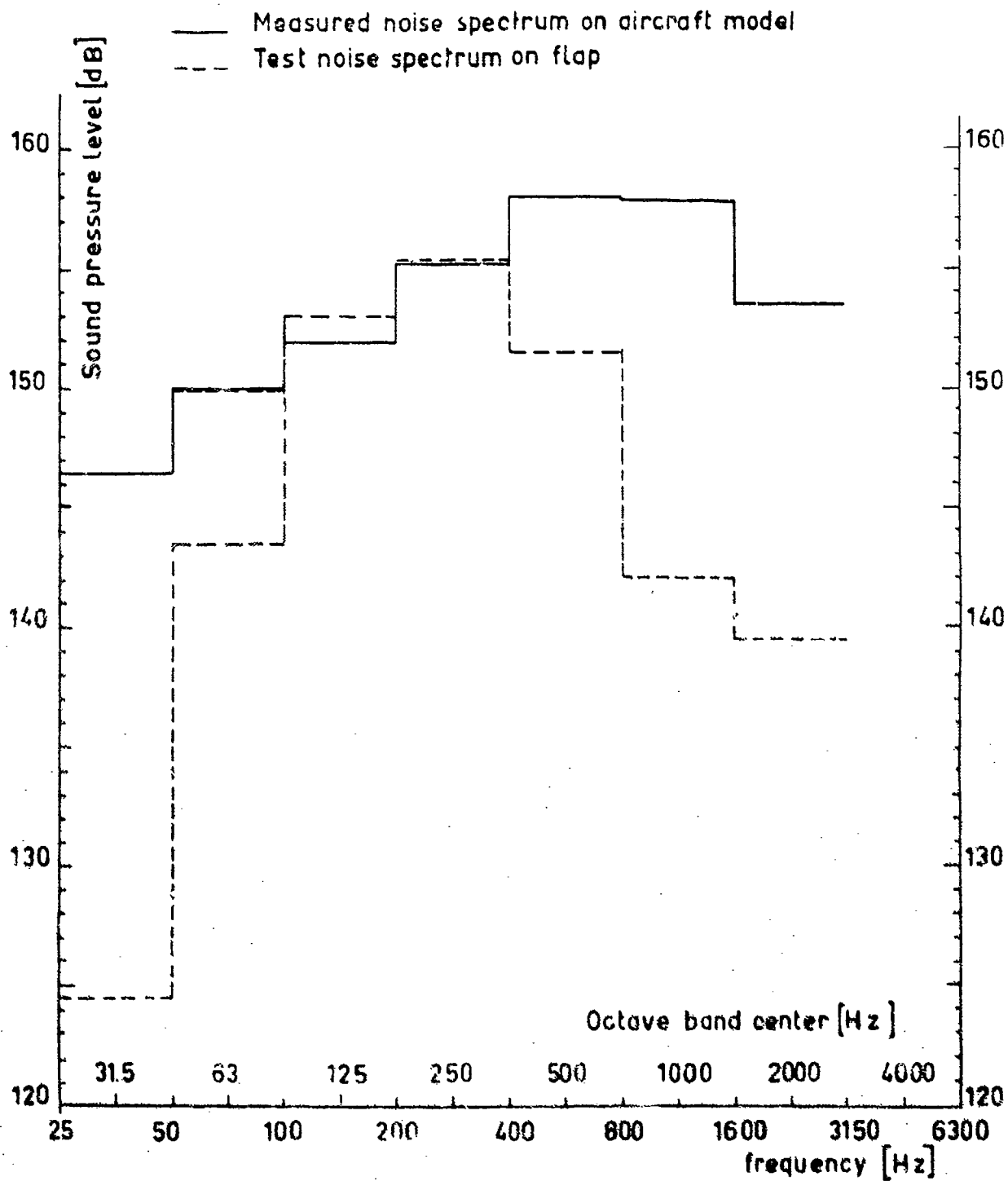
Fig. 12 - VAK 191B - TRAILING EDGE FLAP: Service noise spectrum and facility noise spectrum (STOL configuration)
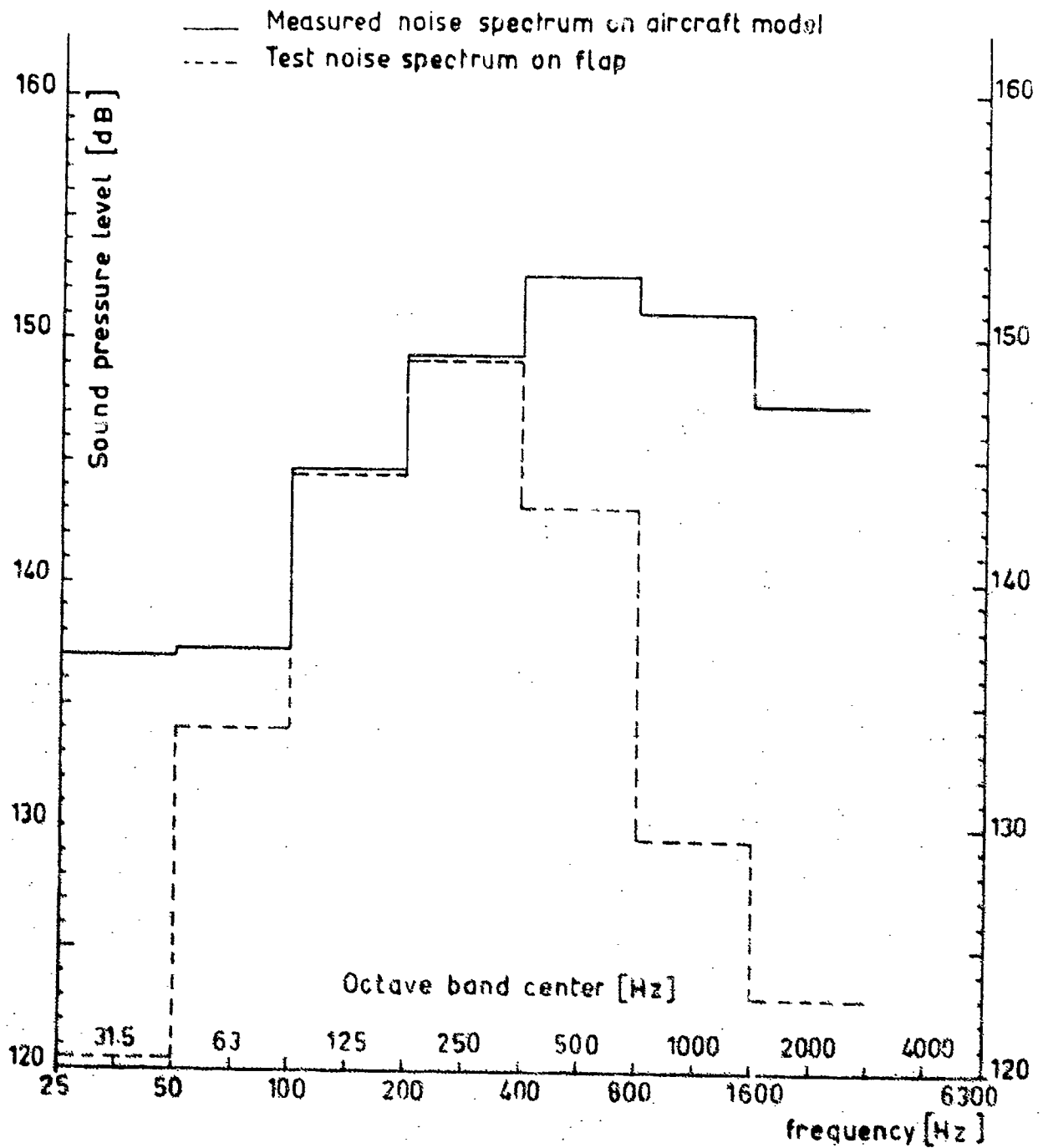
Fig.13- VAK 191 B —TRAILING EDGE FLAP: Service noise spectrum and facility noise spectrum (VTOL configuration)
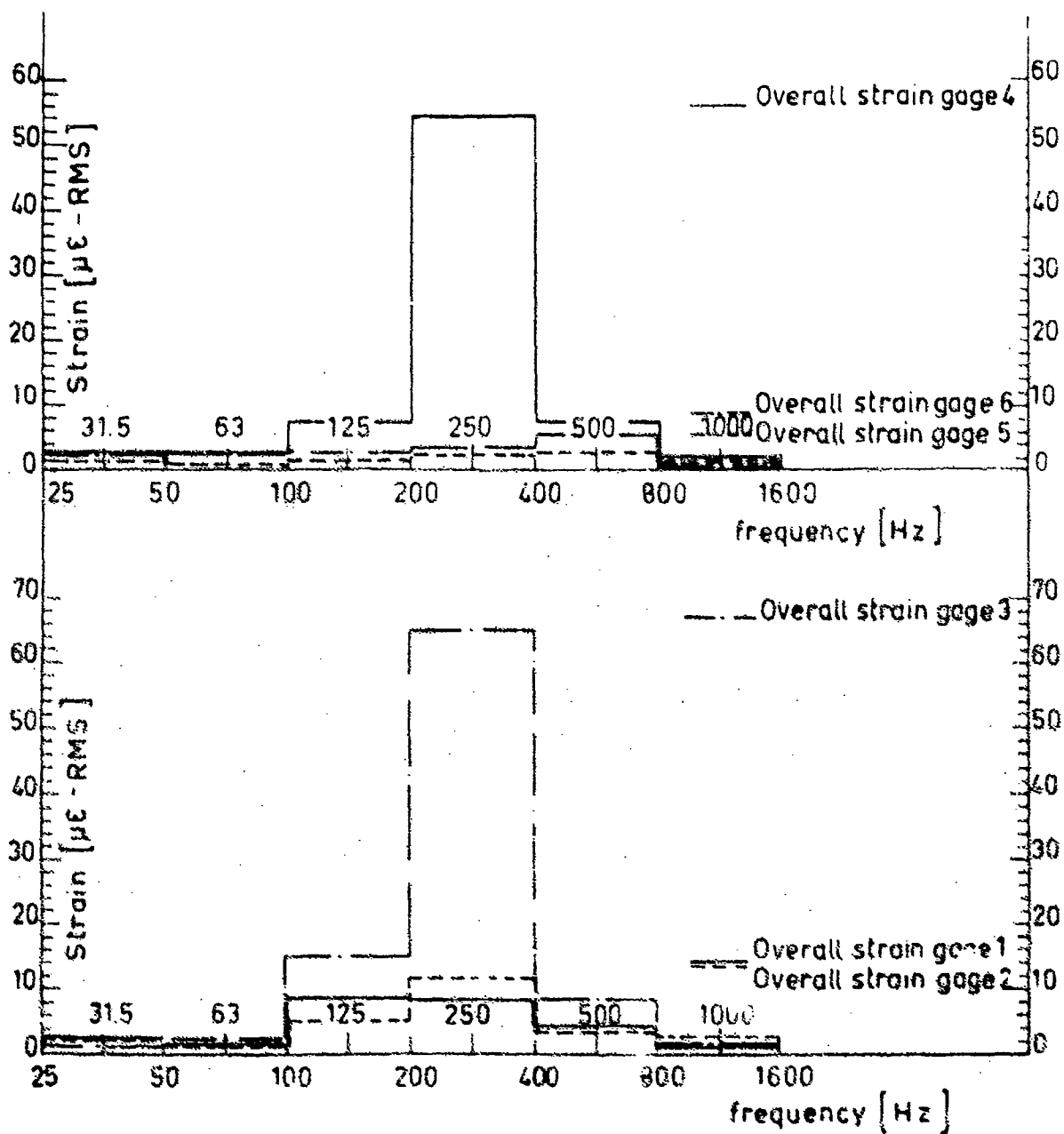
FIG 14 · VAK 191B · TRAILING EDGE FLAP ACOUSTIC FATIGUE TEST

Octave band strains analysis (STOL configuration)
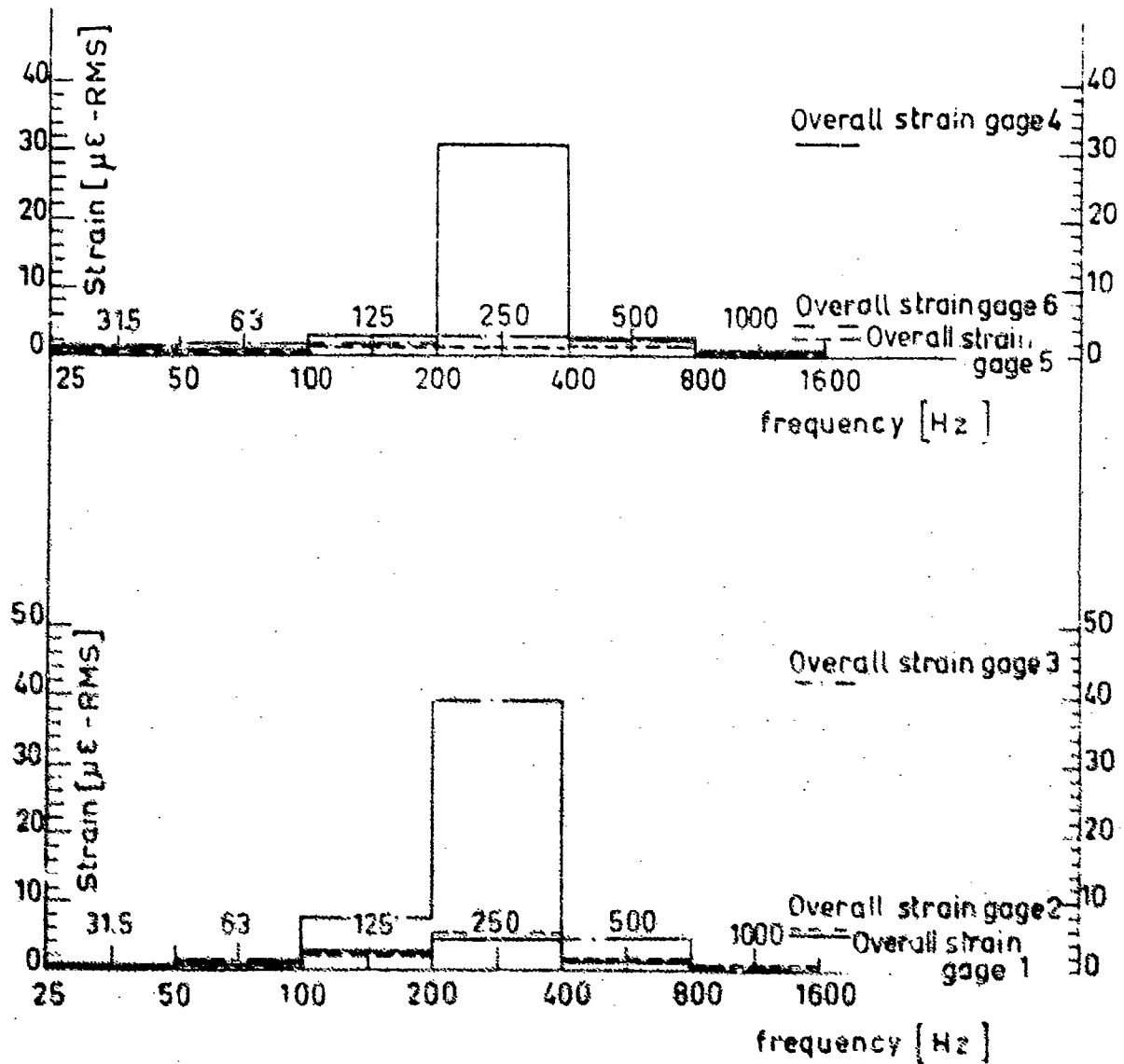
FIG.15 - VAK 191 TRAILING EDGE FLAP ACOUSTIC FATIGUE TEST
Octave band strains analysis (VTOL Configuration)

SOME CONSIDERATIONS OF THE FATIGUE BEHAVIOUR OF ALUMINIUM
ALLOY STRUCTURES UNDER ACOUSTIC LOA TMG

by

W. T. Kirkby
Structures Department,
Royal Aircraft Establishment,
Farnborough, Hampshire England

SUMMARY

In recent years data have been obtained on the fatigue perform.nce of aluminium alloy structural
elements which represent typical skin-stringer attachments, or integrally-milled skin-stiffener con-
figurations, for use in design against acoustic fatigue. The fatigue data have generally been obtained
from tests under narrow-band random loading with zero mean stress in the skin. In this paper some
guidance is given on the allowances which should be made for differences in bandwidth and for effects of
mean stress, when using such acoustic fatigue data. The tentative advice given is based on general
experience of the fatigue behaviour of other types of structural elements under a wider range of random
loading conditions.

Some consideration is also given in the paper to some aspects of crack propagation under acoustic
fatigue loading. In particular the problem of crack propagation under combined fatigue loading actions
is discussed. Predictions of crack growth under cabin pressurisation and acoustic loading are us ! to
illustrate the significance of the problem with reference to aircraft structures which must satisfy fail-
safe requirements. The need for further work on the above aspects of acoust'c fatigue behaviour is
emphasised.

SYMBOLS

K_t	theoretical stress concentration factor
N	number of cycles to failure
N_0	number of positive going zero crossings
N_p	number of positive peaks
n	power to which stress intensity factor is raised to predict crack growth rate
N_{ac}	number of acoustic fatigue stress cycles per flight
S	alternating stress (constant amplitude)
S_p	peak stress in pressure cabin cycle
Δa_{ac}	crack growth per flight from acoustic loading
Δa_{pr}	crack growth per flight from pressure cabin loading
λ	a constant
σ	root mean square stress amplitude

INTRODUCTION

In recent years data have been obtained on the fatigue performance of aluminium alloy structural
elements which represent typical skin-stringer attachments, or integrally milled skin-stiffener configura-
tions, for use in design against acoustic fatigue. In following current design procedure[1], such data are
related to the predicted bending stresses at skin panel boundaries in order to obtain an estimate of
fatigue life to failure. Such fatigue data have generally been obtained from tests under narrow band
random loading with zero mean stress in the skin - in the most commonly used test method, the specimen
itself is excited by a random force input so as to resonate in a mode of vibration in which bending stresses
are induced along a line corresponding to the panel boundary - Fig.1 illustrates the geometry of the
specimens used in such tests and the nature of the response. However, it may be necessary in design to
consider fatigue performance in cases where there is a significant mean stress and also in cases where the
response of the structure to the acoustic excitation may give rise to a multi-modal, or broadband, stress
spectrum. A survey of existing data shows that there is clearly a need for work to provide design data on
the effects of mean stress and bandwidth variation on the fatigue performance of the structural elements
concerned. However, pending the acquisition of such data, some guidance may be obtained from experience
gained on the fatigue behaviour of other types of structural elements under appropriate random loading
conditions.

In the first part of this paper consideration is given to the results of fatigue tests on pin-lug
specimens under narrow-band random loading, and covering a range of positive mean stress, which shed some
light on the effects of mean stress on fatigue performance under such a load spectrum.

In the second part of the paper attention is directed to the information which has been obtained from
tests on several types of structural element under random loading in order to investigate effects of change
in bandwidth. This section of the paper is based to some extent on a comprehensive review of the topic
carried out comparatively recently (1968) by Swanson[2] - this review is up-dated to include other published
results and also to include some results from an investigation currently in progress at RAE.

In the third and final part of the paper consideration is given to some aspects of fatigue crack propagation under acoustic loading. In particular the problem of crack propagation under the acoustic loading action combined with one of the other fatigue loading actions (such as cabin pressurisation) is discussed. Predictions of crack growth under combined cabin pressurisation and acoustic loading are used to illustrate the significance of the problem with reference to aircraft structures which must satisfy fail-safe requirements.

Overall, the considerations and evidence presented in this paper have high-lighted the need for experimental research and data acquisition studies on all of the three above aspects of behaviour under acoustic fatigue loading in order to provide a wider basis for design.

2   EFFECT OF MEAN STRESS ON FATIGUE UNDER RANDOM LOADING STRESS SPECTRA

As far as the author is aware there has been no work carried out to investigate the effect of mean stress on the fatigue performance under random loading of structural elements representing skin-stringer attachments. Before going on to consider any relevant evidence from tests on other types of structural element it is desirable to consider briefly the nature of the failures which occur at such attachments. In the case of fabricated skin-stringer assemblies failures may originate from the combined effects of the stress concentrations and fretting at the rivets - this is generally followed by cracking approximately along the rivet line. Other types of failure may also occur. For example, in such assemblies the type of jointing compound used may provide an appreciable degree of bonding of the stringer flange to the skin. In such circumstances the failure may occur in the skin along a line parallel and close to the edge of the stringer - this mode of failure is associated with the stress concentration arising from the effective change of bending stiffness at this line and there may or may not be some evidence of damage due to fretting between the edge of the stringer and the skin. In the case of integrally-machined skin-stiffener assemblies failure would generally originate in the radius between the skin and the stiffener due to the local stress concentration effect - there would of course be no contribution from fretting in such a situation.

Having these failure modes in mind, it would be worthwhile to consider test results, under the appropriate loading actions, which may exist for other types of structural elements where failure has occurred due to the combined influence of stress concentration and fretting or due to stress concentration effects alone. In section 2.1 which follows, evidence is presented on the fatigue behaviour of a pin-lug assembly under narrow band random loading with a range of positive mean stress conditions. It is considered that this evidence provides some worthwhile guidance which is relevant to situations in which the failures occur from the combined influence of stress concentration and fretting. No corresponding information has been located covering failure from stress concentration effects alone under narrow band random loading.

2.1   Evidence from tests on pin-lug specimens

The information presented in this section was obtained in the course of an investigation by Edwards[3] of the cumulative fatigue damage behaviour of an aluminium alloy lug specimen (see Fig.2) which was loaded through steel pins - the stress concentration factor (K_t) was 3.0. The lug was made from DTD 5014 material having the chemical composition and tensile properties listed in Table 1. Tests were made under both constant amplitude loading and under narrow band random loading, in both cases at a frequency of approximately 110 Hz. The random loading spectrum approximated closely to a Rayleigh distribution of peak amplitudes truncated at a level generally lying between 3.3 and 4 times the rms level (σ) of the stress time waveform. The irregularity factor of the waveform (i.e. number of positive going zero crossings/ number of positive peaks) was approximately 0.98. S/N curves were established under constant amplitude loading for mean stress levels (net) of +69 MN/m^2 (10 ksi), +110 MN/m^2 (16 ksi) and +172 MN/m^2 (25 ksi). Corresponding σ/N curves were obtained under random loading for the same mean stress conditions. On average, some 36 specimens were used in establishing each S/N or σ/N curve with an average of 4 specimens being tested at each condition of mean and varying stress. The curves drawn represented the best fit, as judged by eye, to the log-mean of the values of endurance obtained at each test condition (see Figs.21, 22, 24, 25, 27, 28 and Tables 3, 4, 6, 7, 9, 10 of Ref.3). Information taken from the curves of Ref.3 has been used in order to examine the effect of change of mean stress on fatigue endurance at a given alternating stress, under both constant amplitude loading and under the narrow band random loading. Fig.3 of this paper shows the results obtained, over a range of alternating stress between 10 MN/m^{-2} (1.5 ksi) and 34 MN/m^{-2} (5.0 ksi). Both constant amplitude and random alternating stress are expressed in terms of the root mean square (rms) value of the waveforms concerned. Linear trend lines have been fitted, by eye, to the points plotted - this is not intended to imply that the relationship between mean stress and log endurance is necessarily linear over a wide range of values of mean stress.

The trend lines on Fig.3 suggests that the relationship between mean stress and endurance, over the range of alternating stress concerned, is much the same for both constant amplitude loading and for narrow-band random loading. It may be noted that, under the constant amplitude loading tests, yielding would not have occurred at the stress concentration until a mean stress of 110 MN/m^2 (16 ksi) and an alternating stress of ±10 MN/m^2 (1.5 ksi) rms was reached - it would of course occur to a progressively greater extent at the higher loadings. Under the random loading the higher peaks in the spectrum caused local yielding over almost the whole range of test conditions. Broadly speaking such yielding has a beneficial effect on fatigue endurance[3] - however, at lower mean stress levels when the peak stresses in the random spectrum fall below the value required to cause local yielding it may be expected that the peaks have a detrimental effect on fatigue performance. In such circumstances there is bound to be some element of uncertainty in assuming that the similarity of the effect of mean stress on endurance observed in these tests under the two forms of loading would necessarily apply down to zero mean stress. Nevertheless, in the absence of data at lower mean stresses it is suggested that one of the established methods (e.g. Ref.4) developed in order to correct for mean stress under constant amplitude loading should be used for the time being in design against acoustic fatigue.

Bearing in mind the paucity of evidence on which this tentative advice is given, it is evident that there is an urgent requirement for the acquisition of data to give much more positive guidance on mean stress effects under random loading for use in design against acoustic fatigue.

3 THE INFLUENCE OF BANDWIDTH ON FATIGUE ENDURANCE UNDER RANDOM LOADING

The behaviour of aircraft structures under acoustic loading associated with jet-noise spectra is generally such that, as far as skin panels are concerned, the response will be predominantly in the fundamental mode. As discussed elsewhere in this paper prediction of fatigue life under the resultant narrow-band spectra of bending stresses along the panel boundaries is based on fatigue endurance data for appropriate structural elements under narrow-band random loading. In many cases the contribution to the overall response of the panel from higher modes may be trivial and narrow-band fatigue data may be used with confidence. However in some cases the contribution from one or more of the overtone modes may be too large to be dismissed without further consideration. No data appears to exist, for appropriate structural elements, which may be used in design in such circumstances. In the absence of such data, some guidance may be obtained from consideration of data obtained on other types of structural elements, which may illustrate the nature and probable magnitude of bandwidth effects. Change in bandwidth is taken here to embrace change from uni-modal to bi-modal spectra in addition to the usual meaning of bandwidth change.

Swanson reviewed available data on the effect of bandwidth on fatigue performance under random loading in 1968 [2] and the review covered information taken from the work of Fuller[5], Hillberry[6] and Swanson[7] on plain specimens in aluminium alloy, work by Russa[8] on steel and work by Broch[9] on a non-metallic material. In this present paper, published information from further sources on the fatigue behaviour of aluminium alloy material is also considered – the associated investigations were carried out by Kowalewski[10] on plain specimens and by Clevenson and Steiner[11] on notched specimens. In addition some results are added which have recently emerged from a current investigation by Edwards, at RAE, on the behaviour of pin-lug specimens in which fretting effects are combined with stress concentration effects.

3.1 Summary of available information on bandwidth effects

The principal features of the tests made on aluminium alloy materials and the results obtained are summarised in Fig.4. In this figure plots are given which illustrate the effect of change in the irregularity factor (N_0/N_p) on endurance to failure (N_0). Data points at differing values of N_0/N_p and constant values of rms stress have arbitrarily been joined by straight lines – it is only in the work of Kowalewski, and Edwards, that more than two values of N_0/N_p are covered at the same rms level.

In considering the results it may first be observed that the range of fatigue endurance for which information is given (10^4 to 2×10^6 cycles) falls more than two decades below the endurance considered in designing for acoustic loading. It may also be observed that the majority of the data was obtained on plain specimens whereas actual failure situations involve stress concentration effects and, probably, fretting effects. In this respect the work of Clevenson and Steiner on notched specimens, and the work of Edwards on notched specimens with fretting, is more representative. However, looking at the broad picture presented in Fig.4, for a given rms level it appears that increase of bandwidth, or change from uni-modal to bi-modal response, is unlikely to result in a reduction of fatigue endurance greater than 50%. This is perhaps the best guidance that can be given on the basis of available evidence – it can only be regarded as tentative and there is an evident need for experimental programmes aimed at providing information on representative structural elements at much greater fatigue endurance.

4 SOME CONSIDERATIONS OF CRACK PROPAGATION UNDER ACOUSTIC LOADING

In the first part of the discussion of this section (4.1) consideration is given to the relative merits of adopting a 'fail-safe' or a 'safe-life' approach in designing and testing in relation to acoustic fatigue. It is argued that cracks may nucleate at multiple origins under the acoustic loading with consequent problems in attempting to predict crack growth rates. It is therefore evident that there would be difficulties in implementing a fail-safe approach to the acoustic fatigue problem. In the second part of the discussion (4.2) attention is turned to the contribution that acoustic loading may make to the growth of a 'fail-safe crack' arising from one of the other fatigue loading actions. In this latter case it is assumed that a safe-life philosophy has been adopted in design against acoustic fatigue and that there is no damage initiated by this source of loading.

4.1 Fail-safe or safe-life design in relation to acoustic fatigue

As discussed in section 2 above, a common type of failure is that in which a crack develops along a line parallel to, and close to, the edge of a stiffening member attached to the skin – the failures are initiated in the surface of the skin as a result of reversed bending of the skin along this line. Consider, for example, a typical rectangular fuselage panel (assumed to be flat) bounded on the longer side by stringers and on the shorter side by frame members. The greater part of the acoustic fatigue damage will probably arise from vibratory response in the fundamental 'dishing' mode. In such a mode the longitudinal distribution of bending stress along the failure line between two adjacent frames will approximate to a '(1-cosine)' relationship such that the maximum stress will occur midway between the frame positions – see Fig.5a. This would be the most likely position for cracks to nucleate in the inner or outer surface of the skin, to penetrate through the skin, and to extend in the fore and aft direction along the line of bending. However, for an appreciable distance along the line of bending either side of the central position there is comparatively little reduction in bending stress with the above stress distribution. In a typical size panel the reduction in stress might be little more than 10% over a distance of 5 cm either side of centre. Bearing in mind the scatter in fatigue strength at long endurance – as evident in design data sheets[1] – it is more than likely that fatigue cracks would nucleate at a number of positions along the line of bending over such a ±5cm length. The initiation and development of such an array of cracks into one major crack would be an irregular process lying outside current analytical capability.

Going one step further, consideration of the effects of a significant response contribution from an overtone mode superimposed on the fundamental mode – a not unlikely situation – further complicates the prediction of crack growth behaviour. For example, in the 2:1 mode – see Fig.5b (the first or second overtone mode depending on detail of panel geometry) there would be a nodal line running vertically midway between the frames, with zero resultant stress at the mid-frame position on the line of bending discussed above, but with bending stress maxima in the vicinity of the one third and two thirds frame pitch positions. Whether damage under the combination of this mode with the fundamental mode would be initiated firstly at the mid-frame position or firstly at the third positions would depend on the relative magnitudes of response in the two modes concerned, the relative frequencies and so on. Certainly, in fatigue tests on rectangular panel arrays using broadband siren excitation simultaneous growth of two or more cracks – each measured in centimetres – at different positions in the line of bending has been observed.

It appears therefore that crack growth behaviour may take the form of the linking up of a number of irregularly spaced small cracks into a 'major' crack, which in the worst case might be of unacceptable length. This linking up process could take place 'progressively', but at a virtually unpredictable rate under acoustic loading, or it might take place rapidly and catastrophically under the application of a high quasi-static load. Quite apart from the question of containing such damage from a safety aspects, the problem of predicting damage growth rate, in relation to the fixing of acceptable inspection periods, militates against the acceptance of a fail-safe approach.

The particular panel geometry considered illustrates the nature of the problem that would be encountered in attempting fail-safe design. In other areas of surface structure subjected to acoustic loading panel sizes may be smaller and it could be argued that crack delay, or arrest, would take place at relatively short – and safe – crack lengths. Here again, experience has shown that there may be a multiplicity of damage origins leading to crack growth in the underlying stringers, webs, and cleats, as well as in the skin so that prediction of overall damage growth, as affecting residual strength, would be difficult.

However, consideration of crack growth under acoustic loading does not necessarily end if a safe-life approach is adopted in relation to acoustic fatigue damage and is successfully implemented. It may be that, as a whole, the structure is designed on a fail-safe basis with respect to other fatigue loading actions such as manoeuvre loads, gust loads, ground-air-ground loads and cabin pressurisation loads. In such circumstances it may be necessary to consider for some areas of surface structure whether the acoustic loading is likely to accelerate significantly the growth of any cracks arising from the other fatigue loading actions. If this proves to be the case, then allowance must be made for the contribution made by the acoustic loading to crack growth when establishing the fail-safe characteristics of the areas of structure concerned.

In order to put this potential problem into focus a practical case is discussed in the section which follows – the problem of crack growth in the skin of a pressure cabin under combined pressurisation and acoustic loading.

4.2 Crack propagation under combined pressurisation and acoustic loadings

In this section results are briefly presented of an analysis[12] recently carried out to predict the relative contributions from the pressure cabin ('hoop stress') loads and acoustic loads to crack growth in a typical fuselage panel.

The analysis is centred on the behaviour of a longitudinal crack in a flat panel bounded by frames and stringers; it is assumed that the stringers and frames are continuously attached to the skin and that the crack runs close to and parallel to the edge of one of the stringers – see Fig.6.

Under the pressure cabin load cycle it is assumed that the panel is subjected to in-plane (hoop) stress, the stress field lying normal to the crack. Under the acoustic loading action it is assumed, as in the general design procedure[1], that the panel is responding in the fundamental mode so that reversed bending stresses are induced along the boundaries. The acoustic loading is regarded as being significant only during engine ground running at maximum power and during take-off. Thus, to represent each flight, the crack is taken to be subjected to many cycles of reverse bending associated with the acoustic loads followed by one cycle of in-plane loading representing the cabin pressurisation cycle.

The stress spectrum used to represent the acoustic fatigue bending stresses is assumed to conform to a Rayleigh distribution of peak amplitudes – the rms levels of bending stress chosen are such that freedom from fatigue damage throughout the lifetime of the aircraft would be expected, as judged by the relevant RAeS/ESDU Data Sheets, i.e. a safe-life design is assumed. A range of values of cabin pressurisation stress is taken which covers typical design values.

The analysis is based on the use of linear elastic fracture mechanics and several simplifying assumptions are made. These are discussed at some length in Ref.12 – the most important assumptions are as follows:-

(1) For the range of crack lengths considered, it is assumed that the response of the cracked panel to the acoustic loading is such that the level of bending stresses in the path of the growing crack remains constant.

(2) The stress intensity factor at the crack tip is affected to the same extent by the proximity of the stringer for both the bending case and for the axial loading case. (It is argued that the correction factor on stress intensity lies very close to unity.)

(3) In calculating crack growth, linear summation of growth increment from each cycle is assumed – this is equivalent to the use of Miner's rule. It is considered that cycle-to-cycle interaction effects are not likely to be significant with this particular overall loading action.

On the above basis, an expression for the relative crack growth rate per flight under the two forms of loading action was derived (Eq (15) of Ref.12).

$$\frac{\Delta a_{ac}}{\Delta a_{pr}} = \frac{\lambda^n (2\sigma^2)^{n/2} \Gamma_{x \rightarrow y} \left(\frac{n}{2} + 1\right) N_{ac}}{S_p^n} \tag{1}$$

where Δa_{ac} is the crack growth per flight from acoustic loading

Δa_{pr} is the crack growth per flight from pressure cabin loading

λ is a constant, derived empirically[13] by Roberts and Erdogan to determine 'effective' stress intensity under bending, as opposed to axial loading $(\lambda \approx 0.5)$

σ is rms bending stress

n is the power to which stress intensity is raised in predicting crack growth rate

N_{ac} is the number of acoustic fatigue stress cycles per flight

S_p is the peak stress in the cabin pressurisation cycle.

The incomplete gamma function $\Gamma_{x \rightarrow y}$ is introduced to handle the integration of crack growth under the Rayleigh distribution of peak amplitudes. The lower bound 'x' is associated with a value of stress intensity below which crack growth will not take place – the upper bound 'y' is associated with truncation level.

The above expression has been evaluated for a range of σ lying between 5.2 and 10.4 MN/m^2 rms (0.75 → 1.5 ksi rms) and for three values of S *viz.* 69, 83 and 97 MN/m^2 (10, 12 and 14 ksi). In selecting a value for N_{ac} it is assumed that the fundamental frequency of the panel concerned is 200 Hz and that there is total exposure time per flight of 90 seconds – thus, $N_{ac} = 1.8 \times 10^4$ cycles. A value of n = 3.6 is taken from published data[14] on crack propagation in 2024-T3 material obtained by Hudson. The results of the evaluation of Eq (1) are shown in Fig.7. (It may be deduced from Eq (1) that the values of Δ_{ac}/Δ_{pr} obtained in specific evaluations will not strictly be independent of crack length insofar as Γ_x is dependent on crack length – under the acoustic stress values that we are considering there will be little consequent effect on Δ_{ac}/Δ_{pr}, certainly over a range of crack lengths from, say, 2.5 cm upwards.)

It will be seen from Fig.7 that, over much of the range of acoustic fatigue stress, the contribution to crack growth from the acoustic loading exceeds that from the cabin pressurisation cycle by a considerable margin. For example, with a pressure cabin maximum stress 83 MN/m^2 (12 ksi) and an acoustic fatigue stress of 7 MN/m^2 ($\approx$1.0 ksi) the contributions will be much the same – with an acoustic fatigue stress or 10 MN/m^2 ($\approx$1.5 ksi) the contribution from the acoustic loading is predicted to be some four times greater than that from the cabin pressurisation cycle.

The particular case of the contribution that acoustic loading may make to crack growth in a pressure cabin serves to illustrate the point that it may be necessary to make allowance for the acoustic loading when establishing the fail-safe characteristics of structure even though the acoustic loading is not sufficiently severe to initiate fatigue damage in its own right. The same considerations may also apply to areas of structure other than the pressure cabin, e.g. fin and tailplane structure which may be designed, on fail-safe principles, to withstand the appropriate gust and manoeuvre load fatigue spectra. However, it should be borne in mind that it was necessary in carrying out the foregoing predictions to introduce a number of simplifying assumptions in the analysis. There is clearly a need for experimental work to substantiate the findings. Experimental research programmes currently in progress in the UK at the University of Southampton and at the British Aircraft Corporation, Filton will yield results of direct interest in relation to this potential problem. The former investigation is concerned with the prediction and study of crack growth adjacent to a stiffener in a panel (as in Fig.6), under acoustic loading – the latter is concerned with crack growth in integrally machined skin-stiffener structures under acoustic loading and with the capability of applying in-plane loadings to represent cabin pressurisation stresses.

5   CONCLUDING OBSERVATIONS

Consideration has been given in this paper to the probable effects of change in mean stress, and to the effects of change in bandwidth of the stress spectrum, on the fatigue performance of structural elements which are used to provide basic data for use in design against acoustic fatigue. No directly applicable information obtained on such elements appears to be available and, accordingly, some guidance has been sought from relevant data obtained on other types of fatigue test specimens. Pending the acquisition of directly applicable data on acoustic fatigue test specimens the following tentative guidelines are put forward for use when following current design practice:-

(i)   Corrections for effect of mean stress on fatigue endurance may be undertaken using existing methods developed for application to constant amplitude fatigue data.

(ii)   The effect of increasing bandwidth, or changing from uni-modal to bi-modal stress spectra, is such that the fatigue endurance for the same overall rms level may be halved.

Some aspects of crack propagation under acoustic loading have also been considered. It has been argued that design against acoustic fatigue is more amenable to safe-life, rather than a fail-safe approach. In further discussion of crack propagation, predictions are put forward which show that it may be necessary to make allowance for the acoustic loading actions when establishing the fail-safe characteristics of a structure with respect to other, major, loading actions.

Finally, there is a clear need for experimental research and data acquisition programmes to provide evidence to confirm or modify the foregoing tentative conclusions.

Table 1

MEASURED CHEMICAL COMPOSITION AND TENSILE PROPERTIES OF DTD 5014 ALUMINIUM ALLOY

CHEMICAL COMPOSITION (per cent)

Cu	Mg	Si	Fe	Mn	Zn	Ni	Ti
2.26	1.38	0.25	1.06	0.06	0.02	1.02	0.06

Balance aluminium

Average tensile properties

UTS $\quad$ 404 MN/m^2 (58.5 ksi)

0.1% proof $\quad$ 350 MN/m^2 (50.8 ksi)

Elongation $\quad$ 13%

REFERENCES

No.	Author	Title, etc.
1	-	Royal Aeronautical Society/ESDU Fatigue Data Sheet No.66015
2	S.R. Swanson	A review of the current status of random load testing in America. Proceedings of the Technical Sessions of the Eleventh ICAF Meeting in Stockholm, May 1969, ICAF Doc. No.499
3	P.R. Edwards	Cumulative damage in fatigue with particular reference to the effects of residual stresses. ARC CP 1105, Her Majesty's Stationery Office (1971)
4	-	Royal Aeronautical Society/ESDU Fatigue Data Sheets No. E07.03
5	J.R. Fuller	Research on techniques of establishing random type fatigue curves for broadband sonic loading. ASD TDR 62-501 USAF, October 1962
6	B M. Hillberry	Fatigue life under narrow- and broad-band random loading. Ph.D. Thesis, Iowa State University of Science and Technology, University Microfilms Inc., Ann Arbor, Michigan (1967)
7	S.R. Swanson	An investigation of the fatigue of aluminium alloys due to random loading. UTIA Report 84, February 1962
8	S.L. Bussa	The effect of rms stress level, irregularity factor and power spectrum shape on the fatigue life of SAE 1006 notched specimens under stochastic loading conditions. M.Sc. Thesis, Wayne State University, Detroit Michigan (1967) (Reprinted by MTS Systems Corporation, Minneapolis, Minn. USA)
9	J.T. Broch	Peak distribution effects in random load fatigue. Bruel and Kjaer Technical Review No.1, Copenhagen (1968)
10	J. Kowalewski	On the relation between fatigue lives under random loading and under corresponding programme loading. 'Full scale fatigue test of aircraft structures' edited by F.J. Plant and J. Schijve, Pergammon Press (1966)
11	S.A. Clevenson R. Steiner	Fatigue life under random loading for several power spectral shapes. NASA TR R-266, September 1967
12	W.T. Kirkby	Some predictions of crack propagation under combined cabin pressurisation and acoustic loadings. RAE Technical Report (in preparation)

REFERENCES (concluded)

No.	Author	Title, etc.
13	R. Roberts F. Erdogan	The effect of mean stress on fatigue crack propagation in plates under extension and bending. Journal of Basic Engineering, December 19
14	C.M. Hudson	Effect of stress ratio on fatigue crack growth in 7075-T6 and 2024-T3 aluminium-alloy specimens. NASA TN D5390, August 1969.

Skin

Riveted skin test specimen
(single row of skin rivets)

Excitation

Rib

Skin

Riveted skin test specimen
(double row of skin rivets)

Excitation

Rib

Excitation

Machined stiffener
test specimen
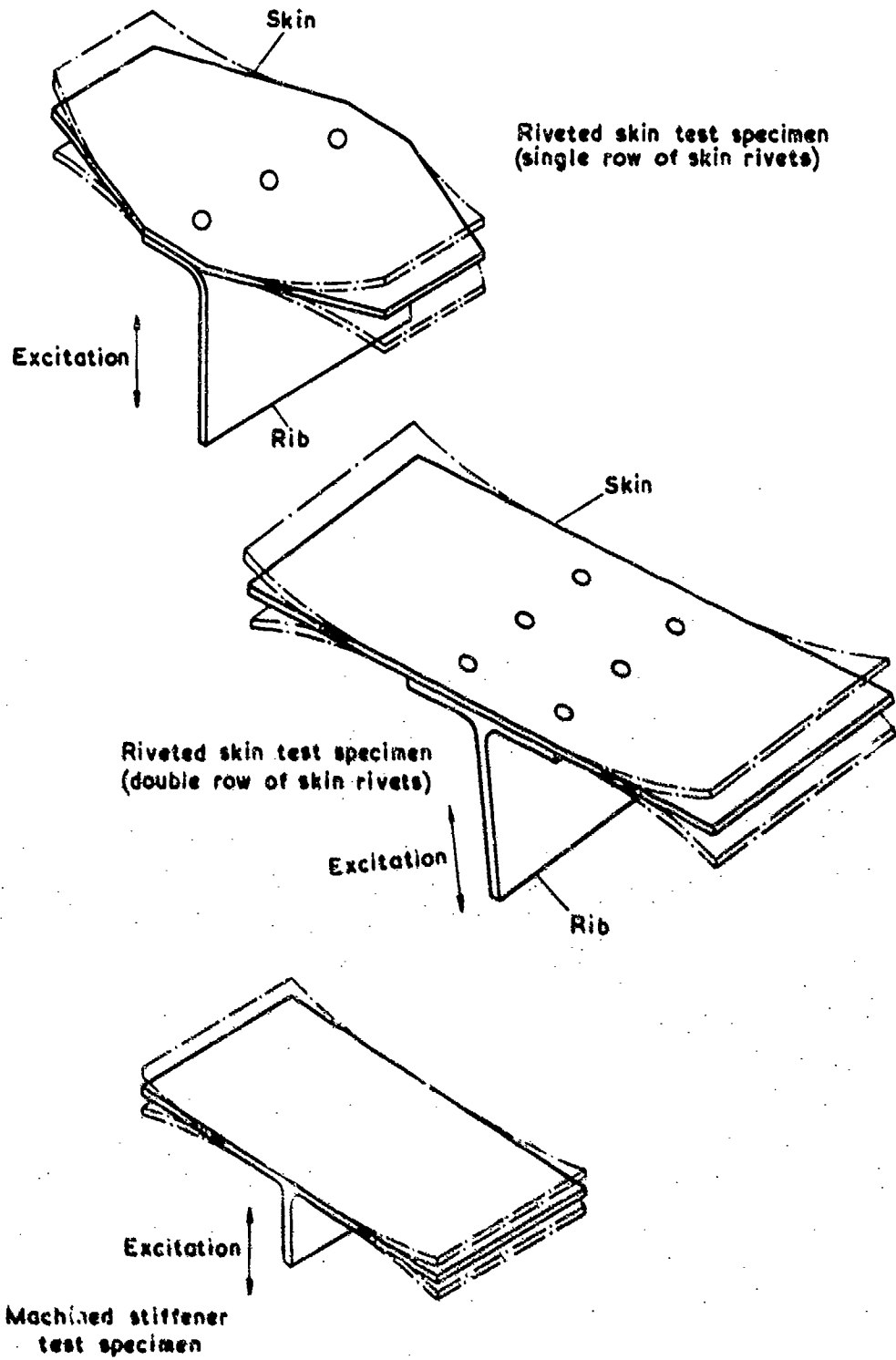
Fig.1 Typical structural elements used in acoustic fatigue tests
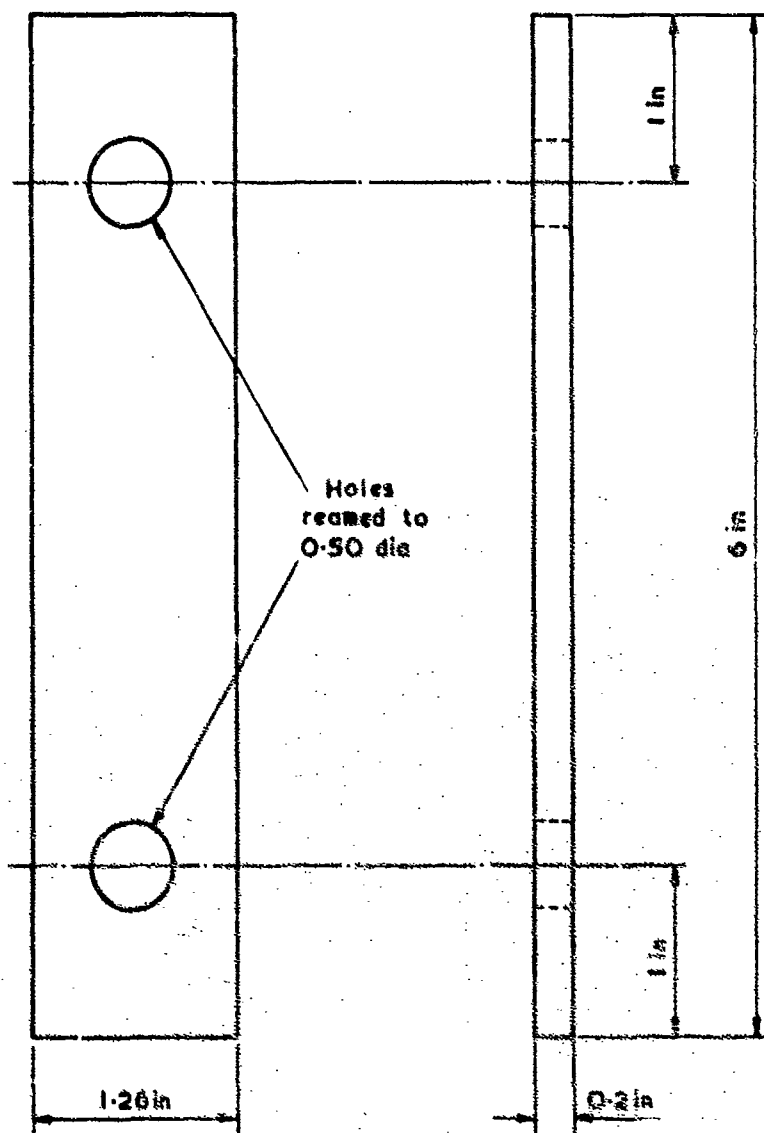
Material   BS 2L65

Fig.2 Lug specimen (Ref 3)

S = rms alternating stress–const amplitude – MN/m²
σ = rms alternating stress–random amplitude – MN/m²
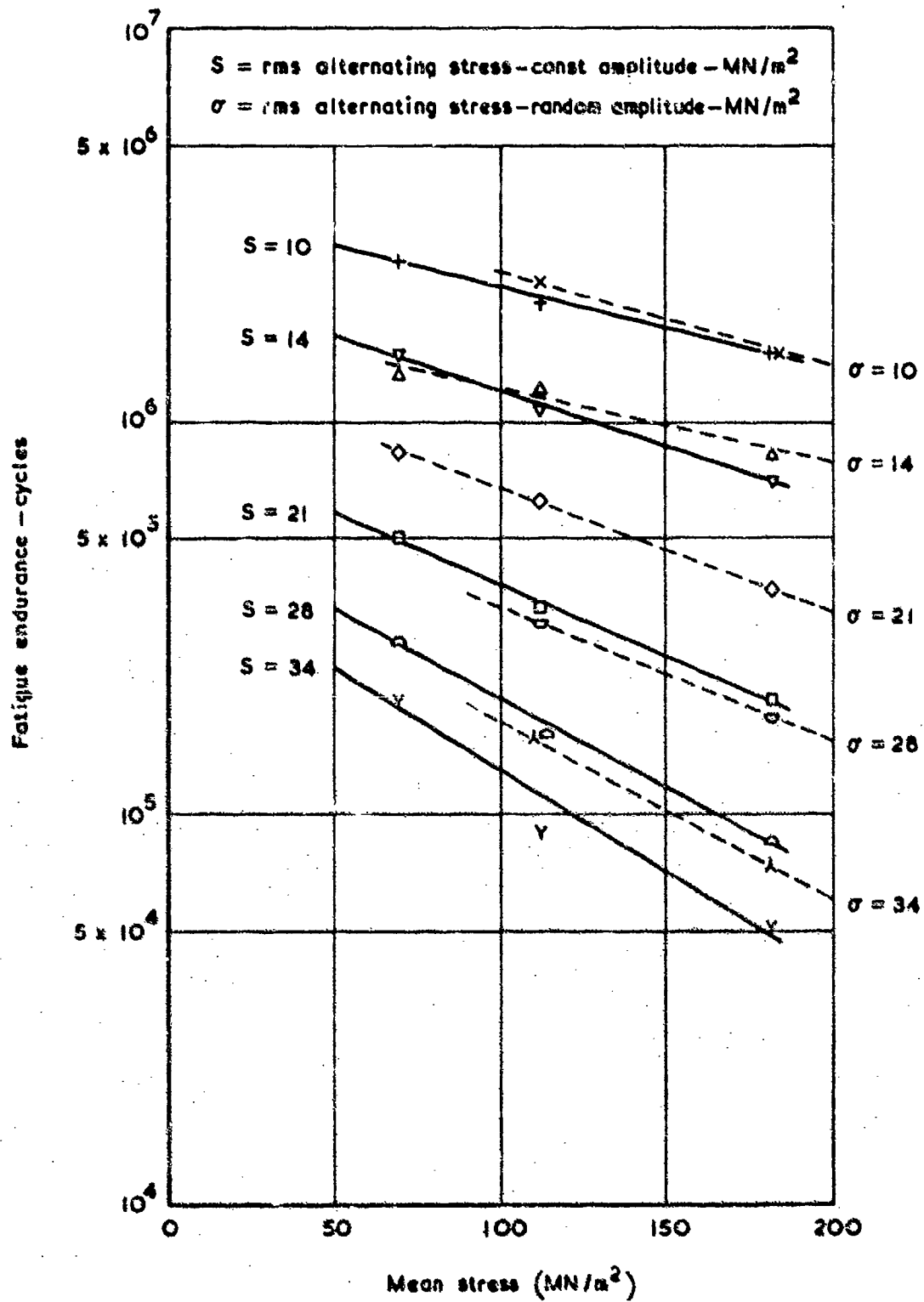
Fig.3 Relationship between mean stress and endurance
for constant amplitude and random loading
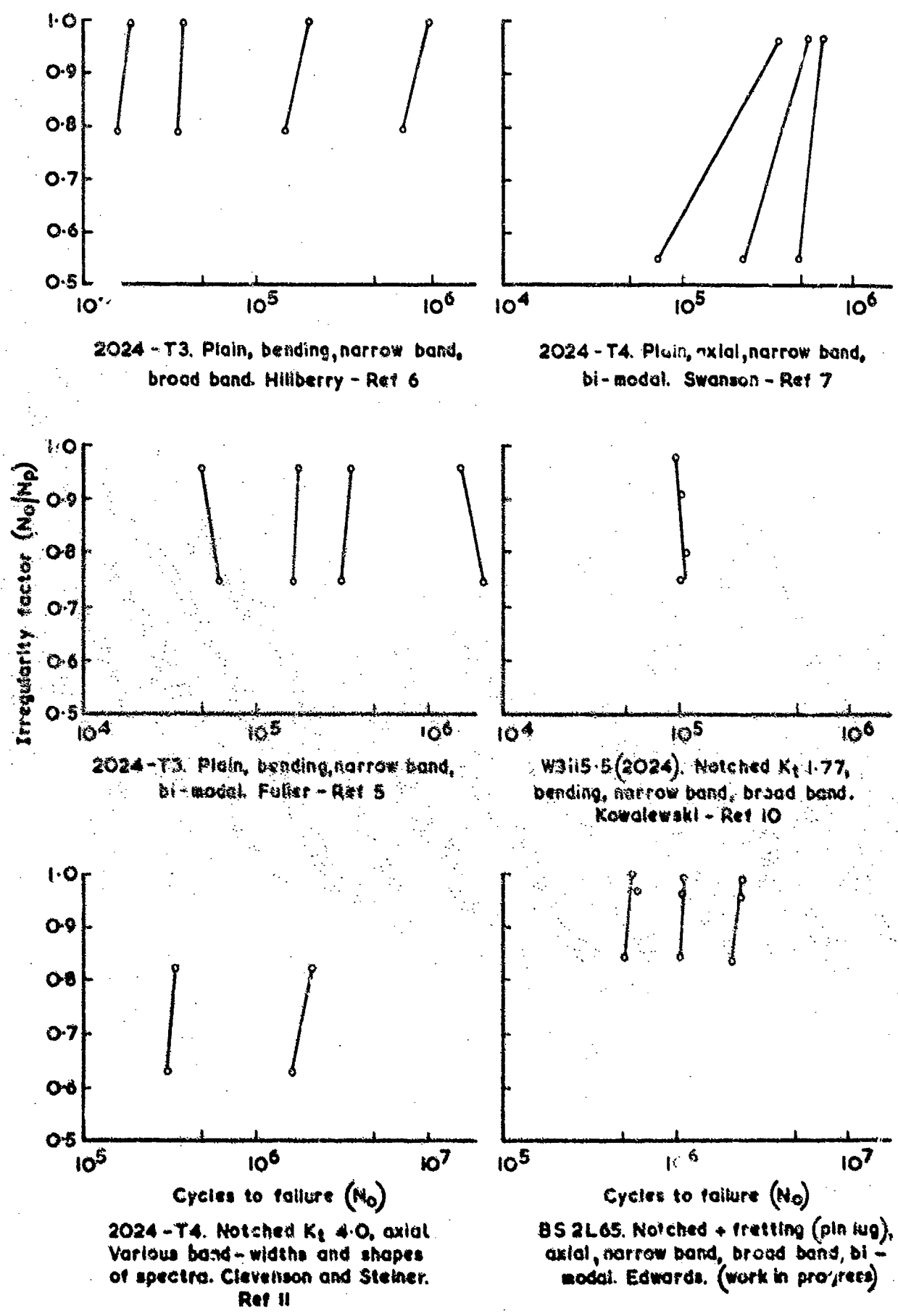
Fig.4 Effect of N_0/N_p on fatigue endurance
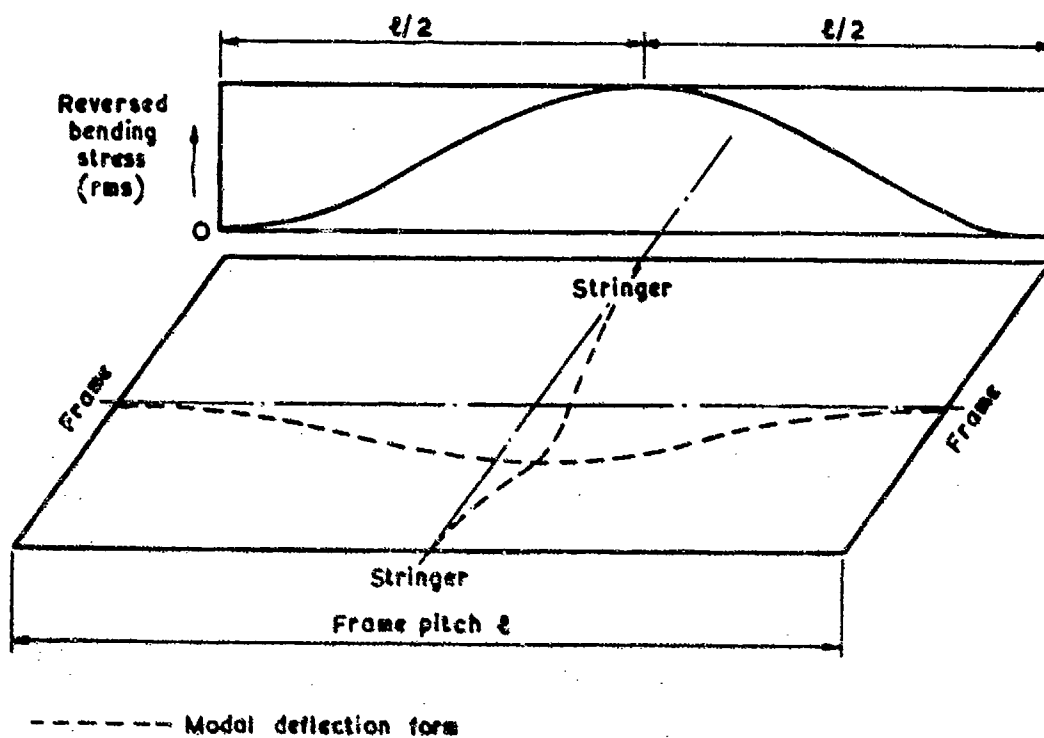
Fig. 5a Distribution of reversed bending stress along panel boundary in fundamental $(1,1)$ panel mode
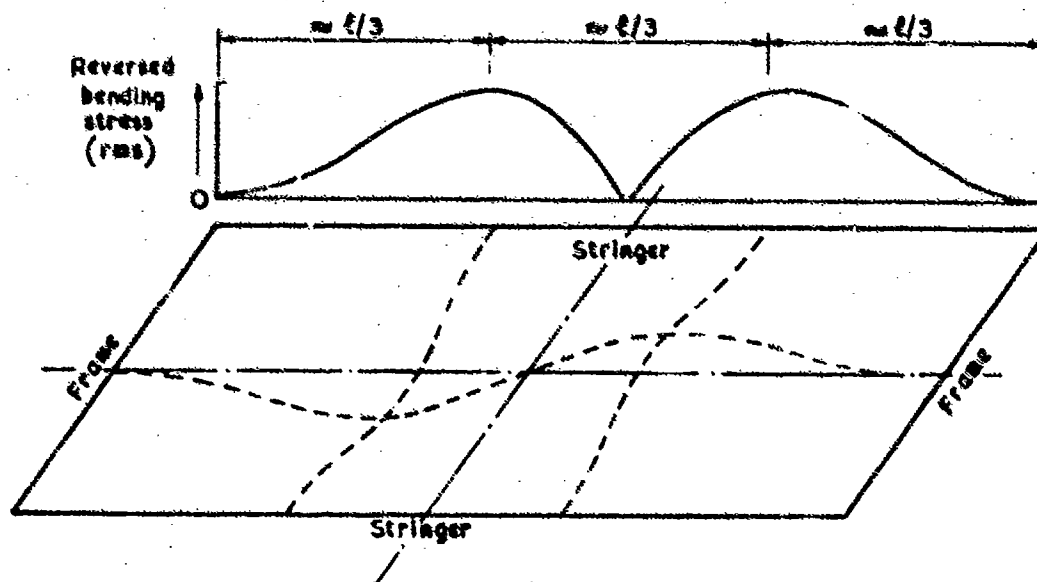
Fig. 5b Distribution of reversed bending stress along panel boundary in overtone $(2,1)$ panel mode
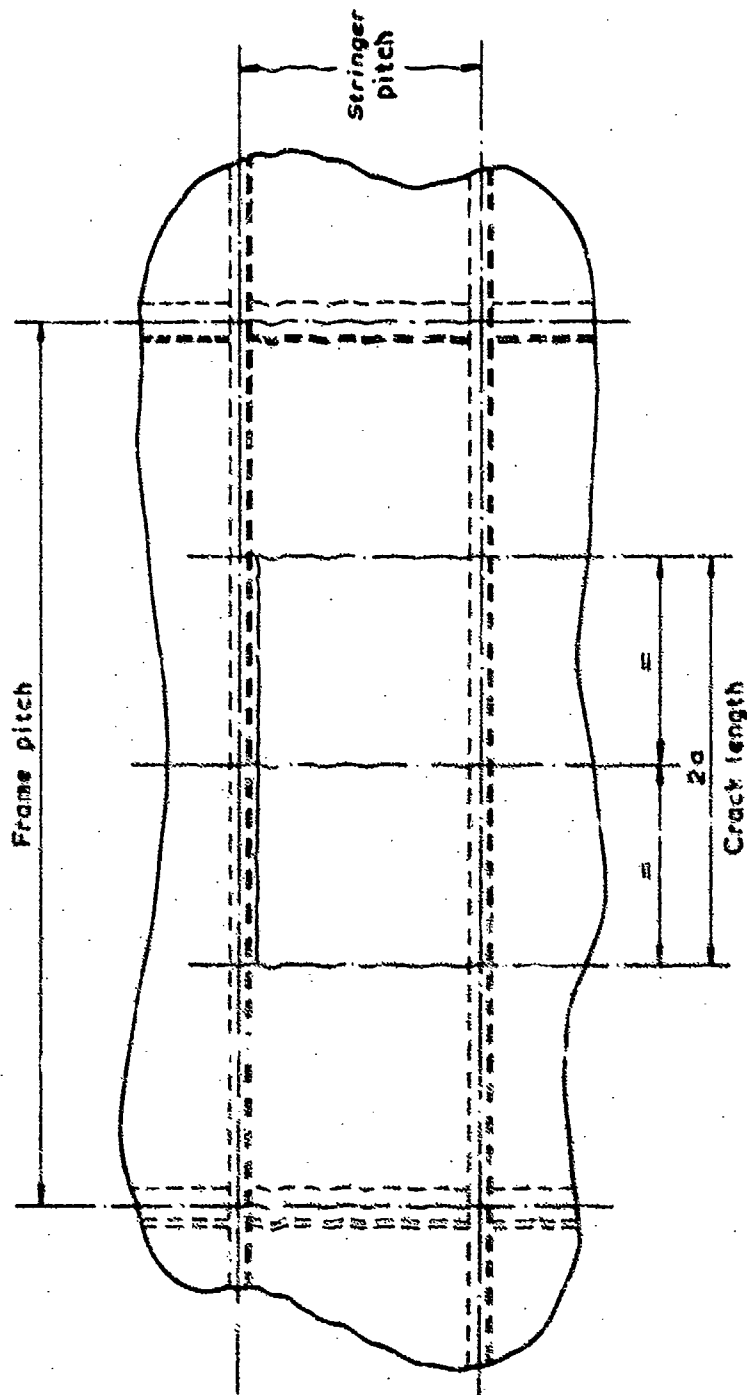
Fig.6 Fuselage panel showing crack running close to stringer edge (Ref 12)
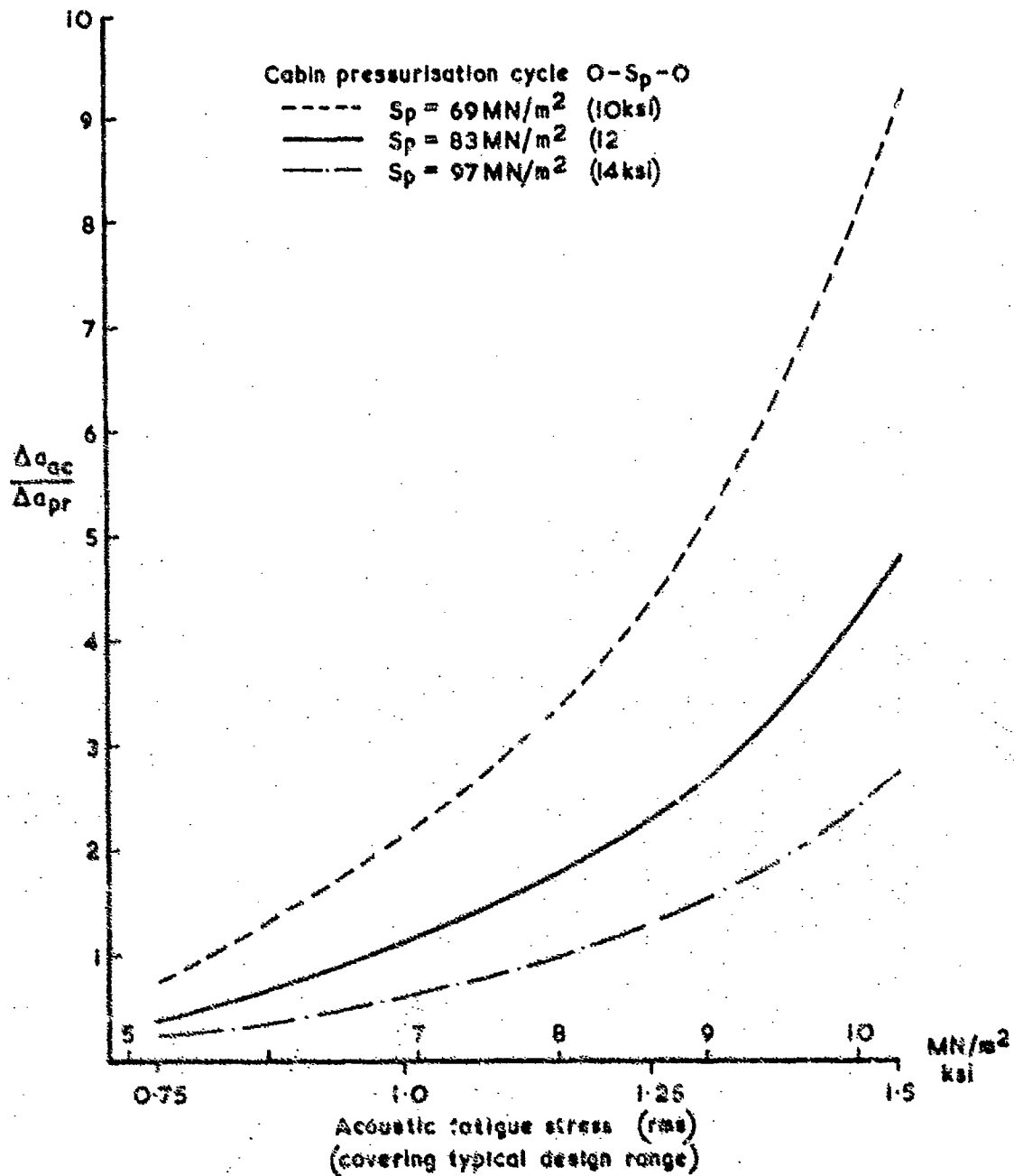
Fig. 7 Relative crack growth rate per flight under acoustic loading and cabin pressurisation loading $\dfrac{\Delta a_{ac}}{\Delta a_{pr}}$ (eq 15, Ref 12)

When asked about the use of conventional stiffened skin-stringer titanium structure for intakes, Mr. Holehouse replied that such structure was heavier and had a shorter life than titanium honeycomb construction.   He added, however, that honeycomb structure could not be regarded as a fail-safe design because, once initiated, failures propagate very rapidly.   Occasionally an edge failure would be slow to propagate but generally it propagated much quicker than a corresponding failure in skin-stringer construction.   Thus honeycomb structure must be designed for safe life. The quality of the bond has a big effect on the life and therefore it is essential to have good quality control of the bond process.   Marginal changes in bond strength may give only marginal changes in mechanical strength but marked changes in sonic fatigue life.   Acoustic emission techniques are being used to assess bond quality.   The results to date are very encouraging.   In the test results shown in the paper only one edge connection design had been used.   This was in order to reduce the number of variables in the test programme.   In actual structures the edge designs would vary.

Mr. Calcagnini, who presented Mr. Selvaggi's paper, was asked if any narrow band analyses of the strain gauge results had been made.   He replied that this had not yet been done as their main interest had been in the fatigue life.   Neither had there been any study of the change in strain response as the structure heated up.   The true temperature-time history had not been simulated in the tests therefore the flap deflection had been limited so as to reduce the area exposed to the hot jet. The adhesives used in this structure could withstand temperatures of $125^{\circ}C$ for a few seconds only.   The original purpose of the tests had been to get some quick estimates of life in order to clear the prototype for flight test.

In the discussion on his paper, Mr. Kirkby emphasised the lack of knowledge on the effect of statistical probability distribution on life.   As most random tests to date had used a narrow band stress time history having a Rayleigh distribution of peaks there was a need for more data to enable us to have a better understanding of the effects of distribution.

There was some discussion of the effect of superimposed static stresses.   Dr. Manson's work had been used to make estimates for combinations of acoustic and thermal stresses.   The static stresses due to preloading in the manufacturing processes could be high.   Mr. Holehouse stated that he measured the assembly-induced stresses and then the acoustically-induced stresses.   The safe allowable acoustic stress was then modified to take into account the static stress.

ASSESSMENT OF SIREN TEST TECHNIQUES

by

Eric James Phillips
Chief Structural Research Engineer
Hawker Siddeley Aviation
Brough
Yorkshire
England

SUMMARY

The objective of the work programme being undertaken is to investigate the siren as a test technique for the determination of response and life of aircraft structures subject to engine noise field excitation.

A flat panel specimen is to be placed in the near noise field of a typical jet engine and its stress response measured. The specimen will then be placed in a siren and the response which was measured in the engine noise field reproduced as closely as possible. The differences in response will be assessed with regard to the extrapolation of measured siren fatigue life to service environments. Specimen responses in the engine noise field and in the siren will be compared with the theoretically predicted response, using methods of varying complexity.

At the time of writing, the theoretical prediction of response is almost complete and some limited discrete excitation testing has been achieved.

1.   INTRODUCTION

A noise testing facility was constructed at Hawker Siddeley (Brough, Yorkshire), in 1963, following concern regarding the effect of acoustic noise on the Buccaneer structure. A considerable amount of acoustic testing has been undertaken since the inception of the facility, mostly comparing the effects of structural design changes. However it became apparent that more fundamental work was required in order to apply the results of siren response and life tests to the determination of structural fatigue life in service acoustic environments.

In 1967, following discussions between representatives of the Society of British Aircraft Constructors and Director General, Structural Research (Aircraft) on the subject of acoustic fatigue, a joint Industry/MinTech working party was formed, tasked with reviewing the situation generally. Amongst the recommendations of the working party, it was thought that further work would be useful on conventional forms of construction, and on a correlation between structural response in near field jet noise and in a siren.

Hawker Siddeley Aviation, Brough, received two contracts for specific work in this area. One contract was concerned with a study of the siren as a test technique, the other with evaluating the effects on fatigue life of small detail design changes to similar test panels.

2.   OBJECTIVES

This paper reports on the investigation of the siren as a test technique. The object of the work is to gain more understanding of the effects, on structural response, of the differences between the noise field of a typical jet engine and a typical siren environment. It is not intended that this particular work programme should provide a complete answer to the problems of translating siren fatigue test results to the estimation of structural fatigue life in service conditions, since many factors are involved, some of which are currently being studied elsewhere. Amongst such factors are the effects of relating test specimen response to the response of an integral part of an aircraft structure, the identification of the significant parameters determining the rate of fatigue damage, and the effects of non-linearities in response.

The response of the specimen will be measured in the near noise field of a jet engine. The one most readily available is a Rolls Royce Spey, but it is hoped to repeat the tests in the near noise field of a high by-pass ratio engine. The response will then be measured in the siren. The exciting noise field will be adjusted, within the limitations of the siren, to reproduce the engine noise field response as closely as possible. The free vibration characteristics of the specimen will be measured by several test methods, for comparison, and additionally the free and forced response will be predicted by methods of varying complexity. The aims are to produce comprehensive, well documented results from carefully controlled tests for comparison with predictions.

At the time of writing, it has not been possible to start the response tests in the engine noise field, and therefore it is only possible to mention the theoretical predictions completed and compare them with the limited discrete frequency test results available. The test rig will also be described in some detail.

3.   TEST PROGRAMME

3.1. DISCRETE FREQUENCY TESTS

Natural frequencies, mode shapes, and modal damping are to be determined by the following techniques.

(a) Mechanical Excitation

(i) Slow frequency sweep using sinusoidal excitation.

(ii) Rapid frequency sweep, using method of reference (1)

(b) Discrete Acoustic Excitation

(i) Using loudspeakers.

(ii) Using a siren.

3.2. ENGINE NOISE TESTS

The specimen will be held at grazing incidence close to the boundary of the efflux of a jet engine, downstream of the engine, in two positions.   The outputs of strain gauges on the specimen, and of two microphones placed near the boundaries of the specimen, on a horizontal centreline, one ahead of and the other downstream of the specimen, will be recorded.

The harmonic and statistical properties of the signals will be determined by narrow band analysis.

The specimen will be tested with the stringers horizontal and vertical, and at two engine power settings.

3.3. SIREN RANDOM NOISE TESTS

The input spectrum of the control signal to the siren transducer will be shaped such that a chosen panel response measured in the engine noise field will be reproduced as closely as possible.

The results will be analysed as for the engine noise tests.

4.   TEST SPECIMEN AND RIGS

4.1. TEST SPECIMEN

The test specimen is shown on figure 1.

The choice of a specimen is often difficult, in this case it was decided to represent a fairly typical piece of fuselage side.   The dimensions of panel width, length, skin and stringer thickness, stringer size, etc., were determined by assuming a typical compressive end load per inch width. One of the considerations in the choice of specimen was that it should be amenable to theoretical analysis. It is fabricated from aluminium copper alloy and mushroom headed rivets are employed to avoid stress concentrations due to countersinking.   With this type of construction failure would normally be expected along the line of skin-stringer attachment and therefore a panel with three by four bays has been chosen so that a typical skin-stringer attachment is in the centre of the panel.   Reference 2 suggests that the number of bays should be sufficient to ensure that the boundary attachment of the panel will not influence the stresses in the centre of the panel.

There is no shear attachment between the stringer web and the frame web since past experience has shown that fatigue failures initiate from the rivet holes in the stringer web in such designs.   A do ler is provided around the stringer cut-out in the frame to reduce bending stresses in the frame flange bend radius.

The specimen has low out-of-plane warping stiffness and is therefore mounted in a frame, which may be attached to test support fixtures, or the siren.   The test frame is designed to eliminate mounting stresses in the specimen.

4.2. TEST BOX

During the engine noise tests, it is necessary that only one side of the specimen should be excited.   Accordingly, thought was given to mounting the specimen in a baffle or in the side of a box. While the former is probably preferable, one large enough to be effective appeared to be impracticable and so the box, shown on figure 2, was adopted.   It is constructed from twelve m m thick mild steel plate and is lined with sound absorbent material.

Tests are proceeding to measure reverberation times of the box and to measure the attenuation of the box with the specimen in position.

4.3. SIREN

The transducer is an EPT94B, and the cross section of the working section is 1.220 m by 76 mm. Extensive tests have been completed to measure the performance of the siren.

The distribution of overall sound pressure levels over the working section aperture was measured, the specimen being replaced by a rigid plate. The results at maximum transducer drive and air conditions are shown on figure 3.

Outputs of several microphones on the horizontal and vertical centrelines have been recorded, with the input signal to the transducer filtered to produce nominally white noise. These records are being subjected to narrow band analysis in a search for duct resonances and other instances of distortion. A typical result is shown on figure 4.

4.4. STRAIN GAUGES

It is imperative that a fairly detailed picture of specimen response should be obtained, but a compromise has to be made between the number of measurements one would like and the recording and analysis facilities available. Since measurements are to be made behind an engine, and engine running time is costly, it was decided that no more than twenty two strain gauge channels would be recorded on test. This requires two runs per test since eleven channels are available per run on the tape recorder.

Gauge positions are shown on figure 1. The object is to measure the principal skin stresses in the centre of a bay, skin stress at the skin-stringer and skin-frame attachment lines, stringer longitudinal stress at the frames and mid way between frames, and the bending stress in the frame attached flange bend radii.

The positions of maximum skin stress were checked by coating the specimen with strain sensitive lacquer, before attachment of the gauges, and exposing the specimen to simulated jet noise in the siren. It was found that high stress levels existed in the skin at the junction of the frames and stringers, and two gauges at right angles were attached at a junction to monitor the stress. The residual and injected electrical noise in the system will be measured by an additional gauge mounted on a metal plate near the specimen and shielded from acoustic noise input.

Each gauge and amplifier are connected by a 25 metre length of twin individually screened cable. Measurements indicate that the system has a signal to noise ratio of 36 dB at 6,89 MN/m².

4.5. RECORDING AND ANALYSIS EQUIPMENT

Signals will be recorded on an Ampex FR 1300 tape recorder.

A Ubiquitous and ICL 1904 are available for narrow band digital analysis and a Panoramic Sonic Analyser, with real time display if required, for analogue analysis.

In addition facilities are available for auto correlation and cross correlation of signals.

5. TEST RESULTS

The only response tests completed to date have used loudspeakers as the source of excitation. The original purpose of these tests was to obtain sand patterns in various modes, however the opportunity was taken to record several strain gauge signals. The specimen was hung by bungee rubber cords.

Figure 5 shows the variation of stringer stress level with frequency, measured during a slow frequency sweep, at normal incidence.

6. THEORETICAL RESPONSE PREDICTIONS

6.1. SIMPLE APPROACHES

Current design practice is often to assume that most of the fatigue damage occurs in the fundamental mode of response. Several papers have been written on this assumption and references (3), (4), (5), (6), were reviewed and used to obtain estimates of stress. Some results are given on figure 6. The method of the Engineering Sciences Data Unit is based predominantly upon work by Miles (3) and Clarkson (4), and is versatile in that allowance may be made if the panel is part of a control surface type structure, or for etched skins. The method of Ballentine (5) is also based upon Miles but the basic equations are modified by the inclusion of empirical results. Arcas (6) attempts to improve the accuracy of Clarkson's predictions by altering the representation of the boundary conditions and mode shapes.

6.2. WAVE GROUP THEORY

In (7), Dr. D.J. Mead of the University of Southampton outlined a method for calculating the free and forced vibration of periodic structures, typically a beam on equi-distant elastic supports. This method has been applied to predict the response of the specimen, the method being given in detail in (8). The method, strictly, may only be applied to a long array of bays, each of which is simply supported at the frames. However, clamped edges at the frames may be allowed for by using Szechenyi's (9) "equivalent wave-length" between the frames. The deflected shape between the frames is represented in the form attributed to Levy:-

$$w(x,y) = \sum_{m=1}^{m=\infty} X_m(x) \sin \frac{m\pi y}{b} \qquad - (1)$$

where, $w(x,y)$ = static deflection at the point (x,y)

$X_m(x)$ = arbitrary functions of x, determined by boundary conditions.

m = number of half sine waves across the plate, between the frames.

b = distance between the frames.

The stringers provide rotational and transverse restraints at their points of attachment to the skin. These stiffnesses are supplied from the existing beam theory of thin walled members of open cross-section.

The distributed transverse load, q, and torque, r, are governed by the expressions given by Lin (10) modified for the effect of the acceleration of the stringer:-

$$q = E_b I_z \frac{\partial^4 w}{\partial y^4} + \rho_b A \ddot{w} \qquad - (2)$$

$$r = G_b J \frac{\partial^3 w}{\partial y^2 \partial x} - E_b \Gamma_s \frac{\partial^5 w}{\partial y^4 \partial x} + \rho_b I_s \frac{\partial^2 w}{\partial x} \qquad - (3)$$

where, E_b = Youngs modulus of the stringer.

I_z = Moment of inertia of the stringer cross-section about the z axis (through centroid).

G_b = Shear modulus of the stringer.

J = St. Venant torsion constant.

Γ_s = Warping constant about the skin attachment point.

I_s = polar moment of inertia about skin attachment point.

ρ_b = mass density of stringer.

A = cross-sectional area of stringer.

The structure is represented by the idealised structure shown on figure 7. For such a periodic structure, under free vibration conditions, the following relationships given by Mead (7) hold:-

$$w_s = e^\mu w_r \quad \text{(displacement)} \qquad - 4(a)$$

$$w_s' = e^\mu w_r' \quad \text{(slope)} \qquad - 4(b)$$

$$M_s = e^\mu M_r \quad \text{(bending moment)} \qquad - 4(c)$$

$$S_s = e^\mu S_r \quad \text{(shear force)} \qquad - 4(d)$$

where, μ is the propagation constant.

The development of these equations can be found in (8) and will not be repeated in this paper. A closed form solution of the forced vibration of an infinite panel, excited by grazing incidence acoustic pressure is given.

The power spectral density of the displacement is given by the expression:-

$$S_w(\omega,k,x,y) = Y_w(\omega,k,x,y) Y_w^*(\omega,k,x,y) S_p(\omega,k) \qquad - (5)$$

where

$$Y_w(\omega,k,x,y) = \frac{1}{\rho_0}\left\{ \sum_{m=1}^{m=\infty} \left[\sum_{n=1}^{n=4} A p_{nm} e^{\lambda_n x} + \bar{w} e^{-ikx} \right] \sin \frac{m\pi y}{b} \right\} \qquad - (6)$$

is the acoustic admittance function of the displacement for the infinite panel.

In this work, which is concerned with the prediction of the r.m.s. stress, the acoustic admittance function of the curvature at a point (x,y) is the important parameter. This is given by:-

$$Y_w''(\omega,k,x,y) = \frac{1}{\rho_0}\left\{ \sum_{m=1}^{m=\infty} \left[\sum_{n=1}^{n=4} \lambda_n^2 A p_{nm} e^{\lambda_n x} - k^2 \bar{w} e^{-ikx} \right] \sin \frac{m\pi y}{b} \right\} \qquad - (7)$$

where, $''$ denotes differentiation twice with respect to x.

The mean square of the curvature $\langle w''^2 \rangle$ is given by:-

$$\langle w''^2 \rangle = \int_{-\infty}^{\infty} S_w''(\omega)d\omega = \int_{-\infty}^{\infty} |Y_w''(\omega)|^2 S_p(\omega) d\omega \qquad - (8)$$

The r.m.s. stress in the x-direction at a point (x,y) in the panel is given by:-

$$\bar{\sigma}(x,y) = \frac{6D}{h^2}\left[\left(\frac{\partial^2 w}{\partial x^2}\right)^2 + 2\eta \frac{\partial^2 w}{\partial y^2} \frac{\partial^2 w}{\partial x^2} + \eta^2 \left(\frac{\partial^2 w}{\partial y^2}\right)^2 \right]^{\frac{1}{2}} \qquad - (9)$$

where $\overline{\sigma}(x,y)$ = r.m.s. stress at point (x,y) in panel.

D = flexural stiffness = $Eh^3/12(1-\lambda^2)$

h = panel thickness.

$\dfrac{\partial^2 w}{\partial x^2}$ = curvature in x -direction.

$\dfrac{\partial^2 w}{\partial y^2}$ = curvature in y -direction.

λ = Poissons' ratio.

This expression has been applied to estimate the stress at the bay edge, and the result is shown in figure 8. The spectrum level of the excitation has been taken at 127.6 dB over the frequency range from 100 - 1,000 Hz so that comparison can be made with the calculated single mode response, assuming band limited white noise over that frequency range. A loss factor of 0.034 has been assumed.

6.3. MODAL ANALYSIS

With the normal mode procedure, it is possible to analyse a finite row of bays, whereas the methods of 6.1 and 6.2 were restricted to a typical bay or an infinite periodic row of bays respectively. Mercer and Seavey's transfer matrix programme (11) was used to obtain the natural frequencies and normal mode shapes of a finite, four bay skin/stringer panel assembly. It was assumed to be simply supported along its long sides and clamped at its short edges. The detailed development of the modal analysis is given in (12), and will not be repeated in this paper.

Following the usual procedure when handling normal modes, the displacement $w(x,y,t)$ of a point, (x,y), in the panel is given by:-

$$w(x,y,t) = \sum_{n=1}^{\infty} \sum_{m=1}^{\infty} q_{mn}(t) f_{mn}(x,y) \qquad -(10)$$

where, $f_{mn}(x,y)$ is the (m,n)th normal mode

$q_{mn}(t)$ is the (m,n)th generalised co-ordinate.

When the structure under consideration is a panel simply supported at its long edges

$$f_{mn}(x,y) = X_n(x) \sin \frac{m\pi y}{b} \qquad -(11)$$

where, $X_n(x)$ are arbitrary functions of x

b is the distance between the long sides (frames).

Assuming that the response occurs predominantly in the modes which exhibit one half-sine-wave between the frames, equation 10 can be written

$$w(x,y,t) = \sum_{n=1}^{4} q_n(t) f_n(x,y) \qquad -(12)$$

where the suffix $m = 1$ has been suppressed for simplicity of notation.

As before $S_w(\omega,k,x,y) = Y_w(\omega,k,x,y) Y_w^*(\omega,k,x,y) S_p(\omega,k)$ $\qquad -(13)$

Assuming that there is no wave number variation

$$S_w(\omega,x,y) = Y_w(\omega,x,y) Y_w^*(\omega,x,y) S_p(\omega) \qquad -(14)$$

Using the modal expression for $w(x,y)$ the response of the system is reduced to the response of a number of single degree-of-freedom systems.

Then the acoustic admittance function can be written as:-

$$Y_w(\omega,x,y) = \frac{w(x,y)}{P_o} = \frac{1}{P_o} \sum_{n=1}^{4} \frac{q_o \int_0^{4b} e^{-ikx} X_n(x) dx}{\pi \int_0^{4b} \rho h X_n^2(x) dx} X_n(x) \sin \frac{\pi y}{b} \qquad -(15)$$

Since we are interested in the r.m.s. stress at a point (x,y) in the panel, the mean square of the bending moment is the parameter required from the analysis.

This is given by:-

$$\langle M_x^2 \rangle = \int_{-\infty}^{\infty} S_{M_x}(\omega) d\omega = \int_{-\infty}^{\infty} Y_{M_x}(\omega) Y_{M_x}^*(\omega) S_p(\omega) d\omega \qquad -(16)$$

where $Y_{M_x}(\omega)$ is the acoustic admittance function for the bending moment and is obtained by differentiating $D Y_w(\omega)$ twice with respect to x, and adding $\lambda Y_w(\omega) D$ differentiated twice with respect to y.

Knowing the mean square of the bending moment the r.m.s. stress is:-

$$\langle \sigma_x^2 \rangle^{\frac{1}{2}} = \frac{6\langle M_x^2 \rangle^{\frac{1}{2}}}{h^2}$$

- (17)

where $\langle \sigma_x^2 \rangle$ is the mean square of stress in the x-direction.

h is panel thickness.

$\langle M_x^2 \rangle$ is mean square of bending moment in the x-direction.

These results have been applied to calculate stress levels in the specimen.

Calculations of the generalised force and mass for the first two modes indicated that their contribution to the r.m.s. stress in the panel could be neglected. Therefore, only modes 3 and 4 were considered, mode 4 dominating the response.

Figure 9 illustrates a typical plot of the power spectral density of the skin stress at the centre of the first stringer.

6.4. FINITE ELEMENT METHOD

The finite four by three bay array will be analysed using a finite element method developed at the Institute of Sound and Vibration, Southampton, by Dr. M. Petyt. At the time of writing the free vibration response is being calculated, it is hoped that the programme for the forced vibration response will be developed at I.S.V.R. before the completion of the contract.

7. CONCLUDING REMARKS

The test programme has suffered serious delays and few meaningful test results are available at the present time.

The loudspeaker tests at normal incidence have indicated a mode at 169 Hz, corresponding to all stringers bending. This compares well with the predicted value of 172 Hz using the E.S.D.U. Data Sheets (clamped edges).

The siren performance tests have shown that overall sound pressure levels over the specimen are satisfactorily constant.

During the discrete frequency loudspeaker tests, the damping of the structure was found to be between 1 and 2 per cent. A value of 1.7 was taken in the theoretical work.

It is expected that most of the test programme will be completed before presentation of the paper.

REFERENCES

1. R.G. White — Evaluation of the dynamic characteristics of structures by transient testing. J. Sound Vib, 15(2), 1971, pp 147-161.

2. T.F. Nelson — An investigation of the effects of surrounding structure on sonic fatigue. NASA CR-1536, May 1970.

3. Miles, J.W. — On structural fatigue under random loading. J. aeronaut. Sci. Vol. 21. No. 11 pp 753-762, November 1954.

4. Clarkson, B.L. — Stresses in skin panels subjected to random acoustic loading. J. aeronaut. Sci. November 1968.

5. Ballentine, J.R. et. al. — Refinement of sonic fatigue structural design criteria. Air Force Flight Dynamics Lab., Ohio, Tech. Rep. AFFDL-TR-67-156, November 1967.

6. Arcas, N. — Prediction of stress and fatigue life of acoustically excited aircraft structures. Shock and Vibration Bulletin, No. 39, part 3, January 1969, pp 37-

7. Mead, D.J. Sen Gupta, G. — Wave group theory applied to the response of finite structures. Proceedings of a conference held at the I.S.V.R., University of Southampton, England, 6-9th July 1970.

8. O'Keeffe, J. — Wave group theory, the solution of the free and forced vibration problems of a skin-stringer panel. Hawker Siddeley Aviation (Brough) Report YSR 270, May 1972.

9. Sgechenyi, G.A. — Approximate methods for determination of natural frequencies and normal modes of stiffened, flat and curved plates. Proceedings of a conference held at the I.S.V.R., University of Southampton, England, 6-9th July 1970.

10. Lin, Y.K. Donaldson, B.K. — A brief survey of matrix transfer techniques with special reference to the analysis of aircraft panels. J. Sound Vib, 10(1), 1969, pp 103-143.

11. Mercer, C.A.   Prediction of natural frequencies and normal modes of skin-stringer panel arrays.
    Seavey, C.   Institute of Sound and Vibration Research tech. Rep. 6, July 1968.

12. O'Keeffe, J.   Prediction of r.m.s. stress levels employing modal analysis techniques.
                     Hawker Siddeley Aviation (Brough) Report YSR 283.
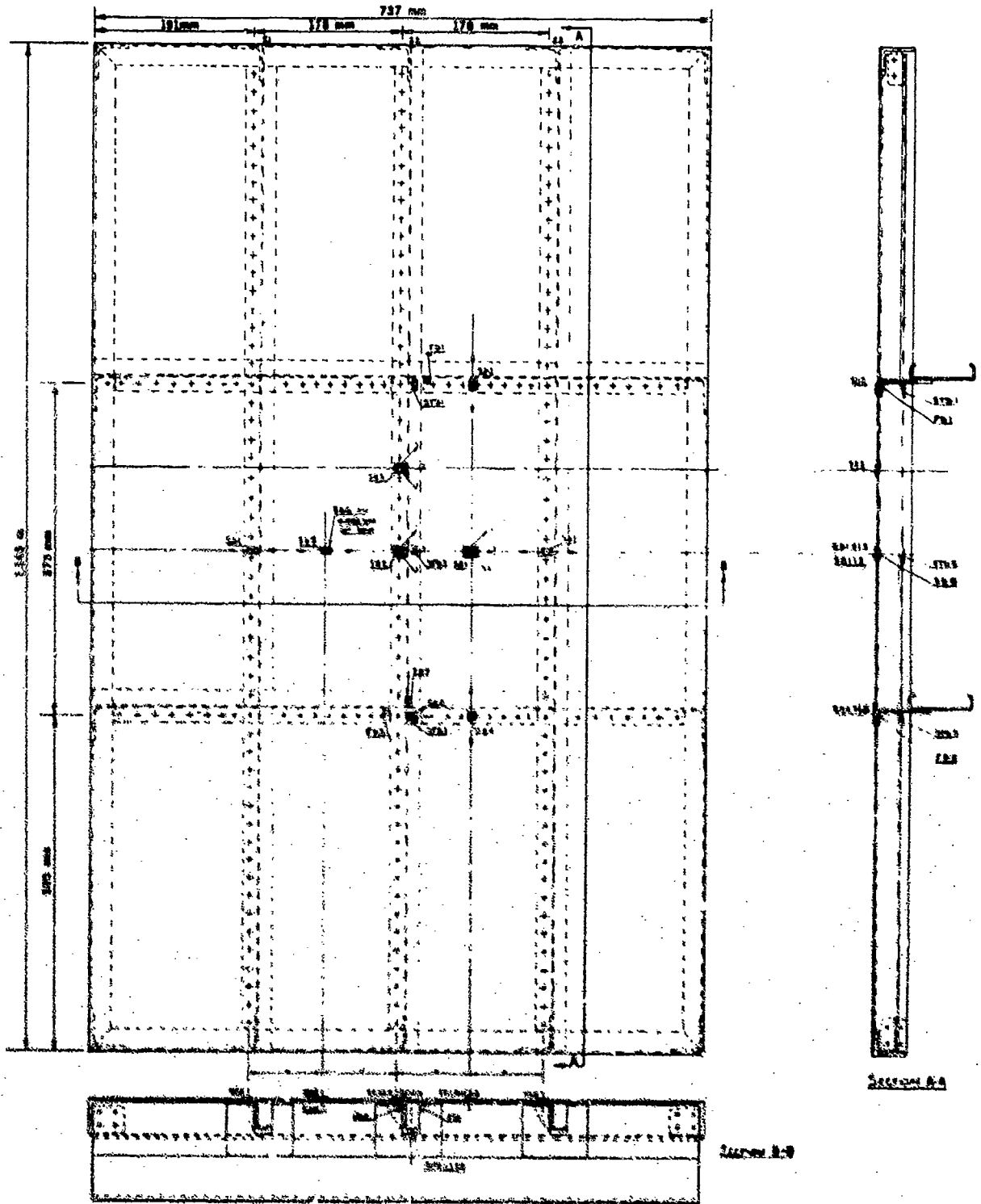
FIGURE 1   TEST SPECIMEN
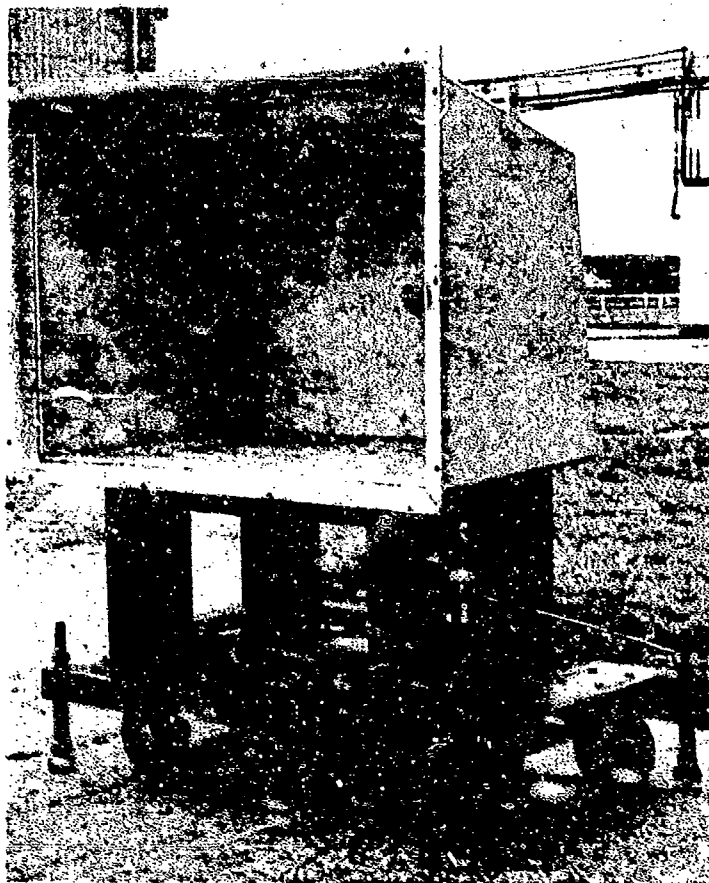
FIG. 2 TEST BOX

	1	2	3	4
A	162·3	162·0	162·8	163·3
B	161·2	159·7	160·0	160·0
C	160·8	159·4	159·3	159·8
D	161·2	161·3	160·0	161·3
E	160·3	160·3	160·3	160·0
F	160·2	159·5	160·1	160·1
G	162·0	161·0	161·4	162·0

FIG. 3 O.A.S.P.L. over working section for
maximum air and transducer conditions.

FIG.4   BAND LIMITED WHITE NOISE INPUT : MICROPHONE   POSITION: D3
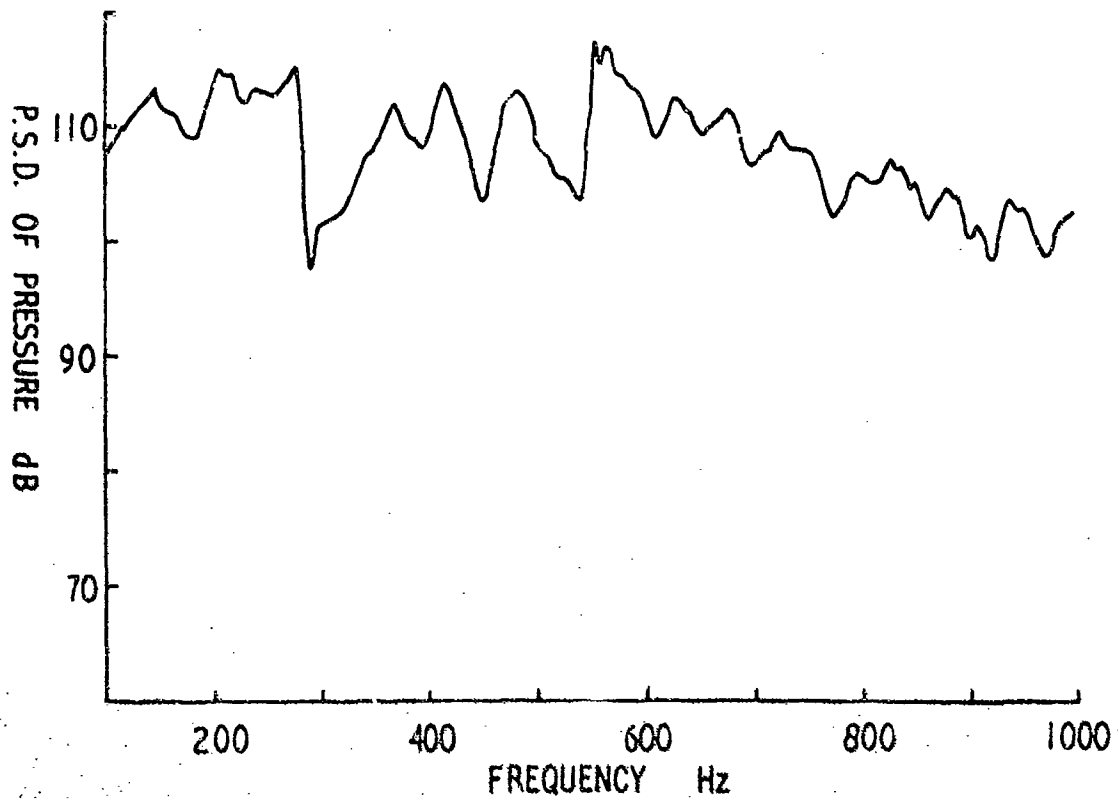
FIG.5   MEASURED FREQUENCY RESPONSE
NORMAL INCIDENCE
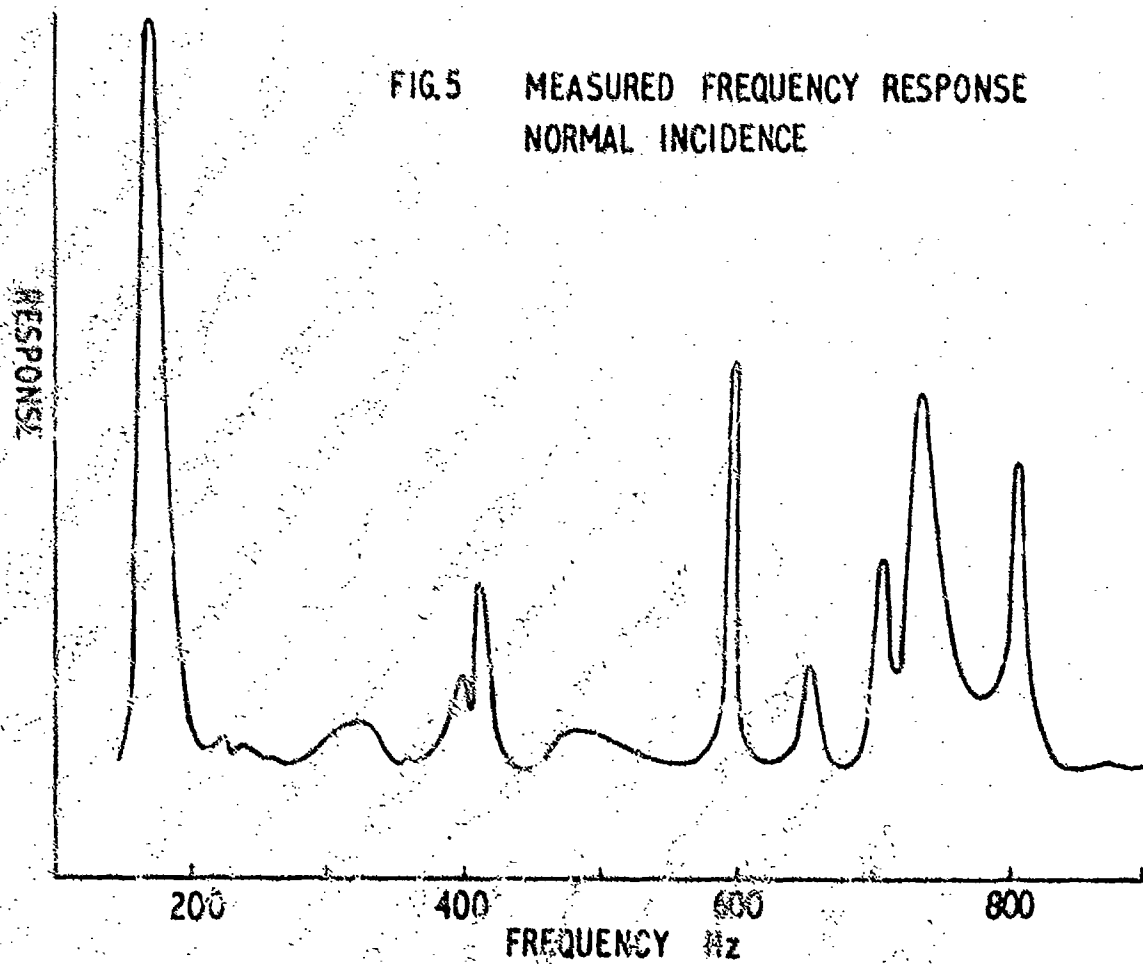
FIG.6 RESULTS OF VARIOUS THEORETICAL METHODS

METHOD	Bay centre r.ms. stress	Bay edge r.ms. stress
Clarkson	40.0 MN/m^2	81.0 MN/m^2
Ballentine	21.0 MN/m^2	41.4 MN/m^2
Arcas	52.5 MN/m^2	80.0 MN/m^2
Wave group	37.3 MN/m^2	78.0 MN/m^2
Modal response	43.5 MN/m^2	61.4 MN/m^2

γ_p = loss factor of plate
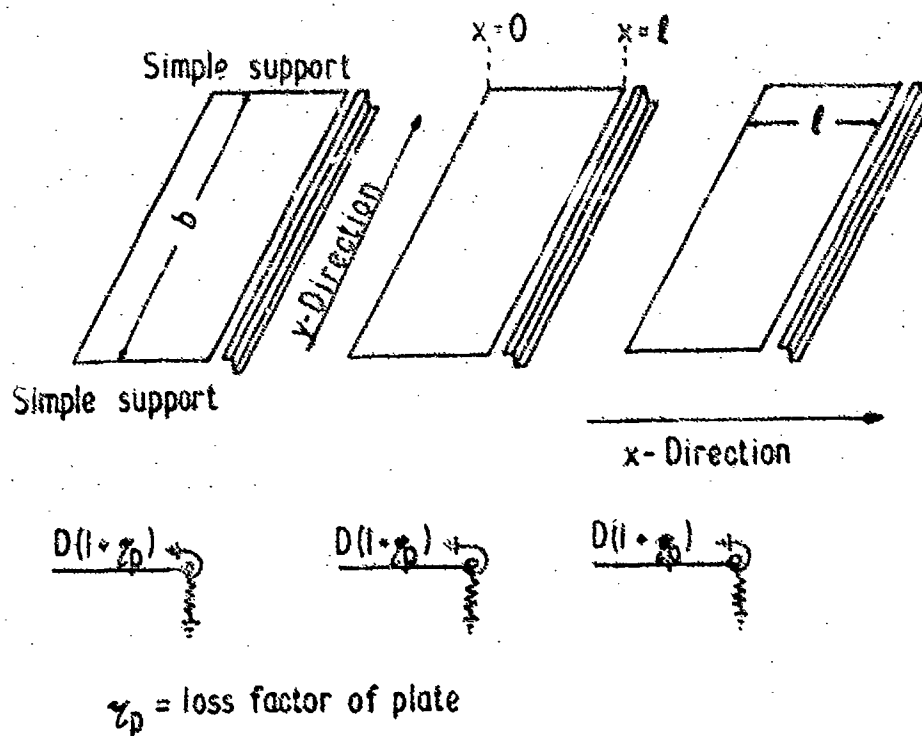
FIG.7 STRUCTURAL IDEALIZATION

FRAMES ACT AS CLAMPED SUPPORTS

FIG.8 SKIN STRESS, WAVE GROUP THEORY

FIG.9 SKIN STRESS, MODAL ANALYSIS
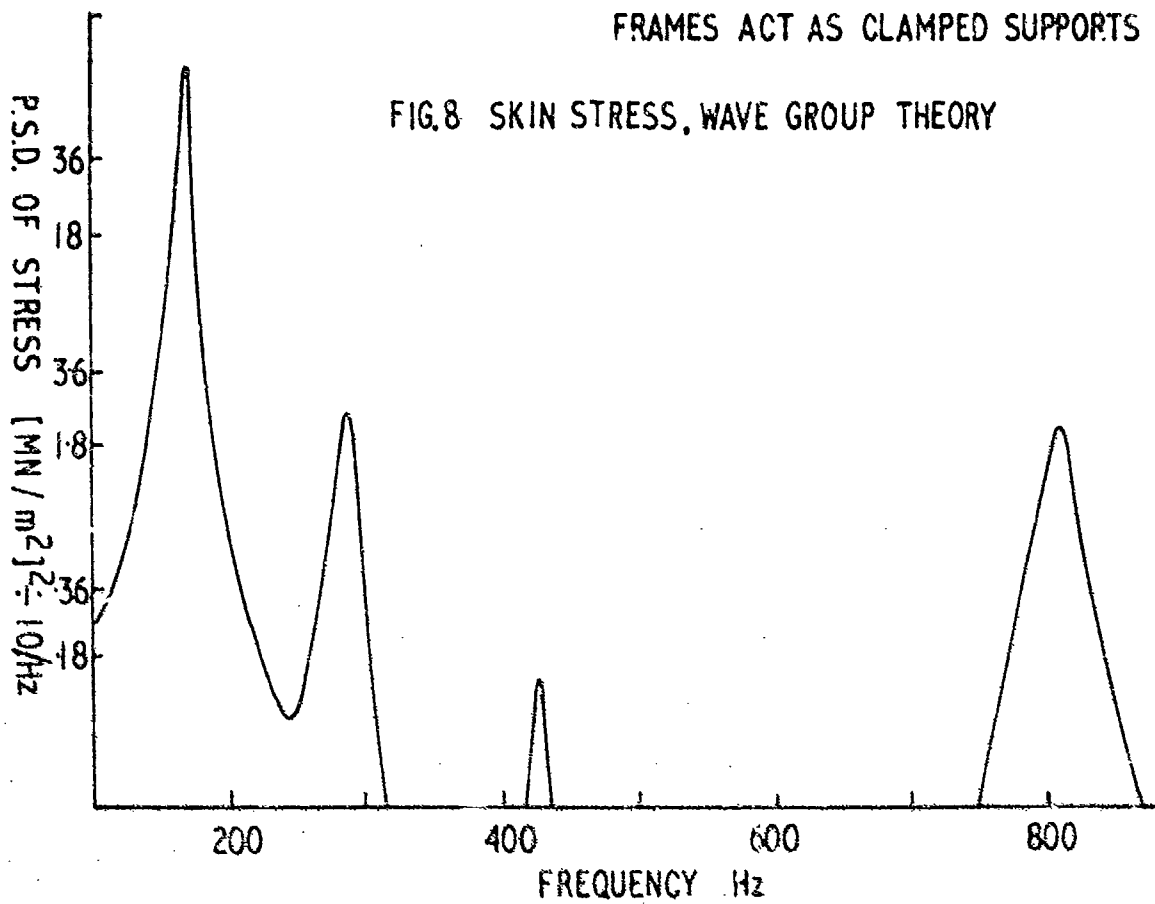
THEORY ASSUMES THAT FRAMES ACT AS SIMPLE SUPPORTS
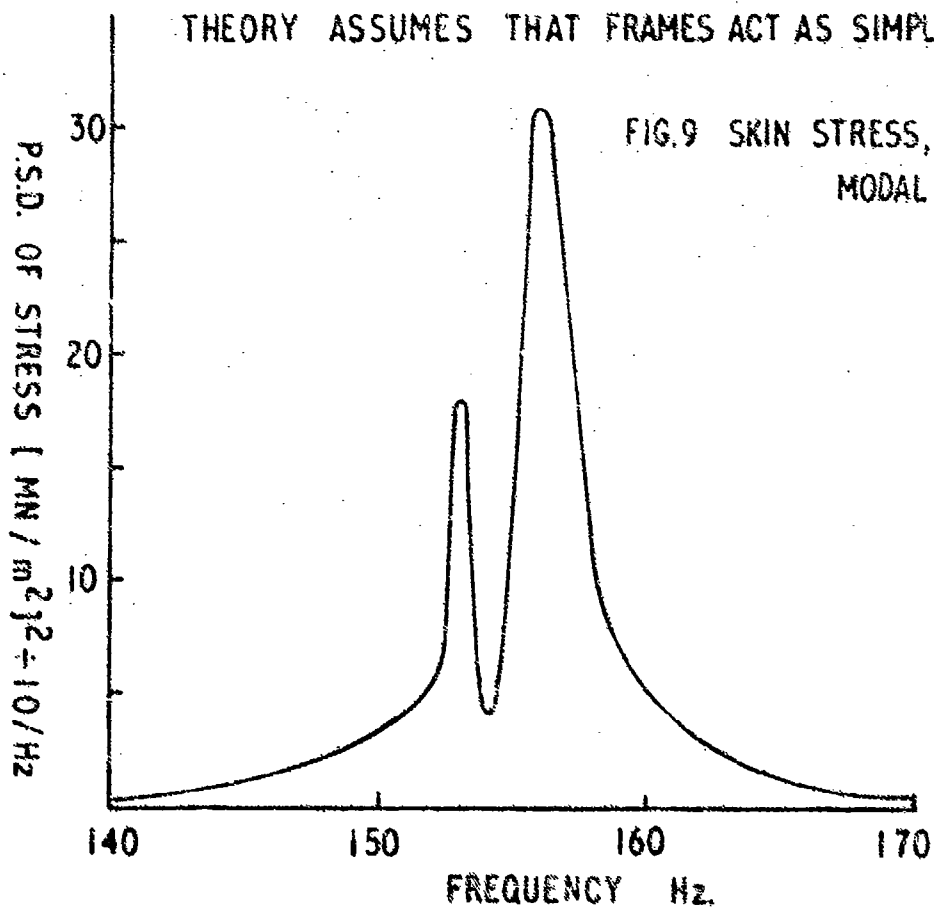
APPENDIX

1. INTRODUCTION

In the period between writing and presenting the paper, additional work was completed on the theoretical prediction of panel response, and on its measurement in the noise field of a jet engine exhaust. Some of this material was presented at the Symposium and is repeated in this appendix.

2. THEORETICAL RESPONSE PREDICTIONS

2.1 Finite Element Method

The free vibration response has been predicted. In the first analysis, each of the twelve bays or sub-panels was divided into a 3×3 array of rectangular plate elements. At each node the displacement w and its derivatives w_x, w_y, w_{xy}, were taken as degrees of freedom. The stiffeners were represented by open section beam elements with two node points, one at each end. The degrees of freedom at each node were taken to be the displacement w, the slope θ, and their first derivatives w_x, θ_x. Each frame was represented by twelve elements and each stringer by nine elements. The external boundaries of the panel were taken to be fully clamped. The natural frequencies obtained are given in Figure A1. Since the stiffeners divide the panel into twelve sub-panels the frequencies occur in groups of twelve, and only the first two groups are presented. The mode shapes obtained indicate that the coupling across the frames is negligible. In the table, modes denoted by an asterisk involve motion in the middle array of sub-panels only. The other modes involve motion in one of the outside arrays only.

The middle array only was then analysed assuming the boundaries to be fully clamped. Each sub-panel was represented by a 4×4 array of rectangular elements, and each stringer by four open section beam elements. The frequencies obtained are given in Figure A2. The mode shapes for the modes with one half sine wave between frames are shown on Figure A3.

The analysis indicated that each array of sub-panels between two frames vibrates independently of the neighbouring arrays, and the frames act as clamped supports. However, because there are a large number of close natural frequencies several modes will appear to respond simultaneously giving the impression that there is strong coupling across the frames. It should be noted that the effect of the finite width of frames and stringers has not been considered.

2.2 Transfer Matrix Method

In addition to the method of Reference 11 a method of normal mode prediction due to Wittrick and Williams has been employed (Williams F W Computation of natural frequencies and initial buckling stresses of prismatic plate assemblies J Sound Vib Volume 21, 1972 pp 87-106). This uses an exact method of analysis to find the natural frequencies of a structure consisting of a set of thin rectangular flat plates of uniform thickness which are rigidly connected together along their longitudinal edges. The panel is assumed to be simply supported at the frames. The frequencies obtained are given on Figure A4.

3. EXPERIMENTAL RESULTS

3.1 Discrete Frequency Measurements

Initially the panel was subjected to sinusoidal acoustic excitation, sweeping slowly through a frequency range from 150 Hz to 500 Hz to obtain its natural frequencies. This was done with the direction of sound propagation parallel and normal to the stringers. The results are shown on Figure A4.

3.2 Engine Noise Tests

The response of the panel has been measured at several positions, and at two engine power settings, in the noise field of a jet engine exhaust, both in the side of the test box shown in Figure 2, and in a simple frame. The frequency bands, in which peaks in the skin response occurred, are shown in Figure A4. Those for the panel in

the simple frame are shown shaded across the table so that a comparison with predicted values can be made. Values of frequency are spotted on a vertical logarithmic scale in the table. During these tests the panel was placed about six feet from the estimated edge of the exhaust jet, in a vertical plane parallel to the jet axis with stringers horizontal.

Initial discrete frequency tests indicated the need to reduce the reverberation time of the box and to this end a 300 mm thickness of 'Stillite' sound absorbent material was attached to the rear wall of the cavity. In this configuration, the overall sound pressure level measured by a microphone inside the box during engine noise tests at maximum r.p.m. was found to be approximately 15 dB lower than that measured by an external microphone at the trailing edge of the panel.

Results indicate that the box has a significant effect upon panel response. Figure A5 gives a comparison of predicted and measured overall stress levels, the former assuming the measured noise spectrum to be acting on one side of the specimen. Position 1 is ten jet pipe orifice diameters downstream of the orifice, and positions 2 and 3 are twenty and thirty diameters respectively. Measured overall sound pressure levels and the band level in the one third octave centred on 160 Hz are also given. Overall levels of stress and sound pressure level are for 0–10 KHz.

Figure A6 shows the power spectral densities of a typical skin stress, measured during excitation under identical conditions with and without the test box. The stress is the direct skin stress, at the bay edge midway between frames, measured by gauge SR2 (see Figure 1). The power spectral densities of the direct skin gauges analysed to date are similar.

The reason for constructing the test box was to provide a means of reducing the overall level of excitation on the rear face of the specimen during engine noise tests to the level which it would experience in the subsequent siren tests. In view of the apparent effect of the box cavity upon the panel response, further testing in the siren and in engine noise fields, under this contract, will probably be carried out with the panel in a simple frame. It is hoped to be able to study the implications of cavity effects upon the design of skin panels forming a side of a cavity in the near future.

4. REMAINING WORK PROGRAMME

Before it is attempted to reproduce the engine noise field response in the siren, the acoustic radiation damping of the panel in the siren will be measured, and a search made for the presence of duct resonances. Finite element theory will be used to predict specimen response. It is felt that the data gathered and experience gained will lead to a greater understanding of the uses and limitations of siren testing techniques.

Mode No.	Frequency	Mode No.	Frequency
1	166.6*	13	220.0*
2	167.5	14	220.1*
3	167.5	15	222.6
4	168.0*	16	222.6
5	169.3	17	222.7
6	169.3	18	222.7
7	180.0*	19	230.7*
8	180.7	20	230.8*
9	18 7	21	233.1
10	181.0*	22	233.1
11	181.7	23	233.3
12	181.7	24	233.3

* Middle array modes

FIGURE A1 – NATURAL FREQUENCIES (Hz) OF THE COMPLETE PANEL

Mode No.	Frequency	Mode No.	Frequency
1	164.5	5	218.1
2	166.9	6	218.4
3	177.7	7	228.6
4	178.7	8	228.8

FIGURE A2 – NATURAL FREQUENCIES (Hz) OF THE MIDDLE ARRAY

MODE 1

MODE 2

MODE 3

MODE 4
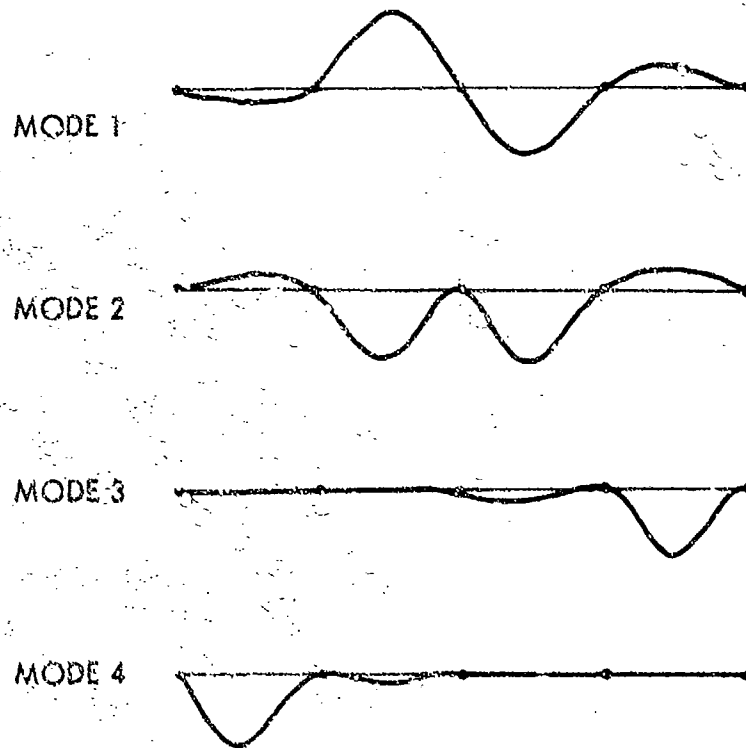
FIGURE A3 – MODE SHAPES FOR A SINGLE ARRAY OF FOUR SUB PANELS

Predicted Frequencies					Measured Frequencies			
		Transfer Matrix Method			Discrete Tests		Engine Noise (Parallel to Stringer)	
Single Bay	Wave Group Theory	Mercer, Seavey	Wittrick, Williams	Finite Elements (Fatyt)	Parallel Stringer	Normal Stringer	Panel Alone	Panel In Box
			• 124					
		• 131						
		• 141	• 140				• 140	• 140
• 155	• 155	• 153 • 156					• 160	• 160
• 165 (3)			• 160	• 164 • 167	• 169	• 169	• 170 • 175	
	• 175		• 170	• 178 • 179				
							• 190	• 190
					• 200	• 200	• 200	
					• 210	• 210	• 210 • 215	
				• 218 (2)	• 225			
				• 229 (2)		• 230	• 240	• 230
	• 275 • 285							
						• 305	• 300	
						• 350	• 375	
					• 380	• 375		• 380
								• 420

FIGURE A.4 COMPARISON OF PREDICTED AND MEASURED NATURAL FREQUENCIES

		Predicted Stress MN/m^2					Measured Stress MN/m^2	
		Clarkson	Ballentine	Arcas	Wave Group Theory	Modal Analysis	Panel Alone	Panel In Box
Pos. 1	Bay Centre	14.47	7.23	16.53	13.10	12.40	7.02	3.86
	Bay Edge	28.60	14.48	31.0	28.22	17.21	10.68	6.20
Pos. 2	Bay Centre	25.45	12.73	27.55	24.08	21.38	10.74	5.85
	Bay Edge	51.0	25.47	55.10	50.30	31.0	14.13	8.52
Pos. 3	Bay Centre	6.41	3.44	7.24	5.92	5.51	1.93	1.64
	Bay Edge	13.09	6.54	14.47	12.40	7.58	2.27	1.65

	Measured S.P.L. [*]	
	O.A.S.P.L. dB	Band Level dB
Pos. 1	148	119
Pos. 2	148	12?
Pos. 3	139	112

* re. 2×10^{-5} N/m^2

FIGURE A5 - PREDICTED AND MEASURED OVERALL STRESS LEVELS
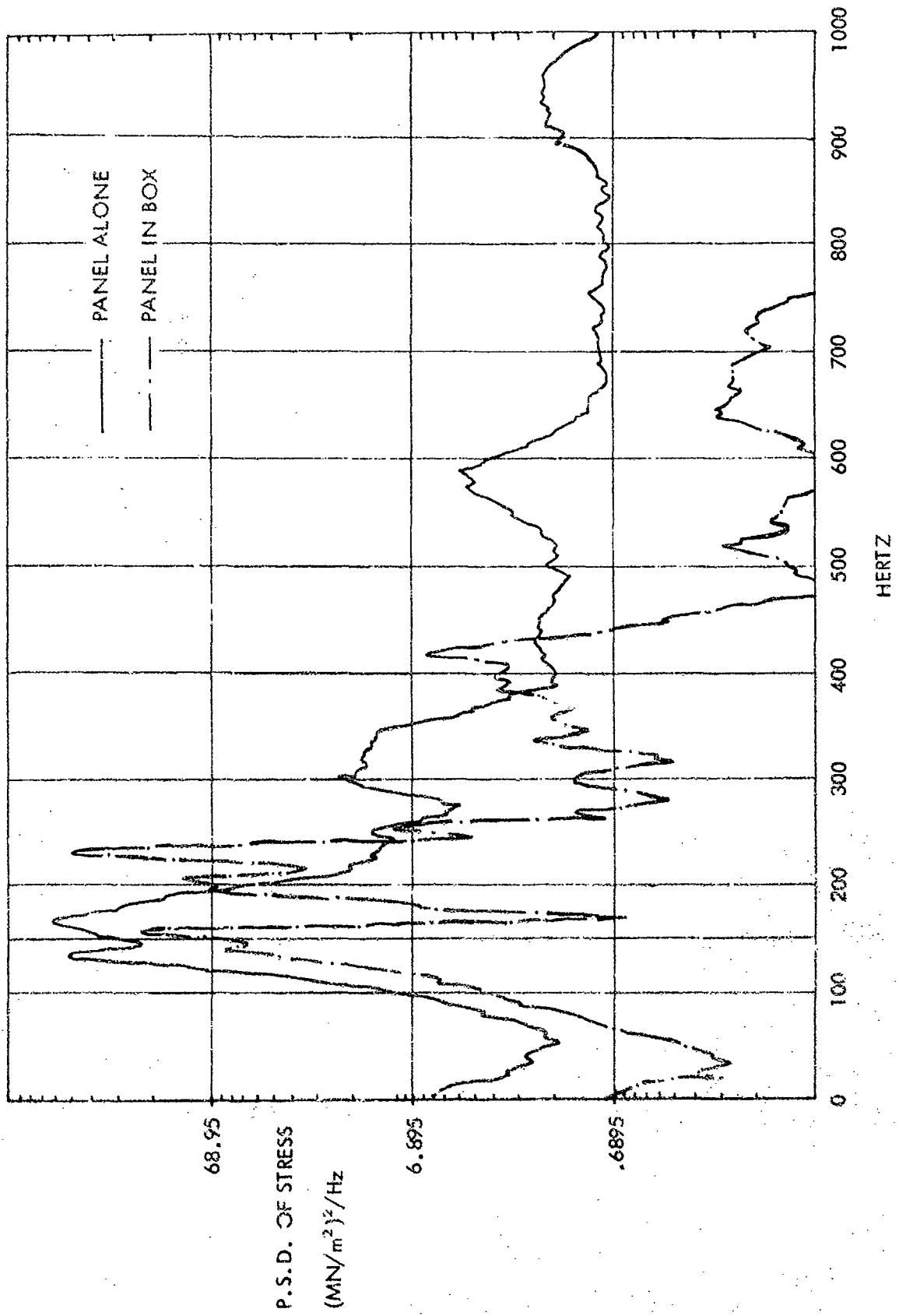
FIGURE A6 – SKIN DIRECT STRESS (GAUGE SR2) – FREQUENCY RESPONSE

SONIC FATIGUE RESISTANCE OF LIGHTWEIGHT
AIRCRAFT STRUCTURES

by

R. C. W. van der Heyde

and

A. W. Kolb

Air Force Flight Dynamics Laboratory (FYA)
Wright-Patterson Air Force Base, Ohio 45433
U.S.A.

SUMMARY

This paper presents results from an experimental program under which the response and sonic fatigue resistance of lightweight aircraft structures were investigated. The program involved a series of aluminum-alloy panels of bonded-beaded and skin-stringer design. A total of 60 bonded-beaded and 60 skin-stringer type test specimens was investigated. The panels were tested in groups of 5 or 10 at 4 different overall sound-pressure levels to obtain test results with a high level of confidence. The data reported include mode shapes, panel damping ratios, linearity of response, fatigue life, and failure location. For some panel configurations, data to above 10^8 cycles were obtained. The test facility, test fixture, noise source, testing technique, and instrumentation used, are described along with the test results. Fatigue failure detection techniques are discussed. The test results are compared with stress predictions from various available methods.

LIST OF SYMBOLS

A   = Assurance

E   = Young's Modulus

f   = Frequency at Resonance

KE   = Ratio of Measured to Estimated Stress

KL   = Ratio of Measured Life to Estimated life

N   = Number of Specimens in Sample

R_{xy} = Correlation Factor Between ϵ_x and ϵ_y

β = Specified Proportion

δ = Damping Ratio

Δf = Bandwidth

The following symbols are used for rosette strain gage data:

ϵ_1 = Measured Static Strain in 0° Direction

ϵ_2 = Measured Static Strain in 90° Direction

ϵ_3 = Measured Static Strain in 45° Direction

$\bar{\epsilon}_1$ = Measured Dynamic RMS Strain in 0° Direction of Strain Gage

$\bar{\epsilon}_2$ = Measured Dynamic RMS Strain in 90° Direction of Strain Gage

$\bar{\epsilon}_3$ = Measured Dynamic RMS Strain in 45° Direction of Strain Gage

$\sigma_{m.x}$ = Maximum Principal Static Stress lbs/in²

$\bar{\sigma}_{max}$ = Maximum Principal RMS Dynamic Stress lbs/in²

μ = Poisson's Ratio

INTRODUCTION

The sonic fatigue failures which occurred on aircraft in the late 1950 time period required the development of techniques to deal with the problem on a broad basis. Numerous investigations were initiated to study the mechanisms which cause sonic fatigue and ways to obtain practical solutions to prevent sonic fatigue failures. Design criteria for many types of structures were developed under U.S. Air Force sponsorship and by Industry. Some of the most important advances are listed in References 1 and 2. These efforts led to sonic fatigue design criteria and design charts which are widely used during the design of aircraft. In general, this information enables the designer to select structural design parameters which result in conservative lightweight structures capable of withstanding the noise levels generated by the powerful jet engines presently in operation. The development of new structural concepts and materials requires continuous updating of sonic fatigue design information. At the same time, existing design data require further refinement and verification. The effort described in this paper falls primarily in the latter category.

The tests described differ from the majority of tests conducted to establish sonic fatigue design information in two ways; first, a large test specimen sample size was used, and second, the duration of the testing was long. While most acoustic test facilities accommodate only one or two specimens at a time the arrangement selected for these tests allowed 5 to 10 panels to be tested simultaneously. This was accomplished by a multiple test panel installation in a large fixture and selecting normal incidence acoustic loading for the test program. This procedure made it possible to test some of the 120 specimens up to 200 hours which is in excess of 10^8 cycles for these panels.

The specimens reported on can be classified in two groups. The first group, bonded-beaded Types I, II and III and skin-stringer Type I consisted of a design with a weight per area of 1 lb/ft^2 and overall dimensions of 24 X 30 inches. The second group of specimens, skin-stringer Type II, featured a thin chem-milled skin with a stiff supporting structure, a weight per area of 3.65 lbs/ft^2 and overall dimensions of 10.5 X 24 inches. This design was used to develop statistical information for sizing of sonic fatigue test samples (Reference 3). While the latter type of panel design is not necessarily typical of an aircraft structure the test data were included since they contribute to the knowledge of sonic fatigue behavior of heavily reinforced chem-milled panels and allow for an additional comparison with prediction methods.

The qualitative and quantitative information presented in this paper can be used as design guidelines and backup information for structures with similar characteristics.

DESCRIPTION OF THE TEST SPECIMENS

Table I presents a summary of the panels tested and their essential dimensions in inches. All specimens were manufactured from standard aircraft materials; their designation and corresponding equivalents used in NATO countries are tabulated in Table II. The bonded-beaded panels Types I, II and III and the skin-stringer panels Type I had the same overall dimensions and weight and were constructed of 7075 T-6 aluminum alloy. The skin-stringer panels Type II were of different weight and dimensions and were constructed of 2024 T-3 aluminum alloy. For the bonded-beaded panels (Figure 1 and Figure 2) only limited sonic fatigue design information was available. Therefore, three designs were tested. These designs included variations in bead length, bead orientation and bead-skin thickness. Consequently the results from the three designs indicate the effect of these parameters on the response and fatigue life of the panel.

TABLE I

CONFIGURATIONS OF THE TEST SPECIMENS

STRUCTURAL PANEL DESIGN	SPECIMEN SIZE INCH	ALUMINUM ALLOY	PANEL SKIN THICKNESS INCH	BEAD SKIN THICKNESS INCH	BEAD HEIGHT INCH	BEAD WIDTH INCH	BEAD LENGTH INCH	NR BEADS	NR SPEC	FIG NR
BONDED-BEADED										
TYPE I	24 X 30	7075 T-6	.032	.032	.80	3.5	21.0	6	20	1
TYPE II	24 X 30	7075 T-6	.020	.045	.80	3.3	21.0	6	20	1
TYPE III	24 X 30	7075 T-6	.032	.032	.80	3.5	37.0	5	20	2
SKIN-STRINGER				STRINGER WEB THICKNESS INCH	STRINGER HEIGHT INCH		NR STRINGERS			
TYPE I	24 X 30	7075 T-6	.032	.040	2.00		2	20	3
TYPE II	24 X 10.5	2024 T-3	.023	.75	.75		4	40	4

TABLE II DESIGNATION FOR U.S. AND SIMILAR FOREIGN ALLOYS[a]

U.S.A. AA	Canada CSA	France	Germany DIN Werkstoff-Nr	Great-Britain B.S. DTD	Italy	ISO
2024	ZC6S	A-Z4GU	AlZnMgCu1.5 3.4365	L.95 L.96		AlZn6Mg-Cu
7075	CG42	A-U4G1	AlCuMg2 3.1355	L.97 L.98	5090	P-AlCu 4.5 -MgMn	AlCuMg1

a Ref. "Aluminum Standards and Data", second edition, Dec 1969 published by Aluminum Association.

The skin-stringer panels Type I (Figure 3) were of a conventional design frequently used in aircraft construction. It should be noted, however, that no sealing or antifretting compounds were used in the rivet joints and therefore an allowance for this fact should be made in the comparison of the test results with panels constructed with these compounds.

Figure 4 shows the skin-stringer panels Type II. In the construction of these panels a chem-milling process was used to obtain the material thickness variations incorporated in the design. The reinforcing structure was riveted to the skin material as shown in Section A-A of Figure. No sealing or antifretting compounds were used in joining the skin to the support structure. The skin-stringer panels Type II had slots of .37 inches cut into each side of the center bay. Preliminary tests indicated that these stress concentrations were necessary to fail the panels with the available noise sources. The test group size was chosen according to the statistical theories developed in References 3 and 4. In these references it is shown that the requirements for statistical confidence may be stated as:

$$A = 1 - N\beta^{N-1} + (N - 1)\beta^N$$

Where A is the degree of assurance that at least 100β per cent of an infinite number of specimens will fail between the longest and shortest failure times encountered in a sample size N. This analysis shows that a sample size of five (5) gives an assurance of 80% that at least 50% of the obtained data fall within these limits.
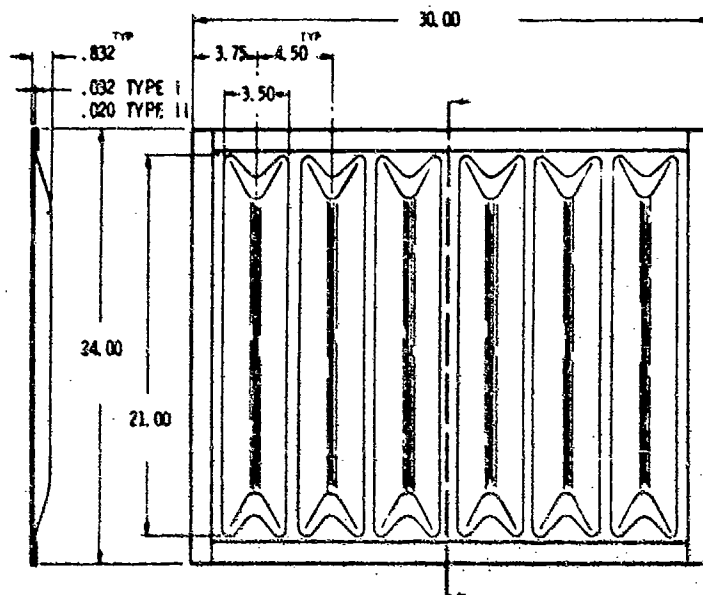
FIGURE 1. BONDED-BEADED PANEL
TYPE I AND TYPE II
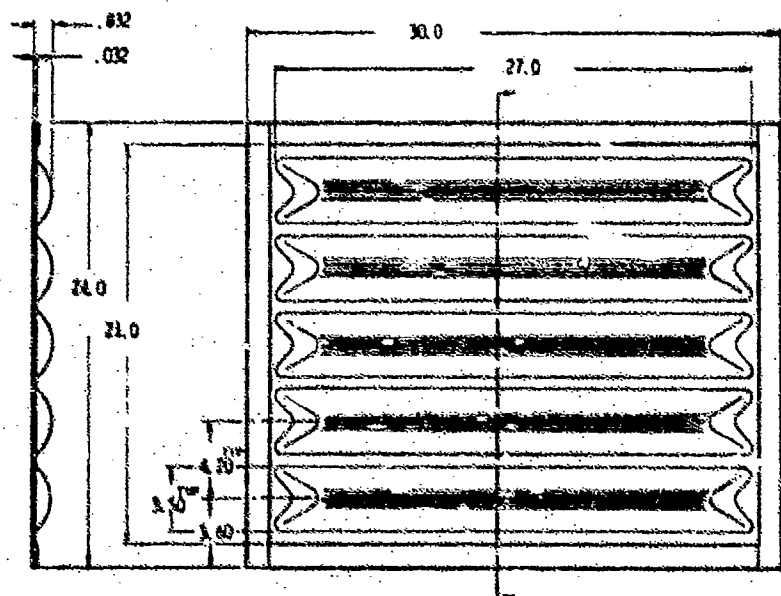
FIGURE 2. BONDED-BEADED PANEL
TYPE III
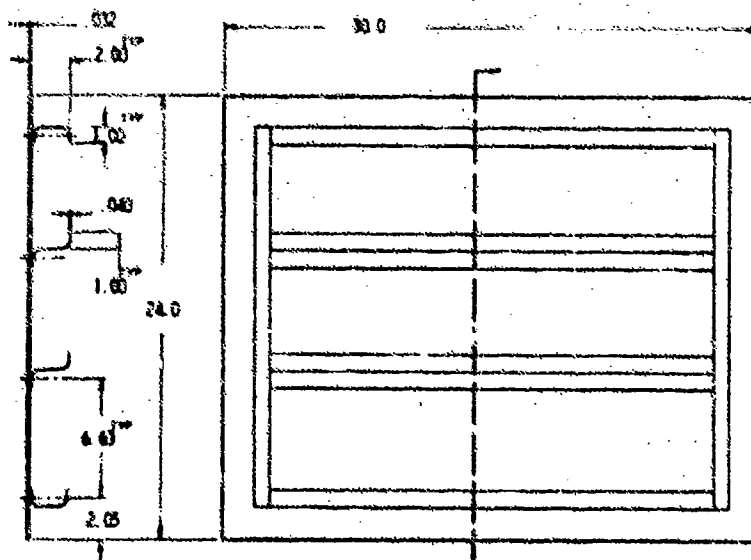
FIGURE 3. SKIN-STRINGER PANEL
TYPE I
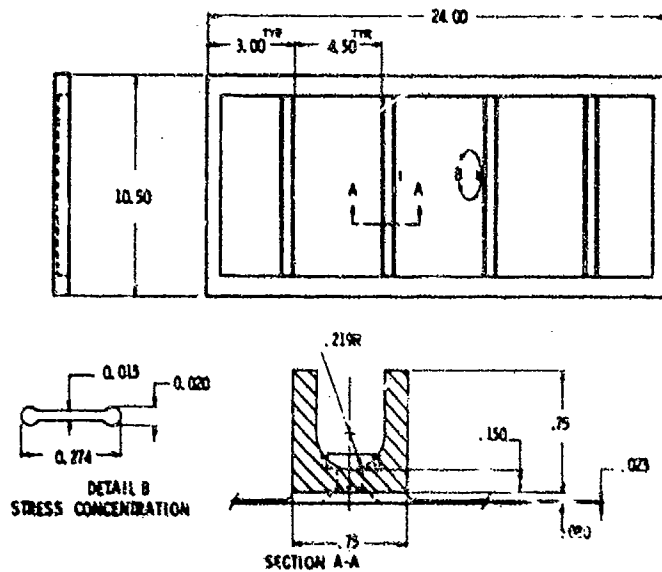
FIGURE 4. SKIN-STRINGER PANEL
TYPE II

TEST FACILITY AND INSTRUMENTATION

The test program was conducted in the Wide Band Noise Test Chamber of the AFFDL Sonic Fatigue Facility which contains a reverberant chamber with a floor area of 231 ft^2 and a volume of approximately 2500 ft^3 (Figure 5). Two high intensity noise sources were used, an air-modulating-valve-type sound-generator delivering sound-pressure levels up to a maximum of 165 dB overall, and a random noise siren which produces a maximum SPL of 160 dB, with a broader sound spectrum.
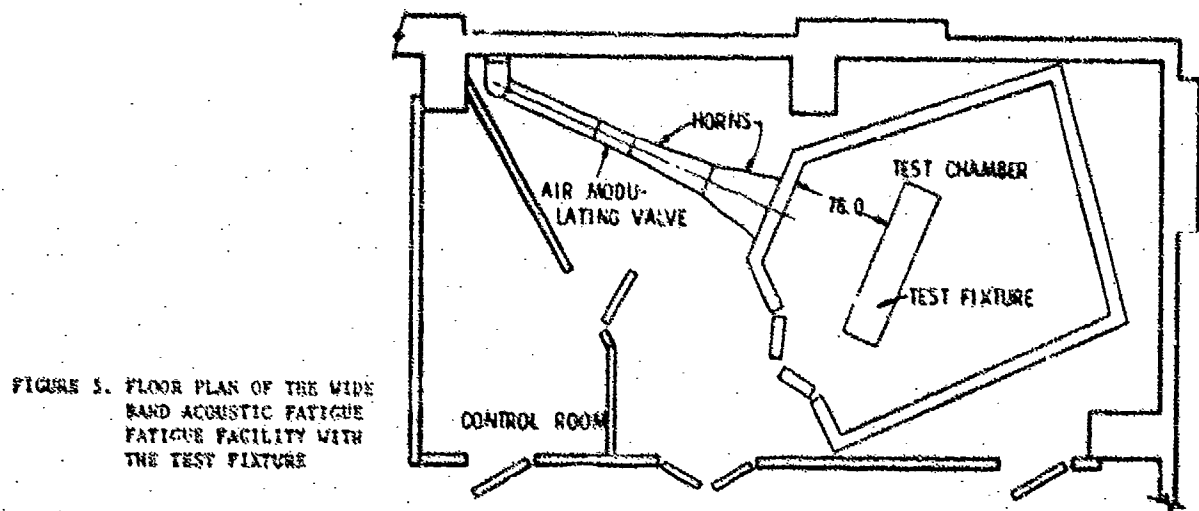
FIGURE 5. FLOOR PLAN OF THE WIDE
BAND ACOUSTIC FATIGUE
FATIGUE FACILITY WITH
THE TEST FIXTURE

The test panels were rigidly mounted in the front of an enclosed steel fixture (Figure 6). This test fixture contained sound absorbing material to prevent standing waves. Access to the rear of the specimens was provided by removable covers. By proper positioning of the fixture, the overall sound pressure level over the test specimens was within ± 1 dB.
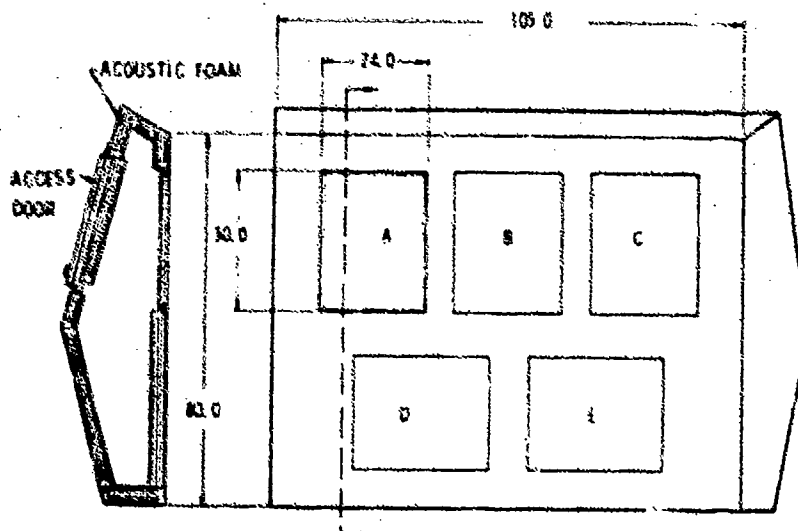
FIGURE 6. TEST FIXTURE

The noise levels were measured with high intensity microphones located 4 inches in front of each test specimen. The strain was measured with rosette strain gages and single element gages (Figure 7). The output from all transducers was recorded on magnetic tape.
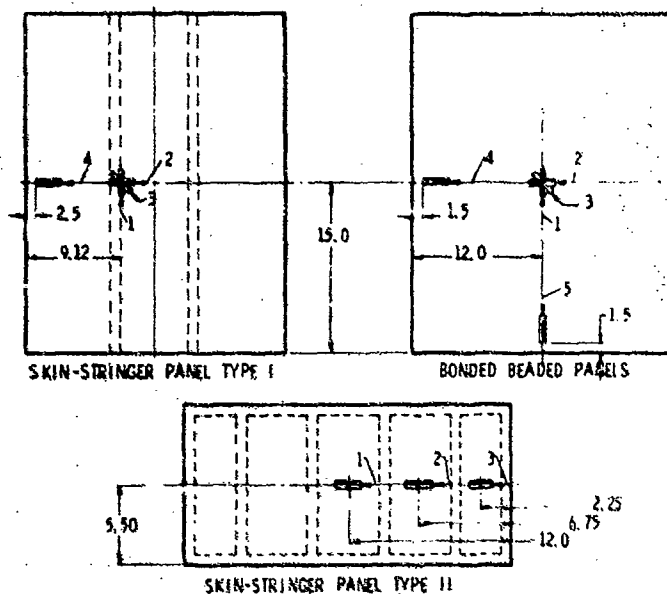
FIGURE 7. STRAIN GAGE LOCATIONS

SKIN-STRINGER PANEL TYPE I

BONDED BEADED PANELS

SKIN-STRINGER PANEL TYPE II

Figure 8 shows a block diagram of the data collection and monitoring system. The microphones and strain gages were monitored before and after recording on tape by means of an oscilloscope and/or octave-band level recorder.
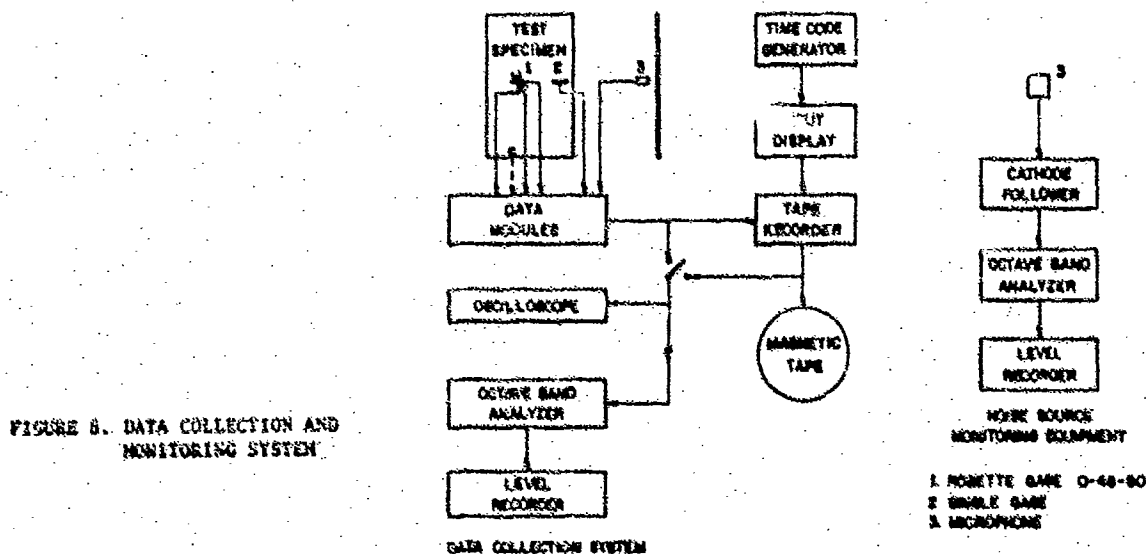
FIGURE 8. DATA COLLECTION AND MONITORING SYSTEM
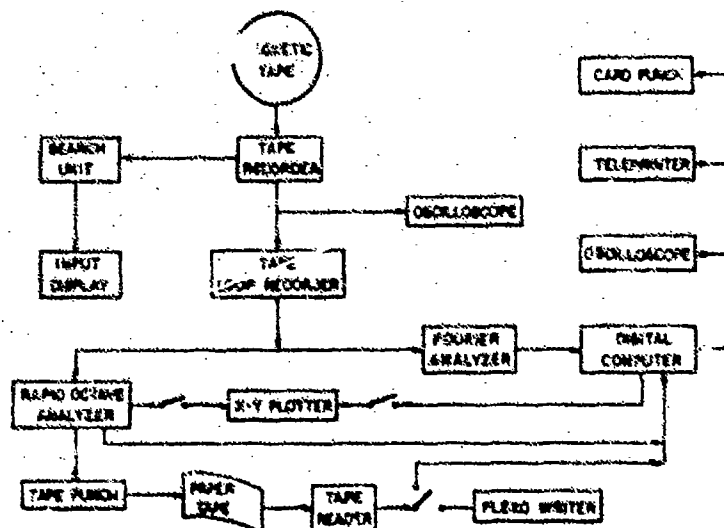
FIGURE 9. DATA REDUCTION SYSTEM

The noise produced by the sound-generator was continuously monitored by an octave band analyzer and periodic recordings were made on a level recorder.

The data recordings were transferred to a tape loop and analyzed with the equipment shown in Figure 9. The Rapid Octave Band Analyzer (B&K P297) was used to obtain 1/3 and 1/1 octave band analyses. The Fourier Analyzer (HP 5450A) was used for time series analysis of the acoustic and strain signals.

TEST AND DATA ANALYSIS PROCEDURE

Groups of five identical panels were tested in the acoustic chamber with the exception of the skin-stringer panels Type II which were tested in groups of 10. One panel of each type was mounted horizontally in a special rig and excited by loudspeaker for low level response tests to determine mode shapes and natural frequencies. The mode shapes were made visible by covering the panel surface lightly with sand. The modal patterns at the resonant frequencies were sketched or photographed. For the skin-stringer panels Type I, however, the mode shapes were determined with the specimen mounted in the test fixture. This was accomplished by attaching one accelerometer to the specimen and surveying the panel with a second accelerometer. The amplitude and phase angle of the signal from the moving accelerometer was measured relative to the stationary accelerometer.

For the dynamic linearity test one panel was mounted at location B of the large test fixture (Figure 6) and subjected to a range of overall sound pressure levels from 130 to 157 dB. After the set of 5 panels was installed, initial data were obtained from all transducers at a specified sound pressure level. These data were used to determine all response and damping information.

The damping ratios were computed from the equation $\delta = \Delta f/2f$, where f is the frequency at resonance, and Δf the width of the resonance peak at the 1/2 power point.

A rosette strain gage was placed on the facing sheet of the panel in order to obtain an approximation of the principal stress. This allows the determination of maximum stress since directionality variations are accounted for. The rms version of the following stress equation was used (References 5 and 6):

$$\sigma_{max} = \frac{E}{2}\left\{\frac{\epsilon_1+\epsilon_2}{1-\mu} + \frac{\sqrt{(\epsilon_1-\epsilon_2)^2 + [2\epsilon_3-(\epsilon_1+\epsilon_2)]^2}}{1+\mu}\right\} = \frac{E}{2}\left\{\frac{\epsilon_1+\epsilon_2}{1-\mu} + \frac{C}{1+\mu}\right\}$$

From which, in terms of RMS, follows:

$$\bar{\sigma}_{max} = \frac{E}{2}\left\{\frac{(\overline{\epsilon_1+\epsilon_2})^2}{(1-\mu)^2} + \frac{\bar{C}^2}{(1+\mu)^2} + \frac{2(\overline{\epsilon_1+\epsilon_2})\bar{C}}{1-\mu^2}\right\}^{\frac{1}{2}}$$

In which:

$$\bar{C} = \left\{\bar{\epsilon}_1^2 + \bar{\epsilon}_2^2 - 2R_{1,2}\bar{\epsilon}_1\bar{\epsilon}_2 + 4\bar{\epsilon}_3^2 - 4R_{1,3}\bar{\epsilon}_1\bar{\epsilon}_3 - 4R_{2,3}\bar{\epsilon}_2\bar{\epsilon}_3 + (\overline{\epsilon_1+\epsilon_2})^2\right\}^{\frac{1}{2}}$$

$$R_{x,y} = \frac{(\overline{\epsilon_x+\epsilon_y})^2-\bar{\epsilon}_x^2-\bar{\epsilon}_y^2}{2\bar{\epsilon}_x\bar{\epsilon}_y} \qquad \text{For: } \begin{array}{l} x = 1,2,3 \\ y = 1,2,3 \\ x \neq y \end{array}$$

The rms values of ϵ_1, ϵ_3 and ϵ_3 were recorded during the tests. These components were added by linear amplifiers.

Spectrum levels were determined from 1/3 octave band analyses, by subtracting $10 \log_{10}\Delta f$, from the 1/3 octave band level which contains the average number of zero crossings per second. Δf is the band width of this 1/3 octave band.

The power spectral density of the sound pressures and strains were obtained by normalizing the output of a 10 Hz band width filter.

TABLE III TEST SPECIMEN INSPECTION SCHEDULE

RUN NO.	LENGTH OF TEST RUN HRS:MIN	TOTAL ACCUMULATED TEST TIME HRS:MIN
1- 6	0:05	:30
7-12	0:10	1:30
13-18	0:15	3:00
19-24	0:30	6:00
25-38	1:00	20:00
39-78	2:00	100:00
79-END	4:00	END

The endurance tests were conducted with broad band noise excitation. The inspections for failures were made according to the schedule of Table III. When a crack was suspected, the area was treated with a special penetrating dye which made surface cracks visible. Fatigue detection wires were attached to the ends of the beads of the bonded-beaded panels where stress concentrations were suspected. The insulated copper wires were connected to a warning light circuit which switched off in case of circuit interruption due to fatigue failure in the bead ends. This simple device proved to be of significant value in the failure inspection procedure. When multiple fatigue failures occurred or the size of the cracks became extensive, the panel was removed and replaced by a wooden dummy panel to maintain an identical acoustic environment for the remaining test specimens.

TEST RESULTS

The test results presented include mode shapes, damping ratios, linearity data, power spectral densities for sound pressure and strain as well as fatigue life.

The panel modes for the dominant resonant frequencies for the bonded-beaded panels are shown in Figure 10. The mode shapes for the higher frequencies resulted in complicated patterns which were not well defined.

TYPE I AND II
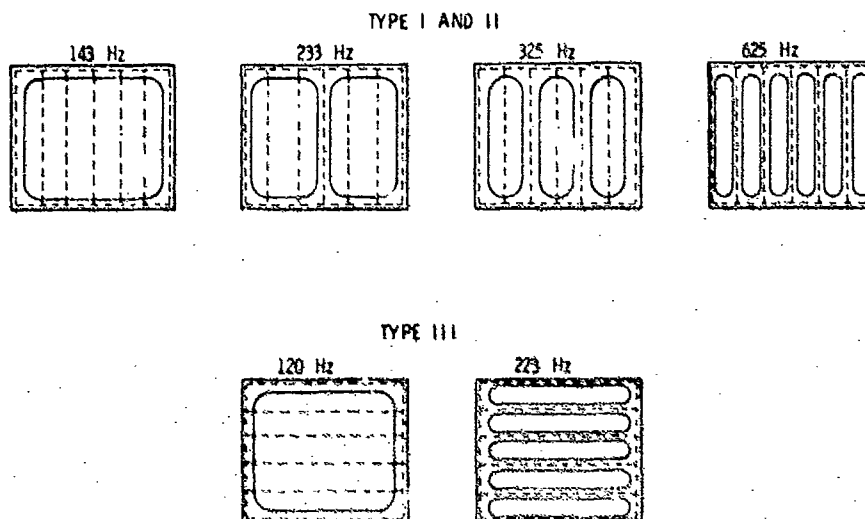
TYPE III

FIGURE 10. MODES FOR BONDED-BEADED PANELS

TABLE IV DAMPING RATIOS OF THE BONDED-BEADED PANELS

	TYPE I			TYPE II			TYPE III	
PANEL	FREQUENCY Hz	DAMPING RATIO	PANEL	FREQUENCY Hz	DAMPING RATIO	PANEL	FREQUENCY Hz	DAMPING RATIO
A	125	.0088	A	142	.0078	A	103	.0116
	142	.0120		181	.0158		116	.006
	164	.0085		228	.0062		125	.0110
	176	.0156					210	.0084
	195	.0036	B	155	.0064		220	.0091
	210	.0070		168	.0104			
				173	.0086	B	104	.0144
B	124	.0141		222	.0050		111	.0130
	132	.0114		263	.0070		125	.0110
	146	.0137					145	.0089
	164	.0079	C	138	.0090		165	.0121
	176	.0114		155	.0090		212	.0075
	196	.0051		168	.0066		252	.0054
	211	.0066		176	.0038		328	.0092
	226	.0040		186	.0036			
	238	.0063		322	.0031	C	111	.0180
				336	.0060		123	.0140
C	138	.0072						
	192	.0052	D	126	.0159	D	102	.0198
	238	.0044		135	.0056		110	.0091
				142	.0123		192	.0078
D	102	.0098		156	.0070			
	132	.0152		173	.0101	E	108	.0232
	148	.0067					125	.0190
	162	.0092	E	136	.0147		200	.0088
	195	.0056		146	.0103		326	.0092
				156	.0064			
E	126	.0127		223	.0067			
	164	.0100		279	.0054			
	186	.0067						
	192	.0062						

The damping ratios for all bonded-beaded panels are listed in Table IV. The average ratios are approximately the same for the panels Type I and II and slightly higher for the Type III panels. Typical response curves for the bonded-beaded panels with the same bead and skin material gage are shown in Figure 11.
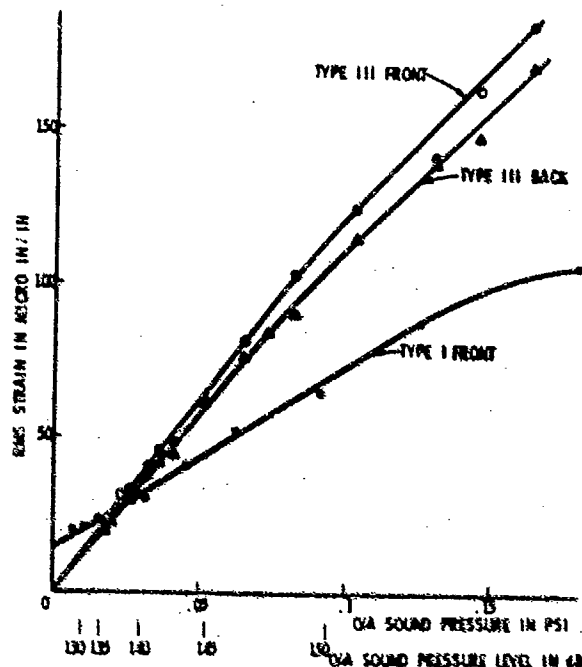
FIGURE 11. TYPICAL RESPONSE FOR
BONDED-BEADED PANELS

Typical power spectral densities for the sound pressures and strains measured are given in Figures 12 and 13. The test data for these panels are summarized in Tables V, VI and VII. In addition to the numerical values listed for sound pressure level, stress and life, the location where the initial fatigue failure occurred is given. Typical failures designated "bead edge" are shown in Figure 14. These failures occurred predominantly on panel Types I and Type III for which skin thickness and bead material gage were identical.
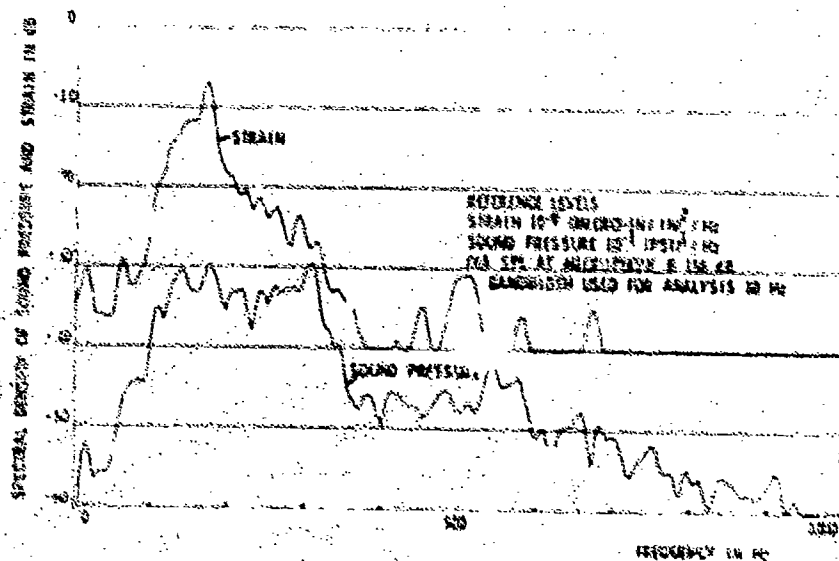
FIGURE 12.
POWER SPECTRAL DENSITY OF
SOUND PRESSURE AND STRAIN
RESPONSE FOR BONDED-BEADED
PANEL TYPE I

The failures on panel Type II occurred in the skin (Figure 13) at sound pressure levels over 150 dB.

At sound pressure levels below 150 dB and test times up to 300 hours, all types of panels failed in the panel to frame connections (edge failures). These failures could conceivably occur in aircraft installations where the supporting structure is rigid. One bonding failure was noted in panel Type III at the lower sound pressure level.

The curves on Figure 16 were determined by the method of least squares and show the relation between overall sound pressure level and life of the bonded-beaded panels. The panels with 21.0 inch long beads have greater fatigue resistance than the panels with 27.0 inch long beads. The principal stresses listed in the tables show less scatter than the stresses measured at the edge of the panels. This is illustrated in Figure 17 for the bonded-beaded Type II panels from the straight line fit where the ratio of the RMS deviations from the straight line fits for the principal and edge stresses is approximately one half. Therefore, the principal stress should allow a better comparison of stress data at various structural configurations.

REFERENCE LEVELS
STRAIN 10^{-9} (MICRO-IN/ IN^2 / Hz
SOUND PRESSURE 10^{-1} (PSI)^2 / Hz
OIA SPL AT MICROPHONE B 162 dB
BANDWIDTH USED FOR ANALYSIS 10 Hz
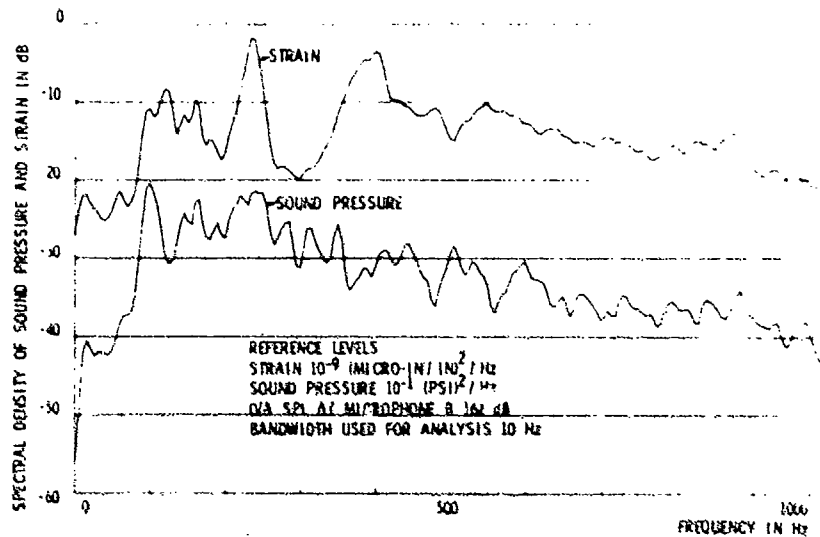
FIGURE 13
POWER SPECTRAL DENSITY OF
SOUND PRESSURE AND STRAIN
RESPONSE FOR BONDED-BEADED
PANEL TYPE III

FIGURE 14. BEAD-EDGE FAILURES

TABLE V STRESS RESPONSE AND FAILURE DATA FOR

BONDED-BEADED PANELS TYPE I (TYPE III)

BEAD LENGTH 21.0 IN, PANEL SIZE .040 IN.

BEAD SKIN .032 IN THICK

STRESS GAUGE LOCATIONS GIVEN IN FIGURE 7.

PANEL NO.	OVERALL SPL dB	SPECTRUM LEVEL dB	STRESS GAUGE 1 PSI	STRESS GAUGE 2 PSI	PRINCIPAL STRESS PSI	STRESS IN -5	STRESS GAUGE 5 PSI	ZERO CROSSINGS SEC⁻¹	LIFE 10⁶ CYCLES	FAILURE LOCATION
A-1	157.0	131.4	1432	1189	1631	1773		210	5,670	Bead Edge
B-1	159.0	130.5	1467	1151	1866	2661		196	5,293	Bead Edge
C-1	157.3	132.2	1412	1085	1680	1269		183	4,817	Bead Core
D-1	158.0	128.0	1592	1584	2458	2155		169	7,170	Bead Edge
E-1	157.0	129.9	2108	972	2584	2052		196	7,023	Bead Edge
A-2	157.5	129.6	863	528	836	1549		172	8,100	Bead Edge/Edge
B-2	153.1	128.4	828	523	543	3003	853	200	18,360	Edge
C-2	153.5	130.3	923	665	852	3493		167	16,750	Edge
D-2	153.5	125.9	1236	395	1170	1498		168	19,930	Bead Edge/Edge
E-2	153.0	125.9	945	503	953	1454		155	20,040	Bead Edge/Edge
A-3	151.5	128.4	833	763	955	1496		183	35,950	Edge
B-3	151.0	128.6	775	633	817	1263	529	173	46,460	Edge
C-3	150.5	128.6	806	510	836	965		166	35,860	Edge
D-3	151.5	124.7	885	628	917	1279		150	39,840	Core
E-3	156.3	123.4	859	527	950	1861		155	8,530	Bead Edge
A-4	149.5	125.5	794	546	898	1450		514	109,248	Edge
B-4	150.0	124.0	663	685	957	1295	93	198	125.	No Failure
C-4	149.0	125.6	698	386	744	1132		168	32,450	Edge
D-4	153.5	129.9				972		145	42,720	Edge
E-4	150.5	123.9	784	552	1237	875		180	71,664	Edge

TABLE VI STRESS RESPONSE AND FATIGUE DATA FOR

BONDED-BEADED PANELS TYPE II (FIGURE 1)

BEAD LENGTH 21.0 IN, PANEL SKIN .020 IN,

BEAD SKIN .045 IN THICK

STRAIN-GAGE LOCATIONS GIVEN IN FIGURE 7

PANEL NR	OVERALL SPL dB	SPECTRUM LEVEL dB	STRESS LOC.1 PSI	STRESS LOC.2 PSI	PRINCIPAL STRESS PSI	STRESS LOC.4 PSI	STRESS LOC.5 PSI	ZERO CROSSINGS SEC^{-1}	LIFE 10^6 CYCLES	FAILURE LOCATION
A-1	157.0	131.4	1748	889	2268	1090		213	5.067	Panel Skin
B-1	158.0	130.2	1423	760	1771	1372		246	1.771	Panel Skin
C-1	157.5	132.4	1603	799	1769	1250		212	2.671	Panel Skin
D-1	158.0	128.3	1546	792	1754			233	3.355	Panel Skin
E-1	157.5	128.8	1413	963	1614	1059		187	2.693	Panel Skin
A-2	152.5	129.4	1243	567	1578	917		259	22.610	Panel Skin
B-2	153.5	128.9	1120	655	1512	1258		310	21.204	Panel Skin
C-2	152.5	130.1	1190	578	1302	1000		256	17.510	Panel Skin
D-2	153.5	126.9	1410	687	1583	613		193	13.201	Panel Skin
E-2	152.0	127.9	1040	702	1208	771		265	18.120	Panel Skin
A-3	151.5	126.1	1090	692	1291	1259	1122	211	12.154	Edge/Bead Edge
B-3	151.0	128.9	1040	641	1331	944	944	258	18.576	Panel Skin
C-3	150.0	129.4	1010	649	1248	335	613	210	34.020	Edge
D-3	151.5	126.0	1075	576	1238		410	247	64.467	Edge
E-3	150.5	127.9	926	673	1194	866	570	315	40.824	Panel Skin
A-4	149.5	126.4	895	440	1241	817		121	119.075	Edge
B-4	150.0	125.1	841	533	994	794		221	>140.	No Failure
C-4	149.0	126.9	882	438	1003	398		199	108.355	Bead Edge
D-4	150.0	129.9	894	531	1033	771		216	>140.	No Failure
E-4	150.0	124.9	796	513	904	562		194	116.679	Edge

TABLE VII STRESS RESPONSE AND FATIGUE DATA FOR

BONDED-BEADED PANELS TYPE III (FIGURE 1)

BEAD LENGTH 27.0 IN, PANEL SKIN .032 IN,

BEAD SKIN .032 IN THICK

STRAIN-GAGE LOCATIONS GIVEN IN FIGURE 7

PANEL NR	OVERALL SPL dB	SPECTRUM LEVEL dB	STRESS LOC.1 PSI	STRESS LOC.2 PSI	PRINCIPAL STRESS PSI	STRESS LOC.4 PSI	STRESS LOC.5 PSI	ZERO CROSSINGS SEC^{-1}	LIFE 10^6 CYCLES	FAILURE LOCATION
A-1	160.8	135.6	2289	2318	4167		4467	133	.954	Bead Edge
B-1	162.2	132.4	2372	1603	3803		4340	344	1.193	Bead Edge
C-1	159.8	136.9	2454	1973	4164		1995	229	1.076	Bead Edge
D-1	161.0	133.4	1929	2511	4201		3072	182	.642	Bead Edge
E-1	160.0	N/A	2919	2289	4864		N/A	N/A	N/A	Bead Edge
A-2	155.8	128.1	2985	1778	4386		3350	336	3.024	Bead Edge
B-2	156.8	129.6	2511	1188	3298		3652	307	1.382	Bead Edge
C-2	156.0	128.9	2441	1334	3330		2371	330	8.118	Bead Edge
D-2	154.8	128.1	2371	1778	3840		3072	341	1.637	Bead Edge
E-2	153.5	125.6	2239	1679	3517		3548	434	4.088	Bead Edge
A-3	151.5	122.9	1939	1180	3087		3073	234	5.476	Bead Edge
B-3	151.8	125.4	1508	686	2203		1333	340	>110.	No Failure
C-3	150.8	124.4	1372	1290	2502		2175	253	34.064	Edge/Bead Edge
D-3	150.0	124.1	1350	1259	2059		1778	253	45.540	Edge/Bead Edge
E-3	150.0	122.1	1708	1429	3177		1778	265	34.344	Edge
A-4	147.0	124.6	1334	1000	2039		1454	143	5.663	Edge
B-4	148.5	126.9	708	178	1213	972	596	163	34.328	Edge
C-4	147.0	124.9	772	631	1294		771	160	112.704	Edge
D-4	146.0	123.6	1000	818	1876		841	130	58.500	Bonding Failure
E-4	146.2	121.9	1841	501	1432		1155	250	76.875	Edge
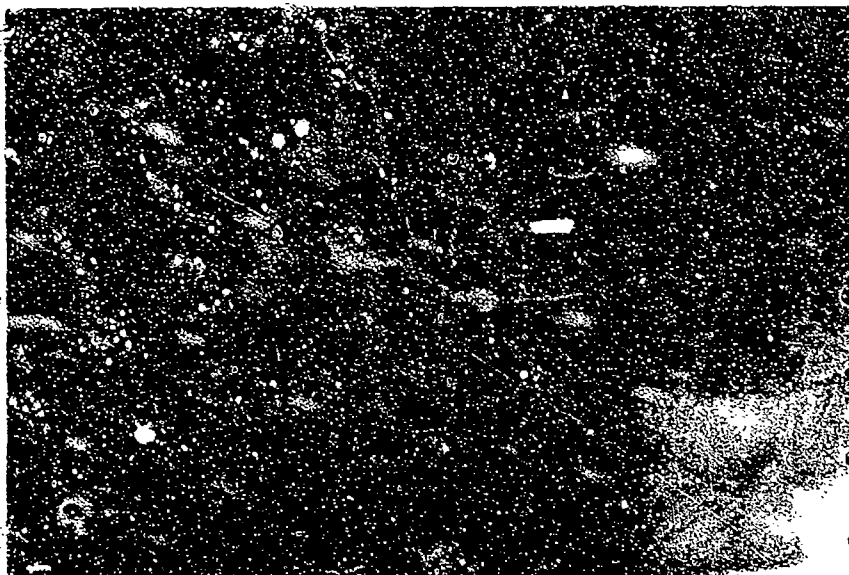
FIGURE 15. SKIN FAILURES
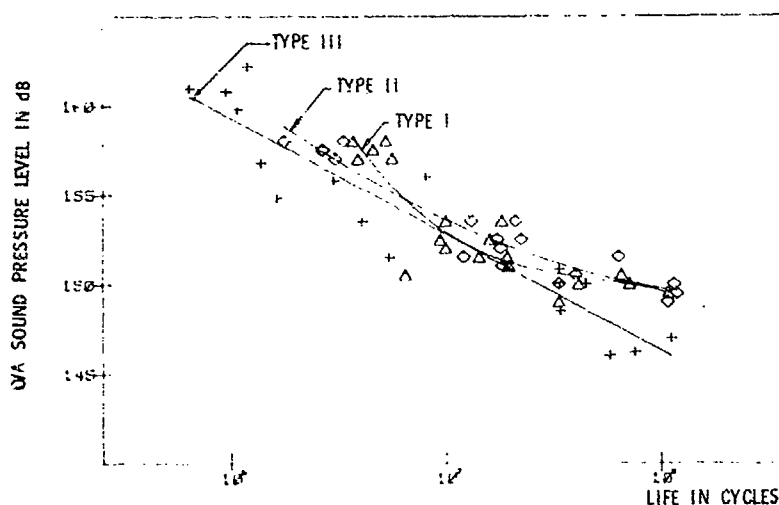
FIGURE 16. OVERALL SOUND PRESSURE
LEVEL VERSUS LIFE FOR
BONDED-BEADED PANELS
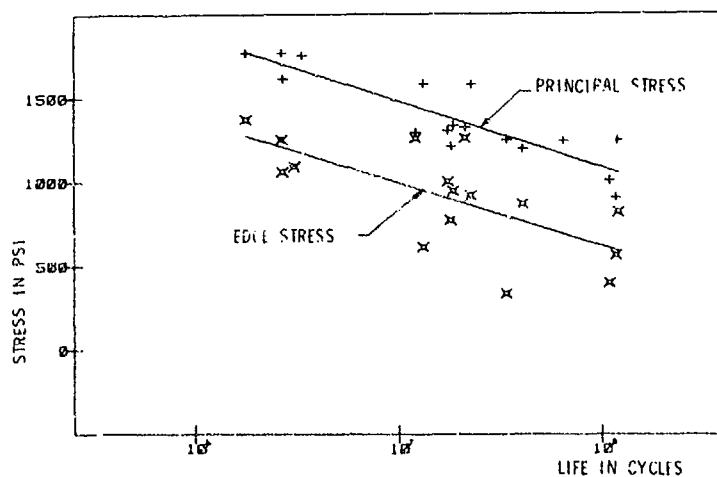
FIGURE 17. PRINCIPAL AND EDGE STRESS
VERSUS FATIGUE LIFE FOR
BONDED-BEADED PANELS TYPE II

The mode shapes, damping ratios and response linearity of the skin-stringer panels Type I are shown in Figure 18, Table VIII and Figure 19. The power spectral densities of the sound pressure and the strain response are plotted in Figure 20.

Table IX summarizes the test data for these panels. The majority of failures occurred in the proximity of a rivet line as shown in Figure 21. The fatigue life of the panels versus overall sound pressure level is plotted in Figure 22. It should be noted that the scatter in life for these panels is considerably less than that shown for the other configurations.

For the skin-stringer panel Type II the mode shape is shown in Figure 18, the damping ratio in Table X, the linearity in Figure 19 and the sound pressure and strain response power spectral density plots in Figure 23. Finally, the test data are tabulated in Table XI and shown in Figure 24. The failure mode observed was primarily located at the stress concentration.

TYPE I

FIGURE 18. MODES FOR SKIN-STRINGER PANELS

TABLE VIII DAMPING RATIOS OF THE SKIN-STRINGER PANELS
TYPE I

PANEL	FREQUENCY Hz	DAMPING RATIO	PANEL	FREQUENCY Hz	DAMPING RATIO	PANEL	FREQUENCY Hz	DAMPING RATIO
A	148	.0186	C	129	.0337	E	127	.0303
	163	.0184		138	.0243		139	.0288
	176	.0199		149	.0252		152.5	.0229
	191	.0157		164	.0198		173.5	.0245
				203	.0160		183	.0224
B	124	.0351		223.5	.0161		193	.0197
	147	.0187					205	.0171
	163	.0190	D	131	.0259			
	193	.0233		148	.0186			
				164	.0183			

FIGURE 19. TYPICAL RESPONSE FOR THE
SKIN-STRINGER PANELS
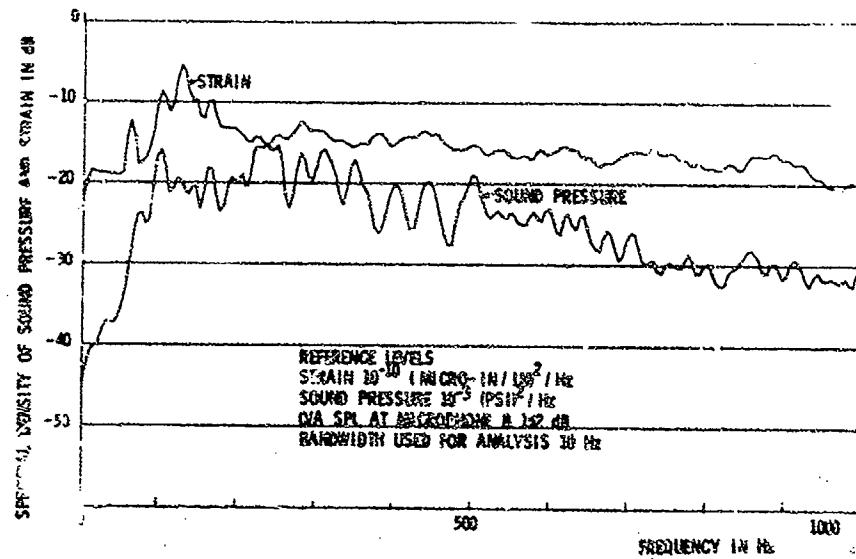
FIGURE 20. POWER SPECTRAL DENSITY OF SOUND PRESSURE AND STRAIN RESPONSE
FOR SKIN-STRINGER PANEL TYPE I

TABLE IX STRESS RESPONSE AND FATIGUE DATA FOR

SKIN-STRINGER PANELS TYPE I (FIGURE 3)

STRAIN-GAGE LOCATIONS GIVEN IN FIGURE 7

PANEL NR	OVERALL SPL dB	SPECTRUM LEVEL dB	STRESS LOC 1 PSI	STRESS LOC 2 PSI	PRINCIPAL STRESS PSI	EDGE STRESS PSI	ZERO CROSSINGS SEC^{-1}	LIFE 10^6 CYCLES	FAILURE LOCATION
A-1	154.5	128.1	2152	632	2532	2085	129	2.438	Rivet Line
B-1	155.0	126.9	2519	673	3097	2294	126	1.678	Rivet Line
C-1	154.1	128.6	2718	455	3308	2156	176	2.344	Rivet Line
D-1	155.0	121.6	2184	705	2479	2482	164	1.535	Edge Line
E-1	154.8	121.1	1883	894	2559	2085	179	1.675	Edge Line
A-2	151.0	123.7	1267	518	1966	1348	183	5.600	Rivet Line
B-2	151.6	124.0	1560	606	1988	1685	160	4.896	Rivet Line
C-2	150.7	123.0	1596	442	2131	1706	194	14.783	Rivet Line
D-2	151.4	126.8	1694	657	2230	1595	132	1.980	Rivet Line
E-2	151.2	126.0	1627	787	2593	1703	143	5.285	Rivet Line
A-3	148.9	121.5	787	427	1092	1269	181	22.806	Rivet Line
B-3	149.4	120.8	1332	416	2342	1179	148	9.324	Rivet Line
C-3	148.5	120.9	938	548	1696	1429	186	23.436	Rivet Line
D-3	149.6	124.8	1087	556	1843	1528	129	9.422	Rivet Line
E-3	149.3	124.5	550	320	809	1258	135	17.010	Rivet Line
A-4	147.1	120.0	1140	1040	1770	772	164	22.532	Rivet Line
B-4	147.6	119.5	1110	312	1460	1122	132	86.288	Rivet Line
C-4	146.4	119.0	846	320	1041	728	182	>130.	No Failure
D-4	147.5	117.7	1438	392	1842	N/A	142	32.546	Rivet Line
E-4	147.4	113.7	1150	274	1482	794	152	25.855	Rivet Line

FIGURE 21. RIVET-LINE FAILURES
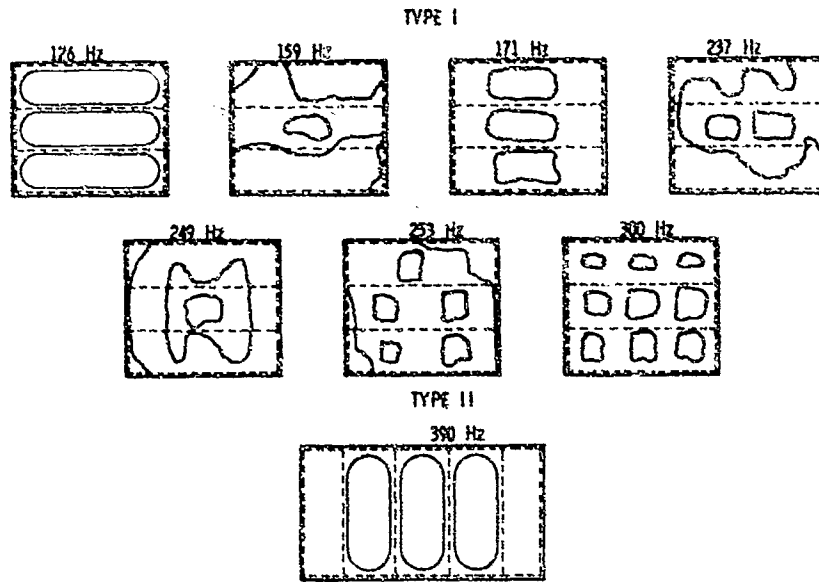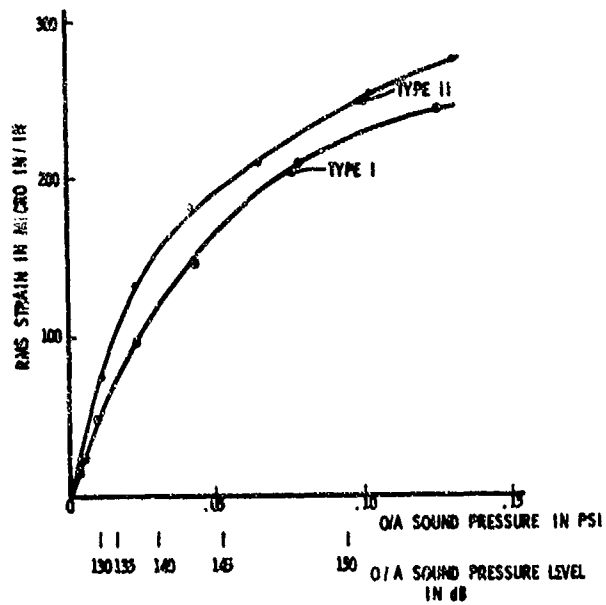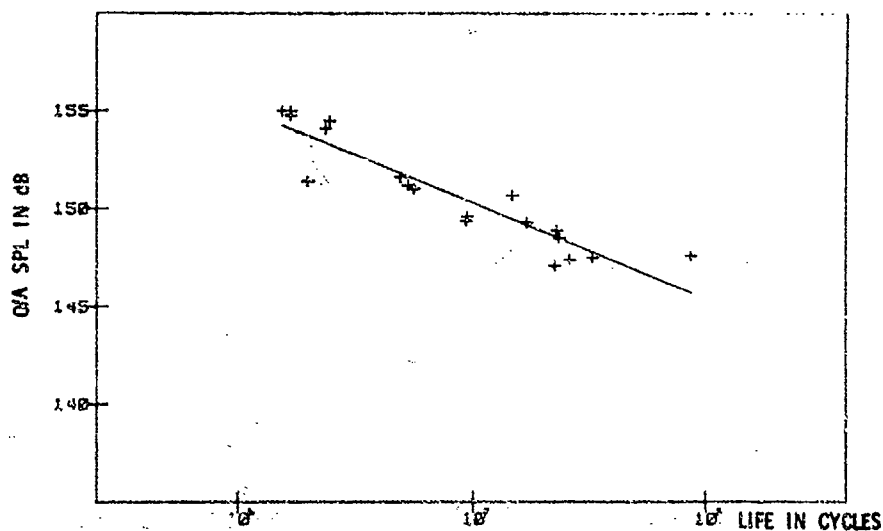
FIGURE 22. OVERALL SOUND PRESSURE LEVEL VERSUS LIFE
FOR THE SKIN-STRINGER PANEL TYPE I

TABLE X DAMPING RATIOS OF THE SKIN-STRINGER PANELS TYPE II

PANEL	FREQUENCY Hz	DAMPING RATIO	PANEL	FREQUENCY Hz	DAMPING RATIO	PANEL	FREQUENCY Hz	DAMPING RATIO
A-1	418	.0072	C-1	352	.0259	E-1	359	.0112
A-2	344	.0151	C-2	396	.0103		364	.0119
	350	.0114		405	.0138		380	.0158
	377	.0159		416	.0144		390	.0113
B-1	380	.0160	D-1	364	.0110	E-2	282	.0142
B-2	371	.0081		390	.0169		300	.0166
	381	.0168	D-2	372	.0140		314	.0104
	389	.0051		418	.0115		318	.0157
	409	.0176						
	420	.0095						
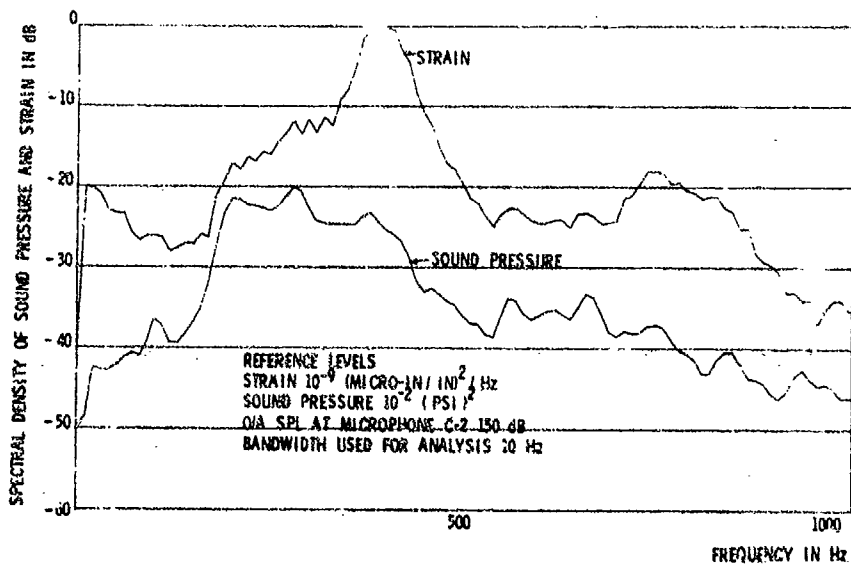
FIGURE 23. POWER SPECTRAL DENSITY OF SOUND PRESSURE
AND STRAIN RESPONSE FOR SKIN-STRINGER
PANEL TYPE II

TABLE XI STRESS RESPONSE AND FATIGUE DATA FOR
SKIN-STRINGER PANELS TYPE II (FIGURE 4)
STRAIN-GAGE LOCATIONS GIVEN IN FIGURE 7

PANEL NR	OVERALL SPL dB	SPECTRUM LEVEL dB	STRESS LOC.1 PSI	STRESS LOC.2 PSI	EDGE STRESS PSI	ZERO CROSSINGS SEC^{-1}	LIFE 10^6 CYCLES	FAILURE LOCATION
A1-1	156.5	127.5	3100		5260	404	21.80	Side Bay
A2-1	153.0	126.0	3320		5650	390	2.34	Stress Conc.
B1-1	157.5	122.0	2070		3520	450	41.30	"
B2-1	157.8	130.0	3160	4870	5370	422	9.12	"
C1-1	155.5	129.0	2260		3840	432	39.70	"
C2-1	156.7	126.5	2650		4500	417	25.50	"
D1-1	157.2	129.5	4350		7400	384	1.84	"
D2-1	156.2	124.5	5680		9650	196	.71	"
E1-1	157.0	129.0	4070	5309	6920	359	5.17	"
E2-1	155.0	129.5	3100		5260	363	2.18	"
A1-2	154.0	125.9	3100	1995	5270	408	6.61	"
A2-2	155.2	128.4	3700		6290	394	5.67	"
B1-2	154.4	127.4	2550		4330	424	7.63	"
B2-2	155.4	127.6	2750	4097	4660	422	5.57	"
C1-2	153.3	126.6	3900		6620	410	6.64	"
C2-2	154.3	124.6	N/A	2985	N/A	N/A	N/A	"
D1-2	153.3	129.4	4550		7240	330	1.76	"
D2-2	154.6	129.0	4800	2738	8150	376	.90	"
E1-2	154.5	126.4	2550	2054	4330	436	16.50	Side Bay
E2-2	153.0	N/A	1600		N/A	N/A	N/A	No Failure
A1-3	149.5	121.0	2020		3430	408	115.00	Stress Conc.
A2-3	149.5	122.0	3150		5350	377	23.80	
B1-3	151.0	123.5	1600		2720	435	265.	No Failure
B2-3	150.5	123.0	2430		4130	409	53.00	"
C1-3	149.5	123.0	2670		4540	351	19.60	"
C2-3	149.5	120.5	1900		3240	416	108.00	"
D1-3	149.0	122.5	2220		3770	369	27.90	Side Bay
D2-3	150.0	123.0	2550		4330	377	76.70	Stress Conc.
E1-3	150.0	121.5	2490		4240	366	87.30	"
E2-3	148.5	122.5	3510		5960	295	16.50	"
A1-4	155.1	125.0	1460		2480	448	N/A	No Failure
A2-4	155.1	127.9	2700		4570	418	18.10	Stress Conc.
B1-4	156.4	129.4	2840		4830	386	.28	S.C./Side Bay
B2-4	156.1	129.1	4480		7640	370	.42	Stress Conc.
C1-4	154.4	127.1	2690		4570	398	1.32	"
C2-4	155.2	126.4	2650		4340	422	10.10	"
D1-4	154.9	128.9	3770		6400	372	.27	"
D2-4	N/A	N/A	2860		4860	396	2.02	"
E1-4	155.5	127.4	2600		4410	420	36.50	"
E2-4	153.3	N/A	N/A		N/A	N/A	N/A	Side Bay

Stress Conc. = Stress Concentration

NOTE: The fixture of Figure 6 was modified for these
tests, each panel opening could accommodate
two 10.5 X 24.0 panels, designated 1 and 2
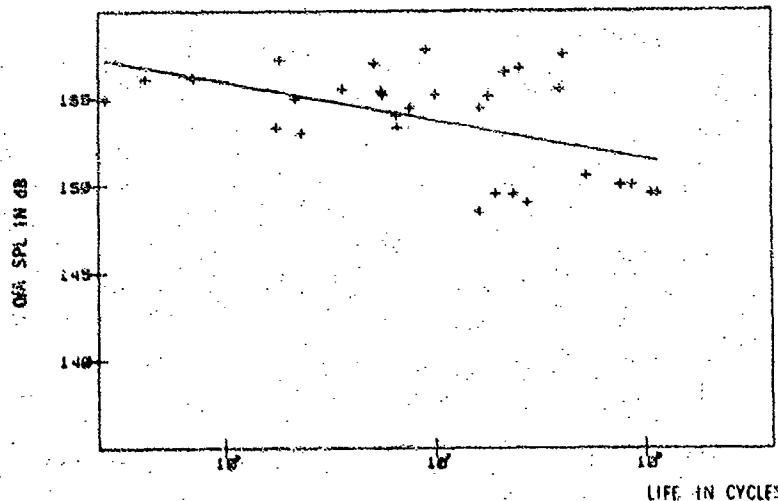e.g., for Location A, Panels A1 and A2.

FIGURE 24. OVERALL SOUND
PRESSURE LEVEL
VERSUS LIFE FOR
THE SKIN-STRINGER
PANEL TYPE II

COMPARISON OF TEST RESULTS WITH STRESS AND LIFE ESTIMATES

The test data were compared with estimates obtained from procedures given in References 1, 2 and the AGARD AG-162 and ESDU AF-17C, References 7 and 8. Reference 1 contains the only applicable prediction method for the bonded-beaded panels. The estimated and measured edge stresses are compared in Figure 25. The comparison indicates that the design chart in Reference 1 predicts conservative values for the edge stress. The measured nominal stress values are within a factor of 2.5 relative to the values predicted, however, the fatigue life predictions are considered to be not comparable with the experimental data presented in this paper. This may be in part due to: (1) differences in structural details which may introduce different stress concentrations in the panels from those which existed in the specimens on which the referenced design chart was based, and (2) the limited number of specimens used in the Reference 1 program. These factors could result in large differences in fatigue life.

The stresses and fatigue lives obtained for the skin-stringer panels Type I are compared in Figures 26 and 27 with the estimations based on the methods published in References 2, 7 and 8. This comparison shows that the ratio between measured and estimated stress ranges from .4 to 2.0. The agreement between the results obtained with both stress prediction methods and the measured data is considered very good.

The ratio between measured and estimated fatigue life for the skin-stringer panel Type I varies from approximately 1 to 100. As these tests were generally conducted at low stress levels, large variations in life resulting from small variations in stress should be expected. Both fatigue life prediction methods yielded shorter life times than the experimental data.

A corresponding comparison between estimated and measured stress for the skin-stringer Type II panels is demonstrated in Figure 28. The same prediction methods as for the first series of skin-stringer panels were used as a basis for comparison. The AGARD method predicted stress values in agreement with the prediction contained in Reference 2. A comparison of the fatigue life of these panels with estimated values was not practical since most failures occurred at stress concentrations which are not directly considered in the prediction methods.
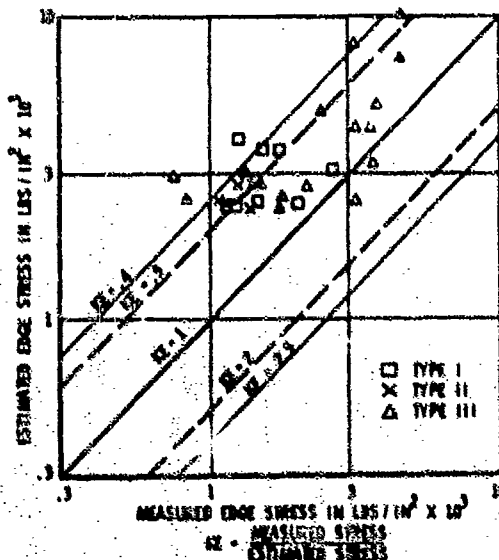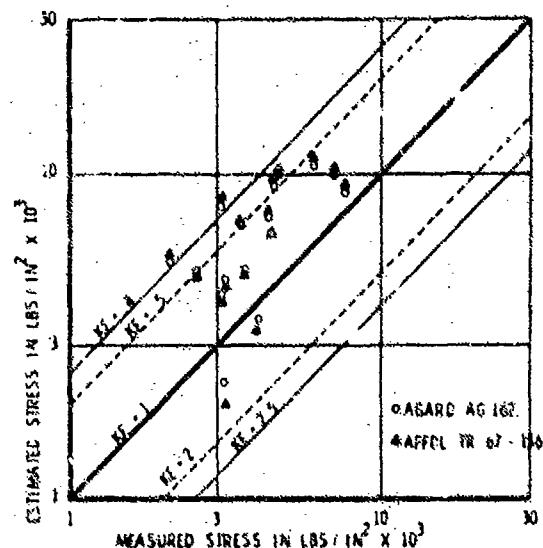

FIGURE 25. COMPARISON BETWEEN ESTIMATED AND MEASURED STRESS FOR THE BONDED-BEADED PANELS

FIGURE 26. COMPARISON BETWEEN ESTIMATED AND MEASURED STRESS FOR SKIN-STRINGER PANEL TYPE I
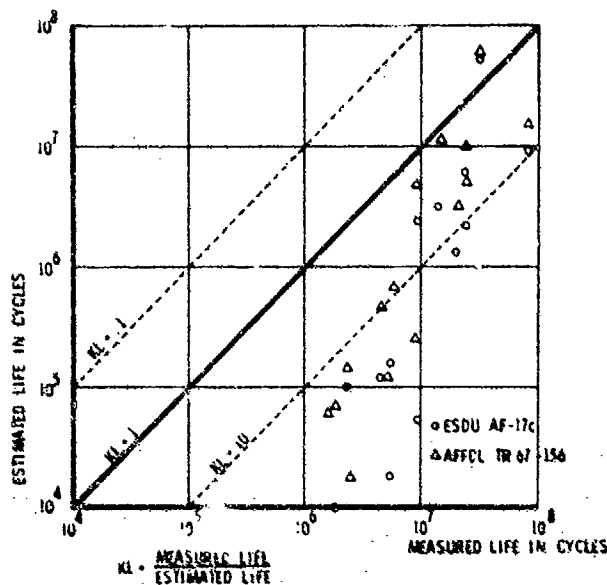
FIGURE 27. COMPARISON BETWEEN ESTIMATED
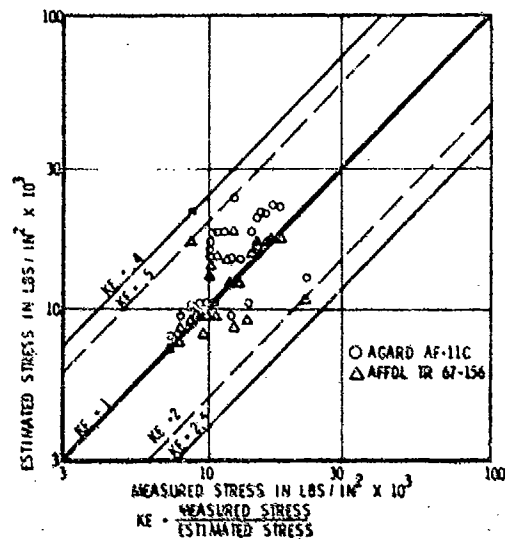AND MEASURED LIFE FOR SKIN-
STRINGER PANEL Type I

FIGURE 28. COMPARISON BETWEEN ESTIMATED
AND MEASURED STRESS FOR SKIN-
STRINGER PANELS TYPE II

CONCLUSIONS

The sonic fatigue data presented in this paper verify and extend design information for which only limited data existed and substantiation was needed. The number of test specimens used in this program, as well as the closely controlled acoustic conditions, justify a high confidence level in the results.

The failure locations of the bonded-beaded panels are well defined at overall excitation sound pressure levels above 150 dB and occur either at the bead edge or in the skin depending on the ratio of skin to bead material gage. Below this excitation level the failure locations become less defined but occur predominantly at the panel edge close to the attachment bolts.

Compared on a weight per area basis of 1 lb/ft², the bonded-beaded panels do not offer significantly longer fatigue life than the skin-stringer panels, however, the panel depth is considerably less for the bonded-beaded panels, a factor which may be of importance where space limitations exist.

Available design methods were well substantiated as far as stress predictions are concerned. This is particularly true for the skin-stringer design methods which proved applicable to conventional lightweight skin-stringer design with semi-rigid supporting structure as well as design with a rigid back-up structure.

The stress predictions for the bonded-beaded panels, as published in Reference 1, were confirmed, however, the fatigue life predictions were not verified and will require updating of the present design charts. The fatigue life prediction methods for the conventional skin-stringer panels given in References 2 and 8 were supported by the test results.

The test specimens were manufactured under observance of the commonly used aircraft manufacturing and inspection specifications. Therefore, the fatigue failures and lifetimes obtained should be indicative of the variability in life to be expected under service conditions.

REFERENCES

1. ASD-TDR-63-820, McGowan, P.R., et al, "Structural Design for Acoustic Fatigue", Oct 1963.

2. AFFDL-TR-67-156, Ballentine, J.R., et al, "Refinement of Sonic Fatigue Structural Design Criteria", Jan 1968.

3. AFFDL-TR-71-113, Serens, A.P. and West, B.S., "Experimental Methods in Acoustic Fatigue" Mar 1972.

4. Wilks, S.S., "Mathematical Statistics", Princeton University Press, Princeton, N.J.

5. Perry, C.C., and Lissner, H.R., "Stress Equations for Strain Gage Rosettes", Product Engineering, July 1955.

6. Timoshenko, S. and Goodier, J.N., "Theory of Elasticity", McGraw-Hill.

7. AGARDograph 162, Thomson, A.G.R., "Acoustic Fatigue Design Data".

8. Engineering Science Data Unit AF-17C, "Endurance of Aluminum Alloy Structural Elements Subjected to Simulated Acoustic Loading".

Mr. Phillips explained that his printed paper only contained the test results which had been obtained up to the time of submission of the paper. Later information was included in the oral presentation. He was questioned about the non symmetrical mode shapes predicted by the finite element analysis. He replied that there was a slight variation in the stiffener spacing and that the stiffeners themselves were unsymmetrical (z section). These two effects had been taken into account in the finite element analysis with the result that an unsymmetrical mode shape similar to that measured was predicted. He commented on the fact that although the Ballantyne method predicted the lowest stresses, it also predicted the lowest endurance. Taking the complete Ballantyne or ESDU procedure gives similar results for life estimates. He also said that a damping ratio of 0.017 (independent of frequency) had been used in the estimates. Dr. Mead pointed out that the wave group theory could be used for a structure having a finite number of bays.

<center>GENERAL DISCUSSION AND WORKSHOP MEETING</center>

The workshop meeting expanded on several points which were raised in the general discussion session and therefore to avoid repetition and to present a more systematic development of the material covered, the main points raised in the two sessions are combined in the following section.

Loading Actions

From the fatigue point of view it is important to know the time history of the loads on the structure. With random loads such as those arising from jet noise or separated flow the appropriate measure of the magnitude is the r.m.s. pressure. Experience on the rear structure of current aircraft has shown that the first part of the take off run when the engines are at full thrust generally makes the greatest contribution to the accumulation of damage. Strain measurement and subsequent damage history have shown that the same is also true of engine intake structure. In these cases the duration of high levels is usually less than one minute per take off.

It was pointed out, however, that where separated flow can occur under certain flight conditions then significant contributions to the accumulation of damage can occur. In these cases the duration can be much greater than that associated with a typical take off. In some military aircraft configurations high noise levels can occur during some flight conditions. These possibilities emphasise the need for a realistic measurement of typical r m.s. strain time histories for typical missions.

The calculations and measurement on vertical take off aircraft have shown that the sound pressure levels in the structure can be increased considerably by the effect of ground reflections. It was suggested that the estimation procedure developed by Dr. Scholten should be used to provide estimates for comparison with the VAK 191 measurements.

Response

I   .e majority of the analytical approaches to calculating the response of structures to random pressure loads the formulation has been based on the normal mode method. In the recent developments reported at this symposium the finite element displacement method has been used to compute the normal modes of the structure. Because of the large number of normal modes in the acoustic frequency range in practical structures, a relatively simple piece of structure has usually been modelled. Substructure analysis has been used successfully to compute the eigenvalues and eigenvectors of more complicated structures but the computing costs increase rapidly as the complexity of the structure increases. Professor Wittrick described a new method (1), which he had developed from his work on the analysis of the buckling of flat and curved stiffened plates. This is similar to the finite element method but like the transfer matrix method it gives an exact solution. It has the advantage that it can determine the number of eigenvalues in any given frequency range and so a more economical use of computer time can be arranged.

In the finite element computations the forcing function can be represented by the cross correlation function of the pressures. Satisfactory estimates of this function can be made in the case of near field jet noise and boundary layer pressure fluctuations. The work described in the papers by Coe and Westley indicate suitable approximations which can be used for impinging jets and separated flows.

Dr. Mead described the development of a new theoretical approach based on the wave group theory. If the structure is periodic (i.e. an assembly of many identical elements such as plates and equally spaced stiffeners or ribs) a closed form solution to the response to a travelling wave excitation field can be obtained. The formulation gives the solution for the total response directly rather than in the form of the response in each of a very large number of normal modes. It also gives a better physical understanding of the travelling wave motion which can be set up in structures excited by acoustic pressure fields. The method can be modified to give an approximate solution for the case of non uniform spacing of stiffeners. The bounds on the frequencies of each type of mode can be obtained exactly. This method has been used in the AGARD data sheets on Acoustic Fatigue for stiffened panels. A further development was described by Mr. Abrahamson in which a Rayleigh Ritz approach is used to determine the predominant features of the fundamental element in the periodic structure. This method allows the designer to use shape functions based on past experience with similar structures or even the results of resonance tests to obtain the response of the structure to a travelling wave excitation. A good approximation to the exact solution is obtained with a relatively few assumed shape functions. More recent developments are using the transfer matrix method and the finite element method to establish the properties of the fundamental element of the periodic structure.

The effect of static, in-plane stresses was discussed. It was considered that this could have a significant effect on the dynamic stresses. In the take off case the static stresses will usually be small at the time of high dynamic loads unless thermal effects in VTOL configurations or high static pressures in externally blown flap configurations give rise to in-plane static stresses. Results from tests on one conventional aeroplane showed that the frequency of the predominant mode changed only a few Hz in going from ground to flight conditions. One company hopes to carry out some tests with a hot structure, and another company is planning tests on integrally machined skin structure with in-plane loads. Professor Wittrick (2) described the results of some of his work which shows that the frequency change due to in-plane stresses is given by

$$n^2 = n_o^2 - \frac{\sigma}{\rho\lambda^2}$$

where n is the new frequency, n_o is the frequency without in-plane stress, σ is the in-plane stress, ρ is the density of the material and λ is the wavelength of the mode of vibration being considered. It was concluded that more experimental work was needed on this topic.

The design procedure proposed in the Data Sheets for the skins of box type structures was discussed. The main reason for the reduction in stress in the skin is that the generalised mass of the structure is increased by a factor of 2.5 to 3 because both skins and the internal rib structure vibrate when sound impinges on one skin. It was pointed out that the load carrying factor of the rib web would affect the distribution of vibration energy in the structure and might affect the stress reduction obtained in the skins.

The next question discussed was the effect of acoustic loads on unusual structural designs. Particular structures of interest are the composite materials used for engine duct liners, doubly curved skew panels and S duct structures in intakes. No specific solutions could be offered although it was felt that finite element methods could be used in the last two cases. A parametric study could be done by the finite element method but this would be very expensive if a reasonably useful range of parameters were to be included. Some work has already been done on the development of a suitable element for use in doubly curved structures but there are no experimental data or analytical results available to check the accuracy. Mr. Holehouse reported that he had carried out tests on 20 specimens of sound absorbing structural design in a progressive wave tube. The structure was of sandwich construction with a perforated face sheet and 1 to 2 in. deep cores. The core depth was based on acoustic criteria. If there was good detail design of the bonding and the edge connections there was not likely to be any failure at sound levels lower than about 180 dB.

The accuracy which might be expected in any comparison of theory with experiment was discussed. It was pointed out that the wide variation in damping provided one limit to the accuracy which might be expected. In this case the errors may not be as high as appears at first sight because the r.m.s. stress is inversely proportional to the square root of the damping ratio. The response to boundary layer pressure fluctuations on a supersonic vehicle generally shows a marked increase in the transonic region. This is because there can be an order of magnitude change in the aerodynamic damping in this flight regime.

It was also pointed out that the manufacturing tolerances on sheet thickness would also lead to variation in results. These tolerances are usually unsymmetric, i.e. +10%, -5%. It was recommended that skin thicknesses should be measured in any control tests on response. Several tests should be carried out on nominally identical structures. The multiple regression analysis described in Mr. Holehouse's paper was based on 16 test panels.

The discussion highlighted a difference of opinion on the strain variation at the centre of honeycomb panels. Some evidence suggests that the effect of the unsymmetrical edge fixing is to give stresses on the inner face which are greater than those on the outer face by a factor of 2 to 2.5. Other workers had not noticed such a difference and failure experience did not suggest that such large differences were common. It was agreed to check this point in future tests on honeycomb structure.

Test Panel

The discussion on the response of structures to random acoustic loading showed that there are many uncertainties in the test procedures which could be leading to discrepancies between the estimated and measured results. It was reported that in one case nominally identical test specimens had given different results in different progressive wave tubes. It was therefore proposed by Mr. Kolb that a systematic comparison of the different test facilities and test techniques should be made. This would be aimed primarily at those who had supplied data on which the Data Sheets were based. It was suggested that this could be done by having a test structure representative of typical stiffened skin design practice which could be passed from laboratory to laboratory. This would have the essential strain gauge instrumentation installed and each laboratory in turn would be asked to carry out their 'standard' test simulating a given jet noise spectrum. They would also be asked to analyse the strain data using their normal data acquisition and analysis system. It was also suggested that a final check could be made by subjecting the panel to a real jet noise environment.

In parallel with this experimental study it was suggested that the different analysis methods be used to estimate the response. Thus the finite element method could be compared with the wave group theory, transfer matrix, and Wittrick method.

Many members of the symposium agreed in principle with this proposal but in further discussion many difficulties were foreseen. When similar exercises have been tried in other fields the results have not been entirely satisfactory although relatively major discrepancies have come to light. If all went well, it would take a long time for the specimen to complete the rounds of the facilities. There was also the question of finance. It was thought that each laboratory might be prepared to fund its own direct involvement but this could not be guaranteed.

In order to carry this one step further forward, Mr. Kolb agreed to circulate an outline proposal on the design of the test panel and the type of test to be conducted. If there was then sufficient interest to justify proceeding, a final agreed proposal could be drawn up and the individual laboratories consider it as part of their own programme of work.

Fatigue Aspects

Definition and detection of failure

Considerable discussion took place on the methods of defining fatigue failure. Several physical changes take place in the structure with the onset of fatigue failure but these are often difficult to identify in their early stages. The same problem exists in classical fatigue but in practice it may not be so important because of the rapid growth of the fatigue crack.

In coupon type specimens there is usually a change in frequency and an increase in damping just before a crack can be determined from a visual inspection. In some tests a 2% change in frequency can be used to define failure, whereas in others a 10% change is used. Unfortunately, built-up structures are not likely to exhibit so marked a frequency change because the change in local stiffness in the region of the crack will be insignificant compared with the stiffness of the remaining uncracked structure.

The use of dye penetrant to detect cracks was mentioned. However, several members objected to this because of the deleterious effect of the dye on the structure and because it was very insensitive. Another suggestion was that failure should be defined as the point at which the static strength of the component had been reduced by 15%. Whilst there was general agreement with this idea, it was felt that in most cases it was impractical to check the static strength at regular intervals during the service life. It was finally conceded by the majority that at present the only possible definition of failure which could be used generally on built-up structures was the point at which a visible (to the naked eye) crack appeared. In a written contribution, Mr. Baratta* pointed out that this definition was conservative because it neglected the significant additional life left in the structure during the crack propagation phase. He went on to suggest that the fracture mechanics approach be used to predict the behaviour during the crack propagation phase and hence determine a more realistic fatigue life. (This aspect of crack propagation was mentioned in Mr. Kirkby's paper - Ed.).

Of the relatively new methods becoming available for failure detection, the stress wave emission technique has been used successfully by one worker in this field. Initial tests have shown conclusively that a marked change in the emission takes place just before a crack is visible to the naked eye.

As a final contribution to this part of the discussion it was pointed out that the S-N curve was very flat in the acoustic fatigue stress range. Thus if a crack goes undetected at one inspection and is then picked up an hour or even a day later there will be little difference in the position of that data point on the S-N curve. This aspect brought forward the strong suggestion from Professor Schjive that we should work to a safe stress level in order to produce a satisfactory design rather than do a cumulative damage computation on a curve which showed considerable scatter.

Fatigue Testing

Coupon tests were considered to be a satisfactory way in which to build up information on the fatigue strength of typical joint configurations. The stress should be random (narrow band random being acceptable) but the wave form would have to be truncated to cut out the rare very large peaks. A truncation point of about 3.2 times the r.m.s. value was considered to be adequate. Mr. Bayerdörfer considered that the test data should specify the probability distribution which had actually been used. In particular the distribution of the higher peaks should be measured and quoted. Comparison of the coupon test results with results from representative built-up structures should be made to assess the accuracy of the structural simulation achieved by the coupon.

Acoustic tests were considered to be an essential feature of any full programme of proof testing. However, the commonly used electro-pneumatic transducer (siren) and progressive wave tube have been shown to give misleading results in some cases. There can be differences in the response level in identical structures tested in different progressive wave tubes. There can even be differences if a different acoustic driver is used. With certain configurations of structural specimen and duct there can be high damping in the lower frequency range due to the radiation of acoustic energy down the duct. A comparison between siren and open air jet tests is being made (see paper by Mr. Phillips) which should help to clarify this problem.

Mr. Bayerdörfer proposed a test procedure which could be used to simulate high intensity noise levels with a relatively small acoustic source. An initial search is carried out at a low sound level to determine the predominant modes of vibration and their natural frequencies. These are then excited separately by a narrow band of noise at a level equal to the spectrum level of the actual environment to be simulated and the responses in the several predominant modes are added to obtain the total response to the complete environment. The fatigue test is then set up so as to simulate the response in the most critical part by exciting one mode with a narrow band of noise. It is usually possible to find a suitable mode. In the simulation it is essential to ensure that the number of zero crossings of the strain waveform in the narrow band tests is equal to the number in the broad band environment.

An additional test procedure to obtain very high dynamic pressures is the use of a wall jet as suggested by Professor Ribner. Several designs on this principle have been made but little operating

experience has been gained to date.

A more complete environmental simulation may be needed for some structures. The Lockheed (Sunnyvale) facility was mentioned as an example of this type of combined thermal, acoustic and vibration environmental test. In cases where the interaction of the structure with the fluid flow is important it is not possible to use these types of facilities. The correct damping in the transonic range can only be achieved in wind tunnel tests.

References

1. W.H. Wittrick   A general algorithm for computing natural frequencies of elastic structures.
   F.W. Williams   Q.J.M.A.M., 24, 263-284 (1971).

2. W.H. Wittrick   General sinusoidal stiffness matrices for buckling and vibration analyses
                    of thin flat walled structures.
                    Int. J. Mech. Sci., Vol. 10, pp. 949-966 (1968).